WOODHEAD PUBLISHING IN TEXTILES

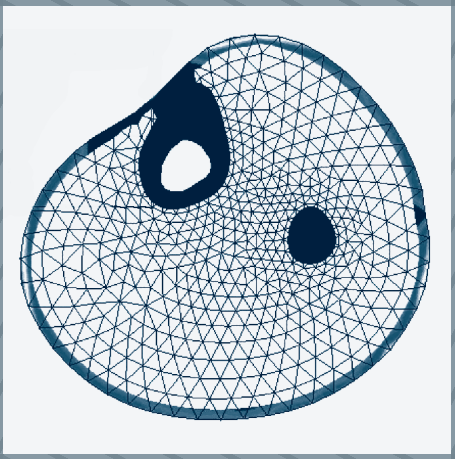

Biomechanical engineering of textiles and clothing

Edited by Y. Li and X-Q. Dai

CRC

The Textile Institute

WP

Biomechanical engineering of textiles and clothing

Related titles:

Effect of mechanical and physical properties on fabric hand
(ISBN-13: 978-1-85573-918-5; ISBN-10: 1-85573-918-6)

This new multiauthored collection addresses the effect of mechanical and physical properties on the way a fabric feels. It begins with concepts and understanding of fabric hand, covering development of fabric hand evaluation, the effect of fibre, yarn and fabric factors as well as finishing on hand, including the mechanical and physical properties. The latter part of the book goes on to cover statistical methods in evaluating hand and a comparison of hand evaluation in different cultures.

Friction in textiles
(ISBN-13: 978-1-85573-920-8; ISBN-10: 1-85573-920-8)

The action of friction in fibres and textiles plays a major role in product performance, from the generation of the fibre through to the way a garment responds to wear. This book addresses both the beneficial and detrimental processes of friction, with chapters on fibre structure, measurement techniques, static electrification, shrink proofing and felting, surface modification treatments, friction in fabrics and fibres and its role in textile processing.

Clothing appearance and fit; Science and technology
(ISBN-13: 978-1-85573-745-7; ISBN-10: 1-85573-745-0)

This comprehensive book provides a critical appreciation of the technological developments and scientific understanding related to clothing appearance and fit. It bridges recent active research and development in beauty and fashion design with garment evaluation technology, drape and human anthropometrics and sizing. It includes many industrial standards, techniques and practices that will make it an essential reference for researchers, academics, professionals and students in clothing and textile academia and industry.

Clothing biosensory engineering
(ISBN-13: 978-1-85573-925-3; ISBN-10: 1-85573-925-9)

Clothing biosensory engineering is a systematic and integrative way of translating consumers' biological and sensory responses and psychological feelings and preferences about clothing into the perceptual elements of design. It is a link between scientific experimentation and commercial application to develop economic solutions to practical technical problems. This book quantifies the decision-making processes through which physics, mathematics, and neurophysiological and engineering techniques are applied to optimally convert resources to meet various sensory requirements. It includes theoretical and experimental observations, computer simulations, test methods and examples of actual product development.

Details of these books and a complete list of Woodhead's titles can be obtained by:

- visiting our website at www.woodheadpublishing.com
- contacting Customer Services (e-mail: sales@woodhead-publishing.com; fax: +44 (0) 1223 893694; tel.: +44 (0) 1223 891358 ext. 30; address: Woodhead Publishing Ltd, Abington Hall, Abington, Cambridge CB1 6AH, England)

If you would like to receive information on forthcoming titles in this area, please send your address details to: Francis Dodds, (address, tel. and fax as above; e-mail: francisd@woodhead-publishing.com). Please confirm which subject areas you are interested in.

Biomechanical engineering of textiles and clothing

Edited by

Y. Li and X-Q. Dai

The Textile Institute

CRC Press
Boca Raton Boston New York Washington, DC

WOODHEAD PUBLISHING LIMITED
Cambridge England

Published by Woodhead Publishing Limited, Abington Hall, Abington
Cambridge CB1 6AH, England
www.woodheadpublishing.com

Published in North America by CRC Press LLC, 6000 Broken Sound Parkway, NW, Suite 300, Boca Raton, FL 33487, USA

First published 2006, Woodhead Publishing Limited and CRC Press LLC

British Library Cataloguing in Publication Data
A catalogue record for this book is available from the British Library.

Library of Congress Cataloging in Publication Data
A catalog record for this book is available from the Library of Congress.

Woodhead Publishing ISBN-13: 978-1-84569-052-6 (book)
Woodhead Publishing ISBN-10: 1-84569-052-4 (book)
Woodhead Publishing ISBN-13: 978-1-84569-148-6 (e-book)
Woodhead Publishing ISBN-10: 1-84569-148-2 (e-book)
CRC Press ISBN-10: 0-8493-9094-X
CRC Press order number: WP9094

The publishers' policy is to use permanent paper from mills that operate a sustainable forestry policy, and which has been manufactured from pulp which is processed using acid-free and elementary chlorine-free practices. Furthermore, the publishers ensure that the text paper and cover board used have met acceptable environmental accreditation standards.

Typeset by SNP Best-set Typesetter Ltd., Hong Kong
Printed by TJ International Limited, Padstow, Cornwall, England

Contents

Contributor contact details

(* = main contact)

Editors

Dr Yi Li,
Institute of Textiles and Clothing,
The Hong Kong Polytechnic University,
Hung Hom,
Kowloon,
Hong Kong, China.

Email: tcliyi@polyu.edu.hk

Dr Xiao-qun Dai,
School of Material Engineering,
Soochow University,
East Ganjiang Road 178,
Suzhou,
China.

Email: daixqsz@suda.edu.cn

Chapter 1

Yi Li (see editors)
Xin Zhang,
Fashion College,
Xian University of Engineering Science & Technology,
Xian,
China.

Email: xianzhangxin@sina.com

Xiao-qun Dai* (see editors)

Chapter 2

Xiao-qun Dai*, Yi Li (see editors)

Chapter 3

Ka-fai Faith Choi,
Institute of Textiles and Clothing,
The Hong Kong Polytechnic University,
Hung Hom,
Kowloon,
Hong Kong, China.

Email: tcchoikf@inet.polyu.edu.hk

Chapter 4

Xiao-qun Dai* (see editors)
Ka-fai Faith Choi (see Chapter 3)
Yi Li (see editors)

Chapter 5

Xiao-qun Dai* and Yi Li (see editors)

Chapter 6

Ameersing Luximon*
General Manager – Sales and Technical,
Milanezy (Excel Last) Co Ltd,
Room A1, Floor 11,
Manning Industrial Building,
116–118 How Ming Street,
Kwung Tong,
Hong Kong, China

Email: ieshyam@yahoo.com

Ming Zhang
Department of Health Technology and Informatics,
The Hong Kong Polytechnic University,
Hung Hom,
Kowloon,
Hong Kong, China.

Email: htmzhang@polyu.edu.hk

Chapter 7

Jason Tak-man Cheung*
Department of Health Technology and Informatics,
The Hong Kong Polytechnic University,
Hung Hom,
Kowloon,
Hong Kong, China.

Email: jason.cheung@mysinamail.com

Ming Zhang (see Chapter 6)

Chapter 8

Xiao-qun Dai* and Yi Li (see editors)
Xin Zhang (see Chapter 1)

Chapter 9

Xiao-qun Dai* and Yi Li (see editors)

Chapter 10

Xiao-qun Dai (see editors)

Chapter 11

Ka-fai Faith Choi (see Chapter 3)

Chapter 12

Yi Li and Xiao-qun Dai* (see editors)

Chapter 13

Ming Zhang* (see Chapter 6)
Jason Tak-man Cheung (see Chapter 7)

Chapter 14

Yi Li and Xiao-qun Dai* (see editors)
Xin Zhang (see Chapter 1)

Chapter 15

Ruo-mei Wang*,
Institute of Textiles and Clothing,
The Hong Kong Polytechnic University,
Hung Hom,
Kowloon,
Hong Kong, China.

Email: tcruomei@polyu.edu.hk

Luo Xiaonan,
Institute of Computer Application,
Zhongshan University,
Guangzhou,
China,
510275.

Email: lnslxn@zsu.edu.cn

Yi Li (see editors)

Xin Zhang (see Chapter 1)

Chapter 16

Ruo-mei Wang (see Chapter 15)
Luo Xiaonan (see Chapter 15)
Xiao-qun Dai* (see editors)
Xin Zhang (see Chapter 1)
Yi Li (see editors)

Chapter 17

Yi Li (see editors)
Ruo-mei Wang (see Chapter 15)
Xiao-qun Dai* (see editors)
Xin Zhang (see Chapter 1)
Luo Xiaonan (see Chapter 15)

Chapter 18

Xin Zhang *
(see Chapter 1)
Yi Li (see editors)
Anthony Wong,
Institute of Textiles and Clothing,
The Hong Kong Polytechnic University,
Hung Hom,
Kowloon,
Hong Kong, China.

Chapter 19

Yi Li (see editors)
Xin Zhang* (see Chapter 1)
K. W. Yeung,
Institute of Textiles and Clothing,
The Hong Kong Polytechnic University,
Hung Hom,
Kowloon,
Hong Kong, China.

Chapter 20

Xiao-qun Dai* (see editors)
Yi Li (see editors)
Rong Liu and Yi Lin Kwok,
Institute of Textiles and Clothing,
The Hong Kong Polytechnic University
Hung Hom
Kowloon
Hong Kong, China.

Chapter 21

Yi Li and Xiao-qun Dai* (see editors)
Ming Zhang (see Chapter 6)
Jason Tak-man Cheung (see Chapter 7)
Xin Zhang (see Chapter 1)

Chapter 22

Ameersing Luximon* (see Chapter 6)
Ming Zhang (see Chapter 6)

Chapter 23

Anthony Wong (see Chapter 18)
Yi Li* (see editors)
Edward Newton,
Institute of Textiles and Clothing,
The Hong Kong Polytechnic
University,
Hung Hom,
Kowloon,
Hong Kong,
China.

Xin Zhang (see Chapter 1)

Part I
Introduction

1

Textile biomechanical engineering

Y. LI[1], X. ZHANG[2] AND X-Q. DAI[1,3]
[1]The Hong Kong Polytechnic University, China
[2]Xian University of Engineering Science & Technology, China
[3]Soochow University, China

1.1 Background

Health and disease-prevention have been and are of major concern to humans, particularly for 21st century consumers regarding their apparel products. Biological health and psychological happiness are critical indexes reflecting quality of life, in which clothing plays very important roles. Clothing is one of the most intimate objects associated with the daily life of individuals, as it covers most parts of our body most of the time. Consciously or unconsciously, our physiological/biological status and psychological/emotional feelings are closely associated with the clothing we wear. A significant proportion of modern consumers understand the importance of clothing and they demand apparel products with higher added values in terms of functional performance to satisfy various aspects of their biological and psychological needs in communication, protection, healthcare, medicine and sensory comfort during wear. Naturally, engineering apparel products for biological and psychological health has become an integrated part of the concept of bioengineering.

What, then, is bioengineering? In February 1998, the United States National Institutes of Health organized a Symposium on bioengineering, at which a definition of bioengineering was formulated as follows: 'Bioengineering integrates physical, chemical, or mathematical sciences and engineering principles for the study of biology, medicine, behavior, or health. It advances fundamental concepts, creates knowledge from the molecular to the organ systems level, and develops innovative biologics, materials, processes, implants, devices, and informatics approaches for the prevention, diagnosis, and treatment of disease, for patient rehabilitation, and for improving health'.[1]

Angnew pointed out that bioengineering is rooted in physics, mathematics, chemistry, biology, computational sciences, and various engineering disciplines.[1] It is the application of a systematic, quantitative and integrative way of thinking about and approaching solutions of problems important in

human biology, physiology, medicine, behavior and health of human populations. From this definition, it is clear that the biological problems are too complex to be solved by biologists alone: partners are needed in many disciplines, including physics, mathematics, chemistry, computer sciences, and engineering. Bioengineering integrates principles from a diversity of fields. The creativity of interdisciplinary teams results in a new basic understanding, novel products and innovative technologies. Bioengineering also crosses the boundaries of academia, science, medicine, and industry.

Considering that clothing has a significant impact on the health and prevention of diseases, and creating appropriate microclimates for living and appearances that influence the perceptions and behaviors of human beings, clothing bioengineering can be defined in a similar way: 'Clothing bioengineering integrates physical, chemical, mathematical, and computational sciences and engineering principles to design and engineer clothing for the benefits of human biology, medicine, behavior and health. It advances fundamental concepts; creates knowledge from the molecular to the body–clothing systems level; and develops innovative materials, devices, and apparel products for a healthy lifestyle fashion with functions of comfort, protection, prevention, diagnosis, and treatment of disease, and for improving health.'

Such a definition shows that clothing bioengineering is rooted in physics, mathematics, chemistry, polymer sciences, biology, computational sciences, and engineering disciplines in polymers, fibers, textiles and clothing. It is the application of a systematic, quantitative and integrative way of thinking about and approaching the solutions in problems of how clothing and textiles can be engineered to the benefits of biology, physiology, medicine, behavior and the health of human populations. From this definition, it is clear that clothing bioengineering needs knowledge and close collaborative research of experts from a diversity of fields, including physics, mathematics, chemistry, polymer science, computer sciences, biology, physiology and psychology, as well as engineering disciplines from such industries as polymer, fiber, textile and clothing. The creativity of interdisciplinary teams can result in new basic understanding, novel products and innovative technologies in a number of areas such as: (i) clothing bio-thermal engineering; (ii) clothing biomechanical engineering; (iii) clothing biosensory engineering; (iv) clothing biomedical engineering; and (v) clothing biomaterial engineering.

Clothing biomechanical engineering is defined as the application of a systematic and quantitative way of designing and engineering apparel products to meet the biomechanical needs of the human body and to maintain an appropriate pressure and stress distributions on the skin and in the tissues for the performance, health and comfort of the wearer. Clothing biomechanical engineering involves not only the design and engineering of fabrics, but also the measurement of body geometric profiles, and the design

and engineering of garments to achieve the required biomechanical functions. Fundamental research to achieve the biomechanical functions involves a number of areas: (i) development of theories, data and models to describe the mechanical behaviors of fiber, yarns and fabric; (ii) development of theories, data and models to describe the geometric and biomechanical behavior of the human body; (iii) development of theories, data and models to describe the dynamic mechanical interactions between the body and garments; (iv) development of computational methods, computing visualization techniques, and engineering databases to integrate all the elements systematically; (v) design and engineering of materials and clothing to achieve desirable biomechanical functions; (vi) development of techniques to characterize the biomechanical functional performances from basic materials to final apparel products.

1.2 History of clothing biomechanical engineering design

Engineering design is an iterative decision-making process in which the basic sciences, mathematics, and engineering sciences are applied to convert resources optimally to meet a stated objective.[2] It is the link between scientific discoveries and commercial applications by applying mathematics and science to research and to develop economical solutions to practical technical problems. Engineering design has been successfully applied in a number of engineering areas such as machine manufacturing, civil engineering, and bridge construction. In 1986, the concept of sensory-engineering (Kansei-engineering) was developed by the Mazda Company in Japan as a development of human factors. Sensory means the psychological feeling or image of a product, and sensory engineering refers to the quantitative translation of consumers' psychological feeling about a product into perceptual design elements. This technique involves determining which sensory attributes elicit particular objective responses from people, and then designing a product using the attributes that elicit the desired responses. Sensory engineering has been applied with great success in the automotive industry, the Mazda Miata (MX-5) being a notable example, and is being extended to other product domains including development of new fibers.[3]

Textile products have been designed by trial and error for thousands of years. However, in the last few decades, industrial and academic experts[4–9] have recognized the importance of systematic engineering design of textiles and textile processes. In 1994, Hearle[7] presented the concept of textile-product design with fabric mechanics as a design tool. He described the different approaches available to tackle fabric mechanics in a hierarchical way and developed the concept of a computer-aided total-design system based on three frameworks: a database of information on fiber and fabric

properties; a knowledge-based system using the pool of available expertise and historical data; and a deterministic suite of programs in structural mechanics. In the 1990s, Matsuo and Suresh[8] proposed the concept of fiber-assembly-structure engineering (FASE) for total material design. Total material design refers to the design of a textile product starting from the conceptual design and going up to the devising of the manufacturing method. The design has three stages: (i) aesthetic-effect or functional design; (ii) basic structure design; (iii) basic manufacturing design.

The close relationship between garment design and fabric selection means that fabric representation and design is a fundamental part of any clothing engineering design system. Fabric is a complex media to model, owing to its complicated microstructure. In the past two decades, cloth modeling has drawn wide attention both from the textile engineering and the computer graphics communities. The textile engineering approach concentrated on the relationship between fabric structure and measurement data. In the 1990s, a series of papers by Dastor *et al.*[4,10,11] presented the computer-assisted structural design of industrial woven fabric, which illustrated the possibility of creating a CAD environment to aid structural design and evaluation of industrial fabric economically. The goal is the engineering design of the ideal quality of suiting on the basis of fiber science, textile mechanics and the objective measurement technology developed. Today, there are numerous existing design programs with various software tools and a wide choice of design functions. For example, Lectra[12] and NedGraphic[13] offer the textile industry a range of CAD/CAM software packages to meet the different requirements of various woven and knitted fabrics, printed fabrics and garment design. However, in such software, the focus is the image effects rather than the geometrical and mechanical models of fabrics and garments. Many existing apparel CAD systems provide assistance in pattern design, grading, marker making and cutting processes. Most of the systems work only two-dimensionally, and the materials' mechanical behavior is not taken into account.[14]

While the textile engineering approach offers precise details of modeling cloth at a microscopic level,[15] the computer graphics approach treats fabric as a deformable object, to develop visually-realistic cloth deformation and animation. Clothing modeling and garment simulation has grown from basic shape modeling to the modeling of cloth complex physics and behaviors. A trend of employing a multidisciplinary approach has started, the two communities having begun to combine their expertise to come up with solutions that can satisfy both of them. With their efforts, 2D apparel CAD systems are extending to 3D. A 3D apparel CAD system often incorporates a suitable fabric model, and enables the designer to assess how a particular type of fabric would interact with the 3D body form. The fabric model may include links to objective data and surface visualization techniques which

allow a fabric design or structure to be superimposed on the garment. Rodel *et al.*[14] pointed out that an excellent CAD system for the clothing industry should comprise three modules: a fabric library relating easy-to-determine fabric mechanical properties; a 3D model for the human body, which can be adapted for people of different sizes; and routines to construct garments from 2D patterns of specific fabrics on the human body with use of the fabric library. A common approach to constructing a garment is to accept 2D pattern shapes from a conventional CAD system, assemble them into a garment and drape or fit it onto a body form for further assessment and adjustment.

Early in 1992, Okabe *et al.*[16] presented details of a 3D CAD system with an energy-based fabric modeler incorporated. They showed examples of simulated garments fitted on a mannequin. The Asahi[17] apparel CAD 3D-PDS system, released in 1995, was also a 3D system that allowed designers to model patterns incorporating a fabric stiffness parameter. Both these systems accept the mechanical properties of fabrics. More recently, Kang and King[18,19] presented details of their 3D apparel system including flat-garment pattern generation, resizable human body modeling and garment-drape shape prediction. There was no evidence that actual mechanical parameters of fabric were used. The computer graphic community seems to be more advanced in 3D clothing modeling. There are many virtual fashion systems developed by different research teams from the computer graphics area, such as the *Virtual try on* system from the Miralab team (Geneva), *DressingSim* from Digital Fashion Ltd (Japan), and 'MayaCloth' from Maya, Spain. Most of these systems focus on generating cloth-like simulation and quick response and animation; accurate interpretation of mechanical properties and real-time performance are of secondary importance.

Although a 3D human body model is essential in all 3D apparel CAD systems, it is often assumed to be rigid, and acts as a geometrical constraint for the garment to drape or closely fit on it. The body deformation due to contact with the garment is rarely taken into account. Modern consumers demand clothing products with superior multi-functional and comfort performance to satisfy their physiological and psychological needs. Garment mechanical comfort such as pressure comfort has been identified as one of the important attributes. For example, Denton[20] pointed out that the discomfort level of clothing pressure was found to be between 20 and 40 g/cm^2, depending on the individual and the part of the body concerned, which is similar to the blood pressure in the capillary blood vessels near the skin surface. Tight-fit sportswear is reported to provide the body with suitable support and compression to accelerate blood circulation, hence improving sports performance.[18] However, the compression exerted on the human body by some medical clothing, such as pressure garments and compression stockings, has been utilized as a kind of physical therapy in clinical practice

for burn rehabilitation[21] and various venous disorders.[22] The biomechanical interaction between the human body and clothing is complicated, involving many aspects. Therefore, engineering design of clothing mechanical performance demands a different kind of logical structure to that of a textile product. An important difference is that human factors (physiological and psychological) have to be accounted for in the engineering design of clothing mechanical performance, because the human is the master in presenting clothing's aesthetic and functional effects.

However, there has not been any CAD system developed for the engineering design of clothing mechanical performance, especially for 3D simulation of the mechanical interaction of the deformable human body and clothing, and sensory evaluation of clothing mechanical comfort. There are not many studies available to express a design methodology and a design process for the engineering design of clothing mechanical performance. Li and Zhang[23] presented a mechanical sensory engineering design system for textile and apparel products, which was developed based on a consideration of human factors. The system had three functional models, namely design, analysis and evaluation. The fundamental work to achieve the system functions was detailed, including the development of mechanical models, development of an engineering database and investigation of psychophysical relationships between mechanical stimulation and comfort perception. The application of the system was illustrated through an example on the design of jeans for mechanical sensory performance. However, there is much room for improvement in this system. Biomechanical engineering design of clothing products is still at the development stage.

1.3 Biomechanical engineering design for fashion products

1.3.1 Clothing design based on human factors

The study of people as a component of an engineering system is called human factors engineering. Human factors engineering is an interdisciplinary science for fitting the product to the person rather than fitting the person to the product, involving specifying design with the requirements of people as the starting point and as the main criterion for effectiveness.[24] It includes taking knowledge from anatomy, anthropometry (the science of dimensions of humans), applied psychology, biomechanics, bioengineering and physiology.

In the concept of mechanical sensory engineering design of clothing performance, human factors are concerned in two design processes: fashion design and clothing materials design, to achieve the desired clothing aesthetic and functional effects. The human factors are mainly concerned

with five aspects: (i) Geometry (such as the body size and the shape); (ii) biomechanics of the human body (such as the deformation of the muscles, skin and soft tissue at different body parts); (iii) physiology (formulating sensory signals from the interactions of the body with the clothing and surrounding environments); (iv) neurophysiology; and (v) psychology (subjective perception of sensory sensation from the neurophysiological sensory signals and leading to formulated subjective overall perception and preferences). The four factors of geometry, biomechanics, physiology and neurophysiology must be considered in pattern design and material design, and the psychological factor must be taken into account in designing aesthetic effects of clothing.

Sensory engineering design of clothing mechanical performance should be based on quantitative investigations of the relationship between clothing mechanical performance and human sensory (physiological and psychological) factors. There are three fundamental investigations required to achieve the concept. The first is the quantitative translation of consumers' psychological feelings about a product into perceptual design elements that will be important attributes in the evaluation of fashion and material design. The second is the investigation of the dynamic mechanism involved in the contact interface between the human body and clothing, which bridges the relationship between human biomechanics and fashion design. The third is deduction of the clothing mechanical characteristics from the dynamic analysis, such as its deformation magnitude, stretch-recovery properties and rheological behavior during wear. These physical and mechanical characteristics of clothing materials are the basic information required for the engineering design of clothing materials.

1.3.2 Computer aiding the iterative decision-making process

Clothing design means creating new clothing by enhancing existing designs or by altering existing ones to perform new functions. The clothing design task consists of selecting the style, color and materials to meet specified functional requirements for the clothing. The conventional procedure of designing clothing without CAD technology is largely based on the experience and intuition of the designer, which has several disadvantages. Firstly, much reliance is placed upon individual designers but not on the knowledge-based design model. It is difficult to require a designer to communicate with interdisciplinary professionals to achieve the developed concept, and the training of new design 'apprentices' is a lengthy, tedious, and costly process. Secondly, it is difficult to achieve an iterative decision-making process in a short design time. Thirdly, the designer does not have the means to make a parametric analysis of the clothing mechanical

performance before it is produced. Finally, it is difficult to maintain a consistently updated information system involving multiple sets of data at several locations within an organization.

A CAD system should overcome these disadvantages by the development of fundamental frameworks. It requires the development of knowledge-based design procedures to guide the user in designing clothing mechanical performance based on human sensory factors. The design starts with a product specification to identify a type of garments (e.g. jeans or bra), followed by selection of garment style and human body parameters from the human factor database and the product database. From the input parameters of the human body and the garment, the deformation characteristics of clothing should be identified, based on mechanical analysis of the dynamic contact between the human body and the garment, which will govern the next steps of selecting fabric structure and selecting mechanical properties of the fiber–yarn–fabric. The selection is a revision of design achieved by searching or reworking some previous fabric structure that reasonably approximates to the current design requirements. Next comes a mechanical model of the body–garment, allowing a numerical simulation and analysis of the mechanical performance of garment and body. The iterative procedure has to be done before the garment is produced, if the design does not satisfy through the simulation and evaluation steps. The iterative design cycle will be shortened through the CAD environment, which is supported by four engineering databases and based on a number of fundamental researches. Through the design process in the CAD system, a sample is manufactured for a wear trial. This aims to further modify the design according to subjective evaluation of the garment before formal production.

1.3.3 Analysis based on 3D virtual prototypes

The design phase determines feasible style and materials parameters; the analysis phase is used to calculate and visualize the mechanical performance of the textile and clothing system, such as distributions of stresses and strains in the garment, the deformation of the skin and soft tissues, and the garment pressure distributions on the skin. This analysis involves computational experiments of the design to test whether it meets the desired functional criteria of clothing. To analyze clothing mechanical performance based on 3D virtual prototypes requires the development of 3D mechanical models of clothing and human body that can simulate the mechanical interactions between them in different wear situations. The saying of ‘A picture is worth a thousand words’ is still true. Visualization of the 3D prototypes undeformed or deformed, and mechanical parameters, such as various strains, stresses and pressure, can give the designer immediate feedback on

design decisions. Based on the visible simulation results, various functional analyses can be carried out. For some special garment items, biomechanical prediction can be obtained.

1.3.4 Sensory evaluation

During wear, clothing comes into contact with the skin at most parts of the body. Li[25] pointed out that the contact has three features: (i) large contacting areas with varying sensitivity; (ii) changing physiological parameters of the body (such as skin temperature, sweating rate, and humidity at the skin surface); (iii) a moving body that induces new mechanical stimuli from the contact between the body parts and clothing. The mechanical stimuli in turn induce responses from various sensory receptors and formulate various perceptions, such as touch, pressure, prickle, itch and inflammation, which affect the mechanical comfort of the wearer. The study of the psychophysical process of perception on clothing mechanical behavior makes it possible to predict and evaluate mechanical sensory comfort of clothing from the mechanical properties and structural features of fibers, yarns and fabrics, as well as garments.

Mechanical comfort should be one of the criteria to decide which design is optimal among several alternatives in the design process. The designer can judge whether the product meets the comfort requirements by comparing the predictions with desirable values, such as desirable pressure distributions and psychological perceptions of comfort pressure. Therefore, in addition to the design and the analysis functions, the system should provide the function of sensory evaluation of mechanical comfort.

Clothing comfort is very subjective. Evaluation of pressure comfort must combine the predicted pressure and the sensation index from a large volume of experiments involving wear trials. It needs much work on psychological evaluation of garment pressure, from which a series of psychophysical models will be developed based on the investigation of the relationship between objective stimuli and psychological perceptions and the investigation of the relationship between the predictions and the objective measurements. For medical clothing items, there are often criteria of specific physical parameters to be met. The evaluation of medical effects is very complicated, and requires more cooperation with clinical practice in a long-term project.

1.4 Fundamental frameworks in clothing biomechanical engineering

To develop Clothing Biomechanical Engineering Design (CBED) systems with the required functions, a series of fundamental developments need to be made by integrating science, engineering and information technologies.

The research involves a number of aspects: material modeling of textile materials of different level (fiber–yarn–fabric); mechanical modeling for the contact system of the human body and clothing; a clothing engineering database; and investigation of the psychophysical relationship between mechanical stimulation and psychological comfort perception.

1.4.1 Textile material modeling

Clothing is made of fabric, which is a flexible material that behaves with complicated deformation. Due to the complicated deformation of fabric and different pattern assemblies, garments show aesthetic appearance of infinite variations. Since fabric is a complicated structure, hierarchically built on yarns and fibers, the investigation of textiles' micro-mechanics is a stratagem whose objective is to achieve the engineering design of clothing performance from fundamental parameters of fiber–yarn–fabric structures. Models of different levels in the hierarchical structure are necessary for the material engineering design. It is also important to understand the relationship between clothing mechanical performance and fabric mechanical properties in simple deformations, such as tension, shearing, bending and compression, because these fabric properties are the basic parameters used in mechanical models of clothing.

1.4.2 Contact model between human body and garment

Clothing mechanical behavior is related to both fabric mechanical properties and the space allowance between the body and the garment during body movement. According to the degree of space allowance, garments can be classified into three types: (i) foundation garments, in which the garment area is less than the body area; (ii) perfect fitting garments, where the garment area is equal to the body area; (iii) loose garments, where the garment area is larger than the body area. Foundation garments are designed to apply a certain level of pressure on the appropriate body part when the body is both active and at rest. Perfect fitting garments have a figure-shaping function but are not designed to apply pressure on the body. Because the body movement can reduce the space allowance, loose garments may also exert pressure on the body in the contact areas. Therefore, the development of 3D geometrical models of human bodies and garments is fundamental for numerical analysis and visualization of clothing mechanical performance.

Generally, clothing behaves mechanically in a non-linear way and is subject to multi-directional stress/strain components. In approaching the complex clothing mechanics, it is usually assumed that the clothing material is a continuum of plate (planar when unstrained), or shell (naturally curved),

or membrane (perfectly flexible plate or shell). This is due to the fact that many studies mainly focused on its macroscopic mechanical behavior that occurs under an external force or prescribed curvatures from a human body.

The mechanical interaction between human body and garment varies significantly for different wearing situations, depending on four factors: (i) garment style; (ii) garment space allowance; (iii) dynamic wearing or pattern assembling processing; (iv) posture of the human body. These factors have to be approached by providing different boundary conditions in the development of contact models. The mechanical system of the contact, which is often non-linear due to the large deformation and complicated contact condition, is usually solved numerically using a finite element method and other discretized methods.

1.4.3 Visualization of the 3D prototypes

A CBED system needs to provide a virtual prototyping environment to enable the designer to visualize a garment prior to making a physical sample. As mentioned previously, geometrical models are essential for the mechanical simulation. Various 3D prototypes need to be generated, positioned properly, and discretized for the further mechanical analysis. Once the mechanical analysis has been completed, the results need to be evaluated. The 3D garment fitted to the human body needs to be visualized for assessing the garment aesthetic shape and fit. The displacements, stresses and other fundamental variables in clothing objects as well as the human body that have been calculated, need to be visualized and plotted for appraising fabric suitability and wearing comfort, and other functional analysis and evaluation. The visualization is generally done interactively utilizing the specific visualization modules for the analysis solvers used, some general graphic tools, or other specifically developed pre- and post-processors.

1.4.4 Clothing engineering database

To support the design, analysis and evaluation phases in a systematic design process with various types of information, it is necessary to develop an engineering database. An engineering database has several important differences from an administrative database or a business database. Firstly, engineering design is an iterative-decision process with analysis and synthesis based on knowledge of basic sciences, mathematics, and engineering sciences. Secondly, engineering design needs a dynamic database that involves two kinds of information: the design environment (rules, methods, standard elements, etc.) and data that are not known previously but defined during the design process. The volume of information increases with the

progress of a design. Thirdly, engineering design deals with a number of data types (text, numbers, equations, diagrams, graphical, photographic images, etc.).

An important characteristic that must be considered in the development of a clothing engineering database is that the clothing design process communicates frequently with the information from the hierarchical construction of a fiber–yarn–fabric–garment and a 3D human body. The structural geometry of textiles is central to all aspects of the computer-aided design and prediction, which should be presented to the designer during the design process. Therefore, the clothing engineering database should support user-friendly program packages to input, store and display the information of fiber–yarn–fabric–garment quickly and effectively in time and space.

1.4.5 Investigation of psychophysical relationship between stimulation and perception

To visualize the sensory perception in the CAD environment, a series of psychophysical experiments have to be carried out to study mechanical comfort of the garment in different wear situations by conducting mechanical sensory comfort perception trials and objective measurement of dynamic pressure distribution. Further, psychophysical models of mechanical comfort have to be developed in different wearing situations, by using statistical methods, neural networks, etc.

1.5 Clothing biomechanical engineering design system: an example

Advances in technology, computer performance and cloth simulation research make the development of a CBED system possible. Now that cloth simulation has been addressed widely from 1D fiber level to 3D garment level, and the physical testing techniques of textiles have been advanced, the challenge is then to integrate these modeling and information techniques logically and effectively and build an interactive and creative system for the engineering design.

The system conceived and developed in the Institute of Textile and Clothing, Polytechnic University of Hong Kong, for the biomechanical engineering design for textile and clothing products is briefly outlined.[23] This system integrates clothing design process, clothing–body biomechanical models, numerical solutions, analysis and evaluation of clothing sensory mechanical performance into a CAD environment based on a collection of well-integrated software tools. There are eight working modules in the system: (i) user interface; (ii) design processing algorithms; (iii) generation

of 3D geometrical primitives, realized using pre-processing software or graphic tools; (iv) definition of boundary conditions of the contact system, performed using preprocessors; (v) mechanical analyzers – can be commercial software, such as LS-DYNA (Livermore Software Technology Corporation), ANSYS (MSC.Software, USA), ABAQUS (Hibbitt, Karlsson & Sorensen Inc., USA) and specifically-developed solvers; (vi) result visualization, performed by using some post-processors; (vii) sensory evaluation; (viii) engineering database. There is also a control communication module connecting with each of the eight working modules, indicating the broad division of the information communication among the working models and the software environment of the system. Each working module accomplishes its purpose with suitable software. A key feature is the integration of relevant software components into the CBED system, because many of the software packages have been developed independently in different industries for their specific purposes, with little knowledge of mechanical engineering design of textiles.

The originality of this system is evident in four major aspects: (i) consideration of human factors (physiological and psychological) in engineering design of clothing products; (ii) simulation and visualization of clothing mechanical comfort performance before the garment is produced; (iii) integration of a range of software components into the system for computer-aided engineering design; (iv) provision of a platform with an engineering database to input, store and display information about the hierarchical mechanical properties and structural features of garments and human bodies. The system aims to provide a design methodology and a tool for fashion designers and textile scientists, engineers and product developers to design new products efficiently with consideration of mechanical performance.

1.6 Outline of this book

This book is divided into five parts. Part I is this chapter as an overall introduction. In Part II, the fundamental scientific theories, principles and models behind the mechanical sensory design technology are described. There is a hierarchical interrelation among textile products, from fiber, yarn and fabrics, to clothing. Two sets of parameters are involved – properties of the constituents and structural geometry. All of these features must be taken into account in garment product design. Micromechanics and macromechanics are the usual tools in tackling the problems of mechanical performance for textile products. Micromechanics covers predicting the fundamental constitutive relations for any textile structure in terms of the two sets of parameters mentioned above, while macromechanics is concerned with predicting the complex response of a material subject to the collection of

forces imposed in practical situations. A fundamental understanding about these micro- and macromechanics in textiles is introduced. The modeling techniques are also overviewed. As the subject for clothing, the human body's geometrical and biomechanical features and sensation, and its contact problem with clothing are also introduced.

In Part III, the brief development history, structural features and mechanical properties of textile materials are described from fibers, yarns, and also the fabrics to clothing, and also the mechanical properties of the biomaterials of the human body. The parameters relevant to clothing mechanical performance are introduced and the major measurements for these properties are reviewed. These parameters will be included in the database for the design system.

In Part IV, the clothing biomechanical engineering design system is discussed, with a detailed explanation of the system construction, including integration of mechanical models, numerical solution approaches, pre- and post-processing and the database constitution.

Finally, in Part V, several practical examples of product development, such as jeans, sports bras, compression stockings, socks, shoes and aerobic sportswear, are provided to illustrate how to carry out the biomechanical engineering design.

This book is the result of the contributions from the authors and the work of other researchers on the important topics of the textile and clothing biomechanical engineering. The authors hope that the book will help interested beginners to carry out research in the area and to motivate current researchers and developers in this area towards further development and applications.

1.7 Acknowledgement

We would like to thank Hong Kong Polytechnic University for funding this research through Projects A188 and G-YD31.

1.8 References

1. Angnew, B., *Science*, 1998. **1516**(5369): p. 280.
2. Woodson, T.T., *Introduction to Engineering Design*. 1966, New York: McGraw-Hill.
3. Honggu, T., *High-Tech Fibers*. 1999, Tokyo, Japan: Woodhead Publishing Limited.
4. Dastor, P.H. *et al.*, Computer-assisted Structural Design of Industrial Woven Fabrics, Part I: Need, Scope, Background, and System Architecture. *Journal of Textile Institute*, 1994. **85**(2): p. 89–109.
5. Hearle, J.W.S., Newton, A. and Grigg, P.J. *Computer-aided Textile Design: A Liberating Prospect*. 1984, Manchester: The Textile Institute.

6. Postle, R., Kawabata, S. and Niwa, M. *Objective Evaluation of Apparel Fabrics*. 1983, Osaka: The Textile Machinery Society of Japan.
7. Hearle, J.W.S., Fabric mechanics as design tool. *Indian Journal of Fibre and Textile Research*, 1994. **19**(3): p. 107–113.
8. Matsuo, T. and Suresh, M.N. *The Design Logic of Textile Products.* Manchester: The Textile Institute, 1997. **27**(3).
9. Kawabata, S., Niwa, M. and Yamashita, Y. Recent Developments in the Evaluation Technology of Fiber and Textiles Towards the Engineered Design of Textile Performance, in *International Technical Symposium '100 Years of Modern Fiber Science'*. 1998. Asheville, North Carolina, USA.
10. Dastor, P.H. *et al.*, Computer-assisted Structural Design of Industrial Woven Fabrics, Part II: System Operation, Heuristic Design. *Journal of Textile Institute*, 1994. **85**(2): p. 110–134.
11. Dastor, P.H. *et al.*, Computer-assisted Structural Design of Industrial Woven Fabrics, Part III: Modeling of Fabric Uniaxial/Biaxial Load-Deformation. *Journal of Textile Institute*, 1994. **85**(2): p. 135–157.
12. Lectra, Lectra's Latest CAD/CAM System. *JSN International*, 2003(9): p. 14–18.
13. Janmaat, M., Textiles by Design. *Textile Technology International*, 1999. **81**(1).
14. Rodel, H. *et al.*, Links between Design, Pattern Development and Fabric Behaviours for Clothes and Technical Textiles. *International Journal of Clothing Science and Technology*, 2001. **13**(3/4): p. 217–227.
15. Tarfaoui, M. and Akesbi, S. Numerical Study of the Mechanical Behaviour of Textile Structures. *International Journal of Clothing Science and Technology*, 2001. **13**(3/4): p. 166–175.
16. Okabe, H. *et al.*, Three Dimensional Apparel CAD System. *Computer Graphics*, 1992. **26**(2): p. 105–110.
17. Niki, T.C. and Grimsdale, R.L.B. The Asahi Apparel CAD 3D-PDS System, One of the Many Exciting New Exhibits at Boobin'95. CAD Developments, *Apparel International*, 1996(12): p. 35–37.
18. Kang, T.J. and Kim, S.M. Development of Three-dimensional Apparel CAD System, Part I: Flat Garment Pattern Drafting System. *International Journal of Clothing Science and Technology*, 2000. **12**(1): p. 26–38.
19. Kang, T.J. and Kim, S.M. Development of Three-dimensional Apparel CAD System, Part II: Prediction of Garment Drape Shape. *International Journal of Clothing Science and Technology*, 2000. **12**(1): p. 39–49.
20. Denton, M.J., Fit, Stretch and Comfort. 1972, *Textiles*. p. 12–17.
21. Ng-Yip, F.S.F., Medical Clothing. *International Journal of Clothing Science and Technology*, 1993. **5**(1): p. 17–24.
22. Ramelet, A.A., Compression Therapy. *Dermatologic Surgery*, 2002. **28**: p. 6–10.
23. Li, Y. and X. Zhang, Mechanical Sensory Engineering Design of Textile and Apparel Products. *Journal of the Textile Institute*, 2002. **93**(2): p. 56–75.
24. Galer, I.A.R., *Applied Ergonomics Handbook*, London: Butterworths.
25. Li, Y., The Science of Clothing Comfort. *Textile Progress*, 2001. **31**(1/2): p. 1–138.

Part II

Theoretical background

2

Fiber mechanics

X-Q. DAI[1,2] AND Y. LI[1]
[1]The Hong Kong Polytechnic University, China
[2]Soochow University, China

2.1 Introduction

Fibers are the fundamental and the smallest elements constituting textile materials. The biomechanical functional performance of garments and devices are very much dependent on the fiber mechanical and surface properties, which are largely determined by the constituting polymeric molecules, internal structural features and surface morphological characteristics of individual fibers. Scientific understanding and knowledge of the fiber properties and modeling the mechanical behavior of fibers are essential for biomechanical engineering of clothing and textile products. In this chapter, we review the knowledge and processes developed in the area of fiber mechanics in relation to biomechanical engineering.

2.2 Fiber morphology

The morphology of fibers includes macrostructure, microstructure, submiscroscopic structure and fine structure of fibers.

2.2.1 Macrostructure

The features of a textile fiber that are discernible to the human eye constitute its macrostructure; these include width, length, and crimp.

Fiber size Fiber size, often referred to as fineness, is one of the most important properties of fibers. It is usually specified in terms of diameter or linear density. The size of natural fibers is often given as a diameter in micrometer units. It reflects the average width along the fiber's length. The sizes of silk and manufactured fibers are usually given in denier or tex units, which specify the linear density based on weight per unit length. *Denier* is the weight in grams of 9000 m of a fiber; *tex* is the weight in grams of 1000 m of a fiber. *Tex* is one-ninth of 1 *denier*.

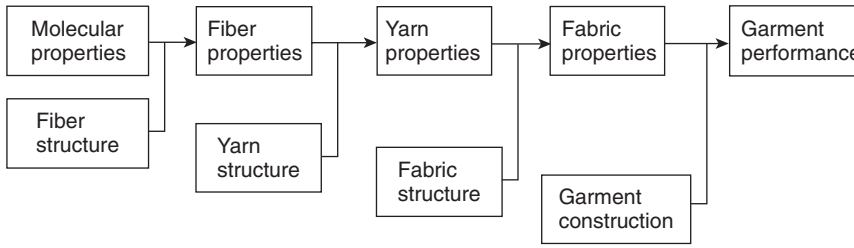

2.1 Hierarchical relationships of fiber, yarn, fabric and garment to the biomechanical function performance of clothing and textile devices.

Fiber size has a very important influence on fiber stiffness, which then affects the stiffness of the fabric made from the fiber and hence the way it drapes and how soft it feels. The fiber stiffness also affects how soft or how prickly the fabric feels when it is worn next to the skin.

Fiber length After size, fiber length is the most important property of a fiber. Fiber length is critical in processing of fibers and yarns and in the translation of fiber strength to yarn strength. In general, a longer fiber length is preferred. Textile fibers are either staple or filament length. Staple fibers range from 2 to 46 cm; filament fibers are of infinite length. All natural fibers except silk are of staple length. Silk and manufactured fibers may be staple or filament fibers.

Fiber crimp Crimp refers to waves, bends, twists or curls along the fiber length. It is expressed as crimps per unit length. Some natural fibers are linear, others form two-dimensional or three-dimensional crimps as shown in Fig. 2.2. Crimped fibers tend to have higher elongation than linear fibers.

2.2.2 Microstructure

Microstructure of fibers includes their surface contour and cross-sectional shape. These features are observable through a light microscope. Surface contour, describing the surface of the fiber along its length, may be smooth, serrated, lobed, striated, pitted, scaly, or convoluted. Surface contour may affect fiber frictional properties and comfort when worn next to the skin.

Cross-sectional shape refers to the shape of a horizontally cut fiber section. It may be round, triangular, dog-bone, kidney-bean, flat, and so on. There is a characteristic shape for each type of natural fiber. The shape of a fiber's cross-section is important in many applications. It has influence on bending stiffness and torsional stiffness of the fiber. Consider the bending

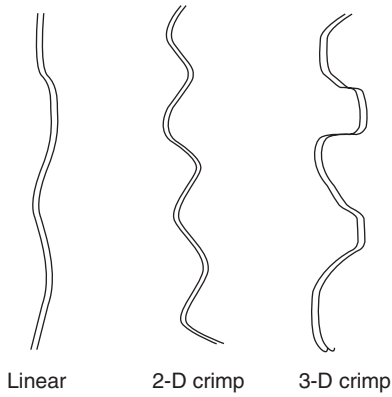

2.2 Fiber crimp.

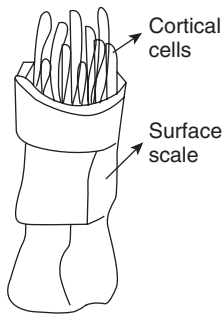

2.3 Fiber submicroscopic structure (wool).

stiffness of the solid fibers, those with round cross-sections offer a high resistance to bending and, hence the fibers are stiff. However, fibers with ribbon-like cross-sections, such as cotton, offer the least resistance to bending.

2.2.3 Submicroscopic structure

Through an electronic microscope, more details of fibers on the surface, as well as in the inner side, are observable. Figure 2.3 shows the schematic microscopic structure of wool fiber.

2.2.4 Fine structure

All fibers are assemblies of macromolecules, called polymers, in the form of hundreds or even thousands of individual chemical units, covalently bonded together one after the other as illustrated in Fig. 2.4. Fine structure

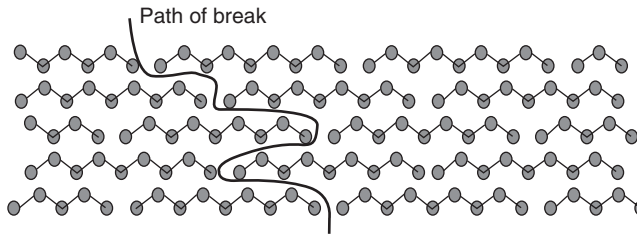

2.4 Fine structure of fiber.

describes the length, width, shape, and chemical composition of these polymers. It largely determines the ability of a fiber to withstand mechanical forces. There are three types of polymers comprising textile fibers: homopolymers, copolymers, and block polymers. In homopolymers, the most common type, one monomer (one chemical compound) repeats itself along the polymer chain. In copolymers, two or more monomers comprise the polymer chain. In block polymers, blocks comprised of homopolymers are repeated along the polymer chain. Polymer length is specified as the number of times the monomer is repeated along the chain, called the degree of polymerization. Polymer length plays a role in fiber tensile properties. If two fibers are alike except for polymer length, the fiber comprised of longer polymers is generally stronger, extends a shorter distance at a given load, and requires more force to cause elongation.

Within fibers, adjacent polymers are found tightly packed together in specially ordered crystalline regions and further apart in amorphous regions. The proportion of crystalline to amorphous regions determines the 'degree of crystallinity'. The thousands of polymers within a fiber lie more or less parallel to the longitudinal axis of the fiber itself. When a relatively high proportion of polymers are aligned with the fiber axis, the fiber is said to be 'highly oriented'. Orientation and crystallinity have a significant impact on various fiber behaviors. If two fibers are alike except for degree of orientation and crystallinity, the fiber that is more crystalline and orientated is stronger and stiffer, and has lower elongation at break.

2.3 Mechanical behavior

The mechanical properties of fibers are their responses to applied forces and to recovery from those forces. They contribute both to the behavior of fibers in processing to yarns and to the properties of the final products so that a knowledge of fiber behavior is essential to an understanding of yarn mechanics and fabrics mechanics.

2.3.1 Tensile properties

Stress–strain curve: Because of the linear shape of a fiber, the tensile properties (the behavior under forces and deformations applied along the fiber axially) are the most important properties and are the most studied. Figure 2.5 illustrates the tensile deformation. In general engineering, the tensile stress = force/area, $\sigma = F/A_0$; the tensile strain = change in length/original length, $\varepsilon = \Delta l/l_0$.

When applying a gradually increasing force along the fiber axis until the fiber breaks, a stress–strain curve is created. It shows many important mechanical characteristics of the fiber. In textile technology, a specific stress is often used instead of the general stress used in engineering area: Specific stress = force/linear density, $\sigma_s = F/d_1$.

Figure 2.6 shows a model stress–strain curve. The curve begins with a straight-line segment that rises as stress is increased (AB) and then suddenly flattens and rises at a slower rate (BC). Close to the failure point, the curve rises steeply (CD). The details of each of the regions is addressed as follows:

- In region AB, the deformation is a result of bond stretching and flexing. It is completely reversible. Hooke's law is obeyed: $\sigma = E\varepsilon$, where E is the slope of the line, called Young's modulus. In this region, the deformation is recoverable, and it is elastic. As the fiber extends along the axial direction, it contracts laterally. Poisson's ratio, defined as the ratio of lateral contraction to axial extension, is another important material characteristic that deals with the behavior in the elastic region.
- After the yield point, deformation becomes nonlinear, and it is usually plastic. The deformation, a result of the polymers slipping by each other, is partially recoverable. In the region BC, the fiber extends more easily.

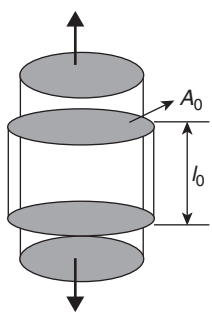

2.5 Schematic tensile deformation of a cylinder.

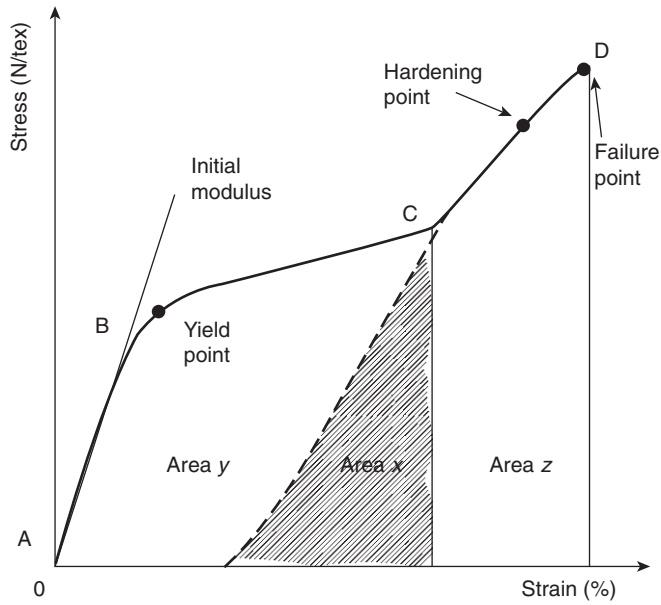

2.6 Schematic stress–strain curve of a fiber.

The slope of the segment BC largely reflects the strength of intrafiber bonding.

- As the polymers become more compact, the fiber reaches a deformation limit, harden point. Following the hardening, the internal structure of the fiber begins to give way and the failure point is reached. The stress and strain at this point give the tenacity and the elongation at break respectively.

Elastic recovery: In the initial segment of the stress–strain curve (AB), the fiber behaves like an elastic spring. Under the applied load, the polymers are being straightened, perhaps becoming more oriented within the fiber. If the load is removed at any point from A to B, the fiber will return to its original length because the polymers can revert to their initial positions. In this case, the elastic recovery is 100%. If the fiber is stretched beyond the yield point but not to its hardening point, and the load is then removed, the fiber will partially recover.

Work of rupture: Work of rupture or toughness is a measure of the ability of a fiber to withstand sudden shocks of energy. The total amount of work required to deform a fiber up to the failure point is indicated by the area under its stress–strain curve, the sum of areas x, y, and z, illustrated in Fig. 2.6.

Resilience: The resilience, also called work of recovery, of a fiber is the ratio of energy returned to energy absorbed when a fiber is deformed and then released. It may be extensional, flexural, compressional, or torsional. In Fig. 2.6, the fiber resilience of extension is the ratio of area x to area $x + y$.

Effects of time, temperature and moisture: The extension caused by a given applied force, or the stress resulting from a given strain in the fiber, depends on how long the force or the strain has been present and on the earlier mechanical history of the fiber; it also depends on the temperature. Time and temperature dependent mechanical behavior is a characteristic of fibers. It is usually called viscoelastic (combined viscous and elastic) and is due to polymers not being ideal elastic solids – they also contain a viscous component. Creep and stress relaxation are the tests developed to probe their time-dependent behavior. In the creep test, the strain increases with time in a sample under constant load. In the stress relaxation test, the stress decays with time after the sample is given an instantaneous strain. Moisture also affects the mechanical behaviors of fibers. Basically, the moisture lodges in the noncrystalline regions and plasticizes them, reducing the modulus.

2.3.2 Forces in various directions

Bending: When a fiber is bent, the polymers must extend and compress to accommodate the bending force. As illustrated in Fig. 2.7, the polymers on the under curvature will compress; those on the upper curvature will extend; and those on the center plane will be unchanged in length.

Flexural rigidity (resistance to bending, stiffness) of a fiber is defined as the couple required to bend the fiber to unit curvature. Thus, in the elastic

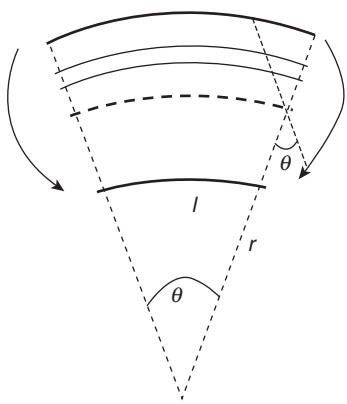

2.7 Bending of a fiber.

region there exists $M_B = BK$, where M_B = force couple, B = flexural rigidity and K = bending curvature. The flexural rigidity can be expressed in terms of the Young's modulus E as: $B = \frac{1}{4\pi}\frac{\eta E T^2}{\rho}$, where, η is a shape factor related to the cross-section of the fiber, and ρ and T are the density and linear density of the fiber respectively.[1] It is convenient to introduce a quantity that is independent of the fineness of the specimen to replace the flexural rigidity. That is the specific flexural rigidity, R_f, equal to the flexura rigidity of a filament of unit tex: $R_f = \frac{1}{4\pi}\frac{\eta E}{\rho}$.

Shear and torsion: Figure 2.8 shows the shear deformation of a solid cube unit. The shear stress τ is expressed as F/A_0 and the shear strain is calculated as $\delta x/y$. Then, in the elastic region, the shear modulus G can be defined as the ratio of shear stress to shear strain: $G = \tau/\gamma$.

Figure 2.9 shows the twisting deformation of a fiber of circular cross-section. If we look at a small region, the fiber is sheared. The torsional rigidity of a fiber, its resistance to twisting, is defined as the couple needed to achieve unit angular deflexion between the ends of a specimen of unit length. Usually the specific torsional rigidity, R_t, the torsional rigidity of a specimen of unit linear density (in tex), independent of the fineness of the particular specimen, is used. Since twisting has the same relation to shearing as bending does to stretching, the torsional rigidity can be obtained in terms of the shear modulus in the same way that the bending rigidity can be obtained in terms of the Young's modulus: $R_t = \eta n/\rho$. Here, ρ and η are the linear density and the shape factor of the fiber respectively. Details can be found in reference 1.

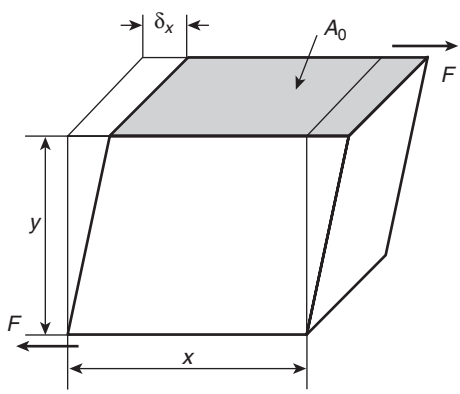

2.8 Shear deformation of a cube.

Compression: Figure 2.10 (a) shows a cylinder under axial compression. A compression stress is simply negative to tensile stress and a compression strain is also a negative one. The initial compressive modulus is generally the same as the initial tensile modulus. However, as the compression force increasing, the fiber will buckle easily. Figure 2.10 (b) shows a cylinder under transverse compression. The transverse modulus is used to reflect the transverse compressive property.

2.3.3 Friction

Fiber friction is the force that holds together the fiber in a spun yarn and the interlacing threads in a fabric. Here, high friction is an advantage to enable a greater proportion of the strength of the individual fibers to be obtained. However, lower friction of a fiber may be desired in other cases,

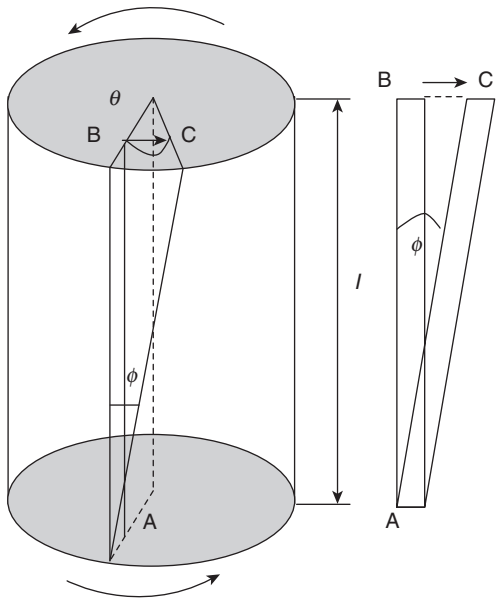

2.9 Shear or torsion on a cylinder.

(a) Axial compression of a cylinder (b) Transverse compression

2.10 Fiber compression.

such as in minimizing wear of fibers and fabrics, providing good fabric drape, and so on. Friction coefficient, μ, is used to denote the friction property of a fiber.

2.4 Modeling of fiber mechanical properties

2.4.1 Structural model

Various models have been proposed to represent the structure of polymers and fibers, and further to calculate fiber mechanical properties on the basis of the properties and arrangement of the components. Fiber scientists often envision a two-phase model, crystalline and non-crystalline, for the structure of polymers and fibers. The three most useful two-phase models for fiber structure are: the isostrain model, the isostress model, and the micellar model, as illustrated in Fig. 2.11. The isostrain model represents a fiber as two continuous phases that are aligned parallel with each other. When the fiber is stretched along the axial direction, the stress will be the appropriate weighted-mean stress contributed by the two components at the same strain, and the modulus of the fiber is a volume-weighted average of the two phases, as the following equation shows: $E_C = E_1V_1 + E_2V_2$. Here, E_C, E_1 and E_2 denote the Young's moduli of the fiber, and the two components respectively.

Figure 2.11(b) show the isostress model, which has the same structure as the isostrain model but is subjected to a stress normal to the fiber direction. In this case, the behavior of the composite system is given by taking the weighted-mean strain with the same stress on each component. The modulus of the composite can be obtained as:

$$1/E_{C\perp} = V_1/E_{1\perp} + V_2/E_{2\perp},$$

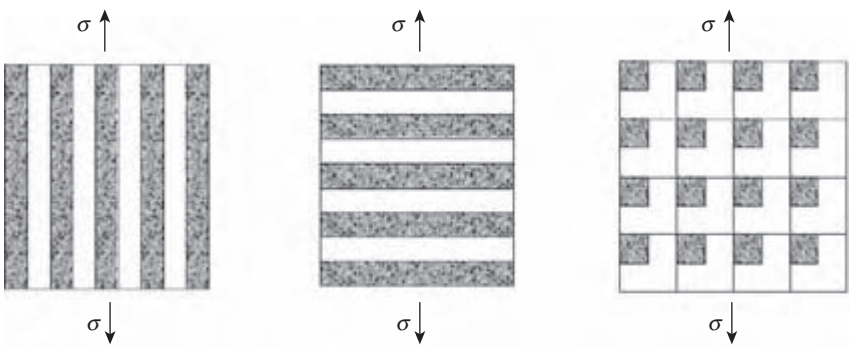

(a) Isostrain model (b) Isostress model (c) Micellar model

2.11 Structural models of fiber.

where $\perp$ indicates that the modulus is measured normal to the axial direction. The micellar model is a little difficult to analyze, and it will give a result between the above two extremes. Details about these models can be found in reference 2.

The two-phase morphology is a reasonable assumption for most fibers. However, there are some problems with these models; for example, the noncrystalline regions are not constant and other phases may be present. Thus, in some cases, three-or-more-phase models may be employed.

Bukosek[3] developed a molecular, supramolecular, and morphological structural model of semicrystalline polymers and the structural factors that influence fiber properties. The contributing effects of wool fiber morphology have been ignored in early mechanical behavioral models, in which the wool fiber has been treated as a two-phase composite with parallel constituents.[4] Liu and Bryson[5] proposed a three-component model of the wool fiber. The stiffness of a wool fiber was derived from the stiffness of the three components: the cuticle, the orthocortex, and the meso/paracortex, and their proportions within the fiber. The developed model may give new insight into the relevance of internal fiber structure to single fiber behavior affecting fiber assemblies in yarns.[5]

2.4.2 Modeling the time-dependent properties

The viscoelasticity of a fiber is often modeled using models composed of ideal springs for the elasticity and ideal dashpots for the viscosity. The springs follow Hooke's law, $\sigma = E\varepsilon$; the dashpots follow Newton's law, $\tau = \eta\dot{\gamma}$. Here, η is a constant, $\dot{\gamma}$ (equaling $d\varepsilon/dt$) is the rate of strain. As shown in Fig. 2.12, if a spring and a dashpot are arranged in series, they make up the Maxwell model; and if they are arranged in parallel, the composed element is called a Voigt–Kelvin model. The Maxwell model can show

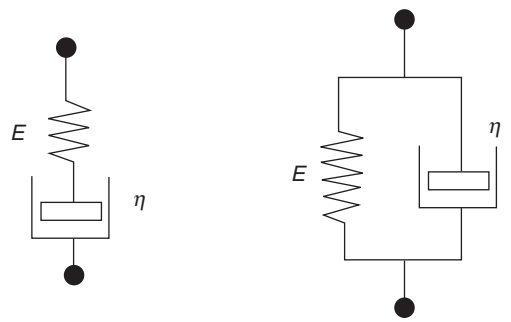

(a) Maxwell model (b) Voigt–Kelvin model

2.12 Spring and dashpot models.

instantaneous extension under the applied load, followed by secondary creep at a constant rate; it can also show stress relaxation at constant length. The Voigt–Kelvin model can show primary creep. The simplest model that can show qualitatively all the features of instantaneous extension, primary and secondary creep and stress relaxation is the four-element model shown in Fig. 2.13(a).

By adding to the number and complexity of arrangements of the springs and dashpots, a complete representation of the mechanical behavior of fibers, exhibiting not only the four effects mentioned above, but also the dynamic properties, which vary with frequency, and nonlinear relations between extension, load, and time, can be obtained. However, there is a limit to such an approach, if all the stress values of a given sequence are doubled, all the strain values will also double. It is often not true for a fiber. Another approach to address this problem is to modify the elements themselves. The three-element system proposed by Eyring *et al.*[9] is the most successful model following this approach. In this model, shown as Fig. 2.13(b), the two springs obey Hooke's law; but the dashpot shows non-Newtonian viscosity, its behavior being represented by a hyperbolic sine law of viscous flow: $d\varepsilon/dt = K \sinh \alpha\sigma$. Here, K and α are constants. Thus, the rate of strain will increase more rapidly with increase of stress than it would do if it were proportional to stress, as in Newton's law. More details about the theories of time-dependence can be found in reference 1.

Applying a three-element model, which has two Hookean springs and a dashpot containing a non-Newtonian power-law liquid, Kumar *et al.*[6] developed equations for creep recovery, stress relaxation and stress–strain behavior of textile fibers. By analyzing the two-element, three-element, four-element and six-element viscoelasticity models, Zhang[7] built up the regression equation of the relaxation curve of Tencel fiber based on the

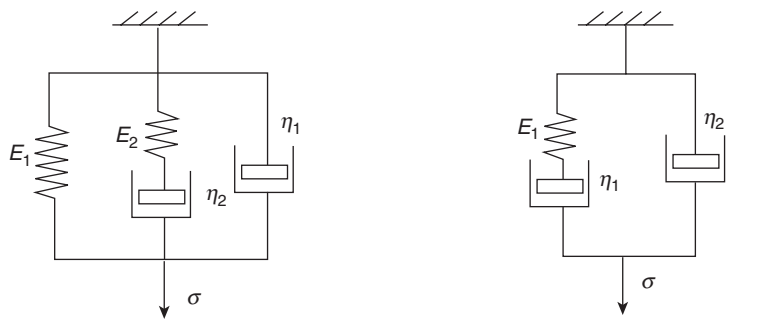

(a) Four-element model (b) Eyring's three-element model

2.13 Viscoelastic models.

six-element model and verified the identity between the six-element model and the test result.

Cai[8] proposed a nonlinear viscoelastic model to describe the time-dependent deformation behavior of fiber assemblies, including braided fiber seals. The models were derived from the standard solid model, but modifications permitted the inclusion of three nonlinear spring and viscous damper elements. For a fiber assembly under a compressive load, the fiber volume fraction characterized the deformation status. The researchers assumed that the elastic spring and viscous damper elements in the proposed model were nonlinear functions of the fiber volume fraction. In the cases of creep and stress relaxation, general deformation solutions were obtained. Baltussen[9] used the Eyring reduced time model to investigate the viscoelastic and yield deformations of polymer fibers, covering the observed tensile behavior of linear polymers in the glassy state, extensions at a constant rate of stress, creep and stress relaxation, and response to complex loading schemes. The experiments showed that the yield deformation and viscoelastic deformation of polymer fibers are strongly related.

2.4.3 Other approaches

The finite element method was also applied to fiber modeling. He *et al.*[10] used a linear elastic finite element model to study the mechanical behavior of irregular fibers. They evaluated the tensile behavior of fibers with simulated dimensional irregularities and determined that variations in fiber diameter affected tensile behavior. They found that greater variation reduced breaking load, Young's modulus, and breaking extension, and increasing the frequency of irregularity reduced breaking load and Young's modulus, but increased breaking elongation.[10]

Komori *et al.*[11] used a curved beam model to investigate the bending behavior of fibers and the micromechanical aspects of fiber compressibility. The analysis was able to reproduce the functional dependence of stress on the strain of a mass by using the structural quantities of assembly density, degree of fiber crimp, and fiber elasticity.

2.5 Conclusion

In this chapter, firstly, the macrostructure, microstructure, sub-miscroscopic structure and fine structure of fibers, which determine the fiber mechanical and surface properties, have been introduced; then the mechanical properties of fibers that contribute both to the behavior of fibers in processing to yarns and to the properties of the final products have been described; finally, several approaches to predict fiber mechanical properties have been briefly reviewed.

2.6 Acknowledgement

We would like to thank Hong Kong Polytechnic University for funding this research through Projects A188 and G-YD31.

2.7 References

1. Morton, W.E. and Hearle, J.W.S., 'Tensile Properties', in *Physical Properties of Textile Fibers.* 1993, The Textile Institute. p. 265–305.
2. Warner, S.B., *Fiber Science.* 1995: Prentice Hall, Inc.
3. Bukosek, V., Importance of Structural Model in Morphology of Fibers. *Tekstilec*, 1998. **41**(5/6): p. 127–133.
4. CSIRO, Models for predicting the mechanical properties of wool fibers, in *CSIRO Annual Report.* 1984: Australia.
5. Liu, H. and Bryson, W.G., A three-component model of the wool fiber – Effects of morphology, elasticity and intermediate filament arrangement on fiber stiffness. *Journal of the Textile Institute*, 2002. **92**(2): p. 121–131.
6. Kumar, S. and Gupta, V.B., Nonlinear viscoelastic model for textile fibers. *Textile Research Journal*, 1978. **48**: p. 429.
7. Zhang, J., The model of viscoplastoelastic behavior of Tencel fiber. *Xibei-Fangzhi-Gongxueyuan-Xuebao*., 1999. **13**(4): p. 399–402.
8. Cai, Z., A Nonlinear Viscoelastic Model for Describing the Deformation Behavior of Braided Fiber Seals. *Textile Research Journal*, 1995. **65**(8): p. 461–470.
9. Baltussen, J.J.M., The Eyring Reduced Time Model for Viscoelastic and Yield Deformation of Polymer Fibers. *Tensile Deformation of Polymer Fibers*, 1996: p. 155–168.
10. He, W., Zhang, S. and Wang, X., Mechanical Behavior of Irregular Fibers – Part I: Modeling the Tensile Behavior of Linear Elastic Fibers. *Textile Research Journal*, 2001. **71**(6): p. 556–560.
11. Komori, T., Itoh, M. and Takaku, A., Model analysis of the compressibility of fiber assemblies. *Textile Research Journal*, 1992. **62**(10): p. 567.

3

Yarn mechanics

K.F. CHOI
The Hong Kong Polytechnic University, China

3.1 Introduction

Yarns are the fundamental elements constituting fabrics. The biomechanical functional performances of garments and devices are very much dependent on the yarn mechanical and surface properties, which are largely determined by the constituent fibers, internal structural features and surface morphological characteristics of individual yarns. Scientific understanding and knowledge of the yarn mechanical properties and modeling their mechanical behavior are essential for biomechanical engineering of clothing and textile products. In this chapter, the knowledge and processes developed in the area of yarn mechanics in relation to biomechanical engineering are reviewed.

There were several reasons for taking a modeling approach to solve yarn mechanical problems. Firstly, yarn models assist the understanding of the structure of yarn and permit exploration of the hidden potential applications of yarns. More importantly, the properties of new yarn structures can be estimated using yarn models, thereby assisting in the mechanical engineering of new textile machines.

3.2 Yarn modeling

The fundamental considerations which were taken into account when deriving the yarn models include the initial yarn structure, material properties, deformed yarn structure, stresses/energy in the yarn, and solution method. In order to study the mechanical response of a yarn, it was necessary to define the initial yarn structure, inclusive of the path and lateral distribution of the constituent fibers.

3.2.1 The fiber path

Most of the researchers in yarn modeling have concentrated on ring spun yarns, although Henshaw[1] presented a model for self twist yarn, Xie *et al.*[2]

published a comprehensive paper on wrap spun yarns and Curiskis, Choi and Shih[3] developed another wrap spun yarn model based on a fiber bundle model.[4] For ring spun yarn, the earliest[5] and also the most popular assumption was that fibers follow a simple helical path. This assumption held that all the helices have the same pitch but have varying helix angles depending on the fiber's radial position in the yarn. According to Morton and Yen,[6] this idealized helical geometry in staple yarns is not practical since fibers on the yarn surface will peel off easily and consequently the yarn will lack cohesion. Morton and Yen performed experiments to determine the yarn structure using a tracer fiber technique. They found that the radial position of a single fiber in the yarn changed along its length. This was termed fiber migration. In contrast, the idealized helical geometry assumed that each of the fibers has a constant radial position.

Morton and Yen[6] explained, 'As the fibers emerge from the front roller of the ring spinning machine at the same rate, those fibers at one instant in the outer layer will follow a longer path, and consequently they will develop a higher tensile stress. The highly tensioned fibers will tend to move towards the yarn axis, displacing the less tensioned fibers already there. When the inner fibers migrate to the outer layer, their tension will build up continuously and they, in turn, will migrate back to an inner position to release tension. As a result, the fiber path is no longer a simple helix, but a helix with a variable helix radius.' Hearle and Bose[7] postulated a geometric mechanism (wrapped ribbon twisting) which explained Riding's[8] experimental findings: the correlation of the migration period in continuous filament yarns with the period of producer's twist. Hearle and Merchant[9] studied the mechanism of filament migration by constructing a seven-ply structure. The first theoretical model relating the migrating frequency with the twist angle, the twisting tension, the free length in the twisting zone, the initial tensile modulus of the filament and the degree of buckling needed to initiate migration was developed. The migration model of the seven-ply yarn was valuable in providing an understanding of what was happening in more complex structures.

Patterns of ideal migration were formulated by Hearle *et al.*[10] and Treloar and Riding,[11] independently, both of them based on the assumption of uniform yarn packing density. The variation of radial position, r, along the yarn length, z, was found to be approximately parabolic, i.e. $z \propto r^2$. Van Luijk *et al.*[12] applied the finite element method to model the long gauge length behavior of staple fiber yarns with the consideration of fiber migration. A V-shaped migration envelope with the fiber ends at the yarn surface was assumed. In addition, the fiber packing density distribution in a yarn cross-section was included in the formulation of the fiber migration path. Treloar and Riding[11] determined the yarn retraction and stress–strain properties based on ideal fiber migration theory. Deviation from the coaxial

helix model was found to be insignificant. Similar work was done by Zurek,[13] and the conclusion did not differ much. As warned by Treloar though, while fiber migration did not have a significant effect on filament yarn retraction and stress–strain properties, for other yarn mechanical properties, fiber migration may have very significant effects.

3.2.2 The fiber distribution

The fiber distribution in the cross-section of an undeformed ring spun yarn depends primarily on the fiber type and the twist level. For an unbulked continuous filament yarn, it was shown[14] that the fibers were virtually close-packed and could be approximated by choosing a uniform packing density. In the case of staple yarns made from crimpy fibers, such as wool worsted yarns, Hickie and Chaikin[15] demonstrated that the packing density varies with the yarn radial position as an inverted parabola with a maximum at a region approximately on a quarter of the yarn radius from the yarn axis. In addition, as might be expected, a high-twist yarn was in general more closely packed than a low-twist yarn.

3.2.3 Material properties

The material properties that mostly affect the yarn's mechanical properties include the fiber stress–strain properties, inter-fiber friction properties and the compressional properties of the fiber mass. The stress–strain properties of fibers have usually been determined by stretching a certain number of the fibers directly using any general-purpose extension machine. The average stress–strain curve can then be obtained.

Staple yarns are the most popular yarn type in the textile and clothing sector. The main difference between staple yarns and continuous filament yarns is that the former are characterized by the discontinuities in fiber length, hence fiber ends will slip relative to the surrounding fibers during yarn extension. The slippage of fibers near their ends hinders the application of energy methods in the yarn mechanical problem because of the energy dissipation against friction involved during fiber slippage. However, it has been pointed out[16] that the build-up of tension from the fiber ends through friction with neighbouring fibers is rapid in most commercially produced yarns, and hence the region of relative slippage of fibers extends only a short distance from the fiber ends. It has been shown that it is possible to make quite successful and accurate models of yarns by treating the fibers as continuous filaments which are arranged in a series of coaxial helices.

Frictional forces oppose relative movement between two contacting bodies. When considering the frictional forces on a fiber in a yarn during yarn extension, the surrounding fibers are moving in different directions

relative to that fiber, so the determination of the resultant frictional force is not straightforward. Hearle[17] introduced a correction factor to take account of the effect of fiber relative movement. Carnaby and Curiskis[4] extended the work further by involving the variation of fiber length. Besides the discontinuity of fiber length, rapid radial migration of fibers also causes fiber slippage. Van Luijk *et al.*[12] worked out the inter-fiber friction differently, and their correction factor for fiber friction was dependent on the type of migration path. The frictional force acting on the fiber surface is a function of the radial position, and its value is constantly changing along a migrating fiber.

Compression properties of fiber strands are highly related to the degree of fiber crimp. Theoretical treatment of fiber mass compression was originated by van Wyk.[18] He first derived the number of the contact points between fibers in a random fiber mass from the probabilistic idea used in the classical kinetic theory of gases. Then he estimated the resistance to compression of the fiber mass from the bending deflection of a fiber segment as supported by two neighbouring contact points. Finally, the fiber mass compression equation was developed. That is: $P = \frac{k \cdot Y \cdot m^3}{36\rho^3}\left(\frac{1}{V^3} - \frac{1}{V_o^3}\right)$, where Y is the Young's modulus of the fiber, m is the mass of the fiber assembly, ρ is the density of the fiber, P and V are the pressure and volume of the fiber mass during compression, and $V = V_o$ at $P = 0$.

In van Wyk's equation, there is an unknown constant k which must be determined experimentally for any particular fiber mass. Experimental studies[19,20] have been carried out to relate fiber properties such as diameter, length, crimp and coefficient of friction to the compressibility of the fiber mass, but no exact relationship has been obtained.

Carnaby[21] modified van Wyk's equation by replacing the bulk volume V by the compressible volume V_c, that is $V_c = V - V_m$, where V_m is the volume of the fiber mass. A better fit to the experimental data could then be obtained.

Stearn[22] modified van Wyk's approach by taking into account the change in fiber orientation during compression of the fiber mass. Komori and Makishima[23] made the fiber mass compression problem more general by introducing the fiber orientation function. Lee and Lee[24] derived the initial compressional behavior of fiber mass in terms of the packing density and a direction density function of the constituent fibers. A large discrepancy between experimental values and theoretical predictions was observed. As explained by the authors, fiber slippage was thought to be one of the main reasons for the big difference. Carnaby and Pan[25,26] described the mechanism of fiber slippage at the microscopic level. The effect of slippage on both the compression and the shear deformation of the fiber mass was expressed analytically, hence the compression and shear hysteresis of the fiber mass was developed.

At present, the micro-mechanics of a fiber mass are still at an early stage of development. Continuous input from research workers is necessary, since a realistic yarn model can only be obtained when the material properties are well defined.

3.2.4 Deformed yarn structure

The lateral strain of yarn can be treated in the following ways:

- unstrained,
- close packed yarn following Hooke's law, mostly with Poisson ratio equal to 0.5 (constant volume),
- compressional pressure inversely proportional to the bulk volume of yarn (van Wyk's equation[18]),
- compression tangent compliance,[27] and
- shortest path principle.[21]

Hearle's initial simple models assumed the yarn lateral strain to be zero, but he realized that this unrealistic assumption should be relaxed. In his later papers, the yarn's lateral strain was determined by the Poisson ratio and the yarn tensile strain. This model worked well only for continuous filament yarn in which close packing of the fibers could be assumed.

For staple yarns, which are more loosely packed, the first two treatments of yarn lateral strain are not appropriate. The lateral strain can be determined by van Wyk's equation,[18] in which the compressional stress is inversely proportional to the cube of the specific volume. The van Wyk equation was derived from the assumption that the fibers in the fiber mass are randomly distributed, and it is valid for small compression strain only. But it has been demonstrated[28,29] that the inverse cubic relationship between the compression stress and bulk volume is quite satisfactory for larger strains and aligned fibers. Even if the orientation function of fibers is taken into consideration,[23,24,30] the result is no better than a modification of the constant factor of the van Wyk's equation.

Compression tangent compliance is a continuum mechanics concept which also enables us to take account of the lateral compression properties of the yarn. At the same time, the compression strain due to axial stress can also be incorporated. This is the continuum approach.

The shortest path analysis was developed by Carnaby.[21] One of the assumptions of this analysis is that fibers will move freely inward to avoid being extended until the fibers are jammed at a particular radial position. This is true if the paths of the fibers in the yarn follow simple coaxial helices. With the shortest-path analysis, quite accurate predictions of load for a semi-worsted wool carpet yarn can be obtained for yarn strain of up to 10%. This is the region of the stress–strain curve where predictions are

dominated by the extent of the lateral movements of the fibers and hence the results provided convincing evidence in support of the shortest-path principle.

3.2.5 Stresses/forces in yarns

In the yarn tensile analysis of Platt,[31] the forces at right angles to the fiber axes were neglected. Hearle[32] pointed out that the transverse forces between fibers played an important part in determining the mechanical properties of yarns. In his model, he assumed that the lateral stress in yarn was hydrostatic and he derived this hydrostatic stress by considering the static equilibrium of a yarn element. The transverse stress distribution in a yarn was expressed in terms of the yarn twist, yarn Poisson's ratio and the yarn strain. The pioneering work of Hearle is the foundation of the continuum approach.

Batra[33] derived the yarn lateral pressure distribution from a different approach, and the contribution of individual helical fibers to the normal force was determined with the consideration of fiber tension, bending and torsional rigidities of the fibers. It was assumed that the yarn is ideally packed in layers and that individual discrete fiber forces can be smoothed out in the layers' surface to give the lateral pressure.

Dogü[34] calculated the transverse pressure distribution in a yarn based on a migrating fiber path and distribution of fiber packing density. The tensions were assumed to be equal along the filaments. Hearle's[35] criticism was that this idealizing assumption could only deal with certain special cases.

Study of the inter-fiber stress is especially important when the recovery route of a textile structure is required. A stress analysis approach is best used to solve yarn mechanical problems which take into consideration inter-fiber friction. Postle *et al.*[36] derived a relationship between the inter-fiber normal force, p, and the external pressure in terms of the mean fiber diameter, the packing fraction of the fiber mass and the coefficient of variation of the fiber diameter. Cox's equation was widely used[2,4,37] by researchers when solving problems of untwisted fiber strand mechanics. In this work, the frictional force, f, between fibers was given as $f = \mu \cdot p + \beta$, where μ and β are related to the surface properties of the contacting pair; β was also related to the self-locking nature of the fiber mass.[37]

3.2.6 Solution method

The solution methods used for yarn mechanical problems can be classified into two approaches: The continuum approach and the discrete fiber approach.

Continuum approach: The continuum concept regards matter as infinitely divisible; thus an infinitesimal volume of material can be referred to as a particle within the continuum. For general engineering purposes, it is convenient to ignore the molecular nature of matter and hence the discontinuity and variation at the microscopic level. The continuum approach makes it possible to formulate the fundamental equations of mechanics with the use of differential and integral calculus. It provides useful results for various practical problems which agree with experience.

This approach has been used by various textile researchers. Under the continuum hypothesis, a yarn is analyzed mechanically as if the contribution of an individual fiber is, in effect, smoothed over a neighbouring region in space. This allows the concepts of stress and strain to be developed. If one is concerned only with effects over distances appreciably greater than the distance between fibers, such an assembly of fibers can be treated as a continuum, in the same way that an ordinary solid is treated as a continuum provided that molecular dimensions are not approached. If this is the case, the well-documented treatment of anisotropic elasticity[38] is directly applicable and apart from the lack of continuity which complicates the constitutive relation, the situation is formally similar to that applying to fiber-reinforced composite materials.

Carnaby and Postle[39] stated that the treatment of yarns as a continuum is divided into two phases: the first phase is to establish the geometrical relationships which connect the external deformation of the yarn to the strain of the continuum in the local co-ordinates of the yarn element, and the second phase is to translate the local strains into stresses. These stresses must combine to match the external loading. The first yarn continuum model was formulated by Hearle *et al.*[32,40] The fibers were assumed to be perfectly elastic and to follow Hooke's Law; the stress at any point was assumed to be constant in all directions at right angles to the fiber axis; further the shear forces acting on the faces of the yarn element were neglected. A more general representation of the stress characteristics of yarns was completed by White *et al.*,[41] and Huang and Funk.[42] The assumptions of no shear forces and hydrostatic pressure acting on the faces of the yarn element were relaxed. Relaxing these two assumptions is not difficult in the formulation part, but one may doubt how this information could be obtained in practice.

Thwaites[43] developed a continuum model to study the tensile and torsional properties of high-twist filament yarn. He concluded that the continuum approach could be used for high-twist filament yarn, since the filaments were very much constrained and the energy loss due to filament slippage was only a small proportion of the strain energy.

Van Luijk *et al.*[44] solved the yarn continuum problem using the finite element method. The yarn was sub-divided into concentric axisymmetric

cylindrical elements, and the longitudinal cross-section of the elements was rectangular. A realistic fiber radial distribution was used in the initial yarn geometry. The problem-solving technique they used can be considered as an informal application of the finite element method. The shear forces between elements were neglected and the lateral stress–strain relationship was determined by a generalized van Wyk's equation. During yarn deformation, they allowed transport of fiber material from one element to another; this was due to the slipping of the fibers. The yarn force was determined using the virtual work principle with numerically calculated derivatives of the work done against slippage.

Djaja *et al.*[27] introduced the tangent compliance matrix for the fiber unit cell into a three-dimensional finite element analysis, so that the fiber strand under combined tensile and torsion load could be estimated. The analysis was confined to small strains only.

The advantage of using the continuum approach is that any complex deformation modes of the yarn can be tackled by applying the well-established theory of continuum mechanics. This approach is successful only if the numerous tangent compliance matrices in different load cases are available. This is generally not the case except for various unrealistically simplified situations.

The relative fiber movement due to fiber end slippage and fiber migration makes the representation of the displacement field in a continuous function impossible. Strictly speaking, the continuum approach cannot be directly used to take account of the fiber slippage and fiber migration effects.

Five independent material parameters are needed for the continuum analysis. An attempt[16] to measure these parameters revealed the considerable difficulties in achieving comprehensive mechanical characterization of the material. As the cohesion of unstrained fiber assemblies is relatively poor, this leads to difficulties both in applying the uniaxial load and in recording the various Poisson ratio parameters.

Since the mechanical responses of a fibrous assembly are highly nonlinear, and the tangent compliance matrix must be updated frequently with the changing yarn configuration, a very large data base containing the values of the compliances corresponding to different load cases is required. This cannot be justified, especially when exploring the mechanical properties of new yarn structures. An alternative route is to derive the compliances theoretically based on the individual fiber's contribution, but here the accuracy of the current models is poor.

Discrete fiber approach: An alternative route used to solve the yarn mechanics problem is the discrete fiber approach. In this approach, each fiber is treated as a discrete component of the structure and the aggregate response

of the assembly is obtained simply by adding the separate contributions of the individual fibers.

The merits of the discrete fiber approach are as follows:

- Phenomena of mass transfer, such as fiber slippage and fiber migration, can be taken into consideration.
- Simple yarn structures can easily be extended to complex geometries and deformations, such as the torsional properties of plied yarns.
- The computational effort is relatively lower than the continuum approach.

Limitations of the discrete fiber approach:

- It is very tedious to take into account every fiber in the yarn.
- A discrete fiber model is mostly for a specific loading situation; for each new load case, a new analysis must be created or an old analysis must be modified.

As for the first limitation, it is not actually necessary to consider the effect of all individual fibers. The fibers can be grouped in a yarn according to their similarities and the effect of each group of fibers determined as a whole. For example, fibers at the same radial position may have roughly the same helix angle and hence the same amount of fiber extension when the yarn is extended. This, in effect, reduces the complexity of the yarn model. In the case of a fiber migration model, not all fibers in the same radial position have the same behavior. This problem may be solved by subdividing the fibers into outwardly migrating and inwardly migrating fibers and treating them separately. However, it is essentially unacceptable to use the continuum approach to solve this aspect of the problem, since the displacement function of the mixed fibers is not a continuous one for the types of yarns found in practice with about 50 fibers in the yarn cross-section.

As for the second limitation, it is the case that in the past, no discrete fiber models were developed for the analysis of combined loading situations. In this chapter, the yarn mechanical model was developed for combined load cases, such as the combined tensile–torsional model for a single ring-spun yarn. The model will be described in a later section, but this is still the most serious limitation of the method.

3.3 Theoretical modeling of a single yarn

A refined singles yarn torsional model was built based on a previously developed singles yarn model.[45] The initial yarn density distribution was found to be a very important yarn parameter governing the torsional property of singles yarns. Detailed study of the differential volumetric changes within the yarn has shown that jamming of the structure is the key factor

initiating longitudinal tensile and compressive strains in the fibers. The yarn model was summarized in the form of a system of non-linear equations.

Huang[46] studied the finite extension of a strand with a central core surrounded by a single layer of helical wires based on the theory of slender curved rods. In his analysis, the distributed moments and distributed forces due to inter-wire contact were included together with the external axial force and twisting moment. Huang's fundamental work is very useful in the analysis of multi-ply structures. However, although it has been applied to mechanical models of helically armoured cables,[47,48] it has not similarly been directly applied to single staple yarns. There are several main reasons. Firstly, in a staple yarn the fibers are not closely packed and the yarn density (especially a staple woollen or worsted yarn) varies with its radial position. Yarn density distribution is a very important yarn parameter; it governs the initial non-linear deformation of the yarn as well as the pattern of fiber strain distribution during yarn deformation. Secondly, many staple fibers are not straight. Wool fibers, for example, are crimpy in nature; this contributes to the handle and warmth of woollen garments. Fiber crimp imposes further complications in the yarn model. Thirdly, the radial position of the helical wires in a cable is constant, so their geometry can be described quite easily. But as revealed by the tracer fiber technique,[6] a staple fiber in a spun yarn does not follow a simple helical path; instead its radial position varies along the yarn axis (fiber migration). This makes a mathematical description of the path of a fiber more complex, and hence the extent of the fiber deformation is harder to calculate. Lastly, the length of fibers in the staple yarn is finite; this implies that the yarn is held together by frictional forces between the fibers. From zero at each end of a fiber, the tensile force builds up with distance along the fiber axis up to a certain value which is large enough to make the fiber extend the same amount as the surrounding fibers.

3.3.1 A tensile torsional model of the single yarn

A singles yarn model developed by Choi *et al.*[49] is described in this section. In brief, the yarn model can be described as follows: A singles yarn is composed of concentric simple helices with equal pitch. The fiber helices are perfectly elastic thin rods and the yarn is assumed to be a conservative system. The fibers are in one of two states; a jammed state or a freely moving state. When a fiber is in the jammed state, its radial movement is restricted. When a fiber is in the freely moving state, its neighboring fibers do not have any interaction with it. It finds its equilibrium state subject to the rule that it remains helical at a prescribed pitch and zero tensile strain.

Only the fibers in the jammed state have tensile strain because the fibers in the freely moving state can readily move inward or outward to avoid

being strained. As the fibers move, the yarn density distribution will change accordingly. If the yarn density of a yarn region reaches a prescribed maximum value, fibers in that yarn region will be in a jammed state.

Notation:

r_A – Initial radial position of outer boundary of jammed region I
r_B, r_C – Initial radial position of inner and outer boundary of jammed region O
r_h – Radius of hollowed yarn region.
r_{yo} – Initial radius of yarn
ϕ_{jam} – Maximum yarn density
e_y – Applied yarn tensile strain
e_θ – Applied yarn rotational strain
L – Length of fiber helix
H_o – Initial helical pitch of fiber in singles yarn
ϕ – Yarn density function
ρ_f – Fiber density
r – Helix radius of fiber
e_f – Fiber extension
θ – Rotation of the fiber helix

The single yarn tensile torsional model can be expressed in terms of a system of equations.

Independent variables : e_y, e_θ, r_A, r_B, r_C, r_h
Given constants/function : H_o, E_f, ρ_f, ϕ_{jam}, $\phi(r)$
Generalized external forces : T_y, T_{or}

Let $\psi(r) = \int_0^r s \cdot \phi(s) \cdot \mathrm{d}s$ and $x_1 = 1 + e_y$, $x_2 = 1 + e_\theta$, $x_3 = r_A$, $x_4 = r_B$, $x_5 = r_C$,

$x_6 = r_h$. The equilibrium configuration $[e_y{*}, e_\theta{*}, r_A{*}, r_B{*}, r_C{*}, r_h{*}]$ of the modeled single yarn under prescribed generalized external forces $[T_y, T_{or}]$ can be determined by solving the following system of non-linear equations:

$\tilde{f}(\tilde{x}) = 0$ where $\tilde{f}: D \subset \Re^6 \to \Re^6$ and $\Re^6$ denotes the real six-dimensional Euclidean space, with

$$\tilde{f} = [f_1, f_2, f_3, f_4, f_5, f_6]^t \quad \tilde{x} = [x_1, x_2, x_3, x_4, x_5, x_6]^t$$

and

$$f_1(x_1, x_2, x_3, x_6) = \frac{2{x_2}^2 \cdot \psi(x_3)}{x_1 \cdot \phi_{jam}} + (x_2 x_6)^2 + \left(\frac{H_o}{2\pi}\right)^2 ({x_1}^2 - 1) - {x_3}^2$$

$$f_2(x_1, x_2, x_3, x_6) = \int_0^{x_3} g(r) \cdot \mathrm{d}r$$

$$f_3(x_1,x_2,x_4,x_5) = \psi(x_5) - \psi(x_4) - \frac{({x_5}^2 - {x_4}^2)x_1 \cdot \phi_{jam}}{2{x_2}^2}$$

$$f_4(x_1,x_2,x_4,x_5) = \int_{x_4}^{x_5} g(r) \cdot \mathrm{d}r$$

$$f_5(\tilde{x}) = \frac{x_1 \cdot \rho_f \cdot T_y}{\pi \cdot E_f} - \int_0^{x_3} g(r) \cdot [3{H_0}^2{x_1}^2 - {L_f}^2(r)] \cdot \mathrm{d}r + \int_{x_4}^{x_5} g(r) \cdot [{L_f}^2(r) - {L_{fo}}^2(x_4)] \cdot \mathrm{d}r$$

$$f_6(\tilde{x}) = \frac{x_2 \cdot \rho_f \cdot T_{or}}{H_o E_f} - \int_0^{x_3} g(r) \cdot [{L_f}^2(r) - {H_o}^2{x_1}^2] \cdot \mathrm{d}r - \int_{x_4}^{x_5} g(r) \cdot [{L_f}^2(r) - {L_{fo}}^2(x_4)] \cdot \mathrm{d}r$$

where

$$L_{fo}(r) = \sqrt{(2\pi \cdot r)^2 + {H_o}^2}$$

$$L_f(r) = \sqrt{{H_o}^2{x_1}^2 + \frac{8\pi^2{x_2}^2}{x_1 \cdot \phi_{jam}} \cdot \psi(r) + (2\pi \cdot x_6)^2} \quad \text{when} \quad 0 \le r \le r_A$$

$$L_f(r) = \sqrt{H_o^2 + (2\pi \cdot x_4)^2 + \frac{8\pi^2{x_2}^2}{x_1 \cdot \phi_{jam}} \cdot [\psi(r) - \psi(x_4)]} \quad \text{when} \quad r_B \le r$$

$$e_f(r) = \frac{L_f(r) - L_{fo}(r)}{L_{fo}(r)}$$

$$g(r) = \frac{r \cdot \phi(r) \cdot [L_f(r) - L_{fo}(r)]}{{L_{fo}}^2(r) \cdot L_f(r)}$$

The system of non-linear equations was solved numerically using Newton–Raphson's Method. A special loading case, yarn torque–rotation property under constant yarn tension, is considered. The model prediction and experimental results are compared in the next section.

3.3.2 Experimental verification

In order to verify the yarn models' applicability of predicting the torsional properties of the yarns which involve a large amount of lateral fiber movement during yarn deformation, a sample of medium-twist woollen spun carpet yarn was chosen for the torsional test. The yarn torque rotation relationship was determined experimentally and the results were compared with the theoretical results based on the model. The inputs of the model include the parameters of fiber properties and yarn structure. As some of these properties are difficult to measure, simplifying assumptions are made.

For example, the fiber axial compressional modulus is very difficult to measure and it is generally assumed that the axial compression modulus of a fiber is equal to its tensile modulus.

The most direct way to determine the torsional properties of a yarn is to measure the torque rotation relationship of the yarn in a torsion meter. The torsion meter, KES-YN1, used in this experiment was manufactured by the Kato Tech Co. Ltd, Japan. The load range is from –500 mgf.cm to +500 mgf.cm. During testing, the yarn specimen is subject to a constant tension and its length is allowed to change freely. The torsion meter is based on the torsion balance principle: a standard metal wire of known torsional stiffness is connected to the yarn at the upper end and the rotational displacement of the wire is measured by a very sensitive displacement transducer. The amplified signals of the transducer output are sent to the plotter and a torsion rotation curve can be obtained.

Specification of yarn:

Yarn type	: Woollen spun carpet yarn
Yarn linear density	: 246 tex
Yarn twist level	: 191 turns per meter (Z-direction)
Yarn state	: Boil-set (almost zero residual torque)
Yarn test length	: 3 cm
Fiber type	: New Zealand Romney Wools
Mean fiber radius, r_f	: 1.805×10^{-3} cm
Density of fiber, ρ_f	: 1.31 g/cm^3
Initial tensile modulus of fiber, E_f	: 3.97×10^7 gf.cm
Shear modulus of fiber, G_f	: 1.391×10^7 gf.cm

The woollen yarns (see Fig. 3.1) and the yarn specifications were supplied by the Wool Research Organisation of New Zealand (Now Canesis Ltd).

A random sample of ten yarn specimens were taken for the torsional test. Each yarn specimen was twisted in a cyclic manner under a constant tension of 20 gf. The mid-points of yarn torque of the upper and lower hysteresis curves at different levels of yarn torsional strain were compared with the output of the yarn torsion model. The singles yarn model gave reasonably accurate predictions of the yarn torque rotation relationship, even though the yarn structure was not fully measured and incorporated into the yarn models. Properties such as the fiber crimp and fiber migration were ignored.

3.4 Conclusion

Research works on yarn mechanics in the past years have been briefly described in this chapter. The discrete fiber approach was considered to be more favorable when compared with the continuum approach. A

3.1 Woollen yarns – longitudinal view.

tensile–torsional singles yarn model developed by Choi *et al.*[49] was described in this chapter. The internal strain energy arising from fiber longitudinal strains has been used to calculate the torque/rotation behavior of the yarn. Bennett and Postle[50] were first to recognize that fiber tensile energy could swamp helical torsion and bending energy effects when yarns are twisted. However, in their work the tensile strain was generated by an unrealistic geometry. This new treatment allows much more realistic freedom of fiber movement in the radial direction, as dictated by the new jamming criterion.

Because this new model allows the initial geometry to have nearly zero twist, there is for the first time a theoretical means of calculating the internal strain distribution in a freshly twisted yarn. This has been cited by Postle, Carnaby and De Jong[16] as one of the great limitations in earlier yarn models since they nearly all assume the fibers to be perfectly set at zero strain in their initial helical geometry. Admittedly the case modeled applies strictly

only to static twisting,[39] since under dynamic twisting, migration effects occurring in the twist triangle below the front roller will drastically alter the developed fiber tensions. However, no previous analysis known to the authors enables this distribution to be realistically modeled for a yarn with an arbitrary initial yarn density.

3.5 References

1. Henshaw, D.E., 'A Model for Self-twist Yarn', *JTI* **62** 1970 p97–107.
2. Xie, Y., Oxenham, W. and Grosberg, P., 'A Study of the Strength of Wrapped Yarns', *JTI* 77 1986 p295–326.
3. Curiskis, J.I., Choi, K.F. and Shih, T.M., 'Mechanics of Wrapped Yarns Using Fibre-bundle Model', *The Proceedings of the 8th International Wool Textile Research Conference*, Christchurch, New Zealand, February 1990.
4. Carnaby, G.A. and Curiskis, J.I., 'The Tangent Compliance of Staple-fibre Bundles in Tension', *JTI* **78** 1987 p293–305.
5. Gegauff, C., 'Force et Elasticite des Files Sur Cotton', *Bull. Soc. Ind. Mulhouse* **77** 1907 p153–212.
6. Morton, W.E. and Yen, K.C., 'The Arrangement of Fibres in Fibro Yarns', *JTI* **43** 1952 T60–66.
7. Hearle, J.W.S. and Bose, O.N., 'Migration of Fibers in Yarns, Part II: A Geometrical Explanation of Migration' *TRJ* **30** 1965 p693–699.
8. Riding, G., 'An Experimental Study of the Geometrical Structure of Single Yarns', *JTI* **50** 1959 T425–442.
9. Hearle, J.W.S. and Merchant, V.B., 'Interchange of Position among the Components of a Seven-ply Structure : Mechanism of Migration', *JTI* **53** 1962 T537–552.
10. Hearle, J.W.S., Gupta, B.S. and Merchant, V.B., 'Migration of Fibers in Yarns, Part I: Characterization and Idealization of Migration Behaviour', *TRJ* **30** 1965 p329–334.
11. Treloar, L.R.G. and Riding, G., 'Migrating Filament Theory : Apparent Variation of Twist with Radial Position', *JTI* **56** 1965 T381–383.
12. Van Luijk, C.J., Carr, A.J. and Carnaby, G.A., 'The Mechanics of Staple-fibre Yarn, Part I: Modelling Assumptions and Part II Analysis and Results', *JTI* **76** 1985 p11–29.
13. Zurek, W., 'Some Properties of Continuous Filament Yarn', *TRJ* **31** 1961 p504–514.
14. Hearle, J.W.S. and Bose, O.N., 'The Form of Yarn Twisting, Part I: Ideal Cylindrical and Ribbon-twisted Forms, Part II: Experimental Studies', *JTI* **57** 1966 T294–320.
15. Hickie, T.S. and Chaikin, M., 'Some Aspects of Worsted Yarn Structure, Part III: The Fibre Packing Density in the Cross-section of some Worsted Yarns', *JTI* **65** 1974 p433–437.
16. Postle, R., Carnaby, G.A. and De Jong, S., *The Mechanics of Wool Structure*, Ellis Horwood Limited 1983.
17. Hearle, J.W.S., 'Theoretical Analysis of the Mechanics of Twisted Staple Fiber Yarns', *TRJ* **35** 1965 p1060–1071.

18. van Wyk, C.M., 'Note on the Compressibility of Wool', *JTI* **37** 1946 T285–292.
19. Chaudri, M.A. and Whiteley, K.J., 'The Influence of Natural Variations in Fiber Properties on the Bulk compression of Wool', *TRJ* **38** 1968 p897–906.
20. Sebestyen, E. and Hickie, T.S., 'The Effect of Certain Fibre Parameters on the Compressibility of Wool', *JTI* **62** 1971 p545–560.
21. Carnaby, G.A., *The Structure and Mechanical Properties of Wool Carpet Yarns*, PhD Thesis (University of Leeds) 1976.
22. Stearn, A.E., 'The Effect of Anisotropy in the Randomness of Fibre Orientation on Fibre-to-fibre Contacts', *JTI* **62** 1971 p353–360.
23. Komori, T. and Makishima, K., 'Numbers of Fiber-to-fiber Contacts in General Fiber Assemblies', *TRJ* **47** 1977 p13–17.
24. Lee, D.H. and Lee, J.K., 'Initial Compressional Behaviour of Fibre Assembly', in *Objective Measurement: Applications to Product Design and Process Control*, Edited by Kawabata, S., Postle, R., Niwa, M., The Textile Machinery Society of Japan, Osaka 1985 p613–622.
25. Carnaby, G.A. and Pan, N., 'Theory of the Compression Hysteresis of Fibrous Assemblies', *TRJ* **59** 1989 p275–284.
26. Pan, N. and Carnaby, G.A., 'Theory of the Shear Deformation of Fibrous Assemblies', *TRJ* **59** 1989 p285–292.
27. Djaja, R.G., Carnaby, G.A., Moss, P.J., Carr, A.J. and Lee, D.H., 'Finite Element Modelling of an Oriented Assembly of Continuous Fibers', *TRJ* **62** 1992 p445–457.
28. Dunlop, J.L., 'The Determination of the Compressive Bulk Modulus from Acoustic-impedance Measurements: The Development of the Technique', *JTI* **65** 1974 p344–346.
29. Dunlop, J.L., 'Characterizing the Compression Properties of Fibre Masses', *JTI* **65** 1974 p532–536.
30. Carnaby, G.A., 'The Compression of Fibrous Assemblies with Application to Yarn Mechanics', *Proceedings of the NATO Advanced Study Institute on Mechanics of Flexible Fibre Assemblies*, Kilini, Greece, August 19–September 2, 1979.
31. Platt, M.M., 'Mechanics of Elastic Performance of Textile Materials, Part III: Some Aspects of Stress Analysis of Textile Structure – Continuous Filament Yarns', *TRJ* **20** 1950 p519–533.
32. Hearle, J.W.S., 'The Mechanics of Twisted Yarns: The Influence of Transverse Forces on Tensile Behaviour', *JTI* **49** 1958 T389–403.
33. Batra, S.K., 'The Normal Force between Twisted Filament, Part I: The Fibre-wound-on-cylinder Model – Analytical Treatment', *JTI* **63** 1972 p209–222.
34. Dogü, I., 'The Distribution of Transverse Pressure in a Twisted Yarn Allowing for the Fiber Migration and Variation of Fiber Packing Density', *TRJ* **42** 1972 p726–733.
35. Hearle, J.W.S., Communications to the Editor, *TRJ* **65** 1974 p394.
36. Postle, L.J., Ingham, J. and Cox, D.R., 'The Measurement of Inter-fibre Friction in Slivers', *JTI* **43** 1952 T77–90.
37. Grosberg, P., 'Strength of Twistless Sliver', *JTI* **54** 1963 T223–233.
38. Lekhnitskii, S.G., *Theory of Elasticity of an Anisotropic Elastic Body*, Holdenday, San Francisco, California, 1963.

39. Carnaby, G.A. and Postle, R., 'Discrete Fibre Versus Continuum Models in the Mechanics of Staple Yarns', *Journal of Applied Polymer Science: Applied Polymer Symposium* **47** 1991 p341–354.
40. Hearle, J.W.S., El-Behery, H. and Thabur, V.M., 'The Mechanics of Twisted Yarns: Theoretical Development', *JTI* **52** 1961 T197–220.
41. White, J.L., Cheng, C.C. and Duckett, K.E., 'An Approach to Friction Effects in Twisted Yarns', *TRJ* **46** 1976 p496–501.
42. Huang, N.C. and Funk, G.E., 'Theory of Extension of Elastic Continuous Filament Yarns', *TRJ* **45** 1975 p14–24.
43. Thwaites, J.J., 'A Continuum Model for Yarn Mechanics', *Proceedings of the NATO Advanced Study Institute of Mechanics of Flexible Fibre Assemblies*, Kilini, Greece, August 19–September 2, 1979.
44. Van Luijk, C.J., Carr, A.J. and Carnaby, G.A., 'The Finite Element Analysis of Yarns, Part I: Yarn Model and Energy Formulation, Part II: Stress Analysis', *JTI* **74** 1983 p343–363.
45. Tandon, S.K., Carnaby, G.A., Kim, S.J. and Choi, K.F., 'The Mechanics of the Torsional Behaviour of Singles Yarns – Part I: Theory', *JTI* 1995 p187–193.
46. Huang, N.C., 'Finite Extension of an Elastic Strand with a Central Core', *Journal of Applied Mechanics* 1978 p852–853.
47. Costello, G.A. and Phillips, J.W., 'A More Exact Theory for Twisted Wire Cables', *Journal of the Engineering Mechanics Division*, *ASCE*, **100** 1974 p1096–1099.
48. Lanteigne, J., 'Theoretical Estimation of the Response of Helically Armoured Cables to Tension, Torsion and Bending', *JAM* 1985 p423–432.
49. Choi, K.F., Carnaby, G.A., Shih, T.M. and Lo, M.T., 'A Theoretical Torsional Model of Singles Yarn', *Research Journal of Textile and Apparel*, **2**, No. 1, Oct. 1998, pp. 1–12.
50. Bennett, J.M. and Postle, R., 'A Study of Yarn Torque and its Dependence on the Distribution of Fibre Tensile Stress in the Yarn, Part I: Theoretical Analysis, Part II: Experimental', *JTI* **70** 1979 p121–141.

4

Fabric mechanics

X-Q. DAI[1,2], K.F. CHOI[1], Y. LI[1]
[1]The Hong Kong Polytechnic University, China
[2]Soochow University, China

4.1 Introduction

Fabrics are the fundamental materials constituting garments and textile devices. The biomechanical functional performance of garments and devices is very much dependent on their fabrics' mechanical and surface properties, which are largely determined by the constituting fibers and yarns, internal structural features and surface morphological characteristics of the individual fabrics. Scientific understanding and knowledge of the fabric mechanical properties and modeling their mechanical behavior are essential for biomechanical engineering of clothing and textile products. In this chapter, the knowledge and processes developed in the area of fabric mechanics in relation to biomechanical engineering are reviewed.

Textile fabrics are manufactured assemblies of fibers and/or yarns that have substantial surface area in relation to thickness and sufficient mechanical strength to give the assembly inherent cohesion. Based on the nature of the yarn or fiber arrangements, fabrics are classified as woven, knitted, twisted and knotted, non-woven, or compound fabric. Among them, woven fabric and knit fabric are the major materials for apparel use. Thus, these two types of fabrics will be focused on.

4.2 Woven fabrics

4.2.1 Structure

Woven fabric consists of two or more sets of yarns that are interlaced at right angles to each other. Figure 4.1 illustrates a small section of a woven fabric; a surface view is presented along with two cross-sectional views, one lengthwise and one crosswise. The yarns in the lengthwise direction are warp yarns, and those transverse crosswise are weft yarns. The bias direction is any direction other than lengthwise and crosswise and a 'true bias' indicates that it runs at a 45° angle to the lengthwise direction.

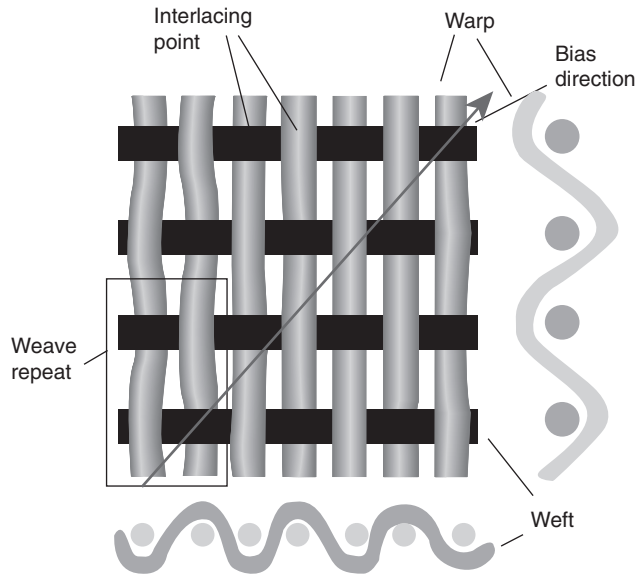

4.1 Woven fabric.

Woven fabrics have a face and back. The face usually has the more attractive appearance and is the side viewed during wear or use. An interlacing pattern is used to describe the movement of the warp or the weft yarns from the surface to the back of the fabric and *vice versa*, and of the manner in which adjacent yarns complete the movement relative to one another. The weave repeat marked in Fig. 4.1 is sufficient to show one pattern. The smallest number of warp and weft yarns can be represented: In this case, two warp and two weft yarns are just sufficient. Besides the description of fabric weave, there are several other parameters to describe fabric geometry:

Fabric count is the number of warp and weft (or filling) yarns per inch (25 mm) of a fabric. It is often written as $W \times F$. Fabric count is an important determinant of the quality of fabric and affects various mechanical properties of the fabric.

Balance is the ratio of warp yarns to weft yarns in a fabric. A balanced fabric has approximately one warp yarn for every filling yarn, thus the ratio is 1 : 1. Balance is helpful in determining the warp direction of fabrics, which usually have more warp yarns than filling yarns.

Fabric thickness is one of the basic properties of a fabric giving information on its warmth, heaviness, and stiffness in use.

Fabric weight is fabric mass per unit area. It is often used commercially as an indicator of thickness instead of fabric thickness itself.

Fabric width depends on the loom on which the fabric is manufactured.

4.2.2 Mechanical behavior

Basic deformation of fabric

Fabrics are complex assemblages of interwoven threads, which are themselves assemblages of twisted fibers. The frictional forces between the fibers and the threads give the fabric a stable structure. Fabrics are therefore anisotropic, inhomogeneous, discontinuous materials. In practical use, fabrics are subject to a wide range of complex deformations. Among them are included such effects as drape, wrinkling, creasing and other aesthetic characteristics. In order to understand fabric mechanics well, it is necessary to split such deformations up into a collection of simpler deformations such as tensile, shearing, bending, and twisting.

Tensile: When a fabric is subjected to a load applied to the warp or weft direction at a constant rate of elongation, it is stretched. Due to the fabric discontinuity, the fabric shows different extension response during the lower and higher extension regions. Figure 4.2 shows a typical load–extension curve, which can be divided into three sections. In the first part, the load increases rapidly along with the elongation; the slope of the curve in this region is taken as Young's modulus to denote this tensile property of the fabric. This initial high modulus is probably due to the frictional resistance to the bending of the thread. Once this resistance is overcome, the extension during the second part is due mainly to crimp redistribution; a

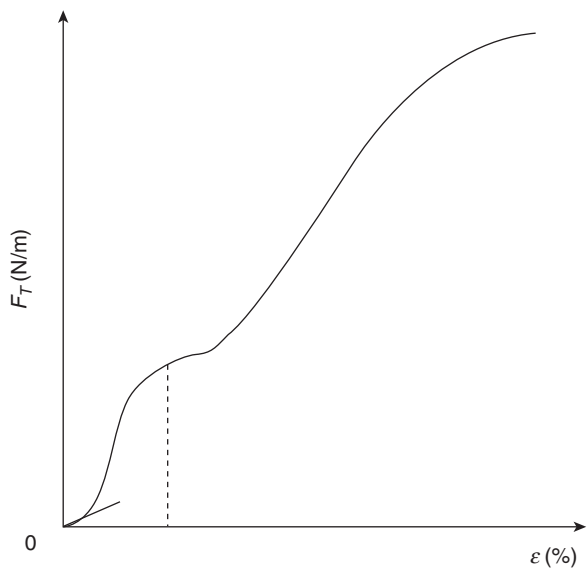

4.2 Modeled load–elongation curve.

relatively low modulus is obtained, which is mainly governed by the force needed to de-crimp the threads in the direction in which the load is being applied (illustrated in Fig. 4.3), and simultaneously the need to increase the curvature in the interlaced threads. As the crimp is decreased, the load rises very steeply and, as a result, the threads in the loaded direction begin to be extended. In this final region, the load–elongation properties of the fabric are almost entirely governed by the load–elongation properties of the yarns themselves. Because a fabric usually has a different construction of warp and weft yarns, the tensile moduli in the warp and the weft directions may differ largely; thus the fabric shows obvious anisotropy of tensile properties.

Shear: The shear deformation of woven fabrics is very different from that of continuous materials such as paper or plastic film. Because there may be slippage between threads at crossover contact regions (Fig. 4.4a), the

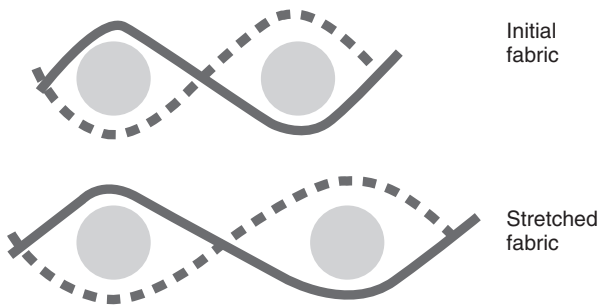

4.3 Stretch deformation.

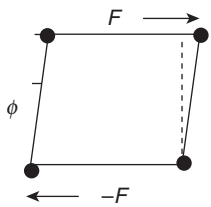

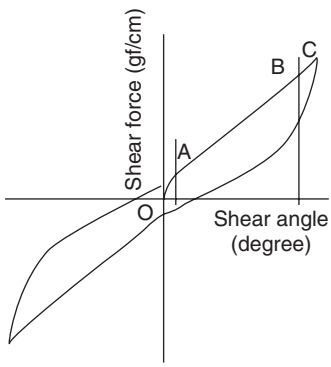

(a) Shear deformation (b) Common representation of shear (c) Schematic shear stress/shear-strain curve

4.4 Fabric shear.

resistance to shear deformation is very low compared with tensile deformation. A common representation of shear is illustrated in Fig. 4.4b: a rectangular element of sheet material is subjected to pairs of equal and opposite stresses F, which are acting parallel to the side of the element; in the case of simple shear, it is assumed that the element deforms in such a way that its area remains constant.[1] The shear strain is defined as the tangent of the change in angle between the sides of the element ϕ. Then, for elastic material, there exists: $F = G\tan\phi$, where G denotes the shear modulus.

However, fabric is not an elastic material, so its shear property also shows nonlinearity. The shear response is often reflected as the shear stress–strain curve (Fig. 4.4c). The curve can be divided into three regions: the initial, nonlinear region, where the shear is governed by the frictional forces resisting the relative rotation of the yarns, coupled with the elastic bending deformation of the yarns; the second, linear region, after the slippage between threads has taken place, where, therefore, the shear is due progressively to this slippage and the intersection of the bent yarns in the crimp requires further bending of the yarns; and the third, nonlinear region, where the shear resistance rapidly increases because of the increasing contact area between the two threads and the jamming of the structure. The slope of the second part of the shear-force/shear-angle curve (the shear rigidity) is often taken to represent the shear property. The curve shows obvious hysteresis.

Bending: Fabrics undergo large deformations for small applied forces. What distinguishes fabrics from other sheet materials is their ability to buckle gracefully in rounded folds and form draped shapes. A complete understanding of the mechanism of the bending of a woven fabric requires knowledge of the relationship between fabric bending rigidity, the structural features of the fabric and the tensile/bending properties of the constituent yarns. Former studies have made it clear that the resistance in the simple warp-wise or weft-wise bending is made up of three components: the bending resistance of the threads, some interaction between the threads, and a frictional restraint.[2] Figure 4.5a illustrates the yarn deformation during fabric bending.

The bending property is represented usually by the relationship of bending moment (M) and bending curvature (K), which is measured in pure bending as illustrated in Fig. 4.5b. If the material is elastic, then $M = BK$, where B denotes the bending rigidity. Figure 4.5c shows a schematic bending curve. The initial bending is governed by the frictional restraint to bending. The frictional force is produced mainly by an inter-yarn pressure acting at the cross-over regions in a woven fabric. The behavior is nonlinear. After the frictional force is overcome, completely free bending begins and it is of

an elastic nature. This final bending rigidity is of the same order of magnitude as (often greater than) the sum of the bending resistances of the crimped yarns in the fabric. The excess bending resistance arises from the increased inter-yarn penetration of the two crossed yarns during bending. The slope taken from the linear part of the bending curve illustrates bending rigidity. The bending curve also shows hysteresis.

Twisting: When a fabric is bent along a bias direction, the deformation is complicated by consisting of warp-wise and weft-wise bending, and twist.[3] As illustrated in Fig. 4.6, twist is a 3D deformation. The twist property is usually represented by the relationship of torsional torque (T) and twist deformation (K_W). If the relationship is linear, then $T = \tau K_W$, where τ denotes the twist rigidity.

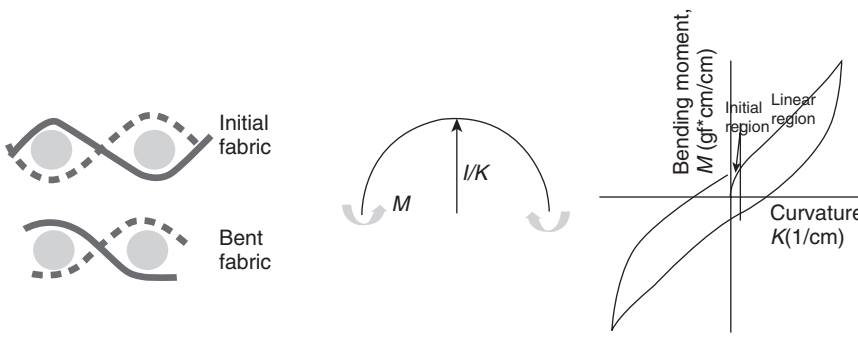

(a) Bending deformation (b) Bending moment and curvature (c) Schematic bending curve

4.5 Bending.

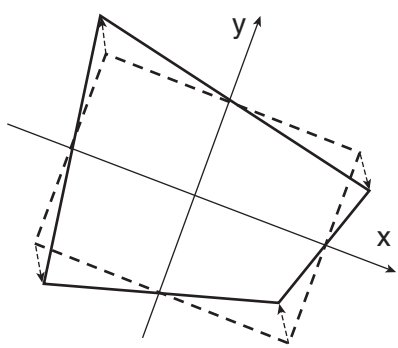

4.6 Twist.

Complex deformation

Buckling: When a fabric is under axial compression, it buckles easily rather than being compressed. The load at which buckling occurs is called the buckling load. Before buckling occurs, the fabric may be compressed a certain distance. This compression at buckling load is called buckling compression. It will be of special importance in determining the formability of a fabric. When a plate fabric buckles, it often takes up a sinusoidal shape. This is called plate buckling. The buckling of a cylindrical fabric will be of a more complex nature. It involves buckling not only in the length direction but also produces a form of wave at the cross-sectional direction. Such deformation is usually called shell buckling.

Rheological behavior: As a fabric is worn, it is subjected to stretching, bending, shearing, twisting, compression, and other distorting forces. These forces will cause wrinkles and creases; consequently, the fabric will bag or sag. Bagging is a typical behavior resulting from fabric rheological properties. It is a type of 3D residual deformation of fabric after prolonged use. Garment bagging often occurs at positions such as the knees, the elbows, the seat and the shoulders, where repeated or prolonged deformations are exerted by moving body parts. Several test methods have been developed to investigate fabric rheological behavior. In the bagging test developed by Zhang,[4] a fabric specimen is clamped in a circle and is deformed repeatedly from the center by a steel ball, and then the bagging height along with the load is recorded. Bagging deformation may involve a number of structural changes: (i) yarn rotation and slippage at the interlacing points during shearing; (ii) yarn bending and compression at interlacing points during tensile and shearing; (iii) yarn extension between interlacing points; (iv) fibre slippage and extension in the yarns at interlacing points and between interlacing points. All of these changes interact with each other to meet the requirements of 3D deformation of the fabric at different bagging stages. Although bagging involves so many sophisticated structural changes and various mechanical deformation processes in fibers, between fibers and between yarns, the deformation during bagging can be classified into three categories: elastic deformation, viscoelastic deformation and frictional deformation.

4.2.3 Model simple mechanical behaviors

There are two major approaches to model woven fabric mechanical behavior: one is to consider a structural weave unit of the fabric (low level) and the other one is to consider fabric deformation of a large-scale shape and neglect the micro-structure (high level). The low-level models are used to

investigate the tensile, shearing and bending properties separately, while the high-level models are often used to predict the whole aesthetic appearance of fabrics such as folding, wrinkling and draping. Here, the focus is on the low-level modeling. High-level modeling will be addressed in the next chapter.

Geometric–mechanical models

Peirce[5] was the first pioneer in cloth modeling research. In the mid-1930s he developed and analyzed a basic modeling cell of fabric geometry, detailing the geometric relationships among yarns at a yarn crossing. He shows that if it is assumed that the bending resistance of the yarns is negligible and that the yarn is circular in cross-section, a purely geometrical model, which involves no consideration of internal forces, can be set up for the determination of the various parameters that are required. This model becomes a basic description of woven fabrics. Peirce derived a set of equations for these parameters. The three equations involve seven parameters; and given four of them, the other three can be obtained.

The basic difficulty in such a calculation when using the Peirce approach arises from the fact that the yarn cross-section is often far from circular. Many attempts have been made to modify Peirce's original relationships by assuming various shapes for the yarn cross-sections. The ellipse and racetrack are the two proposed cross-sections.[6,7] The geometry model of fabric can be used to calculate the weave angles, radii of curvature and crimp height for a plain weave fabric in which the thread spacing and crimps are known, and to estimate the degree of flattening of the yarns. It can also be used to find the minimum value of p_2 for a plain weave fabric made from the same yarn, whose diameter is given, and the value of p_1 is also fixed. Details can be found in reference 6.

Besides the pure geometrical model of a fabric, Peirce also proposed an elastic thread model to take account of the yarn bending resistance. An elastica is used to represent the crimped thread. The physics of elasticas was explored by Euler in 1744 and has been concisely summarized by Konopasek.[8] An elastica is a slender rod, and it is assumed that the bending moment at any point along the central axis of the rod is linearly proportional to the increment of the curvature caused by that moment. The warp and weft threads only touch at the crossing point, and U and V denote the external force components in horizontal (x) and vertical (y) directions. Thus, there is:

$$EI\frac{\mathrm{d}\varphi}{\mathrm{d}s} = -Vx + Uy.$$

Here, EI is the bending rigidity of the thread, $\mathrm{d}\varphi/\mathrm{d}s$ denotes the curvature of the yarn. Only one solution for the equation when U is zero is obtained,

and the yarn crimp for various values of weave angles is calculated. The case where the yarns are in line contact with the cross yarns is also analyzed.

In 1964, Olofsson[9] proposed a model that is structurally similar to Peirce's elastic thread model. He considered that the geometry of yarns in a weave is a function of external forces and reaction forces in the fabric, and assumed that the forces produced by continuous contact between yarns may be approximated with point forces. He studied the general case of bi-axially loaded fabric, wherein both vertical and horizontal forces are present at the yarn crossover points. In addition, he introduced the idea of the permanent deformation of yarns due to bending, leading to 'setting' of the yarn in crimped form. A new parameter, the form factor, φ, is used as a measure of setting. He then assumed a relationship between the curvature of the yarn in the fabric and in the released state:

$$\frac{\mathrm{d}\varphi_0}{\mathrm{d}s_0} = (1+\psi)\frac{\mathrm{d}\varphi}{\mathrm{d}s}.$$

Then the bending moment is modified as

$$M = -E_b I\left(\frac{\mathrm{d}\varphi}{\mathrm{d}s} - \frac{\mathrm{d}\varphi_0}{\mathrm{d}s_0}\right).$$

A bending energy is also derived, based on the mechanics of elastic structures. He also introduced the thread diameters as secondary parameters and suggested that the flattening of the thread should be considered. Through his analysis, he presented equations for the equilibrium conditions and stress–strain relationships within the yarn-crossing structure under low stress. However, no evidence was provided to support the validity of his results.

Grosberg and Kedia[10] also presented a model similar to Olofsson's. The assumptions made are: the length of yarn between two intersecting points remains constant during extension, and its shape is determined by the forces acting at the intersections and can be obtained by assuming the yarn to be an infinitely thin beam. Therefore, the tensile and bending properties are considered, and the effect of compression is ignored. The bending moment equation is solved arithmetically by means of a Taylor series method. The load–extension relationship is obtained by a graphical method. By using this model to investigate the initial load extension modulus of several fabrics, they showed that the theoretical deductions were in accord with experimental findings.

Konopasek,[8,11] in his treatment of the elastica-based model, considered two planar bending curves as the axes of the warp and weft threads. He obtained the equilibrium fabric structure by solving two sets of equations of planar bending curves for warp and weft threads with properly formulated boundary constraints.

In 1985, Leaf and Anandjiwala[12] enhanced Peirce's model by assuming that the yarn in this model can be considered as an elastica with Huang's bilinear bending-moment model. Huang[13] proposed that the moment–curvature relationship of bending fabric can be modeled by two linear segments: the first one has a steep slope in the low-curvature region while the second one has a much lower slope in the high-curvature region. They developed equations that defined the relationship between the geometric parameters of their modeling structure. Their paper provides some data that confirm the ability of their model to predict these geometric relationships. Furthermore, Anandjiwala and Leaf[14,15] use the model to analyze the large-scale load–extension behavior of a plain weave fabric subjected to biaxial forces over repeated cycles of loading and unloading. The yarn bending, extension and inter-yarn compression are considered. They point out that the stress behavior is predominantly influenced by yarn bending parameters. Their theoretical analysis is also confirmed by experiments.

Ghosh, Batra and Barker[2,16,17] proposed a further extension and revision of Peirce's model that is similar to the work of Olofsson, and Leaf and Anandjiwala. Both linear and bilinear bending-moment models were used to study the bending behavior of plain-woven fabrics. The extension they made was to model a line contact between crossing yarns. They produced a set of calculations to predict a range of fabric bending rigidities that reasonably matched the corresponding experimental results. However, the samples were limited to fabrics made of monofilament yarns that closely behave as elasticas.

Lomov *et al.*[18] also proposed a model to predict the fabric-to-yarn bending stiffness ratio of plain-woven set fabric. The model was structurally similar to Peirce's model. A polynomial approximation for the elastica was constructed, and both point contact and line contact were modeled. The fabric deformation was considered as a coordinate transformation. Their model was validated by comparison with published experimental data.

Most of the above-mentioned models try to describe the 2D curve of the loaded thread axis; the cross-threads are often considered by adding various constraints at crossing point or contact line. In 1973, Kawabata, Niwa and Kawai[19–21] proposed a model to describe a 3D yarn crossing structure of woven fabric. The warp and weft yarns can be represented by straight lines that bend at two points on the axis perpendicular to the fabric plane. The equilibrium formula is

$$F_c = 2F_{T1}\cos\theta_1 = 2F_{T2}\cos\theta_2.$$

Here, F_c is the compression force between the warp and weft yarns at the contact point, F_{T1} and F_{T2} denote the tensile forces in the warp and weft yarns respectively, and θ_1 *and* θ_2 denote the bending angles of the two yarns. Additional to the yarn tensile property, the yarn compressibility

under the action of a lateral compressive force is also introduced into the model. Graphic methods are used to solve the equation under different conditions. Their model includes several 'black boxes', which contain mechanical data experimentally obtained from real fabrics. They predicted the biaxial and uniaxial tensile properties and the shearing properties of several fabrics. Comparison of the theoretical and experimental results shows that the compressive properties of yarns have a great influence on the tensile properties. In the uniaxial-deformation simulation, the bending rigidity of the transverse yarn is also considered. The complete load–extension curve from the initial to the ultimate extension is predicted. Neglection of the bending effect of the yarn along the load direction seems to account for the small error for low-extensions. It is stated that the uniaxial-deformation theory is limited to the relatively large-deformation range.

More recently, Realff, Boyce and Backer[22] took an approach similar to Kawabata's, modeling the entire uniaxial tensile stress–strain behavior of the fabric. By applying the beam theory model to the cross-yarn, the yarn curvature is taken into account. The model includes a more complete representation of yarn behavior. The yarn properties used, such as tensile response, flattening, bending and consolidation, are measured out of the fabric; no properties are back-calculated based on the fabric behavior. The tensile behavior of several fabrics of differing weave and yarn construction is investigated. In most cases, there is good agreement between the theoretical and experimental results reported, while they suggested some modification for the tightly woven fabric.

Strain energy methods

In the late 1970s, De Jong and Postle[23–26] presented an energy method to model the shape of deformed yarns, based on the assumption that yarns have simple elastic deformation properties and any fabric structures consisting of such yarns reach equilibrium in a minimum strain energy configuration. In a quarter-wave of the yarn crimp in plain-woven fabric under tension, let P denotes the cloth extension and Q represents half the reaction force of the crossing yarn. Since fabric shear is not taken into account, the 3D problem is reduced to 2D form. The total strain energy stored in the quarter-wave subjected to forces P and Q, includes bending and longitudinal tension, based on the curvature and extension of the yarn geometry: $U = \int_0^1 \frac{1}{2}\left\{(m_1 - m_1^0)^2 + \frac{Y}{B}(m_h - 1)^2\right\}\mathrm{d}s$. Here, Y, and B are the extension and bending rigidities of the yarn; m_1, m_1^0 are the yarn curvature inside the fabric and that released from the fabric respectively; and m_h is the local length of the yarn element (its value is 1 for un-extended yarn). The energy function is minimized by applying methods from optimal control theory. With this model, De Jong and Postle predicted tensile and bending

properties of several materials, producing reasonable results when compared to actual fabrics.

Knoll[27,28] modified the work of De Jong and Postle by including the effects of jamming and contact constraints between cross-yarns. He showed that many of the yarn configurations modeled by Peirce could be reproduced with the same results by using De Jong and Postle's method.

Sinoimeri and Drean[29] applied De Jong and Postle's energy approach to the study of the pure shearing of a plain-woven fabric. One extension was that a rheological model was introduced in the analysis to account for the possible slippage between threads at crossover contact regions. In this model, the slippage threshold and the slippage angle were assumed to be linearly related to the sum of the compression forces between the threads. The predicted shear stress–strain curves agreed well with the corresponding experimental ones.

Hearle and Shanahan[3,30] also developed an energy-based modeling approach very similar to De Jong and Postle's. Their technique employed a somewhat awkward explicit formulation of yarn geometry, as compared to De Jong and Postle's parametric yarn geometry description. Therefore, it is less general than De Jong and Postle's method. They derived equations for the Peirce and Kemp yarn structures, and their own 'lenticular' geometry, which is constructed to avoid the difficulties encountered with Kemp's racetrack geometry. An interactive system called QAS (Question Answering Systems on algebraic equations) was used to solve the sets of non-linear simultaneous equations representing the combination of the three cases: (i) crimp interchange mechanism with or without (ii) yarn stretching and/or (iii) yarn bending rigidity effects. They calculated the load–extension and bending–curvature plots for various yarn structures.

Leaf and Kandil[31] used a model structurally the same as Kawabata's model to analyze the initial load–extension behavior of plain weave fabric. The energy stored in the unit, consisting of bending, extension and compression strain energies, is calculated. Castigliano's theorem is used to solve the fabric extension. Many fabrics of various materials and constructions were investigated, and most of the predicted initial Young's moduli showed good agreement with the experimental results.

Finite element method

Both the geometrical–mechanical approach and energy approach describe the geometry of parts of a weave structural unit, and try to obtain the centerline shape of the thread. The yarn is modeled as a one-dimensional line, not a solid with volume. It is difficult for these models to discuss the deformation of the cross-section and the contact detail among threads. And it is also impossible for them to describe fabrics of other weaves of non-symmetric and complex geometrical structures. To solve these problems,

Tarfaoui[32] tried to apply the Finite Element Method (FEM) to woven fabric modeling. The cross-section of the yarn is meshed by quadrangles with four nodes; the mesh of the yarn is obtained from the basic section, to which is applied adequate translations of well-defined vectors. Basic cells of a plain weave and a twill weave fabric were constructed and their mechanical behavior when subjected to several kinds of stress (uniaxial tensile, biaxial tensile and shear) was investigated. An overload phenomenon was observed.

FEM enables the simulation of complex fabrics subjected to various loads. However, since a single yarn piece between cross-points is represented by a large number of elements, the computational cost becomes a critical issue and thus limits the application of FEM to micro-mechanics of fabrics. FEM is also used in modeling woven composites.[33]

Computational micro-particle model

In the above-mentioned models, only a structural weave unit is considered, and various boundary conditions are added denoting the stress to which the fabrics are subjected. The yarns in fabrics are often assumed to remain in the same plane during extension and bending, and the 3D problem is reduced to a 2D one. This is quite different from the actual state for a piece of fabric under a load. Li and Dai[34] developed an approach to dynamically simulate a piece of fabric subjected to various tensile loads. Similarly to Kawabata's model, the yarn centerline is simplified as straight-line segments and the yarn cross-sections are assumed as circles. Various springs of separation, bending, compression, wrapping and torsion are imaged acting among particles to simulate various yarn behaviors. The model was used to investigate the tensile response under low extension of plain weave fabrics of various fabric counts. The simulated load–elongation curves were compared with the experimental results. A good summary of low-level fabric modeling can be found in reference 35.

4.2.4 Buckling model

When a fabric buckles, it often takes up a sinusoidal shape. By taking a cross-sectional view of a simply buckled fabric, it may be represented by a planar curve. An elastica is often used to simulate this curve. The differential equation for the elastica is $B\frac{\mathrm{d}s}{\mathrm{d}\phi} = -Py$, where B is the fabric bending rigidity, P is the compressive load, and s is the distance measured along the curve. By integrating ds along the length of the curve when the value of s becomes equal to l, the gauge length, the following equation can be obtained:

$$Pl^2/B = 4\{F(k)\}^2,$$

where $F(k)$ is the complete elliptic integral of the second kind of modulus k (= $\sin\alpha/2$). The standard solutions for the curve are usually expressed as the variation of $Pl^2/4B$ with the percentage compression of the fabric. For elastic buckling, the plot is a straight line. However, it has been found that cloth, when buckled, behaves in a different way. Grosberg *et al.*[10,36] have shown that before a cloth bends in a linear fashion, the frictional couple M_0 is needed to overcome the initial friction between the fibers in the interaction. It can be written as:

$$\begin{cases} 1/\rho = 0 & M < M_0 \\ B/\rho = M - M_0 & M > M_0. \end{cases}$$

Here, ρ corresponds to the radius of bending curvature. By assuming this relationship, they derived a series of theoretical buckling curves that were in accord with the actual buckling of cloth. They also found that nearly all the hysteresis seen during buckling and the amount of strain left after one cycle are almost wholly determined by the frictional restraint that arises in the fabric due to inter-yarn pressures.

More recently, Clapp and Peng published a series of papers that attempted to refine the classical models for describing the buckling of woven fabrics.[37–39] Using Timoshenko's elastica theory, they established a differential equation of fabric in which fabric weight is taken into account. The fabric elastica was modeled as a curved beam of constant cross-section; numerical solutions for the differential equation were obtained under two types of boundary conditions at the beam's two ends of (i) symmetrical, free–free ends and fixed–fixed ends, and (ii) unsymmetrical, free–fixed ends. They found that both frictional couple and fabric weight may jointly contribute to determine the buckling state if their values are not negligible.

Shinohara *et al.*[40,41] developed a mathematical model to describe the buckling deformation of a tubular fabric in axial compression. Two groups of contour hyperbolas, which can be determined by boundary conditions for any lobe ratio, can be used to represent the deformed surface on a lobe. They declared that the mathematical model can be used to predict the buckling pattern with any specified lobe ratio and many characteristics of the buckling pattern can be understood with the use of three-dimensional graphics.

4.2.5 Rheological model

Grosberg[42] pointed out that the energy loss during cyclic deformation of a fabric is due to two separate reasons: fiber viscoelastic properties; and the frictional restraint to inter-fiber and inter-yarn movements in fabric during deformation. Theory of fabric rheology was introduced by Olofsson[43–45] and by Grosberg.[42,46,47] They considered the role of inter-fiber and inter-yarn

friction in order to predict fabric hysteresis and recovery from the deformation. In 1969, Olofsson[45] reported an extensive study on fabric rheological behavior. He proposed a series of fabric models that contained elastic, viscous and frictional elements to describe features of bending and shear deformation. In 1977, Grosberg[42] made a detailed analysis on the role of friction in the tension, shearing, and bending deformations of woven fabric at the initial deformation stage. Fabric rheology was further studied by Chapman in the seventies, with the inclusion of fiber viscoelasticity as well as inter-fiber and inter-yarn friction in the models of fabric deformation and recovery.[48–50] He presented a model that took into account the linear viscoelasticity and the frictional moment of fabric, to predict the bending and bending recovery of fabric strip.[50] By measuring the fiber viscoelastic processes of stress relaxation and creep, the deformation of a viscoelastic textile material could be predicted using this model.

More recently, Zhang *et al.* did a systematic study about the rheological mechanism in fabric bagging, and developed a series of models to describe bagging deformation of fabric.[51–56] Their models[4,53] were based on the standard solid model[57] and Olofsson's rheological model of fabric.[45] The stress–strain relations for elastic elements and viscoelastic elements in the models were assumed to be linear. By specifying the fundamental properties of fibers, the measurable parameters of the yarn and fabric structural features, and the geometrical relation between strain and bagging height, their models were able to predict fabric bagging behavior.

4.3 Knitted fabrics

4.3.1 Structure

Knit fabrics are composed of intermeshing loops of yarns. There are two major types of knits: weft knits and warp knits, as illustrated in Fig. 4.7. In weft knits, each weft yarn lies more or less at right angles to the direction in which the fabric is produced, and the intermeshing yarn traverses the fabric crosswise. In warp knits, each warp yarn is more or less in line with the direction in which the fabric is produced, and the intermeshing yarn traverses the fabric lengthwise. Similar to the way that woven fabrics have warps and wefts, knit fabrics have courses and wales, which lie in the crosswise and lengthwise direction, respectively. However, unlike woven fabrics, courses and wales are not composed of different sets of yarns; rather are formed by a single yarn.

'Loop' is the basic unit of knit fabric. As illustrated in Fig, 4.7a, in weft knits, a loop, called a needle loop, consists of a head and two legs, and the section of yarn connecting two adjacent needle loops is called the sinker. In warp knits, the needle loop is divided into overlap and underlap, as

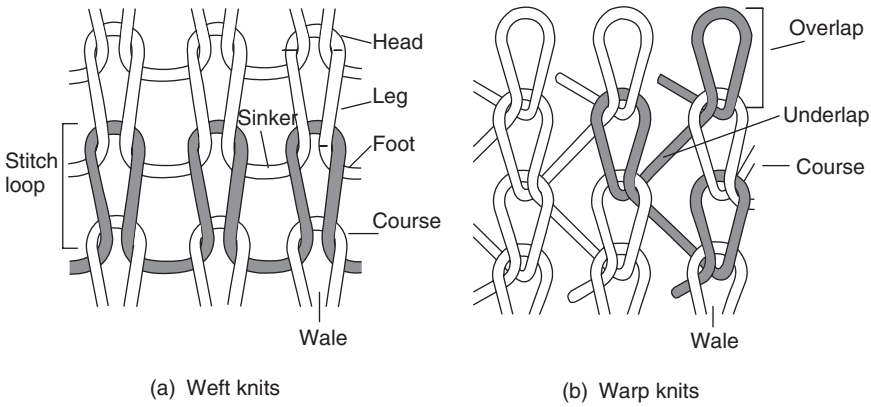

(a) Weft knits (b) Warp knits

4.7 Knit fabric.

illustrated in Fig. 4.7b. Each loop in a knit fabric is a stitch. Alternative to fabric count for woven fabrics, cut (or gauge) and stitch density are used to represent the closeness of the intermeshing loops. Cut or gauge indicates the number of knitting needles per unit length along the crosswise or lengthwise direction. The greater the number, the closer together the loops are to each other. Stitch density is the number of stitches per unit area, obtained by multiplying the number of courses per inch (25 mm) by the number of wales per inch (25 mm). Like woven fabrics, a knit fabric also has a technical face and a technical back and can differ in appearance on each side. The technical face is the side where the loops are pulled toward the viewer. Knit fabric also has an effect side, which is intended to be used outermost on a garment or other textile product. In some cases, the technical face and the effect side are the same; but in others, they are opposite.

4.3.2 Mechanical behavior

The basic factors that govern the mechanical properties of knit fabrics are the same as those that govern the mechanical properties of woven fabrics. In most cases, knitted fabrics are treated as merely variants of woven fabrics; for example, the bending and buckling of knit fabrics has never been treated separately. However, the load–extension behavior of knit fabrics, while similar in kind to the behavior of woven fabrics, shows a large difference of degree in the relative size of the initial extension as well as in the initial modulus. Generally, the resistance of the cloth to extension is mainly due to the resistance of parts of the structure to bending and torsion; therefore it is relatively small. As a result, the relative size of the frictional restraint to the extension is high. Research concerning the warp-wise load–

extension of warp knit fabrics shows that the extension modulus is dependent entirely on the resistance of the yarn to the changes in curvature that take place in the loop during extension. However, the extension of this analysis to plain weft knit seems not to be successful.

Knitted fabrics are usually subject to biaxial stresses under relatively high loads. In such cases, the knitted structure becomes only a tension transmitting body and the internal bending and shear energy changes can be neglected; thus an analysis is available. An analysis of the weft-wise stretching of rib fabrics shows that the mechanical behavior is probably determined almost entirely by the resistance of the link connecting the face and back loop in the fabric, to being twisted or sheared. Furthermore, some analysis leads to a generalization of the mechanical behavior of knitted fabrics: the load to give a fixed extension is proportional to m/l^3 when the resistance is due to bending energy changes, and to G/l^3 when it is mainly due to shear energy changes. Here, l is the loop length, and m and G denote the bending rigidity and the torsional rigidity of the yarn, respectively. More details about the mechanical behavior of knit fabrics can be found in reference 1.

4.3.3 Modeling

Geometrical model

In attempts to understand the dimensional behavior of knitted fabrics, the key element is on the geometry of the knitted loop. Peirce,[58] Leaf,[59,60] Doyle,[61] Munden,[62] Postle,[63,64] and recently Demiroz and Diaz,[65] all have significant contributions to the geometrical analysis of plain knitted fabric.

Peirce[58] extended his geometric model for plain woven fabric to plain knitted fabric. Based on the same assumptions, he deduced that the basic structure of a knitted fabric is one in which the loops consist of parts of circles joined by straight lines and in which the maximum packing of the yarns had taken place. He also assumed that the loops lie on a cylinder, to allow for the 3D properties of the needle loop. From these assumptions, he deduced an equation to describe the relationship between the stitch length l, the course spacing c, the wale spacing w, and the yarn diameter d.

Doyle[61] then suggested that, by using certain dimensionless ratios of the lengths, the properties of knit fabrics could be adequately described in a simple way. He showed that the product of c and w is proportional to l^2. Later work by Munden[62] showed that the relationship can be more universal; the slope of the graph of stitch density against $1/l^2$ is independent of the value of d/l.

Leaf,[59] and Leaf and Glaskin[66] pointed out that there was some intrinsic problem in Peirce's original geometry. They proposed an alternative – that

the loop consists merely of a set of circular arcs. Their model was further improved by assuming that the loop consists of two elasticas joined as mirror images.[59] The success of the model was due to its simplicity and a good description of the actual fabric. Recent innovative work[65] on loop geometry is the application of spline curves to represent the loop. It is especially useful in the visual display of knitted fabric in a CAD system.

Geometric–mechanical model

The dimensional properties of knitted fabric were studied by some researchers alternatively using a force method. In the theoretical models of Postle,[63] Shanahan and Postle[67] and Hepworth and Leaf,[68] yarn was treated as an elastica[69] which is naturally straight. Attempts have been made by MacRory *et al.*[70] and Hepworth and Leaf[71] to tackle the biaxial load–extension problem of knitted fabric. MacRory's model emphasized the slippage between loops and the biaxial load case with the loop elements being straightened, while Hepworth's model concentrated on the effect of yarn jamming.

Energy model

Choi and Lo[72] proposed an energy model with sufficient degrees of freedom for loop deformation, including changes in loop height and width. The yarn forming the loops is perfectly elastic and incompressible, with zero friction. It is naturally curved and its paths in the deformed states are the elements of a prescribed family of space curves. The yarns can be axially compressed or extended at the low-load region. Conditions of loop jamming are taken as the geometric constraints of loop deformation. The total mechanical energy is calculated based on the difference in bending strain and torsional strain of the yarn with respect to the natural curvature and torsion. This model can be applied to determine the biaxial tensile behavior of plain knitted fabric.

Micro-particle model

Eberhardt *et al.* proposed a model to represent knit fabrics based on the assumption that threads bond and interact with each other only at bonding points (BPs).[73] By regarding each BP as a particle, and evaluating the forces exerted by the springs that represent the stretch, compression and bending of the yarns at the bonding points, the dynamics of the particle system corresponding to the micro-structure of the knitting pattern can be simulated. Some simulations taking an initial knit configuration and 'relaxing' it to a minimal energy state were presented in reference 73.

4.4 Conclusion

As the main materials constituting garments and textile devices, woven fabrics and knitted fabrics have been addressed from various aspects, including structure, mechanical behavior and modeling. Tension, shearing, bending and twisting are the basic mechanical behaviors in garment wear. The complex deformation of fabrics includes buckling and rheological behavior. Since the fabric mechanical properties are largely determined by the constituting fibers and yarns, internal structural features and surface morphological characteristics, fabrics' micro-structures and micro-mechanics were focused on here, and the work developed in the area of lower-level fabric modeling was reviewed.

4.5 Acknowledgement

We would like to thank Hong Kong Polytechnic University for funding this research through Projects A188 and G-YD31.

4.6 References

1. Grosberg, P., *The Mechanics of Knitted Fabrics, in Structural Mechanics of Fibers, Yarns and Fabrics*, S. Backer (Editor). 1969, Wiley-Interscience: New York. p. 439–450.
2. Ghosh, T.K., Batra, S.K. and Barker, R.L., The Bending Behavior of Plain-woven Fabric, Part I: A Critical Review, *Journal of the Textile Institute.* 1990. p. 245–254.
3. Shanahan, W.J. and Hearle, J.W.S., Energy Method for Calculations in Fabric Mechanics, Part Two: Examples of Application of the Method to Woven Fabrics, *Journal of the Textile Institute.* 1978. p. 92–100.
4. Zhang, X., (ed.) *Mechanism of Woven Fabric Bagging.* Institute of Textile and Clothing. 1999, The Hong Kong Polytechnic University: Hong Kong.
5. Peirce, F.T., The Geometry of Cloth Structure, *Journal of the Textile Institute.* 1937. p. T45–T97.
6. Hearle, J.W.S., Grosberg, P. and Backer, S., *Structural Mechanics of Fibers, Yarns and Fabrics.* 1969, Wiley-Interscience: New York.
7. Kemp, A., An Extension of Peirce's Cloth Geometry to the Treatment of Non-circular Threads, *Journal of the Textile Institute.* 1958. p. T44–48.
8. Konopasek, M., Classical Elastica Theory and its Generalizations, *Mechanics of Flexible Fiber Assemblies*, J. Amirbayat (Editor) 1980, Sijthoff & Noordhoff, Alphen aan den Rijn. p. 255–274.
9. Olofsson, B., A General Model of a Fabric as a Geometric–Mechanical Structure. *Journal of the Textile Institute.* **55** 1964. T541–T557.
10. Grosberg, P. and Kedia, S., The Mechanical Properties of Woven Fabrics, Part I: The Initial Load Extension Modulus of Woven Fabrics, *Textile Research Journal*, **36** No. 1, 1966, p. 71–79. Part II: The Bending of Woven Fabrics, *Textile Research Journal.* 1966. p. 205–211.

11. Konopasek, M., Textile Applications of Slender Body Mechanics, *Mechanics of Flexible Fiber Assemblies*, J. Amirbayat, Editor. 1980, Sijthoff & Noordhoff, Alphen aan den Rijn. p. 293–310.
12. Leaf, G.A.V. and Anandjiwala, R.D., A Generalized Model of Plain Woven Fabric, *Textile Research Journal.* 1985. p. 92–99.
13. Huang, N.C., Finite Biaxial Extension of Completely Set Plain Woven Fabrics, *Journal of Applied Mechanics.* 1979. p. 651–655.
14. Anandjiwala, R.D. and Leaf, G.A.V., Large-scale Extension and Recovery of Plain Woven Fabrics, Part One: Theoretical, *Textile Research Journal.* 1991. p. 619–634.
15. Anandjiwala, R.D. and Leaf, G.A.V., Large-scale Extension and Recovery of Plain Woven fabrics, Part Two: Experimental and Discussion, *Textile Research Journal.* 1991. p. 743–755.
16. Ghosh, T.K., Batra, S.K. and Barker, R.L., The Bending Behavior of Plain-woven Fabric, Part II: The Case of Linear Thread-bending Behavior, *Journal of the Textile Institute.* 1990. p. 255–271.
17. Ghosh, T.K., Batra, S.K. and Barker, R.L., The Bending Behavior of Plain-woven Fabric, Part III: Thread-bending Behavior and the Effect of Fabric Set, *Journal of the Textile Institute.* 1990. p. 272–287.
18. Lomov, S.V., Truevtzev, A.V. and Cassidy, C., A Predictive Model for the Fabric-to-Yarn Bending Stiffness Ratio of a Plain-woven Set Fabric, *Textile Research Journal.* 2000. p. 1088–1096.
19. Kawabata, S., Niwa, S. and Kawai, H., The Finite Deformation Theory of Plain-weave Fabrics, Part One: the Biaxial-deformation Theory, *Journal of the Textile Institute.* 1973. p. 21–46.
20. Kawabata, S., Niwa, S. and Kawai, H., The Finite Deformation Theory of Plain-weave Fabrics, Part Two: the Uniaxial-deformation Theory, *Journal of the Textile Institute.* 1973. p. 47–61.
21. Kawabata, S., Niwa, S. and Kawai, H., The Finite Deformation Theory of Plain-weave Fabrics, Part Three: the Shear-deformation Theory, *Journal of the Textile Institute.* 1973.
22. Realff, M.L., Boyce, M.C. and Backer, S., A Micromechanical Model of the Behavior of Woven Fabric, *Textile Research Journal.* 1997. p. 445–459.
23. De Jong, S. and Postle, R., An Energy Analysis of Woven-fabric Mechanics by Means of Optimal-control Theory, Part Two: Pure-bending Properties, *Journal of the Textile Institute.* 1977. p. 362–369.
24. De Jong, S. and Postle, R., An Energy Analysis of Woven-fabric Mechanics by Means of Optimal-control Theory, Part One: Tensile Properties, *Journal of the Textile Institute.* 1977. p. 350–361.
25. De Jong, S. and Postle, R., A General Energy Analysis of Woven-fabric Mechanics Using Optimal-control Theory, *Textile Research Journal.* 1978. p. 127–135.
26. De Jong, S. and Postle, R., Modified Equations for the Energy Analysis of the Plain Weave, Including Theory, *Journal of the Textile Institute.* 1979. p. 359–364.
27. Knoll, A.L., The Geometry and Mechanics of the Plain-weave Structure: A Comparison pf the General Energy Method of Analysis and Previous Models, *Journal of the Textile Institute.* 1979. p. 163–171.
28. Knoll, A.L., Modified Equations for the Energy Analysis of the Plain Weave, Including Yarn Extension, *Journal of the Textile Institute.* 1979. p. 355–358.

29. Sinoimeri, A. and Drean, J.Y., A Study of the Mechanical Behaviour of the Plain-weave Structure by Using Energy Methods: Fabric Shear, *Journal of the Textile Institute.* 1996. p. 120–128.
30. Hearle, J.W.S. and Shanahan, W.J., Energy Method for Calculations in Fabric Mechanics, Part I: Principles of the Method, *Journal of the Textile Institute.* 1978. p. 81–91.
31. Leaf, G.A.V. and Kandil, K.H., The Initial Load–extension Behaviour of Plain-woven Fabrics, *Journal of the Textile Institute.* 1980. p. 1–7.
32. Tarfaoui, M. and Drean, J.Y., Predicting the Stress–strain Behavior of Woven Fabrics Using the Finite Element Methods, *Textile Research Journal.* 2001. p. 790–795.
33. Haan, S.I., Charalambides, P.G. and Suri, M., A Specialized Finite Element for the Study of Woven Composites, *Computational Mechanics.* 2001. p. 445–462.
34. Li, Y. and Dai, X.Q., Simulate Woven Fabric Behavior during Low Extension with a Computational Micro-mechanical Model, submitted to *Textile Research Journal.* 2005.
35. House, D.H. and Breen, D.E., *Cloth Modeling and Animation.* 2000, A. K. Paters Ltd: Natick, Massachusetts. p. 55–77.
36. Grosberg, P. and Swani, N.M., The Mechanical Properties of Woven Fabrics, Part III: The Buckling of Woven Fabrics, *Textile Research Journal.* 1966. p. 332–338.
37. Clapp, T.G. and Peng, H., Buckling of Woven Fabrics, Part III: Experimental Validation of Theoretical Models, *Textile Research Journal.* 1990. p. 641–645.
38. Clapp, T.G. and Peng, H., Buckling of Woven Fabrics, Part II: Effect of Weight and Frictional Couple, *Textile Research Journal.* 1990. p. 285–292.
39. Clapp, T.G. and Peng, H., Buckling of Woven Fabrics, Part I: Effect of Fabric Weight, *Textile Research Journal.* 1990. p. 228–234.
40. Shinohara, A., Ni, Q.Q. and Takatera, M., Geometry and Mechanics of the Buckling Wrinkle in Fabric, Part II: Buckling Model of A Woven Fabric Cylinder in Axial Compression, *Textile Research Journal.* 1991. p. 100–105.
41. Shinohara, A., Ni, Q.Q. and Takatera, M., Geometry and Mechanics of the Buckling Wrinkle in Fabric, Part I: Characteristics of the Buckling Wrinkle, *Textile Research Journal.* 1991. p. 94–100.
42. Grosberg, P., The Role of Friction in the Mechanical Behaviour of Fabrics, *Surface Characteristics of Fibres and Textiles, Part II*, M.J. Schick (Editor) 1977, Marcel Dekker Inc: New York and Basel. p. 563–575.
43. Olofsson, B., A Study of Inelastic Deformation of Textile Fabrics, *Journal of Textile Institute.* 1967. p. 221–241.
44. Olofsson, B., The Mechanics of Creasing and Crease Recovery. *Textile Research Journal.* 1968.
45. Olofsson, B., Rheology of Textile Fabrics, in *Rheology – Theory and Application*, B. Olofsson (Editor) 1969, Academeic Press: New York. p. 492–545.
46. Grosberg, P., The Mechanical Properties of Woven Fabrics, Part V: The Initial Modulus and the Frictional Restraint in Shearing of Plain Weave, *Textile Research Journal.* 1966. p. 420–431.
47. Grosberg, P., The Mechanical Properties of Woven Fabrics, Part IV: The Determination of the Bending Rigidity and Frictional Restraint in Woven Fabrics, *Textile Research Journal.* 1966. p. 338–345.

48. Chapman, B.M. and Hearle, J.W.S., The Bending and Creasing of Multicomponent Viscoelastic Fiber Assemblies Part I: General Consideration of the Problem, *Textile Research Journal.* 1973. p. 385–403.
49. Chapman, B.M., The Bending and Creasing of Multicomponent Viscoelastic Fiber Assemblies Part III: The Mechanics of a Two-dimensional Assemblies of Generalized Viscoelastic Fibers of Different Types, *Textile Research Journal.* 1974. p. 306–309.
50. Chapman, B.M., The Bending and Recovery of Fabrics under Conditions of Changing Temperature and Relative Humidity, *Textile Research Journal.* 1976. p. 113–122.
51. Zhang, X. *et al.*, Fabric Bagging, Part I: Subjective Perception and Psychophysical Mechanism, *Textile Research Journal.* 1999. p. 511–518.
52. Zhang, X. *et al.*, Fabric Bagging, Part II: Objective Evaluation and Physical Mechanism, *Textile Research Journal.* 1999. p. 598–606.
53. Zhang, X., Li, Y. and Yeung, K.W., Mathematical Simulation of Fabric Bagging, *Textile Research Journal.* 2000. p. 18–28.
54. Zhang, D. and Yuen, M., Collision Detection for Clothed Human Animation, *Pacific Graphics Conference*, Hong Kong. 2000. p. 328–337.
55. Zhang, X. *et al.*, Relative Contributions of Elasticity and Viscoelasticity of Fibers and Inter-fiber Friction in Bagging of Woven Wool Fabrics, *Journal of Textile Institute.* 2000. p. 577–589.
56. Zhang, X. *et al.*, Fabric-bagging: Stress Distribution in Isotropic and Anisotropic Fabrics, *Journal of Textile Institute.* 2000. p. 563–576.
57. Frindley, W.N., Lai, J.S. and Onaran, K., *Creep and Relaxation of Nonlinear Viscoelastic Materials.* 1976, North-Holland Publications. p. 50–105.
58. Peirce, F.T., Geometrical Principles Applicable to the Design of Functional Fabrics, *Textile Research Journal.* 1947. p. 123–147.
59. Leaf, G.A.V., Models of the Plain Knitted Loop, *Journal of the Textile Institute.* 1960. p. T49–58.
60. Leaf, G.A.V., The Stresses in the Plain Knitted Loop, *Journal of the Textile Institute.* 1961. p. T351–365.
61. Doyle, P.J., Some Fundamental Properties of Hosiery Yarns and Their Relation to the Mechanical Characteristics of Knitted Fabrics, *Journal of the Textile Institute.* 1952. p. 19–35.
62. Munden, D.L., The Geometry and Dimensional Properties of Plain-knit Fabric, *Journal of the Textile Institute.* 1959. p. T448–471.
63. Postle, R., Analysis of the Dry Relaxed Knitted Loop Configuration, *Journal of the Textile Institute.* 1967. p. 329–365.
64. Postle, R., Dimensional Stability of Plain Knitted Fabrics, *Journal of the Textile Institute.* 1968. p. 65–77.
65. Demiroz, A. and Dias, T., A Study of the Graphical Representation of Plain-knitted Structure, Part I: Stitch Model for the Graphical Representation of Plain-knitted Structures, *Journal of the Textile Institute.* 2000. p. 463–480.
66. Leaf, G.A.V. and Glaskin, A., The Geometry of the Plain Knitted Loop, *Journal of the Textile Institute.* 1955. p. T587–605.
67. Shanahan, W.J. and Postle, R., A Theoretical Analysis of Plain Knitted Structure, *Textile Research Journal.* 1970. p. 656–665.
68. Hepworth, B. and Leaf, G.A.V., The Mechanics of an Idealised Weft-knitted Structure, *Journal of the Textile Institute.* 1976. p. 241–248.

69. Szeliski, R. and Teonnesen, D., Surface Modeling with Oriented article Systems, *SIGGRAPH'92*, 1992: Chicago. p. 185–194.
70. MacRory, B.M., McCraith, J.R. and McNamara, A.B., Biaxial Load–Extension Properties of Plain Weft-knitted Fabrics: A Theoretical Analysis, *Textile Research Journal.* 1975. p. 746–760.
71. Hepworth, B. and Leaf, G.A.V., The Biaxial Load-extension Behaviour of a Model of Plain Weft-knitting, *Journal of the Textile Institute.* 1978. p. 101–107.
72. Choi, K.F. and Lo, T.Y., An Energy Model of Plain Knitted Fabric, *Textile Research Journal.* 2003. p. 739–748.
73. Eberhardt, B., Meissner, M. and Strasser, W., Knit Fabrics, *Cloth Modeling and Animation*, D.E. Breen (Editor) 2000, A K Paters: Natick, Massachusetts. p. 123–144.

5

Clothing mechanics

X-Q. DAI[1,2], Y. LI[1]
[1]The Hong Kong Polytechnic University, China
[2]Soochow University, China

5.1 Introduction

Garments and textile devices are the final products that provide biomechanical functions to human bodies. The biomechanical functional performance of garments and devices is very much dependent on the fabric mechanical and surface properties. However, garments and devices are made from pieces of fabrics by sewing them together. Scientific understanding and knowledge of the cloth mechanical properties and modeling their mechanical behavior and their sewing process are essential for biomechanical engineering of clothing and textile products. In this chapter, the knowledge and processes developed in the area of clothing mechanics in relation to biomechanical engineering are reviewed.

5.2 Characteristics of clothing deformation

Garments are made from flat fabrics. By sewing 2D patterns of certain geometric topology, various apparel items can be constructed, and they show variable aesthetic appearances when worn on the human body. According to the degree of space allowance between the body and the garment during the body movement, F, garments can be classified as three types: (i) foundation garments ($F < 0$), as the garment area is less than the body area (e.g. girdles and compression garments); (ii) perfect fitting garments ($F \geq 0$) as the garment area is equal to or slightly larger than the body area (e.g. suits and socks); (iii) loose garments ($F >> 0$) as the garment area is far larger than the body area (e.g. dresses and flared skirts). Postle and Norton[1] pointed out that the mechanical problems in clothing can be roughly divided into two classes. The first is free-form problems, e.g. fabric drape, buckling, wrinkling, in which fabric stresses are essentially limited to those supported by fabric curvature, and where gravitational forces are frequently important. The second is form-fitting problems, often involving prescribed curvatures and larger stresses. Then, type (i) and (ii) garments

belong to form-fitting problems and type (iii) to free-form problems. Different from other sheet materials, such as paper and plastic film, cloth deformation often shows a complex nature of mixed tension, shear and bending, and may form 3D shapes of double curvature. It is this ability that enables fabric to form beautiful draping shapes and to be fitted to a body shape of complicated geometry.

5.2.1 Free-form

Buckling has been discussed in the previous chapter. Here the focus is on drape. Drape is when a fabric deforms under its own weight. It is an important factor that influences aesthetic appearance and has an outstanding effect on the formal beauty of the fabric. Drapability is related to fabric weight, stiffness (flexural rigidity), and shearing rigidity. The greater the fabric weight, the more likely it is to drape. The greater the fabric stiffness, the less likely it is to drape. The greater the fabric shear rigidity, the less the folds formed by fabric drape. However, the draping qualities required from a fabric will differ completely depending on its end use, therefore a given value for drape cannot be classified as good or bad.

5.2.2 Form-fitting

As a subject for garments, the human body surface has very complex geometry. To construct a garment of a certain style, it is often necessary to sew cloth patterns of a certain topology together to build 3D shapes of prescribed curvatures, especially for the perfect-fit garment. Two-dimensional pattern design is a very important procedure in garment manufacture. However, it is out of the scope of this book. Here, the focus is on the deforming ability of fabric. People must be able to move around in the garments they wear, especially sportswear. Discomfort may result if a fabric restrains movement, creates a burden or exerts pressure on the body. Therefore, the form-fitting ability includes not only the ability of a fabric to be perfect-fitted or tight-fitted to a static body, but also its ability to deform dynamically to fit along with the body movement.

When people move, their skin stretches; it elongates and recovers. Skin is a highly elastic material. Fabric placed close to the skin needs to be elastic too. It must elongate to accommodate body movement and then recover. Fortunately, fabric is a flexible material. It can not only form a shape of complicated curvature, but also stretch to a certain extent in two principle directions (warp and weft), even simultaneously. Stretch is the ability of a fabric to stretch when a pulling force is applied and then recover relatively quickly and fully to its original dimensions when the force is removed. Fabric of high stretch will have good form-fit ability. Various stretch fabrics

differing in extensibility are expected to meet the requirement for different special end use.

5.2.3 Sewing

A garment is often made from several pieces of cloth pattern by sewing them together along pairs of prescribed seam lines. This process is realized in a sewing machine by using the sewing thread to stitch pairs of cloth pattern borders together. Failure at a seam makes a garment unusable even though the fabric may still be in good condition. There are many possible causes for seam failure. For example, the sewing thread wears out or fails before the fabric does, or the yarns making up the fabric are broken or damaged by the needle during sewing. These problems are specific to the making-up process and depend on the sewing machine used, the sewing thread, the sewing speed and so on. A typical seam failure that is related to fabric property is seam slippage. It is a condition where a seam sewn in the fabric opens under load. Some of this gap may close on removal of the load but some of it may be a permanent deformation. The resistance to such yarn slippage in fabric is called seam strength. It is an important property for fabric in garment construction and its test will be detailed in a later chapter.

5.3 Clothing modeling

Since fitting formability problems involve contact with the human body, they will be dealt with later, in Chapter 8. Here the focus is on cloth modeling. Many techniques have been developed to model overall fabric shape. Among them, there are two major approaches: to consider fabric as a continuum whole (continuum model) and to discretize fabric into mass points (discrete model).

5.3.1 Continuum models

Even though a fabric is made up of two groups of threads, the discontinuity in the fabric can be neglected when a large piece is considered. Therefore a fabric can be treated as a continuum without its discrete microstructure, and by means of elasticity theory, continuum solid mechanics are used to model it. In 1963, Kilby[2] first applied elasticity theory to fabric modeling. He developed planar stress–strain relationships for a fabric model of a simple trellis, using a conventional elasticity-based analysis. Through his analysis, he predicted that the Young's modulus is a function of angle across a woven fabric surface.

Shanahan, Lloyd and Hearle[3] used the engineering theory of sheets, shell and plates to characterize the elastic behavior of fabrics in complex deformations. The simplest form of the plate and shell theory assumes that the material is homogeneous, that strains and displacements are small, and that the material behavior is linearly elastic. In spite of their concerns with the applicability of this theory to modeling fabric, they derived equations for the generalized tensile, shearing bending, and twisting rigidities of fabric.

$$\begin{pmatrix} F_1 \\ F_2 \\ F_{12} \end{pmatrix} = \begin{Bmatrix} \frac{E_1}{1-\nu_1\nu_2} & \frac{\nu_2 E_1}{1-\nu_1\nu_2} & 0 \\ \frac{\nu_1 E_2}{1-\nu_1\nu_2} & \frac{E_2}{1-\nu_1\nu_2} & 0 \\ 0 & 0 & G \end{Bmatrix} \begin{pmatrix} \varepsilon_1 \\ \varepsilon_2 \\ \varepsilon_{12} \end{pmatrix} \quad \text{(based on Eq. 8 in reference 3)}$$

$$\begin{pmatrix} M_1 \\ M_2 \\ M_{12} \end{pmatrix} = \begin{Bmatrix} B_1 & \sigma_2 B_1 & 0 \\ \sigma_1 B_2 & B_2 & 0 \\ 0 & 0 & \tau \end{Bmatrix} \begin{pmatrix} K_1 \\ K_2 \\ K_{12} \end{pmatrix} \quad \text{(based on Eq. 9 in reference 3)}$$

Lloyd[4] further introduced non-linear extensions into these equations. He applied the finite element method to simulate a series of experiments on fabric structures, and the results compared favorably with actual fabric samples. Their characterization is only valid for the special case of small strains due to the assumption of small strains and deformations; however, it provides a framework for further study.

Accompanying the rapid advance of computer techniques, the finite difference, finite volume and finite element methods are widely used in many engineering fields and computer aided design areas. To aid fabric and apparel design, and to generate clothed character animation, various fabric simulations have been carried out by many research groups from textile areas, as well as by the computer graphics community.

Draping simulation

Draping, where a fabric deforms under its own weight, is an important aesthetic property in garment end-use and has been widely simulated. During draping, fabrics bend through large displacements but are not easily stretched; this leads to classification of draping behavior as a small-strain/large-displacement problem in finite element analysis. When large deformations occur in a finite element solution, the non-linearity due to a change in the geometry of the body has to be considered to obtain the correct load-response. The general approach to handling the geometric non-linearity is the increment method based on the total Lagrangian formulation. Instead

of the one-step solution found in linear problems, the loads are applied incrementally to the system and at each step the equilibrium equation is

$$[K]\{\Delta q\} = \{\Delta f\}$$

Non-linearity is handled by calculating the stiffness matrix $[K]$ in each step as a function of the displacement vector $\{q\}$. In the total Lagrangian formulation, the Green–Lagrange strain and the Piola–Kiechhoff stress refer to the shape and position of the body at the initial time.

$${}^{t}_{0}\varepsilon_{ij} = ({}^{t}_{0}u_{i,j} + {}^{t}_{0}u_{j,i} + {}^{t}_{0}u_{k,i}{}^{t}_{0}u_{k,j})/2$$

$${}^{t}_{o}S_{ji} = \frac{{}^{o}\rho}{{}^{t}\rho}\,{}^{o}_{t}x_{i,\alpha}{}^{t}_{0}x_{j,\beta}\,{}^{t}\tau_{\alpha\beta}$$

In 1988–89, Imaoka *et al.*[5,6] developed a continuum mechanics model of a fabric for their 3D apparel CAD system. Triangular finite elements were employed to investigate the drape of fabrics. To solve the large deformation problem, the total Lagrangian formulation was employed. The tensile, bending, shearing and twisting rigidities of fabrics were used in deriving the strain energy equations for tensile, bending and shear deformations. The energies were then minimized, using a form of Newton's method, to place a 3D cloth structure in a final configuration over a human body. The simulations of a skirt and several blouses were presented.

In 1991 Collier *et al.*[7] used a geometric non-linear finite-element method based on a simple shell theory to predict fabric drape behavior in which fabric deformation is characterized as a non-linear small-strain/large-displacement problem. The fabric is treated as an orthotropic shell membrane. The flat-shell is a four-node quadrilateral bending/membrane element with five degrees of freedom at each node. The generalized displacement is defined in terms of the nodal displacement with an appropriate interpolation function, which is a twelve-term fourth-order polynomial. Three parameters, which are the measured tensile modulus in the two planar principal directions and literature values of Poisson's ratio, are used for material properties. A Newton–Raphson solution procedure is used in the draping analysis, and a non-linear load/deflexion relation is assumed. A traditional drape test on a cotton plain weave fabric is simulated. The result obtained is the projection of the deformed area on the *x-y* plane and from it, the drape coefficient was calculated as 71.0% compared with the experimental value of 68.4%.

Kang *et al.*[8] assumed a fabric to be an elastic material with orthotropic anisotropy and considered it as a thin flexible plate under the plane stress condition. The geometric non-linear phenomenon is dealt with by a total Lagrangian approach. The quadrilateral elements with four nodes and five degrees of freedom for each node are used. A transverse-shear-strain

interpolation method is adopted to avoid the shear-locking phenomenon that is commonly observed in thin-plate analysis. The mechanical parameters used in the simulation are tensile, shear, bending and torsional rigidities. Predicted 2D and 3D draping shapes show reasonably good agreement with those obtained experimentally. The authors also pointed out that the bending properties are more important than the tensile ones in draping simulation.

Chen and Govindaraj[9,10] used a shear flexible shell theory to predict fabric drape. The fabric is considered as a continuous, orthotropic medium. The geometry of the shell is represented by the coordinates and normal vectors at nodes situated on the middle surface. A nine-node, doubly curved shell element with five degrees of freedom per node is used. The kinematics of the shell theory consists of measuring membrane strain on the reference surface from the derivatives of a point position with respect to position on the surface, and bending strain from the derivatives of the unit normal to the reference surface at the point. The strain measures that are used for this purpose are approximations to Koiter–Sanders theory strains. The transverse shear strains are measured as the change in the projections of the normal onto the shell's reference surface. Simulation of a 30×30 cm fabric draped over a 12×12 cm table was carried out. The material characteristics used were Young's modulus in the warp and weft directions, shear modulus and Poisson's ratio. In a number of simulations they varied the values of these quantities and observed the differences in the draped shapes. They concluded that the shear modulus has the greatest influence on draping behavior and Poisson's ratio the least.

Gan and Ly[11] employed a model and a computational approach similar to Chen and Govindaraj's to study fabric deformation. They addressed three issues: (i) proper calculation of shell normals at the finite element nodes, (ii) elimination of shear and membrane locking during element evaluation, and (iii) the definition of an accurate stress–strain relationship for the material. The tensile, bending and shear rigidities are used for the mechanical properties of fabrics in the simulation. The constitutive relation of fabrics is determined mainly on their bending and shear properties. Comparison between the produced results of 2D bending and 3D draping and the corresponding real objects confirms that by using this constitutive relation, the finite element method can give satisfactory results to problems in which bending deformation dominates.

Eischen *et al.*[12] also modeled fabric using the geometrically exact shell theory proposed by Simo *et al.* A woven fabric is considered as an elastic isotropic material. The mechanical properties of fabrics used are Young's modulus, Poisson ratio and the Kawabata bending plots. An adaptive arc-length control algorithm is employed to account for fabric buckling. The non-linear bending response is derived from fifth-order polynomial curves

approximating to KES bend plots. A contact procedure based on a penalty method is used to simulate interactions with solid objects. They developed modeling techniques that allowed the simulation for not only the draping of fabric, but also the picking, placing, and folding of a piece of fabric. They produced several simulations and favorably compared them to photographs of actual fabric drapings and manipulations.

Hu and Chen,[13] and Hu, Chen and Teng[14] predicted the drape behavior of circular fabric sheets over circular pedestals using a geometrically non-linear finite-volume method. An initially flat circular fabric sheet is first subdivided into a number of structured finite volumes, each containing a grid node, by mesh lines along the warp and weft directions. The strains and curvatures and the out-of-plane bending and in-plane membrane strain energies of a typical volume can be evaluated using the global coordinates of its grid node and several neighbors surrounding it. The equilibrium equations of the fabric sheet are derived by employing the principle of stationary total potential energy. The full Newton–Raphson iteration method with line searches is used to solve the non-linear algebraic equations resulting from the formulation. The comparison between the predicted symmetrically deformed shapes and the experimental results is presented to demonstrate the validity and accuracy of the method. The perturbation force is also introduced to simulate the random disturbance in real experiment.

Dynamic continuum model

The previously mentioned finite element or volume approaches are mainly for static draping problems; only static equilibrium equations are involved. However, sometimes dynamic fabric deformation needs to be solved. Since cloth is the most visible object in our daily life, the computer graphics community has shown great interest in dynamic cloth modeling. The goal of their work is not to model any particular deformable material accurately; instead they are interested in creating physically-based models to produce cloth-like deformation for computer animation without expensive computation cost. Measured data of mechanical properties are rarely used in these simulations. Many dynamic finite element and finite difference approaches have been developed.[15–18]

Taking continuum mechanics and differential geometry as their starting point, Terzopoulos and Fleischer[16,19] and Terzopoulos *et al.*[15] developed a wide range of physically-based deformable models that becomes the basis of deformable surface models in the computer graphics area.[15,16,19] They presented a simplified set of equations based on elasticity theory that describe elastic and inelastic deformations, interactions with solid geometry, and fracture for flexible curves, surfaces and solids. For deformable surfaces, the deformation energy is:

$$\varepsilon(r) = \int_{\Omega} \|G - G^0\|^2_{w^1} + \|B - B^0\|^2_{w^2} \, \mathrm{d}a_1 \mathrm{d}a_2$$

Here, $r(a_1, a_2, t)$ denotes the material coordinate of a surface, G is the metric tensor, to measure the local distances and angles between nearby points in the deformable sheet, $\|\cdot\|_{w^1}$, $\|\cdot\|_{w^2}$ are weighted matrix norms, and B is the curvature tensor, defining the local curvature properties of the surface. Lagrange's equations of motion are used to obtain a motion equation for the elastic object.

$$\frac{\partial}{\partial t}\left(\mu \frac{\partial r}{\partial t}\right) + \gamma \frac{\partial r}{\partial t} + \frac{\delta \varepsilon(r)}{\delta r} = f(r, t)$$

Here $\varepsilon(r)$ denotes the deformation energy. To obtain the solutions, the equation has to be discretized by a finite-difference or finite-element method, resulting in a large system of simultaneous ordinary differential equations. By integrating the equations through time, the model simulates the dynamics at each time step. An implicit alternating-direction (ADI) method, which generates a series of tightly-banded linear systems rather than one large sparse system, was used for the large simulations. The produced simulations include a waving flag, a carpet over various objects, and a sequence in which a piece of cloth is torn apart.

A research group from MIRALab, University of Geneva, extended Terzopoulos' general model to cloth modeling.[17,20,21] They developed a cloth simulator for their clothing virtual actors system. The major extension is the way that the damping and collisions are handled. The damping of rigid body motion and the inappropriately springy behavior in collision response that may occur are avoided in Terzopoulos' model. The system uses the midpoint method to advance the simulation. They also developed the computational methods needed for cloth collision detection and producing animations of complete sets of clothing.

Fabric strongly resists stretching deformation while being comparatively permissive in allowing bending and shearing deformations. This results in a 'stiff' underlying differential equation of motion. Explicit methods are not a good choice to solve stiff equations because they require many small steps to stably advance the simulation forward in time. In cloth animation, the computational cost is a critical issue. Many approaches have been developed to increase the time step[22,23] and the most remarkable contribution was made by Baraff and Witkin.[18] They derived the internal cloth forces using a simple continuum formulation that supports modeling operations such as local anisotropic stretch or compression. A unified treatment of damping forces is also included. An implicit integration method (backward Euler method) is used to generate a large, unbanded sparse linear system at each time step, which is then solved using a modified conjugate gradient

method that simultaneously enforces particles' constraints. These techniques allow large time steps in cloth animation. They presented garments including shirts, pants and skirts exhibiting complex wrinkling and folding behavior on both key-framed and motion-captured characters.

5.3.2 Discrete models

Continuum models involve solving large systems of simultaneous ordinary differential equations, and the computational cost is often very expensive. Rather than consider a woven fabric as a whole, another approach is to discretize the fabric into a set of point masses (particles) which interact through energy constraints or forces, and thus model approximately the behavior of the material. The usual way to numerically simulate a mechanically-based particle system is to directly integrate Newton's second law for a mass particle over all particles:

$$F(t) = m\frac{\mathrm{d}^2 X}{\mathrm{d}t^2}$$

where X is the particle position, F is the sum of the forces acting on the particle and m is its mass. The forces exerted on each particle depend on the current state of the system, which is represented by the position and speed of all particles. These forces usually represent all the mechanical effects on the system, which include internal deformation forces, gravity and aerodynamic effects, and different kinds of other external constraints.

Mass–spring systems are the simplest way to design a volume model using a particle system. In this approach, each particle represents a point mass, which is linked to its neighbors by a 'spring' representing the elastic behavior of the material. The springs tend to keep the particles at their initial resting positions. In 1995, Provot[24] proposed a mass–spring system to model cloth. The mass particles, arranged in a rectilinear grid, are connected with three types of springs. The structural springs connect nearest-neighbor particles along thread lines; the shear springs connect nearest-neighbor particles along diagonals; and the flexion springs connect a particle with its second neighbor along thread lines. Provot calculated the dynamic behavior of the springs in order to simulate a cloth hanging from two points and a waving flag. A heuristic method is presented, which first takes a step in time based on the dynamics of the system, then adjusts the positions of the particles that have violated local distance constraints. The enforcement of distance constraints eliminates the unacceptable elongation generally found near fixed model points in elastic models. Removing the elongation makes these kinds of models less 'stretchy' and more cloth-like. Actually, this technique is most widely used in various cloth animations.

In computer graphics applications, curved surfaces are often represented by polygonal meshes. A convenient way to build a mass–spring system from this kind of description is to consider each vertex of the mesh as a particle and the edges or polygons as the interaction forces among several particles. Volino and Thalmann's[25,26] mass–spring model is a typical description of such approaches. They modeled the in-plane elasticity and out-of-plane curvature elasticity and calculated the in-plane deformation within each triangle. By introducing a parameter α ($|\alpha| < 1$), they controled the Poisson coefficient of the simulated fabric. The way to measure the bending curvature in an irregular mesh is to consider the angle θ formed by two triangles about the connecting edge. The resulting curvature force moment is then given by forces applied to the four vertices respectively.

Explicit integration methods are the simplest methods available for solving particle motion equations. The fourth-order Runge–Kutta method is most widely used in particle systems. Since explicit methods are ill-suited to solving stiff equations, various implicit integration methods are proposed to produce real-time cloth animation.[23,25] However, these approaches are mostly used in the computer graphics area, where fast and stable animation is the key issue. The simulated cloth is a 'cloth-like' deformable surface rather than any particular textile material. Parameters of mechanical properties are rarely used in the calculation.

Breen,[27] and Breen *et al.*[28,29] developed a non-continuum particle model for fabric drape that explicitly represents the micro-mechanical structure of a fabric, *via* a particle system. Their model is based on the observation that a fabric is best described as a mechanism of interacting mechanical parts rather than a continuous substance, and derives its macro-scale dynamic properties from the micro-mechanical interaction between threads.

The particle model represents a fabric sheet by particle meshes, where $X_{i,j}$ with three components $(x_{i,j},y_{i,j},z_{i,j})$ denotes the three-dimensional position of a particle. The mass of each particle is the mass of the particle's local regular area and its strain energy represents the aggregate of the strain energies in the local area. Nevertheless, the particle grid still preserves the underlying woven structure of the fabric, and the various inter-crossing strain energies are computed, based on simple geometric relationships among local particle neighbors. The energy functions account for the four basic mechanical interactions of yarn compression, stretching, out-of-plane bending and trellising. The total energy for particle i is given by:

$$U_i = U_{repel_i} + U_{stretch_i} + U_{bend_i} + U_{trellis_i} + U_{\text{gravity}_i}.$$

The energy function U_{repel_i}, prevents particles connected to particle i from approaching it, and the function $U_{stretch_i}$, capturing the energy of tensile

strain between each particle and its four-connected neighbors, are given by generated approximation functions; the energy functions U_{bend_i} and $U_{trellis_i}$ are derived from Kawabata bending and shearing tests.[30] This particle-based approach was first applied to the problem of computing static drape. The simulation was in two stages. In the first stage, particles are allowed to fall freely. Any collision with the object or the ground is determined during this step. The particle positions can be obtained using the equation

$$ma + cv = mg,$$

where a is the acceleration, v is the velocity, m is the mass, c is the air resistance, and g is the gravitational acceleration constant. The result is a rough shape of the draped fabric. In the second stage, an energy minimization process is applied to the inter-particle energy functions to generate fine detail in the shape of the fabric. The final equilibrium shape of the fabric occurs when there is minimum energy over the whole fabric. The simulated tablecloths showed obvious characteristics of materials and agreed with actual ones. However, it is quite slow to compute a drape and it cannot produce the dynamic response.

Several forward dynamics translations of the Breen–House model have been implemented that not only produce cloth motion, but actually compute the final drape more quickly than the original method. One of the most successful of these models was proposed by Eberhardt *et al.* in 1996.[31] They used a Lagrangian dynamics reformulation of the basic energy equations suggested in the Breen–House model, resulting in a system of ordinary differential equations from which dynamics could be calculated. In their energy function, the anisotropy and hysteresis of the fabric are also modeled. A Runge–Kutta method, with adaptive step-size control, was used to solve the differential equations. With their approach, Eberhardt *et al.* simulated a cloth draping over a table top, a sphere and a castle model utilizing significantly less computation time than previously published particle methods. However, there was no comparison with any actual objects reported.

House and Breen[32,33] also extended their model to include dynamics by a force-based formulation approach. Non-linear 'cloth springs' are imagined acting on the yarn segments between crossing-point particles. The magnitude of each spring force or torque is determined by differentiating the corresponding energy equation of the particle model and its direction is determined geometrically. There was no evidence that the measured tensile data was used.

Dias *et al.*[34] proposed a discretized cloth model in which the planar deformation is modeled as the plate under plane stress and the out-of-plane deformation is to model curvature interactions along the edges of neighboring

triangles. This model combines the continuum and discrete models and benefits from both of them. The fabric is described by a mesh of irregular triangles. Each irregular triangle corresponds physically to a set of three linked strain gauges, which are able to evaluate the extensional deformation of the underlying continuum along the angle that the gauge makes with the warp direction. The stress applied on each edge is calculated according to the laws of mechanics of materials. Out-of-plane deformation is the bending interaction between pairs of adjacent triangles along their common edges. The bending curvature was modeled by assuming a cantilever beam's bending, and the Kochaneck–Bartels spline interpolation is used to define the bending curve $\zeta(x)$. Then the curvature increases as the distance from the fixed point increases. Measured data of fabric mechanical properties are used in this model and the non-linearity is included by a piecewise linear approximation approach. Simulated fabrics in tensile, draping and buckling situations are presented but no comparisons with respective real objects are provided.

On the basis of the extended particle model of Breen and House, Dai *et al.*[35] developed a particle model by deriving general force/displacement relationships of various deformations according to fundamental elasticity mechanical laws. Then mechanical data resulting from various tests can be used in this model, and material non-linearity is also included by the piecewise linear approximation. Moreover, twisting, which occurs easily in flexural fabrics, is taken into account. The twist deformation often occurs in clothes such as flared skirts, in which a fabric is subjected to large bending along bias directions. Besides the separation, bending, and shearing springs, a twisting spring is assumed to be acting on each particle square. The twisting spring exerts a torque opposing twisting. As there are no methods to measure the twist rigidity; it is obtained indirectly from known fabric mechanical properties. The heart-loop test is carried out to validate simulation accuracy. The model is also applied to skirt simulation[36]. Fabric anisotropy is visualized by the different draped shapes formed by the skirts made of the patterns of the same shape but with different cutting directions. Various internal forces can also be visualized.

5.3.3 Sewing simulation

It is difficult to simulate the process that a human body is undertaking in a garment with a particular shape by means of a computer. Rather than doing so, to construct a 3D garment worn on a body, a common approach is to first place the 2D cloth patterns that will make up the garment properly around the body. Then to invoke a mechanical simulation to force the patterns to approach each other along the prescribed seam lines. As a result, the patterns are attached and sewn on the borders as specified and attain a shape influenced by the form of the body.

It is slightly difficult for a continuum model to realize the sewing process. Kang and Sung[37] introduced a virtual sewing method by creating new points at the middle of each pair of sewing points and reconstructing the boundary elements using those new points. And the strain reduction method is followed to reshape the elements, especially those in which large deformations are introduced by sewing. Okabe *et al.*[38] developed a 3D CAD system for dresses, in which the topological connections between seam lines on planer cloth patterns are constructed as an initial state for the dress and a succeeding iterative numerical analysis is followed to obtain the mechanical stable state of minimum potential energy.

It is much easier for a discrete model to realize the sewing process. The process often relies on a simplified simulation, where the seaming forces are pulling the matching pattern borders together. There are tasks in sewing simulation: (i) to bring two objects' attachment points progressively together; (ii) to maintain these points together. Volino and Thalmann[26] introduced 'elastics' to bring two extremities together, and then maintain the closest distance between them. 'Elastics' can be either mechanical forces or geometrical constraints. The mechanical approach is to use force-driven elastics directly integrated in the cloth model. An adaptive scheme would then modify the elastic strength force depending on the actual motion and deformation of the concerned objects. The constraint-based interaction is a general scheme that may be implemented in the particular case of collision response effects. The user should be given a very simple way to characterize the effect of the elastics and to describe its strength, using a few parameters, such as the time needed to bring the objects together and the damping of the motion.

Dai and Li[36] have also carried out skirt-sewing simulation by applying a seaming force inversely proportional to the distance between each pair of particles to be attached. After sewing, mechanical properties near seam lines were different from other parts and depended on sewing style and sewing threads. They considered a simple style and neglected the difference, and the sewn parts were regarded as a continuous whole. A seam force was employed to bring the pair of particles together. The direction of the force was along the line connecting the two particles; the magnitude of it only affects the seaming speed. Once two particles approached to a prescribed close distance, they were regarded as one and their neighbourhoods were added to those of each other. When the sewing finishes, all patterns become a continuous whole.

5.4 Conclusion

In this chapter, the characteristics of cloth deformation in garment construction and wear that need to be taken into account in clothing modeling

have been introduced. Drape, stretch and sewing were considered as three major elements in garment formation. The high-level cloth models to predict the whole aesthetic appearance of fabrics and garments were reviewed, including the continuum approach and the discrete approach. Sewing simulation techniques were also briefly considered.

5.5 Acknowledgement

We would like to thank Hong Kong Polytechnic University for funding this research through Projects A188 and G-YD31.

5.6 References

1. Postle, R. and Norton, A.H., Mechanics of Complex Fabric Deformation and Drape, in *Science and Technology of Fibres and Related Materials*, L. Rebenfeld, Editor. 1991, John Wiley & Sons: New York. p. 323–340.
2. Kilby, W.F., Planar Stress–Strain Relationships in Woven Fabrics. *Journal of the Textile Institute*, 1963. **54**: p. T9–T27.
3. Shanahan, W.J., Lloyd, D.W. and Hearle, J.W.S., Characterizing the Elastic Behavior of Textile Fabrics in Complex Deformation. *Textile Research Journal*, 1978. **48**(4): p. 495–505.
4. Lloyd, D.W., The Analysis of Complex Fabric Deformations, in *Mechanics of Flexible Fibre Assemblies*, J.W.S. Hearle, J.J. Thwaites, and J. Amirbayat (Editors.) 1980, Sijthoff & Noordhoff, Alphen aan den Rijn: The Netherlands. p. 311–342.
5. Imaoka, H. *et al.*, Analysis of Deformations in Textile Fabric. *SEN-I GAKKAISHI*, 1988. **44**(5): p. 217–228.
6. Imaoka, H. *et al.*, Prediction of Three-dimensional Shapes of Garments from Two-dimensional Paper Patterns. *SEN-I GAKKAISHI*, 1989. **45**(10): p. 420–426.
7. Collier, J.R. *et al.*, Drape Prediction by Means of Finite-element Analysis. *Journal of the Textile Institute*, 1991. **82**(1): p. 96–107.
8. Kang, T.J., Yu, W.R. and Chung, K., Drape Simulation of Woven Fabric Using the Finite-element Method. *Journal of the Textile Institute*, 1995. **86**(4): p. 635–648.
9. Chen, B. and Govindaraj, M., A Physically Based Model of Fabric Drape Using Flexible Shell Theory. *Textile Research Journal*, 1995. **65**(6): p. 324–330.
10. Chen, B. and Govindaraj, M., A Parametric Study of Fabric Drape. *Textile Research Journal*, 1996. **66**(1): p. 17–24.
11. Gan, L. and Ly, N.G., A Study of Fabric Deformation Using Nonlinear Finite Elements. *Textile Research Journal*, 1995. **65**(11): p. 660–668.
12. Eischen, J.W., Deng, S. and Clapp, T.G., Finite-element Modeling and Control of Flexible Fabric Parts. *IEEE, Computer Graphics and Applications*, 1996. **16**(5): p. 71–80.
13. Hu, J.L. and Chen, S.F., Numerical Drape Behavior of Circular Fabric Sheets over Circular Pedestals. *Textile Research Journal*, 2000. **70**(7): p. 593–603.

14. Chen, S.F., Hu, J.L. and Teng, J.G., A Finite-volume Method for Contact Drape Simulation of Woven Fabrics and Garments. *Finite Elements in Analysis and Design*, 2001. **37**: p. 513–531.
15. Terzopoulos, D. *et al.*, Elastically Deformable Models, in *SIGGRAPH*. 1987.
16. Terzopoulos, D. and Fleischer, K., Deformable Models. *The Visual Computer*, 1988. **4**: p. 306–331.
17. Volino, P., Courchesne, M. and Thalmann, N.M., Versatile and Efficient Techniques for Simulating Cloth and Other Deformable Objects, in *SIGGRAPH*. 1995.
18. Baraff, D. and Witkin, A., Large Steps in Cloth Simulation, in *SIGGRAPH*. 1998.
19. Terzopoulos, D. and Fleischer, K., Modeling Inelastic Deformation: Viscoelasticity, Plasticity, Fracture, in *SIGGRAPH*. 1988.
20. Carignan, M. *et al.*, Dressing Animated Synthetic Actors with Complex Deformable Clothes, in *ACM SIGGRAPH*. 1992. New York.
21. Volino, P. *et al.*, An Evolving System for Simulating Clothes on Virtual Actors. *IEEE, Computer Graphics and Applications*, 1996. **16**(5): p. 42–51.
22. Choi, K.J. and Ko, H.S., Stable but Responsible Cloth. *ACM Transactions on Graphics*, 2002. **21**(3): p. 604–611.
23. Kang, Y.M. *et al.*, Fast and Stable Animation of Cloth with an Approximated Implicit Method, in *Computer Graphics International* 2000. Geneva, Switzerland.
24. Provot, X., Deformation Constraints in a Mass–Spring Model to Describe Rigid Cloth Behavior, in *Graphics Interface*, 1995.
25. Volino, P. and Thalmann, N.M., Implementing Fast Cloth Simulation with Collision Response, in *Computer Graphics International*, 2000.
26. Volino, P. and Thalmann, N.M., Collision Response, in *Virtual Clothing: Theory and Practice*. 2000, Springer. p. 145–182.
27. Breen, D.E., A Particle-based Model for Simulating the Draping Behavior of Woven Cloth, in *Computer and Systems Engineering*. 1994, Rensselaer Polytechnic Institute: Troy, New York. p. 62–63.
28. Breen, D.E., House, D.H. and Getto, P.H., A Physically Based Particle Model of Woven Cloth. *The Visual Computer*, 1992. **8**(6): p. 264–277.
29. Breen, D.E., House, D.H. and Wozny, M.J., A Particle-based Model for Simulating the Draping Behavior of Woven Cloth. *Textile Research Journal*, 1994. **64**(11): p. 663–685.
30. Kawabata, S., The Standardization and Analysis of Hand Evaluation, The Textile Machinery Society of Japan, Japan. 1980.
31. Eberhardt, B., Weber, A. and Strasser, W., A Fast, Flexible, Particle-system Model for Cloth Draping. *IEEE, Computer Graphics and Applications*, 1996. **16**(5): p. 52–59.
32. House, D.H. and Breen, D.E., eds. Cloth Modeling and Animation. 2000, A. K. Paters Ltd: Natick, Massachusetts. p. 55–77.
33. House, D.H. and Breen, D.E., Representation of Woven Fabrics, in *Course Notes of SIGGRAPH'98*. 1998.
34. Dias, J.M.S., Gamito, M.N. and Rebordao, J.M., A Discretized Linear Elastic Model for Cloth Buckling and Drape. *Textile Research Journal*, 2000. **70**(4): p. 285–297.

35. Dai, X.Q., Li, Y. and Zhang, X., Simulation of Anisotropic Woven Fabric Deformation with an Improved Particle Model. *Textile Research Journal*, 2002.
36. Dai, X.Q. and Li, Y., Virtual Visualization of Draping, Fitting and Pressure in Apparel Design, in *International Conference of IFFTI 2002*. 2002. Hong Kong, China.
37. Kang, T.J. and Sung, M.K., Development of Three-dimensional Apparel CAD System, Part II: Prediction of Garment Drape Shape. *International Journal of Clothing Science and Technology*, 2000. **12**(1): p. 39–39.
38. Okabe, H. *et al.*, Transformation from Paper Pattern to Spatial Structure of Dress by Computer-simulation of Sewing and Dressing. *SEN-I GAKKAISHI*, 1988. **44**(3): p. 53–60.

6

The human body

A. LUXIMON[2] AND M. ZHANG[1]
[1]The Hong Kong Polytechnic University, China
[2]Milanezy (Excel Last) Co Ltd, China

6.1 Introduction

The study of the human body, or anatomy, is probably as old as the origin of the human itself.[1] Our earliest ancestors must have observed growth, development and motor behavior as well as the surface anatomy for aesthetic and pleasurable purposes.[2] They would have observed diseases together with their symptoms and they would have experimented by using different herbs. As techniques for making accurate observation evolved, knowledge of the human body increased rapidly. As the amount of knowledge increased and in order to communicate effectively, medical practitioners devised specific terms, many of them originated from Greek and Latin, to describe locations, body parts, and functions.[3]

It is impossible to address the complete anatomy and physiology of the human body in this chapter. Detailed anatomy and physiology can be found in medical books, which are widely available.[1,3–7] Instead, this chapter considers some aspects of human body biomechanics that are important for clothing design. These include anatomical landmarks,[8] skeletal and musculoskeletal system,[1] anthropometry,[9] range of motion,[10] and the human skin.[11] In order to have a complete understanding, an overview of the human systems is provided.[1] These topics are important for clothing design and without their knowledge, the beauty and aesthetic of fashion will be lost.

6.2 Definitions and anatomical landmarks

In order to communicate effectively, a set of terms have been defined to describe anatomical positions with precise meanings. Some of these terms are related to imaginary planes as shown in Fig. 6.1. There are three hypothetical reference planes.[12] The sagittal plane, also called the median plane, is a plane dividing the body into two equal right and left halves. The transverse plane, also called the horizontal plane, is a plane that cuts the body

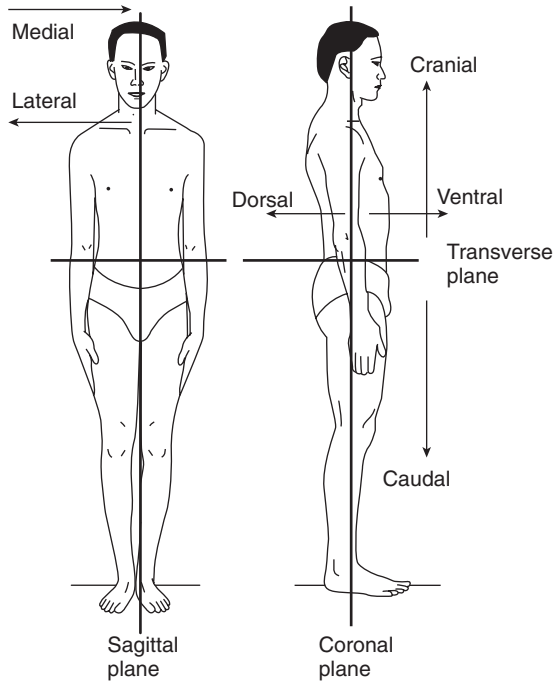

6.1 The planes of reference.

into a 'top' and 'bottom' section as shown in Fig. 6.1. The coronal plane, also called frontal plane, is a plane that divides the body into 'front' and 'back' (Fig. 6.1). Instead of using front, back, top, and bottom, specific terms, such as posterior, inferior, etc., are used to describe relative positions. These are described in Table 6.1.

Figure 6.2 provides the terms used to describe body regions.[8,13] The regions described in Fig. 6.2 are widely used in medical fields whereas the regions described in Fig. 6.3 are rarely used in medical fields but are of immense practical value. They are used by the NASA for anthropometric studies.[12] Knowledge of these terms enables us to understand most text and articles related to anatomy and physiology. Before discussing the skeletal system, some definitions are provided:

- *Cell* This is the basic unit of structure and function in an organism. Some organisms, such as virus and bacteria, are unicellular (one cell) organisms. The cells contains protoplasm (viscous translucent membrane), plasma membrane (cell external boundary), and nucleus (responsible for cell growth, metabolism, and reproduction). In humans, cells are grouped together to form tissues.[14]

Table 6.1 Relative positions

Term	Description
Superior (Cranial)	A body part above another part, or closer to the head.
Inferior (Caudal)	A body part below another body part, or toward the feet.
Anterior (Ventral)	Towards the front.
Posterior (Dorsal)	Towards the back.
Medial	Closer to the Sagittal* plane.
Lateral	Away from the Sagittal* plane.
Proximal	Section of the body part closer to the point of attachment.
Distal	Opposite of Proximal. Section of the body part away from the point of attachment.
Superficial	Situated near the surface.
Deep	Parts that are more internal.
Rostral	Toward the nose.
Bilateral	On both sides of the body or head.
Ipsilateral	On the same side of the body or head.
Contralateral	Opposite of Ipsilateral. On the opposite side of the body or head.

* see Fig. 6.1

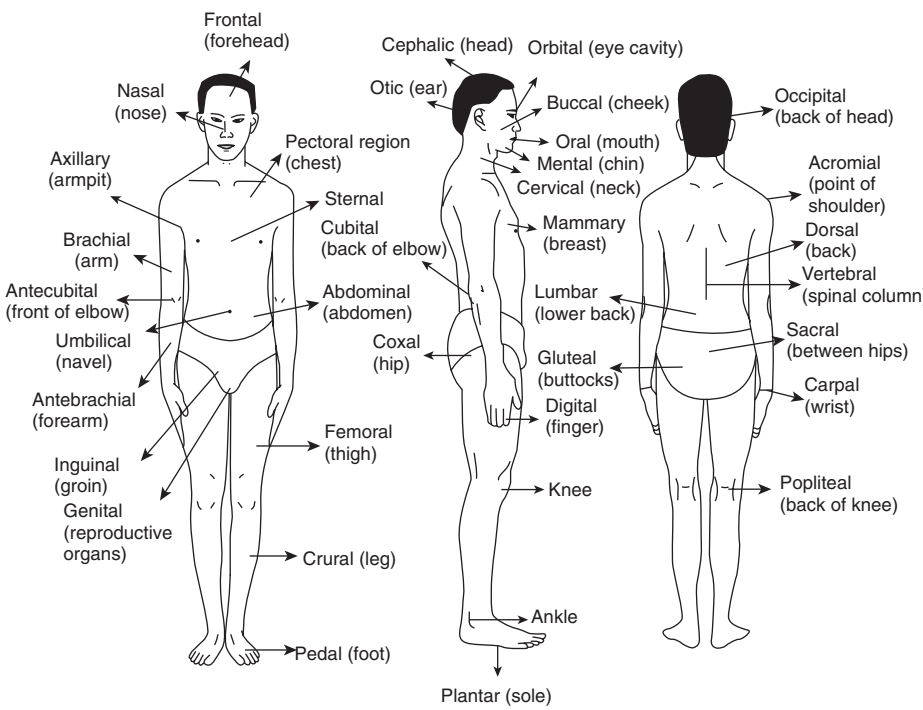

6.2 Body regions.

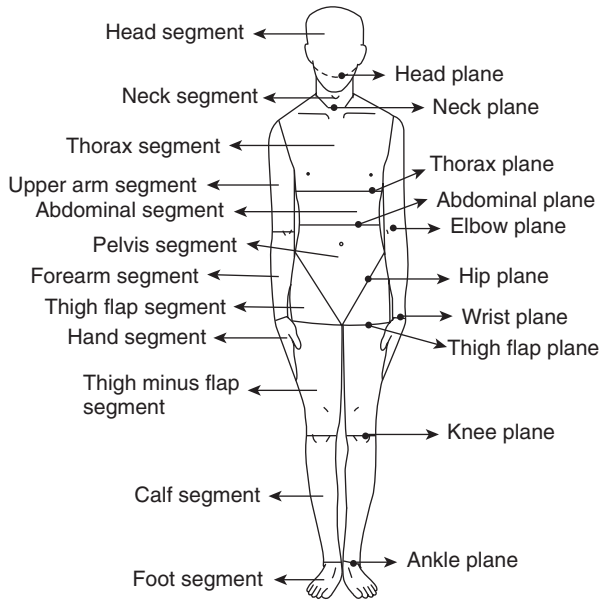

6.3 Body segments and planes of segmentation.

- *Tissue* Tissue is a group of similar cells. They have specialized structure and function. There are four main types of tissues: epithelial, connective, muscle and nervous tissues. Epithelial tissues cover organs, forming a lining. Generally they lack blood vessels. Connective tissue, with a good supply of blood vessels, provides support and protection, serves as a framework, stores fat, produces blood cells, protects against infection, and helps repair tissue damage. The muscle tissues with the help of muscle fibers can contract. This enables movement. Nervous tissues are found in the brain, spinal cord, and peripheral nerves. These tissues are specialized for transmission of nerve impulses.[5,14]
- *Organ* Different kinds of tissue working together in the same place may form an organ such as heart, lungs, eyes, or brain.[5]
- *Bone* Bones consist of bone tissue (connective tissue), blood vessels, bone marrow, and nervous tissue. Nonliving material (mineral salts) in the bone makes it appear inactive. The bones have projections called processes. These projections provide sites for ligament and tendon attachment.[15]
- *Muscle* There are three types of muscle: skeletal, smooth and cardiac. Skeletal muscles, together with the skeletal system, play a vital role in movement. Smooth muscles are somewhat similar to skeletal muscles. They are found in the irises of the eye, and the walls of the blood vessels,

the stomach and the intestines. They are slower to contract and relax compared with skeletal muscles; however, they can maintain contraction longer. Cardiac muscles are found only in the heart.[16]

- *Blood* Blood is used to transport substances throughout the body. It consists of red blood cells, white blood cells, and platelets in a fluid matrix called plasma.[5,14] The red blood cells transport oxygen to the tissues. The five types of white blood cells (neutrophils, eosinophils, basophils, monocytes, and lymphocytes) protect against foreign bodies.[14]
- *Cartilage* Cartilages are connective tissues. They are gel-like structures (look like white plastic) that provide support and protection. They are found at the end of bones in many joints, nose, and ribs.[17] There are three types of cartilage: hyaline, fibrous, and elastic. Hyaline cartilage, also known as articular cartilage, covers bone surfaces at joints. Fibrous cartilage, containing abundant amounts of fibrous material, is strong and rigid. It is used mainly at the intervertebral disks. Elastic cartilage is elastic and resilient. It is used at the auditory canal and external ear.
- *Ligament* Ligament is a dense fibrous connective tissue connecting bones to bones at joints.[17] The ligament can resist tensile forces without considerable elongation.
- *Tendon* Tendons are dense fibrous connective tissues connecting bones to muscles.[17] They are resistant to tension but flexible. They enable bones to move while muscles contract.

6.3 Skeletal system

The skeletal system[1] consists of bony and cartilaginous parts that support and protect the organs. In addition, it is also used for locomotion, together with the muscular system. The skeletal system includes the skull, vertebral column, thoracic cage, upper limbs, and lower limbs. The skull is composed of the cranium and facial bones. The cranium protects the brain, while the facial bones support the teeth and enable us to eat. The vertebral column consists of seven cervical vertebrae, twelve thoracic vertebrae, five lumbar vertebrae, scrum, and coccyx. The cervical vertebrae located at the neck (cervical) region support the head and enable head movement. The first cervical vertebra, the Atlas vertebra, supports the head. Together with the Atlas vertebra, the second vertebra (the Axis), enables head movements. The thoracic vertebrae, larger than the cervical vertebrae, have long transverse process (or projections) on the dorsal side. The two sides of the transverse process provide facets for attachment of rib bones, while the center spinous process is used for muscle attachment. The lumbar vertebrae

are larger, to support the body from above them. The Sacrum is formed of five fused vertebrae and is triangular in shape. The coccyx, composed of four fused vertebrae, is the lowest part of the vertebral column and is usually referred as the tailbone. It provides an attachment for muscles, and also serves as a shock absorber when sitting. The spinal cord, carrying nerve cells from the brain to the body, passes through the vertebral foramen (center hole) of all the vertebrae of the vertebral column except the coccyx.

The thoracic cage comprises the ribs, thoracic vertebrae, sternum, and coastal cartilages. The coastal cartilages connect the ribs to the sternum. The sternum, also referred to as the breast bone, is flat and elongated. It consists of three parts: manubrium, sternum body, and xiphoid process. The ribs form an enclosure to protect the important organs such as the lungs and the heart. Most people have twelve ribs, of which only seven superior ones are attached to the sternum. The next three are attached to the seven ribs via cartilage. Thus, they are indirectly attached to the sternum and are called false ribs. The final two (sometimes three) anterior ones are floating ribs, since they are not attached to the sternum directly or indirectly.

The upper limb (arm and hand) consists of the pectoral girdle, humerus, radius, ulna, and the hand bones. Sometimes the pectoral girdle is grouped in a separate set rather than with the upper limb. The pectoral girdle, also called the shoulder girdle, consists of one pair (left and right side) of clavicles and one pair of scapulae. The clavicles (collar bones) hold the scapula in place and provide attachments for muscles of the upper limb, chest and back. At the medial side, it is attached to the manubrium, while at the lateral side it is connected to the acromion process of the scapula. The scapulae (shoulder blades) are broad triangular bones located at the upper back. The glenoid cavity of the scapula articulates with the head of the humerus. The scapulae provide attachment for the upper limb and chest muscles. The humerus, connected at the proximal side to the scapula at the head, forms the main bone for the upper arm. At the inferior side, the lateral and the medial epicondyle articulates with the radius and ulna forearm bones, respectively. The radius is located at the thumb side of the forearm while the ulna is located toward the small finger side. The hand bones include eight small tarsals that form the wrist, five metatarsals that form the palm of the hand, and 14 phalanges that form the finger. The thumb has only two phalanges, while the other fingers have three phalanges.

The lower limb (leg and foot) consists of the pelvic girdle and the bone forming the thigh, leg, and foot. The pelvic girdle consists of two coxal bones articulated anteriorly to form the pelvis bone. The coxal bones articulate with the sacrum posteriorly. The coxal bones provide attachments for liga-

ments and muscles. The thigh contains the femur bone, the longest bone in the body. The femur articulates at the head with the coxal bone. At the distal end of the femur, the lateral and medial condyles articulate with the tibia bone of the leg. At the distal end, there is also the patella or knee cap that articulates with the femur on its distal anterior surface. The tibia, which is larger than the fibula, is located at the medial side. At the distal end, the tibia form the medial malleolus at the ankle. The long and slender fibula is located in the lateral side of the tibia. The fibula head articulates with the tibia just below the lateral condyle of the tibia. At the distal side, the fibula forms the lateral malleolus at the ankle. The foot consists of seven tarsals (calcaneus, talus, navicular, cuboid, lateral cuneiform, intermediate cuneiform, and medial cuneiform) which form the hind foot. The seven metatarsals of the foot form the mid foot, while the 14 phalanges form the forefoot.

6.4 Musculoskeletal system

Skeletal muscles provide a variety of body movements together with the skeletal system.[4] Each movement depends upon the joint and the degree of freedom at the joint.[18] The joints can be classified, based on function, as synarthrosis (immovable), amphiarthrosis (slightly movable), and diarthrosis (freely movable). There are synarthrosis joints on the skull. Diarthrosis joints are also called synovial joints based on their structure. In a cartilaginous joint, cartilage connects the bones and allows slight movement. Cartilaginous joints can therefore be included with the amphiarthrosis group. The knee and the shoulder are synovial joints, while the joints between vertebrae are cartilaginous joints. The knee can be mechanically modeled as a hinge joint, while the shoulder can be modeled as a ball and socket joint. The cartilaginous joints of the spine (between vertebrae) enable rotation, slight shear, and some compression and extension.

At the synovial joints, in general one end of the muscle is connected to a bone that is movable and other end of the muscle at the other side of the joint to a relatively fixed bone. The immovable end of the muscle is called the origin and the movable end is called the insertion. Muscles can have more than one origin and insertion point. When the muscle contracts (shortens), it pulls the movable bone, thus causing the desired movement. Several muscles work together to generate the desired effect. For a particular movement, one muscle provides the main force and is referred to as the prime mover. Muscles usually work in pairs, so when one muscle contracts the other one relaxes and *vice versa*. The muscle that contracts to generate the prime move is called the agonist or synergist muscle, while the relaxing muscle is called the antagonist. When the antagonist muscle

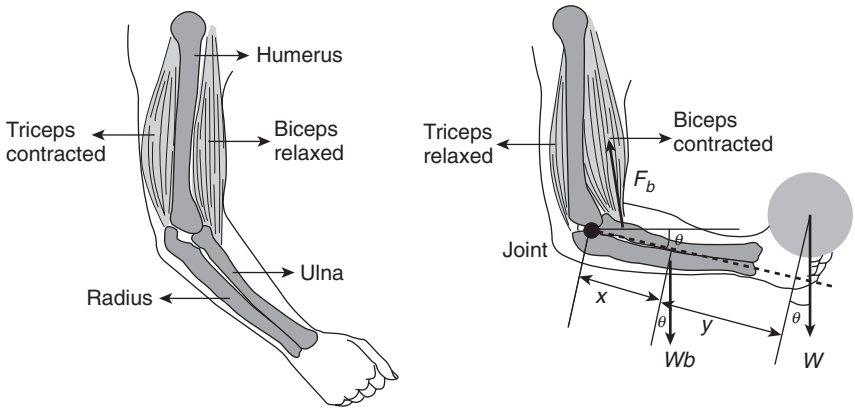

6.4 Simplified musculoskeletal system at the elbow joint.

contracts, motion opposite to the prime movement takes place. Figure 6.4 shows a simplified musculoskeletal system at the elbow joint. The insertion point of the biceps is at the radial tuberosity on the radius bone. The biceps has two origins: coracoid process and tubercle above glenoid cavity of scapula. The insertion point of triceps is at the olecranon process of ulna. The triceps has three origins: tubercle below glenoid cavity, lateral, and medial surfaces of humerus. When the biceps contracts, the triceps relaxes, moving the forearm toward the arm. When the triceps contracts, the biceps relaxes, moving the forearm away from the arm. A simple biomechanical model of the elbow joint can easily be constructed to estimate joint and muscle forces using the distances x (perpendicular distance of center of gravity of forearm from the elbow joint) and y (perpendicular distance of center of gravity of the object from the elbow joint), the angle θ (angle of forearm respective to a given axis system), and the forces W_b (weight of forearm), W (weight of the object lifted), and F_b (force of the bicep muscle).

6.5 Overview of other systems

Several organs can work together in a system. The eleven systems in the human body are the circulatory system, digestive system, endocrine system, immune system, muscular system, lymphatic system, nervous system, reproductive system, respiratory system, skeletal system, and urinary system.[3,5,7,14] The skeletal system has already been discussed sufficiently. It is impossible to describe in detail all the systems in this chapter; however, a brief overview is essential.

The *circulatory system*, the body's transport system, is made up of a group of organs that transport blood throughout the body. The heart pumps

the blood and oxygen-rich blood leaves the left side of the heart and enters the biggest artery, the aorta. The aorta branches into smaller arteries which branch into even smaller vessels called arterioles that travel all over the body. The smallest blood vessels (capillaries), found in body tissue, provide nutrients and oxygen to the cells and take in carbon dioxide, water, and waste. Veins are the opposite of arteries. The capillaries form the venules (small veins) and then veins. The oxygen and nutrient depleted blood goes back to the heart through veins. The veins join together from different branches to form larger veins until they reach the right side of the heart at the vena cava. Blood is pumped from the heart at high pressure, so the arteries have thicker walls than the veins. In addition, veins have valves to assist the transportation of blood back to the heart. These are essential especially when blood has to move 'uphill' from the lower limbs. The oxygen-depleted blood arriving at the right side of the heart is pumped to the lungs, via the pulmonary artery. At the lungs, the blood is oxygenated and arrives to the left side of the heart via the pulmonary vein. The heart beats continuously supplying nutrients and oxygen to all parts of the body.

The *digestive system* is made up of organs that break down macromolecular food particles (protein, carbohydrates, and fats) into simpler molecules (amino acids, glucose, and fatty acids) that can be absorbed by the body. The simpler molecules are 'burned' at the cells to release energy and to facilitate growth and repair. In addition, the digestive system enables the absorption of minerals (calcium, potassium, sodium and others) and vitamins (A, B, C, etc.). After food is chewed in the mouth and swallowed, it goes down the esophagus and enters the stomach. At the stomach, it is broken down by powerful stomach acids. From the stomach, the food travels into the small intestine, where the food is further broken down into nutrients that can enter the blood stream. The excess food that the body does not need or cannot digest is turned into waste and is eliminated from the body via the anus.

The *endocrine system* is a group of glands that produce hormones. Hormones are chemicals that control body functions such as metabolism, growth, and sexual development. The glands (pituitary gland, thyroid gland, parathyroid glands, adrenal glands, thymus gland, pineal body, pancreas, ovaries (in females), and testes (in males)) release hormones directly into the bloodstream, which transports them to organs and tissues throughout the body.

The *immune system* is our body's defense system against infections and diseases. There are three types of response systems in the immune system: the anatomic response, the inflammatory response, and the immune response. The anatomic response physically prevents threatening substances from entering the body. Examples of the anatomic system include the

mucous membranes and the skin. If substances do get by, the inflammatory response goes on the attack. The inflammatory system works by excreting the invaders from the body. Sneezing, running noses, and fever are examples of the inflammatory system at work. When the inflammatory response fails, the immune response goes to work. This is the central part of the immune system and consists of white blood cells, which fight infection by swallowing up antigens. About a quarter of white blood cells, called the lymphocytes, migrate to the lymph nodes, and produce antibodies, which fight disease.

The *muscular system* is made up of tissues that work with the skeletal system to control movement of the body. Some muscles, such as those in the arms and legs, are voluntary, meaning that one decides when to move them. Other muscles, such as the ones in the stomach, heart, intestines and other organs, are involuntary. This means that they are controlled automatically by the nervous system and hormones. The body is made up of three types of muscle tissue: skeletal, smooth and cardiac. Further details may be found in Section 6.4.

The *lymphatic system* is also a defense system for the body. It filters out organisms that cause disease, produces white blood cells, and generates disease-fighting antibodies. It also distributes fluids and nutrients in the body and drains excess fluids and protein so that tissues do not swell. The lymphatic system consists of a network of vessels that help to circulate body fluids. These vessels carry excess fluid away from the spaces between tissues and organs and return it to the bloodstream.

The *nervous system* is made up of the brain, the spinal cord, and nerves. One of the most important systems in the body, the nervous system is the body's control system. It sends, receives, and processes nerve impulses throughout the body. These nerve impulses tell muscles and organs what to do and how to respond to the environment. There are three parts of the nervous system that work together: the central nervous system, the peripheral nervous system, and the autonomic nervous system. The central nervous system consists of the brain and spinal cord. It sends out nerve impulses and analyzes information from the sense organs, which tell the brain about things one sees, hears, smells, tastes and feels. The peripheral nervous system includes the craniospinal nerves that branch off from the brain and the spinal cord. It carries the nerve impulses from the central nervous system to the muscles and glands. The autonomic nervous system regulates involuntary actions, such as heart beat and digestion.

The *reproductive* system allows humans to produce children. Sperm from the male fertilizes the female's egg, or ovum, in the fallopian tube. The fertilized egg travels from the fallopian tube to the uterus, where the fetus develops over a period of nine months.

The *respiratory system* brings air into the body and removes carbon dioxide. It includes the nose, trachea, and lungs. On breathing in, air enters the nose or mouth and goes down a long tube called the trachea. The trachea branches into two bronchial tubes, or primary bronchi, which go to the lungs. The primary bronchi branch off into even smaller bronchial tubes, or bronchioles. The bronchioles end in the alveoli, or air sacs. Oxygen follows this path and passes through the walls of the air sacs and blood vessels before entering the blood stream. At the same time, carbon dioxide passes into the lungs and is exhaled.

The *urinary system* eliminates waste from the body, in the form of urine. The kidneys remove waste from the blood. The waste combines with water to form urine. From the kidneys, urine travels down two thin tubes called ureters to the bladder. When the bladder is full, urine is discharged through the urethra.

6.6 Anthropometry

Anthropometry is a method of assessing the size, proportions, and composition of the human body using simple equipment.[9] It is universally applicable, inexpensive and non-invasive. The anthropometric percentage values are used to compare different populations. Anthropometric measures have been widely used for equipment and workplace design, growth and nutrition evaluation, and for clothing design and sizing.[19–21] Tables 6.2 and 6.3 show anthropometric values for Japanese young males and females collected by Kouchi and Mochimaru.[22] Figure 6.5 shows the location of the measurements. Most of the measurements were taken using anthropometers and tape. In addition, Fig. 6.6 shows the mass and volume of the 12 body segments according to the NASA.[12] This can be used for development of biomechanical models.

6.7 Range of motion

In Section 6.4, the musculoskeletal system was discussed. The amount of movement that occurs at a joint is the range of motion (ROM). Medical practitioners and physiotherapists use ROM to determine abnormality or injury in patients.[10,18] For clothing design, ROM is important for developing items that will be appealing but at the same time do not restrict movement.

6.8 Human skin and temperature regulation

The skin is the largest organ responsible for protecting us against the harsh environment.[11] It is also an element of beauty[2] and racial conflict.[23] Additionally and importantly, it regulates the body's temperature.[24–28] Since

Table 6.2 Anthropometric values for young Japanese males

		Male (N = 109)						
		mean	SD.	Min.	Max.	5th percentile	50th percentile	95th percentile
1	Age	20.5	1.6	19.1	27.1	19.2	19.9	24.7
2	Body mass	59.6	6.9	44.2	82.2	48.2	59.4	68.9
3	Stature	1706.1	53.8	1578.0	1839.0	1619.0	1700.0	1800.4
4	Suprasternal height	1375.7	46.8	1272.0	1504.0	1305.4	1374.0	1460.0
5	Waist height	1030.4	42.0	939.0	1148.0	964.2	1028.0	1110.0
6	Cristal height	995.9	39.1	913.0	1102.0	926.0	999.0	1065.8
7	Iliac spine height, standing	921.6	39.7	821.0	1038.0	860.2	921.0	987.0
8	Trochanterion height	865.0	35.8	788.0	962.0	803.2	865.0	928.2
9	Symphyseal height	851.1	38.5	758.0	959.0	786.4	850.0	914.0
10	Epicondyle height (lateral)	467.3	20.4	418.0	532.0	435.4	467.0	500.4
11	Upper limb length	726.7	29.2	656.0	811.0	683.8	727.0	774.6
12	Forearm length	241.2	11.7	218.0	275.0	223.4	241.0	260.2
13	Upper arm length	307.9	16.4	274.0	353.0	281.0	307.0	337.2
14	Total head height	239.0	7.6	218.0	261.0	225.4	239.0	249.6
15	Head breadth	161.9	5.2	149.0	176.0	154.0	162.0	171.0
16	Head length	189.3	6.3	175.0	206.0	180.0	190.0	200.0
17	Shoulder (biacromial) breadth	396.5	15.5	356.0	440.0	369.6	398.0	418.6
18	Waist breadth	257.1	18.3	213.0	313.0	228.4	258.0	284.2
19	Bicristal breadth	270.4	12.7	240.0	301.0	250.0	272.0	289.6
20	Bicondylar, humerus	64.6	2.8	59.0	72.0	60.4	65.0	69.6
21	Bicondylar, femur	94.6	4.3	84.0	106.0	88.4	94.0	102.0

22	Chest circumference	841.8	44.2	747.0	967.0	777.0	843.0	918.2
23	Waist circumference	730.7	51.9	600.0	884.0	628.6	701.0	780.0
24	Hip circumference	888.6	42.3	799.0	1018.0	814.6	887.0	952.6
25	Upper arm circumference	261.2	19.6	214.0	313.0	230.0	259.0	291.6
26	Upper arm circumference, flexed	273.7	19.0	225.0	330.0	242.0	272.0	305.6
27	Forearm circumference	246.8	11.9	217.0	277.0	229.4	246.0	268.2
28	Thigh circumference	515.1	36.0	441.0	618.0	457.4	515.0	567.4
29	Calf circumference	356.1	23.7	305.0	420.0	318.0	357.0	393.2
30	Foot length	253.2	10.8	226.5	274.0	234.4	254.0	270.3
31	Instep length	182.0	8.1	164.5	201.0	169.5	182.0	194.3
32	Fibular instep length	160.8	7.9	144.5	183.0	148.2	160.0	175.7
33	Ball breadth	99.3	4.4	89.0	108.5	91.9	99.0	106.0
34	Foot breadth	101.6	4.6	90.5	114.0	94.2	101.5	108.5
35	Heel breadth	64.6	3.2	55.0	73.5	60.2	65.0	69.8
36	Foot circumference	250.8	10.2	225.0	269.0	235.0	251.0	266.0
37	Ball angle	78.2	3.1	68.0	86.0	73.2	78.0	83.0
38	Toe I angle	8.7	3.5	–2.0	18.5	2.7	9.0	14.0
39	Toe V angle	11.5	4.8	1.0	23.5	2.2	11.5	19.5
40	Medial malleolus height	82.8	5.1	67.0	98.0	75.0	83.0	91.0
41	Lateral malleolus height	69.7	5.0	57.0	84.0	62.0	69.0	79.0
42	Hand length from crease	180.6	7.2	162.0	198.0	169.4	180.0	190.6
43	Hand length from stylion	189.2	7.8	169.0	212.0	177.8	189.0	202.6
44	Hand breadth	81.8	3.3	74.0	89.0	76.0	82.0	86.6
45	Hand thickness	28.8	1.9	25.0	36.0	26.4	29.0	32.0
46	Subscapular skinfold thickness	11.8	3.6	6.4	27.4	7.6	11.0	18.6
47	Suprailiac skinfold thickness	10.3	5.5	3.6	27.4	4.5	9.0	22.1
48	Triceps skinfold thickness	9.2	3.8	4.2	24.0	5.0	8.2	17.2
49	Calf skinfold thickness	7.5	2.6	3.2	17.8	4.3	7.0	12.2

Table 6.3 Anthropometric values for young Japanese females

		Female (N = 98)						
		mean	SD.	Min.	Max.	5th percentile	50th percentile	95th percentile
1	Age	20.2	1.1	19.2	26.0	19.3	19.9	22.2
2	Body mass	53.1	7.1	37.2	76.4	41.6	52.1	65.0
3	Stature	1583.4	50.6	1440.0	1688.0	1511.0	1578.0	1665.2
4	Suprasternal height	1278.6	44.3	1143.0	1380.0	1216.1	1277.5	1346.3
5	Waist height	991.4	38.7	882.0	1064.0	929.3	992.5	1053.2
6	Cristal height	941.4	39.7	815.0	1022.0	885.6	939.5	1005.0
7	Iliac spine height, standing	848.4	36.0	730.0	919.0	792.4	847.0	908.3
8	Trochanterion height	799.3	35.5	709.0	876.0	740.6	799.0	855.2
9	Symphyseal height	787.1	34.3	685.0	862.0	733.7	787.0	839.4
10	Lateral epicondyle height	428.0	19.1	372.0	479.0	398.7	429.5	459.0
11	Upper limb length	667.4	29.1	605.0	729.0	622.7	668.0	718.2
12	Forearm length	218.1	11.9	185.0	248.0	199.7	218.0	239.2
13	Upper arm length	282.6	14.3	252.0	312.0	256.9	282.0	305.0
14	Total head height	230.7	6.5	215.0	247.0	220.9	232.0	240.2
15	Head breadth	155.8	5.1	144.0	169.0	148.9	156.0	164.0
16	Head length	181.1	6.1	168.0	194.0	171.0	181.0	190.2
17	Shoulder (biacromial) breadth	360.2	16.7	304.0	399.0	331.9	361.0	384.0
18	Waist breadth	237.5	21.1	195.0	348.0	205.0	236.5	268.0
19	Bicristal breadth	276.3	13.6	246.0	323.0	256.9	275.0	300.0
20	Bicondylar, humerus	56.9	3.0	50.0	63.0	52.0	57.0	62.0
21	Bicondylar, femur	89.3	5.1	80.0	101.0	81.9	89.0	97.2
22	Chest circumference	828.3	61.0	678.0	1075.0	735.8	825.0	927.9

23	Waist circumference	657.1	57.7	543.0	937.0	581.5	651.5	744.1
24	Hip circumference	913.5	49.9	777.0	1053.0	834.3	915.0	986.0
25	Upper arm circumference	252.3	24.7	203.0	343.0	215.4	250.0	293.3
26	Upper arm circumference, flexed	257.5	23.6	213.0	338.0	221.9	255.0	297.2
27	Forearm circumference	227.7	13.3	200.0	266.0	210.0	227.0	250.8
28	Thigh circumference	540.9	38.7	458.0	636.0	477.9	544.0	609.1
29	Calf circumference	349.8	24.9	305.0	413.0	314.7	347.0	389.9
30	Foot length	233.3	10.1	209.5	257.0	218.0	233.3	247.2
31	Instep length	168.2	7.9	151.5	187.0	154.9	168.8	180.5
32	Fibular instep length	148.1	7.7	132.0	167.0	137.4	148.3	162.2
33	Ball breadth	91.1	4.0	81.5	103.0	84.9	91.5	97.5
34	Foot breadth	93.2	4.1	85.0	106.0	86.9	93.5	100.1
35	Heel breadth	60.3	3.1	54.0	68.5	56.0	60.0	65.6
36	Foot circumference	231.2	9.3	210.0	256.0	217.0	231.0	245.0
37	Ball angle	77.8	2.5	72.0	84.0	73.4	78.0	81.6
38	Toe I angle	10.9	4.5	1.5	26.0	3.9	11.0	18.0
39	Toe V angle	8.5	5.2	−6.0	21.5	−1.6	9.8	14.0
40	Medial malleolus height	75.5	4.5	66.0	86.0	69.0	76.0	83.3
41	Lateral malleolus height	62.8	4.2	55.0	74.0	57.0	62.5	70.0
42	Hand length from crease	167.3	7.7	146.0	186.0	155.0	167.5	178.0
43	Hand length from stylion	176.6	8.3	154.0	194.0	164.7	177.0	189.0
44	Hand breadth	73.6	3.0	66.0	81.0	69.0	74.0	79.2
45	Hand thickness	25.7	1.4	23.0	29.0	23.9	26.0	28.0
46	Subscapular skinfold thickness	19.8	6.3	8.0	37.8	10.7	18.8	31.5
47	Suprailiac skinfold thickness	24.8	7.5	11.0	38.4	13.0	25.4	37.2
48	Triceps skinfold thickness	18.2	5.2	7.2	34.4	10.3	17.8	26.2
49	Calf skinfold thickness	15.3	4.6	5.8	30.0	8.4	15.2	22.3

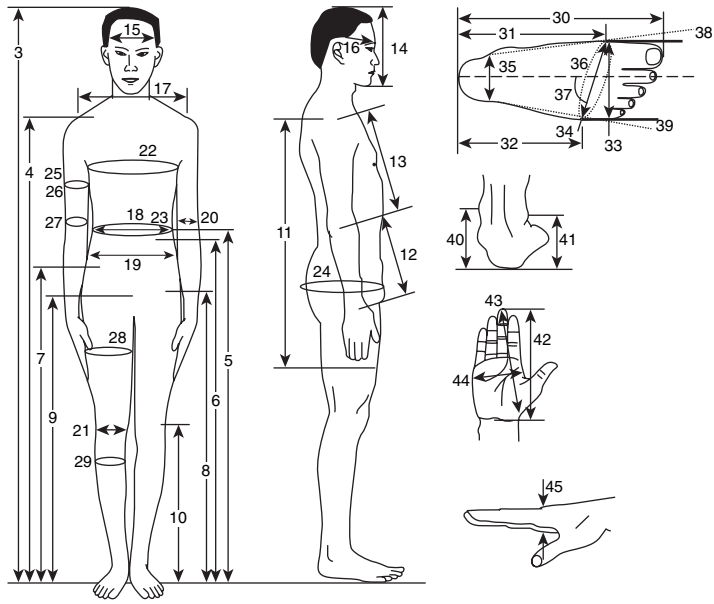

6.5 Anthropometric measures.

Segment	Mass (g)			Volume (cm^3)		
	5th percentile	50th percentile	95th percentile	5th percentile	50th percentile	95th percentile
1 Head	4280	4560	4560	4260	4440	4550
2 Neck	860	1140	1140	930	1100	1270
3 Thorax	20520	26220	31720	20420	26110	31760
4 Abdomen	2000	2570	2850	2030	2500	2960
5 Pelvis	9410	12260	15110	9420	12300	15150
6 Upper arm	1710	2000	2570	1600	2500	2500
7 Forearm	1140	1430	1710	1180	1450	1720
8 Hand	570	570	570	460	530	610
9 Hip flap	2850	3710	4280	2890	3640	4380
10 Thigh	5420	6840	7980	5480	6700	7920
11 Calf	3420	3990	4850	3320	4040	4760
12 Foot	860	1140	1140	840	1010	1180

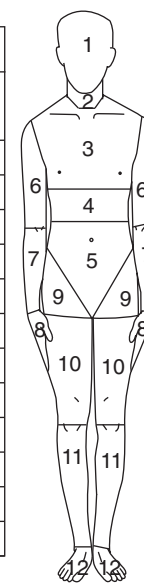

6.6 Mass and volume for different segments.

clothing can influence the temperature of the body, it is essential to know the skin and its properties. The skin has three layers: epidermis, dermis and subcutaneous layer.[11]

The *epidermis* (outer layer), also called cuticle or scarf skin, is non-vascular (does not have blood vessels), and consists of stratified epithelium. However, the deepest epidermal layer (stratum basale), close to dermis, is nourished by blood vessels. The more superficial layers of cells, called the stratum corneum, may be regarded separately from a deeper stratum (stratum mucosum). The epidermis varies in thickness. For example, in the palms of the hands and soles of the feet, it is thick, hard, and horny in texture. Moving from the deep to the outer layer of the epidermis, the nutrient decreases. At the surface, the cells are dead and provide protection against mechanical injury as they can be rubbed away. The epidermis provides protection against water loss, chemicals, and injury. Specialized cells (melanocytes) in the epidermis produce melanin, a dark pigment that absorbs the sun's ultraviolet rays. The amount of melanin in the skin is responsible for the skin color. More melanin causes darker skin. The amount of melanin depends upon genetics, and environmental and physiological factors.

The epidermis is non-vascular whereas the *dermis*, just below the epidermis, is well supplied with blood vessels. The blood vessels provide nutrients to all the skin cells and at the same time are responsible for temperature regulation. The dermis also has nerve ending and specialized nerve cells responsible for detecting mechanical, temperature, pressure, and vibration effects. In hairy skin, the 'root' of the hair (hair follicle) is situated in the dermal layer. The hair inclination can be changed using the arrector pili muscle. The eccrine sweat gland produces sweat which travels along the sweat gland duct and emerges at the pore on the epidermal surface. The sebaceous gland on the other hand secrets an oily liquid (sebum) through small ducts into the hair follicles. This oily liquid keeps the hair and skin soft.

The *subcutaneous layer* consists of loose connective and adipose tissue. There is no sharp boundary between dermis and the subcutaneous layer and, in many cases, the subcutaneous layer is considered part of the dermis. The adipose tissue stores fat and is used for insulation and energy storage.

As previously mentioned, the skin is used for temperature regulation[28] and clothing has much influence in the skin's function.[29] Being warm blooded, the temperature of human deep body parts is kept at 37 °C. Only slight changes of this disrupt the normal body functions, so when the body temperature changes, prompt action is taken. The body can lose heat by three mechanisms: conduction, convection and radiation. When the temperature of the body increases, nerve impulses from the brain (in the

hypothalamus region) cause the blood vessels to dilate.[28] This results in more blood flowing in the dermis. Heat is lost from the skin surface through radiation (more heat is lost from darker skin). At the same time, nerve signals stimulate the eccrine gland to produce sweat. When the sweat evaporates, the skin is cooled further (by convection). In a windy environment, we feel cooler; however, high humidity hinders heat evaporation. Heat is also lost via conduction if the skin is in direct contact with a colder material, especially a heat conducting material. However, when the temperature of the body decreases, nerve signal causes the blood vessels to contract. This decreases blood flow and thus heat loss through the skin is reduced. The sweat glands are inactive and the hair can be erect to create an insulation layer of air on top of the skin. Further reduction in temperature causes shivering, as nerve signals causes the contraction of muscles to produce heat. Thermal regulation is very important for clothing design.[25,26,29]

6.9 Conclusion

Since clothes are designed for humans, it is essential to know the anatomy and physiology of the human body. Only then will we be able to merge the knowledge of clothing mechanics with those of human biomechanics in order to predict the effect of clothing on the human body. This chapter has provided a basic understanding of the human body. First, some terms were defined to enable the user to better understand the human body. Then, the skeletal and musculoskeletal systems were discussed, since it forms the main system for movement and support. Anthropometry and range of motion, together with an understanding of the musculoskeletal system provide the fundamental knowledge for clothing sizing, biomechanical analysis, and fashion design. In addition, the human skin was discussed. The skin not only protects the body but also regulates the body's temperature. Since clothing can influence the skin's function, it is essential to understand the anatomy and physiology of the skin. Sensors in the skin influence the perception of comfort and fit and, as a result, knowledge of the skin enables the design of comfortable clothing for any temperature. In order to make the study of the body complete, an overview of all the human systems (circulatory, digestive, endocrine, immune, lymphatic, muscular, nervous, reproductive, respiratory, skeletal, and urinary) have been provided.

6.10 References

1. Agur, A. M. R. and Grant, J. C. B. (2005). *Grant's Atlas of Anatomy*. Philadelphia: Lippincott Williams & Wilkins.

2. Constance, D. (1993). *An Introduction to Drawing the Nude: Anatomy, Proportion, Balance, Movement, Light, Composition*. London: Apple Press.
3. Gray, H., Williams, P. L. and Bannister, L. H. (1999). *Gray's Anatomy: The Anatomical Basis of Medicine and Surgery*. New York: Churchill Livingstone.
4. Palastanga, N., Field, D. and Soames, R. (1998). *Anatomy and Human Movement: Structure and Function*. Oxford: Butterworth-Heinemann.
5. Sheir, D., Butler, J. and Lewis, R. (1998). *Essentials of Human Anatomy and Physiology*. New York: McGraw Hill.
6. Mader, S. S. and Galliart, P. (2005). *Understanding Human Anatomy and Physiology*. New York: McGraw-Hill Higher Education.
7. Saladin, K. S. (2005). *Human Anatomy*. New York: McGraw-Hill.
8. Tixa, S. (1999). *Atlas of Palpatory Anatomy of the Lower Extremities: A Manual Inspection of the Surface*. New York: McGraw-Hill, Health Professions Division.
9. Pheasant, S. (1994). *Bodyspace.* London: Taylor and Francis.
10. Soames, R. (2003). *Joint Motion: Clinical Measurement and Evaluation*. Edinburgh: Churchill Livingstone.
11. Forslind, B., Lindberg, M. and Norlen, L. (2004). *Skin, Hair, and Nails: Structure and Function*. New York: M. Dekker.
12. NASA (1995). Man-systems integration standards (revision b). USA, NASA Johnson Space Center: (http://msis.jsc.nasa.gov/).
13. Field, D. (2001). *Anatomy: Palpation and Surface Markings*. Oxford: Butterworth Heinemann.
14. Springhouse (2001). *Anatomy & Physiology Made Incredibly Easy!* Pennsylvania: Springhouse Corporation.
15. Behiri, J. and Vashishth, D. (2000). Biomechanics of bone. *Clinical Biomechanics*. Z. Dvir (ed). New York: Churchill Livingstone: 65–82.
16. Dvir, Z. (2000). Biomechanics of muscle. *Clinical Biomechanics*. Z. Dvir (ed). New York: Churchill Livingstone: 83–102.
17. Bader, D. L. and Bouten, C. (2000). Biomechanics of soft tissue. *Clinical Biomechanics*. Z. Dvir (ed). New York: Churchill Livingstone: 35–64.
18. An, K.-N., Chao, E. Y. S. and Kaufman, K. R. (1997). Analysis of muscle and joint loads. *Basic Orthopaedic Biomechanics*. V. C. Mow and W. C. Hayes (eds). Philadelphia: Lippincott-Raven: 1–36.
19. Laing, R. M., Holland, E. J., Wilson, C. A. and Niven, B. E. (1999). Development of sizing systems for protective clothing for the adult male. *Ergonomics*, **42**, (10): 1249–1257.
20. Meunier, P. and Yin, S. (2000). Performance of a 2D image-based anthropometric measurement and clothing sizing system. *Applied Ergonomics*, **31**, (5): 445–451.
21. Luximon, A. (2001). Foot shape evaluation for footwear fitting. *Industrial Engineering and Engineering Management*. Hong Kong: Hong Kong University of Science and Technology.
22. Kouchi, M. and Mochimaru, M. (2002). *Japanese body dimensions data 1997–1998.* Tokyo, Japan: Digital Human Research Center, National Institute of Advanced Industrial Science and Technology.
23. Lappbe, M. (1996). *The Body's Edge: Our Cultural Obsession with Skin*. New York: H. Holt.

24. Kim, H. E., Tokura, H., Nagashima, R. H. S. and Nishizawa, K. (1995). Do cooled women select soft or hard clothing? *Journal of Thermal Biology*, **20**, (4): 327–332.
25. Kraning, K. K. and Gonzalez, R. R. (1997). A mechanistic computer simulation of human work in heat that accounts for physical and physiological effects of clothing, aerobic fitness, and progressive dehydration. *Journal of Thermal Biology*, **22**, (4–5): 331–342.
26. Li, X. and Tokura, H. (1997). Lower critical temperature under the influences of seasonal cold acclimatization due to the two types of clothing. *Journal of Thermal Biology*, **22**, (4–5): 357–363.
27. Noakes, T. D. (2000). Exercise and the cold. *Ergonomics*, **43**, (10): 1461–1479.
28. Clancy, J. and McVicar, A. J. (2002). *Physiology & Anatomy: A Homeostatic Approach*. London: Arnold.
29. Malcolm, S., Armstrong, R., Michaliades, M. and Green, R. (2000). A thermal assessment of army wet weather jackets. *International Journal of Industrial Ergonomics*, **26**, (3): 417–424.

7

Mechanics of the human skin and underlying soft tissues

J.T. CHEUNG AND M. ZHANG
The Hong Kong Polytechnic University, China

7.1 Introduction

Tissues of the human body are often grouped into hard tissues and soft tissues. The hard tissues, i.e. bone and tooth, have been quantitatively characterized at either macro- or micro-levels in many studies. Their mechanical behaviors and properties can be found in many references.[1] Soft tissues refer to a large family of tissues, such as connective tissues, muscle and internal organs. Connective tissues, such as cartilage, ligament, tendon and skin, perform mainly a mechanical function. Their specific functional roles determine the differences in mechanical properties as a result of their diverse combinations of composition and micro-structure.

The human skin directly interacts with external environments, especially with clothes or garments. An understanding of the biomechanical properties of skin and its underlying tissues has considerable impact in the textile and clothing field. This chapter will focus on the biomechanical and structural characteristics of the human skin and underlying tissues. The mechanical behaviors of human skin and underlying tissues, such as its inhomogeneous, anisotropic, nonlinear and viscoelastic properties, and the mathematical models for representing the skin material properties, will be discussed.

7.2 Mechanical behavior of human skin

Soft tissues consist of a network of intertwining fibers with ground substance (matrix of connective tissue) immersed in fluid. The extracellular matrix of fibers contributes mainly to the mechanical properties, which may vary with species, age, hydration, obesity and biological difference between individuals. For the same individual, the properties vary with site and orientation and may be altered by irradiation, drugs, and chemicals.

The human skin possesses complex mechanical behaviors because of its multi-component material constituents, namely collagen fiber, elastin fiber

and ground substance with fluid. It exhibits non-homogeneous, anisotropic, nonlinear, and time-dependent viscoelastic properties. Collagen is a main structural component of connective tissues and accounts for about 70–80% of the dry weight of the skin, depending on age, gender and location.[2] Collagen fibers form a three-dimensional, disordered network of wavy coiled structures, with some preferential orientation. The collagen fibers near the epidermis are finer and randomly oriented, while at the mid zone they are coarser and densely packed.[3] In the deep zone, they are coarse again but are loosely packed. Collagen fibers have high tensile strength, up to 350 MPa, and are stiff with a Young's modulus of approximately 1 GPa.[3]

Elastin accounts for only about 1–2% of the dry weight of skin but is important for the maintenance of skin elasticity and resilience.[2] The elastin fibers are thought to be the first to be stretched when the tissue is strained;[3] they dominate the skin response at very low strain levels when the collagen fibers are still buckled. Elastin fibers appear as fine fibers that intertwine around the thicker collagen fibers in the deep layers of the dermis, but are rather straight close to the epidermis.[3] They are coarser in the dermis layer than close to the epidermis. Elastin is considerably less stiff than collagen and can be reversibly stretched to more than 100%.

The ground substance accounts for about 70–90% of the skin volume.[2] It is gelatinous and imparts viscoelastic behavior. The fluid-like ground substance exudes from the interfiber space while the fibers become reoriented and densely packed upon stretching.[3] This flow of ground substance is associated with the viscosity of the skin, governing the toe region of the nonlinear portion of the stress–strain curve, in which the collagen fibers are not yet fully aligned and stretched. The ground substance shows significant effects on compression, due to the water affinity of the matrix of glycosaminoglycans.[3]

7.2.1 Subject dependent mechanical behavior

Biological variability often dominates the results of mechanical testing. The mechanical properties vary with age, gender, activity levels and healthy conditions.

7.2.2 Site dependent (inhomogeneous) mechanical behavior

The mechanical properties of soft tissue are site-dependent or inhomogeneous. Because the functions of different locations may vary, the skin tissue exhibits inhomogeneous responses to mechanical loading.

7.2.3 Anisotropic mechanical behavior

Skin is an anisotropic material and its characteristics can be described by the directional pattern of pre-stress lines or the so-called Langer's lines (Fig. 7.1). These are related to the visible crease and wrinkle lines of the skin, corresponding to the directions of preferred disposition of collagen fibers.[4] The elastin and collagen fibers along Langer's lines are more stretched than those across the line, so that the extensibility of skin is lower in the directions of these lines and its stiffness is higher in these directions.

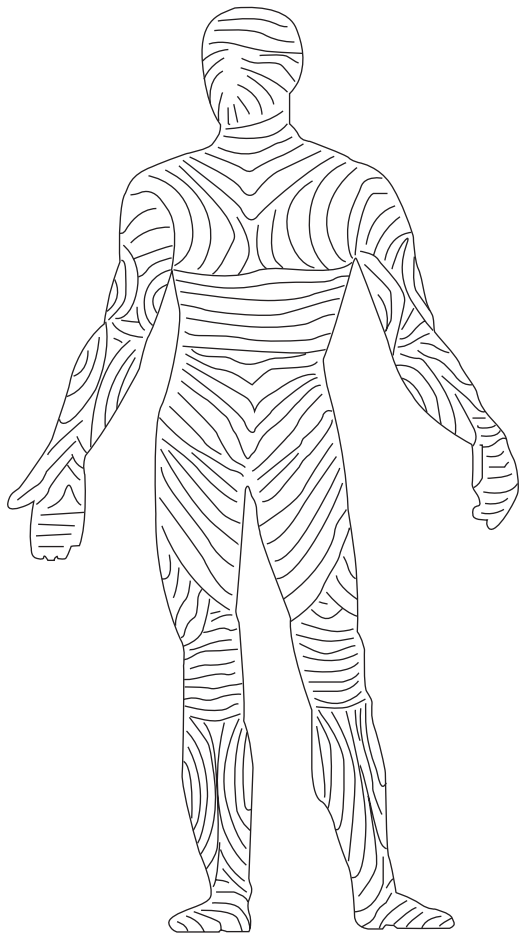

7.1 Langer's lines.

7.2.4 Nonlinear mechanical behavior

Although individual collagen and elastin fibers can be approximated as linearly elastic, non-uniformity of these structures results in nonlinear stress–strain relationships of the skin tissue. This nonlinearity is the result of gradual straightening of the collagen fibers. Figure 7.2 describes a typical stress–strain curve of the skin under tension. At range OA, with very low strains in the skin, the elastin fibers are primarily stretched and the collagen fibers are still coiled, resulting in a very low stiffness and an approximately linear stress–strain relationship. With increasing strains to range AB, a gradual straightening of the originally buckled collagen fibers contributes to the increasing stiffness of the skin tissue. The range OB is often called the toe region. At higher strains to range BC, the collagen fibers are all straightened and the stress–strain relationship becomes linear. Beyond the linear region, skin fibers begin to partially break, until complete tissue rupture occurs. As the skin response exhibits significant nonlinearity, its mechanical behavior depends highly on its state of tension.

7.2.5 Plastic behavior

If the magnitude of deformations is small enough, skin can be reversibly stretched. However, when it is stretched frequently or to a relatively large strain for a long period, permanent deformation occurs, which appears as permanent wrinkles or sutured wounds. The residual deformation after the

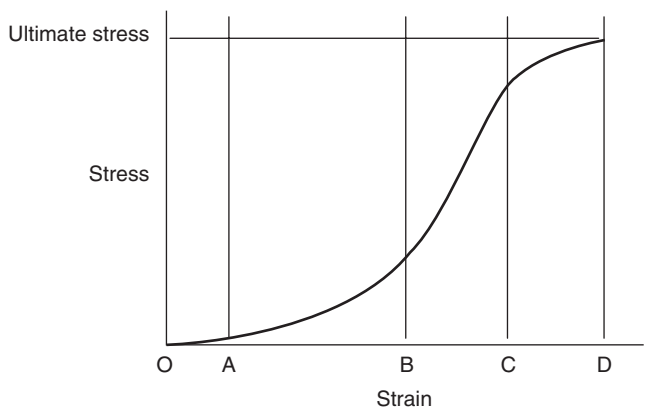

7.2 A typical stress–strain curve of skin tissue under uniaxial tension. From the toe region (O to B), the load increases linearly under initial tension and exponentially with increasing elongation. From the linear region (B to C), the relationship is approximately linear. Going into the plastic region (C to D), the relationship is nonlinear and the tissue will rupture after it has reached its ultimate stress (D).

release of the external loading corresponds to the plasticity of the skin tissue.

7.2.6 Viscoelastic behavior

Viscoelasticity describes time-dependent mechanical properties. Soft tissues consist of both solid and fluid, and behave as viscoelastic material. The mechanical properties are strain-rate-dependent. With increasing strain rate, the material becomes stiffer and stronger. It is necessary to consider and specify the strain rate or load rate when conducting tests and reporting the results. Skin tissues show stress relaxation under constant strain and creep under constant stress. When a tissue is stretched to a certain strain level and kept constant, the stress gradually decreases with time (Fig. 7.3a). This phenomenon is called stress relaxation. Alternatively, when the tissue is stretched to a certain stress level and then kept constant, its strain increases with time (Fig. 7.3b). This phenomenon is called creep. Soft tissues also exhibit considerable hysteresis under a cyclic load, i.e. the stress–strain curve shows two distinct paths during the loading and unloading cycle (Fig. 7.3c). Because of its viscoelastic nature, the stress response at any instant of time depends not only on the tissue strain at that time, but also on the history of the deformation.[4]

7.2.7 Preconditioning

When loading and unloading cycles are applied to the skin tissue successively up to the same stress level, the stress–strain curve is gradually shifted to the right (Fig. 7.3d). After a number of subsequent cycles, the mechanical response becomes reproducible from one cycle to the next. This phenomenon is called preconditioning, a steady state being reached. Preconditioning of the tissues prior to experimentation is important in order to obtain generalized, steady-state response of the materials. Recovery of preconditioning with both initial configuration and initial response will occur provided the specimen has not been damaged or undergone plastic deformation.

7.2.8 Compressibility

The degree of compressibility of skin is determined by the extent of its volume reduction under external pressure. Skin is difficult to compress because it contains a high proportion of chemically-bound water molecules with little free fluid inside. The change in skin tissue volume is extremely small for large changes in pressure; therefore, skin is often considered as incompressible.[4]

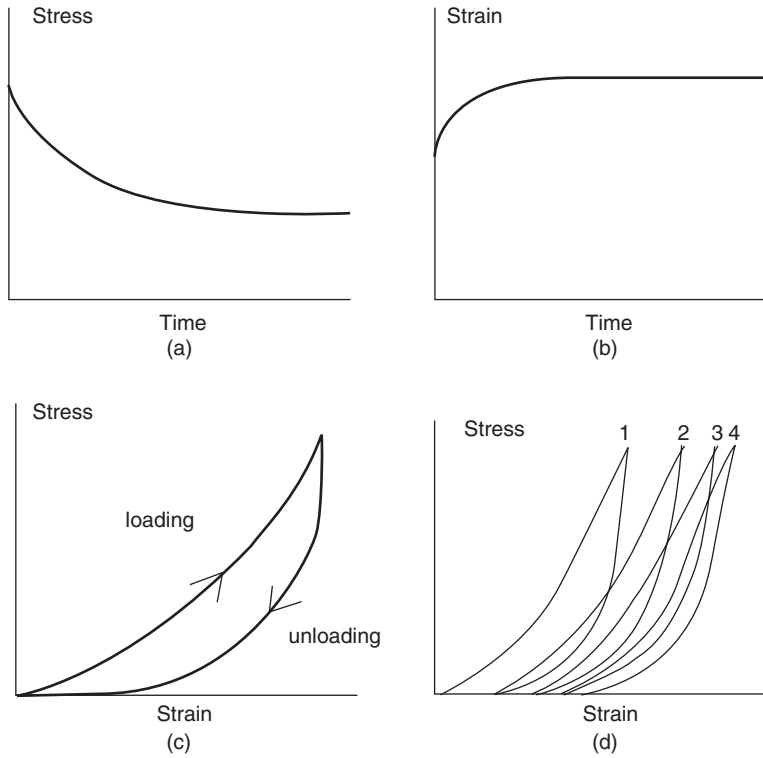

7.3 Typical stress–strain curves characterizing (a) stress relaxation, (b) creep, (c) hysteresis and (d) preconditioning of skin tissue.

7.3 Models of mechanical properties for soft tissues

A linear elastic model is often used for the description of skin mechanical properties. Young's modulus, shear modulus and Poisson's ratio are parameters to specify linear elastic properties. However, soft tissues behave in a more complicated way, such as highly nonlinear and time-dependent. Many more sophisticated models have been developed.

7.3.1 Strain–energy function of nonlinearity

One way to represent the nonlinear stress–strain relationship is the strain energy function method. Let W be the strain energy per unit mass of the tissue, and ρ_0 be the density in the unstressed state. Then $\rho_0 W$ is the strain energy per unit volume of the tissue in the unstressed state. The strain energy function W can be expressed in terms of nine strain components E_{ij} in symmetric forms.[5] The stress components S_{ij}, defined for a unit mass of tissue, can be obtained from the partial derivatives of $\rho_0 W$ with respect to E_{ij}:

$$S_{ij} = \partial\rho_0 W/\partial E_{ij} \quad (i,j = 1,2,3). \qquad [7.1]$$

The general form of the strain energy function W for a material has been given in terms of strain invariants and the extension ratios of the strain tensor as a polynomial or an exponential function.[4]

The commonly used Mooney–Rivlin model has a polynomial strain energy function of the form:

$$U = C_{10}\left(\overline{I}_1 - 3\right) + C_{01}\left(\overline{I}_2 - 3\right) + \frac{1}{D_1}(J_{el} - 1)^2 \qquad [7.2]$$

where U is the strain energy potential,
$\overline{I}_1$, $\overline{I}_2$ the first and second deviatoric strain invariants,
J_{el} the elastic volume ratio, and
C_{10}, C_{01} and D_1 the material parameters.
If D_1 is zero, the material is fully incompressible.

7.3.2 Models of linear viscoelasticity

Models developed to describe a viscoelastic material are a combination of a spring and a dashpot. The spring represents the elastic portion of the material, whereas the dashpot represents the viscous portion. Combinations of spring and dashpot can be used to represent different linear viscoelastic materials. The three most popular models of viscoelasticity are the Maxwell model, a spring in series with a dashpot (Fig. 7.4), the Voigt model, a spring and a dashpot in parallel, and the Kelvin model or the so-called standard linear solid, which is a combination of a spring in parallel with a Maxwell body.

A linear spring instantaneously produces a deformation proportional to the load $\sigma = E\varepsilon$, while a dashpot produces a velocity proportional to the load at any instant $\sigma = \eta\dot{\varepsilon}$. Spring coefficient E and viscous coefficient η are constants. The constitutive relations of the above viscoelastic models can be accordingly derived as follows:[6]

- For the Maxwell model having a series spring-dashpot arrangement, the associated stresses for both spring and dashpot are equal, while the associated strain is the sum of the strains in the two elements; then the constitutive equation is

$$\frac{\sigma}{\eta} + \frac{\dot{\sigma}}{E} = \dot{\varepsilon}. \qquad [7.3]$$

- In a similar manner, the constitutive relation for the Voigt model can be readily shown as

$$\sigma = E\varepsilon + \eta\dot{\varepsilon}. \qquad [7.4]$$

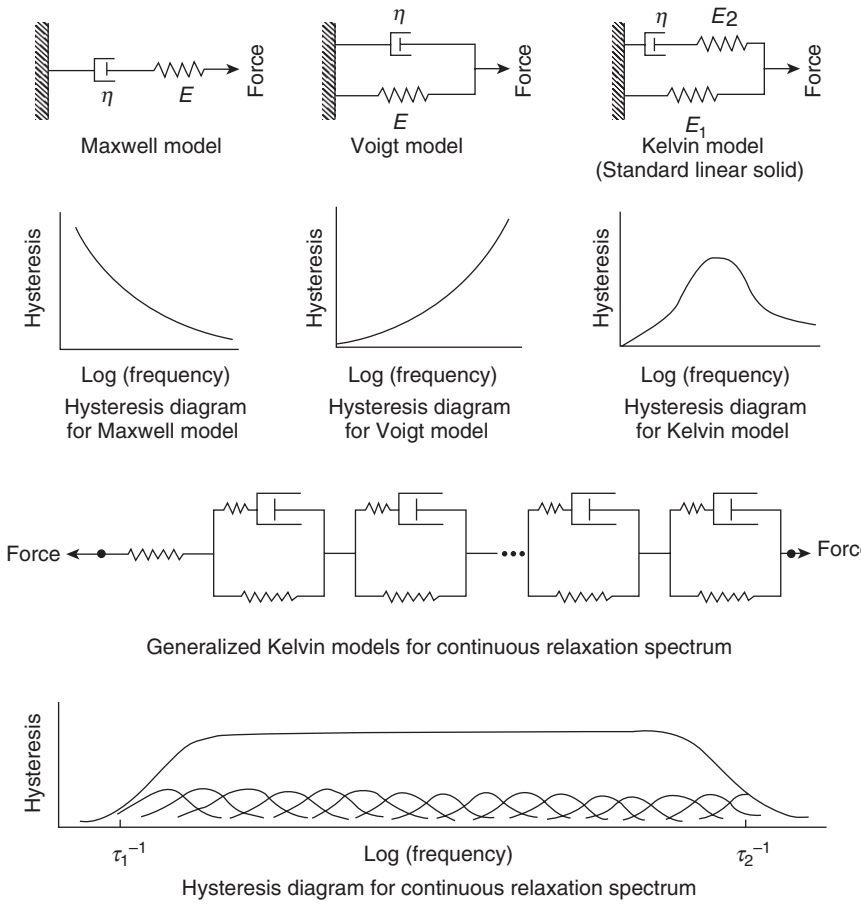

7.4 Viscoelastic models and associated hysteresis diagrams for discrete and continuous relaxation spectra (adapted from Fung, 1993, in Mechanical Properties of Living Tissues, 2nd edition, Springer-Verlag, New York).

- The constitutive relation for the Kelvin model or standard linear solid is

$$\left(1+\frac{E_1}{E_2}\right)\sigma+\left(\frac{\eta}{E_2}\right)\dot{\sigma}=E_1\varepsilon+\eta\dot{\varepsilon}. \qquad [7.5]$$

The above three models have been widely used to describe the viscoelasticity of materials. However, there are limitations for accurate representation of soft tissues.[4] For example, when a material represented by any one of these models is subjected to a cyclic load, the hysteresis will not be

insensitive to strain rate. As loading frequency increases, under the magnitude of load the damping effect exhibited by the dashpot in the Maxwell body decreases with frequency. However, the damping effect of the dashpot in the Voigt body increases with loading frequency. For the standard linear solid, there exists a characteristic loading frequency at which the damping is at a maximum. Therefore, none of these models can represent the nearly constant damping property of soft tissue, which is independent of loading frequency.[7] A model suitable for soft tissues should have more springs and dashpots. Fung[5] described the continuous relaxation spectrum of soft tissues by a generalized Kelvin model in which a large number of Kelvin units are combined in series (Fig. 7.4). The corresponding hysteresis diagram shows an infinite number of bell-shaped curves, which add up to a continuous curve of nearly constant height over a very wide range of frequencies (Fig. 7.4).

Experimental determination of linear viscoelastic properties

For the linear viscoelastic theory, there are different means of expressing the mechanical properties in which the stress–strain properties are given by relaxation and creep functions. Standard testing procedures, such as the relaxation and creep tests, provide the most direct means of obtaining the mechanical properties involved in the linear theory of viscoelasticity.[8] Such tests are usually applied to uniaxial deformation conditions whereby the appropriate constitutive relations are given by

$$\sigma(t) = \int_{-\infty}^{t} E(t-\tau)\frac{\partial \varepsilon}{\partial \tau}\,\mathrm{d}\tau \qquad [7.6]$$

$$\varepsilon(t) = \int_{-\infty}^{t} L(t-\tau)\frac{\partial \sigma(\tau)}{\partial \tau}\,\mathrm{d}\tau \qquad [7.7]$$

where $E(t)$ and $L(t)$ are the respective uniaxial relaxation function and creep function.[8]

In a stress relaxation test, the material specimen is subjected to a strain suddenly applied at time $t = 0$ and maintained constant thereafter. The measured load output can be converted into either true or nominal stress values. If $\sigma(t)$ is measured throughout the experiment, the stress-relaxation function, $E(t)$, is readily determined. In the creep test, the material specimen is subjected to a load which is applied as quickly as possible and is varied in such a manner as to keep the stress, σ_0, at a constant value after load application. With the resulting deformation or strain $\varepsilon(t)$, in the specimen being measured as a function of time elapsed since the load was first applied, the creep function, $L(t)$ can be determined.

7.3.3 Quasi-linear viscoelasticity

The theory of linear viscoelasticity is valid in the case of small deformation. For finite deformations, the nonlinear stress–strain characteristics of soft tissue have to be taken into account. The features of relaxation, creep and hysteresis can be condensed into a mathematical formulation called quasi-linear viscoelasticity theory.[7] In this theory, the instantaneous stress response to strain is nonlinear. The stress at any given time is related to the entire past history of the elastic stress with a linear relationship. The present stress is obtained by multiplying the past elastic stress increment with a relaxation function and integrating the product convolutionally from the beginning of the time to the present. The relaxation function has a continuous relaxation spectrum.

Considering a cylindrical specimen subjected to tensile load, if a step increase in elongation (from $\lambda = 1$ to λ) is imposed on the specimen, the stress developed will be a function of time as well as of the stretch λ. The history of the stress response, called the relaxation function, $K(\lambda,t)$, is assumed to be of the form

$$K(\lambda,t) = G(t) \quad T^{(e)}(\lambda), \quad G(0) = 1, \qquad [7.8]$$

where $G(t)$, a normalized function of time, is called the reduced relaxation function, and $T^{(e)}(\lambda)$, a function of λ alone, is called the elastic response. Assuming that the stress response to an infinitesimal change in stretch, $\delta\lambda(\tau)$ superposed on a specimen in a state of stretch λ at an instant of time τ, is, for $t > \tau$:

$$G(t-\tau)\frac{\partial T^{(e)}[\lambda(\tau)]}{\partial\lambda}\delta\lambda(\tau), \qquad [7.9]$$

and with superposition principles, the stress response is written as

$$T(t) = \int_{-\infty}^{t} G(t-\tau)\frac{\partial T^{(e)}[\lambda(\tau)]}{\partial\tau}\mathrm{d}\tau, \qquad [7.10]$$

where the tensile stress at time t is the sum of contributions of all the past changes, each governed by the same reduced relaxation function. From Eq. 7.10, the stress response is described by a linear law relating the stress T with the elastic response $T^{(e)}$. The function $T^{(e)}(\lambda)$ plays the role assumed by the strain ε in the conventional theory of viscoelasticity.

The inverse of Eq. 7.10 may be written as

$$\varepsilon(T,t) = \int_{-\infty}^{t} J(t-\tau)\frac{\mathrm{d}\varepsilon^{(e)}[T(\tau)]}{\mathrm{d}\tau}\mathrm{d}\tau, \qquad [7.11]$$

which defines the reduced creep function $J(t)$.

The elastic response, $T^{(e)}(\lambda)$.

Assuming $T = \varepsilon = 0$ for $t < 0$ and from Eq. 7.10:

$$T(t) = T^{(e)}[\lambda(t)] + \int_0^t T^{(e)}[\lambda(t-\tau)]\frac{\partial G(\tau)}{\partial \tau}\mathrm{d}\tau. \qquad [7.12]$$

Observing that the steady-state stress–strain behavior of soft tissue is not sensitive to strain rate, its elastic response $T^{(e)}(\lambda)$ may be described using elasticity theory, which can be approximated by its tensile stress response in a loading experiment.[7] By definition, $T^{(e)}(\lambda)$ is the tensile stress instantaneously generated in the tissue when a step function of stretching λ is imposed on it. Strict laboratory measurement of $T^{(e)}(\lambda)$ according to this definition is difficult because, at a sudden application of loading, transient stress waves will be induced in the specimen and a recording of the stress response will be confused by these elastic waves. However, if the relaxation function $G(t)$ is assumed as a continuous function, then $T^{(e)}(\lambda)$ may be approximated by the tensile stress response in a loading experiment with a sufficiently high rate of loading. Besides, the repeatable loading and unloading tensile curves upon preconditioning may be characterized separately using the elasticity theory.

The elastic response function $T^{(e)}(\lambda)$ can be of different forms. A linear stress–strain relationship can be assumed for strains up to about 30% while an exponential or a parabolic form is recommended for larger strains.[4]

The reduced relaxation function, $G(t)$.

With the feature of strain rate independency, a reduced relaxation function of the form:[7]

$$G(t) = \alpha \ln(t) + \beta \qquad [7.13]$$

with $\alpha = -\dfrac{c}{1 + c\ln\left(\dfrac{\tau_2}{\tau_1}\right)}$ and $\beta = -\dfrac{1 - c\gamma + c\ln(\tau_2)}{1 + c\ln\left(\dfrac{\tau_2}{\tau_1}\right)}$

where c, γ, τ_1 and τ_2 are constants with, $\tau_1 \le t \le \tau_2$, has been commonly employed in the quasi-linear viscoelastic theory to incorporate the continuous relaxation spectrum of hysteresis (Fig. 7.4). The two ends of the spectrum, marked by frequencies τ_1^{-1} and τ_2^{-1} define two characteristic times τ_1 and τ_2 which can be determined from experimental data. The quasi-linear viscoelastic theory has been widely applied to characterize the viscoelastic behavior of various soft tissues, including the muscle, ligament and tendon structures.[4]

7.3.4 The poroelastic model of soft tissues

The phenomenon of viscoelasticity can be classified as flow-dependent or flow-independent. Flow-dependent viscoelasticity is the result of the

interaction between the solid matrix of the tissue and the interstitial fluid, whereas the flow-independent viscoelasticity is the result of the intrinsic viscoelastic tissue behavior. The characteristic of flow-dependent viscoelasticity of soft tissue can be described by a poroelastic or a biphasic model.

In the poroelastic model, the diffusive interaction between the solid matrix and the interstitial fluid is assumed to be the sole source of the viscoelastic phenomenon of the tissue in the so-called flow-dependent viscoelasticity. The development of the poroelastic model was based on a consolidation theory introduced by Biot[9] for analyzing the mechanical behaviour of soil structures. This consolidation theory, also known as the poroelastic theory, defined a structure as a porous media consisting of an elastic solid matrix with interconnected fluid saturated pores. A biphasic model for describing the mechanical behavior of soft tissue was introduced by Mow *et al.*,[10] which is based on theory of mixtures.[11] The biphasic theory assumes that tissue is a mixture of two distinct constituents, an incompressible fluid phase (interstitial water) and an incompressible porous solid phase (PG, collagen, and other minor protein molecules). The biphasic model has been recognized to simulate the role of the interstitial fluid in the mechanical behavior of articular cartilage. In the linear biphasic theory, it is assumed that the fluid phase is inviscid and that the solid phase is linearly elastic. The overall viscoelastic behavior of the tissue is mathematically modeled in terms of the diffusive momentum exchange between the fluid phase and the porous solid phase and is dependent on the permeability of the tissue matrix. All of the material parameters, such as the volume fraction of each constituent, permeability, and elastic moduli, are assumed to be constant and independent of tissue deformation. This biphasic theory used a similar approach to that of the poroelastic theory in analyzing the porous media. The poroelastic model of Biot[9] differs from the biphasic model[10] in that the latter does not take into account the compressibility of the individual constituents. The biphasic and poroelastic models are basically the same provided that the described porous media consisted of incompressible elastic solid matrices saturated with an incompressible Newtonian fluid.

A poroelastic model of skin subcutaneous tissue was built by Mak *et al.*[12] to study the effects of epidermal loadings on pressure sores. A layer of skin and subcutaneous tissue on a bony substratum was modeled as a homogeneous layer of biphasic material with uniform thickness. The epidermal surface and the bony interface were taken to be impervious. The cases for surface pressure loadings and displacement-controlled indentations were simulated and the transient tissue response of hydrostatic pressure and tissue compaction were analyzed. The model provided an overview on how various materials, and geometric and loading parameters can affect the transient biomechanical responses of a layer of skin and subcutaneous tissue on a bony substratum; in particular, the hydrostatic pressure build-up

within the tissue and the subsequent tissue compaction as the fluid gradually moves away from the loaded area.

The biphasic model has been extended to include nonlinear behaviors such as strain-dependent permeability and finite deformation.[13–16] Identifying the intrinsic viscoelastic effect on the dynamic behaviour of articular cartilage, Mak[17,18] introduced the poroviscoelastic theory, which took into account the intrinsic viscoelasticity of the solid matrix based on the biphasic theory. Lai *et al.*[19] presented an extended version of the theory, called the triphasic model, to include the dissolved solute concentration, which is known to be responsible for the osmotic pressure and swelling effect of soft tissue.

7.4 References

1. Black, J. and Hastings, G. (1998). *Handbook of Biomaterial Properties*, Chapman & Hall.
2. Elsner, P. (2002). *Bioengineering of the Skin: Skin Biomechanics*, Boca Raton, Fla.: CRC Press.
3. Lanir, Y. (1987). Skin mechanics. In: *Handbook of Bioengineering*, Chapter 11, New York: McGraw-Hill,.
4. Maurel, W. (1998). *Biomechanical Models for Soft Tissue Simulation*, Berlin; New York: Springer-Verlag.
5. Fung, Y.C. (1993). *Mechanical Properties of Living Tissues*. 2nd Edition, New York: Springer-Verlag.
6. Lockett, F.J. (1972). *Nonlinear Viscoelastic Solids*, London, New York: Academic Press.
7. Fung, Y.C., Perrone, N. and Anliker, M. (1972). *Biomechanics: Its Foundations and Objectives*. Englewood Cliffs, N.J: Prentice-Hall.
8. Christensen, R.M. (1971). *Theory of Viscoelasticity; an Introduction*, New York: Academic Press.
9. Biot, M.A. (1941). General theory of three-dimensional consolidation. *J Applied Physics*, **12**, 155–64.
10. Mow, V.C., Kuei, S.C., Lai, W.M. and Armstrong, C.G. (1980). Biphasic creep and stress relaxation of articular cartilage in compression: Theory and experiments. *J Biomech Eng,* **102**, 73–84.
11. Truesdell, C. and Toupin, R. (1960) *The Classical Field Theories, Handbuch der Physik III/I*, Berlin: Springer-Verlag.
12. Mak, A.F., Huang, L. and Wang, Q. (1994). A biphasic poroelastic analysis of the flow dependent subcutaneous tissue pressure and compaction due to epidermal loadings: issues in pressure sore. *J Biomech Eng* **116**, 421–9.
13. Holmes, M.H. (1986). Finite deformation of soft tissue: analysis of a mixture model in uni-axial compression. *J Biomech Eng*, **108**, 372–81.
14. Holmes, M.H. and Mow, V.C. (1990). The nonlinear characteristics of soft gels and hydrated connective tissues in ultrafiltration. *J Biomech*, **23**, 1145–56.
15. Kwan, M.K., Lai, W.M. and Mow, V.C. (1990). A finite deformation theory for cartilage and other soft hydrated connective tissues – I. Equilibrium results. *J Biomech*, **23**, 145–55.

16. Lai, W.M., Mow, V.C. and Roth, V. (1981). Effects of nonlinear strain-dependent permeability and rate of compression on the stress behaviour of articular cartilage. *J Biomech Eng*, **130**, 61–6.
17. Mak, A.F. (1986). The apparent viscoelastic behaviour of articular cartilage – the contributions from the intrinsic matrix viscoelasticity and interstitial fluid flows. *J Biomech Eng*, **108,** 123–30.
18. Mak, A.F. (1986). Unconfined compression of hydrated viscoelastic tissues: a biphasic poroviscoelastic analysis. *Biorheology*, **23**, 371–83.
19. Lai, W.M., Hou, J.S. and Mow, V.C. (1991). A triphasic theory for the swelling and deformation behaviours of articular cartilage. *J Biomech Eng*, **113**, 245–58.

8

Contact mechanics in wearing garments

X-Q. DAI[1,2], Y. LI[1] AND X. ZHANG[3]
[1]The Hong Kong Polytechnic University, China
[2]Soochow University, China
[3]Xian University of Engineering Science & Technology, China

8.1 Introduction

The biomechanical functional performance of garments and devices is determined by the mechanical interactions between clothes and the human body during wear in static and/or dynamic situations. Therefore, how to treat the contact mechanics at the cloth–skin interfaces is critical for establishing scientific understanding and knowledge for the purpose of biomechanical engineering. In this chapter, the techniques and processes developed in the area of contact mechanics in relation to biomechanical engineering are introduced and discussed.

8.2 Contact problems involved in garments

When a garment is worn on a human body, it takes the body shape and follows body movements. During the wearing, cloth deformation is mostly caused by its contact with the body. However, since cloth is a kind of soft and flexible material, it can easily bend and fold to contact itself, especially in free draping. Such self-collision is also an important aspect of the cloth contact problem.

While self-contact is a major determinant of the garment aesthetic appearance, the contact between cloth and the organic human body will have deep influence on the human body. The interaction between fabric and human skin will stimulate various sensory receptors in the skin and may cause uncomfortable feelings, such as tickle, prickle and abrasion of the skin. The pressures exerted on the body will not only affect the person's compression comfort feelings, they will influence physiological performance, such as blood circulation. So it is very important to simulate the geometric and mechanical interaction of cloth contact accurately in biomechanical engineering garment design.

In most garment simulation, the human body is modeled as a shell rather than a solid body. The contact between the body and cloth is usually

considered as a non-penetration geometric constraint rather than a mechanical interaction. A generalized approach is introduced to deal with the contact problem and to generate realistic contact response. In computer simulation, shell or solid objects are often described as polygonal or polyhedral meshes. However, these virtual objects do not occupy any real volume in space, and there is nothing preventing them from occupying the same volume in virtual space, so some collision management is necessary to enable objects to interact, preventing geometrical interference.

8.3 Contact mechanics

When two objects contact, the reaction forces oppose geometrical interpenetration while the friction forces prevent relative sliding. Therefore, dealing with contact involves two types of problems:

(i) collision detection: to find out the locations of geometrical contacts between objects;
(ii) collision response: to integrate the resulting reaction and friction effects in the mechanical simulation.

The two problems are different in nature: the former is essentially a geometrical processing whereas the latter is relevant to the mechanical modeling. They are addressed respectively in the following two sections.

8.3.1 Contact kinematics

Assume two elastic bodies, β^i, i = 1, 2, each occupying the bounded domain $\Omega^i \subset R^3$. The two bodies initially separate from each other. When they come into contact, both of them get deformed and contact at a boundary due to the contact response. Within the contact boundary, the point x^1 in β^1 comes in contact with the point x^2 in β^2, and n^1 denotes the normal of the contact surface at point x^1. In the contact area, constraint equations or the approach function for normal contact have to be formulated, as well as the kinematical relations for the tangential contact.[1]

Normal contact of 3D bodies

As the two bodies come into contact, there are two cases for the contact condition: non-penetration, and a small penetration allowed. Once the point x^1 in contact with x^2 is known, an inequality constraint for the first case can be defined:

$$g_N = (x_2 - x_1) \cdot n^1 \geq 0;$$

or a penetration function for the second case:

$$g_N = \begin{cases} (x^2 - x^1) \cdot n^1 & \text{if } (x^2 - x^1) \cdot n^1 < 0 \\ 0 & \text{otherwise} \end{cases}.$$

Two main techniques can be followed to impose contact conditions in the normal direction. One is the formulation of the non-penetration as a purely geometrical constraint; the normal contact stresses then follow from the constraint equation. And another is the development of an elastic or elasto-plastic constitutive law for the micromechanical approach within the contact area, which yields a response function for the normal contact stresses.

The purely geometrical constraint for the non-penetration can be stated as:

$$g_N \geq 0,\ p_N \geq 0,\ p_N g_N \geq 0.$$

Here, p_N, contact pressure, is the force acting on both surfaces in the normal direction, which obeys the action–reaction principle. For contact, there is $g_N = 0$, and $p_N < 0$. If there is a gap between the bodies, then the relation becomes $g_N > 0$, and $p_N = 0$.

The micromechanical approach takes account of the roughness of the body surface. The mechanical behavior depends in general upon material parameters, such as hardness, and on geometrical parameters, such as surface roughness. Then, the contact pressure can be formulated as:

$$p_N = f(d),$$

where, f is a nonlinear function of the current mean plane distance d. The distance d is related to the geometrical approach g_N, via the relation: $g_N = \zeta - d$ as illustrated in Fig. 8.1.

Tangential contact of 3D bodies

In the tangential direction of the contact interface, there are generally two cases needing to be distinguished: the first is the 'stick state', in which a point that is in contact is not allowed to move in a tangential direction; the second is 'sliding', which means that a point moves in a tangential direction

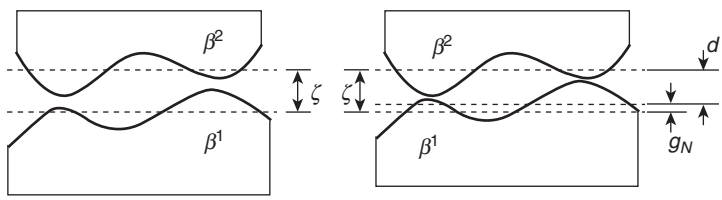

8.1 Physical approach of two bodies.

in the contact interface. The constraint for the 'stick state' can be formulated as: $g_T = 0$, where g_T denotes the relative displacement in a tangential direction. Once the tangential forces are above a certain limit, then the contacting surfaces no longer stick to each other, but move relative to each other. The 'sliding' is usually described by the law of Coulomb:

$$t_T = -\mu |p_N| \frac{g_T}{\|g_T\|}, \quad \text{if} \quad \|t_T\| > \mu |p_N|,$$

where μ is the sliding friction coefficient. The coefficient is a constant in the classical Coulomb law, depending on the material pairing of the solids in contact.

Formulation of contact constraints

The Lagrange multiplier method and the Penalty method are mostly often used to formulate the contact constraints. The Lagrange multiplier method is usually used for the non-penetration contact interface. If contact is active at the surface Γ_c, it adds a contact contribution to the weak form of the system as:

$$\Pi_C^{LM} = \int_{\Gamma_C} (\lambda_N g_N + \lambda_T \cdot g_T) \mathrm{d}A,$$

where λ_N and λ_T are the Lagrange multipliers and λ_N can be identified as the contact pressure P_N. The Penalty method is often used for the contact condition where penetration is allowed. A penalty term due to the penetration is added to the weak form of the system:

$$\Pi_C^P = \frac{1}{2} \int_{\Gamma_C} \left(e_N (g_N)^2 + e_T g_T \cdot g_T \right) \mathrm{d}A, e_N, e_T > 0.$$

Here, e_N and e_T represent the penalty parameters. There are several other variants for the formulation of the normal contact constraint detailed in reference 1.

8.4 Contact detection

Contact takes place between the surfaces of objects. In computer terms, a surface is usually described by polygonal meshes. So the contact detection is carried out between polygonal meshes that may have thousands of polygons. The main problem is to master the computational complexity due to the discretization. Testing each pair of polygons for potential collisions is tremendous work and it is inefficient. Some complexity reduction techniques are necessary in collision detection. There are many different solutions that have been proposed, relying on the geometrical context and situation considered.

Another problem involved in collision detection is that the exact contact locations on the objects are necessary for simulating realistic collision response, which includes preventing geometric interpenetration and generating mechanical interaction. So, to characterize contact geometrically is also an important part in collision detection. It is often a more complicated geometric process compared to just detecting whether two objects are colliding.

8.4.1 Various collision detection techniques

Bounding volumes

As a basic idea for complexity reduction, preliminary collision tests can be performed between simplified bounding volumes containing the complex objects to be tested. A bound volume is a geometric primitive that may contains a group of objects, a complex object, a group of primitives, or just a single polygon. Its construction should be simple and straightforward. Various bounding volumes can be considered, each of them having its own merits and weaknesses. Among them, the most common are bounding boxes, usually axis-oriented, and bounding spheres.

An axis-oriented bounding box is characterized by six parameters describing the minimal and maximal coordinates of the contained objects, as illustrated in Fig. 8.2. They are easy to build, merge, and detect collision with; only linear geometrical calculation is involved. A bounding sphere is described by four parameters: the center coordinates and the radius. They are difficult to build and merge since complex, non-linear geometrical calculations are needed to find the optimal position of the center, but their description is very compact and collision detection is very easy to carry out.

Prior to performing collision detection with the objects contained by the volume, simple and fast collision detection is performed between the volumes. Further detection is carried out only if the volumes intersect. Usually, the

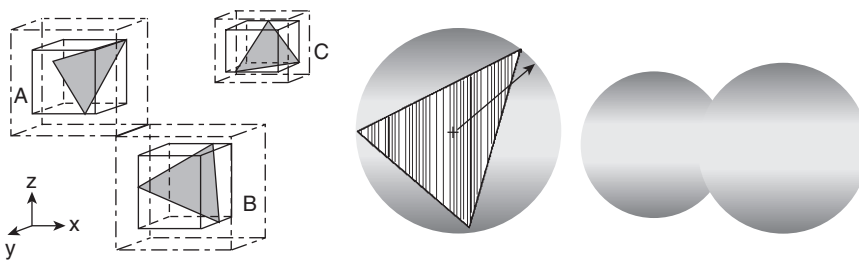

(a) Bounding box (b) Bounding sphere

8.2 Bounding volume.

volume collision detection is integrated to a hierarchical technique. Volume collision detection is performed among bounding volumes of higher level, and further detection among bounding volumes of lower level is carried out only if intersection is detected. Other more complicated bounding volumes aim to optimize the filling efficiency, i.e. to reduce the empty space so that the volume collision may be more representative of the collisions of the contained objects, and be able to describe more complicated shapes.

Axis projection methods

If objects are geometrically colliding, their projections are intersecting. This consideration allows us to carry out quick collision detection in spaces of reduced dimensions. As illustrated in Fig. 8.3, objects are usually projected onto the coordinates. Each object is represented by the intervals on the three axes. Two objects are likely to collide if all three intervals collide with each other, respectively. Here, only a simple interval interference algorithm is needed. Efficient sorting methods can also be implemented for ordering and sorting the intervals along the axes, and detecting the potential for colliding quickly. The technique becomes particularly efficient when integrated with the axis-oriented bounding box technique. Cohen *et al*. used this technique in their collision detection system.[2]

Space subdivision methods

Space subdivision methods are based on a consideration that objects geometrically close to each other are likely to collide. It divides the space into regions and maintains a group of objects contained in each region. Then, the collision detection is performed only between the objects sharing a common region. There are two major methods to divide the space: grid subdivision and hierarchical subdivision.

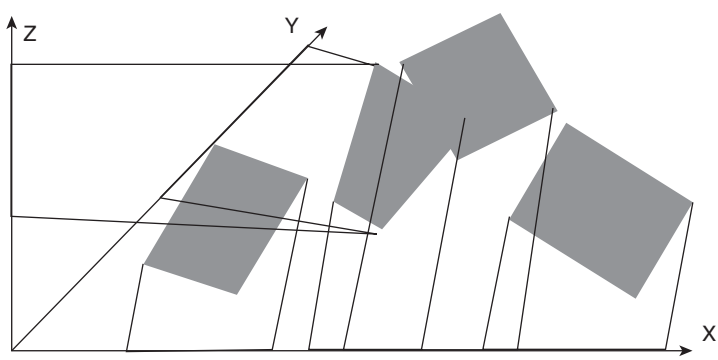

8.3 Projecting objects onto axes.

Grid subdivision divides the space into a regular array of boxes, called voxels, as illustrated in Fig. 8.4a. How to choose the voxel size is the main issue of the method. If the voxel is too large, too many objects may be contained in a same voxel; if it is too small, there will be too many voxels to realize efficient collision detection. The optimal discretization depends on the choice of the collision detection algorithm, the number of objects, and their size and motion. More complicated techniques can be progressive or dynamic grids.

Regular grid subdivision lacks the adaptability to the shapes and geometrical characteristics of objects. The common way to improve the subdivision is to implement a local refinement adapted to the objects' geometrical features, to obtain a hierarchical subdivision. Hierarchical is also the best algorithm technique for improving algorithm efficiency. Octree is the usual hierarchical scheme for space subdivision. As illustrated in Fig. 8.4b, each space box is divided into eight equal sub-boxes by using the three axis-aligned planes at the center of the box. An octree can describe any volume contained in the space at a given resolution represented by the maximal depth of the octree structure. The nodes in an octree structure have three states: *full*, if the corresponding space is contained in the object; *empty* if there is no intersection between the corresponding space volume and the object; *partial* if there is partial intersection. Among the three cases, only in the third one and only if the volume size is bigger than the given resolution, is the space further subdivided in the next step.

The overlap detection between the octree structures is quite simple. Starting from the whole scene, if there is *full–full* or *full–partial* overlap, collision is detected and the test stops; if *partial–partial* overlap occurs, potential collision is detected and further tests on the deeper level are necessary; if there is no overlap, no collision is detected and the test can stop at this level. Meager[3] and Chen and Huang[4] have good descriptions of octree construction.

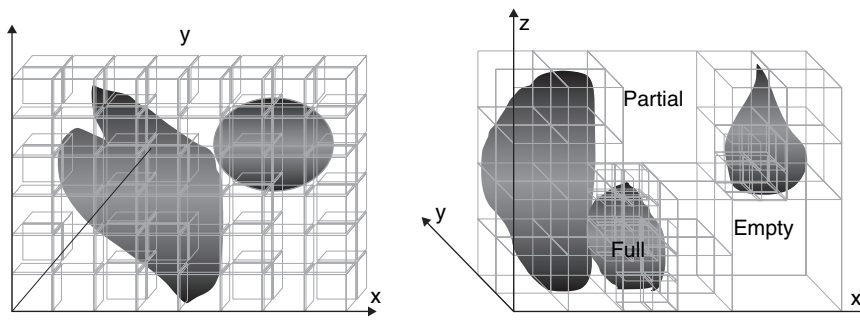

(a) Grid subdivision (b) Hierarchical subdivision

8.4 Space subdivision.

Object subdivision methods

A big problem of the hierarchical space subdivision algorithm is the difficulty of updating the structure efficiently as the objects move. To overcome this problem, one approach is to build the hierarchical structure on the objects themselves rather than based on the time-dependent space. Thus, the hierarchies can be very simply updated as objects move. This approach is only suitable for objects with constant topological structures. Fortunately, both the human body and clothing (deformable surfaces) meet this requirement.

The most common implementation of the object hierarchy technique groups several objects and performs successive tests using the bounding boxes containing the considered groups. If one group collides, collision detection will be performed for the children groups. This process is continued, progressively, until 'no collision' or 'sure collision' is announced for each bounding box. In references 5 and 6 bounding box hierarchy trees are constructed on the objects and dynamically updated as the objects move. Bounding sphere hierarchies are considered in references 7 and 8 for collision detection in animation.

To build an object hierarchy tree efficiently is quite difficult. An efficient tree should have minimum depth, while each tree node of it should correspond to a group of objects being as close as possible to each other in order that the bounding box test will be relevant. As objects move, it may be necessary to change the hierarchy organization using some incremental tree-manipulation techniques to reflect the vicinity changes among objects.

Proximity tracking techniques

An intuitive way for optimized collision detection is to detect collisions only among objects being close to each other. A 'vicinity map' can be built for the whole objects and be updated as objects move, using some computational geometrical techniques. Voronoi domain can be a good choice for this purpose. Figure 8.5 shows a 2D Voronoi domain. A Voronoi domain associated to an object consists of the space points that are closer to it than other objects. Voronoi domain for a group of objects can also be built using some specific techniques. For simplification, bounding spheres can be used instead of the objects themselves in the Voronoi domain calculation. Collision detection is only carried out between objects in neighbored domains. The major difficulty of this algorithm is to update the domains and their neighboring connectivity as objects move around.

A simple variation of the proximity tracking approach is to track the closest distance between bounding spheres containing grouped objects. The

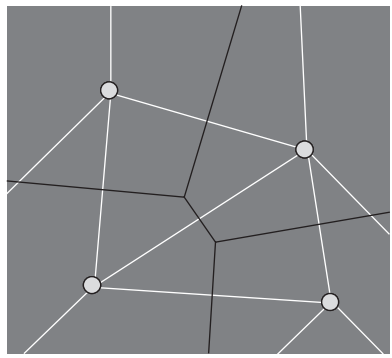

8.5 2D Voronoi domain.

neighborhood can also be roughly determined based on the hierarchical structures. To track the contact efficiently, many Finite Element Analysis software packages use hierarchical global/local search algorithms. For example, in the Finite Element (FE) package ABAQUS (Hibbitt, Karlsson & Sorensen, Inc., USA), a global search determines the globally nearest surface facet for each slave node in a given contact pair. A bucket sorting algorithm is used to minimize the computational expense of this search. A local contact search tracks the motion of a slave node along the nearest facets on the master surface.[9]

Collision detection on polygonal meshes

Both cloth and human body surfaces involved in clothing simulation are usually described in terms of polygonal meshes. By considering each polygon element as an individual primitive, the previously introduced techniques can be applied to the collision detection on polygonal meshes. Actually, the relatively fixed topology of a polygonal mesh is helpful for building a hierarchical tree for a surface. Then the collision detection is to find all the pairs of polygons in contact. For collision between a human body surface and a cloth surface, a 'pair' refers to a polygon on the body surface and a polygon on the cloth surface. However, there will be a big difference for the case of cloth self-collision.

Generally, there is no essential difference between a collision detection between two different objects and that within a single object since, in both cases, groups of elements have to be tested for collisions. Cloth self-collision detection can be performed in a similar way to the body–cloth collision detection. However, some specific algorithm to remove any relevant collisions such as an element colliding with itself is necessary. Collision detection on polygonal meshes has to find all the pairs of polygons in contact. Since

each polygon is naturally adjacent to a certain set of neighbor polygons on a polygonal mesh, these polygons will be detected as collision. Collision detection should not be triggered by these adjacencies and collision should only be tested between polygons that are not topologically in contact in the mesh structure.

Volino *et al*. developed a collision detection algorithm based on a hierarchical bounding-box scheme for polygonal meshes.[10] A hierarchy tree consisting of successive subdivisions of the entire surface is built, taking advantage of the structural continuity of the polygonal description. A node of the hierarchical tree represents a surface region containing a certain number of polygonal elements. Starting from the root of the hierarchy representing the entire surface, the children nodes are recursively built by successively subdividing the surface region of a parent node. Finally, the leaf nodes of the tree are the individual polygons of the surface. A bounding box hierarchical structure is built associated with the tree nodes. Collision detection is performed by testing the bounding box contact between two nodes. If there is a contact, the test is continued by recursively testing the children nodes. The algorithm yields pairs of polygon elements whose bounding boxes are colliding.

This algorithm is optimized for self-collision detection by using the surface curvature evaluation within surface regions defined by the hierarchy tree. As illustrated in Fig. 8.6, the self-collision in (a) can be detected by a standard intersecting test between two bounding boxes, while the collision in (b) within a bounding box cannot be detected in the same way. Further self-collision within a bounding box seems necessary. However, it is not necessary to perform a self-collision test for each leaf bounding box.

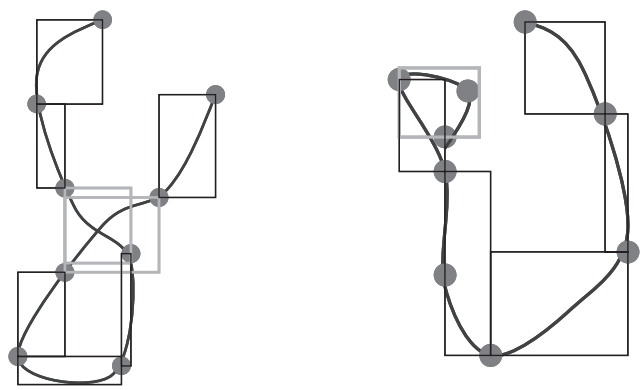

(a) Standard intersecting test (b) Within a bounding box test

8.6 Self-collision detection.

A flat surface cannot have self-collisions. Only if a surface folds is it likely to collide with itself. The curvature of the small piece of surface contained in the bounding box can be the key for achieving efficient self-collision detection. If proper curvature criteria can be set, then self-collision detection within a bounding box is performed only if the corresponding curvature is smaller than the criteria.

A detailed overview of collision detection techniques has been given by Volino and Thalmann in reference 10.

8.4.2 Characterizing collision geometrically

Most of the collision detection algorithms return a bunch of polygon couples that are geometrically close enough to be considered contact. Some further specific process is needed to judge if the pair of polygons are really in contact. If yes, the clear geometrical state of the contact is calculated and is then integrated into collision response. Depending on the application and the response type, two major kinds of contact are often considered:

(i) Penetrations: Objects are penetrating each other. In the case of surfaces, the two colliding surfaces are crossing each other.
(ii) Proximities: Objects are considered colliding when their closest distance becomes less than a given threshold.

Penetration judgment

For polygonal meshes, penetration detection is performed between polygon and polygon. However, it is often simplified as penetration between vertex and polygon. For two objects separated initially, it seems enough to avoid penetration. However, there are some exceptions that cannot be covered by vertex/polygon, as shown in Fig. 8.7, where $P_{a1}(t)$ and $P_{a2}(t)$ denote the positions at time t of two vertices of an edge on object A; $P_{a1}(t + \Delta t)$ and $P_{a2}(t + \Delta t)$ denote the respective predicted positions after a time interval of Δt. In these cases, the two vertices have not penetrated any polygons, but the two objects A and B do cross each other. It can be considered that the edges a_1a_2 and b_1b_2 penetrate each other. To address such problems, penetration detection between edge and edge should be performed in additional to vertex/polygon penetration.

Vertex/triangle has been taken as an example to describe the processing of vertex/polygon penetration detection. Figure 8.8 illustrates the penetration between a vertex on object A and a triangle on object B, where $P_a(t)$ denotes the position of the vertex of A at time t, $P_a(t + \Delta t)$ denotes its predicted position after a time interval of Δt, and $P_{b0}(t)P_{b1}(t)P_{b2}(t)$ represents the position of the triangle at time t. If the line $P_a(t)P_a(t + \Delta t)$ intersects the

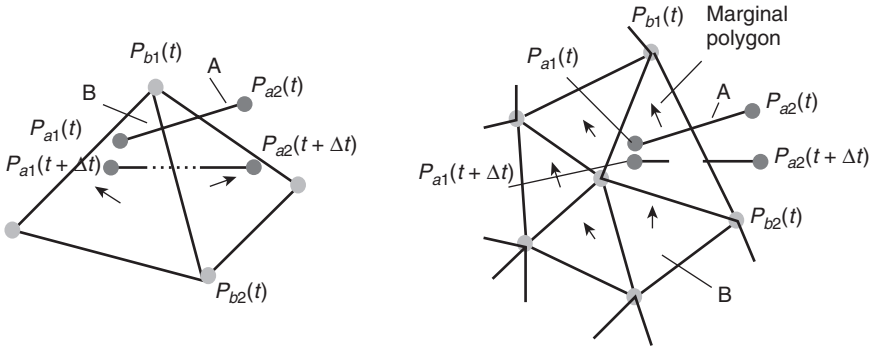

(a) Convex edge (b) Boundary edge

8.7 Edge/edge penetration.

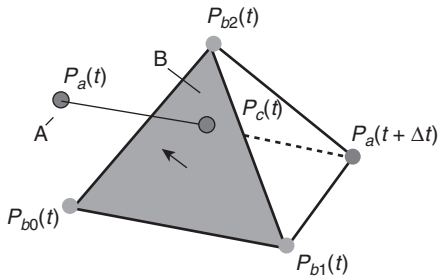

8.8 Vertex/triangle penetration.

triangle, then the vertex of object A is determined to be colliding with the triangle. Whether a line intersects a triangle or not can be judged by using a Euclid 4×4 determinant defined as the following equation:

$$S_{a(t)012} = \begin{vmatrix} x_{a(t)} & y_{a(t)} & z_{a(t)} & 1 \\ x_0 & y_0 & z_0 & 1 \\ x_1 & y_1 & z_1 & 1 \\ x_2 & y_2 & z_2 & 1 \end{vmatrix}.$$

Here, $x_a(t)$, $y_a(t)$, $z_a(t)$ and so on denote the coordinates of the vertex of A at time t and the vertices of the triangle, and $S_{a(t)012}$ is actually the volume of the polyhedron formed by these four vertices. If the vertex locates at the right side of the triangle, $S_{a(t)012}$ is positive and if the vertex locates at the back side of the triangle, $S_{a(t)012}$ is negative. And if the four vertices locate on the same plane, $S_{a(t)012}$ equals zero. Using these characteristics of the equation, it can be judged whether a line intersects a triangle. If either of the following two sets of equations is satisfied, the vertex intersects the triangle.[11]

$$S_{a(t)012}S_{a(t+\Delta t)012} \le 0 \cap S_{a(t)012} \ge 0 \cap S_{a(t)a(t+\Delta t)01} \ge 0 \cap S_{a(t)a(t+\Delta t)01} \ge 0 \cap S_{a(t)a(t+\Delta t)12} \ge 0 \cap S_{a(t)a(t+\Delta t)20} \ge 0,$$

$$S_{a(t)012}S_{a(t+\Delta t)012} \le 0 \cap S_{a(t)012} \le 0 \cap S_{a(t)a(t+\Delta t)01} \le 0 \cap S_{a(t)a(t+\Delta t)01} \le 0 \cap S_{a(t)a(t+\Delta t)12} \le 0 \cap S_{a(t)a(t+\Delta t)20} \le 0.$$

Furthermore, the position of the contact point on the triangle can be calculated as:

$$P_c(t) = P_a(t) + \frac{S_{a(t)012}}{S_{a(t)012} - S_{a(t+\Delta t)012}} \times (P_a(t+\Delta t) - P_a(t))$$

Edge/edge penetration detection can be converted to a line and triangle intersecting problem. In Fig. 8.7, whether the edge $P_{a1}(t)P_{a2}(t)$ is colliding with the edge $P_{b1}(t)P_{b2}(t)$ depends upon whether the edge $P_{a1}(t + \Delta t)P_{a2}(t + \Delta t)$ intersects the two triangles for the case in Fig. 8.7a or the one triangle for the case in Fig. 8.7b connecting to the edge $P_{b1}(t)P_{b2}(t)$. Then the above mentioned approach can be applied.

Proximity judgment

Proximities are represented by the two 'closest distance' points on the elements of the two objects, which can be vertices, edges or polygons. Figure 8.9 illustrates the proximity domains for vertex, edge and polygon. Among the combinations of possible elements involved in the proximities, a collision is set up if both contact points are inside the respective proximity regions, and collision response processing is followed. The possible collision combinations include vertex/vertex, vertex/edge, edge/edge, vertex/polygon, and edge/polygon. Full proximity detection on all the element combinations generates a very dense collision network that can be appreciable for an accurate response simulation. The computational cost is extremely high.

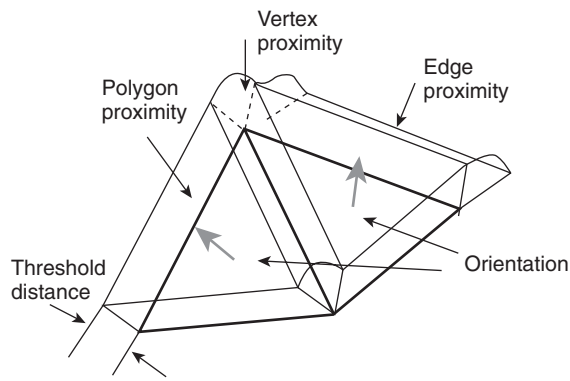

8.9 Proximity domain for vertex, edge and polygon.

However, it is not necessary to carry out all these types of collision detections. The geometrical characteristics of the polygonal meshes can be used to avoid extra processing. A vertex or an edge can be classified as convex or concave as illustrated in Fig 8.10. In cloth simulation, proximities for polygons are always considered. The detection of proximities for concave vertices and edges are covered by the polygon proximities, so they can be omitted. Therefore, edge/edge proximity detection, only for the convex edges, together with the polygon proximity detection, yielding a lighter collision network, is suitable for rapid processing.

In many Finite Element Method (FEM) software packages, the contact is often defined between a 'master' surface and a 'slave' surface, and the penetration detection is then performed between a slave node and a master polygon. A clearance is set; if the distance between the node and the polygon is smaller than the clearance, the two elements are considered in contact.

8.5 Contact response

Once two objects are detected to be interacting, 'feedback' should be performed on their behavior. Collision response aims to visualize the interaction in an accurate way: to avoid interpenetration of the objects and to simulate the bouncing and effects.

8.5.1 Collision on polygonal meshes

In a polygonal mesh, a collision means an interaction between two elements; and each element can be a vertex, an edge, or a polygon. The collision

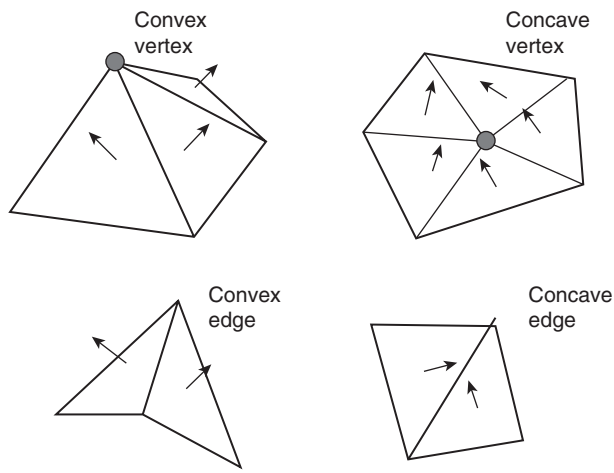

8.10 Characteristics of vertex and edge on polygonal meshes.

itself is applied on specific geometrical locations of the two elements; a pair of contact points. Then a collision is usually identified by both the contact points and a collision distance separating them. A contact point, which may often not be a vertex, can be described by its mass coordinate from the vertices defining the polygon element to which it belongs. Once the position of the contacted point is detected, its area coordinate can be computed using simple geometry. In Fig. 8.11, the area coordinates of the point P_a can be calculated using the following equations:

$$r_{a0} = S_{\Delta P_a P_{a1} P_{a2}} / S_{\Delta P_{a0} P_{a1} P_{a2}},\ r_{a1} = S_{\Delta P_a P_{a2} P_{a0}} / S_{\Delta P_{a0} P_{a1} P_{a2}},\ r_{a2} = S_{\Delta P_a P_{a0} P_{a1}} / S_{\Delta P_{a0} P_{a1} P_{a2}}.$$

As the mesh vertices carry the state of the object position, velocity and acceleration, collision effects need to be distributed on the vertices supporting the colliding elements. Again the area coordinates are used to obtain a linear interpolation.

As for any mechanical interaction, collision interaction obeys some mechanical conservation laws. The major law is the action–reaction equality, which states that the pair of forces exerted on the two objects are exactly opposite. To translate a mechanical response into a geometric effect, it will go through the division by the object mass, where Newton's second law is obeyed. To take the friction effect during contact into account, the Coulombian friction model, which considers a friction force proportional to the normal reaction force and with the direction opposed to the relative sliding speed, is often used.

There are two main approaches for handling collision response:

(i) mechanical reaction: the collision response is simulated by forces or by force adjustments that reproduce the contact effect;
(ii) geometrical reaction: the collision response is simulated by direct corrections on the positions and velocities of the objects.

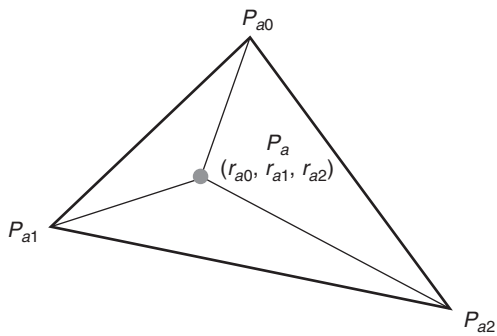

8.11 Area coordinate representation of a point within a triangle.

8.5.2 Mechanical response

The mechanical approach is the most formal way of handling collision response. The forces or energetic contributions generated from the response can be directly integrated into the mechanical model of cloth, and simulated. Collision penalty force or impulse is often employed to simulate the collision behavior. The function for the penalty force is usually designed as a continuous function of collision distance or as a piecewise function using simple linear or polynomial intervals. The penalty force, which acts on the contact point, needs to be distributed to the vertices of the polygon element. A suitable way to perform this response repartition is to use a linear interpolation. The penalty force approach is mostly used in the continuum cloth model, especially in many FEM software packages.

Baraff[12] introduced a non-penetration constraints approach based on rigid body motion to compute the contact forces between contacting bodies.[13] Although neither the cloth nor the human body is rigid, at the colliding moment the elements involved in the collision, which are of small size compared to the dimension of the whole piece of cloth, can be handled as a rigid body. This approach is adaptable for discrete cloth models.

Figure 8.12 shows a particle of object A colliding with a triangle of object B. A particle is imagined existing on the triangle at the contact point B for collision response calculation. The relative velocity between the particles A and B can be obtained as: $v_{rel}^{-} = \hat{n}(t) \cdot (\dot{P}_a^{-}(t) - \dot{P}_b^{-}(t))$. Here, $\hat{n}(t)$ denotes the normal of the triangle, the superior '·' denotes the first order derivative, and we use the superiors '–' and '+' to identify the states of pre-colliding and post-colliding. Depending on this velocity, the contact can be classified as: separating ($v_{rel}^{-} > 0$), resting ($v_{rel}^{-} = 0$), and colliding ($v_{rel}^{-} < 0$). Here the colliding contact is focused on and the impulse is calculated.

To avoid inter-penetration in a colliding contact, a vector quantity J, called an impulse and having the units of momentum, is postulated. To

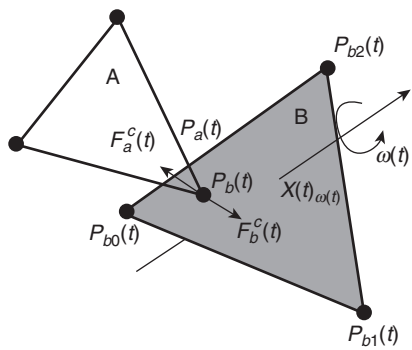

8.12 Vertex/triangle collision.

determine the effect of J, a large force $F_a^C(t)$ is imagined to act on the vertex of A for a small time interval Δt. For frictionless collision, the direction of J will be in the direction of $\hat{n}(t)$, and J can then be described as: $J = F_a^C(t) \cdot \Delta t = j\hat{n}(t)$, where j is the magnitude of J, to be computed. The impulse will change the velocities of the two objects as described in the following equations:

$$\begin{cases} \dot{P}_a^+(t) = \dot{P}_a^-(t) + j\hat{n}(t)/M_a \\ \dot{P}_b^+(t) = \dot{P}_b^-(t) - j\hat{n}(t)/M_b \end{cases}.$$

Here, M_a and M_b denote the mass of particles A and B. The relative velocity between the two colliding particles in the normal direction of the triangle can be described as: $v_{rel}^+ = \hat{n}(t) \cdot \dot{P}_a^+(t) - \dot{P}_b^+(t)$. According to the empirical law for frictionless collision, there are: $v_{rel}^+ = -ev_{rel}$. Here e, called the coefficient of restitution, must satisfy $0 \le e \le 1$. It is usually determined empirically depending on the materials of the colliding objects. Consequently, j can be obtained from the above equations as: $j = \dfrac{-(1+e)v_{rel}^-}{1/M_a + 1/M_b}$.

This impulse acts at the point B, which may often not be the mass center of the triangle, $X(t)$, and will produce an impulsive torque: $\tau_{impulse} = (P_b(t) - X(t) \times J)$. The impulsive torque gives a change in the angular momentum of the triangle ($\Delta L = \tau_{impulse}$), producing a change in angular velocity: $I^{-1}(t)\tau_{impulse}$. Here, $I(t)$ is the inertia tensor, describing how the mass in a body is distributed relative to the element's center of mass. It depends on the orientation of a body, and can be calculated as: $I(t) = R(t)I_{element}R(t)^T$. Here, $R(t)$ is the orientation matrix of the element at time t; and $I_{element} = \sum_{i=0}^{2} m_{bi}(r_{0i}^T r_{0i} I - r_{0i} r_{0i}^T)$ is a constant for a triangular element; r_{0i} denotes a vector from the mass center pointing to a vertex B_i in the triangle at the initial moment.

Since all the effects are taken into account in the same computation step, the resulting simulation by mechanical response approach produces an animation where collision and other mechanical forces add their effects in a compatible way. However, this approach may cause a calculation instability problem. Defining a very small 'response interval' in a small collision region implies the use of very strong and discontinuous reaction forces, which are difficult to simulate numerically. The mechanical response approach is also widely used in the continuum cloth model, especially in many FEM software packages.

8.5.3 Geometric collision response

The geometrical approach is to reproduce directly the effects of collision response on the geometrical state of the objects without making use of

mechanical forces. As mentioned previously, in polygonal meshes, collision often takes place between two elements, A and B, which can be vertices, edges, or polygons; the exact collision positions may locate at specific points, the contact points P_a and P_b. These points can be described by their linear/mass coordinates (r_{ai} and r_{bi}) from the vertices of the respective elements, P_{ai} and P_{bi} as follows:

$$P_a = \sum_i r_{ai} P_{ai}, P_b = \sum_i r_{bi} P_{bi}.$$

The other geometrical quantities for the contact points can be obtained in the same way. Generally, the geometrical collision response is considered to be the difference between the response of the two contact points, a geometrical quantity that can be distance, velocity or acceleration, $Q_{ab} = Q_a - Q_b$. Since it is a geometric value, the conservation laws have to consider the mass of the colliding objects, so the response distribution becomes more complicated. Here, the concept of inverse mass is often introduced. It will allow us to represent fixed and constrained objects as having a null inverse mass rather than an infinite mass. Given the mass M_{ai} for each vertex in the colliding polygon, then the inverse mass of the element A, M_a^{-1}, can be calculated as follows: $M_a^{-1} = \sum_i r_{ai}^2 M_{ai}^{-1}$. Also, it is the same for the other element in contact B, $M_b^{-1} = \sum_i r_{bi}^2 M_{bi}^{-1}$. Then according to conservation laws, the distribution of collision response between the two elements is as follows:

$$\Delta Q_a = \frac{-M_a^{-1}}{M_a^{-1} + M_b^{-1}} Q_{ab}, \Delta Q_b = \frac{-M_b^{-1}}{M_a^{-1} + M_b^{-1}} Q_{ab}.$$

The response ΔQ_a is further distributed to each vertex of element A as: $\Delta Q_{ai} = \frac{-M_{ai}^{-1} r_{ai}}{M_a^{-1}} Q_{ab}$. And the same for ΔQ_b.

Geometrical constraints are directly enforced by a geometrical algorithm, and the simulation process is relieved from high intensity and high discontinuous forces or other mechanical parameters. This makes the simulation faster and more efficient. However, as the collision response changes the geometrical state of the objects separately from the mechanical process, nothing ensures the compatibility of this deformation to be a correct variation of the resultant mechanical state. Therefore, the resulting collision effects may be incompatible with mechanics. These issues have to be addressed for obtaining a collision model with acceptable and steady response.

Volino *et al.* developed an acceleration-based approach for collision response modeling. It performs corrections on position, speed and acceleration simultaneously, ensuring the response is more accurate.[14] Since

the reaction and friction are respectively modeled as a normal and tangent effect along the collision surface, the collision distance, speed and acceleration are decomposed into normal and tangent components as follows:

$$P_{ab}^{N} = P_b - P_a = P_{ab},\ P_{ab}^{T} = 0;$$

$$P_{ab}'^{N} = P_b' - P_a' = \frac{P_{ab}' \cdot P_{ab}}{P_{ab}},\ P_{ab}'^{T} = P_{ab}' - P_{ab}'^{N};$$

$$P_{ab}''^{N} = P_b'' - P_a'' = \frac{P_{ab}'' \cdot P_{ab}}{P_{ab}},\ P_{ab}''^{T} = P_{ab}'' - P_{ab}''^{N}.$$

Position correction is to alter the position of the colliding vertices so that the collision distance is maintained at a given contact distance P_0. The correction is: $P_{0\,ab}^{N} = P_0$.

Speed correction is to alter the speed P' of colliding vertices, ensuring that they will not continue moving toward each other, and further to control the bouncing effect of collision as well as friction effects. To reach the position of the given collision distance P_0 at the next frame, the speed correction should be: $P_{0ab}'^{N} = \frac{P_0 - P_{ab}^{N}}{\mathrm{d}t}$.

Acceleration correction is to alter the acceleration P'' of the colliding vertices so that the desired speeds can be maintained along with time. Given the desired position P and speed P' at the second next frame, the acceleration correction should be:

$$P_0''^{N}(t) = \frac{P_0 - P_{ab}^{N}}{\mathrm{d}t^2} - \frac{0.5P_0' + 1.5P_{ab}'^{N}}{\mathrm{d}t}.$$

The tangential speed and acceleration:

$$P_{0ab}'^{T} = \max\left(1 - \mu \frac{|P_{0ab}'^{N} - P_{ab}'^{N}|}{|P_{ab}'^{T}|}\right) P_{ab}'^{T}.$$

Then, the normal and tangential components are recombined as:

$$P_{0ab} = P_{0ab}^{N} + P_{0ab}^{T},$$

$$P_{0ab}' = P_{0ab}'^{N} + P_{0ab}'^{T},$$

$$P_{0ab}'' = P_{0\,ab}''^{N} + P_{0\,ab}''^{T}.$$

Finally, the corrections to be performed on the current geometrical values are as follows:

$$\Delta P_{ab} = P_{0ab} - P_{ab},$$

$$\Delta P_{ab}' = P_{0ab}' - P_{ab}',$$

$$\Delta P_{ab}'' = P_{0ab}'' - P_{ab}''.$$

8.6 Conclusion

In this chapter, the contact problems involved in simulation of garment construction and wearing have been introduced, including contact between the human body and garment, cloth self-collision, and the mechanical interaction between objects in contact. Various contact detection techniques were briefly reviewed, and also the approaches to characterize collision geometrically. Two major approaches (geometrical and mechanical) to enforce collision response were introduced.

8.7 Acknowledgement

We would like to thank Hong Kong Polytechnic University for funding this research through Projects A188 and G-YD31.

8.8 References

1. Wriggers, P., *Computational Contact Mechanics*. 2002: John Wiley & Sons, 45–91.
2. Cohen, J.D. *et al*., An Interactive and Exact Collision Detection System for Large-scale Environments. in Symposium of Interactive 3D Graphic Process, *ACM SIGGRAPH*. 1995.
3. Meager, D., Geometric Modeling Using Octree Encoding. *Computer Graphics and Image Processing*, 1982. **19**(2): p. 129–147.
4. Chen, H.H. and Huang, T.S., A Survey of Construction and Manipulation of Octrees. *Computer Vision, Graphics and Image Processing*, 1988. **43**(2): p. 409–431.
5. Webb, R.C. and Gigante, M.A., Using Dynamic Bounding Volume Hierarchies to Improve Efficiency of Rigid Body Simulations, in *Communicating with Virtual Worlds, CGI'92 Proceedings*. 1992.
6. Webb, R.C. and Gigante, M.A., Distributed, Multi-person, Physically-based Interaction in Virtual Worlds, in *Visual Computing, CGI'93 Proceedings*. 1993.
7. Hubbard, P.M., Approximating Polyhedra with Spheres for Time-Critical Collision Detection. *ACM Transaction on Graphics*, 1996. **15**(3): p. 179–210.
8. Palmer, I.J. and Grisdale, R.L., Collision Detection for Animation Using Sphere-trees. *Computer Graphics Forum*, 1995. **14**: p. 105–116.
9. Abaqus, V., Chapter 21 Defining Contact Interactions, in *Analysis User's Manual*. 2003, ABAQUS Inc., Pawtucket, RI, USA.
10. Volino, P. and Thalmann, N.M., Collision Detection, in *Virtual Clothing: Theory and Practice*. 2000, Springer. p. 103–144.
11. Yamagutsi, F., *Graphics and Forms Process Technique According to 4-dimensional Theory*. 1995. Nikkan Kougyou Shinbunsya, Japan. p. 301–328.
12. Baraff, D., Rigid Body Simulation, in Course Notes of *SIGGRAPH'98*. 1998.
13. Baraff, D., Rigid Body Simulation, in Course Notes of *SIGGRAPH'98*. 1998. p. D1–D68.
14. Volino, P. and Thalmann, N.M., Collision Response, in *Virtual Clothing: Theory and Practice*. 2000, Springer. p. 145–182.

9

Clothing comfort and compression therapy

Y. LI[1] AND X-Q. DAI[1,2]
[1]The Hong Kong Polytechnic University, China
[2]Soochow University, China

9.1 Clothing comfort

In the past, clothing was something that was kept going for as long as possible. Today, the main consumer purchasing considerations are good appearance and comfort. Comfort is being reinforced as a key parameter in clothing. However, comfort is a complex and nebulous subject that is very difficult to define. The Oxford English Dictionary defines comfort as 'freedom from pain, wellbeing'. Slater[1] defined comfort as 'a pleasant state of physiological, psychological and physical harmony between a human being and the environment'. Therefore, clothing comfort is a neutral sensation, when we are physiologically and psychologically unaware of the clothing we are wearing. There are physiologically and psychologically positive comfort sensations but these tend to be more individualistic and less frequently noticed when we are wearing a garment than discomfort sensations are. Discomfort, which occurs when we are unpleasantly conscious of the garments we are wearing, can be much more easily described in such terms as prickle, hot, and tight. Therefore, a widely accepted definition for comfort is 'freedom from pain and from discomfort as a neutral state'.[2]

Smith[3] pointed out that there are two major types of discomfort sensation: psychological discomfort, when the clothing we are wearing is inappropriate for us personally or for an occasion; and physiological discomfort, when the body feels uncomfortable, as for example when we feel too cold, feel itchy, or the garment is too tight. The psychological comfort depends on the aesthetic appearance of the garment. Psychological factors affecting comfort include color, flattering garment style, proper fit, fashion, suitability for an occasion, and prejudice. A consumer looks at a garment to see if it is the right style, if it is fashionable or traditional, and whether it will be flattering. Decisions are being made on whether the fabric color or print design is acceptable. A garment that is the latest fashion or is in some other way aesthetically appealing, may give the wearer the mental comfort of looking at his or her best. The status of the wearer is also

enhanced by a well-fitting and luxurious garment. An elegant designer gown, a new fur coat, or even the latest brand of jeans, can all confer status on the wearer and thus increase the satisfaction, hence mental comfort, of someone fortunate enough to own such a desirable object. Past experience of fabrics and garment styles also influences the wearer's feeling about the garment.

Physiological discomfort results from thermo-physiological and sensorial aspects. Thermo-physiological reactions include feelings from the temperature of the environment, and the effect of transport of perspiration. Humans must maintain an internal body temperature close to 99.6 °F (37 °C). A rise or fall in this 'core' temperature of up to 9 °F (5 °C) is usually fatal. The body constantly generates heat from the metabolism of food and muscle activity and loses this heat to the environment. A balance must be maintained between the rates of heat production and heat loss. The body is in a state of comfort when the skin temperature is 33–35 °C. The body maintains its comfort state by evaporating moisture to cause cooling when the external temperature or activity increases. A primary function of a garment is to act as a buffer against these environmental changes and to allow the skin to remain free of liquid water. Hatch has given a detailed description about the thermo–moisture interaction between the human body and the environment.[2]

The sensorial discomfort domain includes the feeling of the fabric next to the skin, allergic reaction, abrasion of the skin, tickle, prickle, wet fabric clinginess, and initial cold feel of fabric. Most of the work on clothing discomfort up until now has concentrated on thermo-physiological comfort, of which a researchable level of understanding and background information has been obtained. However, the amount of research work that has been carried out on 'sensorial' discomfort of clothing is very small, although the type of skin sensations produced by next-to-skin apparel are a major factor in determining the overall comfort of a garment. Pressure exerted on the body from garments is also a critical factor causing uncomfortable feelings. In biomechanical engineering design, sensory evaluation of clothing is based on next-to-skin sensorial comfort and pressure comfort.

9.1.1 Sensorial and pressure comfort

Sensory perceptions

As clothing is in direct contact with the human body, it interacts with the body continuously and dynamically during wear and this stimulates mechanical and thermal sensations. Sensorial discomfort, what the fabric/garment feels like when it is worn next to the skin, has been a neglected area. It is

unquestionably a very difficult quantity to assess and define scientifically. The human body is separated from the external environment by the skin, which has a very complex structure. The skin has two layers: the epidermis and the dermis. The epidermis is the outer layer, consisting of several layers of dead cells on top of a single living cell. The dermis is the inner layer, containing most of the nerve endings in the skin. Under the dermis are layers of connective tissue and fat cells.

The various sensations that result from the interaction of skin with fabric are triggered by sensory receptors in the skin. There are three types of sensory receptors, thermo-receptors, mechanoreceptors and nociceptors, and these cover all sensations: the pain group, the touch group of pressure and vibration, and the thermal group of warmth and coolness.

The two types of thermo-receptors are cold receptors and warm receptors. These can respond to both constant and fluctuating skin temperatures. The cold receptors have a peak sensitivity at around 25–30 °C, and the warm receptors have a peak sensitivity at around 39–40 °C.[4] When a fabric is placed on the skin surface, there is a momentary sensation of warmness or coolness due to the apparent difference between the temperature of the fiber and the temperature of the skin. In this case, the thermo-receptors are triggered.

There are two groups of mechanoreceptors: encapsulated receptors, including Pacinian corpuscles, Meissner corpuscles, Krause endings and Ruffini endings, which are all innervated by fast-conducting myelinated fibers; and receptors having an organized and distinctive morphology such as the hair follicle receptors and Merkle discs.[5] Each mechanoreceptor has a distinctive range of properties that enable it to receive and respond to a particular parameter of a mechanical stimulus.

Nociceptors respond to noxious stimuli such as heating the skin, strong pressure, or contact with sharp or damaging objects. These receptors have relatively high thresholds, functioning as warnings of potential damage.

Recent researches in conscious humans by recording directly from single nerve fibers in peripheral nerves have confirmed that isolated activation of an individual sensory receptor can result in distinct sensory perceptions. For instance, Meissner corpuscles cause touch sensation, Merkle receptors generate pressure, and nociceptors evoke pain. The encoding of specific sensory information is begun by these sensory receptors in the skin, and is further passed through neural pathways to the brain to formulate sensation.

Perception of sensations due to mechanical stimuli

Touch and pressure: Any point on our body's surface can evoke the sensation of touch, and our sensitivity of touch varies greatly from one region of

the body to another. Even within a relatively small area of the skin, say the leg, dramatic variations of thresholds are observed. For example, in the lower limb, the highest pressure threshold is at the hallux, and going upward, the threshold decreases. Some researchers have found that even at the same level, for example, the calf, the pressure threshold at the front is higher than that at the back.[6]

Due to the mechanical interaction between fabric and skin during wear, clothing exerts pressure and dynamic mechanical stimulation to the skin that will, in turn, trigger various mechanoreceptors and generate a variety of touch sensations. It further induces subjective perceptions and relevant pressure discomfort, or more serious pain sensations. At times, such discomfort may lead to life-changing consequences. Continuous high pressure may put a person at high risk of the development of various tissue lesions, such as pressure sores and ulcers.[7]

Prickle, itch, and inflammation: Prickle is a sensation caused by coarse and stiff fibers protruding from the fabric surface. It results from the stimulation of the pain group of sensory receptors. The degree of discomfort caused by prickle varies person-to-person and with the wear situation. Itch is a sensation that has been shown to result from the activation of some superficial skin pain receptors. The pain receptors responsible for itch may be of a different type from those responsible for the prickling sensation. Inflammation occurs in a small proportion of the population as a consequence of prickle and itch, resulting in mechanical stimulation of skin pain receptors, most likely through a mechanism termed axon reflex.

Roughness and scratchiness: The sensations of roughness and scratchiness are related to surface geometry, and are perceived when a fabric moves across the skin. During wear, a fabric moves across the underlying skin and friction resisting that movement forces the skin to displace. The skin displacement stimulates the touch group of sensory receptors. As more of the skin is displaced under the fabric moving across it, the perception of fabric roughness becomes greater. The frictional force is related to the roughness of the fabric. High friction makes skin abrasion more likely.

9.1.2 Factors affecting tactile-pressure comfort

The mechanical interaction between clothing and the body consists of two aspects: the local feel of the fabric against skin and the global feeling about the garment. The local feel, also regarded as ‘tactile comfort’, includes prickliness, itchiness, and roughness. The global feeling, relating more to ‘pressure comfort’, includes heaviness and tightness.

Fabric prickliness, itchiness, and roughness

Prickliness: Fabric-evoked prickle has been identified as one of the most irritating discomfort sensations for garments worn next-to-skin. Individual protruding fiber ends from a fabric are responsible for triggering the pain nerve endings when contacting the skin. Summation of responses from a group of pain nerves seems necessary for the perception of prickle sensations. Garnsworthy *et al*.[8] found that the intensity of fabric prickle perception is a function of the density of high load-bearing fiber ends at the fabric surface and the area of contact between the fabric and skin, indicating that both fiber mechanical properties and fabric surface features are important factors determining fabric-evoked sensations. Matsudaira *et al*.[9] compared three techniques for objective measurement of fabric prickle: low-pressure compression testing, laser-counting of protruding fibers, and a modified audio-pickup method. Through the comparison, they found that the third technique was the most effective and the measured mean force per contact correlated well with the subjective perception of fabric prickle. The two classic models, a load cantilever and an Euler column, were used to calculate the pointing force and the critical buckling load of the protruding fiber, which have been identified as the stimuli responsible for triggering the pain receptors. Buckling load can be expressed as: $P_E = \pi^2(EI/4l^2)$, where E is the Young's modulus of the fiber; I is the moment of inertia; and l is the length of the protruding fiber ends. The equation clearly shows that the Young's modulus, diameter, and length of the fiber are the key factors determining fabric prickliness.

Veitch and Naylor[10] also studied the mechanics of fiber buckling in the fabric prickling process, and concluded that the short fiber protruding ends obey Euler's simple buckling theory.

In their investigation into the influence of fabric mechanical properties on the discomfort sensations in wear, Li and Keighley[11] found that fabric prickle sensation was positively correlated with fiber diameter, fabric thickness at low loading, and fabric surface roughness.

Itchiness: Both prickliness and itchiness have been classified as tactile sensory factors. In a number of psychological wear trials, it was found that the perception of itchiness in clothing was highly correlated with the perception of prickliness. Therefore, it could be expected that the factors influencing fabric prickle would affect fabric itchiness as well. Comparing the subjective ratings of itchiness obtained from wear trials with the mechanical properties measured objectively, Li[12] found that the perception of itchiness correlated with fiber diameter, fabric thickness at low and high pressures, and fabric surface roughness.

Roughness: Behmann[13] reported a study on the perception of roughness and textile construction parameters. Roughness was defined as the irregularities in the surface that can be described geometrically by size or mechanically by friction coefficients, and a roughness model was built. A series of subjective perception trials were conducted using single nylon filament woven and knitted fabrics. The author concluded that the perception of roughness was determined by the roughness spacing.

Through comparison between the subjective sensory responses from wear trials with objective measured mechanical properties, Li[12] found that the perception of roughness correlated with fabric surface roughness (mean surface roughness coefficient, and deviation of surface roughness coefficient), compression properties (fabric thickness at high and low pressures, and energy of the compression-thickness curve), fiber diameter and fiber tensile properties (breaking load and elongation), and fabric tensile properties (maximum tensile elongation, elongation recovery load).

Hu and Newton[14] reported that fabric smoothness is related to fabric thickness at low pressure, geometric roughness, bending rigidity, linearity of the compression thickness curve, energy in extending the fabric to 5 N/cm, area density, hysteresis of bending moment, and energy in compressing the fabric under a pressure of 5 kPa.

In summarizing the findings from the literature, Bishop[15] showed that perception of fabric roughness is associated with a number of physical properties objectively measured, such as roughness, friction, prickle, shear and bend stiffness, thickness, and area density.

Garment weight, size and fit

Garment weight is a factor affecting our overall feeling about the garment. If it is too heavy, we can be aware of it as a burden. Since the area of the body supporting the garment is usually small, the pressure generated by the weight on the skin may be above the comfort level. The discomfort can become serious after a period of wearing, especially during walking or sports activity. However, if a garment is too light, it may be easily moved by the wind while walking. The fluttering is not always a pleasant feeling.

Denton[16] pointed out that there is a large difference between the weight of the clothes worn by women and those worn by men; even making an allowance for differences in average body dimensions, men wear heavier clothes than do women. Garment weight depends on the amount of fiber in the garment. In the past, clothes were necessarily heavy, particularly in winter. However, they have now benefited from the advance of the lightweight warmth technique. Sheer weight of outdoor clothing nowadays need not be an important comfort factor.

Slater pointed out that an important aspect of comfort, which is not strictly a textile problem but rather a clothing one, is that of size and fit.[17] When we first put on a garment, before being aware of the feel against skin, we certainly realize if it is too tight or too loose. Thus, no matter how well a fabric is engineered to have optimum values of heat–moisture transfer and feel against skin, any garment made from it cannot be regarded as comfortable if it does not fit properly. There are two distinct factors evident in a determination of whether the fit is good or not. The first one is a subjective one, depending on whether the wearer achieves psychological satisfaction from the garment. Another factor is a physical or physiological one, concerning the conditions of mechanical contact between garment and body. A badly fitting garment can result in high contact pressure concentrating on some regions of body surface, which can restrict cardiovascular flow, cause skin abrasion, cause pressure sores, induce irritation and so on. To achieve correct size selection and hence good fit, proper correspondence between an accurate anthropometric system and a good garment-sizing system needs to be established. Some research has been carried out.[18]

Another aspect affecting fit comfort can be construction factors. The principles of ergonomics are taken into account in clothing design[17] for various specific occupational uses, as well as for handicapped people. For many types of garment items, such as underwear, tights, and socks, variations of construction are designed to improve garment fit.[17] Dimensional change such as shrinkage also needs be taken into account in size selection.

Fabric stretch and body movement

People must be able to move around in the apparel items they wear. Discomfort may result when a fabric restrains movement, or exerts pressure on the body. Denton[16] pointed out that ease of movement is largely dependent on garment design and the relative size between body and clothing. Loose fitting allows freedom of movement but may not be desirable in many situations. Tight fitting may be suitable for certain end-uses, but can exert pressure on localized areas of the body surface and cause discomfort.

When people move, their skin, as a highly elastic material, stretches – it elongates and recovers. As the skin loses elasticity with age, it wrinkles and sags. The critical strain areas of the body are the knee, the seat, the back, and the elbows.[2] Kirk and Ibrahim's[19] study showed that the skin has a high level of two-way stretch and that differences in the percentages of skin stretch are small between men and women. Fabric placed close to the skin surface, especially in tight-fit garments, must

elongate to accommodate body movement and then recover. As elasticity is lost in a fabric, it bags and sags. Kirk and Ibrahim[19] examined the relationship between fabric extensibility and anthropometric requirements of garments. In analyzing the anthropometric kinematics, the authors identified three essential components to meet the skin strain requirements: garment fit, garment slip, and fabric stretch. Garment fit provides the space allowance for skin strain, which is determined by the ratio of garment size and the construction of garment design. Garment slip, influenced mainly by the coefficient of friction between skin and fabric, and between different layers of garments, is another mechanism for a garment to accommodate skin strain. Fabric stretch is the ability of a fabric to extend when a pulling force is applied and then to recover relatively quickly and fully to its original dimensions when the pulling force is removed.

Whether a garment slips or stretches is dependent on the balance of the tensile forces in the fabric and the frictional forces between skin and fabric. If the fabric has a low resistance to stretch and high friction against the skin or fabric, it tends to stretch rather than slip. The opposite is true if the fabric has low friction and high tensile resistance. If the fabric has both high friction resistance and stretch resistance, high clothing pressure is likely to be exerted on the body, which will result in discomfort sensations.

Fabric stretch is an important factor for pressure comfort. If a fabric exhibits more than 15% elongation, it is referred to as a stretch fabric. Use of stretch fabrics that can expand and contract without bucking or wrinkling is another way to fit the body shape. Fabrics exhibiting 15–30% elongation, which meets the requirements of many garments of various end-uses, are referred to as comfort stretch fabrics. These fabrics provide closer-fitting garments by reducing resistance to body movements, particularly around the elbows, knees, back, and seat. Power stretch fabrics have greater extensibility (30–200%) than comfort stretch fabrics, plus the ability to firm and shape body flesh. Body shaping results from compressive pressure of the fabric on the skin, which is useful in swimwear, foundation garments, stretch ski-pants, and active sportswear.

Kirk and Ibrahim[19] investigated the relationship between the pressure exerted on the body and fabric stretch level. The pressure, P, was calculated according to the following equation:

$$P = T_H/R_H + T_V/R_V,$$

where T is the tensile stress measured on an Instron tensile machine at the same level of the strain in the garment, and R is the radius of curvature of the relevant body part; the subscripts H and V indicate horizontal and vertical directions, respectively.

9.1.3 Assessment of sensorial comfort

There is only one accurate method of assessing fabric or garment comfort – wearer-trials. However, wearer-trials are an expensive and time-consuming method of testing a product. The most practical method of textile product assessment, therefore, is to use physical tests that are specially designed to measure a certain property of the fabric or garment that is known to influence a discomfort sensation. In many cases, more than one physical property contributes to producing the sensation, so a weighting factor to indicate the significance of each property has to be applied to the final analysis of results.

In an attempt to establish the relationship between subjective comfort perceptions and fabric properties, Li carried out a series of wear-trials in which three fundamental sensory factors were identified as thermal–wet, tactile, and pressure comfort.[12] Using canonical correlation analysis, Li studied the predictability between ten physical factors, including five transport properties and five mechanical properties, and three psychological factors. It was found that the sensory factors were significantly related to the corresponding dimensions of the physical properties of the fabrics. The tactile comfort factor was mainly related to fabric roughness and fullness, fabric stiffness and wettability; the pressure comfort factor was closely correlated to fabric stiffness, fabric permeability, and fiber tensile stiffness; the thermal–wet comfort factor was related to fabric wettability, fabric roughness and fullness, and fabric water evaporation propensity.

Some researchers aimed to establish relationships between objective measurement and subjective evaluation of fabric sensorial properties.[15] Among them, evaluation of fabric hand (the quality of a fabric or yarn assessed by the reaction obtained from the sense of touch[20]) through fabric objective measurement, which has been developed on the basis of the work of Kawabata and his co-workers, has been recognized and used around the world. The primary measurements use particular expressions, including KOSHI (stiffness), NUMERI (smoothness), FUKURAMI (fullness), SHARI (crispness), HARI (anti-drape stiffness), SOFOTOSA (softness), KISHIMI (scroop), SHINAYAKASA (flexibility), and TEKASA (crepe-like). They developed the KES-F system, consisting of four instruments, to measure fabric tensile, shear, bending, compression, and friction and roughness. Kawabata used a piecewise linear regression procedure to develop his equation between subjective perception and the objective measurements for predicting primary hand values (HVs) in the form of linear and mixed linear–log functions.

Besides the physical tests on fabrics, physiological tests, not directly involving textiles, can also be carried out. They include evaluations of

lung function or efficiency, blood pressure, body mechanical efficiency, and so on.

9.2 Compression therapy

9.2.1 Pressure garments

Pressure treatment for wound care

Normal skin is made up of connective tissues in the dermis that form a three-dimensional mesh, or collagen fibers aligned parallel to the skin's surface. The skin applies pressure against its underlying layers. Under normal circumstances, the pressure that the skin puts upon the body ensures that injured skin is replaced in its original state without scarring. When burns destroy the skin and the papillary dermis, normal pressure by these layers no longer exists. Without this pressure, hypertrophic scars will form irregularly causing possible deformities. Scar tissue consists of young, actively growing cells, which readily respond to changes in stress and external pressure. Various external pressure techniques are used in the treatment of burn scars and contraction. A pressure garment is one of the conventional devices most commonly used by occupational therapists. Instead of skin, pressure garments prevent and control the formation of hypertrophic scars by applying counter pressure to the wounded area, hence reducing scarring and deformities.[21]

It is important that burn patients begin wearing pressure garments while the scar is active and immature. Scar tissue is highly responsive in the early stages so an early application of a pressure garment is imperative. As soon as the wound has healed, wearing of the pressure garment may commence. They are worn continuously, night and day, except for short periods of personal hygiene, until the scar is mature. The length of time required for wearing the garment varies from several weeks up to more than two years, depending on the severity of the injury. The continuous wearing of pressure garments prevents the thickening, buckling, and nodular formations seen in hypertrophic scars. The external pressure applied by the garment decreases inflammatory response and the amount of blood in the scar, reducing itching and preventing collagen from synthesizing. Additionally, pressure garments provide protection against further injury.

Classification and functional requirements of pressure garments

According to the materials, pressure garments are classified into two types: garments made from firm elastic fabric containing Spandex (mainly warp knit powernet or sleeknit) and garments made in 'Tubigrip', a weft knit cotton elastic material containing horizontal rubber yarn, manufactured in

tubular lengths of different diameters.[22] Many doctors and therapists have found that the Spandex garments offer firmer pressure and last longer, whereas 'Tubigrip' garments have greater stretch tolerance and require fewer measurements for proper fitting, which makes them more suitable for the initial stages of treatment.[22]

Pressure garments are either made available as ready-to-wear garments, or manufactured according to the individual measurements of the patient. Ready-to-wear garments are made both in Spandex materials and in Tubigrip. They are generally used for preliminary treatment before custom-made garments can be available. Made-to-measure garments are constructed from Spandex materials in the main. They provide each individual patient with the correct continuous pressure over the scar area, regardless of size or shape and are thus advantageous in conforming precisely and comfortably to the contours of the patient's body, providing maximum benefit.

Early research work revealed that the assessment of the hypertrophic scar relative to the fitting of the pressure garment is subjective, since there is no widely available objective method for measurement of the pressure at the garment–scar interface.[22] The pressure exerted by pressure garments depends on three aspects: shape of the body parts; type and age of the fabric used; and design and fit of the garment.[21] The shape of the underlying body contours is an important influence because the greater the degree of curvature, the greater the pressure exerted. This indicates that it is easier to apply pressure to certain body parts, such as the limbs, rather than to less rounded areas such as the chest wall, pectoral and facial areas. Pressure garments made of different types of fabrics result in pressures of various values on body. The constant stretching and re-stretching of the fabric will eventually wear down the elasticity of the pressure garment and cause it to lose its ability to exert the correct pressure. Even though a pressure garment should be tightly fitted for medical treatment purposes, it should be designed in such a way that it is not too difficult for the patient to put on or take off.

Requirements of pressure garments are based on two aspects: clinical effectiveness and comfort in wear. For clinical effectiveness, a tightly fitting garment made of compressive elastic fabric is necessary to produce the required pressure over the scarred area, and the pressure should be capable of being maintained over a prolonged period of time. However, the acceptability to patients depends on patient mobility, contact and pressure comfort, and ease of wear. Patients are not willing to put on something that will restrict their movements and affect their daily activities. If the pressure values are higher than the patients' pressure pain thresholds, they cannot accept the garments. All these factors are related to the garment materials and design. From the view of mechanical properties,

there are the following requirements for the fabric material. The fabric should be soft and elastic, causing no irritation to the skin, and should fit the body contours like a second skin. It should also be smooth and cause no abrasion to the skin, especially during body movement. It should be easy-care and washable, and its properties should be maintained after multiple washings. With the reference to the manufacturing process, the fabric should be easy to tailor and sew. Both the fabric and the sewing method selected should be strong enough to resist the daily wear and tear.

9.2.2 Compression bandages and stockings

Compression therapy for venous and lymphatic disorders

For over 150 years, external compression therapy (CT) has been used as a treatment for venous and lymphatic disorders, such as deep vein thrombosis (DVT) and superficial phlebitis, as well as in chronic conditions such as chronic venous insufficiency (CVI), gravitational dermatitis, lipodermatosclerosis, leg ulcers and lymph-edema.[23,24] Further indications include thromboembolic prevention and edema prevention in pregnancy, long and microgravity flights, and softening of burns scars. Compression may be achieved by different modalities such as various bandages, wrapped dressings, legging orthosis, and compression stockings. Among them, compression stockings come into our daily life and a wide range of them is commercially available. The mechanism of action of compression therapy remains unclear and is probably multi-factorial. Many hypotheses have been advanced to explain the beneficial effect of compression by stockings, and these have been classified as follows:[24]

Venous: May achieve narrowing of veins, restoration of valvular competence, partial regression of parietal degenerative changes, reduction or suppression of superficial and deep venous reflux, diminution of venous pressure, acceleration of venous flow, improvement of venous pumping, diminution of venous pool, and blood shift into the central compartment.

Arterial: May reduce cutaneous arterial perfusion in a first step, then, paradoxally, improve arterial flow as a result of edema reduction.

Lymphatic: May improve lymphatic function and drainage.

Microcirculatory: May decrease edema, acceleration of capillary blood flow and inflammatory mediators.

Tissular: May increase intra-tissular pression and edema resorption, and decrease protein tissular concentration softening of lipodermetosclerosis.

Hematological: May enhance fibrinolysis.

Bio-functional requirement and classification

The two major compression modalities made of textile materials are bandages and compression stockings.

Compression bandages: There are two main types of bandages: inelastic or short-stretch bandages, and long-stretch elastic bandages. Inelastic bandages exert passive compression and are recommended in the treatment of edema, deep vein thrombosis, or trophic lesions of chronic venous insufficiency (CVI). Long-stretch elastic bandages are much easier to use. Their high resting pressure effectively compresses superficial veins after surgery, sclerotherapy, or thrombophlebitis. There are also some other bandages including four-layer bandages, adhesive dressings, zinc-coated bandages, and cohesive bandages.[24] Four-layer bandages consist of four superimposed layers: (1) padding with orthopaedic wool, absorbing exudates and protecting bony prominences; (2) cotton crepe bandage, holding the former in place; (3) long stretch elastic bandage; and (4) cohesive bandage, strengthening support and holding it all in place. The four-layer bandage provides permanent pressure to the leg in patients with CVI, in particular with leg ulcers.

Compression stockings: Compression stockings may be designed to apply graduated or uniform compression. Graduated compression refers to the application of varying degrees of constant compression to different segments of the leg, with pressure being greatest at the ankle and gradually decreasing proximally. Uniform compression aims to deliver a similar degree of pressure to the whole leg. Graduated compression has been the favoured option since Sigel *et al.*[25] demonstrated small but consistent increases in velocity of flow in the common femoral vein compared with that obtained from uniform compression. Graduated Compression Stockings (GCSs) can enhance venous return and reduce stasis by providing graded compression with the greater pressure applied more distally, as illustrated in Fig. 9.1.

Compression stockings can be further classified into two major types. One is leg-shaped, flat-knitted with a seam. The form of the stocking is achieved by changing the number of needles. This type of stocking can be made tailor-sized, and allows increase and decrease in the number of stitches for each row. Hence, the tension of the threads may not change while the circumference changes. The other type is round-knitted and is seamless. For this type of stocking, the only possibility to form the stocking is by varying the tightness of courses and the tension of the threads.

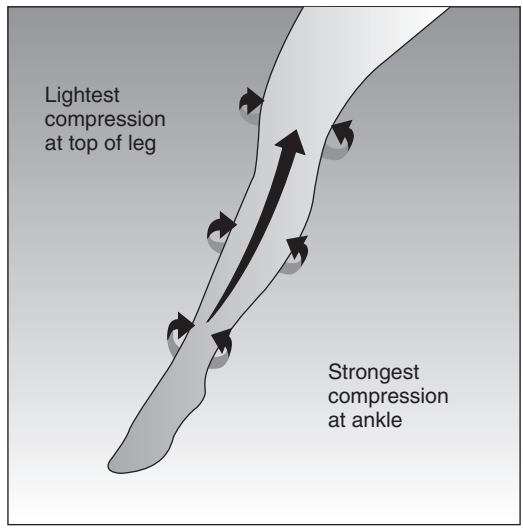

9.1 Graduated compression stocking (GCS).

9.3 Conclusion

In this chapter, the wearing comfort of clothing and compression therapy using textile devices has been discussed. For clothing comfort, the tactile-pressure comfort, which has been an ignored research area but is related directly to mechanical interaction between the human body and clothing, was focused upon. The main factors affecting tactile-pressure comfort include the surface properties of fabrics, garment fit and size, fabric stretch and body movement.

Pressure garments, and compression bandages and stockings, are the major clothing items used for wound care and various venous disorders. The functional requirements and classifications of these devices were also briefly introduced.

9.4 Acknowledgement

We would like to thank Hong Kong Polytechnic University for funding this research through the projects A188 and G-YD31.

9.5 References

1. Slater, K., *Human Comfort*, Thomas Springfield: USA.
2. Hatch, K.L., Chapter 3, Comfort, in *Textile Science*. 1993, West Publishing.
3. Smith, J.E., The Comfort of Clothing. Textiles, 1986. **15**(1): p. 23–27.
4. Iggo, A., Sensory Receptors, in *Sensory Systems II: Senses other than Vision*. 1988, Birkhauser: Boston, USA.

5. Coren, S., Ward, L.M. and Ward, E.J.T., Chapter 7, Taste, Smell, Touch, and Pain, in Sensation and Perception. 2004, John Wiley, p. 179–215.
6. Nakahashi, M. *et al.*, Effect of Clothing Pressure on Front and Back of Lower Leg on Compressive Feeling, in *Journal of the Japan Research Association for Textile End-Uses*. 1999. p. 661–668.
7. Phillips, P., Evans, A. and Popplewell, P., Diabetic Foot Ulcers, A Guide to Treatment. *American Journal of Clinical Dermatology*, 2000. **1**(2): p. 117–123.
8. Garnsworthy, R.K., Gully, R.L. *et al.*, Understanding the Causes of Prickle and Itch from the Skin Contact of Fabrics. *Australian Textiles*, 1988. **8**: p. 26–29.
9. Matsudaira, M., Watt, J.D. and Carnaby, G.A., Measurement of the Surface Prickle of Fabrics, Part I: The Evaluation of Potential Objective Methods. *The Journal of Textile Institute*, 1990. **81**: p. 288–299.
10. Veitch, C.J. and Naylor, G.R.S., The Mechanics of Fiber Buckling in Relation to Fabric-evoked Prickle. *Wool Technology, Sheep Breeding*, 1992. **40**: p. 31–34.
11. Li, Y. and Keighley, J., Relations Between Fiber, Yarn, Fabric Mechanical Properties, and Subjective Sensory Responses in Wear Trials, in *The 3rd International Conference on Ergonomics*. 1988. Helsinki, Finland.
12. Li, Y., *The Objective Assessment of Comfort of Knitted Sportwear in Relationship to Psycho-physiological Sensory Studies*, 1988 Dept. of Textile Industries. The University of Leeds: Leeds.
13. Behmann, F.W., Tests on the Roughness of Textile Surfaces. *Melliand Text.*, 1990. **71**: p. 438–440.
14. Hu, J.L. and Newton, A., A Psychophysical Model for Objective Hand Evaluation: An Application of Steven's Law. *Journal of the Textile Institute*, 1993. **84**: p. 354–363.
15. Bishop, D.P., Fabrics: Sensory and Mechanical Properties. *Textile Progress*, 1996. **26**(3): p. 5–26.
16. Denton, M.J., Fit, Stretch, and Comfort. *Textiles*, 1972. **1**(1): p. 12–17.
17. Slater, K., Comfort Properties of Textiles. *Textile Progress*, 1977. **9**.
18. Fan, J., Yu, W. and Hunfer, L., *Clothing Appearance and Fit*. 2004: Woodhead Publishing Ltd: Cambridge, UK.
19. Kirk, W.J. and Ibrahim, S.M., Fundamental Relationship of Fabric Extensibility to Anthropometric Requirements and Garment Performance. *Textile Research Journal*, 1966. **57**: p. 37–47.
20. McIntyre, J.E. and Damels, P.N., *Textile Terms and Definitions*. 1995, The Textile Institute: Manchester.
21. Pratt, J. and West, G., Chapter 1: Pressure Therapy: History and Rationale, in *Pressure Garments, A Manual on Their Design & Fabrication*. 1995, Butterworth-Heinemann Ltd: Oxford. p. 1–21.
22. Ng-Yip, F.S.F., Medical Clothing. *International Journal of Clothing Science and Technology*, 1993. **5**(1): p. 17–24.
23. Hamilton, O.A.G. and Baker, D., Graduated Compression Stockings in the Prevention of Venous Thromboembolism, in *British Journal of Surgery*. 1999. p. 922–1004.
24. Ramelet, A.A., Compression Therapy, *Dermatologic Surgery*. 2002. p. 6–10.
25. Sigel, B. *et al.*, Type of Compression for Reducing Venous Stasis, *Archives of Surgery*. 1975. p. 171–175.

Part III

Material properties

10
Fibers

X-Q. DAI
Soochow University, China

10.1 Textile fibers

A fiber is a unit of matter with an extremely small diameter and a length at least 100 times longer than its width. There are many fibrous substances. Fibers, that are too fine or too short are difficult to process into yarn. And if they are too coarse and thick, they are uncomfortable if worn next to the skin. Therefore, only the fibers having a minimum length (about ½ inch, or 15 millimeters) and a width range (0.0004 – 0.002 inch, or 10–50 micrometers) can be used as textile materials. Historically, natural fibers were the first textile fibers.

10.1.1 Natural fibers

Wool

Wool refers to fibers from sheep, goats, camels, oxen, and fur-bearing animals. Wool was one of the first fibers to be spun into yarn and woven into fabric. Wool fibers are composed of a protein polymer called keratin. A wool fiber is generally crimped three dimensionally. The crimp ranges from 4 to 10 crimps/cm. The fiber length of wool used for apparel products ranges from 5 to 12 cm and size varies from 14 to 45 μm.

Sheep's wool is the most important type of wool fiber because it is the most plentiful. Specialty wool fibers from the hair of the camel, alpaca, llama, and vicuna are more costly than sheep's wool. Wool is used in both woven and knitted fabrics. The fabrics drape well and are durable; and are used primarily in luxury sweaters, coats, and suits. They are comfortable under a variety of conditions and retain their good looks during wear and care.

Silk

Silk is a fine, strong, continuous filament produced by the larva of certain insects, especially the silkworm, when constructing their cocoons. It is a

natural protein fiber composed of fibroin. Early in 2640 BC, the ancient Chinese learned how to reel the silk and make it into fabric. The silk industry was then monopolized by China for over 3000 years. Today, major producers of silk are China, India and Japan. There are two main types of silk fiber, cultivated and wild. They differ in diameter, cross-sectional shape, and fine structure. The most important commercial silk is cultivated. Silk is the only natural filament fiber. It is linear. Its length may be up to 600 m, but generally averages 300 m. Silk has a very fine diameter of 12–30 μm.

The beauty and hand of silk and its high cost make is known as a luxury fiber. It remains an important fiber in fashion designers' collections. Silk is extremely versatile and can be used to create a variety of fabrics from sheer, gossamer chiffons to heavy, beautiful brocades and velvets. Silk underwear, socks, and leggings are also popular due to silk's soft hand and other comfortable physical properties.

Cotton

Cotton is a seed hair obtained from the boll of the cotton plant. It is a natural cellulosic fiber composed of polymers forming a highly crystalline structure with numerous strong hydrogen bonds. Cotton cloth was used by the people of ancient China, Egypt, India, Mexico and Peru. Today, cotton is the most important apparel fiber. There are also many varieties of cotton fibers differing in staple, length, diameter and so on. The terms 'Pima', 'Egyptian', and 'Sea island' denote the most commonly used cotton fibers. The staple lengths of cotton range from 0.32 to 6.35 cm, and those of 2.22–3.18 cm are used as textile materials. The diameter of cotton ranges from 12 to 20 μm. The microscopic appearance of cotton fiber is a flat, twisted ribbon in the longitudinal direction, and its cross-section shows a kidney-bean shape. Cotton fabrics are used where comfort is of primary importance and appearance retention is not as important, or where a more casual fabric is acceptable. Cotton is often mixed with other fibers to improve its durability and appearance retention; blends of 60 percent or 70 percent cotton are usual.

Flax and ramie

Flax fiber is obtained from the inner bark of the stem of a plant grown in temperate and subtropical regions of the world. It is a natural, cellulosic, multi-cellular bast fiber. Flax fiber is 10–100 cm in length. Its diameter varies from 40 to 80 μm. Flax is stronger than cotton as its polymers lie almost parallel to the fiber axis. Flax is one of the oldest textile fibers. Fabric made from flax is called linen. Remnants of linen were found among the remains

of the Swiss Lake Dwellers, who lived in 8000 BC; linen mummy cloths more than 3000 years old have been found in Egyptian tombs. Actually, the linen industry flourished in Europe until the 18th century. However, with the invention of power spinning, cotton replaced flax as the most important and widely-used fiber. Today, flax is a prestige fiber as a result of its limited production and relatively high cost. Apparel made of linen is usually designed for warm weather use, high fashion aspects, or professional wear.

Ramie is another common bast fiber. It has been used for several thousand years in China. The ramie plant is a tall perennial shrub from the nettle family that requires a hot, humid climate for growth. It grows primarily in China, the Philippines, and Brazil. Ramie fiber is longer than 150 cm. It is a coarse fiber with a fiber size of 4.6–6.4 denier. Ramie fiber is used in a wide variety of apparel items: sweaters, shirts, blouses, and suits. It is often in blends, particularly with cotton or wool.

10.1.2 Regenerated fibers

Regenerated fibers are manufactured cellulosic fibers. These polymers do not naturally occur as fibers; processing is carried out to convert them into fiber form.

Rayon

Rayon was the first manufactured cellulosic fiber. The development of rayon fiber can be traced back to 1664, when the English physicist Robert Hooke suggested it might be possible to spin artificial filaments from a cellulosic gummy substance resembling the secretion of silkworms. In the next two centuries, several inquisitive scientists tried numerous methods to produce an 'artificial' silk. In 1884 in France, Count Hilaire de Chardonnet, called the 'father of rayon', made the first practical commercial production of rayon fiber. After that, various manufacturing processes were developed for its production.

Rayon fiber is available as filament, staple, and tow. Most rayon is used in staple form. Normally, rayon fibers range from 1.5 to 15 deniers. Observed under a microscope, a regular viscose rayon fiber shows a striated surface and a serrated cross-section. Rayon fiber is a manufactured fiber composed of 100% regenerated cellulose, or regenerated cellulose in which chemical substituents have replaced not more than 15% of the hydrogens of the hydroxyl groups. Rayon fiber is soft, comfortable and versatile. It is mostly used in woven fabrics, which have a unique drape that designers love. It is also used in non-woven fabrics.

Acetate

Acetate is another manufactured cellulosic fiber made from the same raw material as rayon, cellulose, but by a different manufacturing process involving a greater degree of chemical modification. Acetate is available as staple or filament. Observed under a microscope, an acetate fiber shows a striated surface and a lobed cross-section. The appearance of acetate fiber is very similar to that of silk: bright, shiny, and smooth to the eye and hand. The low cost and good draping qualities of acetate make it a valuable and beautiful fiber. An important use of acetate is as a lining fabric; another one is in robes and loungewear. Acetate and also rayon are the two oldest manufactured fibers and have been produced in large quantities, filling an important need for low cost fibers in the textile industry.

10.1.3 Synthetic fibers

Synthetic fibers are non-cellulosic manufactured fibers. In producing synthetic fibers, the fiber-forming compounds must be made from basic raw materials (monomers) by a polymerization process. Different chemical compounds are used as the raw materials to make the polymers for nylon, olefin, and acrylic polymers.

Nylon

Nylon was the first synthetic fiber. It was developed by the Du Pont Company in 1939. Nylon is a manufactured fiber in which the fiber-forming substance is any long-chain synthetic polyamide in which less than 85% of the amide linkages are attached to two aromatic rings. Nylon fiber is highly crystalline, oriented, and strongly hydrogen bonded between two types of polar groups in both the crystalline and amorphous areas. So it is very strong, tough and flexible. Nylon is available in multifilament, monofilament, staple, and tow in a wide range of deniers and shapes. There are many variants of the two commonest types of nylon, nylon 6 and nylon 6,6, altering in fiber denier, cross-section and crimp.

Today, nylon is very successful in hosiery and in knitted-filament fabrics such as tricot and jersey, because of its smoothness, light weight, high strength, and good recovery after high elongation. Nylon is also used for lining fabrics in coats and jackets. These linings are more durable; however, their cost is greater than acetate fabrics. In the apparel markets, most nylon is used in filament form rather than staple.

Polyester

The first viable polyester fiber was produced in England by ICI, and it was introduced to the USA in 1951 by the Du Pont Company. Since then, polyesters have undergone significant research and development work. Today, polyester refers to manufactured fibers in which the fiber-forming substance is any long-chain polymer composed of at least 85% by weight of an ester of a substituted aromatic carboxylic acid, including but not restricted to substituted terephthalate units and parasubstituted hydroxybenzoate units.

Polyester is a highly crystalline and well-oriented fiber and its polymers are weakly hydrogen bonded. Therefore, polyester fibers have high tenacity and are highly resilient. At low stress, they have high elastic recovery; at high stress, particularly repeated high stress, they have low elastic recovery. Polyester fiber is smooth and even in diameter and its cross-section is nearly circular. Its diameter varies from 12 to 25 μm, depending on end-use requirements.

Polyester products are available as filament fiber, staple and tow fiber, fibrefill, and non-woven structures. Polyester filament yarns, as well as spun yarns blended with cotton or rayon, are widely used in woven fabric and knitted fabric. These fabrics are attractive, durable, comfortable (except in conditions of high temperature and humidity), retain their appearance well, and are easy care.

Acrylic

Acrylic is a manufactured fiber in which the fiber-forming substance is any long-chain synthetic polymer composed of at least 85% by weight of acrylonitrile units. The first example was made in Germany in 1893. Since then, many efforts had been made to produce improved acrylic fibers. Du Pont started commercial production of the fiber in 1950, and was a major producer for the next 40 years. Acrylic is often available as staple fiber and tow. For apparel products use, its size varies from 1.2 to 3.0 denier. Acrylic fibers are usually slightly crimped, and their cross-section can be dog-bone shaped, kidney-bean shaped, or round.

Acrylic fibers are soft, warm, lightweight, and resilient. Because of their low specific gravity and high-bulk properties, acrylic fibers more successfully duplicate the positive aesthetic attribute of wool fibers. They are superior to wool in their easy-care properties and are non-allergenic. Acrylics are widely used in sweaters, socks, fleece fabrics and fake-fur fabrics.

Polyolefin

Polyolefin fibers are made from polymerized ethylene or propylene. They were originally developed for soled (plastics) applications. Since 1960, polyolefines fibers have been produced for use in textiles, as monofilament, multifilament, staple fiber and tow. They are rod-shaped and smooth-surfaced. However, their cross-section can be modified easily. Polyolefins are the lightest-weight fibers (SG < 1.0). Today, they are used for thermal underwear, socks, sweaters, and active sportswear.

10.1.4 New developments in textile fibers

Despite the long history and maturity of fiber science, new processes, materials and products are still being developed today. Many new fibers with unique characteristics for special use have been developed. Here, some of them are introduced.

Elastomeric fibers

An elastomer is a natural or synthetic polymer that, at room temperature, can be stretched repeatedly to at least twice its original length, and upon immediate release of the stretch, will return to approximately its original length. Spandex and rubber are two major elastomeric fibers used in apparel. Rubber fibers are manufactured fibers in which the fibre-forming substance is comprised of natural or synthetic rubber. Rubber is rarely used as a bare filament; it is generally the core in a covered yarn.

The first synthetic elastic fiber, a spandex fiber called 'Lycra™', was produced Du Pont in 1958 after many years of research. Spandex fibers are superior to rubber in strength and durability. They are produced as monofilament or multifilament yarns in a variety of deniers. Spandex is seldom used alone in fabrics. Other fibers or yarns are added to achieve the desired hand and appearance. Spandex is mostly used in foundation garments, active sportswear, dancewear, hosiery, and narrow fabrics. It also has medical uses, such as surgical and support hose, bandages and surgical wraps (see Chapter 9).

Micro-fibers

One of the most important developments in textiles fibers has been the technology to extrude extremely fine filaments while maintaining all of the strength, uniformity and processing characteristics expected by textile manufacturers and consumers. Micro-fiber is defined as a fiber of less than 1.0 denier, so it is even finer than luxury natural fibers such as silk. It can

be extruded by reducing the polymer output at the spinneret and drawing with a large draw ratio. There are primarily three methods for micro-fiber production: direct spinning, mechanical splitting and solvent splitting.

Micro-fibers are available in two types: continuous filament and random staple. Their designed characteristics are extreme softness, high flexibility and smoothness. Their lower bending rigidity, high surface area and greater number of fibers per unit weight enable the production of fabrics that are softer, quicker drying and have greater cover and cooler hand.

High-performance fibers

High-performance fibers are driven by special technical functions that require specific physical properties unique to these fibers. They usually have very high levels of at least one of the following properties: tensile strength, operating temperature, limiting oxygen index (fire retardancy) and chemical resistance. Here, fibers with high mechanical performance are focused on. Meta-aramids are the most widely used specialized fibers, for their combination of heat resistance and strength at reasonable cost. Nomex from the Du Pont company and TeijinConex from the Teijin company are the well known meta-aramid fibers. Para-aramid fibers have similar operating temperatures to meta-aramid fibers, but have 3–7 times higher strength and modulus. 'Kevlar' (DuPont), 'Twaron' (Akzo) and 'Technora' (Teijin) are typical para-aramid fibers. They are ideal for reinforcement and protective type applications and usually are used in parachutes, bullet-proof vests, ballistic protective fabric, and cut-resistant fabric.

Carbon fiber can vary in both modulus and strength in large ranges depending on the raw material used and final heat treatment temperature. It is mainly utilized in specialized composites for the aerospace and similar industries.

Smart fibers

Shape-memory materials are able to memorize a second, permanent shape besides their actual, temporary shape. After application of an external stimulus, for example an increase in temperature, such a material can be transferred into its memorized, permanent shape. The process of programming and restoring a shape can be repeated several times. Shape memory polymers have been applied to textiles in fiber, film and foam forms, resulting in a range of high-performance fabrics and garments, especially sea-going garments.

There are also some smart fibers that are capable of measuring internal strain, temperature, humidity and so on. They can be made and integrated into textile structures such as yarns, fabrics and composites.

10.2 Structure parameters and measurement

10.2.1 Fine structure

Fine structure is a depiction of the arrangement of the polymers and the bonds that hold them together. The ability of a fiber to withstand mechanical forces is largely determined by its fine structure. Orientation and crystallinity are two major parameters to describe the fine structure of a fiber. Absorption of infra-red radiation, optical and X-ray diffraction studies, electron microscopy, and nuclear magnetic resonance are common methods used to investigate the fine structure of a fiber.

10.2.2 Fiber dimensions

Conditioning and testing of textile fibers must be carried out under constant standard atmospheric conditions. The standard atmosphere for textile testing involves a temperature of 20 ± 2 °C and a relative humidity of 65 ± 2%.

Size

There are a number of different ways of measuring fiber size/diameter, which differ fundamentally in their definitions of size, so that the measurements may not be easily inter-coverted. The gravimetric method is based on the relationship that for a given fiber its mass is proportional to its cross-sectional area. The fiber linear density is measured by weighing a fiber of a certain length on a balance. If the fiber has a circular cross-section, its diameter can then be calculated from the linear density. The projection microscope test (BS 2043) is the standard method for measuring wool fiber diameter, and is also applicable to any other fibers with a circular cross-section. A microscope slide of short lengths of fiber is prepared, and is then viewed using a microscope that projects an image of the fibers onto a horizontal screen for the diameter measurement.

The airflow method is an indirect method of measuring fiber fineness based on the fact that the airflow at a given pressure difference through a uniformly distributed mass of fibers is determined by the total surface area of the fibers.[1–5] The surface area of a fiber is proportional to its diameter but, for a given weight of sample, the number of fibers increases with the fiber fineness so that the specific surface area (area per unit weight) is inversely proportional to fiber diameter.[6] The airflow measurement is often used for wool and cotton fibers. The Shirley fineness and maturity tester (FMT) is also a kind of airflow method for cotton fiber.

The optical fiber diameter analyzer (OFDA)[7] is a microscope-based system which effectively automates the projection microscope. The system was originally developed for wool testing but is also capable of measuring other animal and man-made fibers. The CSIRO fiber diameter analyzer (FDA) is a non-microscopical system of measuring fiber diameter that operates by light scattering.[8,9]

In general, the finer the natural fiber size, the higher the quality of the fiber. Manufactured fibers are available in a wide range of sizes. They are classified as coarse (>7 dtex), regular (2.4–7.0 dtex), fine (1.0–2.4 dtex), micro (0.3–1.0 dtex), and ultra-fine (<0.3 dtex).

Length

The length of natural fibers is not constant but has a range of values. However, man-made fibers can be cut during production to whatever length is required, either with all the fibers of the same length or with a distribution of lengths. In the case of fibers with a distribution of lengths, a mean length is taken. There are two main types of methods to measure fiber length: the direct measurement of single fiber mainly for research purposes and tuft methods that involve preparing a tuft or bundle of fibers arranged paralleled to one another. The Wira fiber length machine is designed for direct measurement. It is an attempt to automate the process of single fiber measurement and is intended mainly for measuring wool fiber.[10] The comb sorter,[11,12] clamped tuft method,[13] Fibrograph,[14] Wira fiber diagram machine, and Almeter[15] are all for the tuft measurement. The comb sorter is used for cotton and wool measurement. The clamped tuft method, the Wira fiber diagram machine and the Almeter are for wool fiber measurement while the Fibrograph is an automatic method of measuring the fiber length of a cotton sample. Some image-based methods have also been developed for fiber length measurement.[16] The Fiber Quality Analyzer (FQA)[17,18] is an image processing system for investigating various fiber properties including length.

A trend in fiber measurement is that several existing instruments for various fiber parameter tests are integrated into a set of instruments, or new types of instruments are developed for measures covering many parameters of the fibers. These sets are known as High-Volume Instruments (HVI). The Spinlab system is one such system, which measures seven parameters of cotton fiber: fiber length, length uniformity, strength, elongation, micronaire, color and trash.[19] The Uster AFIS (Advanced Fibre Information System) is another typical system for single fiber testing covering the assessment of fiber length, fineness, maturity distribution and other dimensional parameters.

Cross-section shape

The shape of a fiber's cross-section is important in many applications. It has a considerable influence on bending stiffness and torsional stiffness of the fiber. Consider the bending stiffness of the solid fibers; those with round cross-sections offer a high resistance to bending and, hence the fibers are stiff. However, fibers with ribbon-like cross-sections, such as cotton, offer the least resistance to bending. The cross-section shape is usually observed under a microscope. Natural fibers usually have characteristic cross-sections determined by nature. The cross-sections of most manufactured fibers can be modified easily.

10.3 Fiber mechanical properties

10.3.1 Testing

Tensile

The stress–strain curve of a fiber is usually obtained by gradually extending it and measuring the tension corresponding to each increase in length. Because of the way in which the elongation and the breaking point of textile fibers varies with time, the method of stretching the specimen is an important factor in determining the results of the test. There are two different ways of carrying out tensile tests with regard to the way of stretching the specimen:

(i) Constant rate of extension (CRE), in which the rate of increase of specimen length is uniform with time and the load measuring mechanism moves a negligible distance with increasing load. The Instron Tensile Tester operates in this way.
(ii) Constant rate of loading (CRL), in which the rate of increase of the load is uniform with time and the specimen is free to extend, the elongation being dependent on the extension characteristics of the specimen at any applied load. The Krais instrument,[20] and the Scott IP testers[21] provide this method.

Universal testers are available in which the principles of constant rate of loading or constant rate of elongation can be used, either of the two modes being selected. The Cambridge Textile Extensometer is of this type.

Properties in various directions

Bending: There are few instruments developed for the bending test of a fiber. However, several approaches to measure bending have been described

in reference 22. A tensile tester can be modified for the measurement of flexural rigidity of coarse fibers. A fiber can also be formed into a circular loop for measuring the bending rigidity by studying the deformation of the loop under an applied load. By measuring the deflexion of filaments of short lengths, clamped at one end and loaded at the other, the bending rigidity can also be obtained. Fiber bending can also be measured dynamically. In this case, a bending stress–strain curve is obtained. Chapman's fiber-bending tester is a successful instrument for such a test.[23,24] The KES-FB2 bending tester, which was developed for a fabric bending test, can also be used to obtain a bending stress–strain curve for fibers.[25]

Torsion and shearing: Morton and Permanyer developed an apparatus to measure the torque–twist relation of a fiber.[26,27] Owen used a double-pendulum method to test the dynamic twisting.[28] By using KES-twist testing, a torque–twist curve can also be produced. Thus, the torsional rigidity can be obtained. It is difficult to measure directly the relation between shear stress and shear strain. The shear modulus is often calculated from the torque–twist curve.

Compression: Axial compression and transverse compressive properties are important in modeling the mechanical behavior of fibers, especially high-strength and high-modulus fibers. The axial compression modulus is often regarded as the same as the tensile modulus. Direct study of axial compression has been made by cutting sections of fibers or monofils and compressing them between plates. The method can also be used to study the transverse properties. The KES-FB3 tester can be used to obtain a pressure–thickness curve of fiber transverse compression.[25]

Friction: Since it is difficult measure the friction of a fiber against another surface or the inter-fiber friction, there are few commercial instruments for friction measurement. However, researchers have designed many apparatuses to deal with this issue. Based on the geometry of the contact area, methods for assessing fiber friction can be divided into four groups: (i) friction between two individual fibers; (ii) friction between a single fiber and one or more fiber assemblies; (iii) friction between two fiber assemblies; and (iv) friction between a single fiber and another surface. In these tests, fiber-to-fiber friction can occur at point, line and area contacts. Figure 10.1 illustrates the three contact modes.

Howell developed many approaches in order to carry out a point contact test for fiber friction: Howell's Method,[29,30] Hanging Fiber Method,[31] Inclined Fiber Method,[32] and Capstan Method.[33] The Cantilever Method[34] is also a point contact method. For the line contact test, there are the Twist Friction Method,[35] Capstan Method,[36,37] and Fiber Pull-out Method.[38–41]

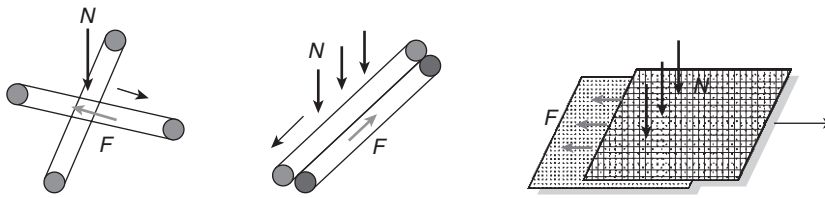

(a) Point contact (b) Line contact (c) Area contact

10.1 Contact modes of fiber friction.

Table 10.1 Fiber-on-fiber friction

Fiber pairs		Friction coefficient, μ	
		Static	Kinetic
Wool-on-wool[50]	with scales	0.13	0.11
	against scales	0.13	0.11
Rayon-on-rayon[51]		0.35	0.26
Nylon-on-nylon[51]		0.47	0.40

Due to anisotropy and viscoelasticity, the line contact and point contact methods may provide different kinds and amounts of contact and thus different frictional responses. Since the area contact method provides small variation in the inter-fiber friction, it may provide more representative and more reproducible results than other methods. There have been many methods and apparatus developed for measuring friction between assemblies.[42–48] It should be mentioned that, depending on the friction measuring device, the values of friction index responses will be different. Hong and Jayaramen have given a detailed review of the developments of fiber friction measurements in reference 49. Table 10.1 lists coefficients of fiber-on-fiber friction for several kinds of fibers.

10.3.2 Properties

The major mechanical properties of various common textile fibers are compared in Table 10.2.

10.4 Conclusion

In this chapter, the brief development history, structural features and mechanical properties of textile fibers have been introduced and the measurement of the relevant properties reviewed.

Table 10.2 Mechanical performance of various fibers

Fiber	Tenacity	Elongation	Initial modulus	Elastic recovery	Flexibility	Stiffness	Resilience	Toughness
Wool	Low	High	Low	High	High	Low	High	Low
Silk	Medium	Medium	Medium	Medium	–	Medium	Medium	High
Cotton	Medium	Low	Medium	Low	Low	Medium	Low	Low
Rayon	Medium	Medium	Low	Low	–	Low	Low	Medium
Acetate	Low	Medium	Low	–	–	Low	Low	Medium
Nylon	High	High	Low	High	High	Medium	High	High
Polyester	High	High	High	High	High	Medium	High	High
Polyolefin	High	Medium	Medium	High	–	Medium	Medium	High
Acrylic	Medium	Medium	High	Medium	–	Low	Medium	Medium

10.5 Acknowledgement

We would like to thank Hong Kong Polytechnic University for funding this research through Projects A188 and G-YD31.

10.6 References

1. BS 3183, *Method for the Determination of Wool Fiber Diameter by the Airflow Method*, British Standards Institution, London.
2. IWTO-28-29, *Detemination by the Airflow Method of the Mean Fibre Diameter of Core Samples of Raw Wool.*
3. BS 3181, *Part I: Determination of Micronaire Value by the Single Compression Airflow Method.*
4. ASTM D 1448, *Micronaire Reading of Cotton Fibers*.
5. Guse, P. *et al*., Optical Measurement of Fiber length in an Airstream. *Melliand Textilberichte/International Textile Reports*, 1995. **76**(3): p. 110–112.
6. Sommerville, P.J., Fundamental Principles of Fibre Fineness Measurement: The Airflow Instrument. *Wool Technology and Sheep Breeding*, 2000. **48**(2): p. 102–1046.
7. Baxter, B.P., Brims, M.A. and Taylor, T.B., Description and Performance of the Optical Fibre Diameter Analyser (OFDA). *Journal of the Textile Institute*, 1992. **83**(4): p. 526.
8. Irvine, P.A. and Lunney, H.W.M., Calibration of the CSIRO Fibre Fineness Distribution Analyser. *Textile Research Journal*, 1979. **49**: p. 97–101.
9. Lynch, L.J. and Michie, N.A., Instrument for the Rapid Automatic Measurement of Fibre Fineness Distribution. *Colourage*, 1981. **28**(14): p. 29–35.
10. BS 6176, *Method for Determination of Length and Length Distribution of Staple Fibres by Measurement of Single Fibres*.
11. BS 4044, *Methods for Determination of Fibre Length by Comb Sorter Diagram*.
12. ASTM D 1440, *Length and Length Distribution of Cotton Fibres (Array Method)*.
13. Anon, The Measurement of Wool Fibre Length. *Wool Science Review*, 1952. **9**: p. 15.
14. ASTM 1447, *Length and Length Uniformity of Cotton Fibres by Fibrograph*.
15. Schenek, A. and Janetzky, I., Almeter Test Method, a Possibility for Fiber Length Measurements on Raw Cotton. *Melliand Textilberichte/International Textile Reports*, 1990. **71**(12): p. 930–938.
16. Ikiz, Y. *et al*., Fiber Length Measurement by Image Processing. *Textile Research Journal*, 2001. **71**(10): p. 905–910.
17. Robertson, G. *et al*., Measurement of Fiber Length, Coarseness, and Shape with the Fiber Quality Analyzers. *TAPPI Journal*, 1999. **82**(10): p. 93–98.
18. Trepanier, R.J., Automatic Fiber Length and Shape Measurement by Image Analysis. *TAPPI Journal*, 1998. **81**(6): p. 152–154.
19. Giddens, B., Spinlab: High-Volume Fiber Testing Instruments. *Textile World*, 1984. **134**(4): p. 123–126.
20. Krais, P., *Journal of Textile Institute*, 1928. **19**: p. T32.
21. Raes, G., Fransen, T. and Verschraege, L., *Textile Research Journal*, 1968. **38**: p. 182.

22. Morton, W.E. and Hearle, J.W.S., Tensile Properties, in *Physical Properties of Textile Fibres*. 1993, The Textile Institute. p. 265–305.
23. Chapman, B.M., *Textile Research Journal*, 1971. **41**: p. 705.
24. Chapman, B.M., *Journal of the Textile Institute*, 1973. **64**: p. 312.
25. Kawabata, S., The Development of the Objective Measurement of Fabric Handle. in *Second Australia–Japan Symposium on Objective Evaluation of Fabric Quality, Mechanical Properties, and Performance.* 1982. Kyoto: Textile Machinery Society of Japan.
26. Morton, W.E. and Permanyer, F., *Journal of the Textile Institute*, 1947. **38**: p. T54.
27. Morton, W.E. and Permanyer, F., *Journal of the Textile Institute*, 1949. **40**: p. T371.
28. Owen, J.D., *Journal of the Textile Institute*, 1965. **56**: p. T329.
29. Howell, H.G., *Journal of the Textile Institute*, 1951. **42**: p. T521.
30. Mogahzy, Y.E.E. and Gupa, B.S., *Textile Research Journal*, 1993. **63**: p. 219.
31. Briscoe, B.J. and Motamedi, F., *Textile Research Journal*, 1990. **60**: p. 697.
32. Howell, H.G. and Mazur, J., *Journal of the Textile Institute*, 1953. **44**: p. T59.
33. Howell, H.G., *Journal of the Textile Institute*, 1953. **44**: p. T359.
34. Basu, S.C., Hazma, A.A. and Sikoski, J., *Journal of the Textile Institute*, 1978. **69**: p. 68.
35. Lindberg, J. and Gralen, N., *Textile Research Journal*, 1948. **18**: p. 287.
36. Roder, H.L., *Journal of the Textile Institute*, 1953. **44**: p. T247.
37. Schick, M.J., *Textile Research Journal*, 1973. **43**: p. 103.
38. Postle, L.J. and Ingham, J., *Journal of the Textile Institute*, 1952. **43**: p. 239.
39. Cox, D.R., *Journal of the Textile Institute*, 1952. **43**: p. T87.
40. Denby, E.F. and Andrews, M.W., *Textile Research Journal*, 1965. **35**: p. 913.
41. Peirce, F.T. and Lord, E., *Journal of the Textile Institute*, 1939. **30**: p. T173.
42. Morrow, J.A., *Journal of the Textile Institute*, 1931. **22**: p. 425.
43. Martindale, J.G., *Journal of the Textile Institute*, 1947. **38**: p. T151.
44. Lord, E., *Journal of the Textile Institute*, 1955. **46**: p. 41.
45. Viswanathan, A., *Journal of the Textile Institute*, 1966. **57**: p. T30.
46. Viswanathan, A., *Journal of the Textile Institute*, 1973. **54**: p. 553.
47. Koza, W.M., *Textile Research Journal*, 1975. **45**: p. 639.
48. Mogahzy, Y.E.E. and Broughton, R.M., *Textile Research Journal*, 1993. **63**: p. 465.
49. Hong, J. and Jayaraman, S., Friction in Textiles, in *Textile Progress*. 2003, The Textile Institute, Manchester.
50. Zurek, W. and Frydrych, I., *Textile Research Journal*, 1993. **63**: p. 322.
51. Olofsson, Bard Gralen, N., *Journal of the Textile Institute*, 1950. **43**: p. 467.

11
Yarns

K.F. CHOI
The Hong Kong Polytechnic University, China

11.1 Introduction

Yarn structure has a strong influence on the biomechanical properties of the fabric produced. It is very difficult to quantify yarn structure and no published literature can be found which gives an unambiguous definition for important yarn quality parameters. Theoretically speaking, the structure of a yarn can be quantified by knowing the spacial arrangement of all the fibers in the yarn. With the incorporation of the fiber mechanical and dimensional properties, the collective behavior of the yarn can then be determined by considering the effect of individual fibers and their interactions. The above work requires tremendous effort and the reward is not attractive enough. Instead of measuring all the fibers in a yarn, a random sample of fibers is taken and the path of those fibers is quantified. This is the famous tracer fiber technique, first introduced by Morton.[1] Another important yarn structural property is the distribution of fibers in the yarn. The highly non-linear mechanical properties are mainly due to the non-uniform distribution of fibers. This can be explained by the shortest path hypothesis.[2]

11.2 General view of today's yarns

Ring spinning is regarded as the conventional yarn production process which has more than 150 years of history and will continue to be the most versatile and important process in the near future until an alternative method has developed to such a stage that it can be replaced over the whole count range. Air jet spinning is taking ground in the fine yarn count region. Rotor spinning has secured its share in the low to medium count sector. Friction spinning is still struggling to get rid of poor yarn strength and low yarn abrasion resistant problems. Other spinning methods, such as wrap spinning by hollow spindle, seem to be quite static in terms of further development. The sole motivation of searching for alternative spinning methods

is to increase productivity, since ring spinning reached its upper limit long ago.

It is expensive to add one turn of twist in the rotor and ring system because it involves one complete revolution of the rotor or the traveler around the ring. The production speed is also limited by the excessive yarn tension arising from the centrifugal force. For friction and air jet spinning, a turn of twist is inserted by rotating the yarn itself; thus it is more energy saving. In addition, the yarn tension is relatively low since the yarn withdrawal force is not directly affected by the action of twist insertion.

Yarns produced by different spinning processes vary quite significantly in yarn properties. As a standard of yarn quality, ring spun yarn is generally used to assess the success of other new processes by quality comparison. The assessment of yarn quality is becoming more stringent. The all-round yarn characteristics are compared. They include the yarn strength, unevenness, abrasion resistance, hairiness, bending stiffness and hand. Those yarn properties will be explained in relation to yarn structure and the measuring methods will be described in the coming sections.

Due to the difference in yarn structure, rotor yarn cannot be compared directly with ring yarn of the same twist level. Rotor yarns require a higher machine twist than ring yarns in order to achieve similar tensile strength levels. Twist measurement of rotor yarn is not straightforward since the wrapper fibers on the yarn surface cannot be untwisted. The direct untwisting method is surely not applicable. The single untwist-retwist method demonstrates large discrepancies. The French type multiple untwist-retwist method has, however, been shown to give accurate measurement of machine twist.

New spinning systems differ from conventional ring spinning systems in regard to the yarn twisting mechanism; they produce yarns with different fiber configuration and packing density distribution. Fibers in ring yarn are well aligned and interlocked with a migratory geometry. In rotor yarn a bicomponent structure can be observed; a regularly twisted core covered by a sheath of entangled fibers which are occasionally wrapped by belt-like fiber.

The yarn-making process has two phases: phase I – Fiber feeding stage (drafting and transport), phase II – Yarn formation stage. Fiber cohesion is obtained by twisting, wrapping, entanglement, bonding or their combinations. (Fiber migration = twist + entanglement). A major drawback of break spinning is lack of sufficient fiber tension during the spinning process. Productivity of rotor yarn is limited by the pull-out tension (proportional to $r \cdot w$), but tension in spinning zone is still low.

In terms of production speed, ring spinning is left far behind to those new spinning methods such as rotor spinning, friction spinning and air jet spinning, and especially by the MVS air jet, where the production speed can

reach up to 400 meters per minute. This is about 20 to 30 times more productive than ring spinning. Nevertheless, ring spinning is still the most popular yarn production method, partially due to the technology inertia. Most people are reluctant to change when the existing system is running fine. Changing will mean further investment and uncertainty. Adopting new technology may cost quite a lot since new versions with certain improvements come out too often. Everyone wants to wait until the technology matures. Another major reason for the popularity of ring spinning is the quality of yarn produced. Ring spinning has its unique yarn formation mechanism such that all the fibers are subject to a certain level of tension. High-tension fibers tend to move toward the yarn center, low-tension fibers tend to buckle out toward the yarn surface. This periodic movement of fibers in a yarn causing a variation of radial position is called fiber migration. The moving in and buckling out mechanisms occur simultaneously, resulting in a self-locking structure. The self-locking structure of ring spun yarn contributes significantly to the high tensile strength and good abrasion resistance.

The self-locking mechanism is enhanced by moderating the fiber tension just before yarn formation. It is the basis of Solospun yarn. A Solo roller with intermittent grooves on the roller surface can enhance the degree of fiber migration such that fibers interlace to a larger extent. It is found that the yarn tensile strength is not further increased, but the abrasion resistance is improved remarkably.

11.3 Yarn structural properties

11.3.1 Fiber path in yarn

The fibers in a ring spun yarn in general follow helical paths with varying helix radii. This is the well known phenomenon called fiber migration. As described by Morton,[1] the spinning tension acting on individual fibers causes the fibers to move away or toward the yarn axis. The migration pattern of ring yarn is very different from other yarn types. For example, open end friction spun yarn (produced using the DREF 2 system) is found[3] to have stronger migration than ring yarn, but the migration is unidirectional, i.e. one end of fiber lies on the yarn surface and the other end in the yarn core. The fibers form conical helices with much intermingling (interlacing), to form a well-locked yarn structure. The fiber migration of friction spun yarn is facilitated by geometrical means instead of mechanical means as for the ring spun yarn. During the yarn forming process, fibers, after passing through the opening roller, are laid on the surface of a conical yarn tail which is rotating on the nip of the suction roller. The so-called 'length utilization' of fiber in friction spun yarn is poor. Quite a number of fibers

wrap loosely around the yarn surface. Tracer fiber technique is an effective way to study the fiber path in a yarn. Together with the image analysis algorithm, a large number of tracer fibers can be sampled and a better representation of the yarn structure can be obtained. The yarn cross-section analysis provides some further information on the yarn structure, for example the fiber packing density distribution[4] in a yarn. It is a very important yarn parameter which is related to the highly non-linear torsional and tensile properties of yarn,[5] and the initial lateral compression modulus of fabric and hence fabric handle.

11.3.2 Packing density distribution of yarn

Some other very interesting results concerning yarn structure can be obtained from yarn cross-section analysis, for example (i) the hollow center[6] of yarn due to ribbon twisting in worsted spinning, (ii) fewer fibers in a cross-section of rotor yarn than that of ring yarn of the same count and twist due to poor alignment of fibers in the rotor yarn, (iii) friction yarn has a loose packing[7] of fibers in the yarn cross-section due to low tension present during yarn formation, and so on.

The packing density distribution has a significant effect on yarn mechanical properties, especially the initial tensile modulus. According to the shortest path principle,[2] fibers will move toward the yarn center to avoid being strained until the yarn core is jammed (i.e. packing density has reached the upper limit). When the yarn is quite loose in the core region initially, it will have room for yarn extension before the yarn core becomes jammed with fibers and forces most of the fibers to extend. The work done to extend the fibers is much larger than that for bending and twisting the fibers. Moving the fibers toward the yarn center only involves bending and twisting fibers. With the same amount of yarn extension, the larger work undertaken means a larger yarn modulus. Methods of measuring fiber packing density are described in the following sections.

Conventional method

The conventional method[4,8] of fiber lateral distribution measurement is called the slice cutting method. The procedures of this method involve fixing the yarn by means of resin and cutting thin slices of the yarn. The fibers in the yarn cross-section can then be analyzed manually or automatically by means of image analysis. In the experiment, the yarn length is under control such that the yarn cannot contract when immersed in the resin. The cross-section of the yarn in an extended or twisted state can also be studied using this method. It is a very useful tool for the analysis of fiber movement in a yarn when subject to external forces.

When a yarn is being deformed, it could be quite compact, so the viscosity of the resin fixing agent should be low enough to penetrate into the spaces between fibers in the yarn. In addition, the fixation process of the fixing agent should take place even though it is at room temperature. Based on the above requirements, an acrylic resin with its catalyst was selected. With suitable proportions of resin and catalyst giving the right amount of setting time, very satisfactory thin slices of the yarn cross-sections can be obtained by use of a microtome.

When a yarn is immersed in a liquid, there will be a change in fiber arrangement. Generally the yarn will increase in diameter but decrease in length. One way to minimize the change in fiber arrangement is by controlling the yarn length. A clamp was specially designed for this purpose. The yarn was threaded through a plastic tube, and then the yarn and the plastic tube were fixed together on the clamp, with the lower jaw closed firmly such that resin would not leak through. By inverting the clamp, the yarn was tensioned under its own weight. The clamp was restored to its upright position after the upper jaw was firmly closed. The resin was mixed with the catalyst according to the proportions stated in manufacturer's manual. The newly prepared resin was injected into the tube as soon as possible. The resin was allowed to set and cool in air for about one hour. The yarn in the resin was then removed from the tube and thin slices were cut using a standard microtome with a steel knife.

The slices were viewed under the microscope and the images were captured. By enlarging the photograph to a scale of 200:1, each fiber cross-section was represented by two quantities: coordinates of the center of mass and area of cross-section. To calculate the mass of fiber at different yarn radial positions, annuli with equal areas were constructed. The area of fiber cross-section at each annulus was determined by representing the fiber cross-sections by circles with same area and center of mass. A computer program was used to perform the calculation and produce the lateral yarn density function.

The disadvantages of the slice cutting method are that, first, the yarn structure may be changed in the resin bath, and secondly this method is a destructive test; as a result the same portion of yarn cannot be used for other tests. In addition, the method is tedious and time consuming to carry out.

Measuring method using computed tomography principle

In this section a novel method of measuring the yarn density distribution is introduced. A technique based on the principle of computed tomography[9,10] (CT, e.g. human body scanning) is introduced. According to a literature search, the principle of CT has never been applied in the textile field

before. The selection of the penetrating source is the most important part in the construction of the measuring device. The penetration power of the source is acceptable when it can penetrate most of the commercial yarn. The sensitivity of the detector is acceptable when the absorption of a single fiber can be detected. The reliability of the new measuring device will be justified by means of the conventional yarn cross-sectional analyzing method which was described in the previous section.

The proposed method could eliminate the shortcomings of the conventional method, which are that, firstly, the yarn structure might be changed by immersion in the resin, and secondly that it is a destructive test. With an automated system for the measurement of yarn structure, any new yarn structures achieved by modifying the spinning methods or spinning conditions may be quantified quickly. This will further assist in future investigations related to yarn mechanics. In addition, the new measuring device could be attached to a spinning machine to provide on-line monitoring of the yarn quality. Since even the packing density distribution of yarn can be measured, all the yarn faults and levels of irregularity can also be measured with ease.

The experimental set-up is shown in Fig. 11.1. An X-ray diffractometer was used for the scanning experiment. The copper target of the X-ray tube was energized at 30 keV, the tube current was limited to 20 mA. A circular, stainless-steel tube and an aperture were used to collimate the X-ray beam to a size of about $2 \times 5\,\text{mm}^2$.

As yarn is produced by twisting fiber strands, it is reasonable to assume the packing density of yarn is axially symmetric. With this assumption, the absorption profile in one direction is enough to reconstruct the cross-section image of the yarn. Obviously, taking the average along the yarn length would get a more representative packing density distribution of the yarn.

The yarn was mounted on a linear positioning stage that was equipped with a digital micrometer of 1 μm reading resolution. It was exposed to the

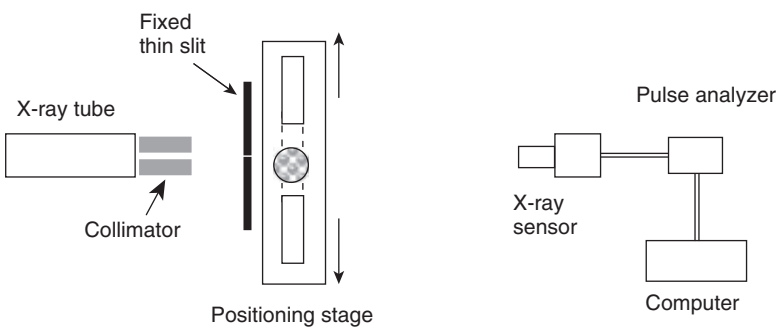

11.1 Schematic diagram for the X-ray scanning experiment.

collimated X-ray radiation at the rear of a 0.1 mm slit. A focusing optic system including a 0.1 mm aperture slit, and a 1/2° field of view slit were used for the X-ray collection. A solid state detector received the X-ray radiation and the signal was fed through a pulse height analyzer and then recorded by a microcomputer. In order to deduct the background, the X-ray intensity was measured by scanning the detector for a small angle in each measurement.

Experimental result: Two woolen carpet yarns were produced at Canesis Network Ltd. (former WRONZ); one was high twist, the other low twist (see Fig 11.2). The specifications of the yarns are given in Table 11.1. The relative X-ray absorption curves of the yarns are shown in Fig. 11.3. The high-twist yarn has a higher degree of absorption at the yarn core region. The absorption region of the low-twist yarn spreads over a relatively larger distance. Another obvious difference of the two yarns is related to the symmetry of the absorption curves. High-twist yarn has a more symmetric absorption curve. It is as expected since twisting a fiber strand would make it more axial symmetric.

Principle of computed tomography: Transmission CT is applied here. A cross-section of the yarn is scanned by a thin X-ray beam whose intensity

Table 11.1 Parameters of yarns

Yarn parameters	Low-twist yarn	High-twist yarn
Linear density (tex)	256	288
Twist level (turns per meter)	115	265
Yarn diameter (mm)	1.16	0.96

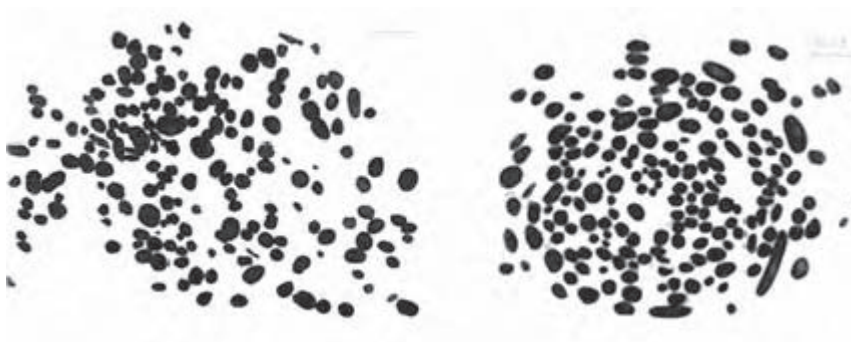

(a) Low-twist yarn (b) High-twist yarn

11.2 Cross-section of yarn.

loss is recorded by a detector and processed by computer to produce a two-dimensional image which is then used for the computation of the yarn density distribution.

The physical model of CT is as follows. Let $f(x)$ be the X-ray attenuation function of the yarn at location x. The X-ray traversing a small distance dx at x suffers the relative intensity loss dI/I, with $\mathrm{d}I/I = f(x) \cdot \mathrm{d}x$. Let I_o be the initial intensity of an X-ray beam L which is a straight line, and let I_1 be its intensity after having passed the yarn.

It follows that

$$\frac{I_1}{I_o} = \mathrm{e}^{-\int_L f(x) \cdot \mathrm{d}x} \qquad [1]$$

The scanning process provides the line integral of the function f along each of the lines L. From all these integrals the function f has to be restructured. The transform which maps a function on R^2 into the set of its line integrals is called the two-dimensional Radon transform. Thus, the reconstruction problem of CT is just the inversion of the Radon transform in R^2. In practice the integrals can be obtained only for a finite number of lines L. In a parallel scanning geometry a set of equally spaced parallel lines is taken for a number of equally distributed directions. It requires a single source and a single detector which move in parallel and rotate during the scanning process. The real problem in CT is to reconstruct f from a finite number of its line integrals, and the reconstruction procedure has to be adapted to the scanning geometry.

Special case: yarn with axial symmetric packing density distribution: When the packing density $\varphi(r)$ is axial symmetric, its determination becomes much simpler. In mathematical terms, the packing density function can be found by solving the following integral equation, with given absorption function $m(x)$, and the unknown function $\varphi(r)$,

$$\int_x^1 \frac{r\varphi(r)}{\sqrt{r^2 - x^2}} \mathrm{d}r = m(x) \quad \text{where} \quad 0 < r < 1, 0 < x < r \qquad [2]$$

The absorption curves as shown in Figure 11.3 were substituted into Equation (2). The packing density functions of the two yarns were determined as shown in Figure 11.4.

The new method provides a convenient way to measure the packing density distribution of yarn. In the preliminary experimental study, the packing density distributions of woolen yarn with two twist levels were measured. When observing the X-ray absorption curve in Figure 11.3 and referring to the corresponding yarn cross-section view in Figure 11.2, the choice of the X-ray source and the conditioning of the X-ray beam were proven to be very appropriate, and the measurement of yarn packing density distribution based on computed tomography is highly feasible.

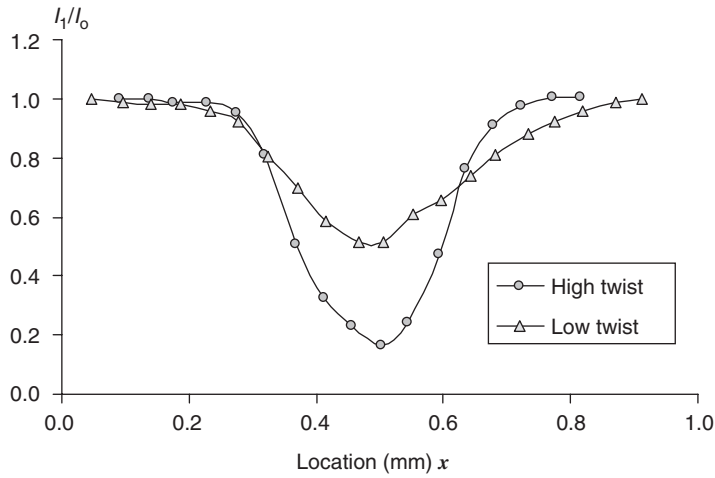

11.3 Relative X-ray absorption of yarns at different yarn locations.

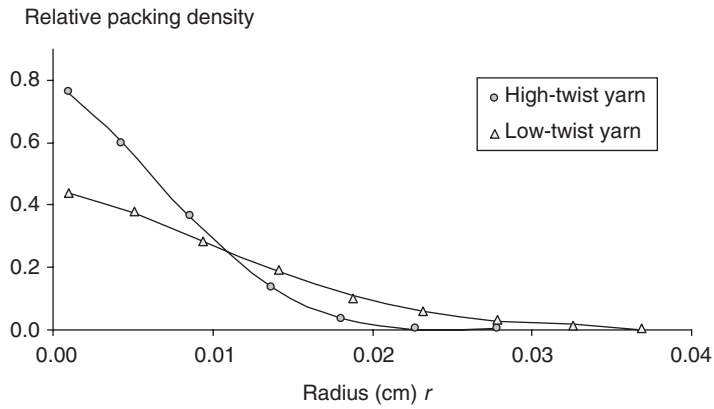

11.4 Packing density distribution of yarns.

11.3.3 Fiber interlacing

Fiber interlacing is the mutual consideration of fiber migration. If nearby fibers migrate in a similar pattern to the way that friction yarn's fibers migrate from core to surface due to the conical wrapping of fibers at the yarn tail during yarn formation, then fibers do not interlace much.

Some new yarn types, such as the Solospun yarns,[11] have proven successful in increasing the abrasion resistance, but the structure of the yarns could hardly be quantified in relation to the eminent properties using conventional method.[12–16] A new yarn structural parameter, average segment length

of fiber on the yarn surface, is proposed and described in this section. An initial experimental trial was performed for the purpose of verifying the usefulness of the new parameter in explaining the variation of abrasion resistance of yarns with different structures. Six types of worsted yarns were produced with varying degrees of fiber migration.

Surface length

A new measurement was introduced to quantify the degree of migration of fibers in yarn. It is the segment length of the fiber on the yarn surface (in short the 'surface length'). A particular fiber coming out of the yarn surface, staying on the yarn surface, and then re-entering into the yarn core would involve two random processes and the length of the fiber segment on the yarn surface would be affected by the surrounding fibers.

Dyed tracer wool fibers have been blended with other wool fibers in the spinning process. They could be observed when they come to the yarn surface. The distribution of segment length of the tracer fibers on the yarn surface reflects the fiber migratory behavior in the yarn. When a fiber undergoes a more idealized migration, it moves from the surface to the core and *vice versa*. If the fibers migrate more frequently, each fiber appears only momentarily on each superimposed concentric layer. Thus, it was postulated that the shorter the fiber exposing on the surface, the more the extent of migration. Consequently, the fibers are more likely to interlock with one another to provide a strong cohesion. It was expected that the shorter the surface length, the more frequent the fiber migration.

Surface length distribution

A segment of tracer fiber is seen on the surface of the yarn. With the aid of mirrors, the starting and ending points of the fiber segment can be located and then the surface length measured. By measuring the length of 100 surface segments of each yarn type, the cumulative distribution of the surface length of yarn type Y1 is plotted as shown in Fig. 11.5a. For the other yarn types, similar results can be obtained as shown in Fig. 11.5b–f. It was discovered that Gamma distribution functions $G(x)$ fit the cumulative distribution of surface length very well. Gaussian distribution functions (cumulative normal distribution) were plotted in Fig. 11.5 as well, for comparison purpose.

The following describes the principle of obtaining the Gamma distribution functions of surface length from the raw data. The generalized Gamma distribution is a three parameters (α, β and γ) distribution. The probability density function (pdf) of Gamma distribution $g(x)$ is the first derivative of the Gamma distribution function $G(x)$ and $g(x)$ is given by:[17]

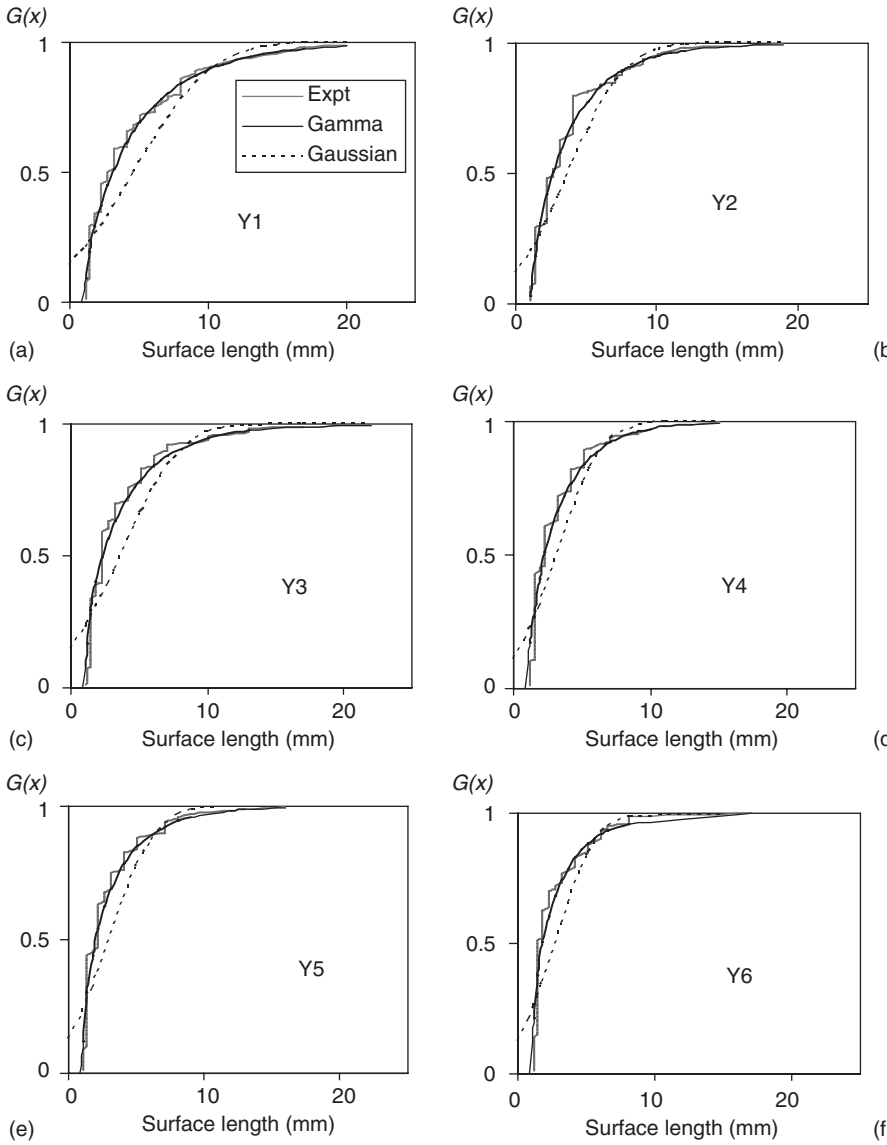

11.5 Distribution functions of surface length.

$$g(x) = \frac{1}{\Gamma(\alpha) \cdot \beta^{\alpha}} \cdot (x - \gamma)^{\alpha - 1} \cdot \mathrm{e}^{-\frac{x-\gamma}{\beta}}$$

where $\Gamma(\alpha) = \int_0^{\infty} y^{\alpha-1} \cdot \mathrm{e}^{-y} \cdot \mathrm{d}y$ and $x > \gamma$.

The mean of the distribution $\mu = \alpha\beta + \gamma$ and the variance $\sigma^2 = \alpha\beta^2$.

From the experimental data of surface length, the minimum surface length was found to be close to but not less than 1 mm. The estimate of the parameter γ was set to that value. The estimates of the remaining two parameters, α and β, could be calculated from the mean and variance of the surface length of the yarn. The means and variances of surface length of the six types of yarns and also the corresponding parameters' values are shown in Table 11.2.

With the values of the parameters given, the pdf for the yarns can be plotted as shown in Fig. 11.6. It was found that yarn type Y6 had the highest proportion of short surface length while yarn type Y1 had the least proportion of short surface length. For the sake of easy visualization, only yarn types Y1 and Y6 were plotted in Fig. 11.6.

Table 11.2 Summaries of surface length distribution for the six types of yarns

Surface length	Yarn type					
	Y1	Y2	Y3	Y4	Y5	Y6
mean (mm)	4.64	3.71	3.58	3.14	3.00	2.69
sd (mm)	4.43	3.17	3.46	2.58	2.67	2.35
Parameters						
α	0.67	0.73	0.56	0.69	0.56	0.52
β	5.40	3.71	4.64	3.12	3.55	3.28
γ	1.00	1.00	1.00	1.00	1.00	1.00

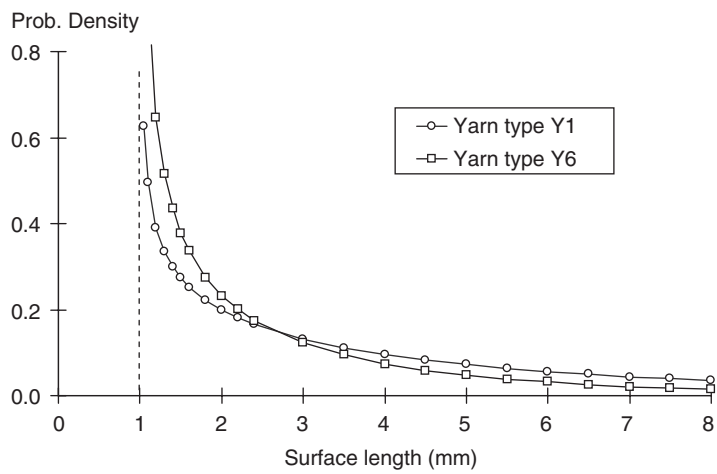

11.6 The surface fiber distribution of the yarns.

11.3.4 Twist and its measurement

Twist affects the yarn structure very significantly; in addition to the geometrical change, the change in fiber tension will affect the packing of yarn and the imposed torsional stress will affect the mechanical stability of the yarn. For a high-twist yarn, when the tension exerted on the yarn is not large enough, the yarn will buckle to become a tortuous shape. Due to the yarn formation mechanism, most yarn will have a large variation of twist at different radial positions, except ring yarn, so that only ring yarn can be untwisted to form a parallel fiber strand. This is the principle of twist measurement using the direct method.

A method based on different principles must be used for the twist measurement of other yarn types (e.g. rotor, friction and air jet). A method such as untwist-retwist, which is based on the twist contraction principle, could be employed, or its refinement; French type untwist-retwist, is a more satisfactory method.[18]

11.4 Yarn mechanics

11.4.1 Tensile properties

The mechanical behavior of yarns affects their suitability in most end uses. The most important yarn mechanical property is the tensile property. The strength of yarn is a crucial yarn specification. When the minimum yarn strength cannot be met, very poor production efficiency in the subsequent processes and inferior product quality will result. The factors affecting yarn tensile strength include yarn structure, fiber strength and fiber surface properties. Yarn mechanics in general refers to the yarn tensile, bending, torsional and abrasion properties. The mechanical properties of yarn include tensile tenacity, extensibility, elastic recovery, tensile modulus, bending stiffness, residual torque, and abrasion resistance under periodic tensile loading. For the measurement of yarn tensile properties a constant rate of extension meter is used – record load extension curve, extend, hold for a period, and release.

The yarn tensile test is well established. Standard testing methods are very popular in the textile field, e.g. the ASTM D2256 Standard Test Method for Tensile Properties of Yarns by the Single-strand Method. This test method describes the determination of tensile properties of monofilament, multifilament, and spun yarns, either single, plied, or cabled with the exception of stretch yarns. This test method covers the measurement of breaking force and elongation of yarns and includes ways of calculating breaking tenacity, initial modulus, chord modulus, and breaking toughness. Conditions of test are included for the testing of specimens that are: (i) conditioned in air, (ii) wet, not immersed, (iii) wet, immersed, (iv) oven-dried, (v) exposed

to elevated temperature, or (vi) exposed to low temperature. In the textile trade, the ultimate tensile strength, or breaking strength is taken into consideration. A yarn technologist would decide on the spinning method and the spinning parameters in order to produce yarns meeting the product specifications with optimum productivity.

The curve of total tensile strength of fibers is the upper bound of the tensile curve of staple yarn (see Figs. 11.7 and 11.8). The tensile load of a

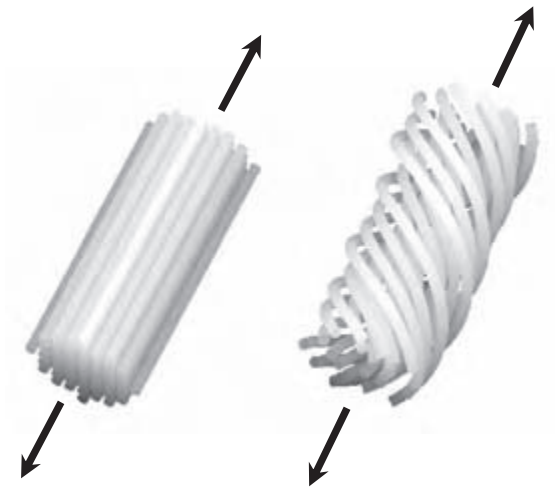

11.7 Fiber strands under tension.

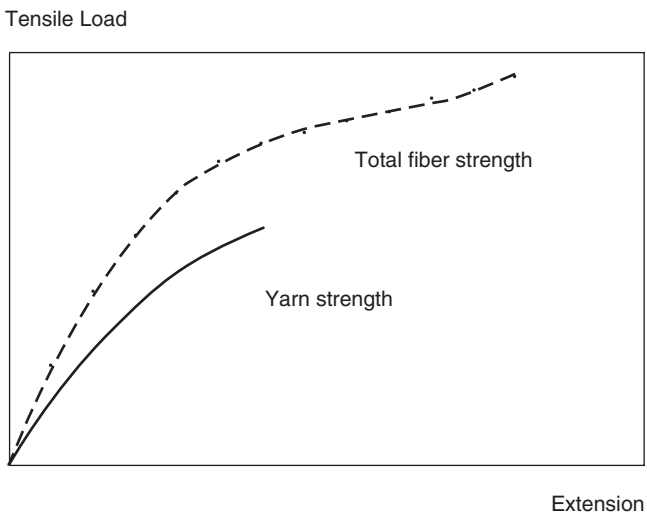

11.8 Load–extension curve.

yarn is always lower than the correspondent total fiber load. The reduction in tensile load is due to a mixture of the following reasons: Fiber slippage, fiber obliquity, loose packing of fiber, weak link effect.[19] Fiber slippage is inevitable for staple yarn; each fiber cumulates tensile stress at both ends from zero up to a stress level which is enough to extend the fiber with the same amount of extension of the yarn. Fiber tension contributes to yarn loading by a fraction of T_f only, which is $T_{//} = T_f \cdot \cos\alpha$, where α is the twist angle (helix angle) of the fiber. At higher twist levels, inter-fiber stress will increase and yarn failure due to excessive fiber slippage can be minimized. At the same time, fibers are more inclined to the yarn axis (with larger twist angle). Fiber load contributes less to yarn tensile load. The loose packing of yarn leads to an extra amount of yarn extension before tightening the fibers to bear the loading. Fibers in the outer yarn region will be straightened in a later stage. When the yarn is being extended, fibers tend to move toward the yarn center to avoid being strained until the yarn core is jammed, i.e. with close packing yarn density. The tensile strain distribution of fibers in a yarn can be calculated at various yarn extension states under the assumption that fibers are simple helices with equal helical pitch.

Even when the fiber is perfectly uniform and the spinning process does not introduce additional variation, the spun yarn will have inherent irregularity. The number of fibers in a cross-section follows a Poisson distribution. Within a length of yarn, there exists a minimum strength point at which the yarn breaks. This is the well-known weak link effect.[19]

11.4.2 Yarn torsional properties

Evaluation of yarn torsional properties is much less popular than that of yarn tensile properties since they are more difficult to measure and their effects are less readily related to the properties of final garment. Normally, people deal with these properties qualitatively. They use words such as twist lively yarn to refer to yarn with a high value of residual torque.

Yarn torsion meter

The most direct way to determine the torsional properties of a yarn is to measure the torque rotation relationship of the yarn with a torsion meter. The torsion meter (KES-YN1) used in this experiment was manufactured by the Kato Tech. Co. Ltd., Japan. The load range is from –500 mgf.cm to +500 mgf.cm. During testing, the yarn specimen is subjected to a constant tension and its length is allowed to change freely. The torsion meter is based on the torsion balance principle: a standard metal wire of known torsional stiffness is connected to the yarn at the upper end and the rotational displacement of the wire is measured by a very sensitive displacement

transducer. The amplified signals of the transducer output are sent to the plotter and a torsion rotation curve is obtained.

Singles yarn torsional properties

Singles yarn torque was measured using the KES-YN1 Yarn Torsion Meter. The twisting head in the instrument twisted the yarn specimen in a cyclic manner. The yarn tension was kept constant at 25 gf.

Specification of low-twist and high-twist yarns

Yarn type	: Woolen spun carpet yarn
Yarn linear density	: 256; 288 tex
Yarn twist level	: 115; 265 turns per metre (Z-direction)
Yarn state	: Boil-set (almost zero residual torque)
Yarn test length	: 3 cm
Fiber type	: New Zealand Romney Wool
Mean fiber radius	: 1.805×10^{-3} cm

The woolen yarns and the yarn specifications were supplied by Canesis Network Ltd (WRONZ) – see Fig. 11.9.

The mid-points of the yarn torque of the upper and lower hysteresis curves at different levels of yarn rotation were plotted in Fig. 11.10. The high-twist yarn has a larger torsional rigidity than the low-twist yarn and the torsional curve of the former is less linear. The low torsional rigidity of the low-twist yarn can be explained by its loose structure. Fibers can freely move to accommodate the overall twisting strain of the yarn before they form a compact yarn core to act against the imposed yarn torque.

11.4.3 Yarn bending properties

Yarn bending rigidity has a strong influence on fabric hand and appearance. The bending properties of yarns differ significantly from those of solid beams. They are strongly influenced by the restraint with which the fibers

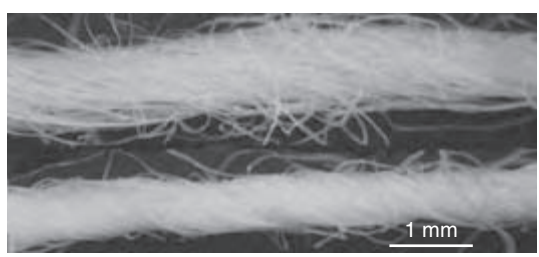

11.9 Longitudinal view of low- and high-twist yarns.

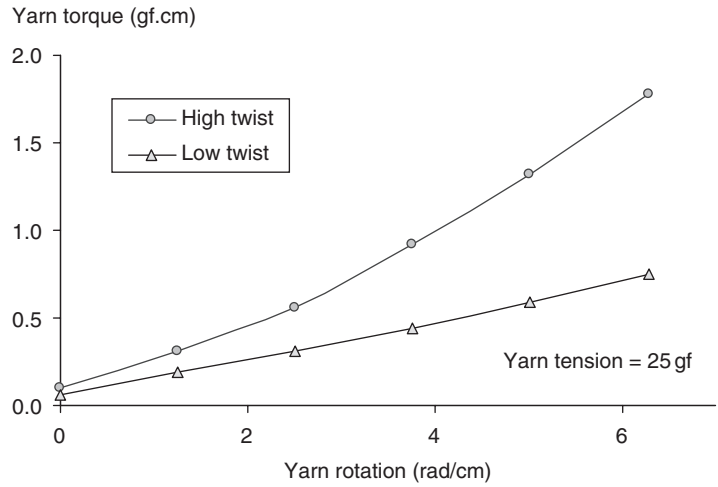

11.10 Torsional properties of yarns with different twist levels.

can move relative to each other in order to accommodate local deformations due to bending. The degree of the constraint is governed by the twist level of the yarn and the surface properties of the fibers. For loose yarns, the fibers can be assumed to bend independently with each other. In this case, the yarn-bending rigidity is effectively equal to the sum of the bending rigidities of individual fibers. Thus, the bending rigidity of such a yarn is proportional to the number of fibers in its cross-section.

In his theoretical study of yarn bending, Backer[20] calculated the local fiber strains for two extreme cases of deformation: complete freedom of relative fiber movement and no relative fiber movement. It was postulated that when the fibers were completely free to change their paths in the yarn, no fiber strain would be developed during yarn bending, and that when complete restriction of fiber movement was imposed, maximum strains would occur in the fibers lying on the outside (with tensile strain) and inside (with compressive strain) of the yarn torus. For real yarns, the mobility of fibers must lie in-between the two extreme cases, and should be closer to the complete freedom case.

Although the Bending Tester is designed to measure fabric bending rigidity, it can also be used to measure the bending properties of yarn. During testing, a number of yarn samples are laid parallel with equal spacing and under uniform tension. Then both ends of the samples were secured using double-side adhesive tapes and paper strips. During testing, the yarns were allowed to bend freely between two clamps spaced 1 cm apart. Bending hysteresis curves were obtained from the KES-FB2. The

bending rigidity and coercive bending moment of the yarns can also be measured.

Specification of yarn

Yarn type	: Woolen spun carpet yarn
Linear density	: 256 tex
Yarn twist level	: 191 turns per metre (Z-direction)
Yarn radius	: 0.05 cm
Yarn state	: Boil-set (almost zero residual torque)
Fiber type	: New Zealand Romney Wool
Mean fiber radius	: 1.805×10^{-3} cm

A total of 64 yarns were laid parallel to one another during the test. The bending hysteresis curve was plotted as shown in Fig. 11.11. The bending curve was unexpectedly linear. This may be due to the fact that the bending deformation was very small since the maximum curvature of the yarn was just equal to 2 cm^{-1}. Comparing with the yarn diameter of 0.1 cm, the curvature should reach 10 cm^{-1}, which is the typical bending deformation of yarn in a knitted fabric. This is a limitation of using the KES-FB2 Tester for the measurement of yarn bending.

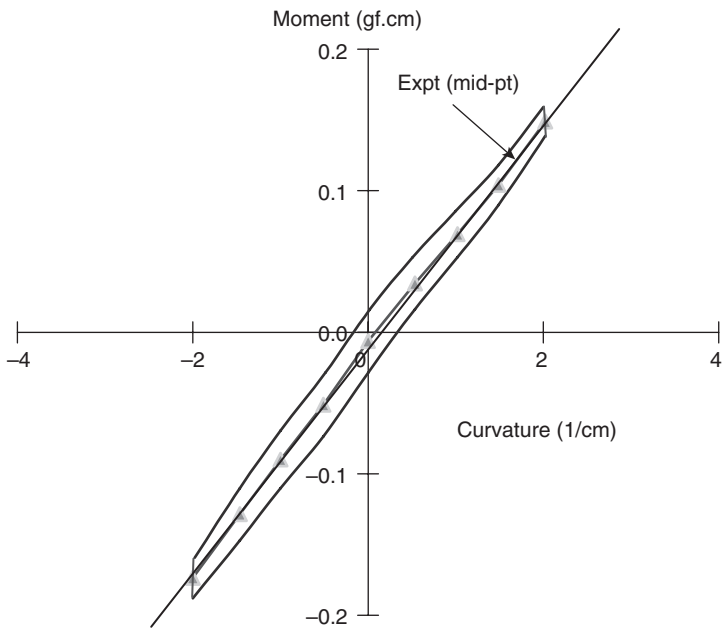

11.11 Bending properties of yarn.

11.5 Degree of fiber interlacing and abrasion resistance

Semi-worsted yarns of 46 tex and 600 turns per meter were processed in Canesis Network Ltd. (WRONZ). The processing parameters were varied such as to obtain a series of yarns with changing abrasion resistance.

Test on yarn abrasion resistance

Brorens *et al.*[21] evaluated the yarn abrasion-resistant properties at WRONZ using their specially designed abrasion tester. Unlike the normal 'rubbing' on the yarn surface, this tester performs the mechanism of yarn failure which is primarily a gradual drafting of the abraded area under abrasion.

In the experiment of yarn abrasion described in this section, the Shirley Yarn Abrasion Tester was used. The tester consists of two reciprocating bars: one is made of hardened steel and the other is covered with the standard abradant used in the Martindale Fabric Abrasion Tester. Eight yarn specimens were tested simultaneously. Yarns were threaded from the fixed holders and clipped onto the flexible holders on which sensors were attached. The initial tension exerted on each yarn was 0.5 N. When a yarn was broken, the flexible holder fell, a signal would be sent to the control unit, and the number of rubs for that particular yarn would be recorded.

The abrasion cycles were set to an upper limit of 10 000 rubs and the elongation of each yarn during test was recorded every 500 cycles. Twenty specimens were taken randomly from each yarn type for the test and the results were summarized in Fig. 11.12. It can be observed that yarns of type Y6 have the highest proportion of yarn specimens lasting for most abrasion cycles before breakage (with extension of more than 12%).

It was found that that yarn abrasion resistance was inversely proportional to the average surface length, and the coefficient of determination R^2 = 0.9481, i.e. around 94.8% of the variation of yarn abrasion resistance can be explained by the variable average surface length. As a result, a simple yarn structural parameter that is closely related to the yarn abrasion resistance properties was discovered. The merits of this new parameter include easy measurement and true reflection of the degree of interlacing of the fibers near the yarn surface. As the surface fibers are to be measured, there is no need to search for a suitable solvent to optically dissolve the fibers in the yarn such as to highlight the tracer fiber for measurement of spatial coordinates. This would save a lot of effort during preparation work and data processing for the generation of migration parameters.[12] In addition, the surface fiber length measurement has eliminated the error of varying yarn diameter which influences the location of the yarn axis and thus the accuracy of the migration parameters. More extensive experimental work

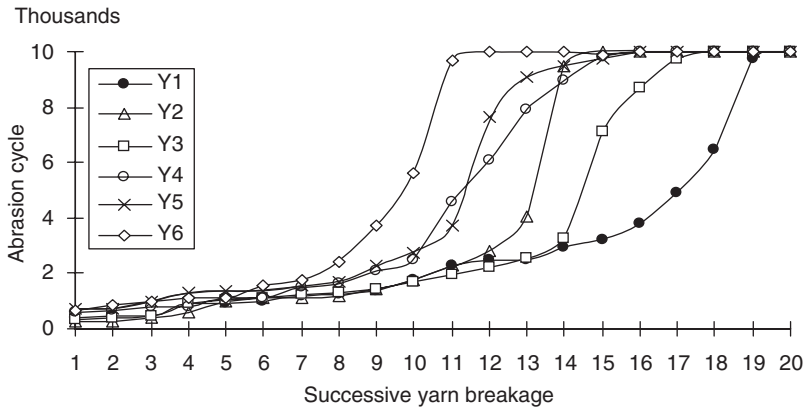

11.12 Abrasion resistance of the yarns.

will be performed to verify the reliability of the new structural parameter for different yarn types, e.g. Solospun.

11.6 Conclusion

In this chapter, a brief development history of yarns has been given, followed by a description of recent studies[22,23] on the most important yarn structural parameters, i.e. surface length distribution and lateral yarn density distribution. The major mechanical properties were briefly described. They include the tensile, bending, torsional and abrasion properties of yarns. The emphasis here is on studies of the inter-relationship between the yarn structure and mechanical properties. For details of the respective yarn properties, many papers can be found in the *Journal of the Textile Institute* and in the *Textile Research Journal*.

11.7 References

1. Morton, W.E., The Arrangement of Fibers in Single Yarns, *TRJ* 1956, **26**, p. 325–331.
2. Carnaby, G.A., The Structure and Mechanical Properties of Wool Carpet Yarns, *PhD Thesis* (University of Leeds), 1976.
3. Lunenschloss, J. and Brockmanns, K.J, Cotton Processing by New Spinning Technologies, Possibilities and Limits, *Int Textile Bull*, Yarn Forming 1986, (2) p. 7–22.
4. Hickie, T.S. and Chaikin, M., The Packing Density in the Cross-section of Some Worsted Yarn, *Journal of the Textile Institute*, 1973, **65**, 433–437.
5. Tandon, S.K., Carnaby, G.A., Kim, S.J. and Choi, K.F., The Torsional Behaviour of Singles Yarns – Part I: Theory, *Journal of the Textile Institute*, 1995, 185–199.

6. Hickie, T.S. and Chaikin, M., *Journal of the Textile Institute*, 1960, **51**, T1120.
7. Alagha, M.J., Oxenham, W. and Iype, C., Influence of Production Speed on the Tenacity and Structure of Friction Spun Yarns, *Textile Research Journal*, 1994, **64**, 185–189.
8. Neckar, B., Ishtiaque, S.M. and Svehlova, L., Rotor Yarn Structure by Cross-section Microtomy, *Textile Research Journal*, 1988, **58**, p. 625–632.
9. Natterer, F., *The Mathematics of Computerized Tomography*, Wiley, 1986.
10. Tasto, M., Reconstruction of Random Objects from Noisy Projections, *Computer Graphics and Image Processing*, **6**, p. 103–122.
11. Lappage, J., Weavable Singles Yarn Potential, *Wool Record* 1999, **158**, (3656) June p. 89.
12. Hearle, J.W.S., Gupta, B.S. and Merchant, V.B., Migration of Fiber in Yarns Part I: Characterization and Idealization of Migration Behavior, *Textile Res. J.* 1965, **35**, p. 329–334.
13. Hickie, T.S. and Chaikin, M., Some Aspects of Worsted-yarn Structure Part IV: The Application of Fourier Analysis to the Study of Single-fiber Configurations in a Series of Worsted Yarns, *J. Textile Inst.*, 1974, **65**, p. 537–551.
14. Morton, W.E., The arrangement of fibers in single yarns, *Textile Res. J.*, 1956, **26**, p. 325–331.
15. Morton, W.E. and Yen, K.C., The arrangement of fibers in fibro yarns, *J. Textile Inst.*, 1952, **43**, T60–T66.
16. Riding, G., Filament Migration in Single Yarns, *J. Textile Inst.*, 1964, **55**, T9–T17.
17. Evans, M., Hastings, N. and Peacock, B., *Statistical Distributions*, 3rd Edition, John Wiley & Sons, Inc., New York, 2000.
18. Schutz, R.A., Kueny, M., LeChatelier, J. and Hunzinger, S., New Type of Twist Determination for Open-end and Ring-spun Yarns, *Melliand Textilberichte International*, 1976, **57**, No. 6, 438–441.
19. Peirce, F.T., Theorems on the Strength of Long and Composite Specimens, *J. Textile Inst.* 1926, T335–368.
20. Backer, S., The Mechanics of Bent Yarns, *Textile Research Journal*., 1952, **22**, 668–681.
21. Brorens, P.H., Lappage, J., Bedford. J., Ranford, S.L., Studies on the Abrasion Resistance of Weaving Yarns, *J. Textile Inst.* 1990, **81**, (2) p. 126–134.
22. Choi, K.F., Wong, Y.W., Luo, Z.X. and Lam, Y.L., Measurement of Lateral Yarn Density Distribution Using Computer Tomography Principle, p. 57 *Proceedings of the 6th Asian Textile Conference Abstract Book*, paper file name: 58.pdf, Proceedings CDROM, Sept. 2001.
23. Choi, K.F. and Kim, K.L., Fiber Segment Length Distribution on Yarn Surface in Relation to Yarn Abrasion Resistance, *Textile Research Journal*, **74**, No. 7, p. 603–606.

12
Fabrics

Y. LI[1] AND X-Q. DAI[1,2]
[1]The Hong Kong Polytechnic University, China
[2]Soochow University, China

12.1 Characteristics and classification of fabrics

12.1.1 Woven fabric

According to the weave structure, woven fabrics are classified into *basic weave* fabrics, consisting of plain-woven fabric, twill fabric, and satin fabric; and *complex weave* fabrics, including leno fabric, crepe woven fabric, dobby fabric, Jacquard fabric and other fabrics of complicated structures.

The three basic weave fabrics are the most commonly used for garment materials. As shown in Fig. 12.1, in the plain weave, each warp yarn interlaces with each weft yarn to form the maximum number of interlacings; in twill weave, warp and weft yarns float over two or more yarns from the opposite direction in a progression of two to the right or left; and in satin weave, warp or weft yarns float over four or more yarns from the opposite direction in a progression of two to the right or left. Leno fabric is mesh-like, and its warp yarns have been made to cross one another between weft yarns during weaving. Dobby fabrics are fabrics with small woven-in geometric patterns. Jacquard fabrics are fabrics with intricate, detailed woven-in motifs.

12.1.2 Knitted fabric

In weft knits, the yarn forming the fabric traverses the fabric crosswise. There are four fundamental stitches forming the diversity of weft knits: knit stitch, purl stitch, float stitch and tuck stitch. The three basic *single weft knits* are jersey, rib and purl, which are composed of all knit stitches or of knit and purl stitch. These fabrics differ in appearance as well as mechanical performance due to their varying stitch structures. The incorporation of tuck and float stitches in the basic structure further introduces a variation of appearances and alters elongation and dimensions. The two *double knits* are rib and interlock, which are rib structures having alternating knit and purl stitches.

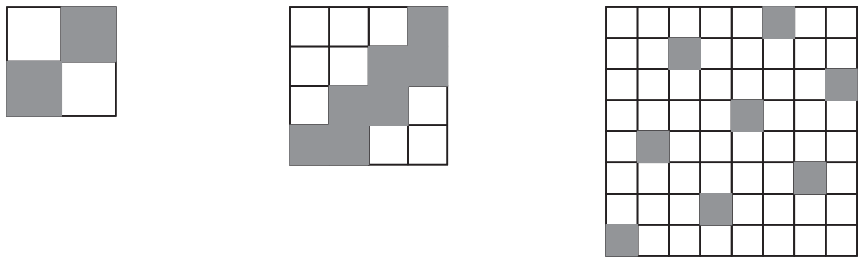

(a) Plain (b) Twill (c) Satin

12.1 Basic weaves.

In warp knits, the yarn forming the fabric traverses the fabric lengthwise. There are three major types of warp knits: tricot, Raschel, and nets and laces. *Tricot*, composed of all knit stitches, represents the commodity warp-knit product. Tricot fabrics vary in the number of sets of yarns in their structure: one-, two-, three- and four-bar. The greatest quantity of tricot produced is two-bar, which is used extensively in a variety of end uses.

Raschel knits are composed of vertical columns of chain stitches and an in-laid yarn that traverses the fabric horizontally between chain stitches. The three main types of Raschel fabrics are those with the basic structure, fall-plate Raschels, and pile Raschels. Both net and lace are open fabrics. Net is an open-mesh fabric in which a firm structure is ensured by some form of twist, interlocking, or knitting of the yarn. Lace is a fine openwork fabric with a ground of mesh or net on which patterns may be worked at the same time as the ground is formed or applied later, and which is made of yarn.

12.1.3 Functional fabrics

There are many kinds of functional requirements for fabrics, varying according to different garment end uses, such as easy care, softness of touch, quick drying, UV-protection, anti-bacteria, long durability, and so on. In regard to the mechanical performance of garments, fabric stretch and recovery are most important. In stretch fabric, a certain percentage of elastic fibers are usually incorporated.

12.2 Fabric construction measurement

Fabric length: The US standard ASTM D3773-90 and ISO 3933 describes the standard test methods for fabric length testing.

Fabric width: The width of a fabric depends on the loom on which the fabric is manufactured. Testing can follow the standard ASTM D3774 and ISO 3932.

Fabric thickness: This is one of the basic properties of a fabric, giving information on its warmth, heaviness, and stiffness in use. Since fabric is sensitive to the pressure used in thickness measurement, it is difficult to measure fabric thickness with satisfactory accuracy. Usually, a thickness gauge, micrometer, FAST-1[1] or KES-FB3[2] are used to obtain standard thickness or a thickness-pressure curve for a fabric. The standards ASTM D1777 and ISO 5084 describe several test methods for fabric thickness testing.

Fabric weight: The heavier a fabric, the more load that is placed on the human body wearing it. Weight can be conveyed as very light (<1 ounce per yard^2), light (2–3 ounces per yard^2), medium (5–7 ounces per yard^2), heavy (>7 ounces per yard^2), or very heavy. Fabric weight is usually measured by using a chemical balance. ASTM D3776, ISO 3801 and ISO 7211-6 describe several standard test methods for fabric weight.

Fabric weave: ISO 7211-1 describes the analysis method for fabric weave diagrams.

Fabric count: This is an important determinant of the quality of fabric and affects various mechanical properties. Generally, the higher the fabric count, the better the technological quality of the fabric. Fabric can also be roughly classified into: tightly woven, closely woven, and loosely woven. ASTM D3775-98 and ISO 7211-2 describe standard methods for determining fabric count.

Fabric crimp: This usually refers to yarn crimp in the fabric. It provides technological data for weaving design and for computation of yarn usage. ASTM D3883-99 and ISO 7211-3 describe the methods for determining yarn crimp in woven fabrics.

Yarn count and yarn twist: To analyze the construction of a fabric, the count and twist of yarn removed from fabric needs to be determined. ASTM D1059-97 and ISO 7211-5 are for testing the count of yarn removed from fabric, and the ASTM D1423-99 and ISO 7211-4 are for testing the twist of the yarn.

12.3 Basic mechanical properties and their measurement

12.3.1 Basic mechanical properties of fabric

In normal garment wear, cloth deformation is a mixture of tension, bending shearing and twisting. Therefore, besides the geometry and biomechanical properties of the human body, garment aesthetic appearance and mechanical comfort depends on these basic mechanical properties. Actually, fabric mechanical-comfort performance has been evaluated by consumers and textile producers subjectively by means of the hand of the fabric. And, fabric handle is used to describe the assessed results. However, fabric objective measurement (FOM) has been widely researched during the past several decades with the aim of specifying and controlling the quality, tailorability, and ultimate performance of apparel fabric. Many test methods, instruments and pieces of apparatus have been developed to measure parameters associated with fabric handle. Most of these parameters point to the basic mechanical properties of the fabric.

Tensile: Fabric tensile properties can be investigated on universal tensile testers. The most commonly used instrument for tensile test is the Instron tensile machine. A fabric specimen is often extended at a suitable rate of extension to its breaking point, and the load–extension curve is produced. There are two major ways to carry out the tensile test – strip test (BS 6176) and grab test (ASTM D1682), as illustrated in Fig. 12.2. Warp-wise and weft-wise specimens are prepared, then the tensile properties in these two principle directions can be investigated.

Figure 12.3 shows the load–elongation curves of two fabrics tested along the warp and weft directions on an Instron tensile machine. From these curves, the Young's modulus (that is the initial slope of the curve), break

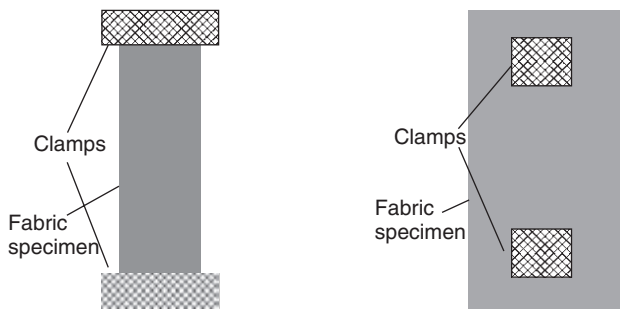

12.2 Instron tensile test.

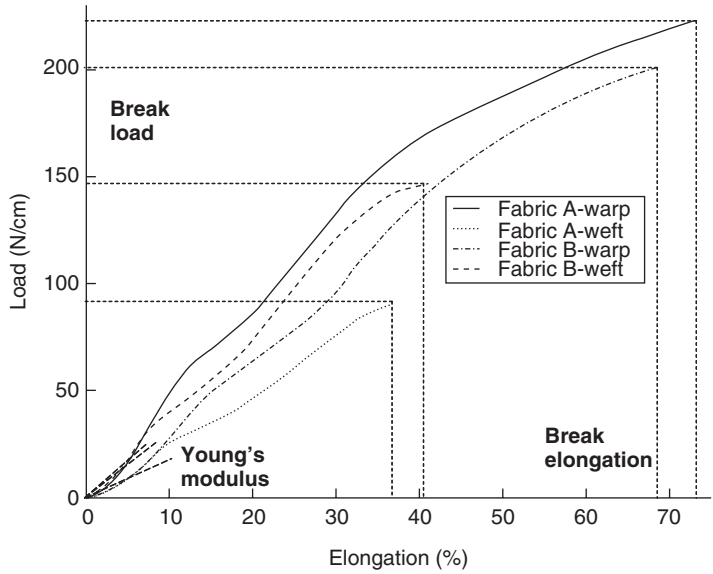

12.3 Instron load–elongation curves.

elongation and break load are often taken as parameters to describe the tensile properties of the fabrics tested. When extending a fabric specimen in one direction, it will contract in the other direction. The ratio of the contraction to the elongation is the Poisson ratio (σ). This can also be obtained by the biaxial tensile test.

Shear: It is the shear property that enables fabrics to undergo more complex deformations than two-dimensional bending and so conform to the contours of the body in garment end use. There are two major approaches to measure the shear property. One was proposed by Morner and Eeg-Olofsson,[3] the other one was developed by Behre.[4] Both of the two pieces of apparatus were attached to the Instron tester. Based on these two methods, many further investigations and improvements have been made.[5–8]

The resistance to shearing, R, is the same in the two methods:[6]

$$R = F - W\tan\theta = F - L\sin\theta.$$

Both of the two approaches produce records on a graph of the angular deformation and the resistance to deformation, and provide a complete hysteresis curve for the shear resistance of the fabric tested. Figure 12.4 shows a typical shear stress–strain curve. Cusick[5] took a number of parameters quantifying shear behavior from the curve: (i) the initial shear modulus, given by the slope of the curve at the origin O; (ii) the shear

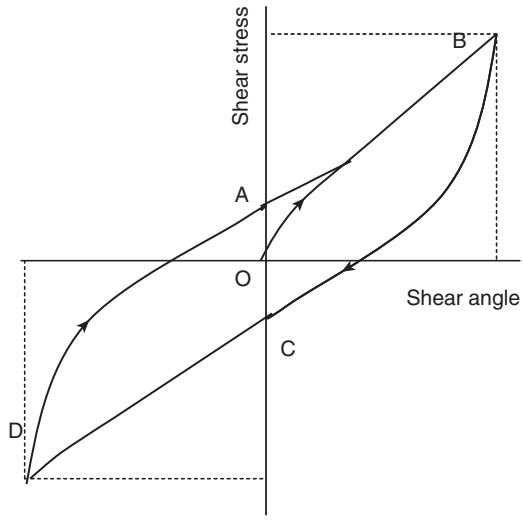

12.4 Typical shear curve.

modulus at zero shear angle, given by the slope at points A and B; (iii) the hysteresis at zero shear angle, given by the length of AC; and (iv) the buckling shear and the buckling angle at B and D, respectively.

Besides these items of apparatus/instruments designed specially for shear property investigations, there is also another approach to measure shear by using tensile testers directly. Killy has derived a formula that gives the Young's modulus (E_θ) for a fabric in the bias directions that are at an angle θ to the warp direction:[9]

$$1/E_\theta = (1/E_1)\cos^4\theta + (1/G - 2\sigma_1/E_1)\cos^2\theta\sin^2\theta + (1/E_2)\sin^2\theta\,.$$

Here, E_1 and E_2 are the Young's moduli of the warp and weft directions respectively, σ_1 denotes the Poisson ratio of the warp direction, and G is the shear modulus. If tensile tests are carried out on specimens of the warp, the weft, and the bias direction at an angle of 45 ° to the warp respectively, then the shear modulus G can be calculated by the above equation.

Bending: Since fabric stiffness has a dominant effect on aesthetic appearance in garment end use, there have been many methods developed to measure it. Peirce first proposed the Cantilever test.[10,11] In that test, a horizontal strip of fabric, one inch wide, is clamped at one end and the rest of the strip is allowed to hang under its own weight. The angle between the horizontal and the chord from the edge of the platform to the tip of the fabric is measured. He defined two quantities calculated from the angle θ:

(i) the bending length $c = l \cdot f(\theta)$, where l = length of fabric overhanging the platform(m), and $f(\theta) = \left(\frac{\cos 0.5\theta}{8 \tan \theta}\right)^{1/3}$;

(ii) the flexural rigidity $F = wc^3$ (Nm), where w = weight (g/m^2).

The higher the bending length, the stiffer the fabric. The Shirley stiffness tester measures the bending length of fabric in another way. A narrow horizontal strip (25 mm × 200 mm) of fabric is allowed to bend to a fixed angle under its own weight. The length of the fabric required to bend to this angle is taken as the bending length.

Peirce also proposed a hanging loop method for fabrics that are too limp to give a satisfactory result by the cantilever method.[10] A one-inch-wide strip of fabric of length L has its two ends clamped together to form loops of different shapes: ring, pear and heart. Figure 12.5 shows a heart loop. The undistorted length of the loop that is under no gravitational or other force, l_0, from the grip to the lowest point, has been calculated by Peirce. The actual length (l) of the loop under the force of gravity is measured. Then, the bending length is calculated as follows for each loop shape:

Ring loop: $l_0 = 0.3183L$, $\theta = 157°$ d/l_0, $c = L0.133f_2(\theta)$;

Pear loop: $l_0 = 0.4243L$, $\theta = 504.5°$ d/l_0, $c = L0.133f_2(\theta)/\cos 0.87\theta$;

Heart loop: $l_0 = 0.1337L$, $\theta = 32.85°$ d/l_0, $c = l_0 f_2(\theta)$.

Here, $d = l - l_0$, and $f_2(\theta) = (\cos\theta/\tan\theta)^{1/3}$. The flexural rigidity is calculated from the bending length in the same way as the cantilever test.

The stiffness of a fabric in bending is very dependent on its thickness, T; the thicker the fabric, the stiffer it is if all other factors are the same. The bending modulus, B (N/m^2), can then be calculated from the flexural rigidity by the following formula:

$$B = 12F/T^3.$$

ASTM D1388 and BS 3356 describe the details of fabric stiffness tests.

To investigate fabric stiffness, Owens *et al.* developed the Shirley cyclic bending tester.[12–15] A bending-hysteresis curve can be obtained from this.

Twist: Since fabric twist always occurs accompanied by bending, it is difficult to measure the pure twist of fabric. Shanahan *et al.* have pointed out that a pure bending along a bias direction is a combination of twist and bending in the warp and weft directions.[16] A formula was derived to calculate the flexural rigidity in the bias direction at an angle θ to the warp:[18]

$$F_\theta = F_1 \cos^4\theta + (4\tau + 2\upsilon_2 F_1)\cos^2\theta \sin^2\theta + F_2 \sin^4\theta$$

where, F_1 and F_2 denote the flexural rigidities in the warp and weft direction, υ_2 is analogous to Poisson's ratio, and τ is the twist rigidity. Then, instead of

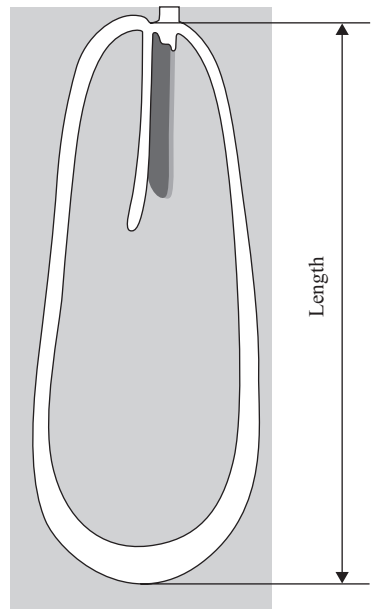

12.5 Heart loop.

measuring twist rigidity directly, it can be obtained by testing the bending of a fabric specimen in a bias direction. With F_1, F_2 and F_θ known, the twist rigidity can be obtained.

Compression: The Schiefer compressometer and universal testers with compression cells can be used to obtain the thickness–pressure curve. ASTM D 6571 discloses a method to measure the compression resistance and recovery properties of any type of high-loft, non-woven fabric using a simple and economically applied static weight loading technique.

Table 12.1 provides a summary of the basic mechanical property tests.

Table 12.1 Summary of basic mechanical property tests

Property	Instruments/methods	Parameter description	Units	References
Tensile	Universal/tensile testers(Instron, Hounsfield, etc.)	Load-elongation curve, Extensibility, Initial Young's modulus, Recovery, Hysteresis	– % N/m width % N/m width	[10]
Shearing	Universal/tensile testers(bias extension) Morner and Eeg-Olofsson's method, Behre's method	Load-extension curve in bias direction, Shear-force/shear-angle curve, Shear modulus, Shear hysteresis	– – N/m*degree N/m	[3–5, 19]
Bending	Cantilever, Hanging loop, Shirley stiffness tester, Shirley cyclic bending tester	Bending length, Felxural rigidity, Bending modulus, Bending hysteresis curve	mm Nm N/m^2	[10, 11, 13–15, 17, 20, 21]
Compression	Universal testers(compression cells), Schiefer compressometer	Thickness-pressure curve, Compressibility, Compressional resilience and hysteresis	– %	[10] [23]

12.3.2 Surface properties

As described in Chapter 9, the basic mechanical properties have an influence on a garment's aesthetic appearance as well as contact comfort through pressure. Besides them, the surface properties (usually roughness and friction) of cloth influence not only the contact state, but also the touch sense of humans. A number of roughness testers have been used for measuring the surface roughness of sheet materials.[13]

There are several approaches for fabric friction measurement. One approach is to carry out friction tests in tensile testers with special friction attachments. The principle of the test is illustrated in Fig. 12.6a, where a block of mass m is pulled over a horizontal flat rigid surface covered with the fabric being tested, and the line connected to the block is led around a frictionless pulley and connected to an appropriate load cell in a tensile tester. Then, the coefficient of friction, $\mu = F/mg$. The Instron machine is most popularly used.[13] An inclined plane method, illustrated in Fig. 12.6b, has also been used for fabric friction testing. Here, $\mu = \tan\theta$. The Shirley Fabric Friction Tester was developed for testing coated fabrics based on this principle.[18]

12.3.3 KES-F system

Kawabata and his co-workers developed the KES-F (Kawabata Evaluation Systems for Fabrics) with the aim of objectively measuring the appropriate fabric properties and then correlating these measurements with the subjective assessment of handle.[19] The system consists of four specialized instruments: (i) FB1 tensile and shearing; (ii) FB2 bending; (iii) FB3 compression; and (iv) FB4 surface friction and variation. The system investigates the responses of various mechanical behaviors under low-load. As is well known, fabric mechanical properties in the low-load region possess a pecu-

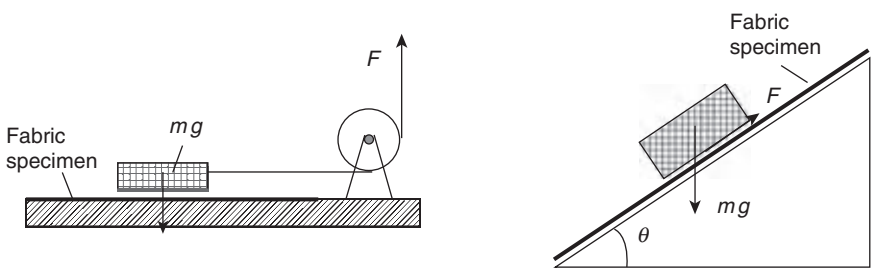

(a) Horizontal pull (b) Friction inclined plane

12.6 Friction test.

liar non-linearity. One example of the non-linearity is the hysteresis behavior in the load–deformation relation. These properties of cloth have significant influences on the aesthetic shape and wear comfort in garment end use. They must be measured exactly and expressed by parameters. Fabric specimens of 20 cm × 20 cm are used for all measurements except compression.

Tensile property

The tensile test is illustrated in Fig. 12.7a. Extension is applied along the 5 cm direction of the specimen up to 500 gf/cm. The transverse contraction is not limited, so the test is a type of biaxial extension. Figure 12.7b shows a typical load–extension hysteresis curve. From this curve, several parameters are derived:

Tensile energy, $WT = \int_0^{\varepsilon_m} F\mathrm{d}\varepsilon$ (gf×cm/cm^2);

Linearity of load–extension curve, $LT = WT/WOT$, where $WOT = F_m \cdot \varepsilon_m/2$;

Tensile resilience, $RT = (WT'/WT) \times 100$, (%), where $WT' = \int_0^{\varepsilon_m} F'\mathrm{d}\varepsilon$;

Extensibility, EM, the strain (ε_m) at 500 gf/cm.

Shearing property

The shear test is carried out using the same tester as the tensile test (KES-FB1). It is illustrated in Fig. 12.8a; a rate of shear strain of 8.34×10^{-3}/sec is applied to the specimen under a constant extension load (10 gf/cm) up to a maximum shear angle of 8°. Figure 12.8b is the obtained shear-force/shear-angle hysteresis curve. From it, the following parameters are measured:

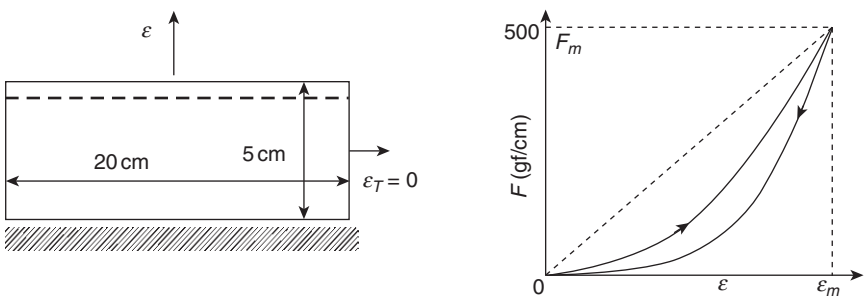

(a) Specimen extension (b) Load–elongation curve

12.7 KES tensile test.

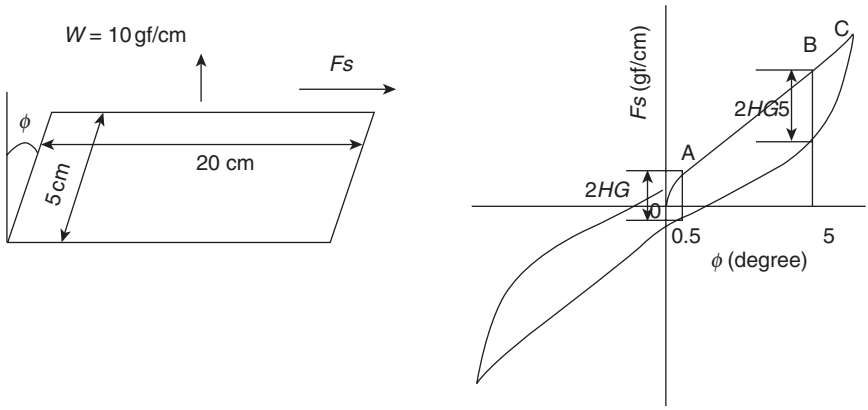

(a) Specimen shearing (b) KES shearing curve

12.8 KES shear test.

(i) G, shear rigidity, mean slope of the curve in the region $\phi = 0.5° \sim 5°$; (ii) $2HG$, hysteresis of shear force at shear angle of 0.5°; (iii) $2HG5$, hysteresis of shear force at shearing angle of 5°.

Bending

Figure 12.9 shows the KES-FB2 bending tester. In the KES bending test, a specimen is bent between the curvatures –2.5 and 2.5 cm^{-1}, as illustrated in Fig. 12.10a. Figure 12.10b is a bending curve, from which two parameters are measured: B, bending rigidity, the mean slope of the curve in the region $K = 0.5 \sim 1.5\,cm^{-1}$; and $2HB$, hysteresis of bending moment, measured at $K = 0.5\,cm^{-1}$.

Compression

Figure 12.11 shows the KES compression tester FB3. The specimen used for the compression test is 2.5 cm × 2.0 cm and the effective pressure region is a circular area of 2 cm^2. The specimen is compressed in the direction of its thickness to a maximum pressure of 50 gf/cm^2, as illustrated in Fig. 12.12a. The shape of the obtained pressure–thickness curve (Fig. 12.12b) is similar to that of the load–extension curve, and the parameters are also defined the same way as those for the tensile property: LC, linearity of compression curve; WC, compression energy; and RC, compression resilience. The fabric thickness at 50 Pa pressure, T_0 and that at 200 Pa pressure T_m can also be obtained from the thickness–pressure curve. The compression tester can also be used for fabric thickness measurement.

12.9 KES-FB2 bending tester.

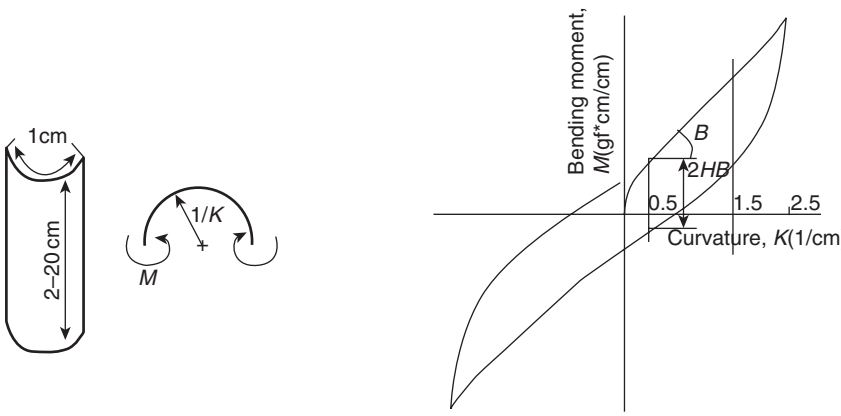

(a) Specimen bending (b) KES bending curve

12.10 KES bending test.

Surface properties

Figure 12.13 is the KES-FB4 tester for evaluating surface properties. Surface roughness is measured by pulling across the surface a steel wire of 0.5 mm diameter that is bent into a U shape, as illustrated in Fig. 12.14a. Figure

12.11 KES-FB3 tester.

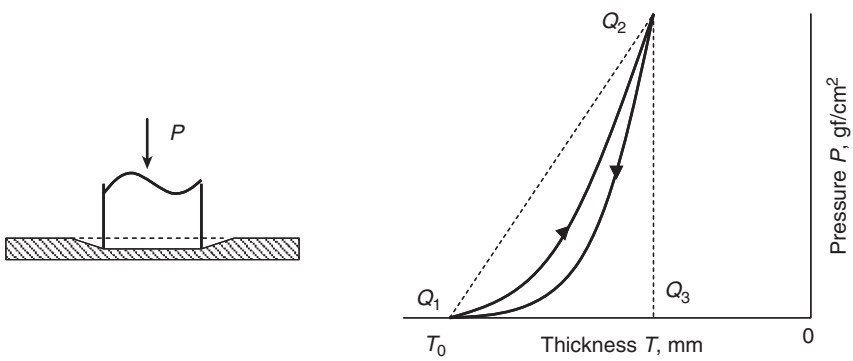

(a) Compression deformation (b) KES compression curve

12.12 Compression test.

12.14b shows a plot of the height variation along the distance. The mean deviation of surface contour, *SMD* is calculated from the plot, *SMD* = hatched area/*X*.

Surface friction is measured in a similar way by using a contactor consisting of 10 pieces of the same wire used in the roughness test, as shown in

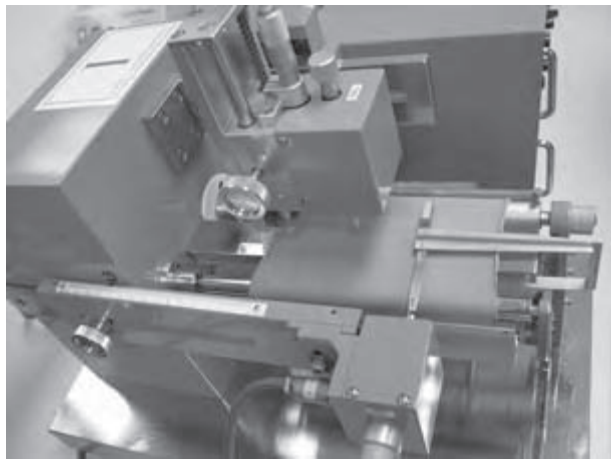

12.13 KES-FB4 tester.

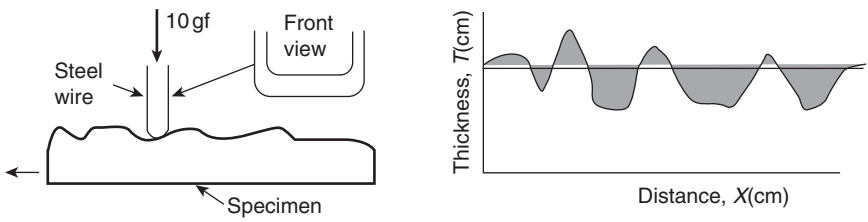

(a) Roughness measurement (b) Surface thickness variation

12.14 KES surface roughness test.

Fig. 12.15a. The force required to pull the fabric passing the contactor is measured. Figure 12.15b shows the obtained plot of friction versus distance travelled, from which two parameters are calculated: the coefficient of friction, *MIU*, the mean value of the curve; and the mean deviation of the coefficient of friction, *MMD*.

12.3.4 The FAST system

Fabric Assurance by Simple Testing (FAST) is a system specifically designed by CSIRO in Australia for use by tailors and worsted finishers to highlight problems that may be encountered in making fabrics, mainly wool and wool-blend, into garments.[1] It is claimed to be much simpler and more robust than the KES-F system, so it can be used as an alternative in many applications. This system comprises three purpose-designed instruments: FAST 1, compression meter, FAST 2, bending meter, and FAST 3, extension

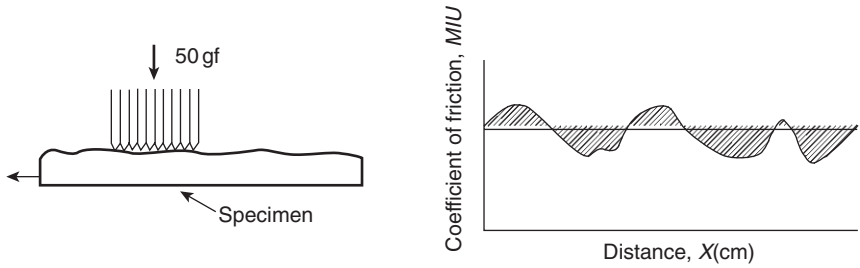

(a) Friction measurement (b) Surface friction variation

12.15 KES surface friction test.

meter; and a test method, FAST 4, dimensional stability test, which requires no specialized equipment.

In the compression test, the thickness of a fabric specimen is measured on a 10 cm^2 area at two different pressures, firstly at 2 gf/cm^2 (0.196 kPa) and then at 100 gf/cm^2 (9.81 kPa). The difference between these two thickness values is regarded as the fabric surface thickness. This is based on the consideration that a fabric consists of an incompressible core and a compressible surface.

The FAST bending meter measures the bending length of a fabric specimen automatically. The flexural rigidity is then calculated from the bending length and the fabric weight as mentioned before.

Using the FAST extension meter, the extension of the fabric is measured in the warp and weft directions at three fixed forces – 5, 20, 100 gf/cm (4.9, 19.6, and 98.1 N/m). The extension at 98.1 N/m is defined as the extensibility. And the extension values at 4.9 and 19.6 N/m are measured for the calculation of the formability, together with the respective bending rigidity. The extension is also measured on the bias in both directions, only at a force of 5 gf/cm (4.9 N/m), to enable the calculation of the shear rigidity.

12.4 Mechanical properties in complex deformation

12.4.1 Bi-extension

In normal garment wear, especially with tight-fit garments, the fabric is often stretched in both the two principal directions. How the fabric responds to such deformation has an important influence on the appearance and comfort of the garments. Kawabata *et al.* developed an instrument to investigate the fabric properties in biaxial extension. Figure 12.16 shows the KES-G2 tester. The test is illustrated in Fig. 12.17a, where two forces are applied continuously to the two axes of the fabric specimen,

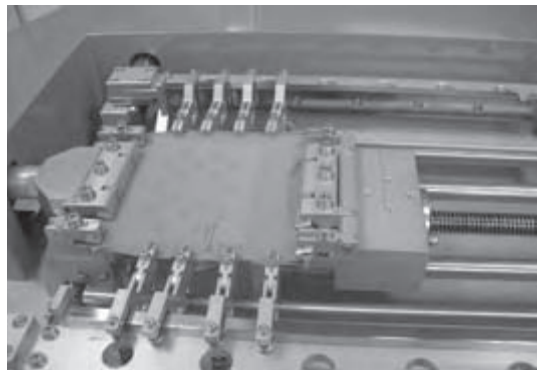

12.16 KES-G2 tester.

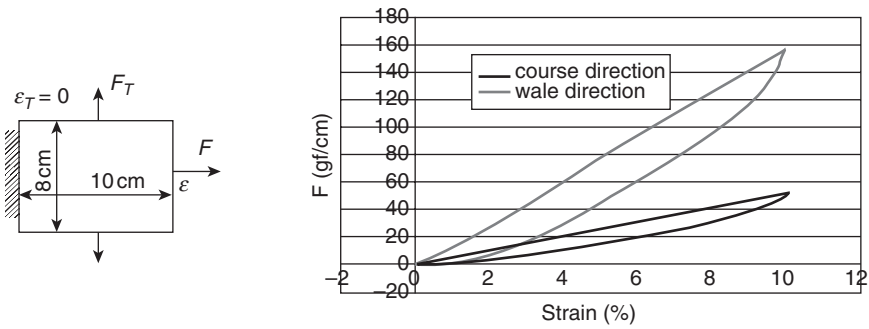

(a) Specimen biaxial extension (b) Load–extension curve

12.17 KES biaxial tension test.

respectively, to keep it constrained on one axis and elongated on the other axis. Figure 12.17b shows the obtained curve of the two forces versus the elongation.

12.4.2 Buckling and formability

Eeg-Olofsson developed a method to measure fabric plate buckling using an Instron tensile testing machine.[21] The test specimen was inserted between two clamps. The lower clamp was rigidly fixed to the movable Instron beam. The upper clamp was guided by means of two rods mounted in bearings on the frame of the Instron machine and suspended by a wire from the strain-gauge. An extra load was hung on the left-hand of the rods in order to maintain tension in the suspension wire throughout the test.

Dahlberg also developed an apparatus as an attachment to the Instron tensile tester for measuring plate buckling and shell buckling of fabric.[22] Both of the tests produced load–deformation curves.

Formability is a measure of the degree of compression in the fabric plane sustainable by it before buckling occurs. Lindberg *et al.* pointed out that it is an important property required in garment construction.[23] Low values of formability indicate that a fabric becomes easily puckered when made into a collar or cuff. The compression force required to buckle a sample of fabric of length l is given by $P = kB/l^2$, where B is the bending rigidity, and k is a constant. Under this compression force, the amount of the fabric compression before it buckles is then given by $CP = kCB/l^2$, where C denotes the longitudinal compressibility (that is often assumed to be equal to the extensibility). Here, CB is a specific property of the fabric determining how much compression it can undergo before buckling. It is defined as the compression formability, F_c.[23] There is no particular instrument for the formability test. It is usually a by-product of the measurements of tensile modulus and bending rigidity.

12.4.3 Drape

The British standard for the assessment of drape of fabrics (BS 5058) describes a method using the 'Drapemeter'. A circular specimen, about 0.3 m in diameter, is supported on a circular disk of 0.18 m diameter. The unsupported area may drape to form some folds. The number of the folds (nodes) is used to describe the drapability directly. The more the nodes, the softer is the fabric. The drape coefficient is the ratio of the projected area of the fabric sample to its undraped area, in which the area of the supporting disk is deduced.

> Drape coefficient = (the area of the shadow – the area of the supporting disk)/(the area of the circular specimen – the area of the supporting disk)

The higher the drape coefficient, the stiffer the fabric.

According to BS 5058, there are three diameters of specimen that can be used:

(i) 30 cm for medium fabrics;
(ii) 24 cm limp fabrics, whose drape coefficients are below 30% with the 30 cm sample;
(iii) 36 cm for stiff fabrics, whose drape coefficients are above 85% with the 30 cm sample.

12.4.4 Stretch and recovery properties

Certain types of garments, particularly sportswear, dancewear, and foundation underwear, are made to be close-fitting or tight-fitting to the body. The fabric for such garments should be able to stretch to accommodate firstly the donning and removal of the garment and secondly any activity that is undertaken while wearing it. To avoid bagging and to remain close fitting, the stretch has to be followed by complete recovery of the original dimensions. For this purpose, usually a small percentage of elastic fibers are incorporated into the fabric structure. There are a large number of methods developed for stretch fabric measurement. Generally, two quantities are measured: one is the extension at a given load, sometimes known as the modulus, which is a measure of how easily the fabric stretches; the other is how well the fabric recovers from stretching to this load, usually measured as growth or residual extension.[24]

The British standard for elastic fabrics (BS 4952) describes a number of test methods using either line contact jaws or looped specimens. The standard covers both woven and knitted fabrics. The measured quantities include: extension at a specified force, modulus, residual extension and tension decay. In the extension test, the sample is cycled twice between zero extension and a specified force. The elongation at the specified force is measured for the extension, and the modulus is obtained by recording the force at specified values of elongation. In the residual extension test, the sample of gauge length L_1 is given a preliminary stretch cycle then extended by a specified force that is held for 10 s. The force is then removed and the sample is allowed to relax on a flat and smooth surface. The length of the sample clamped between the jaws is measured after 1 min (L_2) and after 30 min (L_3) respectively. The following quantities are calculated:

$$\text{Mean residual extension after 1 min} = \frac{L_2 - L_1}{L_1} \times 100\%,$$

$$\text{Mean residual extension after 30 min} = \frac{L_3 - L_1}{L_1} \times 100\%.$$

The tension decay is tested by holding the sample at a specified elongation for 5 min and measuring the decay in force over this period: Tension decay = $\frac{F_1 - F_2}{F_1} \times 100\%$, where F_1 is the maximum force at the specific elongation, and F_2 is the force after 5 min.

The US standard for the stretch properties of woven stretch fabric (ASTM D3107) measures two quantities: percentage stretch, elongation at a fixed

load; and fabric growth, which is the same as residual extension. The US standard for knitted fabric having lower power (ASTM D2594) measures the stretch and the growth after a much longer period.

12.4.5 Strength

Bursting strength

Tensile strength tests are generally used for woven fabrics where there are definite warp and weft directions. However, some other fabrics, such as knitted fabrics, lace or non-woven fabrics do not have such principle directions where the strength reaches a maximum. Bursting strength, in which the material is stressed in all directions at the same time, is an alternative method of measuring strength for such materials. Actually, in many garments, especially at some particular position, such as elbows and knees, the fabric is stressed in all directions during wearing, so it is important to carry out a strength test in a realistic manner.

The BS 4768 describes a diaphragm bursting strength test method, as illustrated in Fig. 12.18a. The fabric specimen is clamped over a rubber diaphragm by means of an annular clamping ring and an increasing fluid pressure is applied to the underside of the diaphragm until the specimen bursts. The operating fluid can be a liquid or a gas. Two quantities are reported: mean bursting strength (kN/m^2) and mean bursting distension (mm). ASTM D3786 describes a similar method. ASTM D3787 describes a ball bursting strength method as illustrated in Fig. 12.18b. The test can be carried out using an attachment on a standard tensile testing machine. In

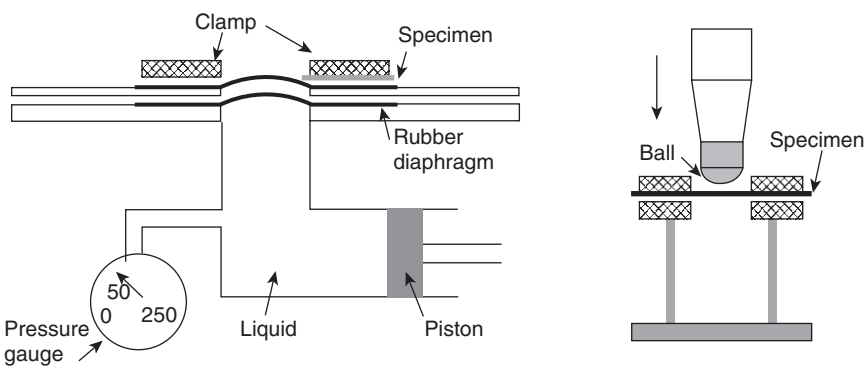

(a) Diaphragm bursting strength (b) Ball bursting strength

12.18 Bursting test.

the test, a steel ball is pushed through the stretched fabric specimen and the force required is recorded. ISO 13938 also describes a hydraulic method and a pneumatic method for determination of bursting strength and a bursting distension.

Tearing strength

A fabric tears when it is snagged by a sharp object and the immediate small puncture is converted into a long rip by what may be a very small extra effort. It is the most common type of strength failure of fabrics in end use. For garment items, such as outdoor clothing, overalls and uniforms, the tearing strength is a very important quantity. The fabric tear property measured is the force required to propagate an existing tear and not the force required to initiate a tear, as this usually requires cutting of threads. In the test, the specimen is cut first and the force required to extend the cut is measured. This is conveniently carried out by gripping the two halves of the cut in a standard tensile tester, and obtaining a tear test force extension curve. The various tear tests carried out in this manner, which are called tongue tear tests, differ mainly in the geometry of the specimen. ASTM D2261 describes a single rip tear test method, and BS 4303 also describes a wing rip tear test method. The results can be expressed as the maximum, the median, or the average tearing resistance.

Another approach to measure tear strength is the ballistic tear test, which measures energy loss (work done) during tearing. ASTM 1424 describes a tear strength test using the Elmendorf tear tester. There is the following equation for the relationship between the tearing force and the energy loss:

$$\text{Energy loss} = \text{tearing force} * \text{distance}.$$

Seam strength

Seam strength is the resistance to yarn slippage in a fabric seam. There are three different types of seam slippage test:

(i) To measure the maximum force to seam rupture.
(ii) To plot a load–extension curve with and without a standard seam and take the difference between the two curves as the slippage.
(iii) To put a standard seam under a fixed load and measure the seam gape.

ISO 13935 describes two methods of the first type. BS 3320 describes a standard test of the second type.

12.4.6 Bagging

There are a few methods developed for evaluation of woven and knitted fabrics' bagging behavior. The Celanese bagging test uses the principle of tensile stretch and recovery and is adaptable to the Instron tensile machine.[25] A 10-inch-diameter specimen is subjected to repeated loads of between 0.5 and 15 pounds. The immediate growth and immediate distortion are recorded, and from them a measure of immediate recovery is obtained. Based on a comparison with wear trials, fabrics with an immediate recovery value greater than 59% are considered to be satisfactory, 53–59% to be on the borderline and less than 53% to be unsatisfactory.

The Zweigle type bagging tester uses the Gronewald and Zoll principle, and enables measurement of bagging tendency under reasonably realistic conditions.[26] The testing apparatus is an artificial arm with an elbow joint. The test fabric, suitably made into tubular form, is drawn onto the tester. With the testing arm bent, the sample is subjected to five hours of static strain. The testing arm is then brought to the straight position and the specimen is allowed to recover. After a 10-minute recovery, the specimen is withdrawn from the arm and the bagging height at the elbow region is measured. For all the fabrics tested, when the bagging height measured in the laboratory was below 5 mm, a fabric was judged to be wearable under practical conditions.

Yokura *et al.*[27] developed an apparatus for the measurement of fabric bagging behavior in terms of increased volume. In the test, a fabric sample is placed on a hemisphere of 14 cm diameter, clamped by chucks and then loaded using a square frame for five hours. The shape of the distorted specimen is measured using the Moiré topographic technique. The volume formed by the bagged fabric is used to evaluate its bagging propensity.

Zhang[28] and Zhang *et al.*[29,30] developed an apparatus that is attached to an Instron tensile machine to investigate the dynamic bagging property of a fabric. A specimen, under a pre-tension force, is stretched to a predetermined height and returned to its original position. This process is repeated continuously many times, followed by a specified recovery time under zero loading. After recovery, the specimen is subjected again to the same pre-tension force and then the non-recovered bagging height is measured. The relative residual bagging height is then the ratio of the non-recovered bagging height to the predetermined bagging height in percentage terms.

12.5 Conclusion

The structural features, classification of woven and knitted fabrics, and the fabric construction measurements have been briefly reviewed. Descriptions of the mechanical properties of fabrics in simple and complex deformations,

which determine the biomechanical performance of clothing, were introduced. The commonly used parameters were derived from these descriptions. To obtain these parameters for biomechanical engineering design, various testing methods and apparatus including the KES and FAST systems were summarized.

12.6 Acknowledgement

We would like to thank Hong Kong Polytechnic University for funding this research through Projects A188 and G-YD31.

12.7 References

1. De Boos, A.G. and Tester, D.H., The FAST Approach to Improved Fabric Performance, in *First International Clothing Conference*. 1990. Braford.
2. Kawabata, S., The Development of the Objective Measurement of Fabric Handle, in *Second Australia–Japan Symposium on Objective Evaluation of Fabric Quality, Mechanical Properties, and Performance*. 1982. Kyoto: Textile Machinery Society of Japan.
3. Morner, B. and Eeg-Olofsson, T., Measurement of the Shearing Properties of Fabrics. *Textile Research Journal*, 1957. **27**(8): p. 611–615.
4. Behre, B., Mechanical Properties of Textile Fabrics, Part I: Shearing. *Textile Research Journal*, 1961. **31**(2): p. 87–93.
5. Cusick, G.E., The Resistance of Fabrics to Shearing Forces: A Study of the Experimental Method due to Morner and Eeg-Olofsson. *Journal of the Textile Institute*, 1961. **52**: p. T395–T406.
6. Treloar, L.R.G., The Effect of Test-Piece Dimensions on the Behaviour of Fabrics in Shear. *Journal of the Textile Institute*, 1965. **56**: p. T533.
7. Spivak, S.M., The Behavior of Fabrics in Shear, Part I: Instrument Method and the Effect of Test Conditions. *Textile Research Journal*, 1966. **36**: p. 1056–1063.
8. Koh, V.K., Shear Behavior of Woven Fabrics. *Textile Research Journal*, 1989. **59**: p. T142–T150.
9. Killy, W.F., Planar Stress–Strain Relationships in Woven Fabrics. *Journal of the Textile Institute*, 1963. **54**: p. T9–T27.
10. Peirce, F.T., The Handle of Cloth as a Measurable Quantity. *Journal of the Textile Institute*, 1930. **21**: p. T377.
11. Abbott, N.J., The Measurement of Stiffness in Textile Fabrics, Part II: A Study of the Peirce Cantilever Test for Stiffness of Textile Fabrics. *Textile Research Journal*, 1951. **21**(6): p. 441–444.
12. Livesey, R.G. and Owens, J.D., Cloth Stiffness and Hysteresis in Bending. *Journal of the Textile Institute*, 1964. **55**: p. T516.
13. Owens, J.D., An Automatic Cloth-bending-hysteresis Tester and Some of its Applications. *Journal of the Textile Institute*, 1966. **57**: p. T435–T438.
14. Owens, J.D., *Journal of the Textile Institute*, 1967. **58**: p. 589.
15. Owens, J.D., *Journal of the Textile Institute*, 1968. **59**: p. 313.

16. Shanahan, W.J., Lloyd, D.W. and Hearle, J.W.S., Characterizing the Elastic Behavior of Textile Fabrics in Complex Deformation. *Textile Research Journal*, 1978. **48**(4): p. 495–505.
17. Cooper, D.N.E., The Stiffness of Woven Textiles. *Journal of the Textile Institute*, 1960. **51**: p. T317–T335.
18. Shirley Institute, *Shirley Fabric Friction Tester(SDL 264), Instruction Manual* (Date unknown).
19. Kawabata, S., The Standardization and Analysis of Hand Evaluation, The Textile Machinery Society of Japan. 1980.
20. Kawabata, S. and Niwa, M., Objective measurement of fabric hand, in *Modern Textile Characterization Methods*, M. Raheel, Editor. 1996, Marcel Dekker, Inc.
21. Eeg-Olofsson, T., *Journal of the Textile Institute*, 1959. **50**: p. T112–T132.
22. Dahlberg, B., Mechanical Properties of Textile Fabrics, Part I: Buckling. *Textile Research Journal*, 1961. **31**(2): p. 94–99.
23. Linberg, J., Waesterberg, L. and Svenson, R., Wool Fabrics as Garment Construction Materials. *Journal of the Textile Institute*, 1960. **51**: p. T1475.
24. Slater, K., Chapter 5, Strength and Elongation Tests, in *Physical Testing and Quality Control*. The Textile Institute, Manchester, 1993.
25. Thomas, W., Celanese Bagging Test for Knit Fabrics. *J. Am. Assoc. Textile Chemists and Colorists* 1971. **3**: p. 231–233.
26. Gronewald, K.N. and Zoll, W., Practical Method for Determining the 'Bagging' Tendency in Textiles. *International Textile Bulletin, Weaving*, 1973. **3**: p. 273–275.
27. Yokura, H., Nagae, S. and Niwa, M., Prediction of Fabric Bagging from Mechanical Properties. *Textile Research Journal*, **105**: p. 748–754.
28. Zhang, X., Mechanism of Woven Fabric Bagging, in *Institute of Textiles and Clothing*. 1999, PhD Thesis, The Hong Kong Polytechnic University: Hong Kong.
29. Zhang, X. *et al.*, Fabric Bagging, Part I: Subjective Perception and Psychophysical Mechanism. *Textile Research Journal*, 1999. **69**(7): p. 511–518.
30. Zhang, X. *et al.*, Fabric Bagging, Part II: Objective Evaluation and Physical Mechanism. *Textile Research Journal*, 1999. **69**(8): p. 598–606.

13

Human skin and underlying soft tissues

M. ZHANG AND J.T. CHEUNG
The Hong Kong Polytechnic University, China

13.1 Introduction

In this chapter, common experimental techniques to quantify the tensile, compression, shear and frictional properties of the human skin and underlying tissues are reviewed. Selected material properties of the human skin tissues are highlighted.

13.2 Biomechanical testing of human skin

Many biomechanical approaches have been developed to test the human skin and underlying tissues. The aims are not only to understand the tissues distinct behaviors, but also to help in clinical diagnosis of skin diseases. Noninvasive measurements of skin mechanical properties provide a possibility for monitoring the temporal effects of disease, drugs, or cosmetics within and across subjects. Establishing objective and quantitative measurements of skin properties is one important aspect for clinical treatment and diagnosis.

Due to the structural variations, the mechanical properties of skin may vary with the subject, body site, direction, testing condition such as strain rate, and ambient conditions. An ideal test should be conducted *in vivo* with controlled specimen size and condition, such as multiaxial tests with uniform strain fields, so that the skin comprehensive properties can be readily associated with the results.[1] However, this can hardly be achieved because it is difficult to obtain a uniform strain field throughout the testing area and to control the loading boundaries in *in vivo* tests. There are difficulties in measuring the resting tension and deformation, the skin dimension and the boundary effects. These difficulties can be solved in an *in vitro* test but the effects of biological behaviors, such as blood pressure, lymphatic drainage, metabolism, and nervous and hormonal controls may be lost. Although *in vitro* testing based on standardized methods can give more repeatable results, *in vivo* skin properties are more relevant to clinical application and

in the fields of textiles and clothing. However, interpretation of *in vivo* tests is difficult because of the measurement constraints and indifferentiable response from boundary and underlying soft tissues.

13.2.1 *In vitro* tests of human skin

An *in vitro* test means that the skin specimen is tested away from the body. *In vitro* methods involve the removal of skin samples from the body and the usual procedure is to excise the skin and to pare off as much subcutaneous fat as possible. Therefore, the tissue cannot be further modulated in *in vivo* situations and thus a significant amount of series measurements of samples from different sites are required for adequate interpretation of results. *In vitro* uniaxial tests or strip biaxial tests are well suited for studies of the anisotropic behavior of the skin because of their better strain uniformity than *in vivo* tests.

The site and orientation of the tested specimen are very important, as anisotropic pre-existing or resting tension of skin exists as a result of structural strain, normal habitual body movements, and underlying joints or musculature. The sample is cut into a dumbbell shape, with the middle portion considered as the test site, and the larger ends are gripped on a tensile testing machine. In this arrangement, the specimen can be stretched under a uniform strain field throughout the skin thickness. It should be noticed that repeating the application of test stresses in both *in vitro* and *in vivo* tests is essential to allow a steady-state response to be achieved, leading to good reproducibility of results.

The ultimate strength and elastic parameters are commonly extracted from *in vitro* mechanical testing of skin. Edwards and Marks[2] summarized the results of selected *in vitro* tests of normal human skin samples of dimensions 4 mm × 2 mm × skin thickness of approximately 1–2 mm. The tensile strength of skin ranged from 5 to 30 N/mm^2, with a maximum mean value of about 21 N/mm^2 at 8 years, declining to about 17 N/mm^2 at 95 years. The ultimate modulus of elasticity ranged from about 15 to 150 N/mm^2. The mean showed a maximum value of about 70 N/mm^2 at age 11, with a decline to about 60 N/mm^2 at 95 years. The ultimate strain varied from about 35 to 115%. The mean value declined in a linear fashion from 75% at birth to 60% at 90 years.

13.2.2 *In vivo* tests of skin

An *in vivo* test means that the skin is tested on body. Though it is difficult to extract consistent mechanical parameters for inter and intra studies comparison, it can provide important information on functional skin mechanics. In fact, the *in vivo* tests have been widely used for the objective

assessment of severity and response to treatment in several diseases. In the following sections, the common measuring techniques and devices for *in vivo* testing of the human skin are discussed.

Tensile test (extensometer, twistometer, cutometer)

Extensometer: The simplest method for measuring the tensile properties of skin is the use of a linear uniaxial extensometer. Tabs are attached to the skin with either cyanoacrylate glue or double-sided adhesive tape and are driven apart to give a preset extension of typically 30%.[2] Strain gauges and a linear variable differential transformer sensor (LVDT) are attached to measure the forces applied to the pads and their displacements.[3] The force required to stretch the skin and maintain the new tab separation can be recorded. Alternatively, the separation of the tabs can be monitored with the application of a constant extension force. This cannot easily be achieved *in vivo*, but a good approximation can be obtained by using attachment tabs that are much wider than their initial separation distance. In this configuration, the skin is prevented from necking in the region of strain application and therefore experiences an effective stress in a direction orthogonal to the extension axis. Modulation of stratum corneum properties by as much as 30% from the effects of emollient applications and different tissue disorders can be evaluated.[2] This method can also be used to study changes due to aging, radiation therapy, steroid application and plastic surgery. Testing of skin properties using the extensometer is practically convenient; however, a pure uniaxial tensile test cannot be achieved as the specimen boundary conditions are not well defined.

Table 13.1 highlights some of the measured material parameters of skin using uniaxial extensometers, in the literature. The uniaxial extensometer has been employed to help evaluate the treatment of postburn hypertrophic skin[4] and the effects of aging and photodamage under sun exposure.[5]

Twistometer: The in-plane response of skin to a torsional stimulus can be measured by a twistometer, which has a central disk within a thin annulus. These are stuck to the skin, usually by means of double-sided adhesive tape, and the inner disk of skin is twisted while the torque required to achieve and maintain this rotation is monitored.[2] The probe of the twistometer consists of a torque motor and an angle sensor. The twistometer may also be configured as electromechanical oscillators connected to a spring exhibiting a variable degree of viscous recoil in the skin, in order to study the dynamic skin response.[3]

When the torque is applied for a given duration via the twistometer, the torque disk moves to a degree dependent on the compliance and viscosity of the tissue, and the resulting angular deformation is recorded. The creep

Table 13.1 Reported skin stiffness using uniaxial extensometers

Research group	Sites and conditions	Measured skin parameters and values
Manschot & Brakkee [55]	Human calf (along and across tibial axis)	Initial stiffness: 1 MPa (along axis), 0.15 MPa (across axis) Effective stiffness: 13 MPa (along axis), 4 MPa (across axis)
Clark *et al.* [4]	Human forearm	Skin stiffness: 0.75 N/mm
Quan *et al.* [5]	Human forearm and thigh (old and young)	Forearm skin stiffness: 1.92 N/mm (young), 2.86 N/mm (old) Thigh skin stiffness: 1.20 N/mm (young), 2.10 N/mm (old)

and relaxation behavior of skin in this test is similar to that obtained from a uniaxial extensometer. The difference between the two methods lies in the fact that the torsional device twists the skin through a small angle in all orientations, thus eliminating differences due to the test direction. With the twistometer, the deformations are applied in the plane of the skin to minimize the contribution of the deep layers. The stresses are applied in rotation, hence with an axis of symmetry. In contrast to uniaxial methods, the contribution of natural skin tensions can thus be averaged and the measurements are independent of the orientation of the imposed stress relative to the Langer's lines.

In the torsional test, a step torque instantaneously applied to the skin is maintained and then released to characterize creep and relaxation of the skin tissue. Typical skin deformation with time is depicted in Fig. 13.1. The parameter *Ue* is the elastic deformation of skin due to the application of an instantaneous load, *Uv* is the viscoelastic creep occurring after the elastic deformation, *Ur* is the elastic recovery, and *Uf* is the total extensibility.

Using a twistometer, Agache *et al.*[6] measured the skin deformation of 138 individuals from 3 to 89 years old and reported that the Young's modulus of the *in vivo* dermis was 0.42 MPa for the young age group and 0.85 MPa for the older age group. Boyce *et al.*[7] measured the deformation and recovery of skin after the treatment of burns with cultured skin substitutes, with the use of a dermal torque meter, in 10 patients. Assessments of burn scars

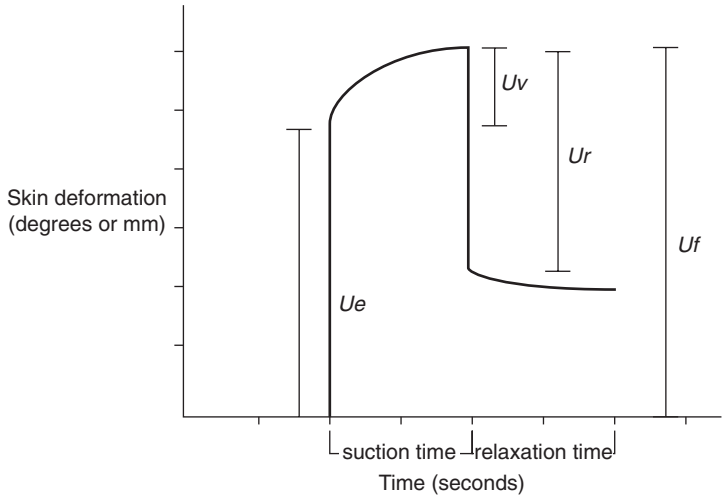

13.1 Graphical representations of the skin deformation–time curve under the mechanical testing of cutometer or twistometer. A suction force (torque for twistometer) is applied on the skin tissue and maintained during the suction time. The suction force is then released to characterize creep and relaxation.

reported time-dependent increases of skin extensibility and elastic recovery during the one-year post-treatment.

The torsional method can be used to determine the basic elastic and viscoelastic properties of skin and for the study of chronic sun exposure, racial differences in skin properties, scleroderma, and effects of cosmetic product application.

Cutometer: A skin pulling device called a cutometer has been used to quantify the mechanical behavior of skin under tension.[2] The device places a suction cup or cylinder perpendicularly on the skin surface and applies a negative pressure through the opening of a probe. The suction head is centered in the probe shield, with the diameter of the probe ranged from 2 to 8 mm, depending on the skin area.[3] The negative pressure is applied via a vacuum pump, which is incorporated with a pressure sensor. The resulting vertical deformation of the dome of the skin surface is measured by determining the depth of skin penetration into the probe. Skin elasticity parameters can be extracted from the applied pressure and the height of the skin dome. The typical skin deformation–time graph obtained is similar to the torsional test as depicted in Fig. 13.1. Cutometers usually provide the ability to alternate the pressure in a dynamic test mode to generate a cyclic suction such that the height of the raised skin can be recorded on each cycle.

The two most commonly used suction cup devices are the Dermaflex A (Department of Dermatology, Rishospital, Copenhagen, Denmark and the Institute of Technical Engineering (ATV), Glostrup, Denmark) and the DermaLab (Cortex Technology, Hadsund, Denmark).[3] These suction chamber devices are usually used to measure distensibility, elasticity and hysteresis of the tested skin.[8,9] Distensibility can be defined as the elevation of the skin under a particular tensile stress, and reflects the stiffness of the stretched skin. The stiffness is thought mainly to be due to the collagen fibers in the dermis. Elasticity defines the ability of the skin to recover from stress/stretch, which can be measured by monitoring the residual skin elevation after the first suction is terminated. Elasticity is also represented by *Ur*/*Uf*. The ability to regain the original shape following exposure to stretch seems to rely mainly on the elasticity fibers of the dermis. Hysteresis describes the irreversible alteration in maximum distensibility resulting from continuous cycles of stress applied on a particular area of the skin. It is determined from the difference between the elevation during the first cycle of suction and the last. Table 13.2 highlights some of the measured elastic parameters of skin using the cutometer, presented in the literature.

The cutometer has frequently been employed to help evaluate the effect of different pathological changes and treatment on skin elastic proper-

Table 13.2 Reported skin elastic parameters using cutometer

Research group	Sites and conditions	Measured skin elastic parameters and values
Jemec *et al.* [8]	Human palm and forearm	Distensibility: 1.76 mm (palm), 2.22 mm (forearm) Elasticity: 58% (palm), 68% (forearm) Hysteresis: 0.21 mm (palm), 0.20 mm (forearm)
Pedersen *et al.* [9]	Human forearm (sex and age)	Distensibility: 2.98 Elasticity: 90% Hysteresis: 0.18 mm Young's modulus: 5.26 MPa (Women), 4.8 MPa (Men) Young's modulus: 3.52 MPa (age 9–29), 4.77 MPa (age 30–39), 6.98 MPa (age 40–58)
Quan *et al.* [5]	Human forearm and thigh (old and young)	Forearm skin stiffness: 1.92 N/mm (young) 2.86 N/mm (old) Thigh skin stiffness: 1.20 N/mm (young) 2.10 N/mm (old)

ties.[10–14] Yoon *et al.*[14] quantified the facial skin elasticity in 96 diabetic patients and 83 normal subjects using a hand-held cutometer. The elasticity in the diabetics was significantly lower than in the non-diabetics. Using the cutometer, Dobrev[10] monitored the effect of therapy with dithranol by measuring the elasticity of 82 psoriatic plaques and of clinically uninvolved psoriatic skin in comparison with the skin of healthy controls. The plaques characterized significantly lower skin distensibility and elasticity compared with adjacent normal skin. After treatment, the mechanical parameters of psoriatic plaques approached the values of adjacent control skin. Van Zuijlen *et al.*[13] studied the effects of dermal substitution in acute burns and reconstructive surgery on skin elasticity measurements in 44 paired burn wounds and 44 paired scar reconstructions. The substituted scar reconstructions demonstrated an elasticity improvement of approximately 20% on a short-term basis but did not yield statistical evidence for a long-term clinical effectiveness of dermal substitution.

In terms of cosmetic skin treatment, Koch and Cheng[11] reported a significant increase of about 18.2% in skin elasticity after skin resurfacing using pulsed carbon dioxide lasers in 32 subjects, demonstrating its positive effect on skin-tightening. Pedersen and Jemec[12] studied the immediate plasticizing effect of water and glycerin on the skin of 23 healthy volunteers. Both water and glycerin were found to cause a significant increase in hysteresis with no significant difference in distensibility.

Indentation test (durometer, indentometer)

Durometer: The durometer is an indentometry device commonly used in the engineering industry to measure hardness of rubbers and other soft materials.[3] It has also been used to assess the degree of skin hardness to help quantify tissue hardness for prognostic and therapeutic reasons. The durometer reading was consistently higher for patients who were clinically judged to show greater induration. Durometry provides an easy to use and reproducible technique for measuring skin hardness on a linear scale. The instrument can thus serve as a standard noninvasive tool to measure skin hardness in systemic sclerosis or other dermatological diseases such as diabetic feet to assess skin involvement and to monitor the efficacy of treatment.

The first instrument used to assess skin hardness was a Rex durometer (model 1700, Rex Gauge Company, Inc., Glenview, IL).[3] This instrument is the international standard for measuring the hardness of rubber, plastic, nonmetallic materials, and soft tissue such as skin. It is a portable, hand-held device, which is provided with a calibrated gauge that registers linearly the relative degree of hardness (Shore hardness) on a scale of units divided from 0 to 100. This feature is the result of a spring-loaded interior that

senses hardness by applying an indentation load to the specimen via a retractable indentor.

Durometry measurements were found to be highly reproducible at the same site in each subject and in different clinical conditions.[3] However, durometer readings are insensitive in some skin areas, such as the forehead and dorsal digit, where subcutaneous tissue is less represented. The relative high stiffness of the underlying bone or tendon structure is suggested as a cause of failure of differentiation between normal and indurated skin tissue.

Romanelli and Falanga[15] measured the degree of skin induration in lipodermatosclerosis on the medial aspect of the leg, on 30 patients, with the use of a durometer. An increase in skin severity scores from 0 to 3 was found to correspond to an increasing durometer reading from 25 to 60. The durometer was suggested as an effective and reliable instrument for measuring skin hardness in patients with lipodermatosclerosis and venous ulceration, for the quantification of skin induration and ulcer healing. The noninvasive determination of skin hardness can be used to help identify patients at potential risk of developing neuropathic foot ulcers. Piaggesi *et al.*[16] evaluated the hardness of plantar skin in diabetic neuropathic feet of 36 patients by means of a durometer. Skin hardness was found to increase with the severity of diabetic neuropathy in patients. An increase in average skin stiffness from 41 (control) to 42 and 51, was measured for patients without and with diabetic neuropathy, respectively.

Recently, Thomas *et al.*[17] reported Shore hardness values ranging from 20 to 60 in different foot sole areas in diabetic subjects, depending on the severity of diabetic neuropathy. Using the Hayes formulation[18] (see page 231), they calculated the corresponding values of Young's modulus to hardness of foot sole soft tissue by measuring the indentation depth, the diameter of the indenter and the applied force. Shore values of 10, 20, 30, 60 and 90 were found to correspond to Young's moduli of 0.3, 0.84, 1.4, 3.85 and 7.9 MPa, respectively.

Indentometer: To obtain the compressive mechanical properties of the skin and underlying soft tissues, the majority of studies reported in literature have used indentation tests.[19–22] A number of indentation studies have been done to quantify the bulk soft tissue response of different regions of the body, using indentation devices of different technologies, such as linear variable differential transformers (LVDT) and ultrasound transducers, to measure the elasticity parameters.

Vannah and Childress[21] conducted an *in vivo* indentor test on the tissue stiffness of the calf of the lower leg, using a device consisting of an indentor with a linear variable differential transformer (LVDT) and a load cell. Prescribed displacement and resulting force were measured simultaneously

and the quantitative data of the nonlinear material stiffness and viscoelasticity occurring in the response of bulk soft tissue was applied for the design of soft tissue support. Zheng and Mak[23] developed a Tissue Ultrasound Palpation System (TUPS) which has a potential for clinical assessment of soft tissues over different regions. The pen-sized, hand-held probe consisted of an ultrasound transducer and a load cell connected in series. The thickness and deformation of the soft tissue layer during indentation were determined from the ultrasound echoes. The force response was monitored by a low profile load cell.

To extract Young's modulus from the force–indentation relationship, the formula developed by Hayes *et al.*[18] is often used. For a rigid, plane-ended and cylindrical indenter, the formula is

$$E = p(1 - \nu^2)/2aw_0\kappa(a/h,\ \nu) \qquad [13.1]$$

where E is the Young's modulus, p the load applied by the indenter, ν the Poisson's ratio, a the radius of the indenter, h the thickness of the measured layer, w_0 the depth of the indentation, and κ a geometric and material dependent factor.

A table of factor κ was given for several values of ratios of indenter radius to tissue layer thickness and the Poisson's ratio. Hayes' solution could be used to consider the layered effect and the lateral expansion of the soft tissue during indentation, based on the assumption of infinitesimal deformation and a frictionless indenter interface. Zhang *et al.*[24] investigated the influence of friction and large deformation during an indentation test of a layered material bonded to a rigid foundation using finite element analyses. Modified κ values were given[24] for the calculation of Young's modulus in the same manner as Hayes' solution, except that the results presented took into consideration the large deformation of the indented tissue and the friction at the skin/indenter interface.

An ultrasound indentation system is an effective tool for the assessment of soft tissue properties. The effective elastic modulus of the skin and subcutaneous tissues at different sites has been reported in the literature (Table 13.3).

Impact test (ballistometer)

The ballistometer employs a dynamic technique for assessing the intrinsic viscoelastic properties of skin.[3] The bulk soft tissue responses, involving contributions from the outermost skin layers to the underlying structures of fat, muscle, or bone, are documented. A lightweight hammer, anchored at one end, free-falls onto the tested skin surface under gravitational force; the resulting hammer oscillatory displacement–time data are recorded and associated physical parameters are determined.

Table 13.3 Reported skin stiffness from indentation tests

Research group	Tested sites	Young's modulus
Krouskop *et al.* [56]	Residual limbs	0.053 to 0.141 MPa
Torres-Moreno *et al.* [57]	Residual limbs	0.027 to 0.106 MPa
Mak *et al.* [20]	Residual limbs	0.021 to 0.194 MPa
Zheng *et al.* [58]	Forearms	0.014 to 0.059 MPa
Zheng and Mak, [59]	Limbs	0.0104 to 0.0892 MPa
Zheng *et al.* [60]	Plantar foot	0.043 to 0.118 MPa
Han *et al.* [61]	Breast	0.029 MPa

A ballistometer usually consists of a rotary transducer and magnet for holding and releasing the ballistic hammer at a fixed angle.[3] The hammer is assumed to be a rigid body, rotating about a noncentroidal axis and its motion can be represented by $\Sigma M_o = I_o\alpha$ where ΣM_o is the algebraic sum of the moments of the external forces about the axis of rotation (o), I_o is the moment of inertia of the hammer about the axis of rotation, and α is the angular acceleration of the hammer. The potential energy of the hammer can be calculated from the mass of the hammer, the distance from the center of rotation to the hammer's center of gravity, and the angular displacement of the hammer with respect to the test surface. The temporal angular velocity and angular acceleration of the hammer can be calculated from the measured angular displacement of the hammer. Alternatively, the angular velocity of the hammer at the instant of impact can be calculated from the conservation of kinetic and potential energy of the rotating hammer. The product of the hammer's moment of inertia and angular velocity is defined as the angular momentum of the hammer. The average force of the hammer during impact can be estimated from the change in angular momentum.

The ballistometer provides a noninvasive method for determining the viscoelastic properties of skin. The four parameters of common interests are amplitude, coefficient of restitution, cutaneous absorption coefficient and stiffness.[3] The amplitude, or angular displacement, measured with respect to the baseline is a measure of elasticity as it relates to the rebound energy of the skin. The coefficient of restitution is a measure of elasticity defined as the ratio between the hammer rebound speed to its speed just before impact on the skin. The coefficient of restitution is calculated either as the ratio of rebound and initial hammer speed or as the square root of the potential energy ratio of two adjacent peaks. The cutaneous absorption coefficient is another measure of elasticity, defined as a dynamic time constant, and presumes that the hammer impact energy is lost exponentially with time and is calculated from the peak height. The Cutaneous Absorption Coefficient, K is defined as

$$K = -(1/t_n)*log((AMP_n + BL)/(AMP_0 + BL)),$$

where t_n is the time at the nth peak, AMP refers to the angular displacement versus the baseline at the peak, and BL the baseline displacement from the horizontal or vertical. Skin stiffness is defined as the ratio of the hammer impact force to the skin deformation, that is the slope of the hammer impact force versus surface deformation curve.

The data obtained in a clinical study on 70 female subjects showed a decrease in the values with age for amplitude and the coefficient of restitution, while the cutaneous absorption coefficient shows a direct increase with age.[3] The stiffness value has an inverse relationship with age until the fourth to fifth decade, after which it increases sharply with age in females.

Using a ballistometer, Tosti *et al.*[25] studied the elastic properties of skin areas of 46 normal subjects ranging in age from 8 to 80 years, as well as on pathologic and cadaveric skin. The results showed a progressive decrease of coefficient of restitution with advancing age, as well as differences related to various skin regions. The tests performed on pathologic skin showed a lowered coefficient of restitution in epidermal hyperplasia, hyperkeratosis, sclerosis, and dermal infiltration. An increase of coefficient of restitution was observed when high water content was present in the skin.

13.3 Frictional properties of human skin

Frictional properties of human skin depend not only on the skin itself, such as its texture, its suppleness and smoothness, and its dryness or oiliness,[26] but also on its interaction with external surfaces and the outside environment. Investigation of skin frictional properties is relevant to several research fields, such as skin physiology, skin care products, textile and clothing industry, human friction-dependent activities and skin friction-induced injuries.

Frictional properties of skin surface may become an objective assessment of skin pathologies. It has been shown that frictional properties can reflect the chemical and physical properties of the skin surface and thus depend on the physiological variations as well as pathological conditions of skin.[26–30] The measurement of skin friction may be useful in studying the progress of individual skin disease.[28] Lodén *et al.*[27] found experimentally that the friction of skin with dry atopic subjects was significantly lower than that of the normal skin.

Skin frictional data have been used to evaluate skin care and cosmetic products.[31] Friction of skin forms an integral part of our tactile perception and plays an important role in the objective evaluation of consumer-perceptible skin attributes.[32,33] Some experiments[31,34–37] investigated friction changes induced by hydration and emollient application and the correlation with perceived skin feel.

Skin friction properties are also relevant to some friction-dependent functions, such as grasping, gripping and movement.[38–41] Such an understanding is very important in the design of handles, tools, controls and shoes. Bucholz *et al.*[42] investigated the frictional properties of human palmar skin to various materials, using a two-fingered pinch grip and effects of subjects, materials, moisture, pinch force. The investigation of the skin frictional properties is also helpful to understand the skin friction-induced injuries.[43–47] The injurious effects of friction on the skin and the underlying tissues can be divided into two classes, those without slip and those with slip. The former may rupture the epidermis and occlude blood and interstitial fluid flows by stretching or compressing the skin. The latter adds an abrasion to this damage. Research showed that the skin shear force produced by frictional force, combining with pressure is effective on occluding the skin blood flow.[48–50] Repetitive rubbing causes blistering and produces heat which may have uncomfortable and injurious consequences.

In lower-limb prosthetic socket and orthotic design, achieving a proper load transfer is the key issue since the soft tissues, such as those over residual limb, which are not suited for loading, have to support the body weight as well as other functional loads. Skin and prosthetic devices form a critical interface, at which skin friction is an important determinant on the mechanical interactional properties. Friction plays significant roles in supporting the load and in causing discomfort or skin damage.[51,52] To optimize frictional actions, there is a requirement to adequately understand the frictional properties between the skin and its contact surface. In textile and clothing industry, skin friction to the clothing materials is an important parameter for the correlation of sensation, comfort or fabric cling.[53]

Frictional properties between human skin and the prosthesis materials were measured using Measurement Technologies Skin Friction Meter (Aca-Derm Inc., California).[54] A spring balance was connected to a hand-held probe to monitor the normal force. An annular disk of the tested material was glued on the rotary end of the frictional meter. The probe sensing surface was annular with an outer diameter of 16 mm and an inner diameter of 10 mm. Five materials namely aluminum, nylon, silicone, sock cotton and Pelite were studied. Ten subjects without any skin problems participated in the study. The measurements were conducted at six anatomical sites, namely the dorsum of hand, palm of hand, anterior side of forearm, posterior side of forearm, anterior leg, posterior leg. The skin was untreated but clean. Various normal forces from 0.25 N to 1 N were applied. The frictional torques were measured at rotation speeds between 25 rpm to 62.5 rpm. Each test was repeated five times.

Tables 13.4 and 13.5 show the coefficients of friction over different sites and with different materials. In all the measurements, the coefficient of friction ranged from 0.24 to 0.65 and the average value for all the tested

Table 13.4 Coefficient of friction at the six anatomical sites (DH = dorsum of hand, PH = palm of hand, AF = anterior side of forearm, PF = posterior side of forearm, AL = anterior leg, PL = posterior leg)

Site	DH	PH	AF	PF	AL	PL
Coefficient	0.47 ± 0.12	0.62 ± 0.22	0.46 ± 0.10	0.43 ± 0.10	0.40 ± 0.10	0.40 ± 0.09

Table 13.5 Coefficient of friction with the five materials

Material	Al	Nylon	Silicone	Sock	Pelite
Coefficient	0.42 ± 0.14	0.37 ± 0.09	0.61 ± 0.21	0.51 ± 0.11	0.45 ± 0.07

Pelite = polyethylene foam

sites and materials was 0.41 ± 0.14. There was no significant difference in friction between the two anatomical sites measured. Among the five materials measured, silicone showed the highest coefficient of friction, and nylon showed the lowest.

13.4 Conclusion

Mechanical measurements of skin properties have progressed considerably in the past several decades. Reliable commercial devices are now available for measuring several different aspects of skin mechanics. With adequate control of the testing instruments, environment and specimens, it is possible to obtain valuable data relating to the effects of treatments, disease states, or the natural aging process. Because of the diversities of instrumental approaches and measured parameters, it is not feasible to set absolute standards for the experimental procedures. Rather, proper control of instrumental and testing parameters, measurement environment, and treatment site should be achieved in order to obtain reliable skin biomechanical measurements.

The noninvasive nature of available techniques provides effective methods for monitoring the temporal effects of disease, drugs, or cosmetics on *in vivo* skin. *In vitro* testing, on the other hand, provides repeatable standardized methods that can supply basic elastic and viscoelastic moduli for skin. Although interpretation of skin parameters measured *in vivo* is difficult, objective evaluations of the changes due to treatment or progress of disease, and the efficacy of competing treatments can be achieved. Measurement of skin mechanical properties is one important aspect of endeavor to help quantify and optimize different treatment modalities.

13.5 References

1. Lanir, Y. (1987). Skin Mechanics. In: *Handbook of Bioengineering*, Chapter 11, New York: McGraw-Hill.
2. Edwards, C. and Marks, R. (1995). Evaluation of biomechanical properties of human skin. *Clin Dermatol.*, **13**, 375–80.
3. Elsner, P. (2002). *Bioengineering of the skin: Skin biomechanics*, Boca Raton, Fla.: CRC Press.
4. Clark, J.A., Cheng, J.C. and Leung, K.S. (1996). Mechanical properties of normal skin and hypertrophic scars. *Burns*, **22**, 443–6.
5. Quan, M.B., Edwards, C. and Marks, R. (1997). Non-invasive *in vivo* techniques to differentiate photodamage and ageing in human skin. *Acta Derm. Venereol.*, **77**, 416–19.
6. Agache, P.G., Monneur, C., Leveque, J.L. and De Rigal, J. (1980). Mechanical properties and Young's modulus of human skin *in vivo*. *Arch. Dermatol. Res.*, **269**, 221–32.
7. Boyce, S.T., Supp, A.P., Wickett, R.R., Hoath, S.B. and Warden, G.D. (2000). Assessment with the dermal torque meter of skin pliability after treatment of burns with cultured skin substitutes. *J. Burn Care Rehabil.*, **21**, 55–63.
8. Jemec, G.B., Selvaag, E., Agren, M. and Wulf, H.C. (2001). Measurement of the mechanical properties of skin with ballistometer and suction cup. *Skin Res. Technol.*, **7**, 122–6.
9. Pedersen, L., Hansen, B. and Jemec, G.B. (2003). Mechanical properties of the skin: A comparison between two suction cup methods. *Skin Res. Technol.*, **9**, 111–15.
10. Dobrev, H. (2000). *In vivo* study of skin mechanical properties in psoriasis vulgaris. *Acta Derm Venereol.*, **80**, 263–6.
11. Koch, R.J. and Cheng, E.T. (1999). Quantification of skin elasticity changes associated with pulsed carbon dioxide laser skin resurfacing. *Arch. Facial Plast. Surg.*, **1**, 272–5.
12. Pedersen, L.K. and Jemec, G.B. (1999). Plasticising effect of water and glycerin on human skin *in vivo*. *J. Dermatol. Sci.*, **19**, 48–52.
13. van Zuijlen, P.P., Vloemans, J.F., van Trier, A.J., Suijker, M.H., van Unen, E., Groenevelt, F., Kreis, R.W. and Middelkoop, E. (2001). Dermal substitution in acute burns and reconstructive surgery: a subjective and objective long-term follow-up. *Plast. Reconstr. Surg.*, **108**, 1938–46.
14. Yoon, H.S., Baik, S.H. and Oh, C.H. (2002). Quantitative measurement of desquamation and skin elasticity in diabetic patients. *Skin Res. Technol.*, **8**, 250–4.
15. Romanelli, M. and Falanga, V. (1995). Use of a durometer to measure the degree of skin induration in lipodermatosclerosis. *J. Am. Acad. Dermatol.*, **32**, 188–91.
16. Piaggesi, A., Romanelli, M., Schipani, E., Campi, F., Magliaro, A., Baccetti, F. and Navalesi, R. (1999). Hardness of plantar skin in diabetic neuropathic feet. *J. Diabetes Complications*, **13**, 129–34.
17. Thomas, V.J., Patil, K.M. and Radhakrishnan, S. (2004). Three-dimensional stress analysis for the mechanics of plantar ulcers in diabetic neuropathy. *Med. Biol. Eng. Comput.*, **42**, 230–5.
18. Hayes, W.C., Keer L.M., Herrmann, G. and Mockros L.F. (1972). A mathematical analysis for indentation tests of articular cartilage. *J. Biomech.*, **5**, 541–51.

19. Reynolds, D.P. and Lord, M. (1992). Interface load analysis for computer-aided design of below-knee prosthetic sockets. *Med. Biol. Eng. Comput.*, **30**, 419–26.
20. Mak, A.F., Liu, G.H. and Lee, S.Y. (1994). Biomechanical assessment of below-knee residual limb tissue. *J. Rehabil. Res. Dev.*, **31**, 188–98.
21. Vannah, W.M. and Childress, D.S. (1996). Indentor tests and finite element modeling of bulk muscular tissue *in vivo*. *J. Rehabil. Res. Dev.*, **33**, 239–52.
22. Vannah, W.M., Drvaric, D.M., Hastings, J.A., Stand, J.A. 3rd. and Harning, D.M. (1999). A method of residual limb stiffness distribution measurement. *J. Rehabil Res. Dev.*, **36**, 1–7.
23. Zheng, Y.P. and Mak, A.F. (1996). An ultrasound indentation system for biomechanical properties assessment of soft tissues *in vivo*. *IEEE Trans. Biomed. Eng.*, **43**, 912–18.
24. Zhang, M., Zheng, Y.P. and Mak, A.F. (1997). Estimating the effective Young's modulus of soft tissues from indentation tests – Nonlinear finite element analysis of effects of friction and large deformation. *Med. Eng. Phys.*, **19**, 512–17.
25. Tosti, A., Compagno, G., Fazzini, M.L. and Villardita, S. (1977). A ballistometer for the study of the plasto-elastic properties of skin. *J. Invest. Dermatol.*, **69**, 315–17.
26. Lodén, M. (1995). Biophysical properties of dry atopic and normal skin with special reference to effects of skin care products. *ACTA Dermato-Venereologica* (suppl.)., **192**, 3–48.
27. Lodén, M., Olsson, H., Axell, T. and Werner, Y. (1992). Friction, capacitance and transepidermal water loss (TEWL) in dry atopic and normal skin. *Br. J. Dermatol.*, **126**, 137–41.
28. Comaish, J.S. and Bottoms, E. (1971). The skin and friction: Deviations from Amonotons' laws, and the effects of hydration and lubrication. *Br. J. Derm.*, **84**, 37–43.
29. Elsner, P., Wilhelm, D. and Maibach, H.I. (1990). Frictional properties of human forearm and vulvar skin: influence of age and correlation with transepidermal water loss and capacitance. *Dermatologica*, **181**, 88–91.
30. Cua, A.B., Wilhelm, K.P. and Maibach, H.I. (1995). Skin surface lipid and skin friction: Relation to age, sex and anatomical region. *Skin Pharmacol.*, **8**, 246–51.
31. El-Shimi, A.F. (1997). *In vivo* skin friction measurements. *J. Soc. Cosmet. Chem.*, **28**, 37–51.
32. Wolfram, L.J. (1983). Friction of skin. *J. Soc. Cosmet. Chem.*, **34**, 465–76.
33. Wolfram, L.J. (1989). Frictional properties of skin. In: *Cutaneous Investigation in Healthy and Disease Noninvasive Methods and Instrumentation*, edited by J. L. Leveque. New York: Marecel Dekker, 49–57.
34. Nacht, S., Close, J.A., Yeung, D. and Gans, E.H. (1981). Skin friction coefficient: Changes induced by skin hydration and emollient application and correlation with perceived skin feel. *J. Soc. Cosmet. Chem.*, **32**, 55–65.
35. Gerrard, W.A. (1987). Friction and other measurements of the skin surface. *Bioeng. Skin*, **3**, 123–39.
36. Hills, R.J., Unsworth, A. and Ive, F.A. (1994). A comparative study of the frictional properties of emollient bath additives using porcine skin. *Br. J. Dermat.*, **130**, 37–41.

37. Highley, D.R., Coomey, M., DenBeste, M. and Wolfram, L.J. (1977). Friction properties of skin. *J. Invest. Dermat.*, **69**, 303–5.
38. Cua, A.B., Wilhelm, K.P. and Maibach, H.I. (1990). Frictional properties of human skin: Relation to age, sex and anatomical region, stratum corneum hydration and transepidermal water loss. *Br. J. Derm.*, **123**, 473–79.
39. Johansson, R.S. and Cole, K.J. (1994). Grasp stability during manipulative actions. *Can. J. Physiol. Pharmacol.*, **72**, 511–24.
40. Smith, A.M. and Scott, S.H. (1996). Subjective scaling smooth surface friction. *J. Neurophysiology*, **75**, 1957–62.
41. Taylor, M.M. and Lenderman, S.J. (1975). Tactile roughness of grooved surfaces: A model and the effect of friction. *Perception and Psychophysics*, **17**, 23–36.
42. Buchholz, B., Frederick, L.J. and Armstrong, T.J. (1988). An investigation of human palmar skin friction and the effects of materials, pinch force and moisture. *Ergonomics*, **31**(3), 317–25.
43. Naylor, P.F.D. (1955). The skin surface and friction. *Br. J. Derm.*, **67**, 239–48.
44. Sulzberger, M.B., Cortese, T., Fishman, L. and Wiley, H.S. (1966). Studies on blisters produced by friction – I. Results of linear rubbing and twisting technics. *J. Invest. Dermatol.*, **47**, 56–65.
45. Dalton, B. (1982). Friction, intermitted or otherwise, the exciting cause of corns and callouses. *Chiropodist*, **37**, 372–80.
46. Armstrong, T.J. (1985). Mechanical consideration of skin in work. *Am. J. Industrial Med.*, **8**, 463–72.
47. Akers, C.W.A. (1985). Measurements of friction injuries in man. *Am. J. Industrial Med.*, **8**, 473–81.
48. Bennett, L., Kavner, D., Lee, B.K. and Frieda, A. (1979). Shear vs pressure as causative factors in skin blood flow occlusion. *Arch. Phy. Med. Rehabil.*, **60**, 309–14.
49. Zhang, M. and Roberts, V.C. (1993). The effect of shear forces externally applied to skin surface on underlying tissues. *J. Biomed. Eng.*, **15**, 451–6.
50. Zhang, M., Turner-Smith, A.R. and Roberts, V.C. (1994). The reaction of skin and soft tissue to shear forces applied externally to the skin surface. *J. of Eng. in Medicine*, **208**, 217–22.
51. Zhang, M., Lord, M., Turner-Smith, A.R. and Roberts, V.C. (1995). Development of a non-linear finite element modelling of the below-knee prosthetic socket interface. *Med. Eng. Phys.*, **17**, 559–66.
52. Zhang, M., Turner-Smith, A.R., Tanner, A. and Roberts, V.C. (1996). Frictional action at residual limb/prosthetic socket interface. *Med. Eng. Phys.*, **18**, 207–214.
53. Kenins, P. (1994). Influence of fiber type and moisture on measured fabric-to-skin friction. *Textile Res. J.*, **64**, 722–8.
54. Zhang, M. and Mak, A.F. (1999). *In vivo* friction properties of human skin. *Prosthet. Orthot. Int.*, **23**, 135–41.
55. Manschot, J.F. and Brakkee, A.J. (1986). The measurement and modelling of the mechanical properties of human skin *in vivo* – I. The measurement. *J. Biomech.*, **19**, 511–15.
56. Krouskop, T.A., Dougherty, D.R. and Vinson, F.S. (1987). A pulsed Doppler ultrasonic system for making noninvasive measurements of the mechanical properties of soft tissue. *J. Rehabil. Res. Dev.*, **24**, 1–8.

57. Torres-Moreno, R., Saunders, C.G., Foort, J. and Morrison, J.B. (1991). Computer-aided design and manufacture of an above-knee amputee socket. *J. Biomed. Eng.*, **13**, 3–9.
58. Zheng, Y., Mak, A.F. and Lue, B. (1999). Objective assessment of limb tissue elasticity: development of a manual indentation procedure. *J. Rehabil. Res. Dev.*, **36**, 71–85.
59. Zheng, Y.P. and Mak, A.F. (1999). Effective elastic properties for lower limb soft tissues from manual indentation experiment. *IEEE Trans. Rehabil. Eng.*, **7**, 257–67.
60. Zheng, Y.P., Choi, Y.K., Wong, K., Chan, S. and Mak, A.F. (2000). Biomechanical assessment of plantar foot tissue in diabetic patients using an ultrasound indentation system. *Ultrasound Med. Biol.*, **26**, 451–6.
61. Han, L., Noble, J.A. and Burcher, M. (2003). A novel ultrasound indentation system for measuring biomechanical properties of *in vivo* soft tissue. *Ultrasound Med Biol.*, **29**, 813–23.

Part IV

Clothing biomechanical engineering design (CBED) system

14

Integration of mechanical models into numerical simulations

Y. LI[1], X-Q. DAI[1,2], AND X. ZHANG[3]
[1]The Hong Kong Polytechnic University, China
[2]Soochow University, China
[3]Xian University of Engineering Science & Technology, China

14.1 Introduction

Mechanical simulation is the heart of the biomechanical engineering design system for textile and clothing products. Mechanical models are key elements in the mechanical simulation. Textile products are of specific hierarchical structure, and each intermediate product may have an influence on the performance of the end product. It is impossible to build a garment model from the fundamental fiber level due to the tremendous demands for the memory and computational cost. Even from the microstructure level of fabric, only a small piece of fabric can be modeled using current computer capacities. However, this does not mean that efforts to model the fundamental structures of the clothing products need be given up. The big problem can be divided into small pieces by separately modeling textile products at different levels. For an end product, the biomechanical design at the highest level of the hierarchical tree can be performed, and then traced backward to the lower level, modeling through the connecting mediate the requirements of geometrical structure and mechanical properties.

Therefore, the system should enable product to be designed from different levels, and fiber, yarn, fabric, and clothing models are fundamental elements in it. Various modeling techniques reviewed in Part II need to be integrated into the system.

14.2 Mechanical simulation system

14.2.1 Components of the system

The aim of mechanical simulation is the virtual reproduction of the mechanical behavior of a textile object subject to various geometrical and mechanical conditions. The object needs to be described through a geometrical representation on a computer. At a given time, the current state of the object is defined by its position and velocity. From these geometrical characteristics, the current deformation state is calculated. The mechanical behavior laws

describing the material properties are then applied on the state to obtain the current internal energy or forces exerted on the object, which is subjected to external forces and constraints. The evolution of the system obeys the laws of mechanical energy conservation and dynamics. The new state of the object at subsequent times is obtained by mathematical integration.

Geometrical modeling

Fiber, yarn and fabric: Geometrical structures of textile products have a determinant influence on their mechanical performance. It is important to describe them accurately. The geometry of the objects involved in textile products can be very complicated, by including 1-D, 2-D and 3-D elements. The description of an object can also vary greatly. For example, for different purposes, a yarn can be modeled as 1-D line[1], 2-D curve, or 3-D curve[2] or solid[3] as illustrated in Fig. 14.1. Line, arc, sine curve, Bezier curve and patch, B-spline curve and patch, and other mathematic curve or surface can all be used to describe the characteristic curves and surfaces of textile products.

Human body: Usually, there are two kinds of human body models: shell and solid. The shell model only describes the surface of the human body while the solid model may contain more information about the inner layers of the body. In biomechanical engineering design, a solid human body is often preferred. There are many commercial graphical tools to generate the human body's geometric data file. The geometric data of a specific individu-

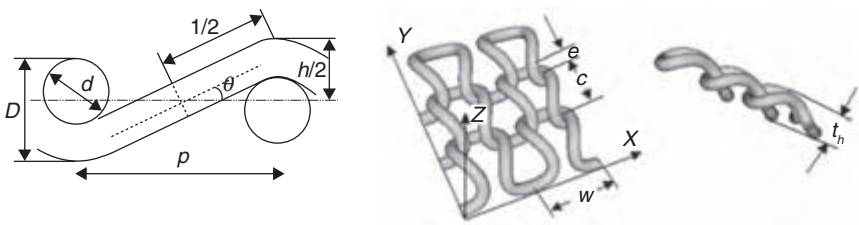

(a) Arc-line (b) 3-D curve of center-line

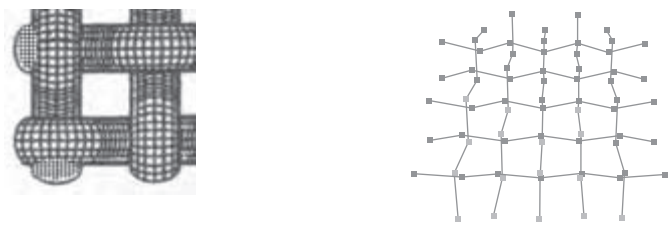

(c) Solid (d) Particle assembly

14.1 Variations of yarn geometry in different models.

al's body can be obtained by using 3-D body scanners, or Computerized Tomography (CT) or Magnetic Resonance Imaging (MRI) scanners. More information about human body modeling is contained in Chapter 16.

Garment prototypes: A 3-D garment primitive can be simply obtained by properly scaling the body surface. It is particularly useful for perfect-fit garments. The 3-D garments are usually described by 3-D mathematic surfaces or polygonal meshes consisting of flat polygons, separated by edges, themselves connected by vertices. A more general approach to obtain a 3-D garment primitive is to arrange 2-D patterns, usually obtained from a 2-D garment CAD system, for the garment properly around a body, and to define the boundaries to be sewn together. If a garment is built from a 2-D pattern assembly, then a description for the 2-D cloth pattern is a necessity. A 2-D pattern can be described as 2-D curves for the boundaries. Seaming information can also be defined on these curves.

Material modeling

The mechanical properties of a material account for how it reacts to given deformations and/or loadings. A material may behave elastically (deformation recoverable), or inelastically (plastic deformation remaining), depending on the range of deformation. During elastic deformation, a material may behave with linear elasticity or nonlinear elasticity. There are various kinds of nonlinear elasticity, such as porous elasticity, hypoelasticity, hyperelasticity, and viscoelasticity. Textile materials are typically time-dependent viscoelastic materials, so the dissipative losses primarily caused by 'viscous' internal damping effects must be modeled in the time domain. Human soft tissues containing lots of vessels need to be modeled as porous elastic material in some cases.

In most cases, for simplification, only the elastic behavior of a material needs to be modeled, so a model of the elastic properties of a material are focused on here. For an anisotropic elastic material, there is the generalized Hooke's law to describe its relationship between strain and stress, as shown in Fig. 14.2, where:

$$\varepsilon_x = a_{11}\sigma_x + a_{12}\sigma_y + a_{13}\sigma_z + a_{14}\tau_{yz} + a_{15}\tau_{zx} + a_{16}\tau_{xy}$$

$$\varepsilon_y = a_{21}\sigma_x + a_{22}\sigma_y + a_{23}\sigma_z + a_{24}\tau_{yz} + a_{25}\tau_{zx} + a_{26}\tau_{xy}$$

$$\varepsilon_z = a_{31}\sigma_x + a_{32}\sigma_y + a_{33}\sigma_z + a_{34}\tau_{yz} + a_{35}\tau_{zx} + a_{36}\tau_{xy}$$

$$\gamma_{yz} = a_{41}\sigma_x + a_{42}\sigma_y + a_{43}\sigma_z + a_{44}\tau_{yz} + a_{45}\tau_{zx} + a_{46}\tau_{xy}$$

$$\gamma_{zx} = a_{51}\sigma_x + a_{52}\sigma_y + a_{53}\sigma_z + a_{54}\tau_{yz} + a_{55}\tau_{zx} + a_{56}\tau_{xy}$$

$$\gamma_{xy} = a_{61}\sigma_x + a_{62}\sigma_y + a_{63}\sigma_z + a_{64}\tau_{yz} + a_{65}\tau_{zx} + a_{66}\tau_{xy}.$$

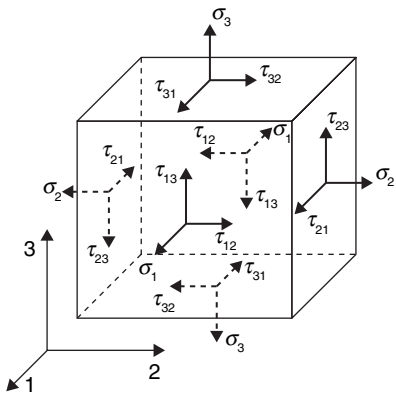

14.2 Stress components.

There are 36 constants a_{ij} ($i,j = 1,2, \ldots, 6$). However, since there is $a_{ij} = a_{ji}$, among the 36 constants, there are only 21 independent constants.

For orthotropic materials, the above equations can be simplified as:

$$\varepsilon_x = a_{11}\sigma_x + a_{12}\sigma_y + a_{13}\sigma_z$$

$$\varepsilon_y = a_{21}\sigma_x + a_{22}\sigma_y + a_{23}\sigma_z$$

$$\varepsilon_z = a_{31}\sigma_x + a_{32}\sigma_y + a_{33}\sigma_z$$

$$\gamma_{yz} = a_{44}\tau_{yz}$$

$$\gamma_{zx} = a_{55}\tau_{zx}$$

$$\gamma_{xy} = a_{66}\tau_{xy}.$$

The number of the independent constants reduces to nine. And these equations are usually rewritten using nine engineering constants as:

$$\varepsilon_x = \frac{1}{E_1}\sigma_x - \frac{\mu_{21}}{E_2}\sigma_y - \frac{\mu_{31}}{E_3}\sigma_z$$

$$\varepsilon_y = \frac{\mu_{12}}{E_1}\sigma_x + \frac{1}{E_2}\sigma_y - \frac{\mu_{32}}{E_3}\sigma_z$$

$$\varepsilon_z = -\frac{\mu_{13}}{E_1}\sigma_x - \frac{\mu_{23}}{E_2}\sigma_y + \frac{1}{E_3}\sigma_z$$

$$\gamma_{yz} = \frac{1}{G_{23}}\tau_{yz}$$

$$\gamma_{zx} = \frac{1}{G_{13}}\tau_{zx}$$

$$\gamma_{xy} = \frac{1}{G_{12}}\tau_{xy}$$

where, E_1, E_2, E_3 are the Young's moduli along the three principle directions, μ_{12}, μ_{13}, μ_{23} are Poisson's ratios, and G_{12}, G_{13}, G_{23} are shear rigidities. And there are relations between Young's modulus and Poisson's ratio as follows:

$$E_1\mu_{21} = E_2\mu_{12},\ E_2\mu_{32} = E_3\mu_{23},\ E_3\mu_{13} = E_1\mu_{31}.$$

For isotropic materials, the generalized Hooke's law can be formulated as:

$$\varepsilon_x = [\sigma_x - \mu(\sigma_y + \sigma_z)]/E,\ \gamma_{yz} = \tau_{yz}/G$$
$$\varepsilon_y = [\sigma_y - \mu(\sigma_x + \sigma_z)]/E,\ \gamma_{zx} = \tau_{zx}/G$$
$$\varepsilon_z = [\sigma_z - \mu(\sigma_x + \sigma_y)]/E,\ \gamma_{xy} = \tau_{xy}/G$$

Since there is $G = \dfrac{E}{2(1+\mu)}$, there are only two independent constants.

To account for the material's nonlinearity, a common approach is to use a piecewise linear approximation for the curve, denoting the nonlinear mechanical behavior.

Mechanical modeling

During the deformation of objects subjected to various loads and constraints, they obey fundamental mechanical laws, such as Newton's second and third laws, and conservation laws. Governed by these laws, both force and moment equilibriums are maintained. Therefore, a series of equilibrium equations can be built to govern the evolution of the mechanical model.

For the unit of a deformable object illustrated in Fig. 14.2, the equilibrium equation is derived as: $\sigma_{ij,j} + f_i = 0$, $i,j = 1,2,3$; and for a dynamic system, the motion equation of the unit is: $\sigma_{ij,j} + f_i = \rho u_{i,tt} + \mu u_{i,t}$, where ρ is the mass density, μ is damping coefficient, and $u_{i,t}$, $u_{i,tt}$ denote the first and second derivatives of the displacement u_i.

For a discrete model, Newton's second law is usually formulated as: $f(t) = m\dfrac{\mathrm{d}^2X}{\mathrm{d}t^2}$, where X is the position of a point mass, and f is the sum of the forces applied to it. This law can be extended to non-point masses by considering the representative action on the mass center and the rotational moment around it. Newton's second law can also be used to describe a deformable object's motion in Lagrange's form:

$$\frac{\partial}{\partial t}\left(\mu\frac{\partial r}{\partial t}\right) + \gamma\frac{\partial r}{\partial t} + \frac{\delta\varepsilon(r)}{\delta r} = f(r,t).$$

Here, $r(X,t)$ is the position of a mass point in the object at time t, μ is the mass matrix of the object, γ is the damping density, $\dfrac{\delta\varepsilon(r)}{\delta r}$ denotes the

internal forces resulting from the deformations, and $f(r,t)$ is the externally applied force.

Derived from Newton's second law, conservation laws apply to motion, rotational moment, and mechanical energy. Energy conservation implies that in a given mechanical system, the internal energy evolves according to the work of the external forces applied on the system. For a deformable mechanical model, the internal energy includes potential energy resulting from the work of the internal conservative forces and kinetic energy resulting from the object's motion. Moment conservation is another aspect of mechanical conservation derived from Newton's second law. This law may manifest in the contact problem between objects.

14.2.2 Simulation scheme

To implement mechanical simulation, the behavioral laws of material have to be combined with mechanical laws in a single framework that works on an appropriate geometrical representation of the involved objects to be simulated. The above mentioned three components need to be integrated into a framework; this yields complex systems of equations, usually ordinary or partial differential equations. The equation system needs to be solved under the boundary conditions denoting various constraints. Mathematics provides analytical solutions for only a limited class of simple equations. For complex mechanical simulations, such analytical solutions are often not available, numerical method being the only practical solution.

The numerical solution requires us to discretize the objects in space domain, and maybe time domain for dynamic cases. Space division can be accomplished either through numerical solution techniques or on the mechanical model itself. Depending on the method of discretization, there are two major schemes for performing mechanical simulation: continuum mechanical models and discrete models.

Continuum mechanical models

An object is considered as a continuum and mechanical laws are represented as a set of partial differential equations defined throughout the volume of the material. Numerical resolution for the equations then requires discretization of the equations in the volume space. Finite difference and finite element methods are common methods for the numerical solutions. The finite element method is most powerful and is widely used today.

Finite element methods discretize an object into elements that are basically defined as interpolation functions over a line, area, or volume piece. The interpolation function has a given order (such as linear or quadric),

and an associated set of parameters (degrees of freedom) that give the actual shape to the interpolation surface over the element. The higher the order, the more accurately the element would fit the real surface shape, but also the more degrees of freedom it has, and hence the higher its computational cost. The energy related to the deformation of the object for given values of the interpolation parameters is calculated from the mechanical properties of the material. Depending on the kind of mechanical simulation to be performed, these values have to be processed globally on the whole volume. The virtual work statement is often used for building equilibrium equations in the finite element analysis.

Continuity conditions between the interpolation curve or surface of adjacent elements imposes constrain relationships on the degrees of freedom of involved elements. All these relationship are summarized in a huge and sparse equation system defined on all the degrees of freedom and completed by additional constraints, such as various boundary conditions. The huge equation system is built by assembling the contributions of all the elements of the object successively. To simulate the mechanical system, the equation system has to be solved. This is done by using various optimized, iterative techniques, such as the conjugate gradient method for the linear system, or the Newton–Raphson method for the nonlinear system.

The Lagrange equations are also the basis of many continuum mechanical models. The mechanical behavior of the material is expressed as the local deformation energy related to material properties at any point (r) on the object. Various mechanical deformation energies are integrated at this point as its internal energy $\varepsilon(r)$. The equation system is then solved numerically using discretization over the whole object. Usually, a regular grid is defined over the object, expressing the partial derivatives; using the finite differences yields a sparse linear system of equations. The system can then be solved using numerical methods, such as the Guass–Seidel method.

Discrete models

Instead of considering the object volume as a whole, another approach is to discretize the object itself as a set of points with mass (particles), which interact with a set of 'forces', or energy constraints, to model the mechanical behavior of the material. A common way to numerically simulate a discrete model system is to directly integrate Newton's second law for a mass particle over all particles. The forces exerted on each particle include internal elasticity and viscosity forces, gravity, and various external constraints. These forces then determine the current mechanical state of the system, which is represented by the position and the speed of all particles.

14.2.3 Numerical solution

Solution of nonlinear problem

To solve the system of equations resulting from the continuum models, a numerical method is the only solution. Since the problem is often nonlinear due to the large deformation, complicated contact boundary, or material nonlinearity, the solution cannot be obtained by solving a single system of equations, as would be done in a linear problem. Instead, the solution is reached by applying the specified loads gradually, and incrementally working toward the final solution. Usually, an approach combining incremental and iterative procedures is used for solving nonlinear problems. The simulation is broken into a number of load increments and finds the approximate equilibrium configuration at the end of each load increment. It often takes several iterations to determine an acceptable solution to a given load increment. The sum of all of the incremental responses is the approximate solution for the nonlinear analysis. The Newton–Raphson method is often used to obtain solutions for nonlinear problems.

Numerical integration

Dynamic analysis yields a system of ordinary differential equations that needs to be solved numerically along time evolution. To perform such simulation, discretization in time domain is necessary. It results from the numerical computation of a sequence of states during the time period. Interpolation of the successive states provides an approximation of the entire trajectory.

The description for a dynamic system is often a second-order ordinary differential equation system in which the variables are positions of the nodes or particles along the evolving time. To solve a second-order differential equation (for example, a motion equation: $f(X(t), X'(t)) = X''(t)$), a common solution is to convert it to a first-order differential equation by employing a new variable: $v(t) = X'(t)$. Then the equation can be rewritten as:

$$\frac{\mathrm{d}}{\mathrm{d}t}\begin{pmatrix} X(t) \\ v(t) \end{pmatrix} = \begin{pmatrix} v(t) \\ f(X(t), v(t)) \end{pmatrix}.$$

To solve a first-order differential equation, there are two families of methods: explicit integration and implicit integration.

Explicit approach: The simplest numerical method to solve a differential equation is Euler's method, which can be formulated as: $X(t + \Delta t) = X(t) + \Delta t X'(t)$. Though Euler's method is simple, it may be inaccurate and unstable. The most widely used explicit methods are the Runge–Kutta family

methods. The fourth order Runge–Kutta method can be formulated as follows.

$$k_1 = \Delta t f(X(t),t),$$
$$k_2 = \Delta t f(X(t) + k_1/2),t + \Delta t/2),$$
$$k_3 = \Delta t f(X(t) + k_2/2),t + \Delta t/2),$$
$$k_4 = \Delta t f(X(t) + k_3/2),t + \Delta t),$$
$$X(t + \Delta t) = X(t) + k_1/6 + k_2/3 + k_3/3 + k_4/6.$$

Inaccuracy and instability are major problems in explicit methods.

Implicit integration approach: Instead of proceeding the evolution forwards, the implicit integration predicts $X'(t + \Delta t)$ and computes $X(t + \Delta t)$ backwards[4]. The backward Euler's method can be formulated as: $X(t+\Delta t) = X(t) + \Delta t X'(t + \Delta t)$. Applying the method to the motion equation yields:

$$\begin{pmatrix} \Delta X \\ \Delta v \end{pmatrix} = \Delta t \begin{pmatrix} v(t) + \Delta v \\ f(X(t) + \Delta X, v(t) + \Delta v) \end{pmatrix}$$

where $\Delta X = X(t + \Delta t) - X(t)$, and $\Delta v = v(t + \Delta t) - v(t)$. Applying a Taylor series expansion to the function $f(X(t),v(t))$ yields the first order approximation:

$$f(X(t) + \Delta X, v(t) + \Delta v) = f(X(t)) + \frac{\partial f}{\partial X}\Delta X + \frac{\partial F}{\partial v}\Delta v.$$

Substituting the first order approximation into the above motion equation and substituting $\Delta X = \Delta t(v(t) + \Delta v)$ into the equation of Δv yields: $\Delta v = \Delta t\left(f(t) + \frac{\partial f}{\partial X}\Delta t(v(t) + \Delta v) + \frac{\partial f}{\partial v}\Delta v\right.$. Letting I denote the identity matrix and regrouping the equation, finally:

$$\left(I - \Delta t \frac{\partial f}{\partial v} - \Delta t^2 \frac{\partial f}{\partial X}\right)\Delta v = \Delta t\left(f(T) + \Delta t \frac{\partial f}{\partial X} v(t)\right),$$

is obtained from which Δv can be solved and further ΔX.

Implicit methods are often unconditionally stable and allow large time step.

Choosing the suitable integration method: Simulation accuracy, time-step, calculation stability, and computational cost are the main factors to be considered in choosing a numerical integration method. For a given problem, an adequate integration method should be defined considering[5]:

(i) the required accuracy of the simulation that may limit the time-step;
(ii) the required accuracy for a given time-step, which is related to the accuracy order;
(iii) the numerical stability that may limit the time-step;
(iv) the amount of time required for the computation of a single time-step;
(v) other factors limiting the time-step, such as contact between objects.

14.3 Numerical simulation systems

14.3.1 Commercial Finite Element Method packages

Commercial Finite Element (FE) software packages are convenient tools to carry out mechanical analysis. Integrating FE software such as 'LS-DYNA' (Livermore Software Technology Corporation), 'ANSYS' (Ansys Inc., USA), 'ABAQUS' (Hibbitt, Karlsson & Sorensen Inc., USA) into a clothing biomechanical engineering system is an effective way to construct the mechanical simulation system. Here, a jeans wearing simulation is taken as an example to briefly introduce how the FE method solves a mechanical problem[6].

Jeans–body contact system

Figure 14.3 shows the time-dependent contact system between a pair of jeans and the human body consisting of three components (skin, soft tissue

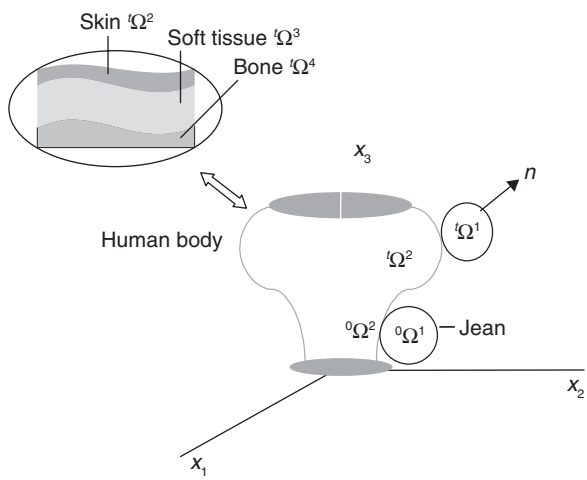

14.3 Contact system of the body–jeans.

and bone) in a fixed global coordinate system $\mathbf{x}$ (x_1, x_2, and x_3). The contact system involves four objects (the jeans, the skin, the soft tissue and the bone) and three contact interfaces (between the garment and the skin, between the skin and the soft tissue, between the soft tissue and the bone). At time $t = 0$, the jeans occupy domain ${}^0\Omega^1$ and the human body occupies domains of ${}^0\Omega^2$ for the skin, ${}^0\Omega^3$ for the soft tissue and ${}^0\Omega^4$ for the bone, respectively.

From time $t = 0$, the jeans start to move from foot to waist to fit the body, during which it is occupying new domains ${}^t\Omega^1$ and contacting the domain ${}^t\Omega^2$ of the skin that corresponds to the domain ${}^t\Omega^3$ and ${}^t\Omega^4$ at any time $t > 0$. The human body and the jeans are all simply connected so that there is no interior boundary in any of them, satisfying physical constraint:

$$ {}^t\Omega^1 \cap {}^t\Omega^2 = \varnothing, \quad {}^t\Omega^2 \cap {}^t\Omega^3 = \varnothing, \quad {}^t\Omega^3 \cap {}^t\Omega^4 = \varnothing, (t \geqslant 0), $$

where $\varnothing$ denotes a null space, indicating that Ω^1 and Ω^2 do not penetrate each other. The boundaries of ${}^t\Omega^n$ are denoted by ${}^t\Gamma^n$, which consists of three distinct components:

$$ {}^t\Gamma^n = {}^t\Gamma^n_d \cup {}^t\Gamma^n_f \cup {}^t\Gamma^n_c, \quad n = 1,2,3,4, $$

where, Γ_d denotes prescribed displacements boundary, Γ_f denotes prescribed load boundary, and Γ_c denotes the contact boundary where contact may occur, and $\cup$ denotes the union operator.

Governing equations

Motion equations: As long as there is no interior boundary for each contact interface, the motion equations remain uncoupled for the objects. Let $u(x)$ be the displacement field within an object n, and $a(x)$ the acceleration field within an object n. The motion equation of an elastic object n at time t is

$$ \frac{\partial^t \sigma_{ji}(\boldsymbol{x})}{\partial^t x_j} + {}^t q_{g_i}(\boldsymbol{x}) = \rho^t a_i(\boldsymbol{x}), \ \boldsymbol{x} \in {}^t\Omega^n, \ n = 1, 2, 3; $$

$$ i = 1 \text{ to } 3 \ \text{ and } \ j = 1 \text{ to } 3, $$

where, ${}^t\sigma_{ij}(x)$ are the Cauchy stress components that give the actual traction on an imaginary plane at a point within object n; ${}^t q_{gi}(x)$ is the ith component of the body force vector ${}^t q_g(x)$ of object n; ρ is the mass density of object n which is assumed constant within ${}^t\Omega^n$, and $a_i(x,)$ is the ith component of the acceleration vector of a material particle within object n.

Constitutive equations: The bone is regarded as stiff, the skin and the soft tissue and the garment are assumed to be linear elastic. For materials with linear elasticity, the stress–strain relation may be given by the generalized Hooke's law, i.e.

$$ {}^t s_{ij} = c_{ijkl}\, {}^t\varepsilon_{kl}, \quad \text{on } {}^t\Omega^n, \quad n = 1,2,3; \quad k = 1 \text{ to } 3 \quad \text{and} \quad i = 1 \text{ to } 3, $$

where c_{ijkl} is the matrix of material constants; s_{ij} is a component of the second Piola–Kirchhoff stress tensor that is related to the Cauchy stress component $\sigma_{ij}(x)$; ε_{kl} is a component of the Green–Lagrange strain tensor to describe the deformation of geometric nonlinearity, which consists of linear and nonlinear components ${}^{t}e_{ij}$ and ${}^{t}\eta_{ij}$:

$$ {}^{t}e_{ij} = ({}^{t}u_{i,j} + {}^{t}u_{j,i}) / 2, \quad {}^{t}\eta_{ij} = {}^{t}u_{k,i}\, {}^{t}u_{k,j} / 2 $$

where, ${}^{t}\mu_{i,j} = \dfrac{\partial^{t}\mu_{i}}{\partial X_{j}}$.

Boundary conditions: Concerning the displacement boundary, the garment fits the body in a constant speed V_0 from the foot to the body waist in the x_3-direction:

$$ V_3\,(x) = V_0, \quad \text{on} \quad {}^{t}\Gamma_{d}^{1}. $$

Concerning the load boundary, the human body is still during the wearing process. Thus the displacement of the bone is zero at x_3-direction in the boundary. These boundary restriction causes boundary force q_b on the bone, which is expressed as:

$$ {}^{t}q_b = {}^{t}\sigma N, \quad \text{on} \quad {}^{t}\Gamma_{f}^{4} $$

where N is a unit normal vector of a fixed boundary point. Gravity exerted on the four objects is expressed as:

$$ q^{n}{}_{g} = \rho^{n} g, \quad \text{on } {}^{t}\Omega^{n}, \quad n = 1,2,3,4 $$

where, g is gravity acceleration.

Contact conditions: For the frictionless contact interfaces, denoting the contact force at contact points by q_c^n, then by Newton's third law, we have

$$ {}^{t}q_{c1}^{n} = -{}^{t}q_{c1}^{n+1}, \quad \text{on} \quad {}^{t}\Gamma_{c}^{n} \cup {}^{t}\Gamma_{c}^{n+1};\ n = 1,2,3 $$

where, ${}^{t}q_{c1}^{n}$ is the component of contact force ${}^{t}q_{c}^{n}$ in the normal direction of contact points.

The mechanical contact condition as a constraint on the normal contact force ${}^{t}q_{c1}^{n}$ is:

$$ {}^{t}q_{c1}^{n} \le 0, \quad \text{on} \quad {}^{t}\Gamma_{c}^{n} \cup {}^{t}\Gamma_{c1}^{n+1};\ n = 1,2,3. $$

This means that the interactive pressure is exerted on the object n against its normal direction of the contact boundary points.

Numerical solution

The mechanical analysis of the body–jeans contact system is carried out using the FE package 'LS-DYNA'. The numerical solution procedure con-

sists of finite element discretization, formulation of the governing equations with the principle of virtual work, contact searching and contact constraint, and numerical solution with an explicit method. The geometrical model discretization, definition of material properties, setting of various conditions of boundary, load and interaction and solution method selection are all performed in a pre-processor for 'LS-DYNA'.

14.3.2 Specific solution systems

The generalized tools for mechanical analysis may sometimes be insufficient to solve the complicated problems involved in textile products so many specific systems and models have been developed for textile products, as reviewed in Part II. These systems and models can be integrated to the design system. Here, a skirt construction is taken as an example to illustrate the frame of a specific clothing simulation system.

A common way to construct a 3-D garment fitted on a human body is to assemble the 2-D cloth patterns according to a given topology. In a skirt construction, two patterns are sewn together along the seam line, and then gravity is added to reach the draping shape. For simplification, only the part of the human body (waist, abdomen and hip) potentially contacting skirt is modeled, it is represented as a triangular mesh. The body is regarded as rigid, the cloth is not allowed to inter-penetrate it. The cloth is represented as a particle collection. During the sewing and draping processes, the motion of the cloth patterns abides by the mechanical laws of cloth material. Various deformations (tension/compression, shearing, bending and twisting) result in internal forces. Besides these inner forces, there are also several external forces acting on the cloth. A seaming force, F_M, acts on the seam lines during the sewing process. As the cloth approaches the body, mechanical interaction occurs at the contact surface between the body and the garment. Conditionally, there are interactive contact forces (F_C) at the normal direction of the contact surface, and friction (F_F) as the garment slips on the surface. These external forces, as well as the cloth gravity G, are balanced by the cloth internal forces, the inertia force and viscous force F_I of the cloth during the dynamic formation of garments, as shown in the following equation:

$$F_T + F_B + F_S + F_W + F_I = G + F_M + F_C + F_F.$$

The cloth mechanical behavior is modeled using a particle model[7], in which various springs are imagined to be acting on joining particles for calculating the internal forces due to deformation. For each particle, the inner forces of stretching ($F_{T_{i,j}}$), bending ($F_{B_{i,j}}$), shearing ($F_{S_{i,j}}$) and twisting ($F_{W_{i,j}}$) are calculated according to its position and the positions of several neighbor particles surrounding it, and the mechanical properties of the

fabric. Let $\dot{X}(t)$ and $\ddot{X}(t)$ denote the velocity and acceleration of the particle, and let m and c represent the mass of the particle and the viscosity resistance; the particle motion equation can be rewritten as:

$$F_T + F_B + F_S + F_W + m\ddot{X}(t) + c\dot{X}(t) = F_M + F_C + G.$$

The ordinary differential equation is then solved along time evolution using the Runge–Kutta method.

14.4 Conclusion

Mechanical models are key elements in mechanical simulation. Textile products are of specific hierarchical structure, and each intermediate product may have an influence on the performance of the end product. Therefore, hierarchical modeling of textile products is necessary. Geometrical modeling, material modeling and mechanical modeling are essential components in the mechanical simulation system. Furthermore, the three components need to be integrated into a framework, yielding complex systems of equations. The equation system, often nonlinear, needs to be solved using various explicit and implicit numerical methods. Integrating commercial FE packages and also various specific solution systems for clothing products is an effective way to construct a mechanical simulation system.

14.5 Acknowledgement

We would like to thank the Hong Kong Polytechnic University for funding this research through the projects A188 and G-YD31.

14.6 References

1. Peirce, F.T., The Geometry of Cloth Structure. *Journal of the Textile Institute*, 1937. **28**: p. T45–T97.
2. Choi, K.F. and Choi, L.T.Y., An Energy Model of Plain Knitted Fabric. *Textile Research Journal*, 2003. **73**(8): p. 739–748.
3. Haan, S.I., Charalambides, P.G. and Suri, M., A Specialized Finite Element for the Study of Woven Composites. *Computational Mechanics*, 2001. **27**: p. 445–462.
4. Baraff, D. and Witkin, A., Large Steps in Cloth Simulation, in *SIGGRAPH*. 1998.
5. Volino, P. and Thalmann, N.M., Chapter 2 Simulation Models, in *Virtual Clothing: Theory and Practice*. 2000, Springer. p. 11–102.
6. Yeung, K.W., Li, Y. and Zhang, X., A 3-D Biomechanical Human Model for Numerical Simulation of Body–Garment Dynamic Mechanical Interactions during Wear. *Journal of the Textile Institute*, 2004. *Accepted*.
7. Li, Y. and Dai, X.Q., Simulate Woven Fabric Behavior during Low Extension with a Computational Micro-mechanical Model. *Textile Research Journal*, 2005. *Submitted*.

15

Database for biomechanical engineering design

R.M. WANG[1,2], X. LUO[2], Y. LI[1] AND X. ZHANG[3]
[1]The Hong Kong Polytechnic University, China
[2]Zhongshan University, Guangzhou, China
[3]Xian University of Engineering Science & Technology, China

15.1 Introduction

'Database' is one of the most important terms in modern technology. It has been widely used in various fields. A database is a logical collection of related information. The collection of related information is used to support a special purpose, business or engineering design. The fundamental difference between an engineering design database and a business database is the stability of the administrative environment as compared to the dynamic engineering environment. The development of an engineering design database management system (EDDBMS) must carefully consider the character of the engineering design process.

15.2 Characteristics of database for engineering design

Engineering design is a many-sided and wide-ranging activity.[1] It is based not only on mathematics, physics and their branches (mechanics, thermodynamics etc.) but also on production technology, materials science, machine elements, industrial management and cost accounting. Such activity includes not only semantic information, as in the case of business databases, but also information details of the engineering design, whereas a business database is a mere collection of related information used for consultation. Figure 15.1 shows the main concept of the engineering design process.

When the basic ideas of the engineering design approach are discussed, it is found that engineering design demands a constant flow of information. It needs to receive rich information to create elaboration of the design specification. The information can be received in different ways, from market analyses, trend studies, patents, technical journals, questionnaires

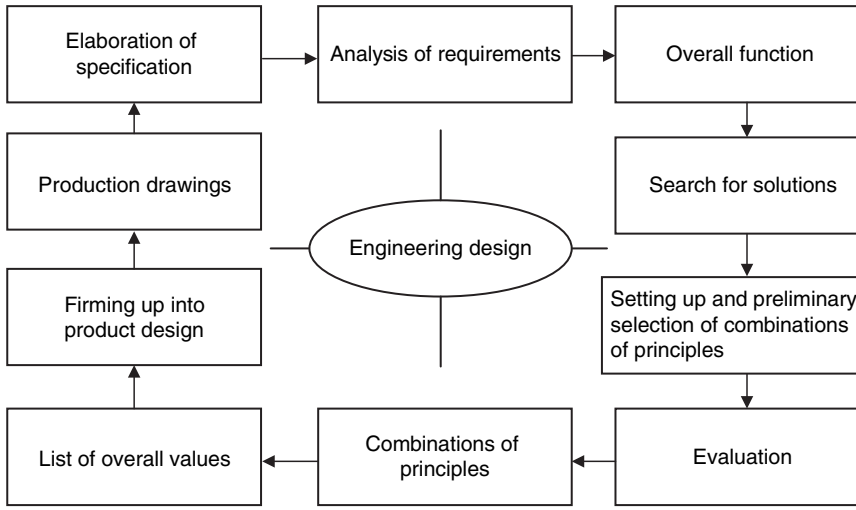

15.1 Main concept of engineering design.

from customers, concrete assignments, design catalogues, analyses of natural and artificial systems, calculations, experiments, analogies, general and in-house standards and regulations, stock sheets, delivery instructions, computer data, test reports, accident reports, and through asking questions.[1] Information can be processed by analysis and synthesis, calculation, experiment, the elaboration of layout drawings and the evaluation of solutions. It can be transmitted by means of drawings, reports, production documents etc.

It will be noticed, however, that the engineering process contains many loops in which activities with a routine character, such as analysis, are followed by activities with a creative character, such as selection. The DBMS should support this process.[2]

Data on engineering design is very dynamic in the sense that they are not known *a priori* but are defined during the design process. So the DBMS should not only deal with a constant area for the storage of standardized parts, design procedures and material properties, but also with structures, machines and installations composed from these elements. Furthermore, the DBMS should be used for storage and retrieval of measured and calculated data in such a way that the origin of these data can be traced. The DBMS should support typical engineering activities such as the analysis and modification of complex structures. Various ways of presenting the database contents must be possible, including graphical, representation of objects and measurement data.[2]

Of all the discussions of engineering design and engineering database, the main concept for developing an engineering database has to support the clothing biomechanical engineering design.

15.3 Functional requirement of database for clothing engineering design

Clothing engineering design means creating new clothing by enhancing existing designs or by altering existing ones to perform new functions; it is a complex, iterative-decision making competitive process in which the basic sciences, mathematics, and engineering sciences, are applied to convert resources optimally to meet a stated objective.[3]

Clothing biomechanical engineering design will be largely based on computer aided design, computer graphics, computer display technology, mathematical models, material sciences and experimental methodology developed for clothing biomechanical design.

Clothing biomechanical engineering design involves rich mathematical models. Different models have different requirement for clothing engineering design, the key technology for using these models is to prepare different data formats, different descriptive ways for data. How to manage these mathematical models and data files is very important during clothing biomechanical engineering design.

The clothing engineering design process generates and uses large volumes of dynamic data, rich data structure and different categories of variables, such as specifications, engineering design orders, technical data, problem reports, design models and analysis files. Each data category contains details of specific information, so that clothing engineering design is a product-oriented functional design process, the work being largely based on the experience and intuition of the designer. In order to support this complex design, it is important to develop an engineering database to support the clothing biomechanical engineering, especially for 3D numerical simulation of the mechanical interaction of the body with the clothing and sensory evaluation on clothing mechanical comfort. The aims of developing a database for clothing engineering design are:

- to create communication between researchers, technologists, designers, customers, manufacturers and other related sectors,
- to provide scientific experience data of clothing performance,
- to design diversity of cloth products, and
- to increase design automation in textile and clothing.

At the same time, it can provide management for (i) product development; (ii) design process control; (iii) quality assurance and (iv) performance evaluation.

15.4 The constitution of clothing engineering design

Clothing engineering design involves different subjects: materials (fabrics, yarns, fibers), human body, garment, engineering simulation, comfort evaluation and so on. Materials are important components in clothing engineering design. The properties of the material will affect the clothing biomechanical characteristics from the dynamic analysis, such as its deformation magnitude, stretch-recovery properties and rheological behavior during wear. These physical and mechanical characteristics of clothing materials are the basic information for the biomechanical engineering design of clothing.

The garment is made from 2D patterns of cloth surfaces. These patterns are constructed through software and discretized into a triangular mesh. The planar patterns are then placed around a 3D virtual body using manipulators. Once the patterns have been placed around the body, a mechanical simulation is invoked to make the patterns approach along the seaming lines. As a result, they become attached and seamed on the borders as specified, attaining the shape influenced by the shape of the body. Thus the garment is constructed around the body.

Human factors are concerned as a component of design. The human body is in direct contact with its clothing. Humans can reflect feelings of comfort through wearing the clothing in special environments in different ways: physical, physiological, biomechanical, neurophysiological and psychological. However, human comfort is a complex process, physics, physiology, biomechanics, and neurophysiology are dealt with in pattern and material design, and psychological factors are attended to in designing the aesthetic effects of clothing and comfort evaluation. This is done by using the physical, physiological, biomechanical, and neurophysiological data during the simulation process, and the psychological data in the evaluation process.

Engineering simulation solving is the core of clothing engineering design. It provides or links special software to create a virtual engineering environment. It gives the relationship between clothing mechanical performance and fabric mechanical properties in simple deformation (tension, shearing, bending and compression). When the design phase has determined feasible style and materials parameters, the simulation procedure is called-on to calculate the mechanical performances of the dynamic simulation system, such as the distributions of stresses and strains in the garment.

During wearing, clothing comes into contact with the skin of most parts of the body. The mechanical simulation induces responses from various sensory receptors and formulates various perceptions: touch, pressure, prickle, itch and inflammation, which affect the mechanical comfort of the wearer. Therefore, the evaluation model will analyze and evaluate the comfort of clothing. Sometimes the project is used to control and manage

the engineering design; it will provide a system design scheme for a design task.

Clothing products depend on the right combination of aesthetic and engineering qualities for their success in the market place. Modern consumers demand clothing products with superior multi-functional and comfort performance to satisfy their physiological and psychological needs. Garment mechanical comfort such as pressure comfort has been identified as one of the important attributes. Therefore, clothing biomechanical engineering design is becoming more and more important.

Figure 15.2 shows the design procedures for clothing biomechanics in detail. The design starts with a project, it defines the specification of clothing biomechanical design (e.g. jeans or bra), and this is followed by selecting the fabric structure and the mechanical properties of the fiber–yarn–fabric. The selection is a revision design, by searching or reworking some previous fabric structure that reasonably approximates to the current design requirements. The next step is to define the garment style, to construct the geometry or mesh data. From the input parameters of the human body and the garment, the deformation characteristics of the clothing should be identified, based on the mechanism analysis of the dynamic contact between the human body and the garment. Next comes a decision mechanical model of the body–garment, then a numerical simulation and analysis of the mechanical performance of the garment and the body. Iterative design has to be done before the garment is produced if the design is not satisfied through the simulation and evaluation steps.

The summary of clothing biomechanical engineering design using a database is shown in Fig. 15.3.

The clothing engineering database (DB) can be separated into four main components:

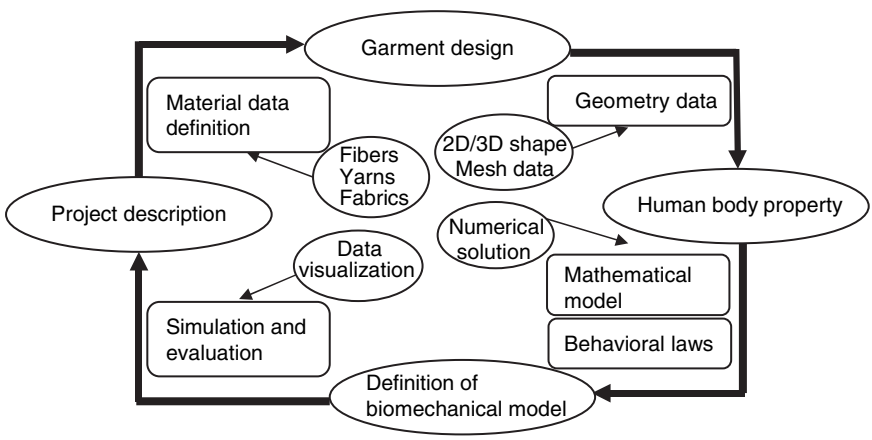

15.2 Clothing biomechanical design.

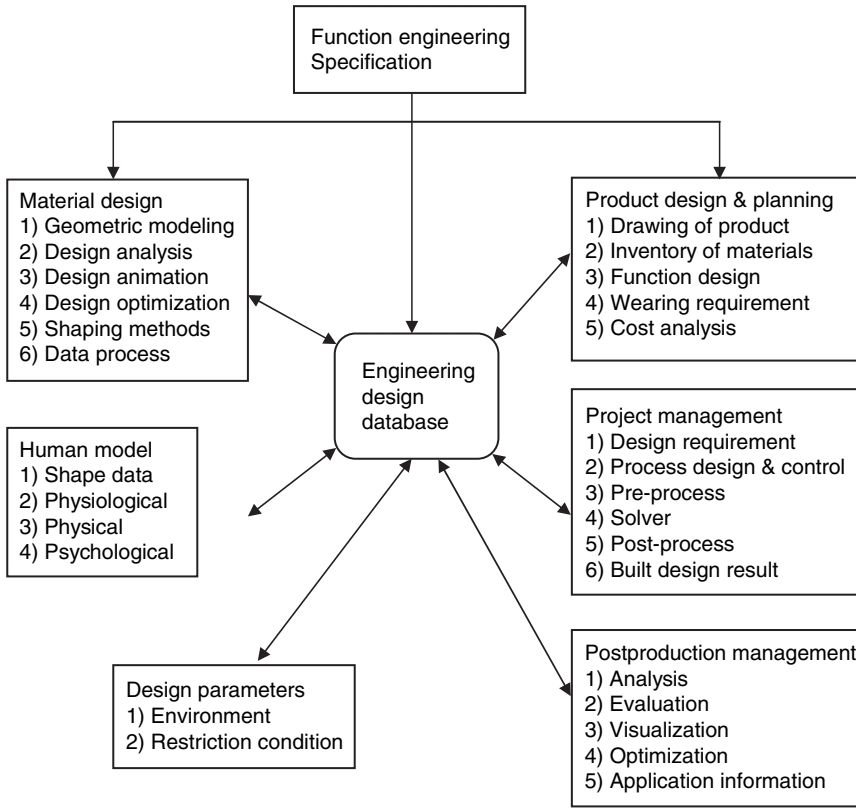

15.3 Main concepts of clothing biomechanical engineering design and EDDBMS.

(i) Garment DB: storing the structure parameters, geometric parameters and images of products (fiber–yarn–fabric–clothing, two-dimensional and three-dimensional data file).
(ii) Human model DB: storing the information of the model used in the biomechanical engineering design (human model factors (physical, biomechanical), manikin model (structure data) or some others).
(iii) Material DB: storing the structure, mechanical and physical parameters (fiber, yarn, fabric) used in the design and analysis processing.
(iv) Project DB: storing the engineering design specification, methodology, design report and analysis file for different design processes.

Textile and clothing engineering function design is concerned with product performance, from characters of mechanical, thermal, sensory, material and so on. According to the requirements and application of

the engineering design, the data can be presented in various categories, as follows:

General data

This is the summary description of the object. Sometimes general data includes the following items:

- Design file and product identification.
- Customer information: name, address and so on.
- Specification of the product's special considerations, and instructions.
- Commerce information.

Property data

This kind of data is about the properties of objects; it includes the following items:

- Objects structure description, including macroscopic and microcosmic: length, thickness, warp count and so on.
- Object mechanical description: warp bend rigidity, shearing modulus.
- Object physical description: thermal conductivity, integral heat of sorption.

Geometric data

This data is about the geometric characteristics of the object; it includes the following items:

- Object's two-dimension geometric description.
- Object's three-dimension geometric description.
- Object's mesh data description.
- Object's other format for analyzing process.

Design data

This kind of data is about design requirements; it includes design environment and specified constraints. The items are as follows:

- Design condition requirement: air density, atmospheric pressure and so on.
- Constraints: specific skin blood-flow rate, thermal conductivity of body tissue.
- Design method description.
- Design processing description.

Project data

This is about design data on previous projects. In cases where a current product has evolved from existing products, duplication of data files should be avoided; the designer can simply build current design data files on the basis of relevant existing ones. The items are as follows:

- Project basic data, designer's name, date.
- Project processing status.
- Project result.
- All documents for this project.

Tables 15.1 to 15.3 describe the fabrics, the fibers, and the human body.

In the database, the fiber–yarn–fabric structure, and mechanical and physical parameters are collated from a series of mechanical experiments using Kawabata and Instron test instruments, including fabric simple deformations by Kawabata instruments, and relaxation deformation of fiber–yarn–fabric and 3D deformation of fabric bagging using the Instron. The major mechanical parameters taken from the experiments are stored in the material database, as shown in Table 15.4. To set up a numerical database of textile properties without any assumption for the material properties, the tension-recovery curves of fiber–yarn–fabric have to be recorded in the material database by direct inputs from the experiments. The experimental curves will be recorded as the images in the database, which can be found during the design process by searching for its identifier number.

Table 15.1 Fabrics

General data	Structural data	Mechanical data	Physical data
Fabric ID	Finishing condition	Poisson's ratio	Surface volume ratio
Fabric name	Length	Warp tensile modulus EA	Absorptivity of outer surface of clothing
Fabric type	Width	Weft tensile modulus EB	Thermal conductivity of fabric
Fabric picture	Thickness	Warp bend rigidity	Thermal capacity
Company	Area density	Weft bend rigidity	Water vapor diffusion
Price data	Volume density	Compression modulus	Liquid water diffusion
	Cover factor	Twisting rigidity	Diffusion coefficient
	Warp count	Shearing modulus	
	Weft count	Hysteresis of shear	
	Warp crimp	Hysteresis of bending	
	…	…	…

Table 15.2 Fibers

General data	Structural data	Mechanical data	Physical data
Fiber ID	Diameter	Tensile modulus	Differential heat of liquid sorption
Fiber name	Volume density	Flexural rigidity	Differential heat of moisture vapor sorption
Fiber type	Length	Shearing modulus	Integral heat of sorption
Fiber picture	Count	Friction factor	Differential radiation absorption constant of the fiber
Company	Effective contact angle between fiber surface and water	Compression modulus	Fiber sorption isotherm
Price data		Bending	Specific heat of fiber
		Torsional rigidity	Volumetric specific heat of fiber
			Diffusion coefficient
			Thermal conductivity of fiber

Table 15.3 Human body

General data	Structural data	Physiological data	Material data
Model ID	Stature	Bone density	Specific heat at constant pressure of blood
Model file	Shoulder	Bone compress mudulus	Specific heat at constant pressure of skin
Model picture	Breast	Torsional rigidity	Diffusion coefficient/Mass diffusivity for moisture vapor diffuse through skin
Model type	Waist	Bone Poisson ratio	Thermal conductance of body tissue
Size	Hip	Soft tissue density	Thermal conductance of the skin
	Arm	Soft tissue shear modulus	Absorptivity of skin surface to the solar radiation
	Leg	Soft tissue Poisson ratio	Emissivity of skin surface
	Neck	Skin density	Dubois body area
	Weight	Skin tensile modulus	Total body mass
		Skin Poisson ratio	

Table 15.4 Items of each database

Human model database items	Garment database items	Material database items	Project database items
Human body ID	Garment ID	Fabric ID	Project ID
Human image ID	Garment name	Fabric bending modulus	Design info.
Stature	Garment image	Fabric shear modulus	...
Shoulder	Garment commercial info.	Fabric Poisson ratio	...
Breast	...	Fabric frictional coefficient	Garment ID
Waist	...	Fabric roughness	Design state
Hip	Garment size	Fabric bagging resist	Pre-process file
Arm	Garment style	Fabric bagging fatigue	Method ID
Leg	Fabric ID	Yarn ID	...
Neck	Fabric ID	Yarn viscoelastic modulus	Post-process file
Weight	...	Yarn relaxation time	Result files
Skin thickness	...	Yarn bending modulus	...
Skin tensile modulus	2D pattern data file ID	Yarn compressor modulus	Evaluation file
Skin density	3D garment data file ID	Yarn torsion modulus	Visualization file
Bone elastic modulus	...	Yarn Poisson ratio	
Bone density	...	Fiber ID	
Soft tissue thickness		Fiber viscoelastic modulus	...
Soft tissue elastic modulus		Fiber relaxation time	
Soft tissue density		Images of experimental curves	
...	...	...	...

15.5 Database design and realization

As mentioned previously, an engineering database has several important differences from an administrative database or a business database. Firstly, engineering design is an iterative-decision process, with analysis and synthesis based on the knowledge and information of basic sciences, mathematics, and engineering sciences. Secondly, engineering design needs a dynamic database that involves two kinds of information: the design environment (rules, methods, standard elements, etc.) and data that are not previously known but are defined during the design process; these are increasing with the design process. Thirdly, engineering design deals with a number of value types (text, numbers, equations, diagrams, graphical, photographic images, etc.).

Therefore, the main thrust in the construction of an engineering design database is to include efficient descriptions of the engineering design of all products and to provide production with the detailed information necessary for manufacturing the final engineering design product. Such descriptions include not only semantic information, as in the case of business databases, but also information details of the engineering design.

15.5.1 Data model

Configuration management and control of the design processes within the engineering environment are complex problems. Effective configuration management involves controlling not only the product data but the processes that create and affect the product design as well.

There are three major data models that are used in the database system: the relational data model, the hierarchical data model and the network data model.[4] The relational data model, in which all entities and dependencies between entities of the reality can be stored, are described, structurally identified by their domains (names and kind of values). The hierarchical data model represents entities and hierarchical relationships among different entities. In this model, each entity is represented as a record and hierarchical relationships by a tree structure. The network data model allows the representation of an arbitrary relationship between entities. Each entity is represented as a record, and it may be owned by more than one record, leading to a network structure.

Based on analysis of the characteristics of the design process for clothing mechanical performance, the hierarchical data model is used in the database system. The hierarchical relationships among fibers, yarns, fabrics and clothing are shown in Fig. 15.4.

In the data model, a material object in different hierarchies (fiber–yarn–fabric–clothing) can be represented by abstractions: the ‘entity’. An entity

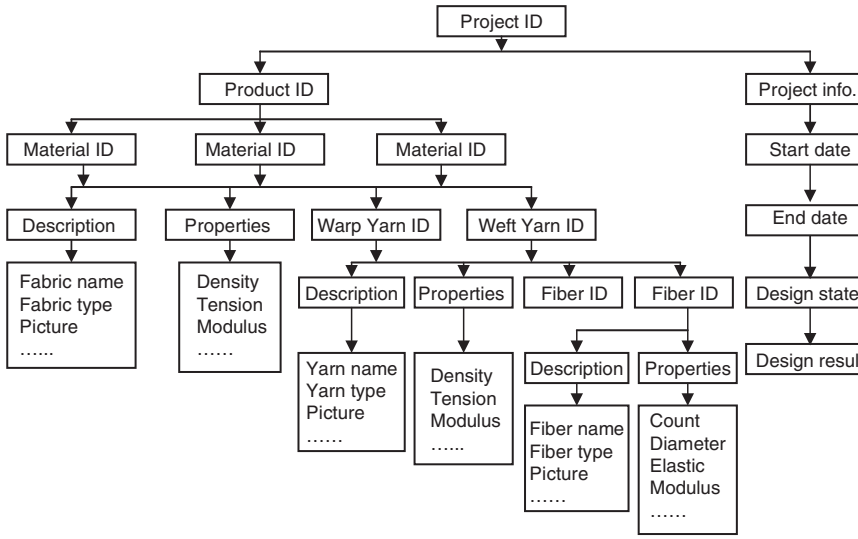

15.4 Hierarchical data model of the clothing engineering database.

has an identifiable number (ID). An entity is a collection of values, each value describing a property of the entity. An ID that involves its father's ID or the tree's node it belongs to indicates the hierarchical relationship. An ID is specified as a unique name of an entity in the engineering database, by which all of its information in the database can be found. As examples of the database, Table 15.5 illustrates the records of nine denim jeans in the product database, and Table 15.6 their mechanical parameters recorded in the material database. For example, the garment ID of 001 is Levis' 3D jeans and its fabric can be identified by the number 001-1. The mechanical parameters of the fabric can be searched in the material database according to the identified number 001-01, and the tension-recovery curves of the fabric in the warp and weft directions, respectively, according to the identified number of Wp001-01 and We001-01, as shown in Table 15.6.[3]

15.5.2 Database description

Each database contains details of specific information. According to the requirement and application of engineering design, the material in the database can be presented in four categories: general information about the material description, and structural, mechanical and physical properties of fibers, yarns and fabrics. These data are recorded and organized in the engineering database according the logical needs of the engineering design

Table 15.5 Records of nine denim jeans in the product database

Price	Garment commercial name	Garment ID	Fabric ID	Fabric image ID	Fabric structure	Fabric weight (g/m^2)	Fabric thickness (mm)	Fabric density		Fiber composite	Yarn count (Ntex)		Fabric cover factor k		Yarn crimp (%)	
								(ends/cm)	(picks/cm)	%	warp	weft	warp	weft	warp	weft
$735	Levi's 3D	001	001-01	E001-01	3 × 1 twill	431	0.88	26	19	25% Ly 75% Cot	6.8	6.0	238.9	191.1	11.7	7.3
$535	Levi's	002	002-01	E002-01	3 × 1 twill	475	1.04	27	20	100% Cotton	6.2	6.2	265.6	192.3	18.0	6.9
$338	Andyrex	003	003-01	E003-01	3 × 1 twill	453	1.12	30	19	100% Cotton	7.0	7.4	274.2	172.1	21.5	8.0
$329.5	Apple	004	004-01	E004-01	3 × 1 twill	451	1.03	27	19	100% Cotton	6.9	6.2	248.2	187.7	18.7	7.1
$148	Mixed	005	005-01	E005-01	3 × 1 twill	438	1.06	28	21	100% Cotton	7.9	7.2	239	189.3	21.4	9.4
$250	Wagner's	006	006-01	E006-01	3 × 1 twill	428	1.04	25	20	100% Cotton	6.7	7.3	237.1	184.4	19.1	10.9
$550	CK	007	007-01	E007-01	3 × 1 twill	458	1.07	27	20	100% Cotton	7.0	6.2	245.9	191.5	20.2	7.7
$679	Edwin	008	008-01	E008-01	3 × 1 twill	459	1.09	28	20	100% Cotton	6.6	7.9	267.8	177.1	23.3	7.8
$190	Giordano	009	009-01	E009-01	3 × 1 twill	400	1.08	27	19	100% Cotton	9.6	5.5	213.1	199.2	21.3	8.9

Table 15.6 Records of nine denim jeans in the material database

Garment commercial name	Garment ID	Fabric ID	Thickness (mm)	Density (kg/m^3)	EA (kgf/m^2)	EB (kgf/m^2)	Poisson's BA	GAB (kgf/m^2)	Curve-Wp	Curve-We
Levi's 3D	001	001-01	0.88	492	50000.0	48000.0	0.38	13179.0	Wp001-01	We001-01
Levi's	002	002-01	1.04	455	40000.0	70000.0	0.48	16645.7	Wp001-02	We001-02
Andyrex	003	003-01	1.12	405	42000.0	80000.0	0.38	20026.4	Wp001-03	We001-03
Apple	004	004-01	1.03	439	36000.0	80000.0	0.45	20771.3	Wp001-04	We001-04
Mixed	005	005-01	1.06	413	40000.0	76000.0	0.38	21974.6	Wp001-05	We001-05
Wagner's	006	006-01	1.04	412	46000.0	52000.0	0.44	25899.6	Wp001-06	We001-06
CK	007	007-01	1.07	427	40000.0	96000.0	0.42	20714.0	Wp001-07	We001-07
Edwin	008	008-01	1.09	421	45000.0	112500.0	0.40	25298.0	Wp001-08	We001-08
Giordano	009	009-01	1.08	370	24000.0	60000.0	0.40	11431.4	Wp001-09	We001-09

process. In the same way, the human model database can present general data, structure data, physiological data and human material data.

The describing and handling of the information elements must both reflect and support the design requirement efficiently, to represent incremental design changes as key elements in an engineering design system's overall ability. This is particularly important when engineering design software is developed for supporting the design process. During the clothing engineering functional design, it will process a large amount of data and this data may involve a number of value types (text, numbers, equations, diagrams, graphical, photographic images etc.). So it is necessary to define the special data type to describe the data used in clothing engineering design. The new definition is shown in Figure 15.5. From this figure, each data is described by five items: data name, data symbol, data type, data value, and data unit.

Data name

Data name is used to identify special data of a material (fiber, yarn, fabric) and human model. For example, the fabric's tension module, the yarn's compressor module, etc. This item value is a string.

Data symbol

Data symbol is a mathematic symbol of data stored in the database, and will be used in the computing process. For an engineering design process, this data can be imported by an expression with a formalized model. This item's value is a string. Table 15.7 shows a data name and its symbol.

Data type

Data type is used to identify the data stored in the database in three types: Value, Equation, Table/Figure. This representation of data is more useful in

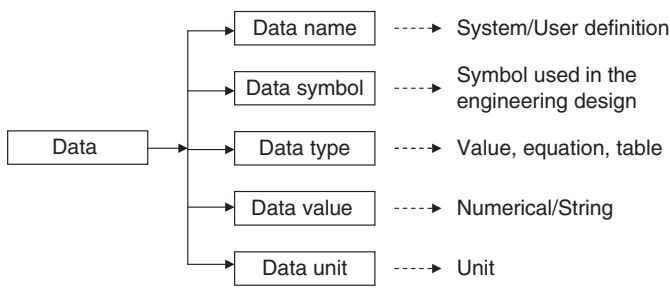

15.5 Data type.

Table 15.7 Data and symbol

Symbol	Data name
S'_v	surface:volume ratio
ε_a	volume fraction of water vapor
ε	porosity of the fabric
ε_f	volume fraction of fiber
δ	$\delta = (\varepsilon_l/\varepsilon)^m$
ε_l	volume fraction of liquid phase
R_f	radius of fiber
C^*	saturated water vapor concentration

design because some data are generated according to engineering experience, and some data are dynamically generated during the engineering design process.

- 'Value' means that this data's value is numerical or a string in the database and this data can be used directly in engineering design.
- 'Equation' means that an equation is stored in the database. When the design process uses these data, the special sub-procedure can compute them using the equation and assign the value to the data variable.
- 'Table/Figure' means there is a table/figure stored in the database. During the engineering design, there are mathematic methods to support the use of these values.

Data value

Data value is the data's real expression. It may be a real value (numerical or string), an equation or a table/figure (file name of table/figure) decided by the item of data type.

Data unit

Data unit identifies this data's unit attribute. Different unit sets are presented in different internal files, and the user can select them directly.

Table 15.8 shows an example that data 'Surface:volume ratio' stored in database. Here, the surface:volume ratio is the woven fabric's physical data; this data is very typical. When it is a real value, it is about 1000/m; however, it can be described in an equation, and the importance of this is that, when the design is begun, it has an initial value, but when the design process is ongoing, its value changes according to the equation. The equation format of surface:volume ratio is:

$$S'_v = 2(\varepsilon_a/\varepsilon)(\varepsilon_f\delta/R_f)\cdot C^*(T)$$

There is another example: data of fabric mechanical (weft tensile modulus EA) stored in database. Sometimes it can be measured to get the result in value, figure, and table style.

Figure 15.6 shows the woven fabric's mechanical data: 'Weft tensile modulus EA' figure description.

Table 15.9 shows the woven fabric's welt tensile modulus EA's table description.

Table 15.10 shows data 'Weft tensile modulus EA' stored in EDDBMS.

Table 15.8 Surface : volume ratio data

Name	Symbol	Type	Value	Unit
Surface : volume ratio	S'_v	Value	1000	1/m
Surface : volume ratio	S'_v	Equation	$S'_v = 2(\varepsilon_a/\varepsilon)(\varepsilon_f\delta/R_f) \cdot C^*(T)$	1/m

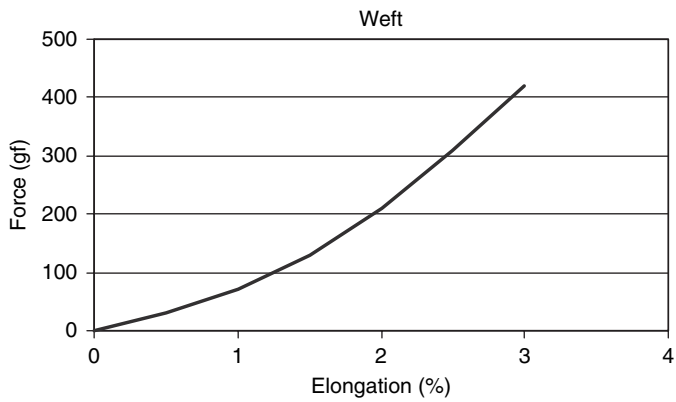

15.6 Weft tensile modulus EA's data.

Table 15.9 Weft tensile modulus EA's data

ε	0.	0.1	0.2	0.3	0.4	0.5	0.6	0.7
F	0.	5.	10.	18.	23.	32.	41.	49.
ε	0.8	0.9	1.0	1.1	1.2	1.3	1.4	1.5
F	60.	71.	80.	90.	102.	114.	130.	144.
ε	1.6	1.7	1.8	1.9	2.0	2.1	2.2	2.3
F	160.	175.	188.	208.	226.	242.	258.	277.
ε	2.4	2.5	2.6	2.7	2.8	2.9	3.0	3.1
F	297.	319.	340.	363.	388.	413.	432.	459.

F = force
ε = elongation

Engineering design is a dynamic process that involves engineering data from a previous engineering experiment, or from the design process, so an engineering database should provide a redefinition function. The designer/user can define their new data in the database and use them as usual in their future design. For this purpose, there is an extra structure attached to each database. When the designer/user wants to define their own data, they can define it through the interface. Figure 15.7 shows the redefinition interface.

Once new data has been added into the database, the designer can input their value through the input window (shown in Fig. 15.8). When this item

Table 15.10 Weft tensile modulus EA data

Name	Symbol	Type	Value	Unit
Weft tensile modulus EA	E_2	Value	50	gf/cm
Weft tensile modulus EA	E_2	Table	t_p1_t_f.txt	gf/cm
Weft tensile modulus EA	E_2	Figure	tensile.jpg	

15.7 The redefinition interface.

15.8 Data input interface.

is stored in the database, all users can use it. This function ensures the engineering database system has a flexible character for the dynamic process. It can provide wide application fields.

15.5.3 Database management systems

Database management systems merge the user's need for sophisticated text, data and graphics manipulation techniques with the technological capabilities offered by the computer. In terms of functionality, they include all the issues associated with retrieving, sorting, updating and filing text, data and graphics. They answer the fairly complex demands posed by engineering applications, running concurrently with the applications programs (processes) in the computer. The engineering database system can be shown in different layers. Figure 15.9 shows these different layers. From this figure, users can operate the database through the input interface to support their application requirements.

15.6 Examples

The aim is to develop an engineering database with a high-performance, system availability and user-friendly interfaces. To provide a simple and intuitive, friendly interface for analysis expertise, the user interface of the

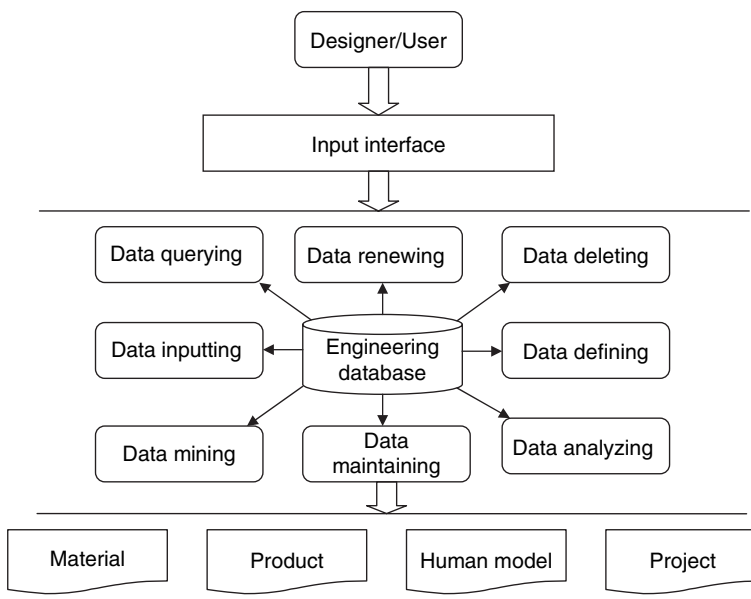

15.9 An engineering database system.

engineering database has been designed with as much image information and associated choices as possible, to clearly present the design environment and the progress of the design process at any time. A high-resolution graphics display is used to meet the geometric information and simulation function in the system. Presentation of choices utilizes pop-up menus with default suggestions to guide the user. The user interface is constructed in the PC operating system by using Delphi + SQL Server. The following figures are the interface windows of the database.

15.6.1 Fabric data management

In this part, fabric data can be managed, by inputting, deleting, modifying, querying and outputting, for the application. Figure 15.10 is the main interface for fabric data input. Four types of data have been put in: general data, structure data, mechanical data and physical data.

Figures 15.11–15.13 are the input windows of fabric structure, mechanical and physical data.

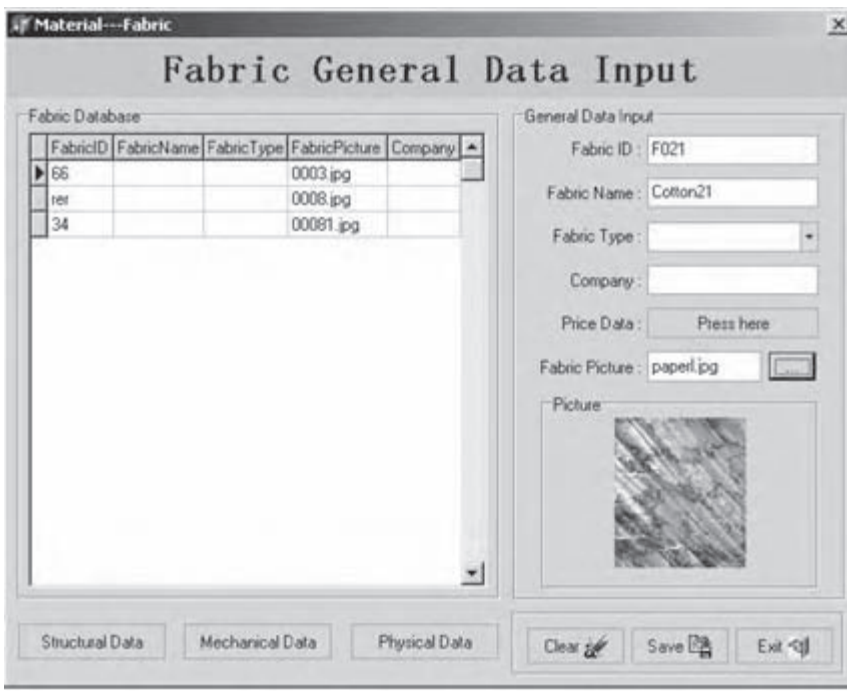

15.10 Fabric general data input interface.

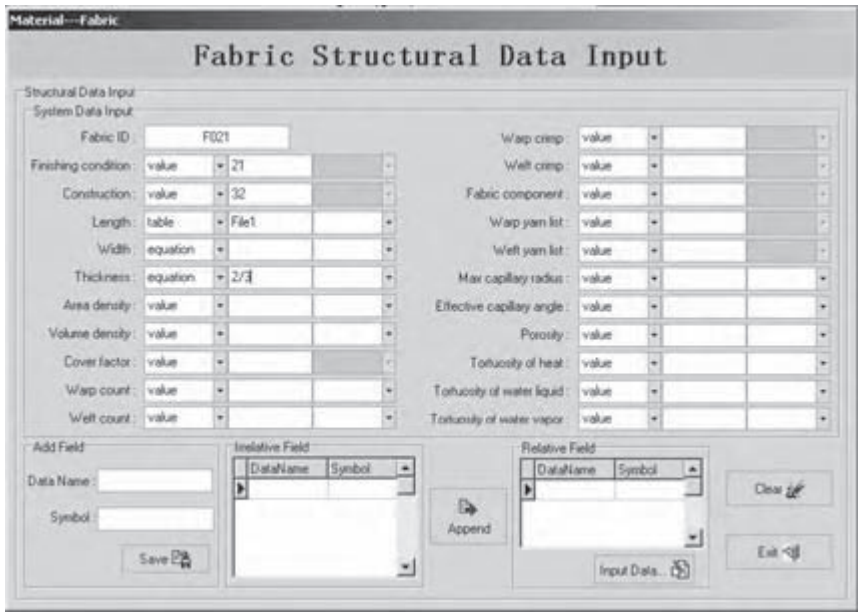

15.11 Fabric structural data input interface.

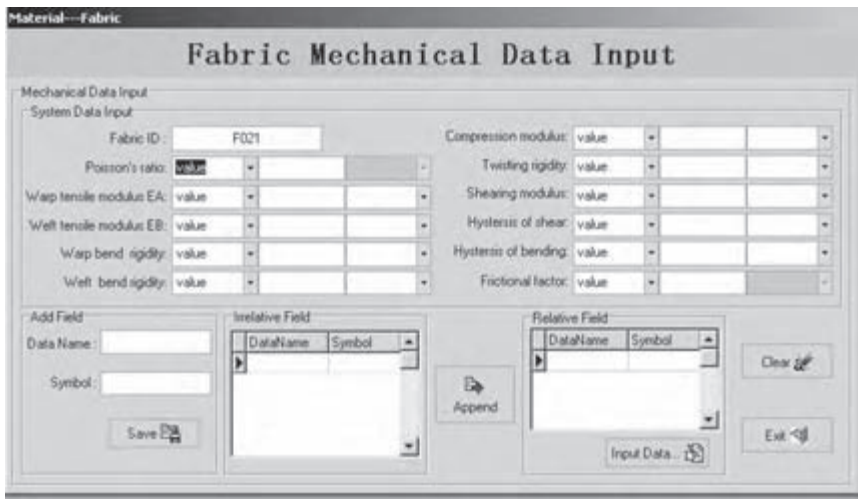

15.12 Fabric mechanical data input interface.

15.6.2 Human data management

In the human model data management, the human model's general data, structural data, physiological data and material data can be managed. Figures 15.14–15.17 show the input interfaces of the human model data.

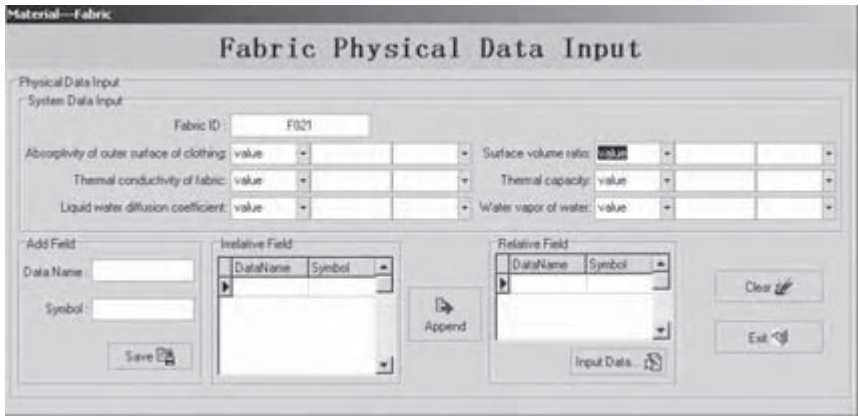

15.13 Fabric physical data input interface.

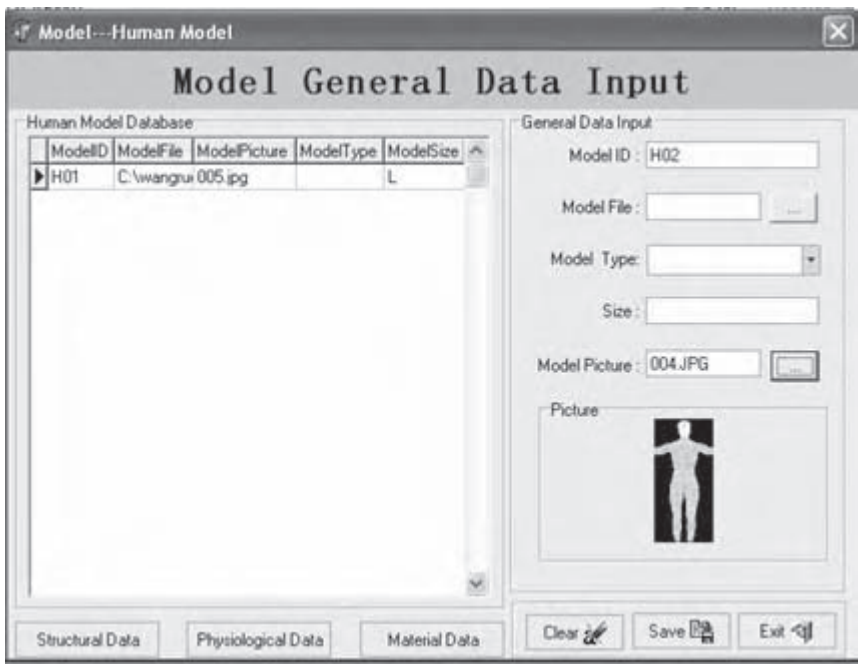

15.14 Human modes main input interface.

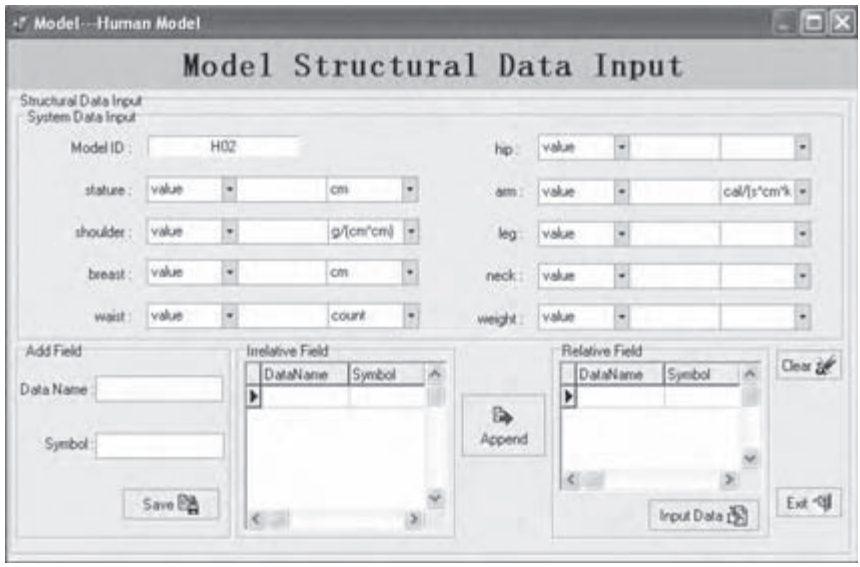

15.15 Structural data input interface.

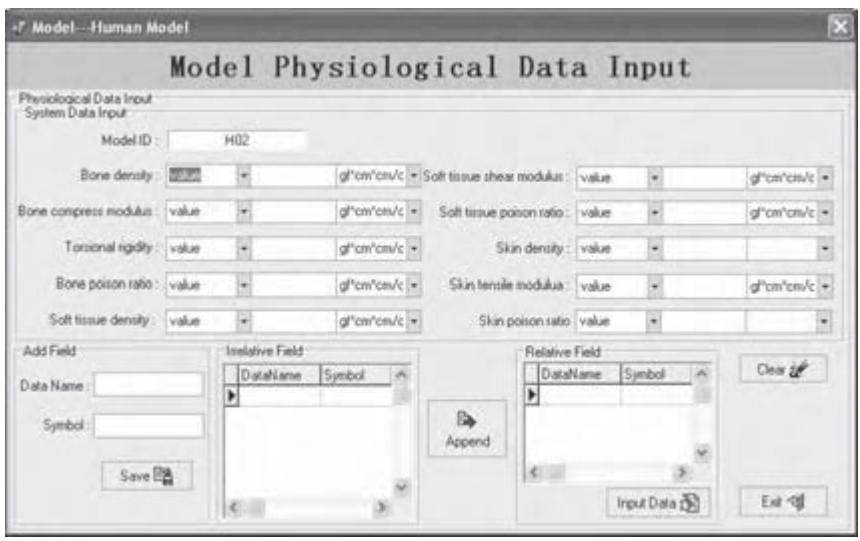

15.16 Physiological data input interface.

15.6.3 Garment data management

In the database, the product object is defined to describe the garment, manikin, and other textile product. Figure 15.18 shows the input window for garment data.

15.6.4 Project data management

Project data management is the management of the engineering design process. It includes the design specification, definition, implementation, and control. Figure 15.19 is the main input interface for project data.

15.7 Conclusion

Textile and clothing function engineering design is a complex and dynamic process. It involves various data, and flexible data types. To support this dynamic and complex design process, it is important to develop an engineering database such as the Engineering Design Database Management System (EDDBMS). This database can store various complex structure data, various formal values of data, and can meet the needs of design requirements from design method, design description, design management and many others. It provides a communication environment for different users. It powerfully supports product development, design process control, quality assurance, and product performance evaluation. The system has

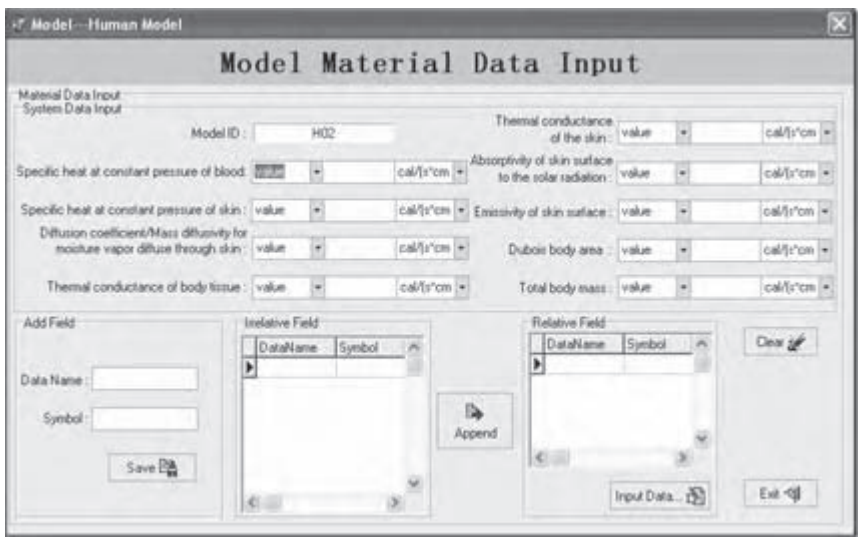

15.17 Material data input interface.

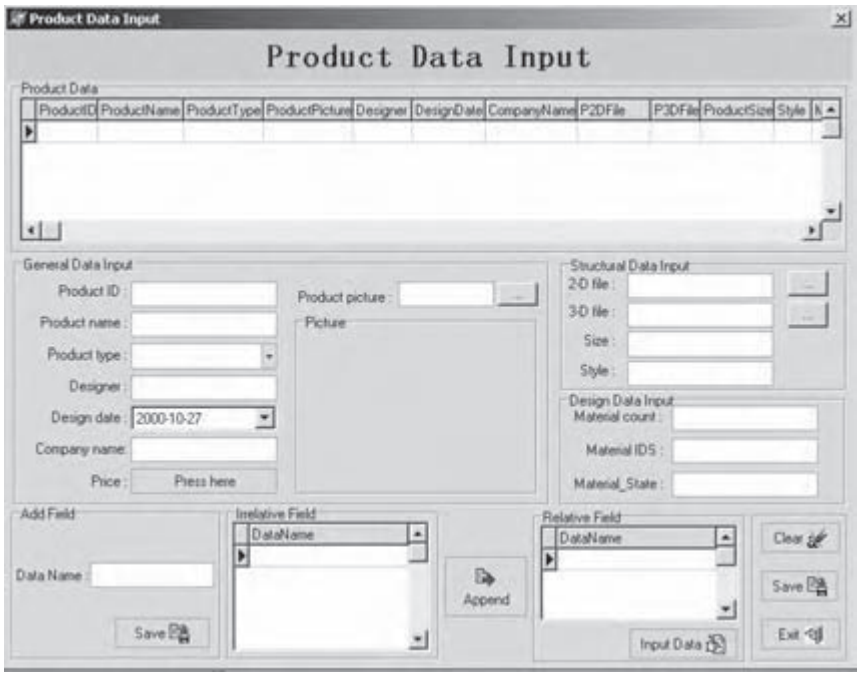

15.18 Main interface of product.

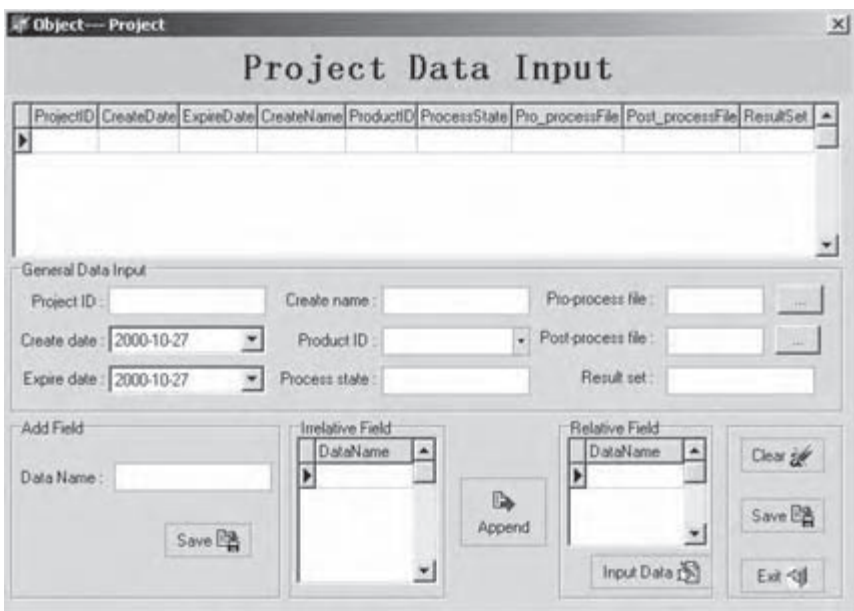

15.19 Project data input interface.

been developed with high-level computer technology, multilayer file structure, integrated description of data, flexible data management and a friendly interface; it is easy to use for different users. The system can be used for different purposes.

15.8 Acknowledgement

We would like to thank the Hong Kong Polytechnic University for funding this research through Project A188.

15.9 References

1. Pahl G., Beitz W., *Engineering Design*, New York Tokyo, Springer-Verlag, 1984.
2. Boerstra M.L., *Engineering databases: Survey of existing engineering database management systems, criteria for selecting a database, and some practical experiences in applying a database system: Report of the CIAD Project Group on Engineering Databases*, Amsterdam, New York, Elsevier, 1985.
3. Li, Y., Zhang, X., Mechanical Sensory Engineering Design System for Textile and Apparel Products, *Journal of the Textile Institute*, 2005.
4. Ullman, J.D., *Principles of database systems*, Second Edition, Maryland, Computer Science Press, 1982.

16

Preparation for mechanical simulation

R.M. WANG[1,4], X. LUO[4], X-Q. DAI[1,2],
X. ZHANG[3] AND Y. LI[1]
[1]The Hong Kong Polytechnic University, China
[2]Soochow University, China
[3]Xian University of Engineering Science & Technology, China
[4]Zhongshan University, China

16.1 Introduction

Clothing simulation and garment animation raise diverse scientific questions; not just the development of a technique or algorithm for solving a single kind of problem.[1] Clothing biomechanical engineering design is a simulation process to analyze and evaluate the functional performance of clothing. The aim of the biomechanical simulation is the virtual reproduction of the mechanical behavior of a textile object subjected to various geometrical and mechanical conditions, or of the interaction between clothing and the human body. This system requires a whole set of advances in a variety of fields: geometric modeling, mechanical simulation, collision detection and response, interaction with environment, numerical solver and others. Therefore, geometric models should be prepared for the garments and the human body, material parameters should be set and various boundary conditions should be defined; and a proper solver should be chosen for the mechanical simulation system. By going through these pre-processes, the whole system is set ready for numerical calculation.

16.2 Preparing geometrical models

16.2.1 Requirements of geometrical models

Geometrical description of the object shape is the fundamental element in the simulation system. In order to simulate an object's mechanical behavior effectively, a good structural framework for its geometry is necessary. For cloth simulation and garment design, as for other objects, one needs to answer the question: what is the best way to represent the shape of the object? There exist different ways to represent the shape and the geometry of objects in computer graphics, such as polygonal representation,

mathematical surface representation and so on. The choice of the representation may not only have to consider the shape alone in a static and passive environment, but may also have to investigate what kind of behavior is being modeled, what the computational requirements of the simulation are, what the details to be shown are, and what rendering method is to be employed. For example, a mere representation of the form of a static garment or a piece of cloth may not be adequate when there is interest in its movement, folds and wrinkles. In fact since a cloth is flexible, it can attain different shapes in different situations, meaning it does not have a fixed shape.

The description of the geometrical models must be accurate enough to capture all the characteristics of the geometry, while minimizing the total amount of geometrical data to be handled. And easy manipulation should also be taken into account. Since the CBED system may integrate various packages, the geometric models need to be convertible for processing in the pre-processors for these packages. So the models should be saved in commonly used graphic formats, such as 'iges', 'dxf', 'sat', '3ds', and so on.

16.2.2 Human body and clothing modeling

Usually, there are two ways to obtain the geometry for a human body: (i) surface shape obtained by using 3-D body scanners; (ii) solid resulting from CT or MRI scanner. Resulting from the first approach, information of discrete points positioned on the body surface are obtained, and they are often reconstructed by using a mathematic surface description, or remain as a discrete description of the points, triangle or rectangle patch. Computerized Tomography (CT) or Magnetic Resonance Imaging (MRI) images contain more information on inner body details. From these images, more complicated 3-D body models consisting of several layers, such as bone, muscle, fat and skin, can be constructed by using 3-D image processing software such as 'MIMICS' (Materilise, Leuven, Belgium). These obtained models, which describe the surfaces of the objects, are shells rather than solids. In biomechanical engineering design, a solid human body is often preferred. The shell models can be converted to solid models by using software such as 'Solidworks' (SolidWorks Corporation, Massachusetts).

Garment models can be obtained in several different ways. Garment items with simple shapes like tubular surfaces, such as sleeves, leggings and trousers, can be built as 3-D prototypes. For close-fit garments, 3-D garment primitives can be simply obtained by properly scaling the body surface using graphical tools. A more general approach to creating a 3-D garment is to simulate the sewing process by assembling 2-D cloth patterns resulting from a conventional 2-D garment CAD system. All these garment models may be described by mathematic curves, surfaces, or polygonal meshes. Any one of them needs to be positioned properly near to the body model for

the body–garment contact simulation. Therefore, both the body and garment models need to be visualized, easily viewed from different view-ports, and easily manipulated. This demands a 3-D interactive interface.

16.2.3 Geometrical discretization

The geometrical models are built for further mechanical simulation. Either in the continuum model or the discrete model approach, the clothing and body models need to be discretized. Geometrical discretization is necessary, not only because numerical solution requires discrete data, but also because it is a convenient way to describe the shape and deformation of the cloth as a compact and easy-to-manipulate set of data.

There are two main types of geometrical descriptions involved in clothing simulation: surface for the clothing object and solid for the human body. The surface is usually represented by a polygonal mesh, which is the simplest data structure for representing geometrical surfaces. The surface is discretized into flat polygons, separated by edges connected by vertices. The vertices are associated with discrete positions representing the sampled geometry. The topological structure of a polygonal mesh corresponds to a locally planar graph. Similarly, a solid is usually represented by a polyhedral mesh consisting of polyhedra separated by polygons.

A 2-D cloth pattern is often described as 2-D curves for the boundaries. The regions enclosed by the curves are then discretized into polygonal meshes. Three-dimensional garment surfaces also need to be discretized. The size and shape of the polygons are chosen to correspond to the desired accuracy of the representation of the 2-D or 3-D objects. The smaller the polygons, the more accurate the mesh, but also the more data are needed to represent them. Several kinds of polygonal mesh can be defined. While it is possible to work with meshes having irregular structures (Fig. 16.1a), imposing the condition of a constant number of edges around each vertex leads to regular meshes, having a globally constant topology. Regular mesh can be triangular (six edges per vertex), quadrangular (four edges per vertex), or hexagonal (three edges per vertex) as illustrated in Fig. 16.1b–d.

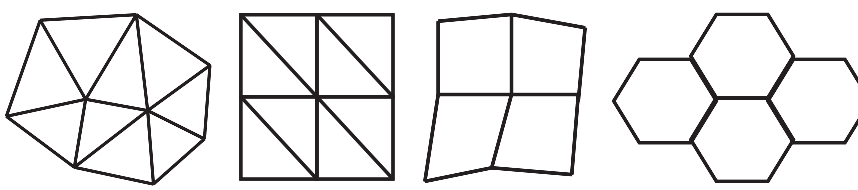

(a) Irregular (b) Triangular (c) Quadrangular (d) Hexagonal

16.1 Mesh variety.

These meshes allow us to take advantage of the local symmetries in performing geometrical computations. Furthermore, global numbering and indexing schemes can be established to provide quick access to any element in the mesh without performing search or traversal operations.

While the most general meshes may be made up of any kind of polygons, it is often useful to restrict them to contain only triangles or quadrangles. This can be helpful in performing certain mechanical analyses on the mesh elements. For example, in numerical calculation, the same formula can be used for elements of the given fixed topology. However, it is not always possible to discretize a surface into mesh containing only triangular or quadrangular meshes. As shown in Fig. 16.2, it is difficult to mesh the boundary part with regular meshes.

In order to reduce the amount of geometrical data to be managed for describing a smoothly curved surface, high-order surfaces are often used. They are described by curved surface primitives, described by a set of curved patches, with a reduced number of control points carrying the geometrical information. The patches may be described by explicit or implicit expressions which have various curvature and continuity

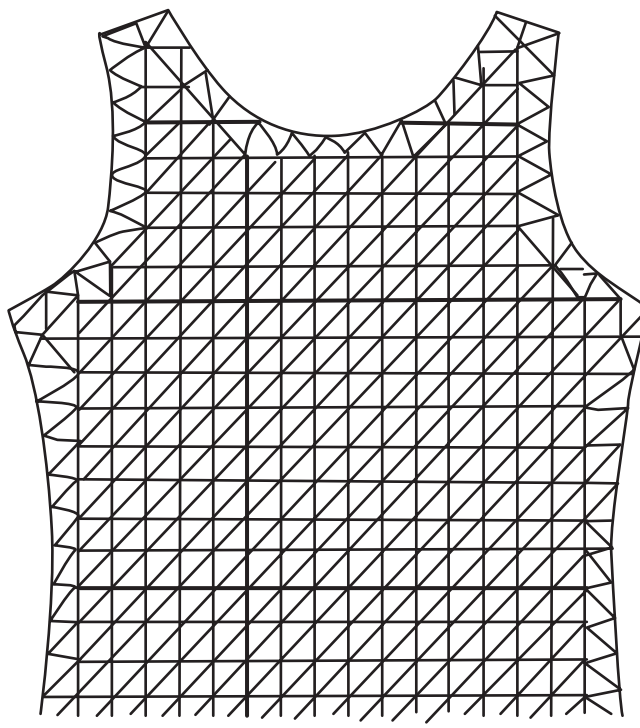

16.2 Mesh of a 2-D pattern.

properties. There are spline and Bezier patches, NURBS, polynomial and rational surfaces, and many of their variations. The patches may also be defined implicitly by a subdivision algorithm which constructs intermediate points hierarchically through a geometrical construction until a given accuracy has been reached. The definition of the patches generally requires that they have a given topology, such as being triangular or quadrangular. Surface continuity between the patches has also to be maintained.

To handle surfaces of complicated geometry, where portions of the mesh may be almost flat interspersed with highly curved portions, or with irregular and sharp deformations, an adaptive topology is often required. The best approach is to subdivide the mesh adaptively, depending on the surface curvature and acceptable geometrical error of the mesh representation. Different levels of detail may be considered, either upward by grouping bigger polygons into bigger and rougher domains, or downward by subdividing mesh polygons into smaller ones. More details about the geometrical representation of cloth surface can be found in reference 2.

Similarly, a solid is usually represented by a polyhedral mesh consisting of polyhedra separated by polygons. The commonly used polyhedra are tetrahedron, wedge and hexagon. The principles concerning polygonal mesh discussed above are also applicable to polyhedral mesh. However, since the human body is of a complicated geometrical shape, the tetrahedron is often used to discretize it. The geometrical discretization can be performed by using general mesh generation tools, a pre-processor for FE software, and specifically designed algorithms.

16.3 Definition of various conditions

Clothing mechanical simulation is the virtual reproduction of the mechanical behavior interacting with its environment. Extended conditions are necessary during simulation. The designer should define these parameters before the simulation.

16.3.1 Material properties

In order to proceed to a mechanical simulation of an object, its mechanical behavior must be described by relevant mechanical parameters and expressed as a set of relations among the geometrical and mechanical values of the object that can be easily manipulated. For clothing objects of different levels, the major elasticity parameters include Young's modulus, Poisson's ratio, bending modulus and shearing modulus. For the human body, the parameters of Young's modulus and Poisson's ratio are usually simplified. For dynamic simulation, the mass density of an object is also

necessary. To address the nonlinearity of the mechanical properties, various stress–strain curves can be approximated by piecewise linear expression, polynomials or tables of test data. All these data can be input from the database, in which a large amount of material data should be stored.

16.3.2 Environment parameters

Cloth behavior in isolation has limited meaning. A cloth's behavior is revealed as a consequence of interaction with its environment. This environment could be the wind or other rigid or flexible objects causing collisions with the cloth. It is necessary to include these aspects into the modeling phase. The most obvious external force exerted on the cloth is universal gravity, which acts to accelerate the cloth towards the ground. This acceleration is usually 9.8 m/sec.[2]

Aerodynamic effects result from the interaction between the cloth and the surrounding air. These interactions are usually modeled as viscosity forces proportional to the speed difference between the cloth and the air, and depend on the local surface orientation. These forces are also highly dependent on the actual shape of the cloth, as well as on all the possible aerodynamic turbulences arising at any distance from the surface.

16.3.3 Interactions

The interaction involved in clothing simulation includes contact between clothing and the human body, contact between clothing/body and other objects, self-contact of clothing, and interaction among different layers within the human body. The mechanical features of these interactions need to be modeled properly in the mechanical system. Usually, all these interactions can be defined on contact interfaces between pairs of surfaces. Generally, there are two types of contact interactions: tied contact and sliding contact.

Tied contact: When a surface pair constrains a vertex on one surface to the closest vertex on the other surface, the two vertices will have equal translational and rotational motion as well as other active degrees of freedom in the duration of a simulation. For example, since soft tissue adheres to the underlying bone tightly, the interface between the two objects can be defined as tied contact.[3]

Sliding contact allows the two contacting surfaces to move separately and only interact through mechanical contact. The interface between a human body and a garment is a typical sliding contact. A contact property characterizing the interaction nature needs to be assigned to a sliding contact. The contact property includes the pressure-overclosure relationship that

governs the motion in the normal direction of the contact interface, friction that defines the force resisting the relative tangential motion of the surfaces, and the damping property that defines forces resisting the relative motions of the contacting surfaces.

16.3.4 Prescribed conditions

Except for the material and environmental properties, and the interactions, there may be other external conditions needing to be prescribed, such as initial conditions, boundary conditions, loads, and constraints and motions.

Initial conditions: Non-zero initial conditions can be defined for many variables in the mechanical system. For example, initial stress can be assigned to close-fit clothing, accounting for the wearing deformation.[4]

Boundary conditions: Boundary conditions are used to specify the values of all the basic solution variables in the mechanical systems, such as displacements and rotations. Usually, boundary conditions are used to constrain portions of the model to remain fixed or to move by a prescribed amount. For example, in a dynamic garment wearing simulation, a displacement amount is often set to simulate the putting-on process.[5]

Loads: Loads deform the physical structure of the object and thus create stress in it. Various concentrated or distributed loads may need to be added to the objects. The load can be concentrated on several single points or distributed to edge, surface or volume. For example, forces are added to points, edges or planes as foot loads during walking.[6,7] Gravity is a typical load added to a volume.

Constraints and motions: Sometimes, it is necessary to define complex mechanical connections between objects, including actuation with prescribed loads or motions. Sewing simulation is a typical example of this kind of constraint. To assemble cloth patterns together, some motion or load constraint needs to be added to the prescribed seam lines.[8]

16.3.5 Analysis type

Before starting a numerical simulation, the kind of mechanical analysis to be performed needs to be determined: static or dynamic, linear or nonlinear? If it is dynamic analysis, how long is the time period to be simulated, which integration method is to be applied (implicit or explicit)? To visualize and analyze effectively the simulated results, output variables need to be specified and clearly structured before performing the mechanical analysis.

16.4 Examples

Most of the previously mentioned processing can be performed using general CAD software. Many commercial packages such as 'Exceed' (Hummingbird Ltd., Toronto, Canada), 'Femap' (UGS, Corp., USA), 'Hyperworks' (Altair Engineering, Inc., Michigan, USA) provide pre-processors that can be integrated with many CAD systems and finite element (FE) solvers. Specifically designed pre-processors can also be developed by integrating 'Visual C++' and 'OpenGL' (Silicon Graphics, Inc., USA), or other programming and graphical techniques. Here, ABAQUS/CAE, which is a pre-processor for the FE package 'ABAQUS' (version 6.4, Hibbitt, Karlsson & Sorensen, Inc., Pawtucket, RI, USA),[9] and 'ST-715', which is a software for clothing simulation developed by the Institute of Textiles and Clothing, the Hong Kong Polytechnic University (Hong Kong, China),[10] are taken as examples to illustrate the pre-processing for the mechanical analysis.

16.4.1 FE packages

An ABAQUS model is composed of several components that together describe the physical problem to be analyzed and the results to be obtained. At minimum, an analysis model consists of the following information: discretized geometry, element section properties, material data, loads and boundary conditions, analysis type, and output requests. As illustrated in Fig. 16.3, ABAQUS provides several modules to deal with the information.

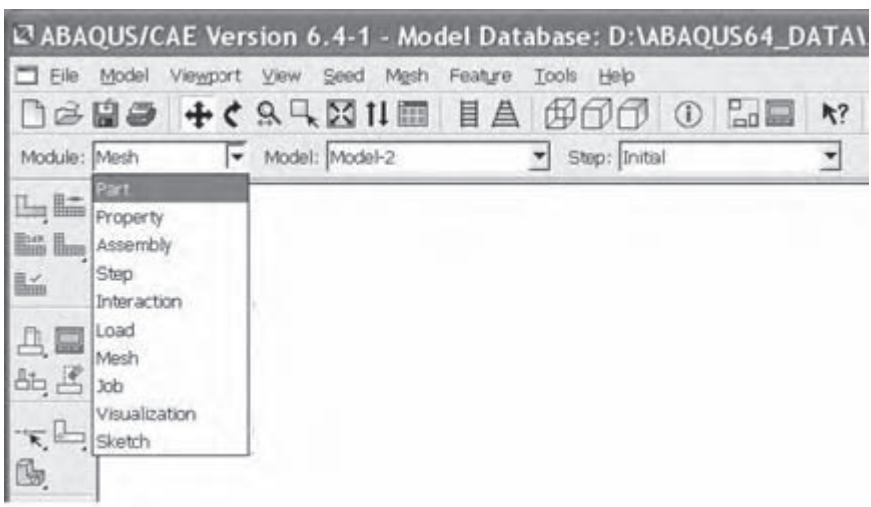

16.3 ABAQUS interface.

Discretized geometry: In FE methods, finite elements and nodes define the basic geometry of the object to be modeled. Elements, connected to one another by shared nodes, represent a discrete portion of the physical structure. The collection of all the elements and nodes in a model is called a mesh. The element type, shape, and location, as well as the overall number of elements used in the mesh, will affect the simulation results. The greater is the mesh density, the more accurate the results. However, as the mesh density increases, the analysis results converge to a unique solution, and the computational time cost increases. Individual objects are created in the 'Part' module, and are then assembled into a global coordinate system in the 'Assembly' module. In the 'Mesh' module, each geometrical model in the assembly is further discretized into a finite element mesh.

Element section properties and material data: ABAQUS has a wide range of elements, many of which have geometry not defined completely by the coordinates of their nodes. For example, the thickness of a shell is not defined by the nodes of the element. Such additional geometric data are defined as physical properties of the element. Material properties for all elements must also be specified. The section and material definitions are created and assigned to regions of a model in the 'Property' module.

Various load and boundary conditions are defined in the 'Load' module. The 'Step' module is used to create and configure analysis steps and associated output requests. Mechanical interactions between regions of a model or between models can be specified in the 'Interaction' module. Once the definition of the model is completed, the simulation is performed in the 'Job' module. And finally, the obtained results can be viewed in the 'Visualization' module.

Taking the simulation of a dynamic stocking as an example, the procedure was introduced using ABAQUS/CAE to prepare for the mechanical analysis. Problem description: a body stands still, the legging of a stocking is put-on from ankle to knee; the bone of the leg is considered rigid and has no displacement during the wearing, and the soft tissue deforms due to the pressure induced by the stocking. It is a nonlinear problem due to the large deformation of the stocking and the complicated contact between leg and stocking. An explicit method is chosen for the dynamic simulation. To construct the model for the simulation, the following modules need to be entered and a series of tasks need to be performed step by step.

Part: Input geometrical model for lower leg, and create the tubular model for the legging.

Property: Define homogeneous solid material of isotropic elasticity for the leg tissue, and homogeneous shell material of orthotropic elasticity for the stocking.

Assembly: Assemble the two parts to a global coordinate system with suitable relative positions as shown in Fig. 16.5.

Step: Configure the analysis procedure (nonlinear dynamic explicit) and output requests.

Interaction: Define a finite sliding surface-to-surface contact between the inner surface of the stocking and the leg surface.

Load: Fix the bone surface, and allow the top edge of the stocking to move upward at a constant speed. The boundary condition is illustrated in Fig. 16.5.

Mesh: Tetrahedron 3-D stress element and quadrangle shell element are used for the leg and the stocking, respectively. The two objects are then discretized into meshes of finite elements.

Job: Create a job and submit it for analysis. A dynamic stress analysis is carried out, and the system is solved using the explicit integration method.

16.4.2 A specifically designed system

The ST-715 package includes simulations of several tests of fabric mechanical properties, such as the heart-loop test and the drape test, and garment simulation. The system is linked to an engineering database. A skirt simulation is taken as an example to illustrate how to construct a 3-D garment from 2-D patterns.

At first, the user needs to prepare the geometric models. Two-dimensional patterns for a skirt described by boundary curves are input,

(a) Lower leg(male) (b) Legging of stocking

16.4 Geometrical models.

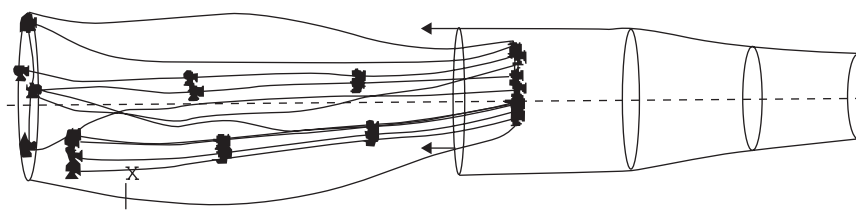

16.5 Boundary condition.

as shown in Fig. 16.6. The patterns are then discretized by the user-defined mesh size. Here, quadrangular mesh is used. After meshing, the points locating within the boundary edges are recorded, representing the cloth patterns for further simulation. Pairs of lines to be sewn together are defined as seam lines (Fig. 16.7).

Figure 16.8 shows the interactive interface to prepare the skirt simulation. The 2-D meshed cloth patterns and the 3-D body model need to be input first. Here, to save the computational cost, only the waist, abdomen and hip parts of a human body that are in contact with a skirt are modeled. The body part is modeled as an elastic shell. The material parameters for both the cloth and the human body can be input from a database supporting the

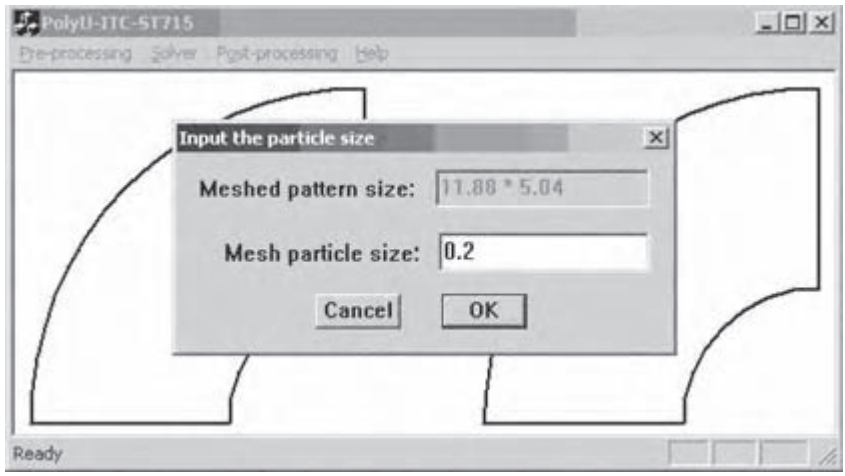

16.6 Mesh 2-D patterns.

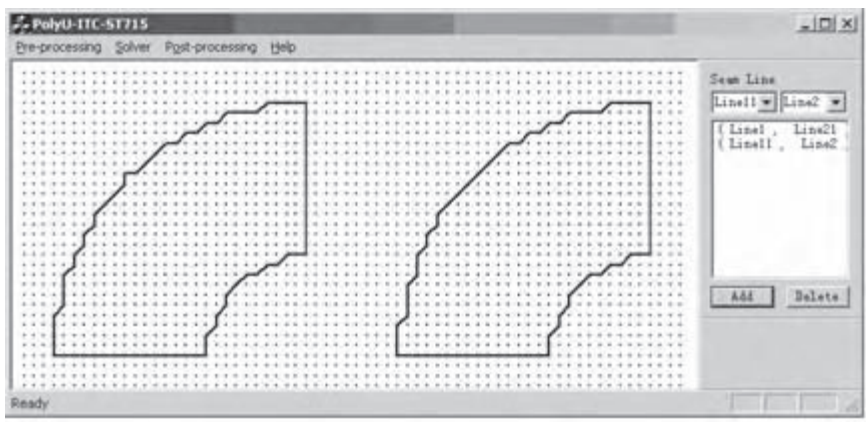

16.7 Defining seam line pair.

system, as illustrated in Fig. 16.9. They can also be input and edited through the interface directly. Usually, the relative positions of the body and the patterns need to be adjusted properly. This positioning process can also be

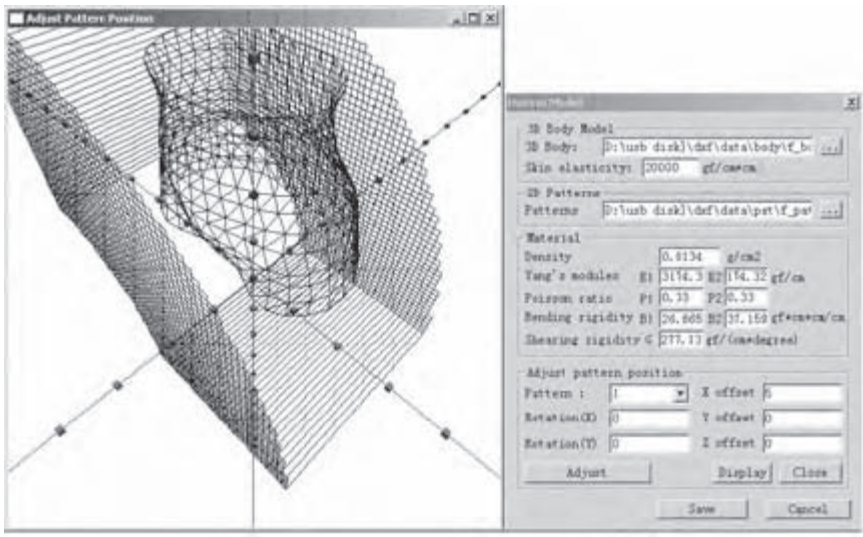

16.8 Editing material parameters and geometric positions of objects.

16.9 Inputting material parameters from database.

performed within this interface. Finally, the whole skirt construction system is set ready for numerical calculation.

16.5 Conclusion

To perform a mechanical simulation, geometric models must be generated to represent the real objects, discretized for the numerical calculation, the material parameters and environment parameters set, various conditions such as interactions, load and boundary conditions defined and a proper solver for the mechanical system chosen. An interactive interface for the pre-processing is necessary. Many general pre-processors for CAD systems or FE solvers can be used for this purpose. Some specifically-designed software can also serve this purpose. Two examples were used to explain how to prepare for a numerical simulation.

16.6 Acknowledgement

We would like to thank the Hong Kong Polytechnic University for funding this research through Project A188.

16.7 References

1. Volino, P. and Thalmann, N.M., Chapter 1 Introduction, in *Virtual Clothing: Theory and Practice*, New York, Springer, 2000, p. 1–9.
2. Volino, P. and Thalmann, N.M., Chapter 2 Simulation models, in *Virtual Clothing: Theory and Practice*. New York: Springer, 2000, p. 11–102.
3. Dai, X.Q., Li, Y., Effect of sock on biomechanical responses of foot during Walking. *Clinical Biomechanics*, 2005. Submitted.
4. Dai, X.Q., Liu, R., Li, Y., Zhang, M., Kwok, Y.L. Numerical simulation and prediction of skin pressure distribution applied by graduated compression stockings. *17th IMACS World Congress, Scientific Computation, Applied Mathematics and Simulation.* 2005. Paris.
5. Dai, X.Q., Li, Y., Zhang, X., Numerical simulation of mechanical interaction between lower-limb and compression stocking. *Journal of Information and Computational Science*, 2004(1): p. 15–19.
6. Jacob, S. and Patil, M.K. Stress analysis in three-dimensional foot models of normal and diabetic neuropathy, *Frontiers of Medical and Biological Engineering*, 1999 **9**(3): p. 211–238.
7. Cheung, J.T., Zhang, M. and An, K.N., Effect of Plantar Fascia Stiffness on the Biomechanical Responses of the Ankle–Foot Complex. *Clinical Biomechanics*, 2004 **19**: p. 839–846.
8. Volino, P. and Thalmann, N.M., Collision Response, in *Virtual Clothing: Theory and Practice.* 2000, Springer. p. 145–182.
9. Hibbit, Karlsson and Sorensen, Inc., Chapter 2 ABAQUS Basics, in *Getting Started with ABAQUS.* 2003. 2-1-2-44.
10. Zhou, X., *ST715 particle system user manual.* 2003. The Hong Kong Polytechnic University: Hong Kong.

17

Visualization for mechanical analysis

Y. LI[1], R.M. WANG[1,4], X-Q. DAI[1,2], X. ZHANG[3] AND X. LUO[4]
[1]The Hong Kong Polytechnic University, China
[2]Soochow University, China
[3]Xian University of Engineering Science & Technology, China
[4]Zhongshan University, China

17.1 Understanding the role of visualization

Visualization in scientific computing and engineering design is getting more and more attention from many people. Especially in relation to the fast increase of computing power, graphic tools are required in many cases for interpreting and presenting the results of various simulations, or for analyzing physical phenomena.[1] Visualization of scientific data has become a very important topic for many researchers. Scientists, engineers, medical personnel, business analysts, and others often need to analyze large amounts of information or to study the behavior of certain processes. Numerical simulations carried out on supercomputers frequently produce data files containing thousands and even millions of data values. Similarly, satellite cameras and other sources are amassing large data files faster than they can be interpreted. Scanning these large sets of numbers to determine trends and relationships is a tedious and ineffective process.

The appropriate way to analyze and understand these results is to visualize the data. If the data is converted to a visual form, the trends and patterns are often immediately apparent. Visualization is not just graphics, which itself has the power to present large amounts of numerical information in an efficient and effective way to allow an insight into the numbers, but is concerned with exploring data and information graphically, as a means of gaining understanding and insight into data. Visualization of data is an emerging visual computing technology that uses intuitive and innovative graphical user interface and visualization techniques. This technology helps engineers, scientists, and technicians to access, analyze, manage, visualize, and present large and diverse quantities of data to get information from raw technical data. The technology has evolved from the combination of powerful desktop computers, statistical and analysis tools, graphics and visualization, and sophisticated interaction tools. The data visualized enables

scientists to explore their research data, to gain new scientific insight, and to communicate their discoveries to others. Visualization allows the conversion of information that cannot be perceived by the human eye into forms suitable for this most highly developed human sense.

Visualization of data includes a well-defined set of graphics and visualization tools for visually interpreting the data and producing a hard copy of the results. The environment of data visualization includes analysis tools for a better understanding of the data, data management tools for generating, reducing, saving, and restoring the data, and data access techniques to help get the data into and out of the visual data analysis environment. As visualization environments mature, they focus more on integrating the analytical and visual technologies into more complete data interpretation systems. Examples of visualization integrated into CAD, GIS, and spreadsheet software have already been seen. The idea behind visualization data is to put the user in the center of the analysis process, using visualization as a tool to navigate through data.

The biomechanical engineering for textile and clothing products is a typical kind of human factors engineering, in which humans are the most important element. The design should be based on quantitative investigations of the relationship between the mechanical performance of textile and clothing products and human sensory factors, including physiological and psychological aspects. Visualizing and analyzing the results of the mechanical simulation using a broad range of interaction techniques is crucial to the effectiveness of the product development in the CBMD system.

17.2 Methods of visualization

Visualization is to transform experimental data into graphical primitives. There are many different kinds of data sets, and effective visualization schemes depending on the characteristics of the data. A collection of data can contain scalar values, vectors, high-order tensors, or any combination of these data types. And data sets can be two-dimensional or three-dimensional. Graphing and visualization techniques can vary from simple chart-ing to volume visualization. Several academic visualization classification schemes have been proposed. A simplified classification is used here to explain popular graphing and visualization types. The focus is on technical data and real examples of how various graph types are being used, with an interest in both basic and more advanced visualization techniques. Basic techniques include the familiar types of graphs such as scatter, line, contour, as well as 3D surfaces, and various combinations of these. Advanced visualization methods include 3D geometric rendering, volume visualization, multidimensional visualization, vector fields, and animation.

17.2.1 Charts and graphs

Traditional graph types frequently used in technical or business applications include the scatter, curve, bar, area, pie, and polar charts. The X-Y plot is the most often used curve chart in clothing biomechanical engineering. An X-Y data object is a collection of ordered pairs stored in two columns: an X-column and a Y-column. The X and Y can be any geometrical or physical variables in the mechanical system. For example, an X-Y data object can be stress values versus strain values or time. Attention also needs to be paid to the graph annotation. For presentation graphics, the detailed layout of the graph is an essential component of visual communication. Without the ability to perform detailed annotation of the graph, the entire visual message might be lost. Important layout features include title, notes, legend, axes labeling, fonts, and maybe color scales and some special symbols. Figure 17.1 illustrates two different kinds of presentation graphs: (a) is a fabric load–elongation curve with measured results compared against simulated ones and (b) shows garment stress varying with time during wearing process.

17.2.2 Geometrical modeling

Mechanical simulation is based on geometric data, which describe from 1D to 3D objects that are often constructed out of one or more primitives (lines, curves, polygons, meshes, polyhedra, or spheres).

Contouring

Contouring is the most commonly used basic visualization display technique for 3D objects. Contour maps are normally derived from a two-

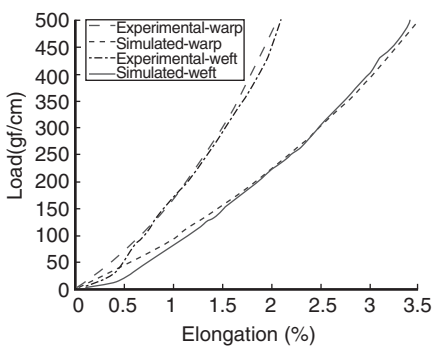

(a) Load–elongation curves: Measured results compared with simulated ones

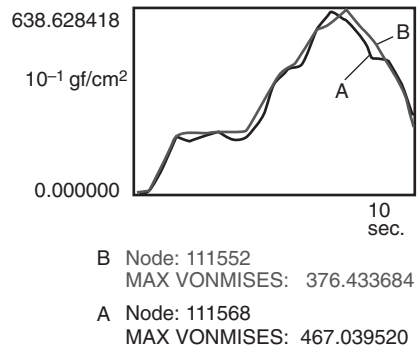

(b) Garment effective stress versus time

17.1 X-Y plots.

dimensional matrix of gridded data. If the data are scattered, various interpolation algorithms are used to construct the data into regular gridded data. The data is then displayed as a contour map with lines of constant height (isolines) showing the shape of the surface, or as a shaded contour map. Shaded contouring is a contour map technique where colors fill in the areas of constant height between isolines.

3D surfaces

A three-dimensional surface is another of the most commonly used basic visualization display techniques for 3D objects. It provides a representation of the surface displayed as a polygonal mesh or a shaded surface.

Rendering

Rendering makes a visualized object look more realistic. A geometric rendering process requires two tasks: hidden surface and shading. Shading is to fill meshes with color; it can be flat shading or smooth shading. Another useful method for adding detail to a 3D model is texture mapping. With texture mapping, arbitrary 2D images can be mapped onto 3D graphics objects. It is a technique very often used in clothing simulation. Various printing patterns can be mapped to garments to show cloth variety.

Volume and multidimensional visualization

In mechanical simulation, the objects involved are not limited to surfaces. In most cases, 3D solid objects are simulated, and the internal structures are considered. For example, in biomechanical analysis, the inner mechanical state of a body subjected to external loads needs to be investigated. Therefore, volume visualization becomes a necessity. Most often the volumetric dataset is defined on a three-dimensional lattice with one or more scalar values, and possibly one or more vector values, at each grid point (x, y, z) on the lattice.

Plane section slicing and dicing is a simple visualization technique to inspect a large 3D data volume. Generally, only display 2D or 3D objects can be displayed on a 2D screen. However, additional variables and data components can be shown through color, icons or other media.

17.2.3 Vector field

In mechanical simulation, many applications involve some kind of magnitude and direction; a vector. Geometrical variables such as displacements

and strains, and physical variables such as forces, stresses and velocity are all vectors. Arrows are icons for vectors. An arrow can indicate both the magnitude and the direction of a vector. A complete view of a vector field can help us understand the deformation and state of a mechanical system well.

17.2.4 Animation

An animation is a collected sequence of slightly varying images that show movement through time. In mechanical analysis, changes can be shapes or positions of objects along time or deformation. Animation brings the data to life, helping us to discover things that we cannot see from the static chart or pictures. It is often crucial for understanding complex 3D scenes. Moving 3D objects in relation to each other, or in relation to other fixed-scene attributes, enables insight and understanding.

Animations can be produced either in real time, or simply by play-back of a series of pre-computed images called frames. In real time animation, rendering of each frame is done during display. It has the advantage that the animation may be interactively controlled by the user. A disadvantage is that the screen update time usually depends on image complexity, which may vary per frame. To realize real time animation, the rendering techniques are also limited. Usually, the frame play-back technique is used to produce animation.

17.3 Post-processing: an example

Clothing biomechanical engineering design is a complex procedure. At the end of the design, large number result data will be generated; these then go to the post-processing part to be analyzed and to evaluate the mechanical performance. The post-processing procedure is relatively straightforward. It simply involves obtaining the results from the analysis program, selecting appropriate views, modifying options on these views, and manipulating and/or reporting output. Visual information can be communicated through color, form, plot and animation.

To visualize and analyze the results of the mechanical simulation effectively, the following features are considered essential for the post-processors: linear and logarithmic axis scales, axis annotation, simultaneous display of data and visualization, diverse range of plotting modes, diverse range of 3D display modes, superimposition of mathematical functions, and intuitive user interface.[2] Most finite element (FE) packages have their own visualization modules to view the results of the mechanical analysis. Here, the ABAQUS/Viewer is used as an example to illustrate what is necessary for a typical post-processor for mechanical analysis, and what can be done with it.

17.3.1 Visualization module basics of ABAQUS/Viewer

ABAQUS/Viewer is a post-processor incorporated into ABAQUS/CAE as the visualization module.[3] The user interacts with ABAQUS/Viewer through the main window. Figure 17.2 shows the components that appear in the main window. The toolbar contains a convenient set of tools for managing the data files and viewing the model. The viewer obtains all model data and analysis results from the output database of ABAQUS. The database manipulation tools allow one to open and save output databases, and to print viewport. The view manipulation tools allow one to specify different views of the model or plot. For example, the user can pan, rotate or zoom the model or plot. The view and display options tools allow one to customize the appearance of the model. For example, the user can specify whether wireframe, hidden line, filled, or shaded render style will be used and whether perspective will be applied. The display group tools allow one to selectively plot one or more output database items.

ABAQUS/Viewer offers several distinct types of plots for viewing a model and results.

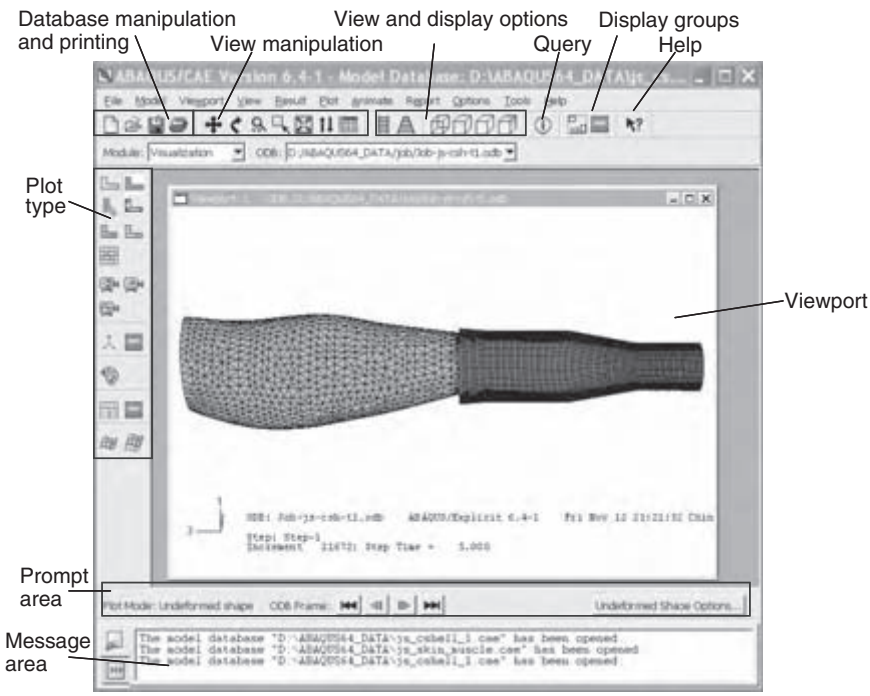

17.2 ABAQUS/Viewer interface.


A fast plot is a quickly drawn representation of the model.


An undeformed shape plot displays the initial shape or the base state of the model.


A deformed shape plot displays the shape of the model according to the values of a nodal variable such as displacement.


A contour plot displays the values of an analysis variable such as stress, strain or pressure at a specified step and frame of the analysis. The visualization module represents the values as customized colored lines, colored bands, or colored faces on the model.


A symbol plot displays the magnitude and directions of a particular vector or tensor variable at a specified step or frame of the analysis. The visualization module represents the values as symbols, for example arrows, at locations on the model.


A material orientation plot displays the material directions of elements in the model at a specified step and frame of the analysis.


An X-Y plot is a two-dimensional graph of one variable versus another.

The animation tools display a series of plots in rapid succession, giving a movie-like effect. There are also several additional capabilities. Visualizing diagnostic information helps to determine the causes of non-convergence in a model. Probing displayed model data and analysis results as the cursor moves around a model plot; probing an X-Y plot displays the coordinates of the graph points. The user can define a path by specifying a series of points through the model, then view results along the path in the form of an X-Y plot.

17.3.2 Analyzing simulation results

To understand the visualization module for the CBED system well, the dynamic simulation of wearing a stocking is taken as an example, to go through the general post-processing procedures.

The initial shape for the stocking is tubular, after wearing simulation it takes the shape of the leg surface. This pressure distribution is crucial for compression stocking.

The simulation of the dynamic wearing process can be recorded as animation. By using the X-Y data plot, more detailed information can be visualized. Figure 17.3a plots the changes of the Mises stress of the stocking at three nodes during wearing. Figure 17.3b shows that the pressure varies along a path in the front center of the leg from ankle up to knee.

Not only can the cross-sectional distribution of the pressure on the skin surface be investigated, but also the mechanical state of the volume interior

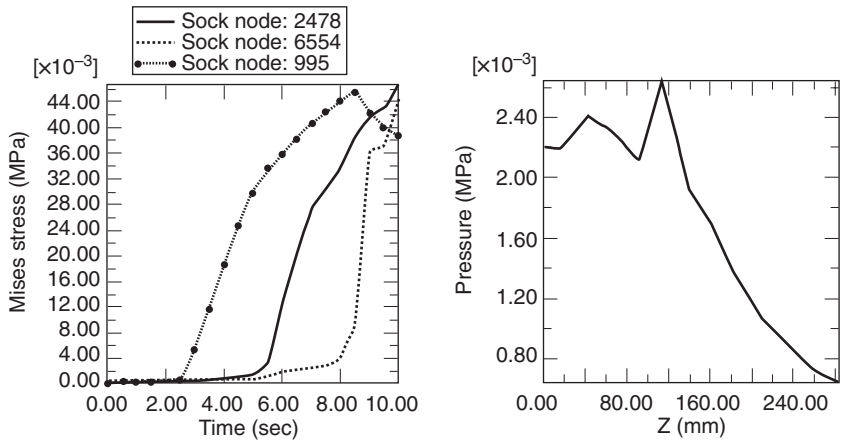

(a) Changes of stocking stress at several nodes

(b) Skin pressure distribution along a path

17.3 X-Y data plots.

can be looked into. Moreover, by using the probing function, detailed information can be obtained of any a node or an element, such as node/element number, coordinates, stress, pressure and so forth.

17.4 Conclusion

To analyze and understand the results of mechanical simulation effectively, it is necessary to transform numerical data into graphical primitives. Data visualization includes a well-defined set of graphics and visualization tools for visually interpreting the data. Graphs and charts, contour plots, surface modeling and rendering, and color coding are common tools for visualization and visualizations of volume interiors. Additional techniques include visualizations of volume interiors, multidimensional and animations. Through an example to analyze the simulated results of dynamic stocking wearing using the ABAQUS/Viewer, the requirements for a typical post-processor for mechanical analysis have been illustrated, along with what can be done with it.

17.5 Acknowledgement

We would like to thank Hong Kong Polytechnic University for funding this research through Projects A188 and G-YD31.

17.6 References

1. Earnshaw, R.A., Vince, J. and Jones, H., *Visualization and Modeling*, San Diego, Calif.: Academic Press 1997.
2. Brown, J.R., *Visualization*, *Using Computer Graphics to Explore Data and Present Information*, New York: John Wiley & Sons, Inc. 1995.
3. ABAQUS, Inc., *ABAQUS/CAE Users' manual*, Pawtucket, USA: ABAQUS, Inc. 2004.

Part V

Applications in product development

18

Biomechanical engineering of jeans

X. ZHANG[1,2], Y. LI[1], AND A. WONG[1]
[1]The Hong Kong Polytechnic University, China
[2]Xian University of Engineering Science & Technology, China

18.1 Introduction

18.1.1 Need for numerical simulation of jeans' mechanical performance

Jeans have become more and more popular in the world because they provide a satisfactory level of comfort and durability for consumers. Their fitness and pressure comfort have been identified as important attributes of mechanical comfort to satisfy the wearer's physiological and psychological needs. To quickly respond to the jeans market, it is necessary to predict jeans' mechanical performance at the design stage by using engineering design technology, for the optimal design of jeans in terms of functional performance and pressure comfort. This engineering design application involves two aspects of development: (i) the need to develop a mechanical model that is able to describe the dynamic mechanical interaction between jeans and the human body in the design stage with satisfactory accuracy; (ii) the need to develop a computational methodology to solve the model and to visualize the 3D distribution of the mechanical performances of the jeans.

The mechanical comfort of a garment during wear is determined by a complex process, in which the human body interacts dynamically with the garment on large surface contact areas. The interaction force generated during the dynamic interactions between the clothing and the human body induces the perception of various mechanical sensations. Therefore, the engineering design of jeans' mechanical performance based on the development of the mechanical model requires interdisciplinary knowledge and technologies mainly in four aspects: human physiology and psychology, clothing mechanics, contact mechanics and advanced computing technologies. Extensive research has been carried out experimentally on garment mechanical comfort, such as garment pressure. However, very little has been reported on the theoretical inverstigation of jeans' mechanical performance during wear by integration of the knowledge and technologies

for the development of advanced engineering design technology for jeans products.

18.1.2 Biomechanical features of body parts covered by jeans

Jeans cover the hip, the lower abdomen and the lower limbs of the human body. The abdomen consists of the abdominal cavity, of which the volume changes with respiration, and the digestion of food and drink. The lower limbs play an important role in supporting the whole body and in walking and other movements. Like other body parts, the lower limbs consist of skin, tissue, fat, bones, and so on. They also consist of muscles. The thicknesses of skin, fat, and muscles vary greatly among the abdomen, hip, thigh and shank, and even among different regions of the same part. For example, the hip and thigh have a much thicker layer of fat than the shank; and the thigh has a skin layer of different thickness at the front, the back, and the side, the skin at the side being the thickest. Actually, the skin elasticity also varies among different regions. All these differences lead to different sensibilities about pressure at different positions.

When the body is subjected to small external force, such as garment pressure during wearing, the bone can be considered as a stiff material without deformation. The skin may have tensile, shearing and bending deformations. The soft tissue, which consists of the adipose tissue and the skeletal muscles in passive condition, can be regarded as incompressed rubber, indicating that its shape distortion is much easier than its volume change. Therefore, to describe the interactive mechanics between a deformable human body and a garment, it is assumed that the human body consists of three major components: skin, soft tissue and bone.

18.1.3 Sensory perceptions and preference in jeans' wearing

Generally, by their nature, jeans are perfect-fitting or tight-fitting; at least they have close contact with the waist and thigh of the body. The mechanical interaction stimulates neurophysiological impulses of touch and pressure through the mechanical receptors in the deep layer of the skin, which further induces subjective perceptions and relevant pressure discomfort sensations of the human body. Growther[1] pointed that classic jeans are characterized by body-hugging or tight fitting, which may result not only in a sculptured form, but also in possible body malfunction in the long-term. The author suggests that (i) the fabric construction and the chosen angle of bias along the back-rise seam of a pair of jeans may directly contribute to clothing fit and body comfort, and (ii) that cotton denim may be pre-

shaped to accommodate body contours and so reduce the compressive forces of the fabric on the body in the jeans with close-fit styling.

The results reported by Makabe *et al.*[2] indicated that the pressure at the waist is influenced by the area covered, respiration and the ability of the garment to follow bodily movements. The subjective evaluation of clothing pressure at the waist showed that no sense of discomfort is perceived when the pressure is in the range of 0–15 gf/cm^2. Negligible or only slight discomfort is perceived when the pressure is in the range of 15–25 gf/cm^2, and extreme discomfort is perceived when the pressure exceeds 25 gf/cm^2. Through their study on girdle pressure,[3] they found that subjects complained of discomfort when the clothing pressure reached more than 40~54 gf/cm^2, and the discomfort areas are at the waistline, the thigh base, and the thigh front. The relation between waistband-pressure and wearing time was examined by a series of subjective experiments.[4] The results show that both the waist girth and the clothing pressure changed according to the time of day and increased significantly after eating. A linear relation between the increment of waist girth and the increment of waistband-pressure was observed.

18.2 Biomechanical modeling

Denton[5] pointed out that the level of garment pressure is a mechanical parameter that mainly depends on four factors: (i) design and fit of the garment; (ii) the different radii of curvature of body parts; (iii) the mechanical properties of the underlying tissue and (iv) the extensibility of the garment. Therefore, it is possible to predict garment pressure in terms of the geometrical and mechanical parameters of individual people wearing garments. The basic work is to develop a mechanical model of garment pressure for optimizing the design of a garment in terms of functional performance and pressure comfort at the design stage. Numerical simulation of garment pressure based on the model will help designers and consumers to see the pressure distribution of the garment on a body before the actual garment is produced. There is also a need for quick response to the changes of clothing marketing. This simulation has two objectives. The first is to predict jeans' mechanical performance on a human body in a 3D display by development of a jeans–body dynamic contact model. The second one is to study the mechanical interaction of the contact interface between the jeans and the human body.

18.2.1 Model description

During the process of wearing a garment, the human body deforms the garment and, in return, the pressure induced from the garment deforms the

skin and soft tissue of the body. The interactive deformations between the human body and the garment can be disintegrated into three deformation components. First, the garment is stretched to fit the human body, which induces pressure on the body. Secondly, the pressure compresses the elastic components of the body and makes the soft tissue flow or redistribute, and the skin is stretched accordingly. Thirdly, the rigid bone restrains the deformation of the skin and the soft tissue. The pressure distribution is changing dynamically with the garment stretch that accommodates the body shape and the body deformation during the wearing process.

Garment pressure is closely related to specific shapes of individual human bodies and garment styles. To obtain simulation results that are able to represent actual situations, a specific 3D geometric model for a particular individual female body needs to be developed and a specific 3D geometric model for a particular garment. For this simulation, 3D models of a female human body and jeans were generated by using commercial graphic software. The body is modeled with three layers of materials that have different properties, representing the bone, the soft tissue and the skin respectively.

As the basis of the analysis, there are the following assumptions:

(i) The human model consists of three components: the bone, the soft tissue and the skin. The bone is regarded as a stiff shell, the skin as a thin elastic shell and the soft tissue as an incompressible rubber shell.
(ii) The displacements of the skin and the soft tissue are the same when subjected to compression from the garment and the displacements cannot be permeated to the bone.
(iii) The mechanical performances of the skin and the soft tissue are assumed to be of material linearity and geometrical non-linearity.
(iv) The garment is regarded as a thin elastic shell of material linearity and geometric non-linearity, and the stress in its thickness direction is assumed to be negligible.
(v) The garment is moving up along the human body from the foot to the waist without friction while the human body stands still during the wearing process.
(vi) The contact between the human body and the garment is a dynamic process of coordinated contact, which is related to the overall stress distribution in the contacting objects.

The time-dependent contact system involves four objects (the garment, the skin, the soft tissue and the bone) and the three contact interfaces (between the garment and the skin, between the skin and the soft tissue, and between the soft tissue and the bone). At time $t = 0$, the garment occupies domain ${}^0\Omega^1$ and the human body occupies domains of ${}^0\Omega^2$ for the skin, ${}^0\Omega^3$ for the soft tissue and ${}^0\Omega^4$ for the bone, respectively. From time $t = 0$,

the garment starts to move from foot to waist to fit the body, during which it is occupying new domains ${}^{t}\Omega^{1}$ and contacting the domain ${}^{t}\Omega^{2}$ of the skin that corresponds to the domain ${}^{t}\Omega^{3}$ and ${}^{t}\Omega^{4}$ at any time $t > 0$.

18.2.2 Contact modeling

Contact interfaces inside the body

Shell elements are used in the discretization of the 3D human body. Figure 18.1a shows a schematic diagram of the constraint methods used in the contact interfaces inside the body. The method of merging matched nodes is used in the geometrical structure of the contact between skin and soft tissue. As the shell elements have no true thickness, the mid-surfaces of the skin and the soft tissue are regarded as coincident, as shown in Fig. 18.1a. Then, the elements of the skin and the soft tissue can be tied by merging the matched nodes at the mid-interfaces, which are marked with the circles shown in Fig. 18.1a. The merged nodes on the mid-surfaces will have the same degrees of freedom during the wearing process but have different stress–strain distributions due to their different mechanical properties, such as Young's modulus E_t for the soft tissue and E_s for the skin.

The method of offset tying is used in the geometrical structure of the contact between soft tissue and bone, to make the soft tissue and the skin both deform and show no penetration through the bone during the wearing process. A geometrical control distance d_c between the mid-surfaces of the bone and the soft tissue is constructed, as shown in Fig. 18.1b, where the soft tissue is defined as the master surface and the bone as the slave surface. This d_c can be regarded as the maximum compressive allowance of the skin and the soft tissue against the normal direction of the bone. The tying will work if the surfaces are close to each other. Therefore, a distance d is used to determine whether a slave node is tied down or not. The distance d is defined as 1 mm in the simulation, with consideration of the size of the shell

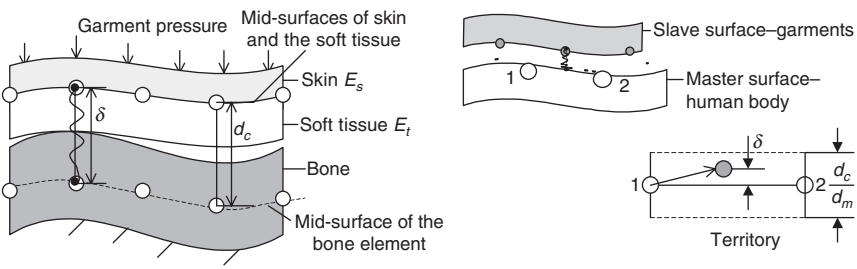

(a) Contact interfaces in the body model (b) Contact between body and garment

18.1 Contact interface.

elements used. The soft tissue must be tied to the bone if $\delta \leq d$, where δ is the distance between the slave node and the master segment.

The penalty constraint method[6] is used in the contact interface between the soft tissue and the bone. The contact constraint consists of placing normal interface springs between all penetrating nodes and the contact point, as shown in Fig. 18.1b. In the constraint, a contact force q_{ci} applied between the slave node and its contact point is represented as $q_{c1} = -k_i\delta$, where k_i is the stiffness factor for the master surface as spring stiffness. This k_i is given in terms of its bulk modulus, the element volume, the segment area, and the penalty scale factor. Because the element sizes in the three layers are similar, each master node on the soft tissue can coincide with a slave node on the bone to ensure complete displacement compatibility along the interface. Therefore, no nodes on the bone interpenetrate through the surface of the soft tissue in the numerical simulation.

Contact between body and garment

Contact between the human body and the garment is modeled as a dynamic sliding interface. In the sliding contact algorithm, the human body is defined as a master surface with a target boundary and the garment is defined as a slave surface with hitting boundary, as shown in Fig. 18.1b. A slave node on the slave surface is assumed to be in contact with a master segment if $-d_m \leq \delta \leq d_c$. Here, δ is the distance between the slave node and the master segment, d_c is control distance, and d_m is the maximum penetration allowed. The equation defines a domain, which may be referred as a contact territory as shown in Fig. 18.1b. Thus, a node is considered as a contacting node if it is within the contact territory. In explicit analysis with the penetration method, it is natural to set d_c to zero. Thus, the value of δ is equal to the penetration ${}^tp^1$ as a slave node passing through a master segment. The penalty constraint method consists of placing normal interface springs between all penetrating nodes and the contact surface, as shown in Fig. 18.1b. If the slave node does not penetrate, nothing is done. If it does penetrate, a contact force ${}^tq_{ci}$ is applied between the slave node and its contact point: ${}^tq_{c1} = -k_i{}^tp^1$, where, k_i is the stiffness factor for the master surface, such as a spring stiffness, which is given in terms of the human body's bulk modulus K_i, its element volume V_i, its segment area A_i and the penalty scale factor *fsi* that can be controlled. The spring stiffness matrix must be assembled into the global stiffness matrix.

Since the penetration ${}^tp^1$ depends only on the displacement of the contact system at time t and k_i as a chosen parameter, the normal contacting force ${}^tq_{ci}$ can be calculated by knowing the configuration of the contact system at t time. Therefore, the contact force vector ^{t}Rc can be evaluated as a function of the displacement U.

18.2.3 Numerical solution

The solution of the mechanical contact system is complicated by (i) dynamic balance on space domain and on time domain; (ii) geometry non-linearity of the garment deformation; (iii) contact non-linearity due to the unknown contacting boundaries prior to the solution of the problem. Therefore, the model needs to be solved numerically using the finite element method in the space domain and the finite difference method in the time domain. The mechanical analysis of the model is performed using LS-Dyna Finite Element Method (FEM) software. The Belytschko–Lin–Tsay shell element[6] is used in the discretization of the 3D human body and the jeans, because of the large displacements and large rotations of the elastic objects. The total element number of the human body is 13362 (7221 elements for the bone, 3145 for the soft tissue, 2996 for the skin) and 1585 for the garment. Since the simulation is a non-linear problem, dynamic explicit analysis is carried out.

18.3 Computational experiments

18.3.1 Material properties

To validate the model, it is applied to simulate mechanical performance during wearing jeans of two different materials. Table 18.1 shows the mechanical parameters of the materials used in the simulation.

For lifting the trousers, the top of the trousers is given a speed 100 mm/s for moving from foot to the waist. The termination time is 6.5 seconds to make the garment fit to the body. The time step size is 3.5E-4 second, which can be adjusted according to the needs of computing stability.

Table 18.1 Mechanical parameters of the materials used in the simulation

The soft tissue	Density (kg/m^3)	*937
	Shear modulus (kg/m^2)	^3300
	Poisson's ratio	0.49
The skin	Density (kg/m^3)	*1060
	Tensile modulus (kg/m^2)	^2000
	Poisson's ratio	0.3
Denim A	Density (kg/m^3)	492
	Tensile modulus (kg/m^2)	54000
	Poisson's ratio	0.48
Denim B	Density (kg/m^3)	370
	Tensile modulus (kg/m^2)	42000
	Poisson's ratio	0.40

*[7, 8]

18.3.2 Mechanical performance of jeans

Jeans' deformation

The simulation indicates the jeans stretch and recover during the wearing process. Also, the simulation shows the jeans wrinkle in the wearing process. To describe the process of the dynamic deformation, three nodes were selected on the jeans (A at the center front waist, B at the pelvis and C at the knee). Figure 18.2 shows the curves of the displacements of the three nodes, (a) for the displacement at *x*-direction of the body wide direction and (b) for the displacement at *z*-direction of the body thickness direction. The scale in the graphs is presented in the unit used in the finite element model, which is transformed into centimeters by multiplying by 16. The positive and negative values of the displacement are relative to the *x*-axis and *z*-axis. For the three nodes, the displacements at the *x*- and *z*-directions are all increasing to a maximum value and then decreasing, indicating the jeans stretch-recovery on passing the hips and finally fitting to the body. For node A at the center front waist, the positive value at the *z*-direction indicates that the jeans stretch; this increases to a value around 5.7 cm on passing the hips, then to 6.8 cm when finally fitted to the waist. For node B at the pelvis, a maximum stretch of 6.8 cm is observed in the *x* direction when passing the hips. This decreases to 3.2 cm in the *x*-direction and 3.3 cm in the *z*-direction when finally fitted to the waist. For node C at the knee part, the maximum stretch is observed in the *z*-direction, finally recovering to 2.7 cm. Small displacements in the *x*-direction are observed at nodes A and C, as shown in Fig. 18.2a, due to their center positions on the jeans.

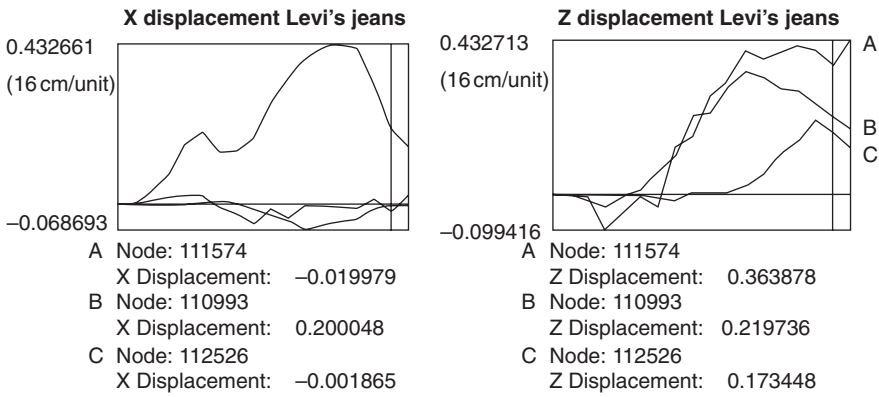

(a) *x*-displacement of the three nodes (b) *z*-displacement of the three nodes

18.2 Displacements at the three nodes of jeans A.

Jeans' pressure distributions

The pressure distribution of the two pairs of jeans was visualized. Negative values of pressure showed the pressure on the body induced by the garment; positive values of pressure showed the force in the garment to move it towards the skin when the garment did not contact the body at a specific point. From the pressure contour plots of the two pairs of jeans, it could be seen that the pressure does not distribute uniformly over different parts of the body. The pressure on most of the front waist area and the pelvis area covered by the clothing was in the range of 20 to 60 gf/cm^2. The pressure on most of the leg area and knees is in the range of 2 to 20 gf/cm^2. The pressure distribution on the front waist area and the upper leg area covered by jeans A showed some difference with the pressure distribution on the same areas by jeans B.

Figures 18.3a and b show the dynamic pressure changes at the three nodes of jeans A and jeans B, respectively. For the two pairs of jeans, the pressure on node A at the center front waist and node B at the pelvis is increasing until the garment passes the hip area, and then decreasing as they fit to the waist. The pressure on node C arises when fitting to the waist. When jeans A are fitted the body, a high-pressure value of 62 gf/cm^2 is observed on node B, followed by a value of 51 gf/cm^2 on node A and 3.5 gf/cm^2 on node C at the knee. When jeans B are fitted to the body, a high-pressure value of 61 gf/cm^2 is observed on node B, followed by a value of 44 gf/cm^2 on node A and 2.3 gf/cm^2 on node C at the knee. The results indicate that the pressure distribution is different for the two pairs of jeans, but high pressure is observed at the pelvis and lower pressure at the knees

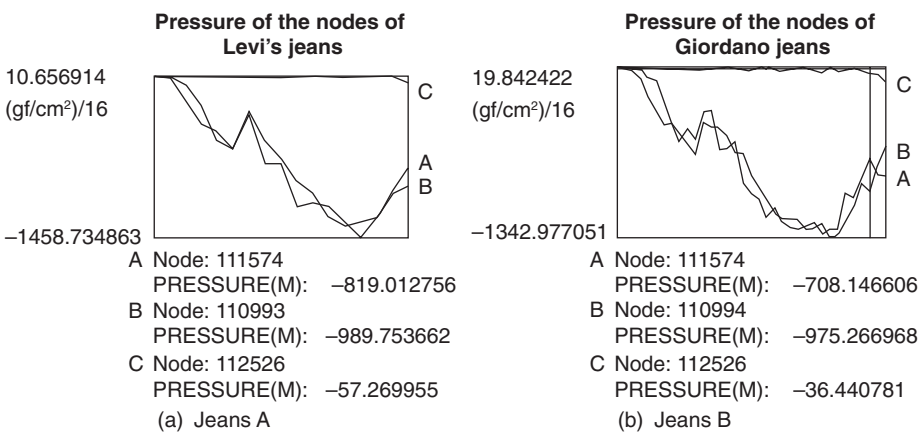

18.3 Pressure change.

for the two pairs of jeans. It corresponds to the fact that the two pairs of jeans in the simulation are of the same style but different material properties. The pressure on the waist area and the pelvis area exceeds 25 gf/cm^2, which may cause extreme discomfort sensations according to the report by Makabe *et al.*[2]

18.3.3 Mechanical behavior of the human body

Displacement of the skin

In the wearing process, the human body is deformed under pressure from the garment. The displacements did not distribute uniformly over different parts of the body. Most of the areas covered by the jeans had displacements in the range 0.3 to 2.8 mm. High-deformation zones of 8 mm were observed on the front of the thigh. The distribution of the displacement was different for the two pairs of jeans, especially at the front of right thigh. The results indicated that the jeans have a different trimming function for the human body.

Skin pressure distributions

The distributions of the skin pressure in wearing the two pairs of jeans was visualized. A positive value of pressure showed that the skin pressure was towards the normal direction of the skin and the interface or against the garment pressure on the skin. A negative value showed the areas subject to the pressure from the garment or the areas not subject to pressure. The pressure distributions were similar to the distribution of skin displacement in the z-direction as observed for skin displacement, suggesting that the skin deformation induces pressure on the soft tissues (defined as the skin pressure).

In the case of wearing jeans A, many areas show a pressure value in the range 0.25 to 2.8 gf/cm^2, and values higher than 8 gf/cm^2 are observed at the front of the thigh and the hip back. In the case of wearing jeans B, many areas show pressure values in the range 0.75 to 3.6 gf/cm^2, and values higher than 9.4 gf/cm^2 are observed at the front of the thigh and the hip back. Compared with Fig. 18.3a and b, the trends of pressure change correspond to the jeans pressure changes, respectively. A high skin pressure of 6.8 gf/cm^2 is observed when wearing jeans B, and a lower skin pressure of 2.7 gf/cm^2 is observed at the node when wearing jeans A, while the garment pressure at node B shows similar values of 61 gf/cm^2 and 62 gf/cm^2 for the two pairs of jeans. It suggests that the skin pressure is not only induced by local contact but also by the overall contact situation. The results illustrate how the skin deformation induces the inner pressure on the soft tissues during wearing.

18.3.4 Model validation

From the simulation results, it is clear that the biomechanical human body provides quantitative descriptions of the mechanical interaction between the human body and the garment during wear, which can be neither simulated by using a rigid model of the human body nor easily measured by experimental methods. The mechanical interaction induces two pressure components: the pressure on the skin by the garment deformation and the pressure on the soft tissue due to the skin deformation, which determine the perception of pressure related comfort sensations.

To validate the simulation results, the predicted jeans pressures at the three nodes have been compared with the objective measurements at corresponding nodes on the Levi's jeans and Giordano jeans in a wearing experiment by Kwok *et al.* (private correspondence) where the geometrical model of the jeans used in the finite element analysis was constructed similar to the jeans styles in the experiment. Figure 18.4 shows comparisons with the two pairs of jeans respectively. The trends of the nodes' pressure show good agreement between the prediction and the experimental measurement; node B at the pelvis had high pressure, followed by node A at the center of the front of the waist, and C at the knee had lower pressure. However, for the two pairs of jeans, the predictions show nearly five times the measurement at node A, twice the measurement at node B, and four times the measurement at node C.

The factors influencing the deviation between the prediction and the measurements need examination. From previous experience in measuring garment pressure, the authors found that there are two major factors influencing the validation method. The first one is the difference between the wearer's actual body shape in the experiment and the geometrical model of the female human body used in the simulation. The second one is the distortion degree of the sensor insertion and the accurate degree of the sensor used that influences the level of garment pressure measured.

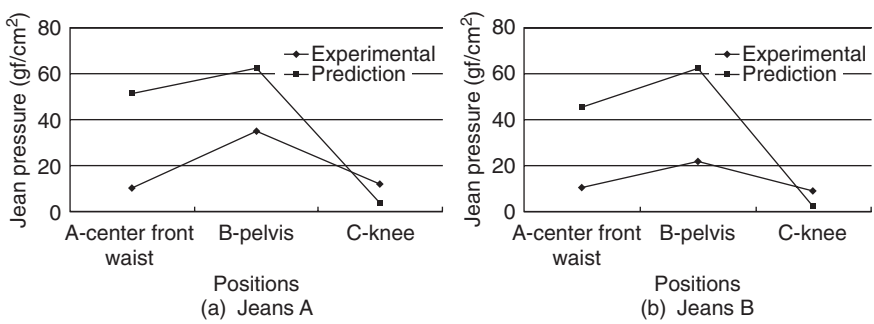

18.4 Pressure comparison between predicted and measured results.

Therefore, development of an experimental method is needed to obtain a map of the deformation of the garment and the pressure contours on the body and the garment. Also, the geometric models of a human body and a garment should be generated from the 3D measurements of the human body and the garment for individuals. All of those will be further work in this research direction.

18.4 Application in jeans' design

Numerical simulation on the basis of the biomechanical human model is able to generate quantitative descriptions of mechanical behaviors such as the garment deformation process, the garment pressure distribution, the human body deformation and the inner stress of the skin. The simulation results based on the model can help the design and evaluation of a garment at the design stage and in e-business use before it is manufactured.

From the simulations of garment deformation in the fitting process, the fit of a garment on a body can be evaluated. The quantitative description of the displacement of garment 3D directions, as shown in Fig. 18.2, may give designers a guide to adjust the garment size.

The predicted pressure distribution of a garment provides a map of the mechanical function of the jeans on a body. It helps to optimize the design of jeans in terms of functional performance and pressure comfort. With the numerical data from the solution of the model, visualization of mechanical sensory perceptions can be achieved based on the investigation of the relationship between objective stimulus and subjective perceptions, and the investigation of the relationship between the predictions and the objective measurements. Designers can judge whether the jeans meet the comfort requirements by comparing the predictions with desirable values, such as desirable pressure distribution or subjective perception of comfort pressure.

The validation of the work has more limitations because jeans pressure varies with individual human situations and pressure comfort is a very subjective sensation. The authors have found that the type of jeans and body posture have a significant influence on the pressure comfort rating. Therefore, to model jeans of various types the dynamic change of body posture is necessary in the simulation to aid sensory engineering design.

18.5 Acknowledgement

We would like to thank Hong Kong Polytechnic University for funding this research through Project A188.

18.6 References

1. Growther, E.M., Comfort and Fit in 100% Cotton-Denim Jeans. *Journal of the Textile Institute*, 1985: p. 323–338.
2. Makabe, H. *et al.*, Effect of Covered Area at the Waist on Clothing Pressure. *Sen'i-Gakkaishi*, 1991. **49**(10): p. 513–521.
3. Makabe, H. *et al.*, A Study of Clothing Pressure Developed by the Girdle. *Journal of the Japan Research Association for Textile End-uses*, 1991. **32**(9): p. 424–438.
4. Mitsuno, T., Changes in the waistband-pressure according to time of day – In special reference to diet and the phase of menstrual cycle. *Journal of Japan Research Association for Textile End-uses*, 1999. **40**(10): p. 57–66.
5. Denton, M.J., Fit, Stretch, and Comfort. *Textiles*, 1972. **1**(1): p. 12–17.
6. Hallquist, J.O., *LS-DYNA Theoretical Manual*. 1998: Livermore Software Technology Corporation.
7. Yamada, H., *Strength of Biological Materials*. 1970: The Williams & Wilkins Company Baltimore. 226.
8. Zheng, X.Y., *Advances in Sports Biomechanics*. 1998, Beijing: Guo Fang Gong Ye Press. p. 145–147.

19

Biomechanical engineering of a sports bra

Y. LI[1], X. ZHANG[2], AND K. W. YEUNG[1]
[1]The Hong Kong Polytechnic University, China
[2]Xian University of Engineering Science & Technology, China

19.1 Designing a sports bra

19.1.1 Introduction

A bra is the most feminine of foundation garments, required to satisfy the aesthetic needs and physiological health and comfort of the wearer. Generally, sports activity puts tremendous stress on breasts and the tissue surrounding them. A good bra offers the best support and protection against damaging breast tissue. Most women wear their bras between 10 and 12 hours every day from puberty until death. Therefore, it is important to select and wear a bra that is a good fit with support and pressure comfort. To optimize the design of a bra with such properties, the mechanical mechanisms involved in the dynamic contact between breast and bra need to be studied experimentally and theoretically. There is a very limited amount of literature in this area, particularly in theoretical investigation. A number of papers have been published in Japan on the measurement of garment pressure and relevant subjective sensations in wear trials.[1–4] Makabe *et al.* studied the pressure of brassieres by letting subjects wear brassiere samples that were designed in different shapes, materials and patterns.[1] Pressures were measured at 6 points under the bra. The pressure of the most comfortable brassiere sample was 24 mm Hg (32.40 gf/cm^2) at the point where the strap and the shoulder line cross, and 11–16 mm Hg (14.85–21.60 gf/cm^2) at the points under bust line and lateral top areas of the cup.

To achieve design optimization, a thorough theoretical understanding of the mechanisms and processes concerning the physiology, psychology and physics of the breast and bra are needed as the foundation of engineering design, which involves a number of aspects of research. Firstly, the human body needs to be scanned and digitized as the actual shape and dimension of the body and breast have a critical influence on the garment–skin contact process. Secondly, biomechanical models of the body and breast need to be developed as different parts of the body have different structural and material features. Thirdly, mechanical models need to be developed to

describe the dynamic mechanical interaction between the body (breast) and garment with satisfactory accuracy. Finally, computational methodology to solve the models and computing technology needs to be developed to visualize the dynamic interactions.

19.1.2 Biomechanical characteristic of breasts

Breasts comprise a number of different structures, each with their own specific function. One-third of the breast is composed of fatty tissue. The other two-thirds are made up of structural components called ducts and lobules. Fat fills the spaces between lobules and ducts. There are no muscles in the breast, but muscles lie under each breast and cover the ribs. Each breast also contains blood vessels and vessels that carry lymph. The breast increases in volume during pregnancy and generally weighs between 400–600 grams, increasing up to 800 grams during lactation.[5] Very weak ligaments, which stretch easily, support the breasts. The overlying skin of the breast offers only secondary support.

During walking, breasts bounce with each foot-strike, and this repeated action accelerates permanent stretching of the skin and sagging. Easily stretched ligaments cause the breast to sag. Excessive breast motion is the most common cause of movement discomfort during physical activity. Therefore, the breast structures, lacking internal anatomical support, require some type of external support, including weight support, movement restriction and compression by flattening the breast against the body, depending on an individual's needs and shape.

19.1.3 Mechanical characteristics of a bra

A good design of a 3D structural bra is probably the most important factor influencing the bra's functional performance and dynamic comfort during wear. It needs to be constructed with an appropriate structure that induces basic load distribution in the bra. The front straps should be positioned so that they lie in a direct line of lift over the nipples, allowing for optimal vertical breast support. The strap fabric should also be wide to allow for greater force distribution to prevent the straps digging into the shoulders. Fasteners, hooks and wires should be covered to avoid irritation. A good bra does not chafe around the arms or ribcage. Actually, most sports bras come without wires as these can puncture the skin during physical activity. All of these factors should be considered in a 3D-structural design of a bra. The contact interface between the breast and bra can be regarded as a dynamic coordinated contact. It represents the contact feature that the magnitude of the contact interface is comparable to the effective surfaces of a woman's body and bra.

Fabric stretch is another important factor influencing the effectiveness of the support. A bra should have enough elasticity to accommodate upper torso movement but prevent breast movement. It should be sufficiently elastic in the horizontal plane to allow for chest expansion while breathing. However, elasticity in the vertical plane should be limited to minimize vertical breast movement. Straps should have limited elasticity for the same reason. Fabric-stretch in multi-directions and frictional slippage generate pressure from a bra over the skin surface. Generally, the mechanical properties of desirable bra fabrics are both lower tensile modulus with large deformation and effective elastic recovery, which can be regarded as the mechanical properties of material linearity but geometric non-linearity.

19.2 Biomechanical modeling

19.2.1 Mechanical interactions between breast and bra

To optimize sports bra design, a biomechanical model for numerical simulation of mechanical interactions of bra and breast during wear was developed.[6] Based on analyzing the mechanical characteristics of breast and bra, a mechanical model was developed based on the theory of contact mechanics. The finite element method is used in the time domain for deriving a numerical solution of the dynamic contact model. A female wearing a bra and walking at a constant speed is simulated. During walking, breasts may bounce with each foot-strike, causing mechanical deformation in the breast. Meanwhile, mechanical interaction occurs at the contact surface between the breast and bra that supports and compresses the breasts. The external forces on an element of the breast involve gravity q_g, the interactive contact force q_c at the normal direction of the contact surface, the friction q_f of the bra as it is slipping on the breast surface. Contact force q_c and friction q_f are interaction forces between breast and bra. The mechanical forces will cause the internal strain–stress and the inertia force q_i within the breast and the bra respectively.

By analyzing the characteristics of the breast and bra, the authors developed a mechanical model to simulate the mechanical interaction as a female body wears a sport bra and walks at a constant speed V_z, which results in an up–down cycling motion of the body with speed V_y, according to analysis of the sports biomechanics during human walking.[7]

19.2.2 Model development

Model assumptions

On the basis of the analysis, the following assumptions are made:

(i) The female body is assumed to be a bi-material body that consists of two material components within an object: elastic material for the breast part and rigid material for the other part.
(ii) The bra is considered as a thin elastic shell with material linearity and geometric non-linearity; the stress in the fabric thickness is assumed to be zero.
(iii) The body always keeps in contact with the highest point of the bra's shoulder strap.
(iv) The contact between breast and bra is dynamic coordinated contact, due to the contact feature that the magnitude of the contact interface is comparable to the effective surfaces of the breast and bra.[8]
(v) The friction between the human body and the garment is neglected.

Model descriptions

Figure 19.1 shows the time-dependent contact system between the female human and the bra in a fixed global coordinate system $\mathbf{x}$ (x_1, x_2, x_3). In this system, the bra is regarded in a domain Ω^1, and the human body in a domain Ω^2 that consists of two connecting sub-domains of elastic breast Ω_e^2 and rigid body Ω_r^2, as shown in Fig. 19.1. At time $t = 0$, the bra and the human occupy domains ${}^0\Omega^1$ and ${}^0\Omega^2$ in their unreformed configuration respectively. The human body and the bra are all simply connected so that there is no interior boundary in any of them, satisfying physical constraint:

$$ {}^t\Omega^1 \cap {}^t\Omega^2 = \varnothing \quad (t \geqslant 0), $$

where $\varnothing$ denotes a null space, indicating that Ω^1 and Ω^2 do not penetrate each other.

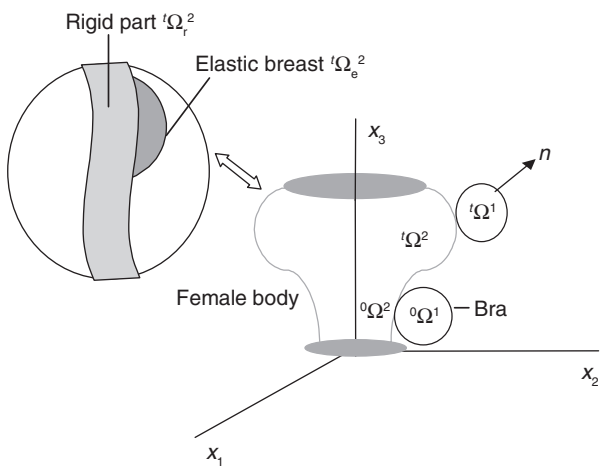

19.1 Global coordinate system of the contact system.

From time $t = 0$, the human body moves to occupy new domain ${}^t\Omega^2$, contacting the domain ${}^t\Omega^1$ of the bra at any time $t > 0$. The boundaries of ${}^t\Omega^1$ and ${}^t\Omega^2$ are denoted by ${}^t\Gamma^1$ and ${}^t\Gamma^2$, respectively, which consists of three components:

$${}^t\Gamma^n = {}^t\Gamma^n_d \cup {}^t\Gamma^n_f \cup {}^t\Gamma^n_c \quad n = 1,$$

where Γ_d denotes prescribed displacements boundary, Γ_f denotes prescribed load boundary, and Γ_c denotes the contact boundary where contact may occur, and $\cup$ denotes the union operator.

Governing equations

The motion equation of the bra at time t is:

$$\frac{\partial {}^t\sigma_{ji}(x)}{\partial {}^t x_j} + {}^t q_{g_i}(x) = \rho\, {}^t a_i(x), x \in {}^t\Omega^1; i = 1 \text{ to } 3 \quad \text{and} \quad j = 1 \text{ to } 3$$

For the female body of bi-material, the motion equation is written in the two sub-domains of elastic breast $\Omega_e{}^2$ and rigid body $\Omega_r{}^2$ respectively:

$$\frac{\partial {}^t\sigma_{ji}(x)}{\partial {}^t x_j} + {}^t q_{g_i}(x) = \rho\, {}^t a_i(x), x \in {}^t\Omega^2_e; i = 1 \text{ to } 3 \quad \text{and} \quad j = 1 \text{ to } 3 \quad \text{and}$$

$${}^t q_{g_i}(x) = \rho\, {}^t a_i(x),\ x \in {}^t\Omega_r{}^2;\ i = 1 \text{ to } 3 \text{ and } j = 1 \text{ to } 3,$$

where t denotes time; x a position vector; $a(x)$ the acceleration field; ${}^t\sigma_{ij}(x)$ is the Cauchy stress components that give the actual traction on an imaginary plane at a point within an object; ${}^t q_{g_i}(x)$ is the i-th component of the gravity ${}^t q_g(x)$ on an object, ρ is the mass density of an object which is assumed constant, and $a_i(x)$ is the i-th component of the acceleration vector of a material particle within an object.

For the bra and the breast of linear elasticity, the stress–strain relationship is given by the generalized Hooke's law,[9] i.e.,

$${}^t s_{ij} = c_{ijkl}\, {}^t\varepsilon_{kl}, \quad \text{on} \quad {}^t\Omega^1 \quad \text{and} \quad {}^t\Omega_e{}^2,\ k = 1 \text{ to } 3 \quad \text{and} \quad i = 1 \text{ to } 3,$$

where c_{ijkl} are material constants; s_{ij} is a component of the second Piola–Kirchhoff stress tensor that is related to the Cauchy stress component $\sigma_{ij}(x)$; ε_{kl} is a component of the Green–Lagrange strain tensor to describe the deformation of geometric non-linearity, which consists of linear and non-linear components ${}^t e_{ij}$ and ${}^t\eta_{ij}$:

$${}^t\varepsilon_{ij} = {}^t e_{ij} + {}^t\eta_{ij}$$

$${}^t e_{ij} = ({}^t u_{i,j} + {}^t u_{i,j})/2, \qquad {}^t\eta_{ij} = {}^t u_{k,i}\, {}^t u_{k,j}/2,$$

where, ${}^t u_{i,j} = \dfrac{\partial {}^t u_i}{\partial X_j}$, on ${}^t\Omega^1$ and ${}^t\Omega_e{}^2$; $k = 1$ to 3 and $i = 1$ to 3.

Various conditions

Initial speed: Initial speed is exerted on the rigid body part, which consists of two components: horizontal motion with speed V_z at x_1-direction and up–down motion with speed V_y in x_3-direction, which are presented as:

$$^0\mathrm{V}_1(x) = \mathrm{V}_z \quad \text{and} \quad ^0\mathrm{V}_3(x) = \mathrm{V}_y \quad \text{on} \quad {}^t\Gamma^2_d.$$

Displacement boundary condition: According to assumption (iii), the shoulder strap of the bra has the same movement as the body. The displacement boundary conditions on these contact points are represented as follows:

$$^tu_1(x^1) = {}^tu_1(x^2), \quad \text{and} \quad {}^tu_3(x^1) = {}^tu_3(x^2), \quad \text{on} \quad {}^t\Gamma^n_d,\ n = 1,2.$$

External force: Gravity exerted on the bra, the breast and the rigid body part is expressed as:

$$q^n_g = \rho^n g, \quad \text{on} \quad {}^t\Omega^1,\ {}^t\Omega_e{}^2,\ {}^t\Omega_r{}^2, \text{ where } g \text{ is gravity acceleration.}$$

Contact conditions: For the frictionless contact interfaces denoting the contact force q^n_c, then by Newton's third law, we have:

$$^tq^n_{c1} = -{}^tq^{n+1}_{c1}, \quad \text{on} \quad {}^t\Gamma^{1\cup}_c\ {}^t\Gamma^2_c,\ n = 1,$$

where $^tq^n_{c1}$ is the component of contact force $^tq^n_c$ in the normal direction of contact points. The mechanical contact condition as a constraint on the normal contact force $^tq^n_{c1}$ is:

$$^tq^n_{c1} \le 0, \quad \text{on} \quad {}^t\Gamma^{1\cup}_c\ {}^t\Gamma^2_c,\ n = 1,2.$$

This means the interactive pressure is exerted on the object n against its normal direction of the contact boundary points.

19.2.3 Numerical simulation

3D geometrical models

The 3D geometrical models are described by B-spline surfaces. The Belytschko–Lin–Tsay shell element[10] is used in the discretization of the 3D surfaces of the female body and the garment. The bi-material model of the female body is constructed by tying the nodes of the elastic breast to the rigid chest. The total element number of the female body is 24790 (5770 elements for the breast, 19120 for the rigid part), and 2386 for the bra.

Table 19.1 Mechanical parameters of the materials

The bone	Density (kg/m^3)	*1579
	Compression modulus (kg/m^2)	*489000
	Poisson's ratio	0.3
The breast	Density (kg/m^3)	2250
	Tensile modulus (kg/m^2)	2500
	Poisson's ratio	0.45
Bra	Density (kg/m^3)	455
	Tensile modulus (kg/m^2)	3500
	Poisson's ratio	0.32

*[11] and [7]

Material properties

The mechanical properties of the human body were estimated from the published data in the literature.[7,11] The breast density was estimated from its weight and volume. The tensile modulus of the fabrics were tested on an Instron tensile machine and the Poisson's ratio was estimated from the measurements of a Kawabata bi-tensile test. Table 19.1 shows the mechanical parameters of the materials used in the computing.

Simulation conditions

In the simulation, it is assumed that the female model is walking at an initial speed V_z, which results in a cycling motion of the body in the y-direction with speed V_y. The V_z is specified as 10 cm/s and V_y as 30 cm/s, and the time period of motion is 0.05 seconds. Thus, the movement amplitude of the human body in the y-direction is about 1.5 cm in the motion period. The time step size is 1.08E-4 second, which can be adjusted according to the needs of computing stability. The numerical computation is implemented by using the commercial finite element software, LS-DYNA.[10]

19.3 Biomechanical analysis

19.3.1 Breast bounce process

Simulation shows that during the dynamic deformation, the breast bounces with the body movement. The bra stretches to conform with the breast dynamic deformation. The displacements do not distribute uniformly over both breast and bra in the body movement.

19.3.2 Mechanical behavior of the bra

The displacement of the bra

A bra will accommodate the breast deformation by fabric stretch and recovery. Figure 19.2 shows the bra displacement of three nodes (A_1, B_1, C_1). For node A_1 at the shoulder strap, the displacement appears increasing linearly with the body movement until reaching a level of steady slow increase. For the nodes B_1, C_1, the displacements are zero at the initial stage of the body movement, which is related to the bra accommodating the upward movement of the body, the downward movement of the breast and the space allowance between the breast and the bra. Then, the displacement of node B_1 is gradually increasing to accommodate the displacement of node B of the breast. The displacement of node C_1 is decreasing to –1.8 mm then recovering to zero value, indicating the stretch and recovery property of the bra in accommodating the bouncing process of node C of the breast.

Figure 19.3 shows the bra displacement of two nodes (at A position of right and left shoulder) in the shoulder straps' x-direction. One positive value and one negative value in the x-direction means that the shoulder straps of the bra are slipping on the skin surface during the movement of the body. In the initial stage of body movement, the displacements of the two nodes are zero, indicating that no slipping occurs between the bra and the shoulder. Comparing them with the displacement in the y-direction of node A_1, it is found that the slippage is a factor causing the slow displacement in the final stage of the movement as shown in Fig. 19.2.

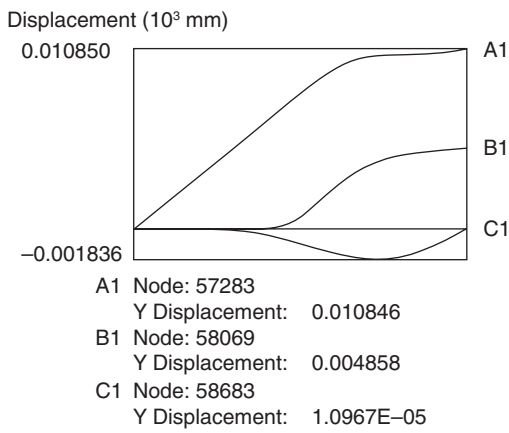

19.2 Bra displacement at three nodes in *y*-direction.

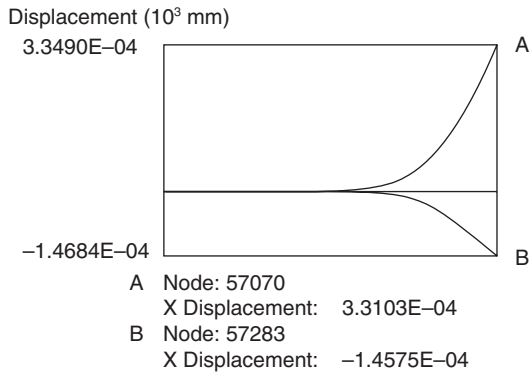

19.3 Displacement of the shoulder strap in *x*-direction.

Bra pressure

The stretch of the bra in multi-directions induces pressure on the human body. From a pressure contour plot, it could be seen that the pressure did not distribute uniformly over different parts of the bra. The pressure on most of the areas was in the range of 4 to 20 gf/cm^2. When the breast was falling, high-pressure zones were observed in the lower part of the bra with a value of about 14 gf/cm^2. When the breast was bouncing, high-pressure zones were observed in the upper part of the bra with a value of about 20 gf/cm^2.

Bra stress

Garment pressure is related to the strain–stress in the deformed fabric.[12] The effective stress is a scalar by integrating all the internal stress components, such as tension, shearing and bending, which are shown by positive values. Simulation suggests that the garment pressure distributions are directly related to the effective stress distributions in the garments. The effective stresses in the bra vary from 0 to 12 gf/cm^2 with the breasts falling, while with the breasts bouncing they vary in the range of 0 to 20 gf/cm^2. For the three nodes, the maximum value is observed at node A_1 with 18.7 gf/cm^2, followed by node B_1 and C_1, indicating that the front straps are subject to the maximum strain–stress in a vertical direction.

19.3.3 Mechanical behavior of the breast

Responding to the dynamic movement and the bra pressure, there are stress–strain distributions in the breast. Simulation showed the distributions of effective stress in the breast during wearing the bra for the case of the

breast falling and for the case of the breast bouncing. In the case of the breast falling, a higher value of stress is observed in the root area around the breast. When the breast is bouncing, a higher value of stress appears at the upper area of the breast. Many areas with effective stress of about 1000 gf/cm^2 are observed.

19.4 Validation of the model

To validate the model, the simulation results were compared with the measurements from the experimental measurements of bra pressure reported by Makabe *et al.*[1] In their experiment, pressures were measured at six points under the bras that were of four styles and different material compositions. Six points were then selected on the simulation model which corresponded to the points used in the experiment: point a under bust line and mammary line cross, b under bust line and anterior axially line cross (seam), c under bust line and scapular line cross, d at the lateral area of cup and ribcage band cross, e at ribcage band and anterior axially line cross (seam), f at strap and shoulder line cross.

The corresponding pressure changes are shown in Fig. 19.4. For the points of d, e and f at the lateral area of cup and strap of bra, good agreement is observed between the simulation and the experiment. For the points of a, b and c that are all at under-bust line, the simulated values appear to be much smaller than the experimental measurements. The major reason causing the deviation is due to the difference in bra-styles used in the

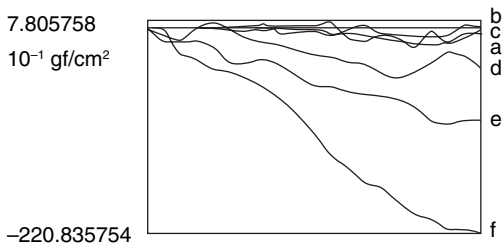

a Node: 57853
PRESSURE(M): –1.810685
b Node: 56967
PRESSURE(M): 0.095988
c Node: 56903
PRESSURE(M): –4.811592
d Node: 57062
PRESSURE(M): –43.935020
e Node: 57065
PRESSURE(M): –98.521759
f Node: 57070
PRESSURE(M): –220.835754

19.4 Pressure changes of the six measuring points on the bra.

experiment and in the simulation. In Makabe's experiment, the bra was of a very tight-fitting style with a stiff ring along the underbust line, while in the current numerical model, only a one-piece style sportsbra can be simulated. Therefore, the pressure under the under-bust line is predicted to be small. The prediction of bra pressure at the upper parts of the bra is close to the magnitude of the measurements from the experiments of bra pressure, indicating that the model is able to predict and simulate bra pressure during wear with reasonable accuracy.

19.5 Conclusion

A 3D biomechanical model of a female body, which consists of an elastic breast and a rigid body, has been developed on the basis of analyzing the biomechanical characteristics of the human body. The bra is regarded as having material linearity and geometric non-linearity. The contact between the human body and the bra is modeled as a dynamic sliding interface based on the theory of contact mechanics. A finite element method is used in the time domain for deriving a numerical solution of the dynamic contact problem.

An example is presented to illustrate the simulation results of the computational model: a female human model is walking at a constant speed when wearing a bra. The computational model can simulate and characterize the dynamical mechanical behavior of the breast and bra during the body movement with the breast falling and bouncing, in terms of the bra deformation, pressure and stress distributions and breast stress distributions. With the distributions of the variables, the effects of the bra on the dynamic deformation of the breast during the body movement can be studied. Compared with the quantity of measured garment pressure reported in the literature, the predicted pressure is close to the magnitude of experimental measurements, indicating that the model is able to simulate bra pressure during wear with reasonable accuracy. The model can be used as an engineering design tool for optimizing the structure and material in the bra design process.

19.6 Acknowledgement

We would like to thank Hong Kong Polytechnic University for funding this research through Project A188.

19.7 References

1. Makabe, H. *et al.*, A Study of Clothing Pressure Developed by the Brassiere. *Journal of the Japan Research Association for Textile End-uses*, 1991. **32**(9): p. 416–423.

2. Makabe, H. *et al.*, A Study of Clothing Pressure Developed by the Girdle. *Journal of the Japan Research Association for Textile End-uses*, 1991. **32**(9): p. 424–438.
3. Makabe, H. *et al.*, Effect of Covered Area at the Waist on Clothing Pressure. *Sen'i-Gakkaishi*, 1991. **49**(10): p. 513–521.
4. Mitsuno, T., Changes in the waistband-pressure according to time of day – In special reference to diet and the phase of menstrual cycle. *Journal of Japan Research Association for Textile End-uses*, 1999. **40**(10): p. 57–66.
5. http://mesomorphosis.com/home.htm. 2001.
6. Li, Y., Zhang, X. and Yeung, K.W., A 3D biomechanical model for numerical simulation of dynamic mechanical interactions of bra and breast during wear. *Sen'i-Gakkaishi*, 2003. **59**(1): p. 12–21.
7. Zheng, X.Y., *Advances in Sports Biomechanics*. 1998, Beijing: Guo Fang Gong Ye Press. p. 145–147.
8. Johnson, K.L., *Contact Mechanics*. 1992, Beijing: High Education Press.
9. Xu, X., Guo, Y.M. and Shen, Y.X., *Non-linear Finite Element and Program Design*. 1993, Hong Zhou, China: Zhejiang University Press.
10. Hallquist, J.O., *LS-DYNA Theoretical Manual*. 1998: Livermore Software Technology Corporation.
11. Yamada, H., *Strength of Biological Materials*. 1970: The Williams & Wilkins Company, Baltimore. p. 226.
12. Zhang, X., Yeung, K.W. and Li, Y., Numerical simulation of 3D dynamic garment pressure. *Textile Research Journal*, 2002. **72**(3): p. 245–252.

20

Biomechanical engineering of compression stockings

X-Q. DAI[1,2], Y. LI[1], R. LIU[1] AND Y.L. KWOK[1]
[1]The Hong Kong Polytechnic University, China
[2]Soochow University, China

20.1 Introduction

20.1.1 Bio-functional requirement and classification of compression stockings

As introduced in Chapter 9, as a type of compression therapy, elastic compression stockings come into our daily life, and there is a wide range of them available commercially. Among them, Graduated Compression Stockings (GCSs), which provide graded compression with the greater pressure applied distally, have been reported as more effective in enhancing venous return, reducing stasis, etc.[1] Usually, the specification of a GCS only describes a range for the pressure exerted at ankle level. However, the pressure profile for a GCS has pressure ranges at several levels: ankle, calf, knee and maybe thigh. Figure 20.1 shows the pressure profile for GCS proposed by the European Normalization Committee (CEN). Depending on the pressure exerted at the ankle, the GCS is then classified into four compression classes, I being the weakest and IV the strongest. The choice of a stocking depends on both medical indication and the patient's tolerance and acceptance. According to the European Standardization Commission, there are classifications and indications for GCS.[1]

Compression stockings are available as different styles: full-length, thigh-length, and knee-length. Earlier research has shown that there is no increase in deep venous flow velocity when whole limb compression is applied, compared with below-knee compression.[2,3] Moreover, since thigh or full length stockings are more difficult to put on and less tolerated than knee-length ones, and maybe more easily ill-fitted, they may actually be inferior to knee-length ones.[4] So knee-length stockings are expected to replace thigh-length stockings for DVT treatment and prophylaxis, being equally effective, cheaper, more likely to fit correctly and better tolerated by patients.

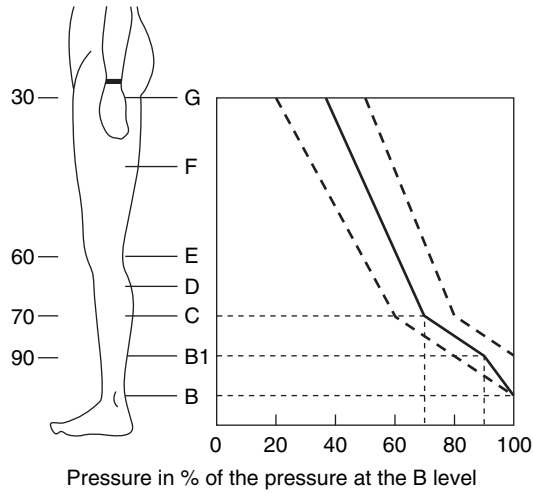

20.1 Pressure profile for GCS fulfilling the CEN criteria.

20.1.2 Demand for a biomechanical model

GCS therapy has not been as effective in clinical practice as it has been in research studies, in part due to poor patient compliance due to painful, hot, and itchy reactions; and some potential complications such as impairment of subcutaneous tissue oxygenation, peroneal nerve damage, skin necrosis, pressure ulcer, induced arterial hypoxia, and even DVT.[5] Some investigations show that poor fit, and incorrect size are major causes for these negative effects.[6] Stocking fit is of utmost importance in order for the pressure gradient to be effective.

However, as a key factor in compression therapy, the pressure itself has not been investigated sufficiently. The pressure exerted by a GCS may vary among individuals, different leg levels, and also different regions at the same level. The size selection based on the simple measurement of leg length and circumference is insufficient to evaluate the pressure exerted on an individual leg. There are three major approaches for pressure determination of compression stockings. The early approach was to stretch a stocking on a tensile tester to a suitable size, and then calculate the pressure according to the fabric tension indirectly, based on Laplace's law.[7] Another approach is to determine pressure by using air-filled leg segments to counterbalance the stocking pressure.[7] A more common approach is to measure pressure *in situ*, based on the insertion of a pressure sensor in the form of a fluid or air filled balloon (connected to a manometer), or other pressure sensor.[8–10] All these techniques have several intrinsic defects. As the limb dimensions of humans are infinitely variable, the same stocking fitted to various individuals results in different pressures. To obtain the pressure, the measurement

must be carried out on each individual body. Accuracy is also a problem because the pressure sensors may themselves distort the limb dimensions and produce incorrect pressure measurements. Only the pressures at several measured points are obtained, not the overall pressure distribution.

Based on the above considerations, a mathematical model to simulate the mechanical interaction between a leg and a stocking is necessary to theoretically evaluate the pressure *in situ*, and further to fundamentally understand the mechanism of the compression therapy exerted by stockings. The design of GCS also demands a tool to evaluate what will be the overall pressure distribution exerted on a leg before the stockings are produced.

20.2 Biomechanical simulation

20.2.1 Mechanical modeling

A common way to obtain the final leg-fitting shape for a stocking is to simulate a dynamic wearing process. Two objects are involved in the simulation; one is the leg, which is solid, and the other is the stocking, which can be regarded as a sheet material. It is too difficult to include the foot in the wearing simulation due to the complex definition of boundary conditions. Since the focus is to investigate the pressure exerted on the leg, only the process of putting the stocking on from ankle to knee, or upper part was simulated. As boundary conditions, the body is assumed to stand still; the top welt of the stocking moves upwards at a constant speed until it reaches a fixed displacement. The dynamic contact takes place in a large space and period of the time domain. During the wear process, the stocking is slipping over the surface of the body with friction. To prevent the stocking interpenetrating the lower limb and generating a frictional effect, it is necessary to enforce a kinematical constraint in the normal direction as well as in the tangent direction of the contact surface. The simulation is performed using 'ABAQUS', a commercial Finite Element Method (FEM) software from ABAQUS Inc., Pawtucket, RI, USA.

20.2.2 Numerical simulation

3-D geometric models of lower leg and stocking

The lower leg consists of bones, cartilages, ligaments, soft tissue (muscle, fat, and skin), etc. A simplified model including soft tissue and two bones (the medial tibia and the lateral fibula) is used to model a lower leg during standing. The surfaces of a lower limb and inner bones are reconstructed from Magnetic Resonance Imaging (MRI) coronal images, and

then the solid bone and soft tissue are created using 'SolidWorks', a 3-D drawing tool.

Commercial knee-length stockings with medical effects to prevent and manage varicose veins were taken as samples and their dynamic wearing on a male and a female lower leg simulated. The stocking sizes were chosen properly according to the lower legs' geometrical shapes. The legging of the stocking was of cylindrical shape. A cylindrical tube was built as the initial geometry of the stocking, its size being taken from the actual sample.

Material model

Even though both the materials for the lower limb and stockings may behave with material non-linearity when undergoing large deformation, to simplify the problem, it is assumed that there is material linearity for all materials involved. An assumption is made that the medial tibia and the lateral fibula do not deform due to wearing the stockings, so the bones are assumed to be rigid. The soft tissue material is assumed to be homogeneous, isotropic and linear elastic. For the soft tissue, the Young's modulus, Poisson ratio, mass density are taken as 0.01 MPa, 0.49, and 9.37×10^{-10} tonne/mm^3, respectively.[11,12]

Since knitted fabrics often have significantly different mechanical properties in the wale and course directions, the material properties for stockings are defined as orthotropic and linearly elastic. Different kinds of knit stitches are used for the ankle part and the calf part of the sample stockings. Hence the two parts have different mechanical properties. All the parameters needed in the numerical analysis are listed in Table 20.1, where E_1 and E_2 denote the Young's moduli in the course and wale directions respectively, G_{12} and v_1 are the shear modulus and Poisson ratio, and t denotes the fabric thickness.

Finite Element Analysis

The Finite Element Method was used for numerical analysis of the model due to its unique capability to analyze structures of complicated shape, loading and material behavior. The model was elaborated using the ABAQUS 6.4 FE software package (ABAQUS Inc., Pawtucket, RI, USA).

Table 20.1 Mechanical properties of the stocking materials

Part	W (tonne/mm^3)	E_1 (N/mm^2)	E_2 (N/mm^2)	G_{12} (N/mm^2)	v_1	t (mm)
Ankle	2.1E-10	0.098	0.147	0.052	0.113	0.8
Calf	2.0E-10	0.093	0.059	0.029	0.369	0.76

Contact constraints: The interface between the stocking and the lower limb is considered as surface-to-surface contact; the surfaces can undergo finite sliding relative to each other. Finite sliding allows arbitrary motion of the surfaces forming the contact pair. A penalty method is employed to enforce a kinematical constraint that the slave surface nodes (inner surface of stocking) do not penetrate the master surface (lower limb surface).

Boundary condition: Since the medial tibia and the lateral fibula are assumed not to deform due to wearing the stockings, the displacements of all the nodes on the two bones are constrained in all directions as a boundary condition in the simulation. Thus, for the stockings along the lower leg length direction, the displacements of both the top and the bottom lines are defined while in the cross-sectional plane they can deform freely according to the shape of the lower leg.

Numerical solution: The dramatic change in contact pressure that occurs when a contact condition changes from open (a positive clearance) to closed (clearance equal to zero), may make it difficult to complete contact simulations. The geometric non-linearity due to the large deformation of the stocking, and the boundary non-linearity due to the discontinuous contact constraints make the mechanical simulation complicated. A nonlinear explicit dynamic analysis was performed for the numerical simulation using ABAQUS/Explicit.

20.2.3 Dynamic wearing simulation

The wearing simulation is set to complete within 10 seconds. Once the contact occurs, the interaction between the lower leg and the stocking stretches the stocking, meanwhile inducing pressure on the lower leg. As the contact area increases, the pressure also spreads. And as the stocking gets much more stretched, the pressure value increases. However, even at the final state, the pressure does not distribute uniformly over all the lower leg. Due to the complicated geometrical features of the lower leg surface, the stocking is not in contact with the underlying body everywhere. Only the surface of convex curvature supports the stocking, and the surface of concave curvature does not come into contact with the stocking.

20.2.4 Model validation

To validate the model, the wearing of two stockings on two legs was simulated respectively. Meanwhile, the two subjects whose lower limbs were scanned for the simulation participated in the wearing trial for pressure measurement. As with commercial stockings having medical effect to

prevent and manage varicose veins, the stocking sample used has a specified pressure value. It has graduated compression on the lower leg, the highest pressure of about 15–19 mmHg (1995–2527 Pa) being at the ankle level, and then while moving upward, the pressure decreases. The pressure at the maximum calf level will decrease to 65% of the specified value. The pressure was measured by using apparatus developed in the laboratory of the Institute of Textiles and Clothing at the Hong Kong Polytechnic University, in which the 'Flexiforce Sensor Model A201',[13] a piezoelectric sensor, was used for the compression receptors. The sensor is shaped as a thin ribbon. Air- or fluid-filled devices are not used because they may cause localized ballooning, raising the pressure spuriously.

The pressure was measured at the following positions, as illustrated in Fig. 20.2, showing where the maximum calf (Cf) contour is crossed by the front central line (F), inside line (I.S), back central line (B) and outside line (O.S) and where the minimum ankle (Ak) contour is crossed by F, I.S, B and O.S. The measurement results are given in Fig. 20.3, where 'M' and 'S' correspond to 'measured' and 'simulated', respectively. The peak pressures

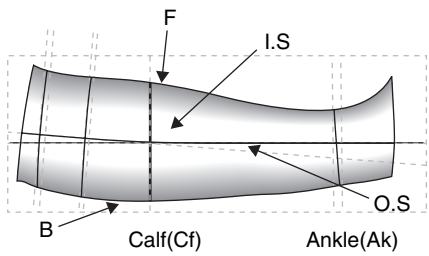

20.2 Pressure measurement position.

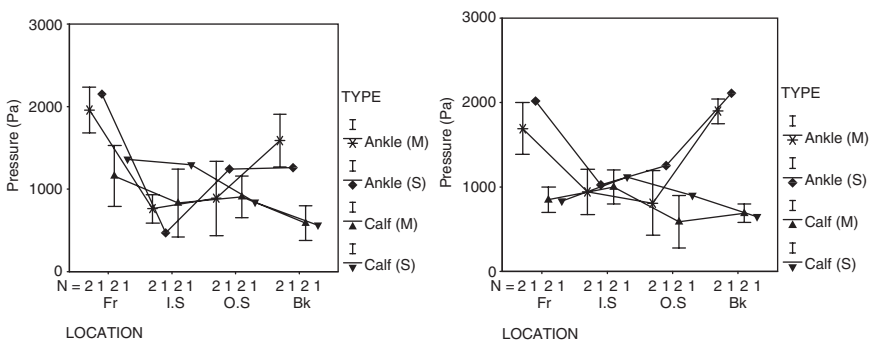

20.3 Pressure exerted on lower leg.

for both the male (1960 Pa) and female (1896 Pa) cases are close to the lower limits of the specified pressure ranges. And as the stocking moves upward, the pressure decreases. At the maximum calf level the peak pressure is 1160 Pa, which is 59.2% of the respective one at the ankle for subject A; and 998 Pa, which is 52.6% of the respective one at the ankle for subject B. These results generally agree with the specification for the stockings though the measured results are a little smaller than the specified values. This indicates that the pressure measurement is successful. Comparing the measured pressure values with the respective simulated results, good agreement is obtained as shown in Fig. 20.3a and b.

20.3 Analysis and discussion

20.3.1 Pressure induction

Figure 20.4 shows the dynamic changes of the mises stress and pressure of three nodes, which are at the top (995), middle (2478) and bottom (6554) on the front central line of the stocking. From these plots, observations and considerations were made as follows: (i) other than at the top node 995, which shows fabric stretch and recovery as it passes through the maximum calf, the stress curves show monotonic increases during the wearing process; (ii) the pressure curves show obvious rising and falling, due to the change of the contact interface; (iii) in Fig. 20.4b, for all the three curves, the peaks

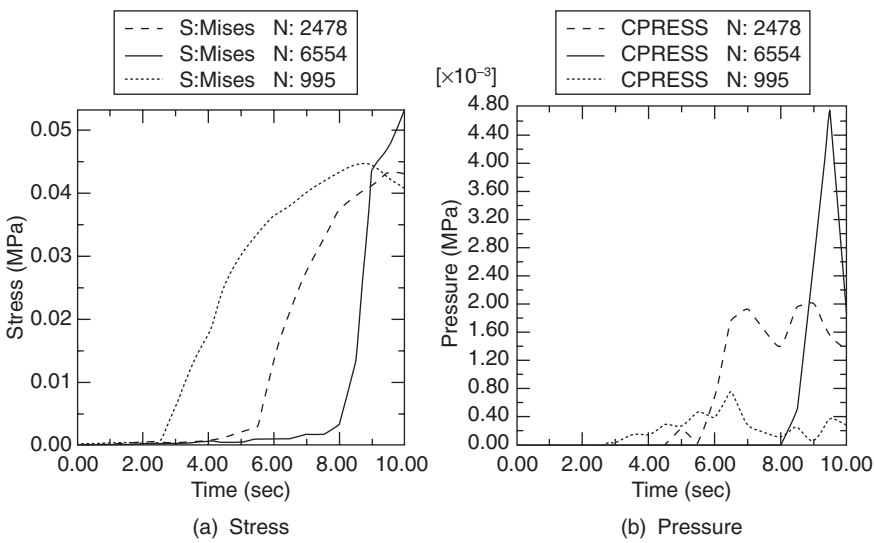

20.4 Dynamic changes of stress and pressure.

occur in the middle rather than at the end of the simulation, indicating that the dynamic pressure value during the wearing process is higher than the final values; this is consistent with our thoughts of compression perception when wearing stockings; (iv) as the stress increases, the respective pressure increases generally, indicating that the pressure is balanced against the fabric stretch in multi-directions; (v) when the wearing is complete, the stress at the bottom node 6454 is the highest; second is the middle node 2478; and then the top node 995. Correspondently, this results in graduated pressure at the three nodes.

20.3.2 Stress and pressure distributions

From the pressure and stress distributions resulting from the wearing simulation on male and female legs, it was found that: (i) In the two cases, the pressures show significant gradient distributions; from the ankle to the knee, the pressure value decreases; (ii) similar stress distributions in the two simulations indicate that the fabric stretch in the two stockings are roughly the same; (iii) the two pressure distributions differ from each other, the contact area on the female leg seems relatively larger than that on the male leg; therefore the pressure distributes more evenly on the whole lower leg of the female subject.

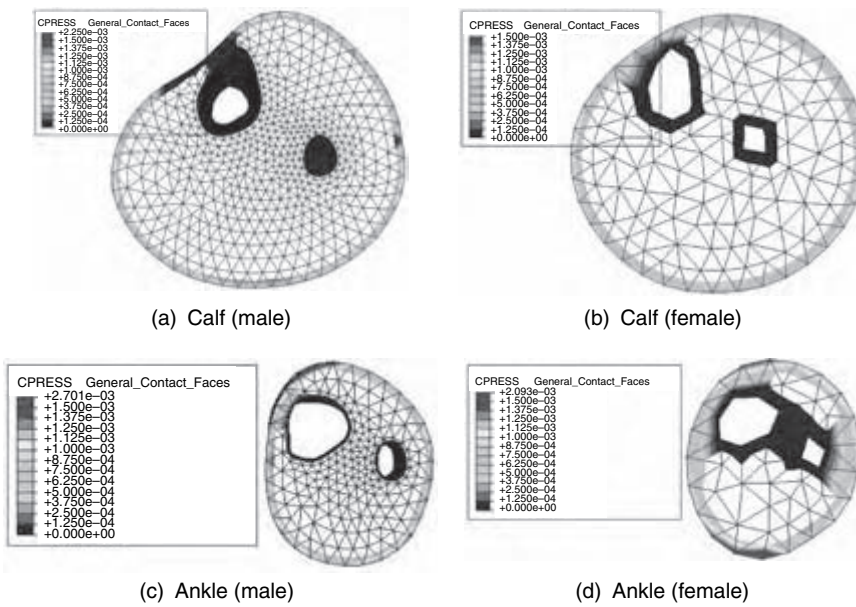

(a) Calf (male) (b) Calf (female)

(c) Ankle (male) (d) Ankle (female)

20.5 Cross-sectional pressure distribution.

In Fig. 20.5, the cross-sectional pressure distributions at the maximum calf and at the ankle of the two legs are looked into further. At the ankle level, for leg A, the highest pressure occurs at the front, and then at the back, finally, at the two sides; for leg B, the highest pressure occurs at the back, then at the front, and finally at the two sides. At the calf level, for leg A, the highest pressure occurs at the front, then at the inner side, then the outer side, finally at the back; however, for leg B, other than the pressure value at the inner side being a little higher than at other places, the pressure distributes evenly. These observations are consistent with the measured results shown in Fig. 20.3. It can also be seen that the curvatures of calf cross-sections agree well with the respective pressure distributions. This indicates that the curvature of the lower limb surface has significant influence on the pressure.

20.3.3 Pressure determination

As discussed, the graduated pressure is due to the graduated stress. Table 20.3 lists the measured stretch in the cross-sectional direction at the maximum calf and at the ankle for the two subjects. The longitudinal stretch is very small for the two cases, and can be neglected. Although the stocking has a much larger stretch at the calf part than that at the ankle, the resulting stress at the calf is lower than that at the ankle. Referring to Table 20.2, it is known that this occurs due to the difference of mechanical properties of the materials for the calf part and the ankle part, especially the significant difference between the Young's modulus in the longitudinal directions. Therefore, the graduated pressure is created by using different materials (in this case, different stitches) for the ankle and the calf parts.

The above discussions make it clear that the pressure exerted on the leg by the stocking depends on the curvature of the leg surface and the stress rather than the stretch of the stocking, as has been indicated by the equation $P = K_1T_1 + K_2T_2$.[14] Here, K_1 and K_2 are the curvature of the leg surface along the cross-section direction and the length direction; T_1 and T_2 denote the stress along the two directions, respectively.

Table 20.2 Stretch of the stockings

Subject	Ankle	Calf
Male	40%	70%
Female	38.5%	75%

20.4 Investigation of the mechanism of compression therapy

20.4.1 Leg deformation

Fig. 20.6 shows the deformation at four feature nodes, front (196), inside (205), outside (269), and back (28) of the maximum calf contour. The

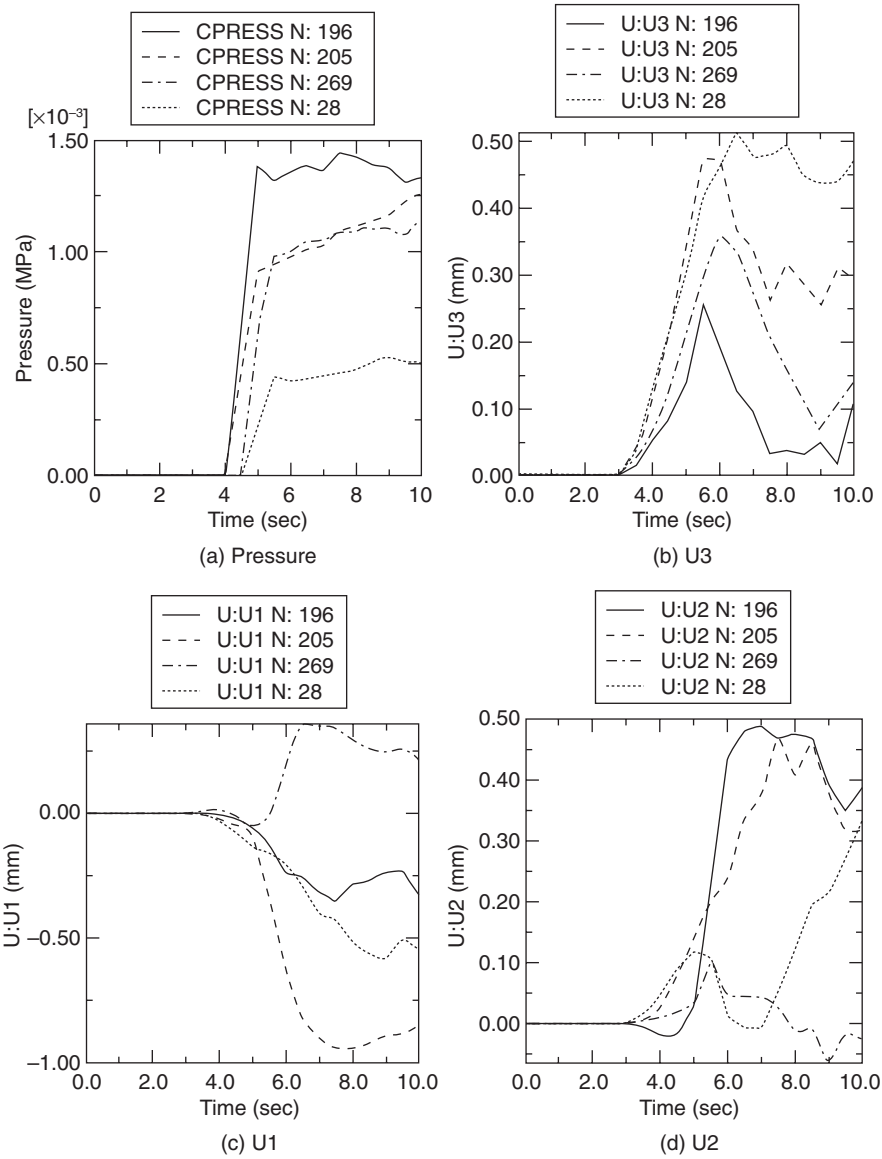

20.6 Leg displacements.

pressure plot shows that these nodes begin to be covered by the stocking at about 4.0 seconds. However, the displacements take place earlier than this, soon after that the stocking begins to come into contact with the leg. The displacements in the '3' direction (vertical) at the four nodes increase rapidly, and then decrease, vibrate, and finally reaches positive values. This indicates that during the wearing process, the whole calf is shifted upwardly due to the compression force spreading from ankle to calf. And once the upper region of the four nodes is also compressed by the stocking, the upward shift begins to recover. However, the recovery is not completed; part of the shift displacements remain, especially at the inside (205) and the central back (28).

Due to the external pressure exerted by the stocking, the calf is compressed at both sides; the displacement at the inside is greater than the outside due to the higher pressure, and both the front and the back nodes (196 and 28) are shifted toward the outside, maybe also due to the higher pressure at the inside. The displacement in the '2' direction shows more complication. The calf at node 196 seems to be stretched before it is covered by the stocking, due to the shift mentioned above; soon after that, it is covered by the stocking, at a time of about 4.0 seconds; the displacement begins to turn to become positive, meaning it is being compressed, and increases rapidly due to the higher pressure at the front. The node 205 is shifted to the back due to the pressure. The node 269 is shifted backward and then forward; finally the shift deformation almost recovers. The calf at node 28 shifts backward at first, due to the upward shifting, then recovers from the shift due to the stocking pressure; finally it turns to be shifted backward again. Since it is assumed that the soft tissue is incompressible in the simulation, the volume of the leg will remain constant during the dynamic wearing. The cross-section also tends to keep its area roughly constant. Therefore, when the calf is compressed at the front and both sides of the surface, the soft tissue is shifted toward the inner center until it reaches the fixed bone surface, and then turns toward the back side, where there is no bone, and relatively smaller pressure is exerted. However, since the whole calf is shifted upward, especially at the back and the inside, the areas of the leg cross-sections reduce to some extent. The upward shift helps the calf muscles pump. The reduction of the cross-sectional area results in the narrowing of the vein, and improvement of coaptation of the valvular cusps, which have the major positive effects of accelerating the venous flow and reducing venous reflux.

20.4.2 Pressure distribution along superficial veins

Venous diseases, such as varicose vein or edema, develop after long-periods of standing or sitting, due to an increase in hydrostatic pressure. One purpose

of wearing GCS is to add compression on superficial veins to bring the venous walls close together, and then to help the return of blood in the superficial venous system. Figure 20.7 shows the pressure distributions along the courses of the great and the small saphenous veins in the male and the female legs respectively. Figure 20.7b shows a trend that the pressure on the superficial veins decreases as the course goes upward from ankle to the calf. This is expected. However, in Fig. 20.7a, there is no such trend; the pressure distribution shows irregular variation. From Fig. 20.5, it can be learnt that leg B has more circular cross-sections, and is similar to a cylinder, so the gradient stress distribution in the stocking results in graduated pressure distribution on the leg surface. Leg A is of a much more irregular shape, hence the contact condition and curvature varies greatly along the vein paths from ankle to maximum calf due to the complicated geometry of the leg surface. For legs of very irregular shapes, to augment the local pressure on the veins, some compression enhancers such as pads and rolls are added over the concave areas to change the local contact condition.[15,16]

20.4.3 Inner leg stress

Referring to the respective cross-sectional pressure distribution in Fig. 20.5a, it is found that high pressure values induce high compression deformations (and therefore stresses) on the underlying leg surface. At the surface, normal pressure further transmits to the inner body; when going into the deeper layer of the leg, the stress decreases gradually. It is helpful to shift blood into the central compartment, and divert blood from

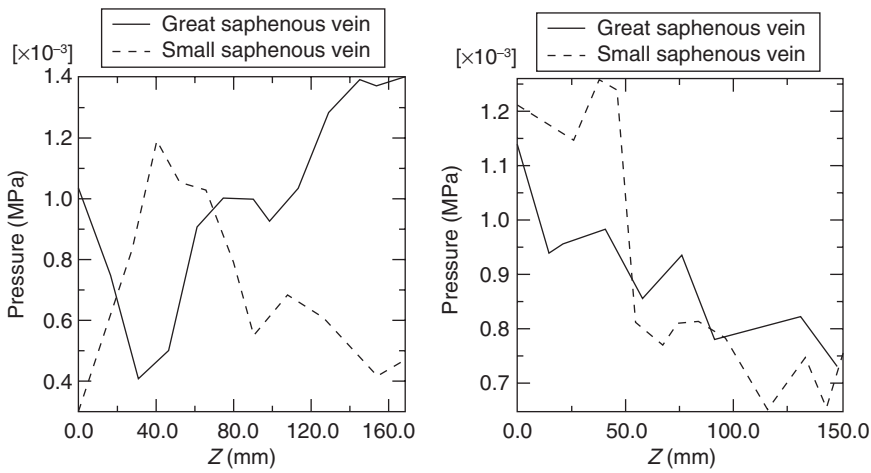

20.7 Pressure distribution along great and small saphenous veins.

superficial distended veins. Comparing the stresses at the calf and the ankle, it can be found that the stresses at the ankle are much higher than the respective ones at the calf. This indicates that the inner stresses decrease when going upward due to the graduated pressure distribution. The graduated stress distribution will shift blood upward, hence helping blood flow back to the heart through the veins.

Pressure sores are one of the complications of wearing compression stockings. Early researchers have concluded that if the normal capillary pressure exceeds 32 mmHg (4230 Pa),[17,18] ischemia will result, followed by occlusion or collapse of capillaries, leading to tissue destruction over a period of time. Although this limit value of 32 mmHg is questionable, and various higher or lower values have been established,[19,20] it is still the generally accepted value for relevant products. Usually, tissue interface pressure (the normal surface pressure) must be lower than 32 mmHg to prevent pressure sores. However, it is seen in simulations that, as the bones are approached, the stress increases. If the Mises stress is looked at, which is the effective stress integrating all the stress components in the three directions, the concentration of high stress at the bone prominences is significant. This is consistent with the former research findings in buttock contact simulation.[21,22] It indicates that the interface pressure is not representative of the internal mechanical state of the soft tissues involved. Pressure sores may develop easily in the deep layer, especially near the bone prominences.

20.5 Conclusion

Simulation demonstrates that pressure exerted on the leg by a compression stocking is induced due to fabric stretch; its value depends on fabric tension and the curvature of the leg surface. Therefore, the pressure distribution on a leg is non-uniform. Even though at the same cross-section the fabric stretch is the same, due to the irregular non-circular shape the pressure varies at different points. With the stocking-wearing model, the overall pressure distribution can be predicted in a quick and easy way. It is helpful in stocking size selection and it can aid the physician to know the inner mechanical state of leg subjected to stocking pressure. The model also enables parametrical design of gradient compression stockings.

The mechanism of compression therapy is discussed through investigating the lower leg deformation and its internal mechanical state. Reasonable correspondence between the mechanical state of the leg and the medical effects of compression exerted by the stockings is established. Since the mechanical properties of skin, fat, and muscle may vary greatly, a biomechanical leg model describing more details about the leg structure is necessary to quantitatively investigate the internal mechanical state of the leg, thus to demonstrate the medical effects of GCS. Nonlinearity of knitted

materials as well as of the soft tissue of the leg should also be taken into account.

20.6 Acknowledgement

We would like to thank Hong Kong Polytechnic University for funding this research through Project A188 and the Research Grant Council through Project PolyU 5157/02E.

20.7 References

1. Ramelet, A.A., Compression Therapy. *Dermatologic Surgery*, 2002. **28**: p. 6–10.
2. Lawrence, D. and Kakkar, V.V., Graduated, Static, External Compression of the Lower Limb: A Physiological Assessment. *British Journal of Surgery*, 1980. **67**: p. 119–121.
3. Porteous, L.M.J. *et al.*, Thigh length versus knee length stockings in the prevention of deep thrombosis. *British Journal of Surgery*, 1989. **76**: p. 296–302.
4. Williams, A.M. *et al.*, Knee-length versus Thigh-length Graduated Stockings in the Prevention of Deep Vein Thrombosis. *British Journal of Surgery*, 1996. **83**: p. 1553.
5. Geerts, W. *et al.*, Prevention of Venous Thromboembolism. *Chest*, 2001. **119**: p. 132S–175S.
6. Hayes, J.M., Lehman, C.A. and Castonguay, P., Graduated Compression Stockings: Updating Practice, Improving Compliance. *Medsurg Nursing*, 2002. **11**(4): p. 163–167.
7. Stolk, R. and Salz, P., A Quick Pressure Determining Device for Medical Stockings based on the Determination of the Counterpressure of Air Filled Leg Segments, in *2nd International Symposium, Compression Bandages and Medical Stockings – Clinical and Practical Results; Measuring Methods and Standards*. 1987. Zurich.
8. Momota, H. *et al.*, A Study of Clothing Pressure Caused by Japanese Men's Socks. *Journal of the Japan Research Association for Textile End-uses*, 1993. **34**(4): p. 175–186.
9. Momota, H. *et al.*, A Study of Clothing Pressure Caused by Japanese Women's High Socks. *Journal of the Japan Research Association for Textile End-uses*, 1993. **34**(11): p. 603–614.
10. Harries, C.A. and Pegg, S.P., Measuring pressure under burns pressure garments using the Oxford Pressure Monitor. *Burns*, 1989. **15**(3): p. 1879.
11. Dai, G.H., Gertler, J.P. and Kamm, R.D., The Effects of External Compression on Venous Blood Flow and Tissue Deformation in the Lower Leg. *Journal of Biomechanical Engineering*, 1999. **121**(12): p. 557–564.
12. Xiu, Y., *Advances in Sports Biomechanics*. 1998, Beijing: Guo Fang Gong Ye Press. p. 215–240.
13. Tekscan, *http://www.tekscan.com/flexiforce.html*.
14. Inoue, M., Sukigara, S. and Niwa, M., Prediction of 'Wearing Pressure' by Linearizing Method. *Journal of the Japan Research Association for Textile End-uses*, 1992. **33**(5): p. 254–260.

15. Tazelaar, D.J., Neumann, H.A.M. and De Roos, K.P., Long Cotton Wool Rolls as Compression Enhancers in Macrosclerotherapy for Varicose Veins. *Dermatologic Surgery*, 1999. **25**: p. 38–40.
16. Goldman, M.P., Sclerotherapy for Superficial Venules and Telangiectasies of the Lower Extremities. *Dermatologic Clinics*, 1987. **5**: p. 369–379.
17. Hussain, T., An Experimental Study of Some Pressure Effects on Tissues, with Reference to the Bed-sore Problem. *Journal of Bacteriology and Pathology*, 1953. **66**: p. 347–357.
18. Landis, E., Microinjection Studies of Capillary Blood Pressure in Human Skin. *Heart*, 1930. **15**: p. 209–228.
19. Defloor, T., The Risk of Pressure Sores: A Conceptual Scheme. *Journal of Clinical Nursing*, 1999. **8**: p. 206–216.
20. Young, J.B., Aids to Prevent Pressure Sores. *British Medical Journal*, 1990. **300**: p. 1002–1004.
21. Chow, C. and Odell, E., Deformations and Stresses in Soft Body Tissues of a Sitting Person. *Journal of Biomechanical Engineering*, 1978. **100**: p. 79–86.
22. Oomens, C.W.J. *et al.*, Can Loaded Interface Characteristics Influence Strain Distribution in Muscle Adjacent to Bony Promiences? *Computer Methods in Biomechanics and Biomedical Engineering*, 2003. **6**(3): p. 171–180.

21

Biomechanical engineering design of socks

Y. LI[1], X-Q. DAI[1,2], M. ZHANG[1], J.T. CHEUNG[1], AND X. ZHANG[3]
[1]The Hong Kong Polytechnic University, China
[2]Soochow University, China
[3]Xian University of Engineering Science & Technology, China

21.1 Introduction

21.1.1 Foot lesions

The human foot is an immensely practical, beautifully designed structure built to bear many times its weight, thousands of times a day and bounce back ready for more. It has been suggested that an individual takes about 8000–10 000 steps a day and in a day, the average walker generates about ½ pint of moisture through foot perspiration.[1] During walking, a foot rubs against its footwear and can be susceptible to malfunction. There are at least 300 types of foot problem. Many of them result from poorly fitting footwear. The most frequent foot problems are blisters, corns and calluses, and all of them are related to friction in shoes. Blisters are fluid-filled sacs that develop between the top layers of skin after prolonged pressure or rubbing against the skin, which causes irritation. Blisters occur most often on the heel, the toe, and the ball of the foot. Corns normally occur over toe joints, when there is friction associated with localized pressure. Calluses appear as broad areas of hardened, sometimes yellow, skin on pressure points that develop after prolonged wear-and-tear or rubbing against a shoe. Calluses usually form on the ball of the foot, the heel, and the inside of the big toe.[2]

At times, such foot problems can have life-altering consequences, especially for people with diabetes. Diabetes patients may not be able to recognize the painful event due to a condition called neuropathy. Diabetic neuropathy can cause insensitivity or a loss of ability to feel pain, heat, and cold. Diabetics suffering from neuropathy can develop minor cuts, scrapes, blisters, or pressure sores that they may not be aware of due to the insensitivity. If these minor injuries are left untreated, complications may result and lead to ulceration and possibly even amputation. Fig. 21.1 illustrates the ulcer development. Calluses occur when there is intermittent pressure at some part of the foot. This causes the outer skin to thicken and become hard, as illustrated. During rubbing, the shearing forces rupture the flesh under a callus, the outer skin becomes loose and fluid collects beneath it,

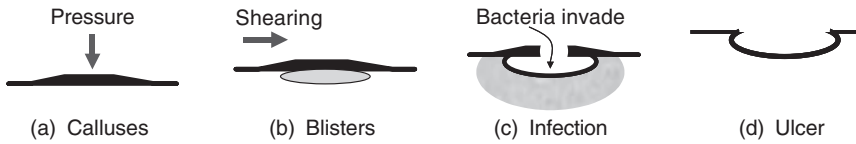

21.1 Foot lesion development.

forming a blister. If the pressure and shearing continue, the blister breaks down and bacteria invade. The necrotic area gets infected. Finally, a deeper cavity forms as an ulcer.[3] It is reported that about 15% of diabetics will experience significant foot problems during their lives, and each year 86 000 will have a lower limb amputated because of foot complications.[4]

Foot lesions are common and costly complications in people with diabetes.[5] Most people with diabetes are beginning to understand the importance of protecting their feet. Bad footwear has been identified as a major cause of ulceration in diabetes.[6] In a European study, footwear was implicated as being contributory to 21% of all ulcers in a large survey.[7] So an effective way to protect feet is to wear proper footwear. Actually, various preventive and therapeutic modalities, including shoes and insoles, have been developed for diabetics. Much research has been carried out to investigate the role of footwear in the prevention of foot lesions. Most of the researchers conclude that appropriate footwear helps to redistribute and reduce peak plantar pressure, which is a major cause of calluses, sores and ulcers.[5,8–14] Further research on foot care shows that good shoes and insoles are not enough, attention must also be paid to socks.[3,15,16] People with diabetes are advised that they should never wear shoes without socks. Hosiery plays a number of roles: removing perspiration from the skin, helping regulate foot temperature, providing pressure relief by increasing thickness, and protecting the skin from abrasion. However, except for a few research investigations into the effect of padded socks on plantar pressure,[15,17] research has rarely focused on socks. The part socks play in foot care remains unclear.

21.1.2 Socks for foot care

Compared with shoes and insoles, socks are much simpler to apply and are less expensive. However, the questions to answer are: how do socks work, and what kind of socks should people with diabetes wear? Firstly, socks should be fitted properly. Socks that are too large bunch up in the shoe; those that are too small squash the feet. During the wearing of a sock, the foot stretches the sock and, in return, the pressure induced from the sock deforms the skin and soft tissue. This mechanical interaction stimulates neurophysiological impulses of touch and pressure through the mechanical receptors in the deep layer of the skin,[1] which further induces subjective

perceptions and relevant pressure discomfort or more seriously, pain sensations. Sensitivity to pressure also differs in different small regions of the foot. For example, the absolute pressure thresholds at the hallux and the heel are higher than for the middle sole.[18] Due to difference of skin thickness, sensitivity to pressure should be higher at the instep than at the sole. However, suitable pressure is needed to keep close contact between the sock and foot. There should be no lumps or folds to irritate the foot. How to provide suitable pressure to the foot while not causing an uncomfortable compressive feeling is important in sock design and engineering.

Regarding sock materials, many people believe that natural fibers, such as cotton, are better than synthetic fibers.[5] However, other researchers disagree with this opinion. Although cotton absorbs water well, it retains it. Some researchers have found that the friction coefficients of many textile materials, especially natural fibers (cotton and silk), increase along with increase in temperature and humidity.[19] This may result in a more severe friction situation. Therefore, for sock materials, two aspects need to be considered. Firstly, wearing socks of good heat and moisture transfer, and moisture absorption properties, can help to keep the foot dry during the day, hence avoiding moist feet that tend to 'stick' to the shoe and exacerbate rubbing. Secondly, socks of low friction material can directly reduce friction. By imparting a low friction value to the contact areas, abrasion of the foot skin is diminished as well as the shearing between the contact interfaces. Friction-free technology is being developed in sock manufacture.[20] Du Pont's Teflon fibre of extremely low friction is now available for socks. How to utilize this technology in socks design for foot care is an important issue.

21.2 Biomechanical modeling

21.2.1 Model development

Various pressure measurement methods have been developed to measure static and dynamic plantar pressure.[21] There are also biomechanical foot models built for predicting the plantar pressure to aid clinical practice.[22,23] However, unlike plantar pressure that can be measured directly, there are only a few experimental devices for shear measurement.[24] Knowledge of shoe rubbing remains minimal. Since direct measurement of friction and shearing *in situ* is difficult, an approach is to build 3-D models to theoretically investigate the mechanical interactions in footwear. The focus is on normal walking rather than active sports. There is very little modeling work on foot–sock interaction reported in sock engineering. In the biomechanics research area, various 2-D and 3-D foot models using the Finite Element Method (FEM) approach have been developed, and the foot–insole interface is modeled with the aim of investigating plantar pressure and stress in

the foot during various stance phases of gait. Gefen,[25,26] Chen *et al.*,[27] and Jacob and Patil[28] developed 3-D biomechanical foot models consisting of bones, soft tissues, cartilage and ligaments and analyzed stress distribution in the foot during various stance phases of gait, mainly for clinical applications. Furthermore, Chen *et al.*,[23] and Lemmon[22] modeled the foot–insole interface to investigate the insole effect on the plantar pressure distribution. Some other researchers focused on the in-shoe pressure during walking, running or doing other sports, in order to provide guidance for sports shoes design.[29,30] There is no report on modeling foot rubbing and slippage in shoes. And since the mechanical contact between a foot and a flexible sock is difficult to model, there are also few 3-D sock models reported. A 3-D foot, sock and insole contact model has therefore been developed here to investigate the sock pressure exerted on the foot, stress in the sock, plantar pressure, plantar shearing force, and the forward slippage of the foot at push off.

21.2.2 Simulation of wearing a sock

Modeling of foot and sock interaction

Since the purpose of the foot–sock interaction model is to investigate the pressure and stress in the foot resulting from wearing socks, it is assumed that foot deformation is limited to soft tissue. Therefore, some reasonable simplification was made: all the bones and cartilages were combined as a whole skeleton and the remaining parts of the foot were considered as soft tissue. The toes were also combined as a whole. The surfaces of the foot and inner skeleton were reconstructed from Magnetic Resonance Imaging (MRI) coronal images of a male in his twenties and a solid bone and soft tissue model was created. The bone and soft tissue materials were assumed to be homogeneous, isotropic and linear elastic. For bones, the Young's modulus was taken as 7300 MPa, and Poisson ratio as 0.3, and for the soft tissue, the values were taken as 1 MPa and 0.49, respectively.[28] Since a sock takes the shape of the foot surface when it is fitted, the foot surface is used as the sock geometry. Knitted fabrics often have significantly different mechanical properties in the wale and course directions, so the materials for socks were defined as orthotropic and linear elastic shell. Two cases of a sock of crew length, worn on a foot, using two materials, nylon and cotton, were simulated. The material parameters for the sock are listed in Table 21.1, where E_1 and E_2 denote the Young's moduli in the course and wale directions respectively, G_{12} and υ_1 are the shear modulus and Poisson ratio, W is the mass density and t is the fabric thickness.

The interface between sock and foot is considered as surface-to-surface contact; the surfaces can undergo relatively finite sliding in relation to each

other. A penalty method is employed to enforce the kinematical constraint that the slave surface nodes (inner surface of sock) do not penetrate the master surface (foot surface); friction between the two surfaces is also taken into account. The friction coefficient is set as 0.1 in the simulation. The sock welt is often made of tightly knitted fabric to prevent slipping, so it adheres to the underlying foot surface. A tie constraint between the sock welt and the surface of the ankle was defined.

Boundary condition: Since the purpose is to investigate the pressure exerted by the sock, pressure due to the supported body weight should be avoided. Therefore, the foot is simulated as 'hung' and has no contact with other objects except for the sock. It is assumed that the bone part of the foot does not deform due to the wearing of the sock, therefore the displacements of all the nodes on the bone are constrained in all directions as a boundary condition in the simulation.

As the initial condition, the initial stress needs to be added to the sock, accounting for the sock deformation due to the wearing process. It is difficult to measure the stress in socks due to biaxial extension. However, with the Finite Element (FE) approach, the stress according to the stretch and the mechanical properties of the material can be predicted. The biaxial extension of a piece of fabric (5 cm × 10 cm rectangle) using a mesh of 4-node quadrilateral shell elements, which is the same as the sock, was

Table 21.1 Parameters of knitted fabrics

Sock	E_1 (N/mm)	E_2 (N/mm)	G_{12} (N/mm)	υ_1	t (mm)
Nylon	0.0446	0.061	0.02	0.195	0.5
Cotton	0.061	0.0728	0.028	0.155	0.85

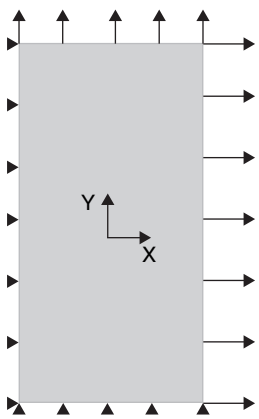

21.2 Biaxial extension of fabric.

simulated. As illustrated in Fig. 21.2, displacements corresponding to the stretch in the wale and course directions are set to the nodes on the right and top edges, while the displacements of the nodes on the left edge are constrained in the *X* axis direction and those on bottom edge are constrained in the *Y* axis direction. The resulting stresses in the two directions are taken as initial stresses for the sock in the wale and the course directions. A non-linear general static analysis is performed for the bi-extension simulation.

For each sock case, static general nonlinear analysis was performed in ABAQUS/Standard using the Newton–Raphson method.

Experimental results and discussions

Both of the two sock samples have foot-like shapes. Therefore, the sock model is divided into four parts and it is assumed that the fabric is evenly stretched in each part. Then, according to the sock sizes and the dimension of the subject's foot, it is calculated that the fabric stretches in two directions for each part. The stress in the nylon sock is found to be higher than that in the cotton sock. Before numerical analysis, the sock is in an unbalanced state, but after the numerical analysis, the sock stress is balanced by the contact pressure and frictional force due to the interaction between sock and foot, and reaches a balanced redistribution.

The stress in the sock, pressure on the foot, and stress in the foot show significantly different distributions. The Mises stress in the cotton sock varies from 0.0043 to 0.0347 MPa, and that in the nylon sock varies from 0.00625 to 0.0399 MPa. This indicates that the sock is stretched everywhere and no part rests on the foot surface. Higher stress concentrates at the heel part. The stretched sock induces pressure on the underlying foot. From the pressure distributions, it was noticed that the pressure does not distribute uniformly over all the foot. The pressure range for the cotton sock was 0–0.0039 MPa, and for the nylon sock 0–0.0046 MPa. Zero pressure indicates 'no contact' between the foot and sock. Due to the complicated geometrical feature of the foot surface, as well as the tightly-stretched state of fabric, the sock is not in contact with the underlying foot everywhere: only the convex surface of positive Gaussian curvature supports the sock, and the concave surface of negative Gaussian curvature does not contact the sock. Moreover, high pressure occurs where the curvature of the foot surface is high, such as the end of the toes, and the two lateral sides of the foot. As a whole, the two socks result in similar pressure distributions. The pressure on the foot deforms the foot. The stress in the foot caused by the cotton sock ranged from 0–0.00299 MPa, and the nylon sock from 0 to 0.00399 MPa. High stress concentrates at the toe part.

Comparing the two socks, it was found that the stress in the nylon sock is higher than that in the cotton sock. As a result, it was found that the stress

and pressure in the foot for the nylon sock are also higher than those for the cotton sock, especially at the toe part. These distributions demonstrate that the pressure depends on the curvature of the body surface and the stress in the fabric. This observation has been confirmed by Inoue *et al.*'s work,[31] in which reasonable pantyhose pressure was predicted according to the body curvature and the biaxial extension of fabrics, and was compared with subjective test results. However, it is difficult to calculate the curvature of the body surface as it is often of complicated shape. Therefore, in that work, the thigh was simplified as a cylinder and was focused upon.

Comparison with measured results

Pressure measurement was carried out by using an apparatus developed in the laboratory of the Institute of Textiles and Clothing at The Hong Kong Polytechnic University, in which the sensor 'Flexiforce Sensor Model A201'[32] was used as a pressure receptor. According to reference 33, the pressure was measured at the following positions: Malleolus medialis (Mm), Malleolus lateralis (Ml), Instep (Ins), Ball of foot (Ba), facies mediales of the Digitus 1 (D1), facies lateralis of the Digitus 5 (D5), facies mediales of the Planta (Pl), and facies posterior of the Calx (Ca). These points are the characteristic points of the foot surface geometry; the curvatures at these points are relatively high. At these points, the pressure is the highest within the vicinity around them. The measured results are shown in Fig. 21.3, and 'M' and 'S' means 'measured' and 'simulated', respectively.

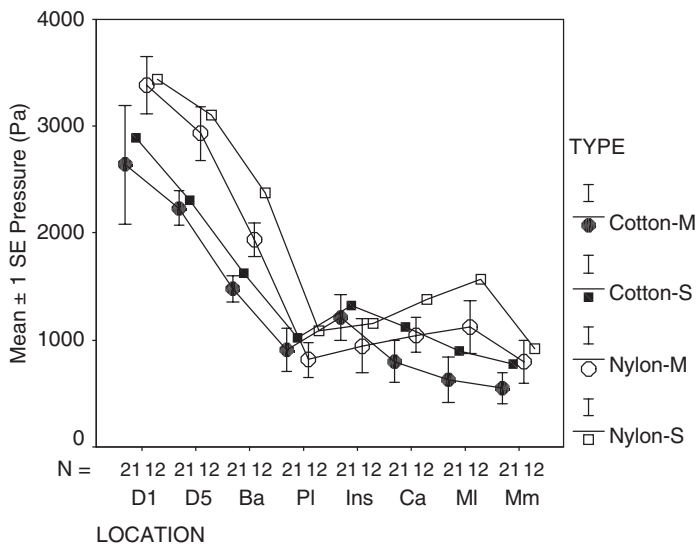

21.3 Pressure in the sock.

Both of the socks showed the same trend of pressure change: the highest pressure occured at D1, then D5. These pressures were greater than the rest. This trend is consistent with that reported in references 33, 34. When comparing the two socks, it was found that the pressure in the nylon sock was significantly higher than that in the cotton sock due to the higher strain, especially at D1. The simulated pressure results agreed roughly with the respective measured ones. The difference between the simulated and measured results, especially at the positions, where the pressure is low, is considered to be because the measure positions in simulation and in reality may not be exactly the same; and the measurement error also accounts for the difference. The error of stretch measurement for each sock part is also a main factor causing the difference between the simulation results and the actual state of the sock. The agreement between real measurement results and simulated ones confirms that the model is useful in predicting the pressure on the foot caused by wearing the sock. By using the model, not only the pressure values of several feature points, but also the overall pressure distribution in a sock of complicated geometry can be predicted.

Pressure control

To avoid causing uncomfortable compressive feelings, the high pressure at the toe part needs to be reduced. However, lumps or folds resulting from loose-fitting socks may irritate the foot. A certain pressure is necessary to provide tight contact at the sole. However, both the socks show lower pressure at the facies mediales of the Planta (Pl). An ideal design for a sock provides tight contact at the sole part and relatively loose contact at the toe part. Using higher Young's moduli for the sole part and lower Young's moduli for the toe part, and assuming the sock has uniform stretch, the initial stress distribution can then be obtained. After the numerical simulation, the stress is redistributed so that the higher pressures concentrate at the sole and instep rather than the toe; stress in the toe part is also reduced. The simulation indicated that it is easy to predict the overall pressure distribution exerted by a sock assembled by various materials, by using the foot–sock contact model.

21.2.3 Dynamic walking simulation

Modeling of foot, sock and insole interaction

During walking, the gait cycle is usually subdivided into a stance phase and a swing phase. The swing phase is the period of time when the foot under consideration is not in contact with the floor. The stance phase is the period of time when the foot under consideration is in contact with the floor. The

stance phase can be further subdivided into five stages: heel-strike (initial foot-floor contact), foot-flat, mid-stance, push-off, and toe-off. According to our perception, slippage takes place easily when the phase turns from foot flat to mid-stance, and then to push-off. Therefore, the phase transition from foot-flat to push-off is simulated. Since the shoe is not the focus of this study, only a barefoot or a foot wearing a sock standing upon an insole lain over a supporter is simulated rather than in a shoe.

To allow bone deformation, proper partition is performed on the skeleton, and the thinner pieces between parts are defined as soft cartilages. The bone, cartilage, and soft tissue materials are assumed to be homogeneous, isotropic and linear elastic. The Young's moduli, Poisson ratios, and mass densities for these materials are listed in Table 21.2.

For the loads on the foot, the loads at the mid-stance phase are used. According to reference 28, only ankle joint force and the forces of several major muscles are considered. The muscle forces include triceps surae (TS), reaction at the medial pulley due to the muscles flexor hallucis longus (FHL), flexor digitorum longus (FDL), tibialis posterior (TP), reaction at lateral pulley due to muscles peroneus longus (PL), peroneus brevis (PB), and flexor hallucis longus (FHL).

Three computational experiments were carried out: one barefoot and two sock simulations. There are several objects involved in the mechanical system: bone, tissue, insole, support and in some cases, sock. In the barefoot simulation, there is only a pair of surfaces involved in the contact problem: the foot surface and the top surface of the insole. The friction coefficient is set as 0.5. In the sock simulation, there are two pairs of surfaces involved: the foot surface and the inside of the sock; and the outside of the sock and the top surface of the insole. It has been reported that the friction coefficient between skin and Teflon fabric can be as low as 0.04 while that between skin and cotton fabric is as high as 0.54.[35] These two friction coefficients are chosen in the simulation. Two cases differing in friction arrangements are simulated: in case I, the coefficient of the friction between sock and foot is set as 0.54, and that between sock and insole is set as 0.04; in case II, the two friction coefficients are arranged *vice versa*. Usually, the soft tissue

Table 21.2 Material properties of foot and insole

Parameters	Soft tissue	Bone	Cartilage	Supporter	Insole
Young's modulus (MPa)	1.0	7300	10	50	0.5
Poisson ratio υ_1	0.49	0.3	0.4	0.36	0.85
Mass density (kg/m^3)	9.37×10^3	1.5×10^3	2.0×10^3	5.0×10^3	2.0×10^3

adheres tightly to the underlying bone; the two objects are not free from each other in motion. A tie constraint between the surface of the skeleton and the inside of the soft tissue model is defined, and also the interface of the insole and the supporter is defined as a tie constraint.

The simulation is divided into two steps: the first step is to calculate the sock–foot interaction, and reach a stable mechanical state of sock on foot; the second step is to simulate the phase change from mid-stance to push-off. The time period is set as 0.5 second and 0.75 second for the two steps, respectively. To make the simulation results comparable, the step set for the bare foot simulation is the same as the one for the foot wearing the sock. During the first step, no foot load is added, and the foot is fixed at three points. At the end of this step, the initial stress is redistributed in the sock and is balanced by the contact pressure, indicating that the sock is worn on the foot. In this simulation, it is assumed that the fabric is stretched evenly all over the sock, and the obtained stresses in the wale and the course directions are 0.03 MPa and 0.04 MPa respectively. In the second step, the loads mentioned above are added to the foot to simulate the foot phase change from mid-stance to push-off. Since the stress distribution in the bones is not examined as in reference 28, to simplify the calculation the loads are applied at single points rather than in areas. The magnitudes of loads are listed in Table 21.3. To allow for the foot motion during the phase changing from mid-stance to push-off, the constraints on the foot length direction at the fixed three points are released.

Simulation results

The frames taken from the bare-foot simulation were examined. The foot is flattened and then turns to take off. There was a similarity between the stress distributions and the respective pressure, demonstrating that the high pressure induces high stress in the foot. However, the pressure only occurs where the foot sole comes into contact with the insole: the stress distributes on larger regions than the pressure does, indicating that the mechanical response to pressure spreads to large areas on foot.

The sock simulation at the end of the first step was also examined. The uniform initial stress is redistributed in the sock and is balanced by the contact pressure. The pressure does not distribute uniformly; the pressure

Table 21.3 Loads on foot skeleton

Positions	L1	L2	L3	L4	L5
Load	1800 N	1200 N	850 N	200 N	100 N

magnitude varies from 0 to 0.005 MPa. The foot displacement in the simulation of foot wearing the sock I is compared with that in the barefoot simulation. Significantly, the foot wearing the sock slips to a larger distance upon the insole. In Fig. 21.4, it can be seen that the shearing force distributions in the two simulations are similar while the magnitudes of the shearing forces differ greatly. Fig. 21.4a shows the change of pressure on foot at two nodes, 651 at the heel, and 2587 at the forefoot; the pressure values peak in these vicinities. When the foot phase turns from mid-stance to push-off, the heel lifts up, only the forefoot is in contact with the insole, and the decrease of contact area leads to the increasing of pressure at the forefoot. The peak forefoot pressure is also higher than at the heel. It is consistent with many measurement results.[36] Compare the two simulations: at the forefoot, the plantar pressure reduces for the foot wearing the sock while the situation is the converse at the heel. This observation needs to be confirmed by further experimental measurement. Some former research has shown that a peak plantar pressure of larger than 12.3 kg/cm^2(12.05 MPa)[37] has the highest specificity in identifying patients at risk of foot ulceration, while a recent piece of research regarded 6 kg/cm^2(0.588 MPa) as a threshold.[38] No matter what the exact value of the threshold is, the pressure change plot will be helpful in identifying the risk.

In the simulated distribution of the shearing force on the foot sole, the shearing force occurring accompanied by the pressure showed a significant difference between the barefoot and the foot wearing the sock I. Both at

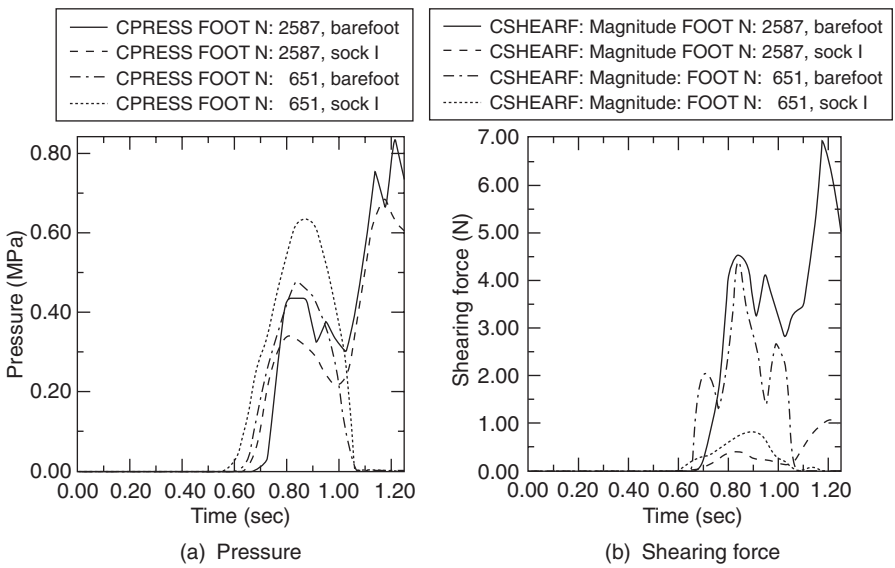

21.4 Changes of pressure and shearing force at two foot nodes.

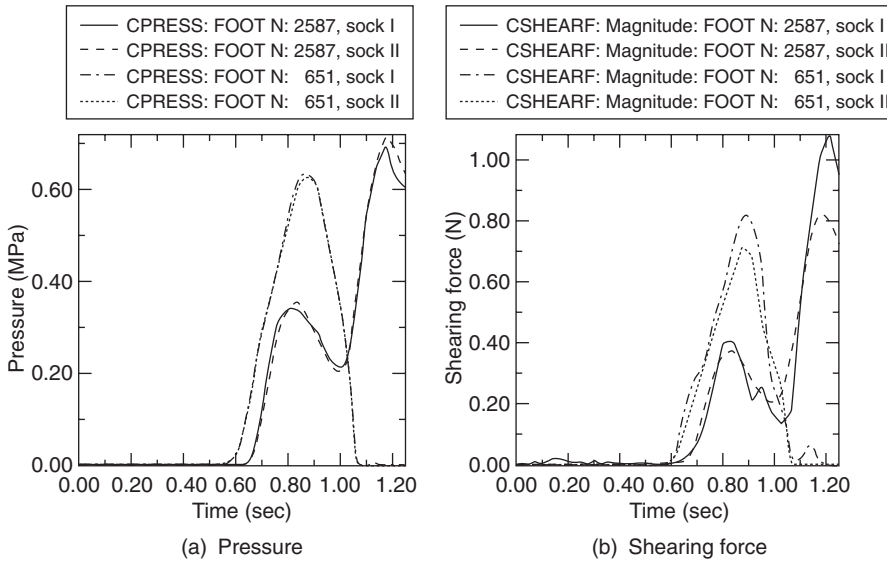

21.5 Comparison between two socks.

the heel and at the forefoot, the shearing force reduces dramatically for the foot wearing the sock. Although the magnitude of the shearing force depends on the pressure, its change trend is not always the same as the pressure. Comparing Fig. 21.4a with b, at the heel node, the shearing force for the foot wearing the sock reduces significantly while the pressure change increases.

In Fig. 21.5a, the two simulated results for the two socks are compared. The plots of plantar pressure are almost the same for the two cases, indicating that the difference in friction arrangements have no influence on the plantar pressure. Figure 21.5b shows that the shearing force for sock II is significantly lower than that for sock I: at the heel, the peak shearing force reduces from 0.84 N to 0.71 N, and at the forefoot, it reduces from 1.09 N to 0.78 N.

The change of foot and sock displacement is further looked into in Fig. 21.6, which shows the changes of the displacements along the foot length direction of the forefoot node (2587) and the sock node (5050) initially close to it. In the two sock simulations, the foot has the same slippage distance of 9.8 mm, while the barefoot has a very smaller displacement (1.34 mm). The slippage difference is 8.46 mm. At the node 5050, sock I has the same displacement as the underlying foot node, indicating that the foot adheres to the sock due to the high friction (0.54), and they slip upon the insole together. However, sock II has no forward displacement, indicating that it sticks to the insole, and the foot slips in the sock due to the low friction (0.04). The different foot movement in the sock results in completely

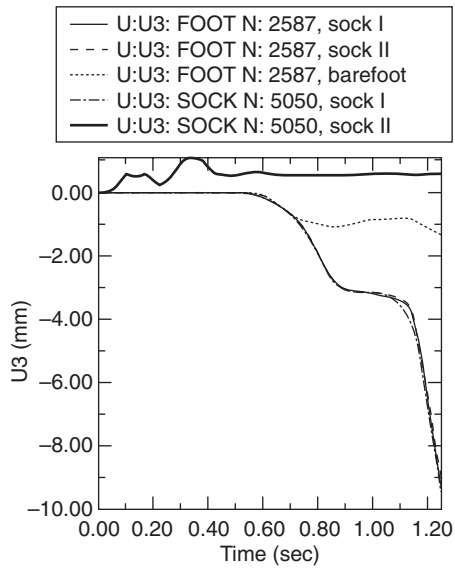

21.6 Displacement of foot and sock.

different stress distributions in the two socks. Due to the high friction between the sock and the skin of the foot, sock I adheres to the underlying foot during the phase changing, and slips together with the foot upon the insole. Therefore, the differences of displacement for different regions of the sock sole are not significant. The stress in the sock shows a similar distribution to that of the shearing force and the change of the stress in the sock also shows the same trend with the respective change of the shearing force, indicating that the sock stress is increased to balance the shearing force resulting from the friction against the foot as well as the insole. The situation for sock II is completely different. On the one hand, as demonstrated in Fig. 21.6, the sock sticks to the insole at the metatarsal heads during the phase changing of the foot. On the other hand, pushed by the advancing toes of the foot sliding inside the sock during walking, the sock at the toe part is stretched. Hence, the stress of the sock toe increases, accompanying the foot slippage.

Plantar pressure measurement

Besides the numerical simulation, a plantar pressure measurement using the pedobarograph (Tekscan, Inc, Boston, USA) was carried out. The subject whose foot is used in the simulation walks on the sensor mat with bare feet or wearing polyester socks of lower friction. The plantar pressures of the bare feet were consistent with the patterns shown in the simulated values

while the magnitude was lower due to the sensor losing accuracy. The slippage distance of the foot was further investigated. A peak phase pattern was used to show the largest measured values of each sensing point. The pattern illustrates the accumulated contact area during walking. The difference in the length between the peak pattern of barefoot and that wearing the socks is taken as the difference of slippage distance between the two walking situations. The length is calculated through the ASCII data file, in which the pressure value of each sensing points is recorded in a fixed rectangular array. The range of the non-zero column is counted and converted to length. The resulted difference was 9.04 mm. It is close to the simulated results of 8.46 mm.

21.3 Implications in sock design

21.3.1 Sock pressure

In days gone by, socks were something that were kept going for as long as possible. Today, the main consumer purchasing considerations are fit and comfort. For people with diabetes, socks are essential medical devices for foot care. We have seen some of the foot problems that may be caused by high sock pressure. To choose socks of the correct size and that fit the feet properly is very important.

21.3.2 Plantar pressure and shearing force

Through the numerical experiment, it was demonstrated that high plantar pressure and shearing force occur at the forefoot and heel during walking. The magnitudes of the plantar pressure and shearing force are large at the forefoot as well as at the heel. Since the tissue thickness at the forefoot is smaller than that at the heel, blisters and ulcers form more easily at the forefoot. The shearing force distribution at the forefoot compares with the blister and ulcer areas. To avoid foot ulceration, reducing the plantar shearing force is as important as reducing the plantar pressure. Soft and thick padded soles are often used to reduce the plantar pressure. To reduce the shearing force, an easy and effective approach is to wear socks of low friction.

The barefoot simulation demonstrated that high friction between the foot skin and the insole make the barefoot stick to the insole easily, and that this sticking leads to extremely high shearing forces. Due to the foot load, there is a potential for forward slipping in the shoe. If the slipping is completely resisted by rubbing against the insole and the shoe sides and tops, the high pressure and shearing force will soon results in calluses and blisters, especially at the forefoot. If the foot is allowed to slide upon the insole to a

certain distance, the shearing force will be reduced, hence reducing the potential for the formation of various foot lesions. This demands both a low friction and a certain space kept in the shoe to allow the foot to slide. Wearing a sock can reduce friction and allow the foot to slide upon the insole, hence reducing the shearing force.

Friction between the shoe insole and the sock or foot can influence a walkers' definition of comfort and the risk of injury. If it is too low, the foot will move easily in the shoe. But excessive movement gives rise to a feeling of underfoot insecurity, and may well generate pressure and rubbing between the top and upper part of the foot and the shoe.[39] Rubbing in the shoe includes friction between the foot and the inner surface of the sock, and that between the outer surface of sock and shoe. Friction that is too low in both of the interfaces may lead to excessive movement of the foot in the shoe, and cause discomfort and feelings of insecurity. An ideal way is to allow low friction on one side to allow foot sliding, and high friction on the other side to provide an appropriate level of resistance to avoid excessive movement. The numerical simulations demonstrated that this is more effective by reducing the plantar shearing force in the sock II simulation with low friction set against the foot skin than that in the sock I simulation with high friction set against the foot skin. This consideration has been confirmed by the socks using the low friction Teflon fiber.[20] By keeping the Teflon fiber against the skin to reduce rubbing between the foot and the sock's inner surface, and using high friction to provide the required resistance between the outside of the sock and the insole to prevent excessive movement of the foot in the shoe, the socks reduced the occurrence of blisters by around 90 percent in athletes.[40] The benefit of this technique in diabetic foot care needs to be confirmed in clinical practice. However, as observed above, the toe part of sock II shows large alternating stretch and recovery due to the foot sliding inside the sock during walking. This deformation and recovery may cause the fabric at this part to get looser or wear out easily. So, in sock design using friction-free fibres, a material of good elasticity and stretch recovery is necessary for the sock, especially at the toe.

21.3.3 Sock design

For different end uses, there are large variations of functional requirements. For each foot part, there are also different requirements. For normal use, the sole needs to be soft and durable; the instep of the sock can be loose-fitting to reduce the pressure where the skin is thin and the pressure threshold is relatively lower. For athletes, it is important to reduce calluses and blisters, and prevent tendons from injury. Sports socks often have thick cushioned soles, and reinforced elastic material to fully encompass the arch

and instep for a snug fit and support and also to protect the Achilles tendon. For diabetic patients, any tiny lesion will lead to ulceration. There should be no elastic or tight welt which can interfere with blood flow. There should also be no seam felt. Any holes in the sock can be a source of additional friction. There should be no lumps or folds to irritate the foot.

Regarding sock material, it must be able to wick moisture away from the foot leaving skin dry and reduce sticking. Materials such as Coolmax™ have been used in sock manufacture. For the foot arch part, reinforced elastic materials such as Lycra™ have been used to support and protect the foot arch. For the sock sole, soft and thick cushioning is necessary to reduce plantar pressure; 'friction free' construction, such as the use of Teflon™ fiber, needs to be imparted to the forefoot and heel to reduce rubbing. For the sock instep, loose fit can help reduce the sock pressure for comfort.

The present biomechanical foot, sock and insole interaction model can help us to design a sock of complicated structure and material assembly, and predict the pressure and shearing. Further development of the model can be focused on sock thickness, to quantitatively investigate the effect of thickness on plantar pressure. Integration with the shoe model is also expected, in order to study the mechanical interaction of footwear systematically.

21.4 Acknowledgement

We would like to thank the Hong Kong Polytechnic University for funding this research through the Projects A188 and G-YD31.

21.5 References

1. Anon., Hot under the Foot. *World Sports Activewear*, 1999. **5**: p. 58.
2. Anon., *Skin and Toenail Problems.* Foot Care Basics, A Special Health Report from Harvard Medical School, 2001: p. 21–27.
3. Phillips, P., Evans, A. and Popplewell, P., Diabetic Foot Ulcers, A Guide to Treatment. *American Journal of Clinical Dermatology*, 2000. **1**(2): p. 117–123.
4. Anon., *Foot Care Basics.* Foot Care Basics, A Special Health Report from Harvard Medical School, 2001: p. 1–2.
5. Litzelman, D.K., Marriott, D.J. and Vinicor, F., The Role of Footwear in the Prevention of Foot Lesions in Patients with NIDDM. *Diabetes Care*, 1997. **20**(2): p. 156–162.
6. Apelqvist, J., Larsson, J. and Agardh, C.D., The Influence of External Precipitating Factors and Peripheral Neuropathy on the Development and Outcome of Diabetic Foot Ulcers. *Journal of Diabetes Complications*, 1990. **4**: p. 21–25.
7. MacFarlane, R.M. and Jeffcoate, W.J., Factors Contributing to the Presentation of Diabetic Foot Ulcers. *Diabetic Medicine*, 1997. **16**: p. 867–870.

8. Perry, J.E. *et al.*, The Use of Running Shoes to Reduce Plantar Pressures in Patients Who Have Diabetes. *The Journal of Bone and Joint Surgery*, 1995. **77-A**: p. 1819–1828.
9. Boulton, A.J.M. and Jude, E.B., Therapeutic Footwear in Diabetes. *Diabetes Care*, 2004. **27**(7): p. 1832–1833.
10. Lord, M. and Hosein, R., Pressure Redistribution by Molded Inserts in Diabetic Footwear: A Pilot Study. *Journal of Rehabilitation Research and Development*, 1994. **31**: p. 214–221.
11. Maciejewshi, M.L. *et al.*, Effectiveness of Diabetic Therapeutic Footwear in Preventing Reulceration. *Diabetes Care*, 2004. **27**(7): p. 1774–1782.
12. Mueller, M., Strube, M.J. and Allen, B.T., Therapeutic Footwear Can Reduce Plantar Pressures in Patients with Diabetes and Transmetatarsal Amputation. *Diabetes Care*, 1997. **20**(4): p. 367–371.
13. Praet, S.F.E. and Louwerens, J.W.K., The Influence of Shoe Design on Plantar Pressures in Neuropathic Feet. *Diabetes Care*, 2003. **26**(2): p. 441–445.
14. Viswanathan, V. *et al.*, Effectiveness of Different Types of Footwear Insoles for the Dianetic Neuropathic Foot. *Diabetes Care*, 2004. **27**(2): p. 474–477.
15. Scheffler, N.M., All about Socks. *Diabetes Forecast*, 2001. **54**(9): p. 78,80–81.
16. Mayfield, J.A. *et al.*, Preventive Foot Care in People with Diabetes. *Diabetes Care*, 1998. **21**(12): p. 2161–2177.
17. Veves, A. *et al.*, Use of Experiment Padded Hosiery to Reduce Abnormal Foot Pressures in Diabetic Neuropathy. *Diabetes Care*, 1989. **12**: p. 653–655.
18. Dohi, M., Mochimaru, M. and Kouchi. M., The Tactile Sensitivity and the Elasticity of the Sole of the Foot as Factors of the Shoe Comfort, in *IEA2003*. 2003.
19. Morooka, H. *et al.*, Relationships of Slip in Shoes to Frictional Property and Cloth Thickness of Men's Socks. *Journal of the Japan Research Association for Textile End-uses*, 1994. **35**(12): p. 682–689.
20. Anon., More Comfort from Socks with Low-friction Teflon. *Textile Magazine*, 1999. **28**(2): p. 8–9.
21. Cavanagh, P.R., Hewitt, F.G.J. and Perry, J.E., In-shoe Plantar Pressure Measurement: A Review. *Foot*, 1992. **2**: p. 185–194.
22. Lemmon, D., The Effect of Insoles in Therapeutic Footwear – A Finite Element Approach. *Journal of Biomechanics*, 1997. **30**(6): p. 615–620.
23. Chen, W.P., Ju, C.W. and Tang, F.T., Effects of Total Contact Insoles on the Plantar Stress Redistribution: A Finite Element Analysis Clinical Biomechanics. *Clinical Biomechanics*, 2003. **18**: p. s17–s24.
24. Hosein, R. and Lord, M. A Study of in-shoe Plantar Shear in Normals, *Clinical Biomechanics*, 2000, **12**, p. 46–53.
25. Gefen, A., Biomechanical Analysis of the Three-dimensional Foot Structure During Gait: A Basic Tool for Clinical Applications. *Journal of Biomechanical Engineering*, 2000. **122**(12): p. 630–639.
26. Gefen, A., Stress Analysis of the Standing Foot Following Surgical Planter Fascia Release. *Journal of Biomechanics*, 2002. **35**: p. 629–637.
27. Chen, W.P., Tang, F.T. and Ju, C.W., Stress Distribution of the Foot during Mid-stance to Push-off in Barefoot Gait: A 3-D Finite Element Analysis. *Clinical Biomechanics*, 2001. **16**: p. 614–620.

28. Jacob, S. and Patil, M.K., Three-dimensional Foot Modeling and Analysis of Stresses in Normal and Early Stage Hansen's Disease with Muscle Paralysis. *Journal of Rehabilation Research and Development*, 1999. **36**(3).
29. Aguinaldo, A. and Mahar, A., Impact Loading in Running Shoes with Cushioning Column System. *Journal of Applied Biomechanics*, 2003. **19**(4): p. 353–360.
30. Geil, M.D., The Role of Footwear on Kinematics and Plantar Foot Pressure in Fencing. *Journal of Applied Biomechanics*, 2002. **18**: p. 155–162.
31. Inoue, M., Sukigara, S. and Niwa, M., Prediction of 'Wearing Pressure' by Linearizing Method. *Journal of the Japan Research Association for Textile End-uses*, 1992. **33**(5): p. 254–260.
32. Tekscan, *http://www.tekscan.com/flexiforce.html*.
33. Momota, H. *et al.*, A Study of Clothing Pressure Caused by Japanese Men's Socks. *Journal of the Japan Research Association for Textile End-uses*, 1993. **34**(4): p. 175–186.
34. Momota, H. *et al.*, A Study of Clothing Pressure Caused by Japanese Women's High Socks. *Journal of the Japan Research Association for Textile End-uses*, 1993. **34**(11): p. 603–614.
35. Buirski, Just Slip into Something a Little More Comfortable. *World Sports Activewear*, 2000. **6**(4): p. 49–50.
36. Caselli, A. *et al.*, The Forefoot-to-Rearfoot Plantar Pressure Ratio is Increased in Severe Diabetic Neuropathy and Can Predict Foot Ulceration. *Diabetes Care*, 2002. **25**(6): p. 1066–1071.
37. Veves, A. *et al.*, The Risk of Foot Ulceration in Diabetic Patients with High Foot Pressure: A Prospective Study. *Diabetologia*, 1992. **35**: p. 660–663.
38. Pham, H. *et al.*, Screening Techniques to Identify People at High Risk for Diabetic Foot Ulceration: A Prospective Multicenter Trial. *Diabetes Care*, 2000. **23**(5): p. 606–611.
39. Draper, D., Coming down to Earth. *World Sports Activewear*, 1999. **5**(1): p. 53–55.
40. Delporte, C., New Socks Offer Relief, Blister Guard System with Teflon Reduces Friction between Foot and Sock. *America's Textiles International*, 1997. **26**(12): p. K/A 10.

22

Biomechanical engineering of footwear

A. LUXIMON AND M. ZHANG
The Hong Kong Polytechnic University, China

22.1 Introduction

It is not very clear why or when humans started wearing footwear. Many scientists believe that the first shoe, probably a bag-like wrapping made from animal skins,[1–3] was used to protect against the cold temperatures during the Ice Age about 500,000 years ago.[4] Ever since people started to wear footwear, there has been a constant progression in its use and design. The impact and influence of footwear have changed over the years. During the Stone Age, footwear was probably used to protect the feet against rocks, thorns, and harsh weather, whereas in the ancient Egyptian time, footwear depicted rank and was a status symbol.[4] Initially, footwear production was completely manual. Then, during the Industrial Revolution, the mechanization of the footwear industry started after the invention of sewing machines and equipment to roll sole-leather.[5] From that time, the number and variety of footwear have drastically increased. Foot coverings have become increasingly specialized for a variety of tasks and functions. For example, nowadays it is not surprising to have more than 200 models of running shoes.[6] Since footwear has become an integral part of our daily life, it is nearly impossible for many people to go out without footwear or even to stay in their room without some sort of foot covering.

During most of the early years of footwear development, style and fashion have played a huge part in the design of footwear. Since designs were based on aesthetic and sensual appeal rather than scientific studies, it is not surprising to find several examples of beautiful but 'badly-designed' footwear. In the Middle Ages, men were wearing long-toed footwear called *poulaine* to show their masculine sexuality;[4] however, the toe extensions were so long that it made walking almost impossible. Similarly, during the fifteenth century, beautifully decorated *chopine* footwear was designed to increase the height of ladies. It was short-lived because ladies could easy fall over while wearing it, resulting in miscarriages.[4] Furthermore, *chopine* footwear caused changes in posture and eventually the start of medical interest in problems with

elevated footwear. Although we cannot find *chopine* footwear today, a variation of it, the high heel, is widely available. As a result, there is still medical interest in elevated footwear. Of course, there are other parameters of footwear design that are of medical interest. Another classic example of 'beauty footwear' occurred during the tenth century (continuing until 1911) in China. In the name of beauty, Chinese female children's feet were bound with cloth to stop them from growing. The aim of the foot binding was to obtain feet resembling a 'three-inch golden lotus' and the women would be able to wear tiny footwear. Foot binding causes damage to the foot structure resulting in severe life-long disability for many elderly Chinese women.[7] Today, there are no extreme cases of foot torture such as foot binding; however, the incompatibility of footwear and the feet usually causes some sort of foot injury and illness. This chapter provides some basic information on the feet and footwear, so that footwear is designed to have aesthetic as well as fit, comfort, and functional design elements.

22.2 The human foot

Humans have evolved and have adopted an upright posture by walking on their hind-limbs and leaving the fore-limbs free for other uses. The development into bipedalism was a major step in human evolution, as many things associated with being human became possible – including fine manipulation with the hands and more mobility.[8] During the developmental stages, the foot lost the climbing ability and evolved into an organ of weight bearing, support, and locomotion. In early hominids or humans, the weight was carried along the side of the foot, while now the body weight is transmitted internally from the heel along the outside (lateral) of the foot. Also, in early hominids the body was pushed forward through the middle of the toes, while now the push-off is made generally by the big toe. This is a much more efficient arrangement for striding.[8] The detailed discussion of the development of hominids falls outside the scope of this chapter; instead, the foot structure of the 'modern' human foot is discussed in more detail.

22.2.1 Foot skeletal structure

The human foot (Fig. 22.1), an unsymmetrical object, comprises a complex arrangements of 26 bones, cartilage, muscles, tendons, ligaments, nerves, and blood vessels, and has evolved from a generalized grasping organ to an organ specialized in weight bearing, locomotion, and support.[9] The 26 bones are divided into three major groups: hind-foot (tarsal), mid-foot (metatarsals), and fore-foot (phalanges). The hind-foot consists of seven short bones (calcaneus, talus, navicular, cuboid, medial cuneiform, lateral cuneiform, and intermediate cuneiform) as shown in Fig. 22.1. The calcaneus, also

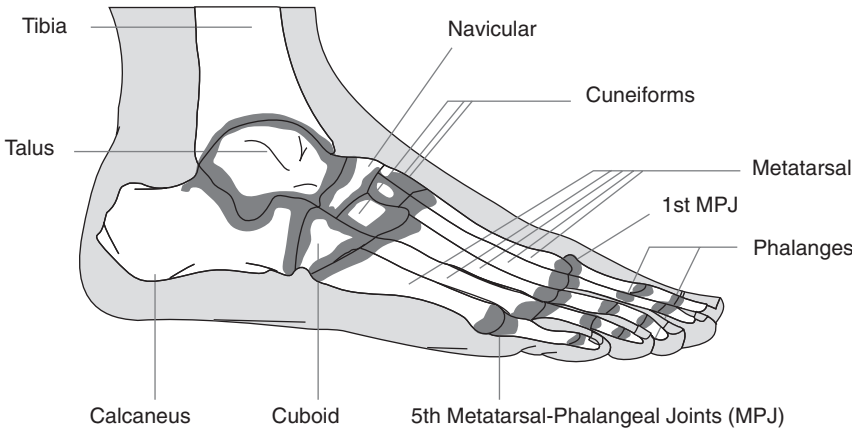

(a) Side view of foot

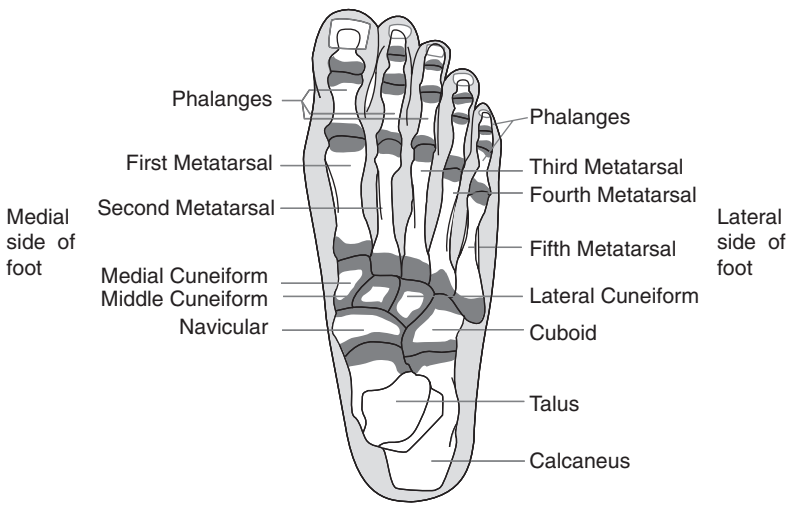

(b) Top view of foot

22.1 Basic foot structure.

known as the heel bone, carries a large proportion of the body weight. The talus is connected to the tibia and fibula (leg bones), and helps to distribute the weight of the body on the foot. The mid-foot consists of five metatarsals. The first three metatarsals are joined to the cuneiform bones (lateral, medial, and intermediate), while the last two metatarsals are joined to the cuboid. The fore-foot consists of fourteen phalanges that form the toes. Even though the three-section classification of the foot is more prevalent, some studies have separated the foot into four groups[10] for biomechanical

purposes. The four foot sections are: hind-foot (calcaneus and talus); mid-foot (navicular, cuboid, medial cuneiform, lateral cuneiform, and intermediate cuneiform); fore-foot (5 metatarsals); and phalanges (14 phalanges).

The bones are joined together at joints where some degree of motion is possible. The main foot joints are the ankle joint, the subtalar joint, the midtarsal joint, the metatarsal-phalangeal joint, and the phalangeal-phalangeal joints. The ankle joint is between the tibia and the talus. The subtalar joint involves talus, calcaneus, and navicular bones, whereas the midtarsal joint involves the talus, calcaneus, and cuboid bones. The ankle, metatarsal-phalangeal joints (MPJ) and phalangeal-phalangeal are hinge-type joints. At the joints, cartilage covers the ends of the bones and acts as a shock absorber. Cartilage also allows motion at the joints while being lubricated by synovial fluid. In order to have movement at the joints, muscles attached to the bones by tendons are used to create the pulling force. These muscles are stimulated by nerve endings through voluntary, involuntary or reflex actions. Ligament attaches a bone to another bone and thus restricts the bone motion resulting in enhanced support and locomotion. The complex arrangement of bones, muscles, ligaments, and other tissues are enclosed in a protective layer – the skin. The skin has nerve endings, blood vessels, sweat glands, and hair follicles, to enable its function of protection, temperature control and the sense of touch. Due to the complexity of the foot structures, the human foot has wide variations in size, shape, and proportion, within and between persons under different conditions, which affect the footwear fit.[11]

Within-subject variation

For a given person, the feet are different between the right and the left foot. Individuals working with their right hand have the tendency to use the left foot as a support. Thus, some people assume that the left foot might be longer. Rossi[12] reported that differences between the feet are prominent, based on a study using 6800 participants. Rossi states that 'no individuals are likely to have two feet exactly alike in terms of size, shape or proportions'. There are differences of 5 to 10% between the right and left foot. Similarly, several studies have found differences between the left and right foot of individual people; however, some people will have their right foot longer than their left foot and some *vice versa*. On average, there is no *overall* difference between right and left feet. Since previous studies have only considered length and width dimensions, more studies are required to look into the 3-D shape differences between the left and the right feet.

For an individual, in addition to differences in left and right feet, the feet undergo changes under different conditions such as loaded versus unloaded; functionality; and thermal conditions.[12] The foot normally increases in shape

and size when moving from no-load to semi-load to full-load weight bearing. A no-load, unloaded or no-weight condition is when the foot does not carry any body weight. This situation can be obtained by sitting and removing all weight from the foot. The semi-load, half load or semi-weight bearing condition is when one foot carries half of the body weight. This situation occurs while standing normally. The full-load, loaded, or full-weight bearing situation is when the foot is subjected to the full weight of the body. This situation can be obtained while the person is standing on one foot.

When comparing both feet in a fully loaded state, one foot elongates more than the other for 80% of people.[12] For example, this foot stretches half a shoe-size (1/6 inch) more than the other for about 85% of women, while it stretches 1 shoe-size (1/3 inch) or more for the rest. Since both the length and width increases in dimension under loading condition, fitting trials must include wearing both shoes and testing the fit under different weight-bearing conditions.[13] The foot shape is also different under different functions.

The foot functions can be separated into two main conditions: static and dynamic. Previous sections have considered the foot in static conditions (standing and sitting). Dynamic conditions include walking, running, jumping, other such activities; and the foot shape is different depending on the functions. The foot shape is different due to several motions at the joints, notably the ankle, the sub-talar, the mid-tarsal, the metatarsal-phalangeal and the phalangeal-phalangeal joints. These joints allow a different range of motion and thus the foot shape changes. At the ankle joint, a hinge type mechanism allows dorsiflexion (upward movement) and plantarflexion (downward movement) as shown in Fig. 22.2. The sub-talar and the mid-tarsal joints, located below the ankle, play a major role in supination and pronation.[14] Pronation is composed of three movements: eversion, abduction and dorsiflexion (Fig. 22.2), and it results in an upwards and inwards movement; while supination, the opposite of pronation, is composed of inversion, adduction and plantarflexion, and it results in a down and outwards movement. Furthermore, the metatarsal-phalangeal joints (MPJs) and the phalangeal-phalangeal joints (PPJs) are hinge joints. The MPJ allows dorsiflexion and plantarflexion of the toes, while the PPJ permits toe grasping. During any given dynamic condition, heat, friction, and sweat are produced which change the interior-shoe condition. The foot shape is also influenced by changes in environmental conditions.

The foot shape is affected by interior-shoe conditions such as heat, friction, humidity, and moisture. The foot volume changes by 5% at the end of the day compared to early morning, due to these thermal conditions.[12] Perspiration plays a major role in controlling body temperature. When the body becomes heated from muscular activity an even larger quantity of moisture is produced.[14] During perspiration, the sweat glands produce half

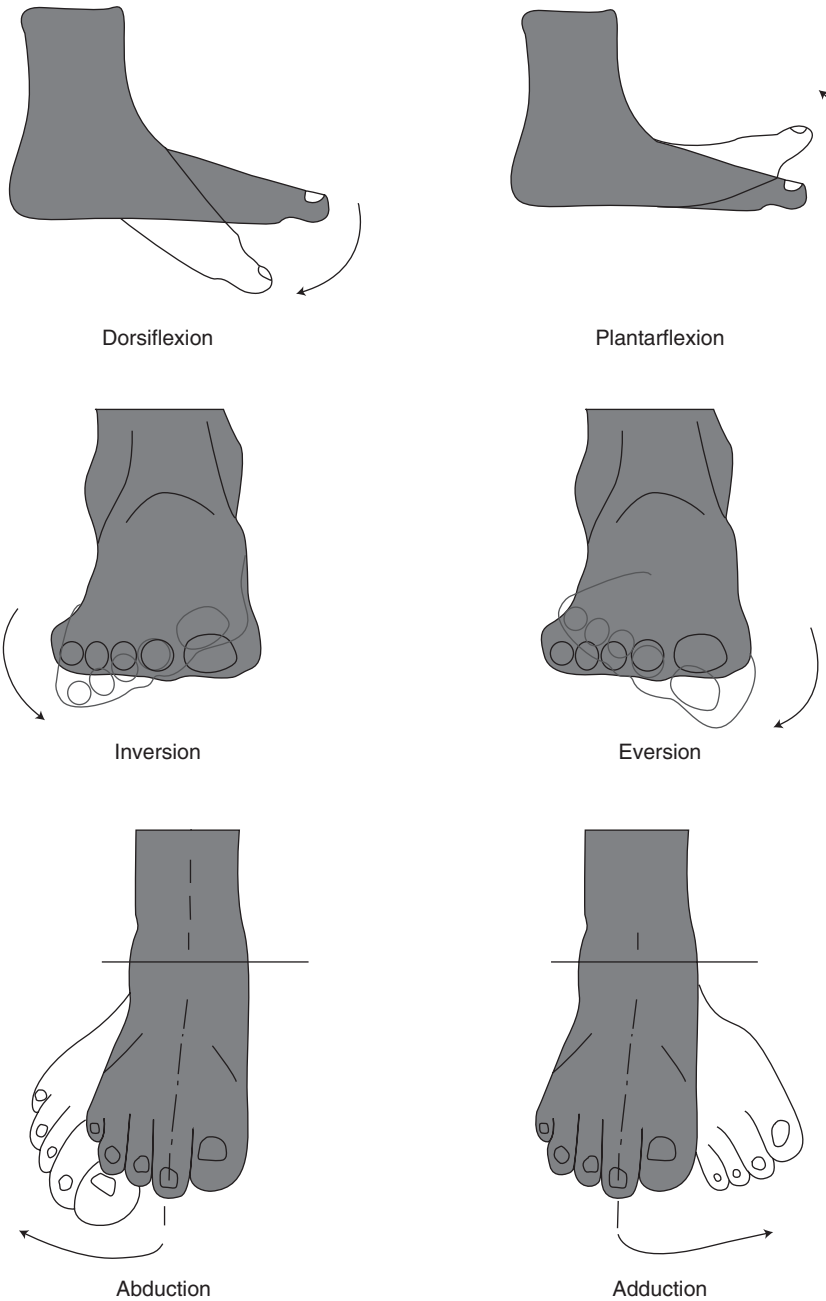

22.2 Foot dynamics.

a pint of moisture, salts, and acid into the shoes each day, changing the interior-shoe conditions drastically. So far the inter-subject variations have been considered: in contrast the between-subject variations are larger.

Between-subject variation

There are variations between people depending on gender, age, and race.[14] The mean length of the female foot is about 92% of the mean length of the male foot, while the mean volume of the female foot is about 81% of the mean volume of the male foot.[15] Even when comparing children between the ages of 6 to 11, boys have consistently a larger foot length and foot breadth than girls.[16] As far as the age variation is concerned, the foot stops growing after 14 years in boys and 13 years in girls even though the height is still increasing.[15] Dahlberg and Lander[1] studied men's feet as they aged between 17 and 47, and found that there were no differences in 18 foot-measurements showing that the feet had stopped growing. It is very evident that the foot size (length and width) changes for children, but does the foot shape change proportionately? This remains to be seen. In addition to gender and age, the feet are also different among different races.

Cheskin[14] grouped the feet into 3 main groups: Negroid foot; Oriental foot; and Caucasian foot. The Negroid foot is broad at the forepart and narrow at the heel. The oriental foot is short and broad in the forepart and heel. The Caucasian foot is broad with straight toes. There have been several studies on age and gender; however, studies on racial differences are few. Thus, a comprehensive study to quantify the racial differences would be useful.

22.2.2 Foot classification

Human feet have wide variations and, in order to simplify analysis, feet have often been classified according to arch height;[14,17,18] flare angle;[19,20] rear foot position[21] and big toe length.[17]

Arch height

When considering arch height, the foot can be grouped as high arched (Pes Cavus), normal arched and low arched (Pes Planus) as shown in Fig. 22.3. Figure 22.3 also shows typical plantar pressure distribution for feet with different arch heights. Pes Cavus and Pes Planus (flat foot) are developed when the balance between the muscles and ligaments of the foot is somehow disrupted.[18] In the high arched foot, the forefoot and the heel generally carry more weight, while for the normal arched foot the body's weight is distributed evenly throughout the foot.[14] However, in the low arched foot,

22.3 Classification based on arch height.

the weight is distributed over the total area of the foot. This causes extra pressure on the outside border areas, especially the medial side of the foot, resulting in pain, discomfort and decrease in function. The percentage of different arch types may vary between races but all types are found in all races.[14] The arch height can be determined from footprints. The various stages of the development of the Pes Cavus and Pes Planus are also shown in Fig. 22.3. Since Pes Cavus and Pes Planus feet are structurally weak, there have been several methods developed to quantify the percentage or degree of flat footedness. A simple method involves measuring the arch height[22] while others involve taking measurement from the plantar pressure prints.[23] The results obtained from the measurement techniques can vary for different conditions, e.g. static and dynamic; or loaded versus unloaded. In other words, an accurate method for quantification of flat footedness should account for age, gender, race, and different conditions, and existing results should be used with caution.

Foot flare

The foot can be classified as based on foot flare, which is a measure for the planter curvature of the foot similar to last flare (discussed in later sections). In order to calculate the amount of foot flare, we need to define a flare axis. For the purpose of calculating foot flare, the heel center line has been used. Freedman *et al.* (1946) have defined foot flare as the ratio of the horizontal distance between the heel center axis and the medial ball point to the foot width (horizontal distance between the heel center axis and the medial ball point + horizontal distance between the heel center axis and the lateral ball point). According to this definition, a straight foot is one which has a ratio of 50%, an out-flared foot is one which has a ratio of less than 50%, and an in-flared foot is one which has a ration greater than 50%. Goonetilleke and Luximon[20] used principal component analysis and found that the foot center is located at approximately 52% of the foot length, and that Hong Kong males have a mean in-flare of 3.2 degrees (standard deviation 2.73). According to Goonetilleke and Luximon's method, a negative angle value shows in-flare, while positive values show out-flare. Their method has higher sensitivity and is highly correlated with Freedman's ratio measure.

Rear foot position

Nigg[21] classified the foot according to rear foot position (Fig. 22.4). If the foot rear position is 0° to 6° toward the medial side, it is called a normal foot. If the foot is inclined more than 6° toward the medial side, it is called Pes Valgus. It is called Pes Varus if it is inclined toward the lateral side. In most cases, Pes Valgus occurs in combination with Pes Planus; thus some

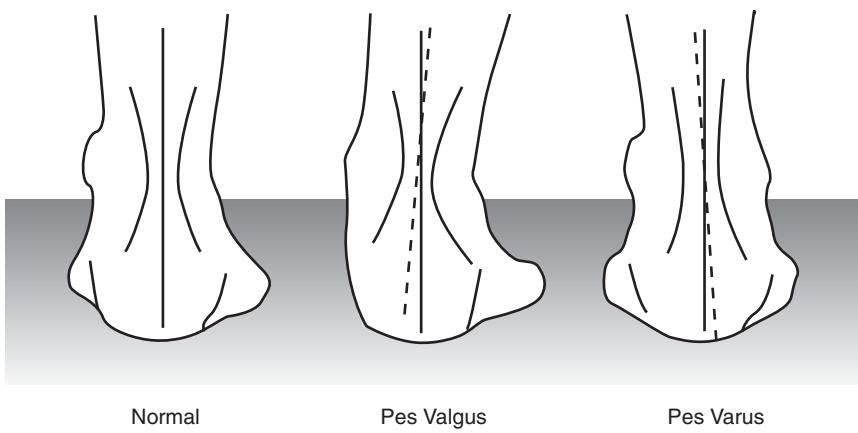

22.4 Classification based on rear foot position.

people use the measurement of the rear foot angle to quantify the degree of flat footedness.

Toe length

Feet can be classified in terms of big toe length, as shown in Fig. 22.5.[24] If the big toe length is the longest compared to the other toes, then the foot is called an Egyptian foot. If the second toe is the same length as the big toe, then the foot is called a Square foot. However, if the second toe is longer than the big toe, the foot is called a Greek foot. Kaplan[25] has attributed the differences in toe length to genetics, with long toe lengths being recessive. Due to the different toe lengths, the walking pattern and foot pressure of these different types changes. Figure 22.5 shows the typical pressure print of the three types of feet. For extreme cases of Greek feet (i.e. when the second toe are significantly longer), plantar pressure is higher at the second MPJ location. This might result in pain, discomfort, and skin break down.

22.2.3 Human gait

After considering the variation in feet and foot classification, the foot primary function is now considered. The foot is used primarily for walking and the human walking gait is very important. Foot, limb, and other muscu-

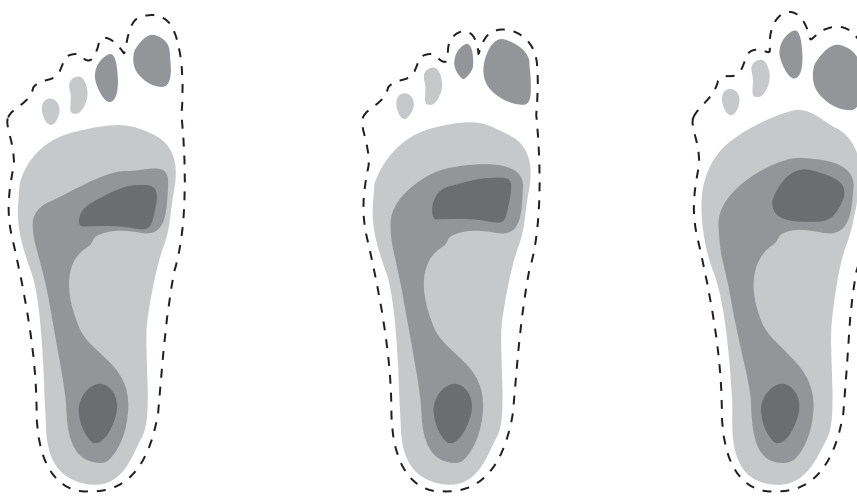

22.5 Classification based on toe length.

loskeletal problems can be identified by gait cycle evaluation. The gait cycle begins when one foot touches the ground and ends when the same foot touches the ground again (Fig. 22.6). The gait cycle is divided into two main phases, the stance phase and the swing phase. The stance phase is when the foot is touching the ground, while the swing phase is while the foot is not touching the ground and is in motion. The stance swing phase starts when the foot touches the ground, usually at the heel (heel strike), and ends when the foot leaves the ground, usually at the toe (toe off). During the stance phase, three periods can be identified: initial double limb support, single limb support, and terminal double limb support. Each double limb support period accounts for about 10% of the gait cycle (20% total), while the single limb support is 40% of the gait cycle. During the double limb support, the two limbs usually do not share equal load. There is always a shift of load from one foot to the other during the gait cycle. The swing phase for the same limb is the remaining 40% of the gait cycle. For different walking

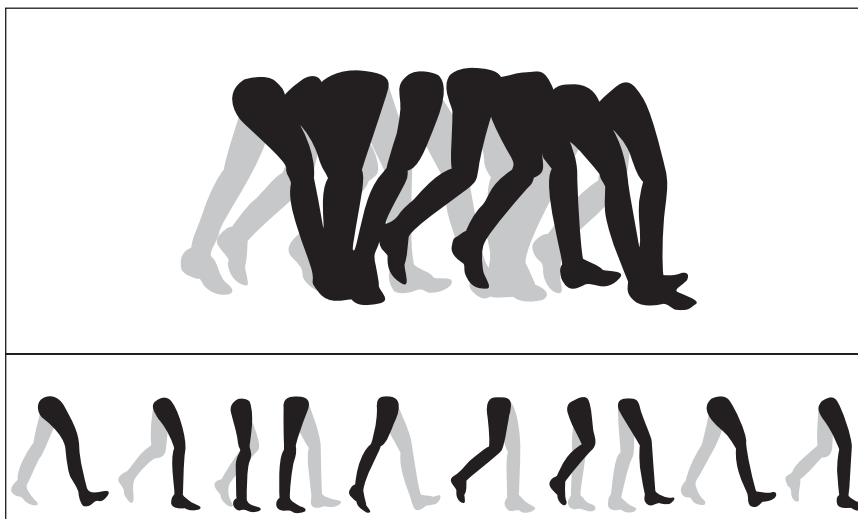

22.6 Gait cycle.

speeds, there are slight variations in the percentage of stance and swing phases. Also, when changing from walking to running, the duration of double limb support decreases until it is eliminated while running. A stride or gait is the interval between sequential initial floor contacts by the same limb (Fig. 22.6). A step is recognized as the interval between sequential floor contacts; thus, two steps make up each gait cycle.

22.3 Footwear

In today's society, footwear has become increasingly specialized for a variety of tasks and functions. There are shoes for most sports, ranging from running to golf. Footwear design and manufacture have been influenced by function but also by fashion and technology. In the following sub-sections, the main components of footwear (Fig. 22.7) and footwear manufacturing will be discussed.

22.3.1 Anatomy of footwear

Shoe upper

The shoe upper includes toe box, vamp, tongue, lining, collar, and fastening mechanisms (lacings, zipper, etc). The toe box covers the toe region and affects the fit at the toes. The function of the toe box is to protect the toes,

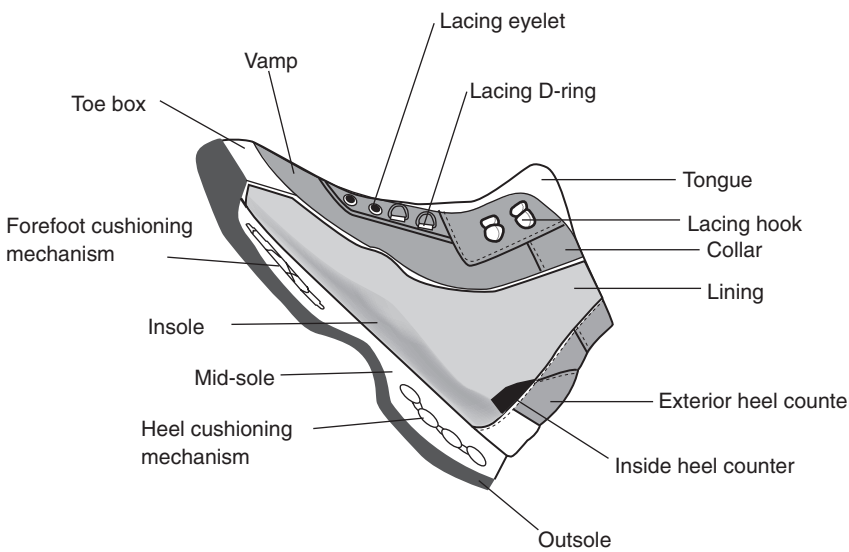

22.7 Anatomy of footwear.

allow their movement, and retain the shape of the shoe around the toe. The toe box may include a metal toecap in order to protect the toes against injury, especially in working boots. The vamp covers the dorsum of the foot including the tongue piece and superior aspects over the toes. This section is reinforced to give the shoe its shape as well as protection. The vamp is often made of more than one piece, creating a decorative pattern. There are various types of vamps suited for different styles of shoes.

The construction of shoe upper depends on style and fashion; however, the shoe *last*, a 3-D mould that represent the foot shape, determines the shape of the shoe upper. The uppers are made with leather or synthetic materials such as polyurethane-coated fabrics (PUCFs), polyvinyl chloride coated fabrics (PVC-CFs) or leather-like materials called poromerics. Leather, due to its inherent properties such as plasticity and breathability, is a better choice for the shoe upper and has been used through the ages. Leather can easily take the shape of the foot after sometime in use. It can also absorb perspiration and allow air-flow from the surrounding. This provides good aeration and can keep a suitable climate inside the shoe. Even though leather seems to be the perfect choice for shoe upper, PUCF, PVC-CF, and poromerics are also used because of cost and fashion trends. Synthetic uppers are cheaper and are used in most mass-produced footwear. PUCF is soft, light and comfortable to wear, but not so durable. PVC-CF is cheap, easy to clean, durable, but not breathable and does not change shape to fit the foot. Poromerics, even though synthetic, have leather-like properties. They are used widely as a leather substitute.

Shoe sole

The main components of the bottom are the outsole, the mid-sole, and the insole. The outsole is designed to give durability and traction but also contributes to shock absorption. The mid-sole is designed exclusively for shock absorption. Sometime a wedge is added at the heel for shock absorption and heel lift. The insole board is covered with a thin layer of material called a 'sock-liner' or an insole. This provides some cushioning, but its importance is during lasting (pulling the upper part of the shoe on the *last* and sticking on the insole board). Since many sports movements produce forces of considerable magnitude, most sports footwear has some sort of cushioning mechanism making use of air or gel.

Common soling materials are leather, rubber, polyvinyl chloride (PVC), ethylene vinyl acetate (EVA), and polyurethane (PU).[26] EVA is light weight and has good cushioning abilities. PU is heavy and inflexible, though it is more durable than EVA and still has cushioning abilities.

22.3.2 Shoe last

The word *last* (Figure 22.8) comes from the old Anglo-Saxon word *laest*, meaning a footprint or foot track. While shoemaking is an age-old craft rich in tradition, heritage and prestige, the foundation of shoes – the *last* – has been recognized as an important fashion and health factor only within the past few decades.[5] The *last* is the very heart, the single most important element, of the shoe.[12] It is the most scientific and complex part of the whole shoemaking process and it is the foundation upon which much shoe-related foot health depends.[27] It is responsible for the size, fit, shape, feel, wear, style, tread, and even the making of the shoe.[28]

The *last* is a reproduction, generally in maple wood, of the approximate shape of the human foot over which a shoe is produced which, when properly constructed, furnishes support and protection without undue pressure,

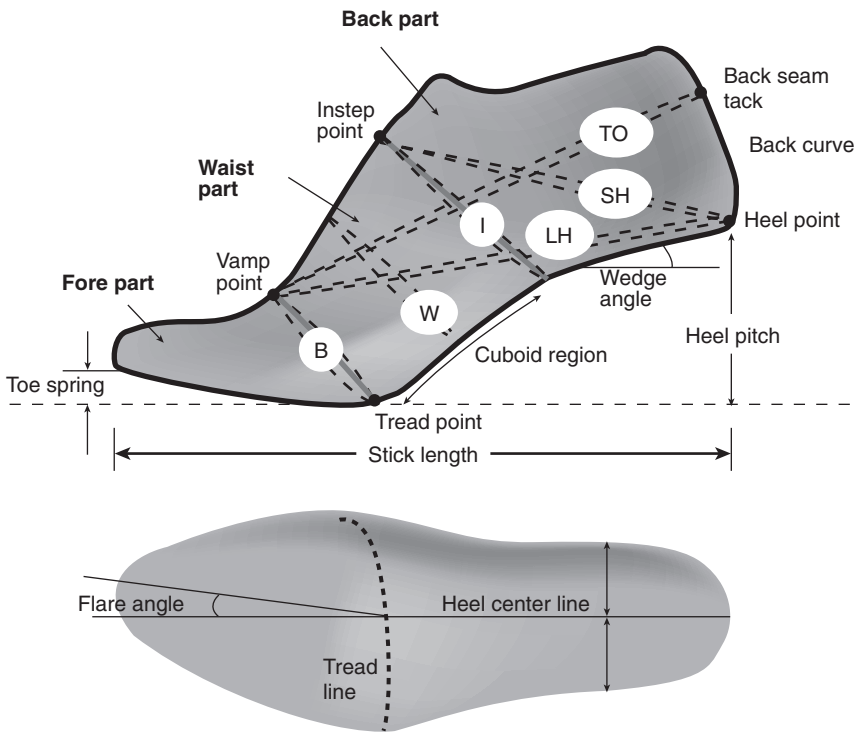

Note:
I : Instep girth W : Waist girth B : Ball girth
LH : Long heel girth SH : short heel girth TO : Throat opening

22.8 Ladies shoe-last with basic last measurements.

binding or constriction at any point.[5] The first *last* maker in the USA whose name is on record was William Young of Philadelphia, Pennsylvania, who was granted a patent for a minor *last* improvement in the year 1807. In 1840, *lasts* were slightly improved. By adding a pad over the front of the shoe they created two sizes called 'slim' and 'fat'. Now, shoes are made on *lasts* graded in width from AAA (small) to EE (large) (The widths are AAA, AA, A, B, C, D, E, EE).

During the 19th century until about the time of the American civil war, the same wooden *last* was used in the construction of both right and left shoes. The *lasts* were straight in shape with no allowance for the foot contour. The shoes could be swapped from left to right. Before 1880, shoes were made in full sizes and seldom more than three widths. After 1880, half sizes were introduced. In the twentieth century, quarter sizes were introduced but were unsuccessful due to inventory costs.

In 1815, Thomas Blanchard, Sutton, Massachusetts invented a lathe for the turning of irregular shaped objects. It was first used for turning out gunstocks but was later adopted for *lasts*. The Gilman lathe, now used throughout the *last* industry, was an improvement on the Blanchard lathe. By reason of the fact that no feet are exactly alike, one can readily appreciate the necessity of making shoes on scientifically designed *lasts* – *lasts* that will conform to the great majority of feet of any given type.[5]

Even after 60 years, most master *lasts* are still made by a master *last* maker, who uses his/her artistic skills to generate a *last* using few foot parameters. Currently, wood, aluminum, or plastic (high density polyurethane) are used for shoe *lasts*. The wooden *last*, which has a high price and low durability, is the traditional material for *last* making. It has the disadvantage of changing its shape due to temperature and humidity. Currently, it is usually used for the model, master or designer's *last*. However, the plastic *last* is widely used. It has a medium durability, but it is difficult to handle due to its heavy weight. Aluminum *lasts* are relatively cheap and have high durability, however, their shape is temperature dependent.

Difference between foot and last

It is essential to understand the difference between a *last* and a human foot. The *last* has a smooth surface to enhance the appearance of the shoe and enable the upper to be moulded more easily to shape. The surface of the foot is irregular and varies with individuals. The outline of a *last* is regular and continuous with a sharp featheredge around the seat and forepart to assist lasting and give a clear defined edge to the finished shoe. The foot has no featheredge. The *last* is hard and firm, while the foot is softer and more flexible. The foot has separate toes, while the toe end of a *last* is solid. The heel curve is greater on the *last* to help the shoe grip the foot. Heel pitch

is present in the *last* but not on the foot. The front part of the *last* is thinner to help the shoe to grip the foot around the quarters. The *last* length is greater than the foot to prevent pressure on the foot. Toe spring is not present on foot but is on the *last.* Girth and size intervals are regular on *lasts* but irregular on feet. The dimensions are identical on a pair of *lasts* but rarely identical on a pair of feet. At the toes, the *last* increases gradually in height from the feather line, but not in the foot. The *last* is for shoe making while the foot is used for weight bearing and locomotion.

Basic last measurements

The American Footwear Manufacturers Association (AFMA) defines as many as 61 terms related to *last* dimensions. However, there is no direct mapping from the foot to the *last*. The model maker rarely starts from scratch. A previous *last* is used as a starting point, and thus foot studies have little impact on *last* making.[17] Although the *last* is a complex 3-D shape with no straight lines on it, the *last* maker first marks the four points vamp, instep, ball break, and heel point as the reference points[17] as shown in Fig. 22.8. Then only six dimensions are used to guide the last maker in the *last* making process. Five of the six measures are circumference measures: ball girth, waist girth, instep girth, long heel girth, and short heel girth. The final measurement is the overall heel-to-toe length on the *last*, which is also called stick length. The model maker shapes, sands and files until the six measurements match and the model 'looks right'.[17] The way the model has been sanded will affect the fit. The *last* making is evolved on a man's size 9D *last* or a woman's size 7D *last*. The other sizes are generated by a procedure known as grading.[28]

It is important to note that the stick length used in *last* making is dependent upon heel height, toe spring, and toe style. The degree of toe spring in a *last* depends on several factors, namely the heel height, the shoe style, the upper material and the general flexibility of the shoes. When the heel height is high, the toe spring is lower. Stiff upper material requires more toe spring. Furthermore, toe spring depends on the purpose of the footwear. Normally, walking shoes need more toe spring than dress shoes, while ballet shoes do not have toe spring.

Sizing and grading

Sizing basically involves the construction of footwear of different sizes in order to *fit* the selected population. A *last* is measured by the 'stick length' shoe size. The exact sizing of footwear in order to have perfect physical *fit* is complicated since there is a large range of variations in the dimensions

of the human foot. In order to make the sizing simple, a combination of foot length and foot width is used. However, the size markings are rarely exact.[26] Foot length is measured as the maximum distance from the heel point to the toes. Foot measuring devices such as the Brannock, the Ritz stick, and the Scholl have concentrated on two areas by measuring the length along the foot and the maximum width around the MPJ joint area.

In the US and British systems, the shoe size length changes by 1/3″ (8 mm) per size and the girth by 1/4″ (6 mm) per size. In addition there is an increase in 1/4″ (6 mm) between different width grades. For example, from shoe size 9D to shoe size 10D the length will increase by 1/3″ (8 mm) while the girth will increase by 1/4″ (6 mm). However, from shoe size 9D to shoe size 9E the girth increases by 1/4″ (6 mm) while the length is not increased. Apart from the US and British systems, most European countries use the French system, also known as the continental system or the Paris points. The ratio of length increase to girth increase is the same as in the other two systems. However, the metric increment is not the same. The length grade is 2/3 cm and the girth grade is 1/2 cm between sizes. The Mondopoint system is a foot sizing system proposed by the International Standards Organization (ISO). This uses the metric system for sizing the length and the width dimensions.[29] Different from the other system, the projected length of a foot, around which the shoe should *fit*, is used for sizing.

There are three types of grading system: the arithmetic grade, the geometric grade, and the proportional grade. In an arithmetic grade, the increment of a dimension per increase in foot size is a constant.[28] The arithmetic grade is currently used for US and British shoe standards. In the geometric grade, the increment per size and/or width of any dimension is a specified percentage of the dimension. Proportional grading is a system in which the increments of all dimensions per size within a size run are a constant.

Different last shape

There are an enormous number of shoes, but most of them can be classified into six toe types. These are square, oblique, round, circle, oval and crescent (Fig. 22.9). Moving from round to crescent passing through circle and oval, the toe shape becomes more pointed. The square shape shoe *last*, as the name suggests, does not have a rounded toe box. The oblique toe box provides more space at the big toe and less space at the fifth toe. If properly designed, it can provide the best comfort. In addition, the shoe-last can be different based on different toe heights, as shown in Fig. 22.9. Due to the shape of the *last*, especially at the toe, shoes of the same size may not have the same length and width. As a result, shoes manufactured with different shoe-last do not have the same *fit*.

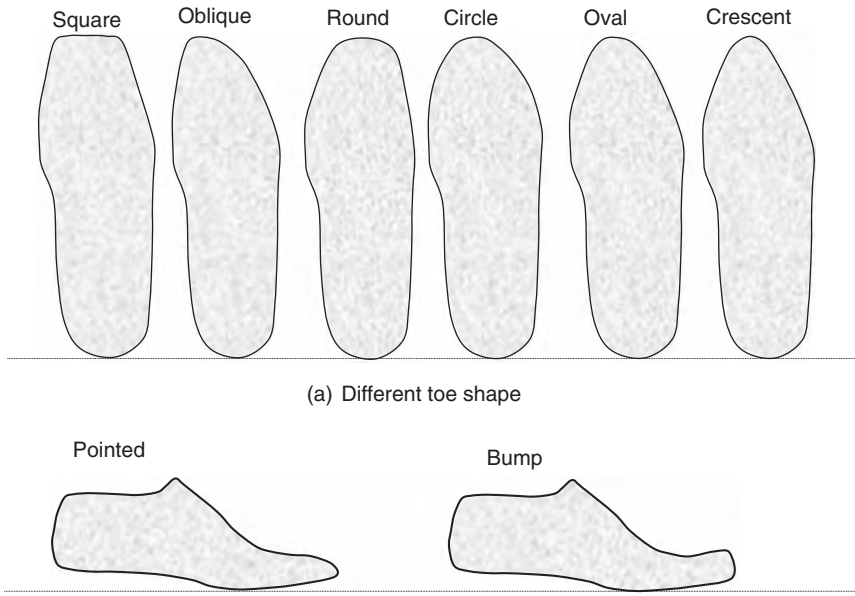

22.9 Shoe-last shapes.

Curve and straight last

In addition to *last* shape, shoe-lasts can have different plantar curvature (Fig. 22.10). The shoe 'curvature' or flare can be seen while looking at the shoe outsole or the bottom of a *last*. The flare can be quantified as an angular measure,[19] ratio,[30] or an angular measure with a center.[20] Most *lasts* have a distinct inward turn towards the medial side of the foot and are known as curved, racing or inflared *lasts*. Most shoes have a 6 degrees inflare.[31] The flare angle, which is typically 3 degrees for a straight *last*, can be up to 12 degrees.[17] Different shoe manufacturers build-in different flares in their shoes (Fig. 22.10); thus different shoes with the same size can have different fittings.

22.3.3 Footwear manufacturing

SATRA[26] provides 12 simple steps to make footwear. The first step in shoe production is to have a shoe *last*. The *last* is covered with paper tape and a pattern is drawn on it. The tape is then removed from the *last*. Various allowances are added. The patterns are then encoded into knives and cutters. This can be used in a press to cut the leather or synthetic material. After

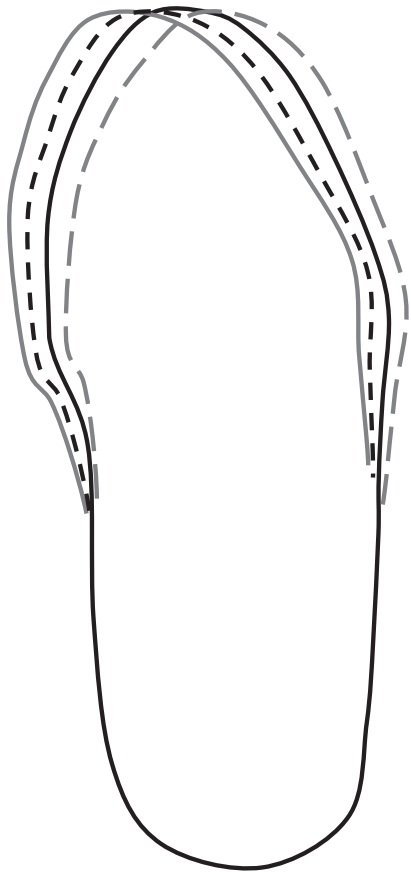

22.10 Shoe-last with different curvatures.

the upper material is cut, it is stitched together to form the upper part of the shoe. The upper part may include toe puffs and heel stiffeners. The insole is attached to the *last.* The upper part is lasted. Lasting is basically the pulling of the upper part and sticking in on the insole attached to the *last*. The sole unit is attached. In some cases the sole and heel are attached. The shoe is cleaned and sprayed. The shoe is checked and dispatched. This procedure is for the cemented shoe construction method, the most common shoe manufacturing method (Table 22.1). There are different types of shoe construction based on shoe style, cost and quality.[32]

Shoe classification

There are numerous shoe styles and new styles of footwear are created every day. Independent of the number of shoes in the market, there is a fixed shoe

Table 22.1 Type of shoe construction

Name	Construction method
Cemented	Most shoes are constructed using this method. – The insole is attached using staples or adhesives to the last bottom. – The shoe upper is placed on top of the last. – The free ends of the upper are pulled, turned on the insole and glued. – The outsole is cemented to the bottom of the lasted shoe upper. – The heel is attached if needed.
Veldtschoen stitch down	The upper is flanged outwards and stitched to the insole. The outsole is cemented to the lasted shoe.
Welted	A special insole with a rib or wall is used. The upper is attached to the ribs usually by wires or staples. The sole is then stitched to the upper. This method is usually used to make better grade men's dress shoes and requires high skills, especially if manual.
Slip-lasted	The last is placed inside after the upper has been stitched with the insole and a sock or cover. Most infant shoes and slippers are constructed using this method.
String lasted	A strong string is used to stitch the edge of the upper. The upper is fitted to the last and then the string is drawn and its ends tied. Then the soles are attached.
Vulcanized	Usually the upper is made of canvas and the insole is attached to the canvas by sewing. – The last is forced inside the upper. – The sole and mud-guard rubber foxing are attached. – The shoe is vulcanized (placing the lasted shoe in a vulcanization tank which is set to a temperature of 150 °C, pressure 3 kg/cm^3 for about 50 minutes.) For some shoes, such as work shoes and outdoor boots, the outsole is directly vulcanized and moulded to the shape of the sole.
Injection	Soles are directly heat-sealed to the upper by machine.

classification system. In general, seven categories are used, except in Hong Kong where ten categories are used for footwear classification. The categories, as shown in Fig. 22.11, are Oxford, pump, boot, sandal, mule, clog, moccasin, infant (Hong Kong classification), children (Hong Kong classification), and sports (Hong Kong classification). Figure 22.11 also provides a simple drawing for each shoe category. Traditionally, Oxford was worn by men only; however, this trend has changed. Now even ladies wear Oxford shoes. Pump, mule and clog are usually worn by ladies, while Oxford, boots, moccasin, sports shoes, and sandals are worn by both ladies and gentleman. Babies' and children's footwear need to have allowance for foot growth and should also include attractive components (lights, sounds, and attractive colors).

Oxford		For many people, Oxford shoes are basically dress shoes and are worn by men, ladies and children. Oxford shoes can be sub-categorized into Balmoral Oxford, Blucher Oxford, Saddle Oxford, Derby, Work shoe, Loafer, and Monk shoe.
Boot		Worn by men, ladies, children and infants. This footwear covers the ankle and was designed for industrial and military work, and outdoor activities. These days, it is worn for all purposes. Boots can be further categorized into Desert boot, Wellington boot, Work boot, Military boot and Cowboy.
Moccasin		Shoe constructed with leather wrapped around the last to form the bottom, sides and upper. Include Deck shoes.
Sandal		Sandals are worn by men, ladies and children. Sandals are open shoes which consists of a decorative or functional arrangement of straps. These include Casual sandals, Sport sandals and Thong sandals.
Pump		Pumps are ladies' shoes. They include Pump, Sling-back court, Open Shank court, Open back court, Open toe court, and Platform court.
Mule		These are shoes without a back strap and slippers with or without heel.
Clog		Clogs are shoes with thick wooden soles.
Infant		Shoes designed for young children. These are soft, with lots of room for the foot to move and grow.
Children		These shoes may have special design for beauty and fun such as sounds and lights.
Sport		There are more and more specific shoe designs for different sports such as Badminton, Baseball, Basketball and others. Since these sports have different dynamics, the shoes are designed to enhance performance and reduce injury, as well as to provide comfort.

22.11 Shoe classification.

22.4 Foot and footwear interface

The interface between the foot and the shoe determines the footwear fit and comfort. When there is a mismatch between the foot and the shoe, the foot is deformed resulting in injury and foot-related illness. It has often been stated that babies are born with perfect or near perfect feet, and many of the foot deformities are due to ill-fitting footwear.

22.4.1 Foot problems

Some of the foot deformities related to footwear are hallux valgus, ankle valgus, hallux rigidus, lesions, corns, calluses, blisters, chilblains. Hallux valgus is associated with abnormal pressure at the MPJ joint of the great toe.[33] The joint is enlarged and there may be formation of a bursa sac of fluid at the joint. In advanced cases, the first toe can overlap or underlay the second toe and the first metatarsal may be deflected away from the other metatarsals. In addition, the MPJ may dislocate and the metatarsal head can be exposed. Moreover, the bursa can be inflamed and it is then known as a bunion. Hallux valgus is caused by footwear that is too narrow or too short. The footwear squeezes the toes together. Ankle valgus (pes valgus) may not be painful in itself. It is caused by the inward rotation of the back of the foot such that the body weight falls on the inner side of the foot, causing the arch to flatten. The condition is self-aggravating, since the more the foot twists the more the weight is on the inner side of the foot. Hallux rigidus include deformities such as hammer toe, clawed toe, retracted toe, mallet toe. It occurs when the footwear is too short and thus limits the movement of the toe at the joints. Calluses, corns, blisters and chilblains belong to the deformities known as lesions. Calluses occur when there is intermittent pressure on some part of the foot. This causes the outer skin to thicken and become hard. Usually, there is pain and a burning sensation when the calluses are under pressure. Corns normally occur over toe joints, when there is friction associated with localized pressure. Blisters are caused by friction. During friction, the outer skin becomes loose and fluid collects beneath it. If the friction continues, the blister breaks, causing an inflamed area. This occurs normally at the back of the heel due to heel slip. Chilblains are caused by pressure, normally at the back of the heel in cold weather.

Many deformities can be eliminated if the offending footwear is discarded early enough. For mild cases, custom insoles, wide toe-box shoes, and arch supports can be used, while surgery might be needed for severe cases.

22.4.2 Consumer consideration

Several surveys have shown that footwear *fit* is a very important factor when purchasing footwear. The characteristics that may affect the choice of footwear depend upon footwear related factors (material, weight, quality, durability, flexibility, traction, shock resistance, etc.), society related factors (fashion, style, brand, store, peer pressure, self esteem, etc.), and foot related factors (comfort, fit, function, softness, cushioning, perceived flexibility, breathability, etc.).[33] Furthermore, subjects rate *fit*, minimal perspiration, good thermal insulation, sole flexibility, upper flexibility, and protection

against the elements as the main elements of comfort (Bolanger, 1974, cited in reference 17). According to Clarks,[28] major consumer needs are appearance and fashion content, *fit* and comfort, price, quality and store. Chong and Chan,[2] in a footwear survey using 70 subjects, required the subjects to rank the importance of six factors (attractive style, function, affordable price, famous brand, material quality, and comfort) when buying a pair of shoes. 27.8% of the subjects gave the highest rating to comfort. When computing the weighted average from Chong and Chan's study,[2] Luximon and Goonetilleke[34] found that comfort was rated higher than quality, price, function, and brand. Since comfort is affected by *fit*, it can be deduced that *fit* is an important factor. The footwear fit can be quantified using dimensional differences between footwear and foot.[34] Fit is just one of the consumer considerations; the whole footwear has to be assessed to select a proper choice for a given function.

22.4.3 Footwear assessment

Experienced fitters check 14 points when fitting footwear.[11] Most of the *fit* trials show that the toes and the ball areas are the most critical to an individual's perception of *fit*. In addition to footwear fit, comfort, flexibility and cushioning have also been evaluated subjectively and objectively.[35] Luximon[33] has considered comfort and fit at the toe box, waist, instep region, and heel region. Table 22.2 shows the different parameters and the footwear regions that can be used to assess footwear comfort, fit, and function.

Table 22.2 Footwear assessment

Footwear region	Parameters		
Toe region or toe box	Width	Height	Volume
MPJ region	Width	Height	Girth
Instep region	Width	Height	Girth
Arch	Height		
Topline or Collar	Height	Comfort	
Heel	Width	Back curve	Heel cup fit
Sole	Flexibility	Flexion point	Tread pattern
	Overall cushioning	Cushioning at heel	Cushioning at forefoot
	Traction	Comfort	
General	Flexibility	Material	Construction
	Overall comfort	Fastening mechanism	Stability

22.5 Biomechanical model

Due to the advancement of technology, it is possible to generate a complex 3-D biomechanical model of the foot including its structures. Generally, the 3-D model of the human foot and ankle is generated from coronal sections of MRI images. Zhang *et al.*[36] used MRI images at 2 mm intervals to create a 3-D geometrical accurate ankle–foot model using MIMICS™ (Materialise Inc., Leuven, Belgium) and SolidWorks 2001™ (SolidWorks Corporation, Massachusetts). Then, ABAQUS™ (ABAQUS Inc. Pawtucket: Rhode Island, USA), a Finite-Element (FE) analysis software, was used for FE mesh generation and subsequent FE analysis.[36] The FE model consisted of 28 distinct bony segments and all major ligaments embedded in homogenous soft tissue.[37] In order to simplify, as well as to have computational convergence, all elements had homogeneous, isotropic, and linearly elastic material properties. The bony structure had a Young's modulus of 10 000 MPa and the Poisson ratio was 0.34, while the plantar soft tissues had a Young's modulus ranging from 0.05 MPa to 0.3 MPa and a Poisson ratio of 0.49.[38] The foot biomechanical model, together with mechanical models of insole,[39] *last*, and footwear,[40] can be used to evaluate internal stresses/strains of the ankle–foot complex. FE analyses can be used efficiently to determine design parameters of footwear without the need for expensive experimental study. In addition, the material properties of the insole and foot model can be varied to study the impact on the foot.

22.6 Conclusion

Footwear has become an integral part of our life and it will remain so for many years to come. Although, footwear has become very sophisticated, footwear comfort and fit has often been neglected. This might be due to the wide variation in feet and the cost of production. It is very expensive to produce individual footwear, so footwear is produced in different sizes. In addition, shoes are produced in different styles depending on fashion. This might further aggravate footwear comfort and fitting. As people become more health conscious, more research is being undertaken into understanding the human foot and its biomechanics. Several biomechanical models are being constructed to help design better footwear. In addition, advancement in technologies will reduce the cost of production; thus perfect fitting footwear will be possible. In conclusion, footwear design should consider fashion and style as well as fit, comfort, and function.

22.7 References

1. Dahlberg, G. and Lander, E. (1948). Size and form of the foot in men. *Acta Genetica*, **2**(I): 8–162.

2. Chong, W.K.F. and Chan, P.P.C. (1992). *Consumer Buying Behaviour in Sports Footwear Industry*. Hong Kong, Business Research Centre: Hong Kong Baptist College.
3. Carlson, M. (2001). Footwear of the Middle Ages. *http://www.personal.utulsa.edu/~marc-carlson/shoe/SHOEHOM1.HTM*.
4. Kippen, C. (2004). The History of Footwear. *http://podiatry.curtin.edu.au/history.html*.
5. Quimby, H.R. (1944). *The Story of Lasts*. New York, National Shoe Manufacturers Association.
6. Luximon, A. and Goonetilleke, R.S. (2001). A fit metric for footwear customization. *World Congress on Mass Customization and Personalization*, Hong Kong.
7. Cummings, S.R., Ling, X. and Stone, K. (1997). Consequences of foot binding among older women in Beijing, China. *American Journal of Public Health*, **87**, (10): 1677–1679.
8. Hunt, K.D. (1994). The evolution of human bipedality: Ecology and functional morphology. *Journal of Human Evolution*, **26**, (3): 183–202.
9. Morton, D.J. (1935). *The Human Foot*. New York, Columbia University Press.
10. Abboud, R.J. (2002). Relevant foot biomechanics. *Current Orthopaedics*, **16**, (3): 165–179.
11. Rossi, W.A. (1988). The futile search for the perfect shoe fit. *Journal of Testing and Evaluation*, **16**: 393–403.
12. Rossi, W.A. (1983). The high incidence of mismated feet in the population. *Foot and Ankle*, **4**, (2): 105–112.
13. Tsung, Y.S. (2003). *Insole design based on pressure distribution and foot shape under different weight bearing conditions.* Hong Kong, The Hong Kong Polytechnic University.
14. Cheskin, M.P. (1987). *The Complete Handbook of Athletic Footwear*. New York, Fairchild Publications.
15. Kouchi, M. and Mochimaru, M. (2002). *Japanese Body Dimensions Data 1997–1998*, Digital Human Research Center, National Institute of Advanced Industrial Science and Technology.
16. Malina, R.M., Hamill, P.V.V. and Lemeshow, S. (1973). Selected measurements of children 6–11 years. *Vital Health Statistics, Series 11*. Washington, DC., USDHHS, US Government Printing Office.
17. Cavanagh, P.R. (1980). *The Running Shoe Book*. Mountain View, CA, Anderson World.
18. Palastanga, N., Field, D. and Soames, R. (1989). *Anatomy and Human Movement: Structure and Function*. Oxford, Heinemann Medical Books.
19. Freedman, A., Huntington, E.C., Davis, G.C., Magee, R.B., Milstead, V.M. and Kirkpatrick, C.M. (1946). *Foot Dimensions of Soldiers.* Fort Knox, Kentucky, Armored Medical Research Laboratory.
20. Goonetilleke, R.S. and Luximon, A. (1999). Foot flare and foot axis. *Human Factors*, **41**, (4): 596–607.
21. Nigg, B.M. (1986). *Biomechanics of Running Shoes*. Champaign, Ill, Human Kinetics Publishers.
22. Clarke, H.H. (1933). An objective method of measuring the height of the longitudinal arch in foot measurements. *Research Quarterly*, **4**: 99–107.
23. Cavanagh, P.R. and Rodgers, M.M. (1987). The arch index: A useful measure from footprints. *Journal of Biomechanics*, **20**, (5): 547–551.

24. Kreighbaum, E.F. and Smith, M.A. (1996). *Sports and Fitness Equipment Design*. Champaign, Ill., Human Kinetics.
25. Kaplan, A.R. (1964). Genetics of Relative Toe Lengths. *Acta Genet. Med. Gemellol*, **13**: 295–304.
26. SATRA (1993). *How to Fit Footwear*. UK, Shoe and Allied Trades Research Association (SATRA), Footwear Technology Centre.
27. Rossi, W.A. (1980). The Last: Heart of the Shoe. *Journal of American Podiatrist Association*, **70**: 533–534.
28. Clarks (1989). *Manual of shoe making*. UK, Training Department Clarks.
29. ISO9407 (1991). *Shoe Sizes – Mondopoint System of Sizing and Marking*. Switzerland, International Organization for Standardization.
30. Yavatkar, A.S. (1993). *Computer aided system approach to determine the shoe-last size and shape based on statistical approximated model of a human foot.* Medford MA, Tufts University.
31. Holscher, E.C. and Hu, K.K. (1976). Detrimental results with the common inflared shoe. *Symposium on Pitfalls in Foot Surgery*: 1011–1018.
32. Hong Kong Productivity Council (2001). *Information Handbook for Merchandisers of the Hong Kong Footwear Industry*. Hong Kong, Publisher Hong Kong Productivity Council.
33. Luximon, A. (2001). Foot shape evaluation for footwear fitting, in *Industrial Engineering and Engineering Management*. Hong Kong, Hong Kong University of Science and Technology.
34. Luximon, A. and Goonetilleke, R.S. (2003). A 3-D methodology to quantify footwear fit (Chapter 28), in *The Customer Centric Enterprise – Advances in Customization and Personalization*. M.M. Tseng and F. Piller (eds). New York, Berlin, Springer: 491–499.
35. Mundermann, A., Stefanyshyn, D.J. and Nigg, B.M. (2001). Relationship between footwear comfort of shoe inserts and anthropometric and sensory factors. *Medicine and Science in Sports and Exercise*, **33**, (11): 1939–1945.
36. Zhang, M., Cheung, J.T.M., Fan, Y.B. and Leung, A.K.L. (2002). Development of 3D finite element model of human foot and ankle. *IVth World Congress of Biomechanics*, Calgary, Canada.
37. Cheung, J.T.M. and Zhang, M. (2004). A 3-D finite element model of the human foot and ankle for insole design. *Archives of Physical Medicine and Rehabilitation*: Accepted 2004.
38. Gefen, A., Megido-Ravid, M. and Itzchak, Y. (2001). *In vivo* biomechanical behavior of the human heel pad during the stance phase of gait. *Journal of Biomechanics*, **34**, (12): 1661–1665.
39. Cheung, J.T.-M., Zhang, M. and Luximon, A. (2004). *Computational Model for Foot Orthosis Design. 11th World Congress of International Society for Prosthetics and Orthotics*, Hong Kong.
40. Luximon, A., Cheung, J.T.M. and Zhang, M. (2004). Biomechanical effects of shoe last design on the ankle–foot structures, *International Society for Prosthetics and Orthotics*, Hong Kong.

23

Biomechanical engineering of aerobic sportswear

A. WONG[1], Y. LI[1], E. NEWTON[1] AND X. ZHANG[2]
[1]The Hong Kong Polytechnic University, China
[2]Xian University of Engineering Science & Technology, China

23.1 Introduction

In relation to clothing construction, Kirstein *et al*.[3] stated that the term 'fit' means to adjust the measurements of a garment to those of the body. Zhang *et al.*[15] stated that garment pressure is closely related to the space allowance between the body and the garment during body movement. When a garment girth measurement is smaller than the human body, the space allowance between body and garment is less than or equal to zero, hence pressure is generated. Skin is extremely sensitive to pressure and, under ideal conditions, skin displacement that is less than 0.001 mm can result in a sensation of pressure or touch.[9] Denton[2] found the level of clothing pressure discomfort to be in the range 20 to 40 g/cm^2, depending on the individual and the part of the body concerned. According to Pratt and West,[8] there are three factors influencing the pressure exerted by garments: (i) shape of the body parts, the greater the degree of curvature, the greater the pressure exerted; (ii) type of fabrics used; and (iii) design and fit of the garment. A badly designed garment may lead to the body suffering by perceiving unnecessary pressure.

In general, investigations of pressure distribution on the human body can be classified into two categories: experimental and numerical. The experimental category, can be divided into psychological and physical sections. Morooka *et al.*[7] found that perception of clothing pressure of females in their forties was twenty percent less than for females in their teens and twenties. Furthermore, the influence of leg circumference on the clothing pressure tended to become lower with increasing age. Zhang *et al.*[11–14] carried out a series of investigations in relation to pressure by using the force–deformation of relationship fabric bagging – a planar fabric being forced to conform to a spherical surface. Mitsuno *et al.*[6] used a hydrostatic pressure-balanced method to measure clothing pressure qualitatively. Makabe *et al.*[5] investigated clothing pressure developed by a girdle. They found that subjects perceived pressure discomfort mainly on the front waist

line and the thigh base. They also noticed that when clothing pressure reached more than 30 to 40 mm Hg, subjects began to complain of pressure discomfort. The previous chapter investigated the psychological pressure perception of tight-fitting sportswear in young adults.[10] A group of subjects wearing different sets of tight-fitting sportswear and required to perform different postures gave scores at nine pressure points on the perception of pressure comfort on the body after each posture. The results show that subjects perceived most pressure discomfort around the thigh. We also carried out a physical pressure distribution investigation, when five female subjects participated in a wear trial.[10] Each subject was connected to nine pressure sensors, which were placed between the subject's skin surface and the inner layer of the garment at nine different body locations. By assuming different postures, the results show that subjects perceived most pressure at the side waist while they were standing, arm-lifting and stretching. However, subjects perceived most pressure at the front waist while they were curling-up their legs.

Although these experimental results indicate that there are differences in the pressure perception, they do have disadvantages, including: (i) many subjects have to be used in order to obtain a reliable result, (ii) subjective judgments may be influenced by many psychological factors, which vary from person to person, and (iii) the variations in subjects' body curvatures influence the placement of pressure sensors. Cheng *et al.*[1] stated that the distortion degree of sensor insertion and the degree of accuracy of the sensor used were found to be important factors influencing the measured level of garment pressure. These experiments provide evidence and clues on what factors influence the garment pressure and the perception of pressure comfort. However, they cannot explain the physical mechanisms involved.

Theoretical investigations can be carried out to develop an understanding of the mechanisms by establishing mechanical–mathematical models on the basis of physical laws. The models can be solved by numerical computation, and can be used for numerical simulation of the wear process. In the numerical simulation, the 3D human body model can be generated through a commercially available virtual human model or a scanned human body, and pressure distributions of a garment can be predicted on the basis of fabric properties. A series of biomechanical models have been developed by Zhang *et al.*[15] and Li *et al.*[4] to investigate the dynamic interactions between the human body and garments in various wear situations, such as a bra and tight-fitting trousers, by considering the biomechanical structures of the human body, and the contact mechanics between body, garment and 3D garment constructions.

In this chapter, a theoretical investigation of garment pressure comfort is conducted by applying a dynamic model for the numerical simulation of

pressure in tight-fitting garments during wear. By analyzing the contact characteristics between a human body and a tight-fit garment, the process of a female body wearing three well-fitting tight-fit garments, which have the same design but are made from different fabric, is simulated. The predicted pressure distributions are compared with the objective garment pressure measurements and psychological pressure perception ratings.

23.2 Biomechanical modeling

Clothing pressure is a combination of garment, human body and the mechanical interactions between them. Denton[2] stated that true fitting to the body shape can only be achieved by the use of stretch fabrics that can expand and contract without buckling or wrinkling to accommodate body movement. Zhang *et al.*[15] held that garment pressure is closely related to the space allowance between body and garment when the body is moving. Furthermore, Zhang classified garment into three categories on the basis of space allowance.

Therefore, the assumption of stretch-to-fit garment is to be a thin elastic shell with material linearity and geometric non-linearity, and the human body to be a rigid body. The stress in the direction of fabric thickness is assumed to be zero. This simulation only considers the female body in a steady standing state. All the garments have the same style but are made of different materials.

Figure 23.1 shows the model developed by Zhang *et al.*,[15] which describes the interaction between human body and a tight-fit garment. During wear, mechanical interaction occurs at the contact areas between the body and the garments. The figure shows the external forces on the tight-fit shorts during wear, including an interactive contact force q_c in the normal direction to the contact surface, the friction q_f as the garment slips on the surface and the gravity q_g on the garment. The external forces will be balanced by fabric internal stresses (tension, shearing and bending) and the inertia force q_I of the garment during a dynamic deformation process.

In the simulation of a human body, three major components (skin, soft tissue and bone) were considered. A human body is constructed from a skeleton covered by a layer of skin, which is the largest organ in a human. Between the skeleton and skin is a layer of tissue. A 3D finite element model of a female human body was developed on the basis of a commercially available virtual human model.

The process of a female human body wearing a pair of tight-fit shorts from the foot level to the waist was simulated. The process was divided into three steps: (i) the waistline of the garment just reaching the subject's shank; (ii) the waistline of the garment reaching the subject's pelvis; and (iii) the garment completely fitted to the subject. In practice, a human's body and

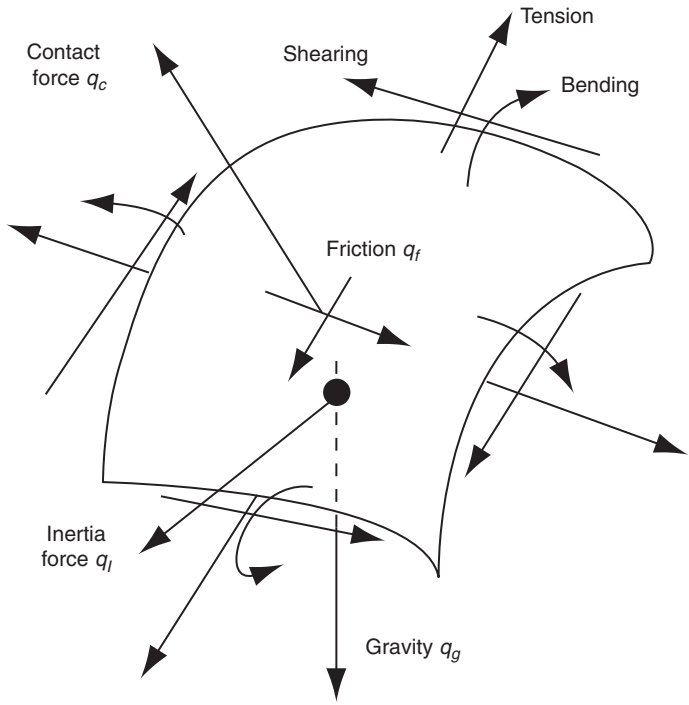

23.1 External forces on tight-fit shorts during wear.

legs are moving continuously during the wearing process. This might cause external force to be applied to the shorts, which begin to deform. As the amount of force acting on the shorts is unknown, therefore, the female body was assumed to remain still in the standing position throughout the wearing process. It was also assumed that the frictional force between body skin and the shorts is negligible.

23.3 Physical properties of aerobic wear

The physical properties of the two tight-fit garments used in this study are shown in Table 23.1. Two fabrics made of different fibres with completely different mechanical properties were selected in order to study the influence of the garments on dynamic clothing pressure distribution. Each fabric sample was kept in a conditioned room for more than 24 hours with temperature and humidity of 20 ± 2 °C and 65 ± 3%, respectively. In order to test the mechanical properties of the garments, which relate to the development of the numerical model, the KES tensile and shear tester, KES-FB-1, was used. The mechanical parameters of both tests were modified from the

original setting of the machine. The maximum force was set at 50 gf/cm, the sensitivity was 5 × 5, the tensile speed was 0.1 mm/sec, and the size of the fabric was 20 × 20 cm^2. The characteristic property values and the measurement conditions for these parameters are listed in Table 23.2.

23.4 Biomechanical simulation

23.4.1 Simulated pressure changes at measured body locations

Dynamic pressure changes of two garments, C98L2 and P98L2, at seven pressure points during the wearing process were simulated. A positive pressure value indicates the force in the garment moving towards the skin when the garment does not contact the body at a particular point. A negative

Table 23.1 Basic description of selected garments

Garment	Thickness (mm)	Weight (g/m^2)	Fibre content (%)	Construction
C98L2	0.73	179.00	Cotton (98) & Lycra™ (2)	Plain knitted
P98L2	1.27	220.00	Polyester (98) & Lycra™ (2)	Rib knitted

Table 23.2 Tensile and shear properties of selected garments

Property	Symbol	Unit	Garment	
			C98L2	P98L2
Tensile	LT	–	0.83 ± 0.15	0.78 ± 0.11
	WT	gf/cm·cm^2	3.76 ± 1.62	6.28 ± 1.58
	RT	%	57.26 ± 12.17	54.02 ± 15.10
	EMT	%	24.56 ± 6.12	56.40 ± 37.90
Shear	G	gf/cm·degree	0.77 ± 0.02	0.46 ± 0.10
	2HG	gf/cm	2.21 ± 0.14	1.47 ± 0.18
	2HG5	gf/cm	2.47 ± 0.22	1.57 ± 0.19

LT = Linearity of load–extension curve
WT = Tensile energy
RT = Tensile resilience
EMT = Tensile strain
G = Slope measured between $\phi = 0.5$ and 5.0 degrees
2HG = Hysteresis of Fs at $\phi = 0.5$ degrees
2HG5 = Hysteresis of Fs at $\phi = 5.0$ degrees

pressure value indicates that pressure on the body is induced by the garment. The pressure distribution at individual pressure points among the two garments was similar. For the pressure points on the waist girth, the pressure changes had an increasing trend until the garment passed through the hip and the trend began to decrease until the garment was totally fitted onto the body. On the other hand, the changes of pressure on garment side pelvis and thigh girth points had relatively flat and stable trends, which began to increase when the garment passed through the hip. The maximum pressures on the waist were 29 and 30 gf/cm^2 for garments C98L2 and P98L2, respectively.

23.4.2 Maxima of the predicted garment pressure measurements

Figure 23.2 compares the maxima of the predicted garment pressure measurements at different locations on the two garments. The general patterns of the two garment trends are similar. It appears that the maximum garment pressure of C98L2 is greater than P98L2 for most of the body locations except back waist. C98L2 has a lower value of tensile strain than P98L2, suggesting that more force has to be applied in order to put on C98L2 during the wear process, especially when the waist girth of the shorts passes through the pelvis of the simulated body.

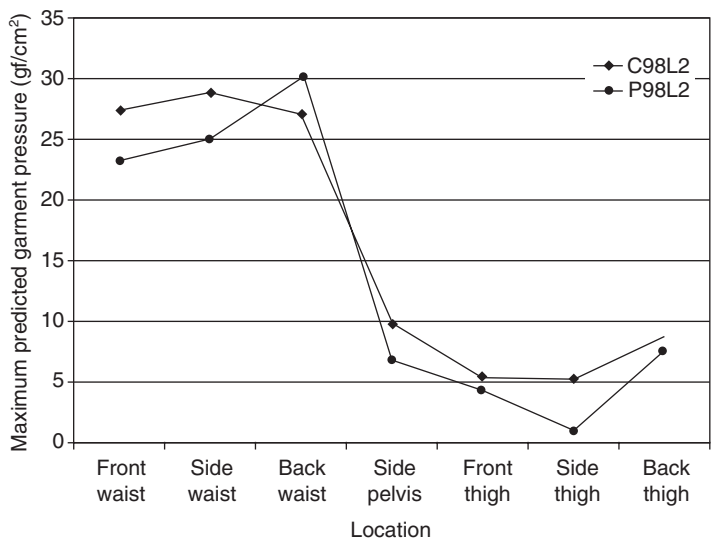

23.2 Predicted garment pressure, maximum measurements.

23.4.3 Simulated pressure distribution in 3D

The simulated pressure distributions of C98L2 and P98L2 from the front and back in the fitted position were determined. Based on the contour plot, the simulated pressure acting on the subject body was not uniformly distributed and was within the range of 6 to 30 gf/cm^2. High-pressure zones were observed on the waist girth for both garments, with a range between 18 and 30 gf/cm^2.

23.5 Validation of the model

23.5.1 Objective measurements of pressure distribution

Figure 23.3 compares the objective pressure measurements for the two tight-fit garments. Among the three pressure locations on the waist girth, back waist has least pressure for both garments. The subjects perceived significantly greater pressure at the front waist with C98L2 than P98L2. On average, the pressure at the waist girth is greater than at the thigh girth. ANOVA shows that there is a significant difference ($p < 0.05$) between pressure measurements of the two garments, suggesting that these two garments, which were made of different type of fabrics, provided significantly difference objective garment pressure to the wearers. In Chapter 6, the detailed ANOVA table shows that garments have a significant influence on garment pressures. Location also has a significant ($p < 0.05$) influence on this.

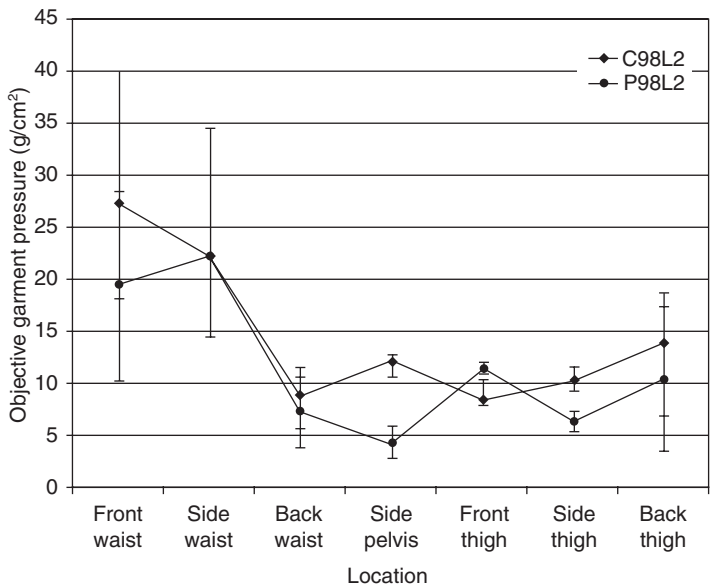

23.3 Objective pressure measurements on two garments.

23.5.2 Subjective assessments of pressure distribution

Figure 23.4 compares the subjective pressure comfort rating of two tight-fit garments. It is obvious that subjects are more comfortable with C98L2 than with P98L2 when comparing the pressure comfort rating around the thigh girth. The subjective clothing pressure comfort rating and objective clothing pressure measurement have relatively larger variations at the front and side waist than other body locations. This might be explained by the variation of the subjects' waist measurements. In other words, the difference in waist measurement is larger than thigh measurement for the objective clothing pressure measurement. Furthermore, the skin sensitivity also has to be taken into account for the subjective clothing pressure comfort rating.

23.5.3 Comparison between experimental and simulated pressure distribution

The experimental and simulated pressure distributions of both garments were compared at seven pressure points. The trends of experimental and simulated pressure distributions are similar for both garments over the seven body locations except at the back waist. At the back waist, predicted garment pressure was higher than the measured values for

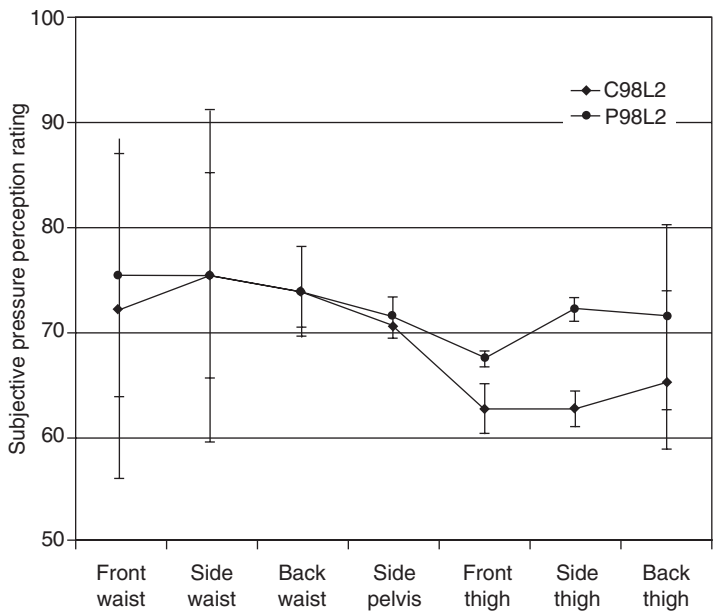

23.4 Subjective pressure perception rating of two garments.

both garments. This might be explained by the difference in the geometric contours between the simulation and the experiment. Practically, there is a hollow place between the skin and garment at the back waist, the depth of which varies from person to person. Hence, the contact force and area between skin and garment are expected to be small. However, the simulated body has no such variation, as the depth is small and garment is closely contacted with skin. Therefore, the predicted garment pressure was greater than experimental garment pressure measurement in both garments. In C98L2, both subjective pressure perception rating and predicted garment pressure measurement peaked at the front waist, followed by the points at the side waist. On the other hand, subjective pressure perception rating and predicted garment pressure measurement of P98L2 peaked at the side waist and the back waist, respectively.

23.5.4 Relationship between subjective garment pressure perception and predicted garment pressure measurement

Figures 23.5 and 23.6 illustrate the relationship between subjective pressure perception ratings and predicted garment pressures. Positive linear relationships between subjective rating and predicted pressure distribution are observed for both garments. For the garment made of cotton and Lycra™ (C98L2), the correlation between the two sets of data has $r = 0.90$, significant at the 0.05 level. For the garment made of polyester and Lycra™ (P98L2), the correlation between the two has $r = 0.78$ at a significance level of 0.05. This suggests that the predicted pressure of C98L2 has a slightly closer linear relationship with the subjective pressure perception rating than the predicted pressure measurement of P98L2.

The gradients of two slopes is different due to the fact that the garments are made of two different types of fabric, the mechanical properties of which are different, although the design and size are the same for both garments in the wear trial and simulation process. This suggests that the mechanical properties play an important role in clothing pressure. The measuring conditions and physical parameters of the two garments are shown in Table 23.2.

The significant relationship between subjective pressure perception and predicted pressure shows: (i) theoretical modeling is effective for prediction of pressure comfort; (ii) the physical mechanisms developed in the model are valid for the description of the perception of pressure comfort; and (iii) fabric mechanical properties influence the garment pressure distribution, and thus the subjective pressure comfort perceptions.

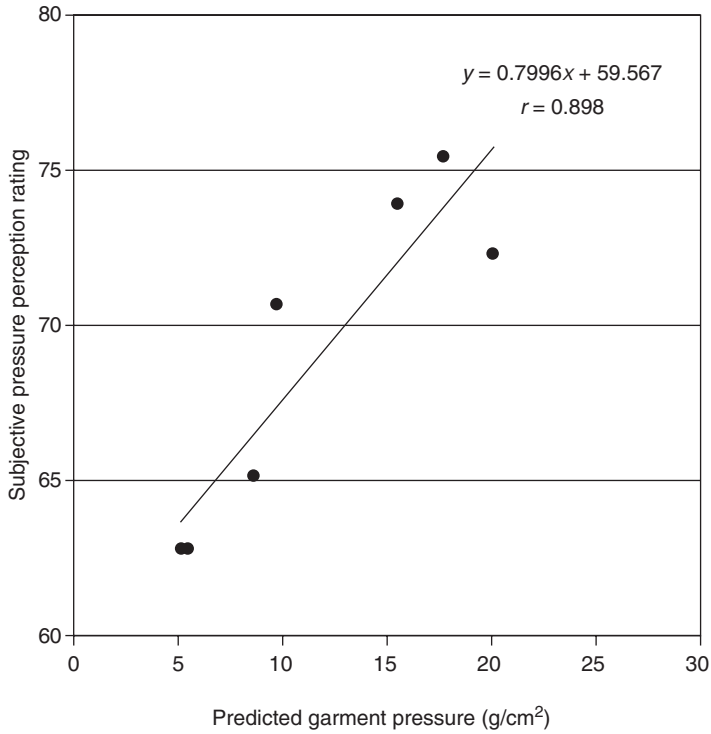

23.5 Relationship between subjective pressure perception rating and predicted garment pressure (cotton/Lycra™ garment).

23.6 Conclusion

Clothing pressure distributions of two sets of tight-fit sportswear have been investigated by theoretical modeling and simulation. In the numerical simulation of clothing pressure, we found that pressure increased more at the waist girth than at other body locations. The pressure begins to decrease when the waist girth passes through the pelvis. Meanwhile, pressure at side pelvis and thigh girth begins to increase during the wearing process. Based on the pressure contour plot on the subject body, pressure was not uniformly distributed and a high-pressure zone was found on the waist girth for both garments. Garments made from different fibres have different pressure distributions during wear and pressures are significantly different at different body locations. Good correlations were observed between subjective pressure perception rating and predicted garment pressure, indicating that the physical mechanisms proposed in the model are valid in describing the dynamic mechanical interaction between body and garments so as to predict garment pressure comfort. Fabrics with different mechanical

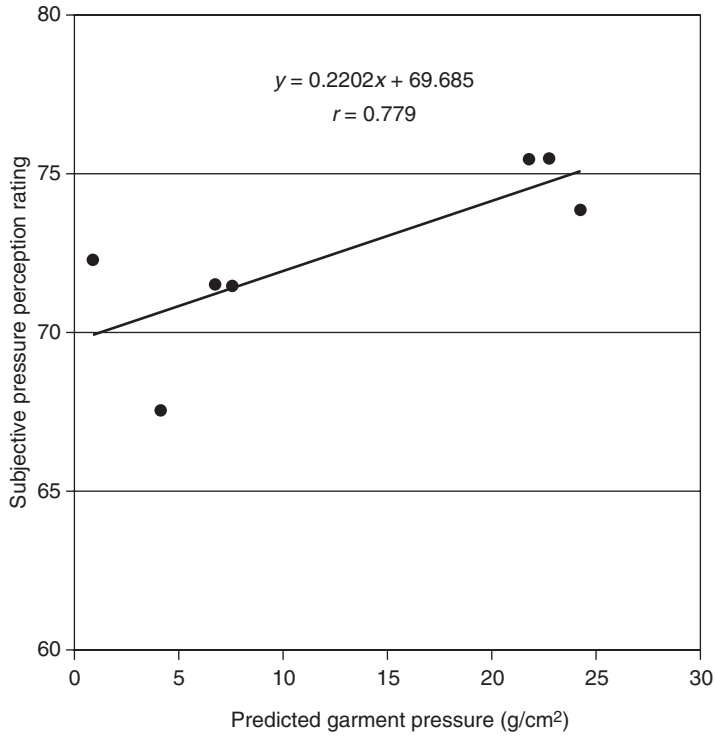

23.6 Relationship between subjective pressure perception rating and predicted garment pressure (polyester/Lycra™ garment).

properties influence the dynamic pressure distributions at contacts with the body during wear. Good agreement was found between predicted and measured garment pressure.

23.7 Acknowledgement

We would like to thank the Hong Kong Polytechnic University for funding this research through the projects A188 and A714.

23.8 References

1. Cheng, J.C.Y., Evans, J.H., Leung, K.S., Clark, J.A., Choy, T.T.C., and Leung, P.C. Pressure Therapy in the Treatment of Postburn Hypertrophic Scar – A Clinical Look into Its Usefulness and Fallacies by Pressure Monitoring. *Burns*, 1984. **10**(3): p. 154–163.
2. Denton, M.J., Fit, Stretch, and Comfort, in *Textiles*. 1972. p. 14.
3. Kirstein, T., Krzywinski, S. and Rodel, H., Fit optimization for close-fitting garments with regard to material properties. *Texsci-'98*, 2001. **3**: p. 398–403.

4. Li, Y., Zhang, X. and Yeung, K.W., A 3D Bio-Mechanical Model for Numerical Simulation of Dynamic Mechanical Interactions of Bra and Breast during Wear. *Ergonomics*, 2001.
5. Makabe, H., Momota, H., Mitsuno, T. and Ueda, K., A study of clothing pressure developed by the girdle. *Journal of the Japan Research Association for Textile End-Uses*, 1991. **32**: p. 424–438.
6. Mitsuno, T., Makabe, H., Momota, H. and Ueda, K., Studies on the Clothing Pressure (Part 1) – Measurements by a Hydrostatic Pressure-Balanced Method. *Journal of the Japan Research Association for Textile End-Uses*, 1991. **32**: p. 362–367.
7. Morooka, H., Nakahashi, M. and Morooka, H., Compressive property of legs and clothing pressure of pantyhose from the view point of difference in age. *Journal of the Japan Research Association for Textile End-Uses*, 1997. **38**: p. 324–332.
8. Pratt, J. and West, G., *Pressure garments – A manual on their design and fabrication*. 1995: Butterworth Heinemann.
9. Schiffman, H.R., The Skin, Body, and Chemical Senses, in *Sensation and Perception*, R.L. Gregory and A.M. Colman, Editors. 1995, Longman: London and New York. p. 70–96.
10. Wong, A.S.W., Li, Y. and Zhang, X., *Influence of fabric mechanical property on clothing dynamic pressure distribution and pressure comfort on tight-fit sportswear.* Sen-i Gakkaishi, 2004. **60**(10): p. 293–299.
11. Zhang, X., Li, Y., Yeung, K.W., Miao, M.H., and Yao, M., Fabric Bagging: Distribution of Stresses of Isotropic and Anisotropic Fabrics. *Journal of Textile Institute*, 2000. **91**(4): p. 563–576.
12. Zhang, X., Li, Y., Yeung, K.W. and Yao, M., Fabric Bagging Part I: Subjective Perception and Psychophysical Mechanisms. *Textile Research Journal*, 1999. **69**(7): p. 511–518.
13. Zhang, X., Li, Y., Yeung, K.W. and Yao, M., Fabric Bagging, Part II: Objective Evaluation and Physical Mechanism. *Textile Research Journal*, 1999. **69**(8): p. 598–606.
14. Zhang, X., Li, Y., Yeung, K.W., Miao, M.H. and Yao, M., Fabric Bagging: Simulation and Test Method. *International Journal of Clothing of Science and Technology (submitted)*, 1998.
15. Zhang, X., Yeung, K.W. and Li, Y., Numerical Simulation of 3D Dynamic Garment Pressure. *Textile Research Journal*, 2002. **72**(3): p. 245–252.

Index